INTERNATIONAL COUNCIL FOR RESEARCH AND INNOVATION
IN BUILDING AND CONSTRUCTION

WORKING COMMISSION W18 - TIMBER STRUCTURES

CIB - W18

MEETING FORTY-FOUR

ALGHERO

ITALY

AUGUST 2011

Ingenieurholzbau und Baukonstruktionen
Karlsruhe Institute of Technology
Germany
Compiled by Rainer Görlacher
2011

ISSN 1864-1784

CONTENTS

0 List of Participants

INTERNATIONAL COUNCIL FOR RESEARCH AND INNOVATION IN BUILDING AND CONSTRUCTION
WORKING COMMISSION W18 - TIMBER STRUCTURES

MEETING FORTY-FOUR

ALGHERO, ITALY

29 AUGUST – 01 SEPTEMBER 2011

LIST OF PARTICIPANTS

AUSTRALIA

K Crews	University of Technology, Dural
C Gerber	University of Technology, Sydney

AUSTRIA

M Augustin	holz.bau forschungs gmbh, Graz
T Bader	TU Wien
T Bogensperger	holz.bau forschungs gmbh, Graz
G Hochreiner	TU Wien

CANADA

G Doudak	University of Ottawa
T Joyce	University of New Brunswick
F Lam	University of British Columbia, Vancouver
M Popovski	FPInnovations, Vancouver
A Salenikovich	Universite Laval, Quebec
I Smith	University of New Brunswick

CZECH REPUBLIK

P Kuklik	Czech Technical University

DENMARK

H J Larsen	Copenhagen
J Munch-Andersen	Danish Timber Information, Lyngby

FINLAND

A Ranta-Maunus	Hämeenlinna

FRANCE

F Rouger	FCBA, Paris

GERMANY

S Aicher	MPA University Stuttgart
H J Blaß	Karlsruhe Institute of Technology (KIT
F Brühl	University Suttgart
M Frese	Karlsruhe Institute of Technology (KIT)
R Görlacher	Karlsruhe Institute of Technology (KIT)
C Hall	TU Braunschweig
P Janßen	TU Braunschweig
U Kuhlmann	University Suttgart
M Merk	TU München

P Mestek	TU München
J Müller	Bauhaus Universität, Weimar
M Sieder	TU München
P Stapel	TU München
G Stapf	MPA University Stuttgart
J W van der Kuilen	TU München
S Winter	TU München

ITALY

M Ballerini	University of Trento
A Ceccotti	IVALSA-CNR
M Follesa	University of Cagliari, Firenze
M Fragiacomo	University of Sassari, Alghero
A Polastri	IVALSA-CNR
F Sarti	Venegono Inferiore

JAPAN

K Kobayashi	Shizuoka University
M Yasumura	Shizuoka University

NEW ZEALAND

A Buchanan	University of Canterbury, Christchurch
B Franke	University of Auckland
J Jensen	University of Auckland
S Pampanin	University of Canterbury, Christchurch
F Scheibmair	University of Auckland
T Smith	University of Canterbury, Christchurch

NORWAY

E Aasheim	The Norwegian Institute of Wood Technology, Oslo
S Eide	The Norwegian Institute of Wood Technology, Oslo
K A Malo	NTNU, Trondheim
K Nore	The Norwegian Institute of Wood Technology, Oslo

SLOWENIA

B Dujic	Contemporary building design, Celje
J Jancar	Contemporary building design, Celje
I Sustersic	Contemporary building design, Celje

SWEDEN

C Bengtsson	SP Trätek, Boras
U A Girhammar	Lulea University
N Jacquier	Lulea University
A Just	SP Trätek, Stockholm
J Schmid	SP Trätek, Stockholm
E Serrano	Linnaeus University, Växjö
R Ziehten	SP Trätek, Boras

SWITZERLAND

G Fink	ETH Zürich
A Frangi	ETH Zürich
S Franke	Berner Fachhochschule, Biel
R Jockwer	EMPA Dübendorf
M Klippel	ETH Zürich

J Köhler	ETH Zürich
C Sigrist	Berner Fachhochschule, Biel
R Steiger	EMPA Dübendorf
T Theiler	ETH Zürich

THE NETHERLANDS

A Jorissen	TU Eindhoven

UNITED KINGDOM

R Harris	University of Bath
K K Ranasinghe	TRADA, High Wycombe
J Skinner	University of Bath
V Enjily	Enjily International, Oxford

USA

T Skaggs	American Plywood Association, Tacoma
B Yeh	American Plywood Association, Tacoma

1. Chairman's Introduction

2. General Topics

3. Stress Grading

4. Stresses for Solid Timber

5. Timber Joints and Fasteners

6. Laminated Members

7. Structural Stability

8. Fire

9. Statistics and Data Analysis

10. Research Notes

11. Any Other Business

12. Venue and Program for Next Meeting

13. Close

INTERNATIONAL COUNCIL FOR RESEARCH AND INNOVATION IN BUILDING AND CONSTRUCTION

WORKING COMMISSION W18 - TIMBER STRUCTURES

MEETING FORTY-FOUR

ALGHERO, ITALY

29 AUGUST – 01 SEPTEMBER 2011

M I N U T E S
(F Lam)

1 CHAIRMAN'S INTRODUCTION

Hans Blass welcomed the delegates to the 44th CIB W18 Meeting in Alghero, Italy. He thanked M Fragiacomo for hosting the meeting.

Prof. V Maciocc, Dean of Faculty of Architecture University of Sassari gave a welcome address. Prof. H Spano, representative of the Vice Chancellor of the University of Sassari also offered welcome to the participants.

Over 80 participants are attending the meeting. The presentations are limited to 20 minutes each, allowing time for meaningful discussions after each paper. The Chair asked the presenters to conclude the presentation with a general proposal or statements concerning impact of the research results on existing or future potential application and development in codes and standards. R Görlacher will deal with questions regarding the meeting proceedings.

Papers brought directly to the meeting would not be accepted for presentation, discussions, or publication. Papers presented by non-authors or non-coauthors are not recommended except in exceptional situations because the discussion process might be compromised.

There are 11 topics covered in this meeting: Limit State Design Codes (1), Stress Grading (1), Stresses for Solid Timber (3), Timber Joints and Fasteners (9), Timber Beams (1), Laminated Members (5), Structural Stability (4), and Fire (3).

M. Fragiacomo discussed organizational matters for the meeting.

2 GENERAL TOPICS

The large number of interested participants attracted many abstracts. The number of accepted paper was limited to 30 to keep the characteristics of the CIB W18 meeting. 60 submitted abstracts meant a large number of submissions were rejected. The chair discussed JL Jensen's suggestions offered in a letter to the chair. Suggestion 1 considered the option of accepting presentations at CIB W18 based on the quality of the work. This means a strict deadline of sending in full paper for peer review. Participants are sought to volunteer as reviewers on specific topic of interest. Open discussion with the participant took place regarding the merit of this alternative system. The final agreement was to submit two page detailed abstracts for review. The Chair will choose the reviewers for specific topics and the abstracts must arrive on time. No more than 10 abstract for each reviewer and clear guidelines for the review with check box rating system will be issued. Suggestion 2 concerns the accessibility of CIB W18 papers as there are wishes to allow the older papers to be made accessible electronically. Scanned old proceedings and newer proceedings in pdf version will be available from CIB W18 home page: www.CIBW18.com within one year. This website will be maintained by the Danish Timber Information Website. Printed proceedings will be available on a limited basis only to the participants and library requests etc. Suggestion 3 concerns arranging the excursion on the last day of the meeting allowing participants not interested in such activity to depart earlier. H Blass stated that the host may want to showcase their city etc to the participants. J Munch Andersen suggested a compromise of 1/2 day excursion. H Blass encouraged the host of the next meeting to consider this option.

A Jorissen gave a short presentation of the developments in EC5. M Fragiacomo added developments in the timber part of EC8. J Köhler added that as there are many developments there should be discussions about the basis on the development of design codes where a 1/2 day discussion of such topic may be appropriate. G Hochreiner discussed using CIB W18 as an avenue to further facilitate and enhance the process of changes to standards.

3 STRESS GRADING

44 - 5 - 1 *Assessment of Different Knot-Indicators to Predict Strength and Stiffness Properties of Timber Boards* - **G Fink, M Deublein, J Köhler**

Presented by G Fink

H Blass commented that P Glos did similar work and asked if there was any comparison with Glos' results. He also asked about the length of the knot section under consideration. G Fink responded that comparison with Glos' results has not yet been done and the length of the knot section was 150 mm.

R Harris asked and received clarification that in addition to knot parameters and stiffness additional indicators included MOE_F, MOE_{ws} and density etc.

P Stapel and G Fink discussed suggestion on possible changes in grading practice.

F Lam commented that there commercial machines such as Continuous lumber tester and Cook Bolinders are available to measure the bending stiffness along member length. It would be useful to consider such system for obtaining MOE rather than using a predictive approach.

JW Van de Kuilen received clarification that the six strain measurements within a measurement zone were averaged for the calculation of localized MOE.

R Harris commented on the influence of juvenile wood could be significant as the current paper did not consider material with pith presence. His experience with UK Douglas fir indicated that variation in stiffness when considering juvenile wood seemed to be significant.

44 - 5 - 2 *Adaptive Production Settings Method for Strength Grading* - **G Turk, A Ranta-Maunus**

Presented by A Ranta-Maunus

JW Van de Kuilen commented that the interest is to minimize the number of rejects. The problem here was that it was far too optimized as we would have to ask whether it would be acceptable that 20% of the material did not meet the requirement.

F Rouger commented that the impact of the method was less than 0.5%. There were discussions on the accuracy of the simulation method. As Table 12 was based on simulated results and showed 20% of the samples did not meet requirements why there was not corresponding influence on yield. A Ranta-Maunus responded that although there were a number of rejects but yield could go up or down between grades. P Stapel agreed that there were movements between grades. S Aicher agreed that the results seemed logical.

J Köhler commented that references were not complete and there was a need to move from counting pieces to consider structural design issues; extend the work to consider what would be the influence on the capacity of the structural elements. He commented also that method should be based on robust IP.

44 - 5 - 3 *Initial Settings for Machine Strength Graded Structural Timber* - **R Ziethén, C Bengtsson**

Presented by R Ziethén

V Enjily asked why C16 was not considered. R Ziethén responded that the principles would be the same regardless of grade or grade combinations. Further C16 is not common in Sweden. A Ranta-Maunus commented that he did not like the example where the material was graded to C18 alone. R Ziethén responded that this topic is frequently discussed and may be hard for the producers to change.

P Stapel and R Ziethén had discussion about the common practice of always grading to the highest grade and the question why characteristic values and yield were compared. R Ziethén confirmed that not more than two settings per combination for each location were recommended even though strength settings depended on the grade combinations.

4 STRESSES FOR SOLID TIMBER

44 - 6 - 1 *Impact of Material Properties on the Fracture Mechanics Design Approach for Notched Beams in Eurocode 5* - **R Jockwer, R Steiger, A Frangi, J Köhler**

Presented by R Jockwer

H Blass commented that different size of specimens may influence findings and asked if size effects were considered. R Jockwer responded that it was not yet studied. I Smith added that member thickness could influence fracture energy and commented that although the Canadian approach appeared to look like shear strength design, in effect it was just the format of the equation. I Smith also commented that in service behaviour would also be important not just short term behaviour.

44 - 6 - 2 *Interaction of Shear Stresses and Stresses Perpendicular to the Grain* – **R Steiger, E Gehri**

Presented by R Steiger

G Hochreiner commented that TU Wien work on this area should be considered. R Steiger agreed and commented that they are aware of the work; however, there is no design provision in codes except the Swiss code and the German approach is not continuous. There were discussions that the compression strength perpendicular to grain depends on the actual deformation allowed and therefore not real material properties.

S. Aicher and R Steiger discussed the merits of tensor polynomial approach in comparison to the Swiss approach.

5 TIMBER JOINTS AND FASTENERS

44 - 7 - 1 *Pull-through Capacity in Plywood and OSB* - **J Munch-Andersen, J D Sørensen**

Presented by J Munch Andersen

F Lam commented that the statement that density of the panel did not influence pull through capacity was too strong. J Munch-Andersen responded that the analysis did not find any correlation. F Lam stated since the analysis considered reported data from different sources with a range of connectors and panel material, the influence of density was masked. If one were to consider a single connector type with panels of density, one would find density influence.

G Hochreiner and J Munch-Anderson discussed the issue that failure mode considerations may be important and modelling approach would be useful.

H Blass commented that KIT has additional results and questioned whether the head diameter of 18 mm is valid.

S. Aicher followed up on F Lam's point and commented that the range of applicability of plywood made from hardwood may not be valid. J Munch Andersen responded that that the results would be lower bound.

44 - 7 - 2 *Design Concept for CLT - Reinforced with Self-Tapping Screws* - **P Mestek, H Kreuzinger, S Winter**

Presented by P Mestek

H Blass commented that considering the average k_{R90} behaviour for comparison between test and model would be okay. For final design considerations, would it be possible to consider characteristic values by shifting the whole line. P Mestek agreed.

H Blass commented about the stiffness of screws in relationship to the rolling shear load path and asked whether screw withdrawal was observed. P Mestek responded mostly screw tension failures were observed and only one case of withdrawal was seen. H Blass asked how one would know that the screws were loaded to their capacity. P Mestek responded that this was a simplification for the practical design concept.

F Lam commented reporting r^2 values with two data clouds as shown in Figures 6 and 7 is not appropriate.

U Kuhlmann received explanations about that the effective width was based on elastic theory.

44 - 7 - 3 *Fatigue Behaviour of the Stud Connector Used for Timber-Concrete Composite Bridges* – **K Rautenstrauch, J Müller**

Presented by J Müller

G Hochreiner questioned the choice of frequency as different frequencies would influence the results. He also asked about the shear area for design.

H Müller responded that the choice of frequency was based on standard/typical procedures from literature as they are logistics limitations. Also there were discussions that compression perpendicular to grain stresses existed from the test set up and they wanted to simulate the possibility of such load in the structure. However they could not say how much the level of such load would be.

A Ceccotti commented that references from Finnish colleagues should be considered from structural engineering literature.

K Crews asked and received confirmation that the span of the bridge of interest was 15 mm. K Crews commented that the system would not be suitable for span over 30 m. Based on the span one should consider frequency of 8 to 10 Hz or higher.

R Harris commented that the volume wood used in the bridge seemed to be large and questioned why concrete composite. J Müller responded that it was for stiffness consideration. R Harris stated that then fatigue should not be an issue of concern.

U Kuhlmann stated that there is a fundamental difference between dynamic loading and behaviour under cyclical loading where there is a strength change. She commented that the low run out level did not give a real S/N curve and one should increase the load level to get real fatigue failure to draw the S/N line. J Müller responded that work would be continued at higher load level.

I Smith commented the whether such isolated test could be applied to actual structure.

M Fragiacomo stated that there was information from Colorado State University in this area and suggested exchange of information.

44 - 7 - 4 *The Stiffness of Beam to Column Connections in Post-Tensioned Timber Frames* - **T Smith, W van Beerschoten, A Palermo, S Pampanin, F C Ponzo**

Presented by T Smith

H Blass asked about the energy dissipation or q factor for such system. T Smith responded that they are looking at equivalent viscous damping values in the range of 12 % to 16%.

I Smith discussed the local failure influence on the behaviour of system. T Smith stated that the system can be designed and installed for other moment resisting systems and walls.

B Dujic asked what would be the level of damage in the joint and how could one evaluate the damage. T smith stated that damage could be evaluated from visual inspection if the energy dissipation devices were not hidden in the member. The damaged devices can then be replaced. Also instrumentations can be installed in the building to evaluate movement and hence damage. B Dujic and T Smith further discussed the practicality of such practice in real buildings.

M Fragiacomo and S Pampanin discussed further the applicability of the approach to other building systems.

B Dujic stated that one could design this as elastic case if the damage was so low.

A Ceccotti said that in real building how could one clad over this. T Smith responded it would be an issue for the architect.

M Yasumura asked about the control of the relaxation of the timber on post tensioning. He stated that based on the shown hysteresis curve, energy dissipation would be very low. T smith stated that the relaxation could be controlled by periodic re-tensioning. The amount of damping would not be an issue as it can be controlled by the size of the steel devices. It is more important that pinching effect is minimal.

M Popovski asked about the interest of application of such concept to CLT. S Pampanin responded that there are interests in New Zealand and F Lam in Canada will also be working on this issue.

44 - 7 - 5 *Design Approach for the Splitting Failure of Dowel-Type Connections Loaded Perpendicular to Grain* - **B Franke, P Quenneville**

Presented by B Franke

A Jorissen commented that the fracture energy seemed to be dependent on connection lay out and geometry. B Franke responded that fracture energy was known for Mode I and II but not for combined stresses and fracture energy may be related to stress states in mix mode and this approach may be okay for practical reason. Furthermore curve of normalized fracture energy was used.

A Jorissen commented that there were significant developments of theoretical equations in the last decade. This study was based on experimental approach this be justified. B Franke responded that situation was configuration dependent and if analytical based approach was available, one could consider them.

A Jorissen asked whether the ductile and brittle failures in experimental separated. B Franke replied that no and they always used the combinations of both failure modes.

M Ballerini received clarifications about how the crack surfaces for mode I and II and how to calculate some of the parameters.

I Smith asked how the current approach compared with past results. B Franke stated that they try to consider the more complex cases to arrive at rational solutions.

S Winter commented that design approach based on fracture mechanics with unit-less factors would be difficult to justify in codes. B Franke responded that the factors in this study did not have such problems.

G Hochreiner asked about overlaying of shear stresses and B Franke responded that CIB W18 last year addressed the issue.

6 LAMINATED MEMBERS

44 - 12 - 1 *Properties of CLT-Panels Exposed to Compression Perpendicular to their Plane* - **T Bogensperger, M Augustin, G Schickhofer**

Presented by T Bogensperger

H Blass asked why reinforcement techniques were not considered. T Bogensperger responded that they were well aware of reinforcement techniques but wanted to consider basic properties first.

H Blass asked what the failure criteria were for FEM. T Bogensperger responded that failure criteria were based on deformation.

S Franke and T Bogensperger discussed the fact in some configuration one edge could not have bending of the fibres and the elasto-plastic behaviour. T Bogensperger stated that the next step would have to consider shear behaviour.

44 - 12 - 2 *Strength of Spruce Glulam Subjected to Longitudinal Compression* **– M Frese, M Enders-Comberg, H J Blaß, P Glos**

Presented by M Frese

J Köhler and M Frese discussed the procedures used to consider the lengthwise correlation of material properties.

R Harris asked how one would know the specimens were of sufficient poor quality to be representative. M Frese responded that the comparisons of density should the material are representative and further comparisons between simulations and experiments showed good agreement. R Harris questioned the high influence of moisture content on compression strength parallel to grain and questioned again whether the tested material was at too high a quality. M Frese stated it might be good to perform tests on glulam with wider range of density and H Blass confirmed that the glulam material was not of particular good quality.

F Lam commented that compared to clear wood values the influence of moisture content on compression strength parallel to grain is of the same magnitude; however, the COV of the compression strength seemed to be low. M Frese responded that it could be explained by homogenisation of material via the lamination process. J Munch-Andersen commented that the variation of the simulation agreed with the experiments.

A Jorissen commented that the moisture content on compression strength of wood is well known and asked whether one sought another k_{mod} for compression. M Frese explained about the proposed model. Currently the same k_{mod} is used for service class 1 and 2. The work aimed to study the limit of the moisture to assess the influence.

A Frangi asked whether the results were compared to older results. M Frese responded no and they only used the test results from 50 specimens in the current study.

44 - 12 - 3 *Glued Laminated Timber: A proposal for New Beam Layups* - **F Rouger, P Garcia**

Presented by F Rouger

R Harris commented that he was pleased to see the utilization of lower grade material. He commented that if one changed the requirement of the number of high grade lamina, one could create different grades of glulam material such that the product with 2 pieces of high grade lamina would be better than the product with one piece of high grade lamina. F Rouger responded that there would be a market for such product and the industry was demanding it.

P Stapel asked how one would make sure that the C14 is not a C24. R Rouger stated that they were machine graded with additional checks.

A Ranta-Maunus commented that this would be important for the industry.

G Hochreiner asked about the use of 80 mm thick laminae. R Rouger said that such thick laminae would not be used for glulam beams.

44 - 12 - 4 *Glulam Beams with Internally and Externally Reinforced Holes – Test, Detailing and Design* – **S Aicher**

Presented by S Aicher

A Buchanan asked what if the screws were installed in an inclined angle. S Aicher stated that it might create an issue in terms of placement of the screws that could not be matched with the high stress fields of both tension perpendicular to grain and shear. Although increases might be possible but not sure about how big an increase could be achieved.

BJ Yeh asked whether there could be an orientation effect for the reinforcing panel. S Aicher confirmed that panels were failing in tension but stated that the effect of orientation of the panel could be minimal.

F Lam received confirmation that 3-D FEM analysis was used with large number of nodes and elements.

S Franke asked whether softening behaviour from cracking considered. S Aicher responded no and pure elastic simple approach was used in the analysis and it would be interesting to see how far the internal cracks went.

44 - 12 - 5 *Size Effect of Bending Strength in Glulam Beam* - **F Lam**

Presented by F Lam

S Aicher received clarification that the tension strength of the T1 laminae was approximately 29 MPa and the characteristic bending strength of the glulam was similar.

J Köhler asked why the simulated results were not smooth for the strength to volume relationship. F Lam responded that the simulations considered the actual grades of the laminae in different layup. In some layups the percentage of the high grade laminae exceeded the minimum requirement.

I Smith asked whether the small beams failures were similar to the large beams. F Lam responded they failed the same way.

S Aicher and F Lam discussed the observation of failures in the interior laminae. S Aicher asked about the implication of the results for European consideration of glulam size effect. F Lam responded that the direct application of the results is limited to Canadian glulam. Nevertheless, in the case of European glulam, one should be careful with size effects consideration especially if the design of larger beam is governed by bending strength.

I Smith commented on dynamic failure mechanism and it might not be a Weibull based consideration.

7 STRUCTURAL STABILITY

44 - 15 - 1 A Proposal for Revision of the Current Timber Part (Section 8) of Eurocode 8 Part 1 - **M Follesa, M Fragiacomo, M P Lauriola**

Presented by M Follesa

V Enjily commented that this work just covered CLT but an important class of building products insulated panels consisting of I- beams were not considered. M Follesa replied that other building systems can be used provided that the ductility can be achieved.

A Ceccotti suggested that in EC8 there should be the possibility for designers to demonstrate the appropriate q factors for alternative systems. He expressed concern that the over strength factor of 1.6 for CLT may be too high based on his experience in the shake table test project in Japan where an engineered guess of 1.3 would be more reasonable. M Fragiacomo responded that based on single component test results it seemed that the over strength factor of 1.6 was appropriate. The work was still in progress.

A Buchanan provided explanation of the basis of the over strength factor of 2 used in New Zealand for nailed plywood connections in most timber structures. As there were difficulties in putting precise factors for different systems in the code, it would be more important to have the proper design philosophy recognized in the code. It would be important in codes to allow designers to come up with justifiable q factor.

S Pampanin further discussed the seismic design issues related drift values, yield displacements, stiffness, displacement based design and nonlinear design methods.

44 - 15 – 2 Influence of Vertical Loads on Lateral Resistance and Deflections of Light-Frame Shear Walls - **M Payeur, A Salenikovich, W Muñoz**

Presented by A Salenikovich

F Lam commented that given the seismic motions are three dimensional where upward accelerations can be expected, it might not be appropriate to rely on vertical loads for lateral resistance of wall systems. A Salenikovich agreed and commented that more discussions and studies on the topic would be needed.

B Dujic asked what force would be acting on the damaged stud as the information would be useful to gain understanding the rocking, uplift and shear mechanisms. A Salenikovich clarified that the forces in the damaged studs were not monitored.

44 - 15 – 3 *Modelling Force Transfer Around Openings of Full-Scale Shear Walls* – **T Skaggs, B Yeh, F Lam, Minghao Li, D Rammer, J Wacker**

Presented by T Skaggs

S Pampanin discussed the compression forces in the straps and the possibilities to make the straps work both in tension and compression. T Skaggs stated that flat straps would buckle in compression; alternative systems with rod would be possible; however the purpose of the bracket system used in the study was for experimental investigations only.

I Smith commented that there were full scale tests done in the US and asked what happened in full scale building system in relation to accuracy of the component evaluations. T Skaggs responded that the full scale building system test in US did not consider the force transfer around openings issues.

44 - 15 - 4 *Design of Bottom Rails in Partially Anchored Shear Walls Using Fracture Mechanics* - **E Serrano, J Vessby, A Olsson, U A Girhammar, B Källsner**

Presented by E Serrano

V Enjily stated it would be more useful to have more details of the tests, for example, were bottom plates all cracked in the tests. E Serrano responded that for small washer size vertical sill plate cracks were observed and for large washer sizes horizontal sill plate cracks were observed.

S. Aicher commented about the why such construction was made. With a simple modification of construction detail/technique one could avoid such problem even though the analytical work is valid. E Serrano stated that the work was also curiosity driven.

44 - 15 - 5 *Notes on Deformation and Ductility Requirements in Timber Structures.* **- K A Malo, P Ellingsbø, C Stamatopoulos**

Presented by K Malo

J W van de Kuilen and K Malo discussed about the time dependent deformations which would be partly recoverable were considered. This would be an important issue because part of the plastic deformation capacity would have been taken up by creep and one would only have the remaining deformation capacity available for the overload.

44 - 15 - 6 *Enhanced Model of the Nonlinear Load-bearing Behaviour of Wood Shear Walls and Diaphragms* - **M H Kessel, C Hall**

Presented by C Hall

M Yasumura and C Hall discussed the pin joint at the bottom of the panel. C Hall responded that there were boundary conditions for the vertical members for uplift considerations. These methods could be applied in general such that one could consider hold-downs etc.

F Lam asked whether the approach had been compared with results from experimental data or verified model predictions to support the conclusions. C Hall responded that on-going work with FEM was underway.

H Blass commented that considering our criteria for paper acceptance, this work should have been accepted as research note.

44 - 15 - 7 *Seismic Performance of Cross-Laminated Wood Panels* - **M Popovski, E Karacabeyli**

Presented by M Popovski

A Buchanan stated that this work made comparisons between CLT and light wood frame systems. In case of light wood frame system there are many nail connectors helping the structure resist the lateral forces. In CLT only few hold down and brackets devices were available such that the entire system relied on few connectors. For CLT case with a nail strip, it is more similar to the light frame wall but still not the same. A Buchanan stated that more care would be needed to treat the CLT system. M Popovski agreed and stated in general CLT system connections are more localized but there can still be a lot of nail available.

B Dujic S Pampanin and M Popovski discussed where sliding occurred in the load CLT walls.

A Ceccotti asked about the equivalent viscous damping. M Popovski answered that it was not calculated yet.

I Smith stated that in Canada the type of building for CLT use is still unknown and 2015 target for CLT information to be in the Canadian CSA code might be too optimistic.

44 - 15 – 8 *Evaluation of Plywood Sheathed Shear Walls with Screwed Joints Tested According to ISO 21581* **- K Kobayashi, M Yasumura**

Presented by K Kobayashi

F Lam received confirmation that the calibration of the hysteresis rules for the model was based on single connection test results.

E Serrano asked about the single spring model and the influence of load direction in relation to wood grain. K Kobayashi responded that test results corresponding to perpendicular to grain direction was used and there could be influence from grain direction but was not considered in the study.

J Munch-Andersen asked about the brittle fracture of the screws and how much bending of the screws was experienced. K Kobayashi responded that in monotonic tests the single screws seemed ductile.

44 - 15 – 9 *Influence of Connection Properties on the Ductility and Seismic Resistance of Multi-Storey Cross-Lam Buildings* - **I Sustersic, M Fragiacomo, B Dujic**

Presented by I Sustersic

I Smith and I Sustersic discussed that estimating the lower strength such as 5th percentile would be easier than estimating the higher end strength and its relationship with over strength factor.

8 FIRE

44 - 16 - 1 *Gypsum Plasterboards and Gypsum Fibreboards – Protective Times for Fire Safety Design of Timber Structures* – **A Just, J Schmid, J König**

Presented by A Just

A Frangi commented that the ETH data on start time of charring t_{ch} was based on mean values and the proposed equation here was very conservative. He questioned whether one would need to go with such high level of conservatism. He also question how the 1%

criterion in the fire test was measured and whether 5% could be used. A Just and J Schmid responded that the high degree of conservatism was desired and the 1% was more or less a subjective criteria and difficult to assess. They claimed that there would be less difference between 1 to 5 % or 10% criteria.

S Winter commented on the issue of starting time of charring from test and supported A Frangi's point. He stated that one has to look the total system behaviour and discussed EI calculations in comparison with DIN specifications. He stated that results from Eurocode are already conservative. It would be incorrect to adopt such high degree of conservatism and 5% criterion may be more appropriate. Finally he commented that the density of gypsum board was missing in the report which would be an important parameter that could explain the validity. A Just responded that density was considered but they found no correlation.

A Buchanan commented that information of the fastening to the gypsum to the assembly was missing which could have an influence. A Just responded that the fastening of course could have an influence but they did not have more information. Also he did not believe the influence would be large.

9 STATISTICS AND DATA ANALYSIS

44 - 17 – 1 Influence of Sample Size on Assigned Characteristic Strength Values –
P Stapel, G J P Ravenshorst, J W G van de Kuilen

Presented by P Stapel

J Köhler questioned about 1) the confidence intervals to the design of the structure an 2) whether each subsample would be expected to have the target strength values.

P Stapel answered that question 2 should be directed to the users as to what would be their expectations. J W van de Kuilen added that on average one would like to see the samples meet the target level; however, this could not be checked if there was not enough data. Also the checks needed to be done based on the limited available data and this did not have to do the design issues.

F Rouger asked whether the approach of Ks or CI and Weibull based for 5%tile calculations in relation to the stability of small sample size. P Stapel responded that the Weibull based for 5%tile did not matter as they also tried different approaches.

R Harris commented on the representativeness of the sample with respect to the location etc. Ks should be location dependent. P Stapel agreed and stated that this would be especially problematic for tropical hardwood where the source of the material might not be known and producers wanted to reduce testing costs.

10 RESEARCH NOTES

Considerations for the inclusions of expressions to assess the vibration performance of TCC floors - **J Skinner, R Harris, K Paine, P Walker**

Presented by J Skinner

Splitting of beams loaded perpendicular to grain by connections – some issues with EC5 - **J L Jensen, P Quenneville**

Presented by JL Jensen

Mechanical behaviour of the in-plane shear connections between CLT wall panels – **T Joyce, M Ballerini, I Smith**

Presented by J Joyce

Compression perpendicular to the grain – the Norwegian approach – **S. Eide, K Nore, E Aasheim**

Presented by S Eide

Bending strength of finger jointed solid lumber – **G. Stapf, S Aicher**

Presented by G Stapf

Performance of timber buildings in the 2010, 2011 New Zealand earthquakes – **A Buchanan**

Presented by A Buchanan

Opportunities for rebuilding Christchurch with damage-resistant multi-storey timber buildings – **S Pampanin**

Presented by S Pampanin

Damage of wooden houses due to Tsunami caused by the 2011 off the Pacific coast of Tohoku Earthquake – **M Yasumura**

Presented by M Yasumura

Mineral wool in timber structures exposed to fire - **J Schmid, A Just**

Presented by J Schmid

Basis on reliability based code calibration – **J Köhler**

Presented by J Köhler

11 ANY OTHER BUSINESS

H Larsen gave a presentation on the new CIB W18 Homepage.

12 VENUE AND PROGRAMME FOR NEXT MEETING

C Bengtsson and E Serrano gave a presentation of the next venue and invited the participants to come to Växjo Sweden for the 2012 CIB W18 meeting.

Chairman also announced that F Lam will host the 2013 CIB W18 meeting in Vancouver. UK has also offered to host either the 2014 or 2015 CIB W18 meeting.

13 CLOSE

M Fragiacomo thanked the participants for coming to Alghero and provided further information for participants that opted to continue their travel on the island.

Chairman thanked M Fragiacomo and the supporting group for hosting and organizing the excellent meeting.

14. Peer Review of Papers for the CIB-W18 Proceedings

14. Peer review of papers for the CIB-W18 Proceedings

Experts involved:

Members of the CIB-W18 “Timber Structures” group are a community of experts in the field of timber engineering.

Procedure of peer review

- Submission of manuscripts: all members of the CIB-W18 group attending the meeting receive the manuscripts of the papers at least four weeks before the meeting. Everyone is invited to read and review the manuscripts especially in their respective fields of competence and interest.

- Presentation of the paper during the meeting by the author

- Comments and recommendations of the experts, discussion of the paper

- Comments, discussion and recommendations of the experts are documented in the minutes of the meeting and are printed on the front page of each paper.

- Final acceptance of the paper for the proceedings with
  no changes
  minor changes
  major changes
  or reject

- Revised papers are to be sent to the editor of the proceedings and the chairman of the CIB-W18 group

- Editor and chairman check, whether the requested changes have been carried out.

15. List of CIB-W18 Papers, Alghero, Italy 2011

List of CIB-W18 Papers, Alghero, Italy 2011

44 - 5 - 1 Assessment of Different Knot-Indicators to Predict Strength and Stiffness Properties of Timber Boards - **G Fink, M Deublein, J Köhler**

44 - 5 - 2 Adaptive Production Settings Method for Strength Grading - **G Turk, A Ranta-Maunus**

44 - 5 - 3 Initial Settings for Machine Strength Graded Structural Timber - **R Ziethén, C Bengtsson**

44 - 6 - 1 Impact of Material Properties on the Fracture Mechanics Design Approach for Notched Beams in Eurocode 5 - **R Jockwer, R Steiger, A Frangi, J Köhler**

44 - 6 - 2 Interaction of Shear Stresses and Stresses Perpendicular to the Grain - **R Steiger, E Gehri**

44 - 7 - 1 Pull-through Capacity in Plywood and OSB - **J Munch-Andersen, J D Sørensen**

44 - 7 - 2 Design Concept for CLT - Reinforced with Self-Tapping Screws - **P Mestek, H Kreuzinger, S Winter**

44 - 7 - 3 Fatigue Behaviour of the Stud Connector Used for Timber-Concrete Composite Bridges – K **Rautenstrauch, J Mueller**

44 - 7 - 4 The Stiffness of Beam to Column Connections in Post-Tensioned Timber Frames **– T Smith, W van Beerschoten, A Palermo, S Pampanin, F C Ponzo**

44 - 7 - 5 Design Approach for the Splitting Failure of Dowel-Type Connections Loaded Perpendicular to Grain - **Bettina Franke, Pierre Quenneville**

44 - 12 - 1 Properties of CLT-Panels Exposed to Compression Perpendicular to their Plane- **T Bogensperger, M Augustin, G Schickhofer**

44 - 12 - 2 Strength of Spruce Glulam Subjected to Longitudinal Compression – **M Frese, M Enders-Comberg, H J Blaß, P Glos**

44 - 12 - 3 Glued Laminated Timber: A proposal for New Beam Layups - **F Rouger, P Garcia**

44 - 12 - 4 Glulam Beams with Internally and Externally Reinforced Holes – Test, Detailing and Design – **S Aicher**

44 - 12 - 5 Size Effect of Bending Strength in Glulam Beam - **F Lam**

44 - 15 - 1 A Proposal for Revision of the Current Timber Part (Section 8) of Eurocode 8 Part 1 - **M Follesa, M Fragiacomo, M P Lauriola**

44 - 15 - 2 Influence of Vertical Loads on Lateral Resistance and Deflections of Light-Frame Shear Walls - **M Payeur, A Salenikovich, W Muñoz**

44 - 15 - 3 Modelling Force Transfer Around Openings of Full-Scale Shear Walls - **T Skaggs, B Yeh, F Lam, Minghao Li, D Rammer, J Wacker**

44 - 15 - 4 Design of Bottom Rails in Partially Anchored Shear Walls Using Fracture Mechanics - **E Serrano, J Vessby, A Olsson, U A Girhammar, B Källsner**

44 - 15 - 5 Notes on Deformation and Ductility Requirements in Timber Structures. - **K A Malo, P Ellingsbø, C Stamatopoulos**

44 - 15 - 6 Enhanced Model of the Nonlinear Load-bearing Behaviour of Wood Shear Walls and Diaphragms - **M H Kessel, C Hall**

44 - 15 - 7 Seismic Performance of Cross-Laminated Wood Panels - **M Popovski, E Karacabeyli**

44 - 15 - 8 Evaluation of Plywood Sheathed Shear Walls with Screwed Joints Tested According to ISO 21581 **- K Kobayashi, M Yasumura**

44 - 15 - 9 Influence of Connection Properties on the Ductility and Seismic Resistance of Multi-Storey Cross-Lam Buildings - **I Sustersic, M Fragiacomo, B Dujic**

44 - 16 - 1 Gypsum Plasterboards and Gypsum Fibreboards – Protective Times for Fire Safety Design of Timber Structures **–A Just, J Schmid, J König**

44 - 17 - 1 Influence of Sample Size on Assigned Characteristic Strength Values **– P Stapel, G J P Ravenshorst, J W G van de Kuilen**

Notes:

Considerations for the inclusions of expressions to assess the vibration performance of TCC floors - **J Skinner, R Harris, K Paine, P Walker**

Splitting of beams loaded perpendicular to grain by connections – some issues with EC5 - **J L Jensen, P Quenneville**

Mechanical behaviour of the in-plane shear connections between CLT wall panels **– T Joyce, M Ballerini, I Smith**

Compression perpendicular to the grain – the Norwegian approach **– S. Eide, K Nore, E Aasheim**

Bending strength of finger jointed solid lumber **– G. Stapf, S Aicher**

Performance of timber buildings in the 2010, 2011 New Zealand earthquakes **– A Buchanan**

Opportunities for rebuilding Christchurch with damage-resistant multi-storey timber buildings **– S Pampanin**

Damage of wooden houses due to Tsunami caused by the 2011 off the Pacific coast of Tohoku Earthquake **– M Yasumura**

Mineral wool in timber structures exposed to fire - **J Schmid, A Just**

Basis on reliability based code calibration **– J Köhler**

16. Current List of CIB-W18(A) Papers

CURRENT LIST OF CIB-W18(A) PAPERS

Technical papers presented to CIB-W18(A) are identified by a code CIB-W18(A)/a-b-c, where:

a denotes the meeting at which the paper was presented.

1 Princes Risborough, England; March 1973
2 Copenhagen, Denmark; October 1973
3 Delft, Netherlands; June 1974
4 Paris, France; February 1975
5 Karlsruhe, Federal Republic of Germany; October 1975
6 Aalborg, Denmark; June 1976
7 Stockholm, Sweden; February/March 1977
8 Brussels, Belgium; October 1977
9 Perth, Scotland; June 1978
10 Vancouver, Canada; August 1978
11 Vienna, Austria; March 1979
12 Bordeaux, France; October 1979
13 Otaniemi, Finland; June 1980
14 Warsaw, Poland; May 1981
15 Karlsruhe, Federal Republic of Germany; June 1982
16 Lillehammer, Norway; May/June 1983
17 Rapperswil, Switzerland; May 1984
18 Beit Oren, Israel; June 1985
19 Florence, Italy; September 1986
20 Dublin, Ireland; September 1987
21 Parksville, Canada; September 1988
22 Berlin, German Democratic Republic; September 1989
23 Lisbon, Portugal; September 1990
24 Oxford, United Kingdom; September 1991
25 Åhus, Sweden; August 1992
26 Athens, USA; August 1993
27 Sydney, Australia; July 1994
28 Copenhagen, Denmark; April 1995
29 Bordeaux, France; August 1996
30 Vancouver, Canada; August 1997
31 Savonlinna, Finland; August 1998
32 Graz, Austria, August 1999
33 Delft, The Netherlands; August 2000
34 Venice, Italy; August 2001
35 Kyoto, Japan; September 2002
36 Colorado, USA; August 2003
37 Edinburgh, Scotland, August 2004
38 Karlsruhe, Germany, August 2005
39 Florence, Italy, August 2006
40 Bled, Slovenia, August 2007
41 St. Andrews, Canada 2008
42 Dübendorf, Switzerland 2009
43 Nelson, New Zealand 2010
44 Alghero, Italy 2011

b denotes the subject:

1 Limit State Design
2 Timber Columns
3 Symbols
4 Plywood
5 Stress Grading
6 Stresses for Solid Timber
7 Timber Joints and Fasteners
8 Load Sharing
9 Duration of Load
10 Timber Beams
11 Environmental Conditions
12 Laminated Members
13 Particle and Fibre Building Boards
14 Trussed Rafters
15 Structural Stability
16 Fire
17 Statistics and Data Analysis
18 Glued Joints
19 Fracture Mechanics
20 Serviceability
21 Test Methods
100 CIB Timber Code
101 Loading Codes
102 Structural Design Codes
103 International Standards Organisation
104 Joint Committee on Structural Safety
105 CIB Programme, Policy and Meetings
106 International Union of Forestry Research Organisations

c is simply a number given to the papers in the order in which they appear:

Example: CIB-W18/4-102-5 refers to paper 5 on subject 102 presented at the fourth meeting of W18.

Listed below, by subjects, are all papers that have to date been presented to W18. When appropriate some papers are listed under more than one subject heading.

LIMIT STATE DESIGN

1-1-1	Limit State Design - H J Larsen
1-1-2	The Use of Partial Safety Factors in the New Norwegian Design Code for Timber Structures - O Brynildsen
1-1-3	Swedish Code Revision Concerning Timber Structures - B Noren
1-1-4	Working Stresses Report to British Standards Institution Committee BLCP/17/2
6-1-1	On the Application of the Uncertainty Theoretical Methods for the Definition of the Fundamental Concepts of Structural Safety - K Skov and O Ditlevsen
11-1-1	Safety Design of Timber Structures - H J Larsen
18-1-1	Notes on the Development of a UK Limit States Design Code for Timber - A R Fewell and C B Pierce
18-1-2	Eurocode 5, Timber Structures - H J Larsen
19-1-1	Duration of Load Effects and Reliability Based Design (Single Member) - R O Foschi and Z C Yao
21-102-1	Research Activities Towards a New GDR Timber Design Code Based on Limit States Design - W Rug and M Badstube
22-1-1	Reliability-Theoretical Investigation into Timber Components Proposal for a Supplement of the Design Concept - M Badstube, W Rug and R Plessow
23-1-1	Some Remarks about the Safety of Timber Structures - J Kuipers
23-1-2	Reliability of Wood Structural Elements: A Probabilistic Method to Eurocode 5 Calibration - F Rouger, N Lheritier, P Racher and M Fogli
31-1-1	A Limit States Design Approach to Timber Framed Walls - C J Mettem, R Bainbridge and J A Gordon
32 -1-1	Determination of Partial Coefficients and Modification Factors- H J Larsen, S Svensson and S Thelandersson
32 -1-2	Design by Testing of Structural Timber Components - V Enjily and L Whale
33-1-1	Aspects on Reliability Calibration of Safety Factors for Timber Structures – S Svensson and S Thelandersson
33-1-2	Sensitivity studies on the reliability of timber structures – A Ranta-Maunus, M Fonselius, J Kurkela and T Toratti
41-1–1	On the Role of Stiffness Properties for Ultimate Limit State Design of Slender Columns– J Köhler, A Frangi, R Steiger

TIMBER COLUMNS

2-2-1	The Design of Solid Timber Columns - H J Larsen
3-2-1	The Design of Built-Up Timber Columns - H J Larsen
4-2-1	Tests with Centrally Loaded Timber Columns - H J Larsen and S S Pedersen
4-2-2	Lateral-Torsional Buckling of Eccentrically Loaded Timber Columns- B Johansson
5-9-1	Strength of a Wood Column in Combined Compression and Bending with Respect to Creep - B Källsner and B Norén
5-100-1	Design of Solid Timber Columns (First Draft) - H J Larsen
6-100-1	Comments on Document 5-100-1, Design of Solid Timber Columns - H J Larsen and E Theilgaard
6-2-1	Lattice Columns - H J Larsen
6-2-2	A Mathematical Basis for Design Aids for Timber Columns - H J Burgess

6-2-3	Comparison of Larsen and Perry Formulas for Solid Timber Columns- H J Burgess
7-2-1	Lateral Bracing of Timber Struts - J A Simon
8-15-1	Laterally Loaded Timber Columns: Tests and Theory - H J Larsen
17-2-1	Model for Timber Strength under Axial Load and Moment - T Poutanen
18-2-1	Column Design Methods for Timber Engineering - A H Buchanan, K C Johns, B Madsen
19-2-1	Creep Buckling Strength of Timber Beams and Columns - R H Leicester
19-12-2	Strength Model for Glulam Columns - H J Blaß
20-2-1	Lateral Buckling Theory for Rectangular Section Deep Beam-Columns- H J Burgess
20-2-2	Design of Timber Columns - H J Blaß
21-2-1	Format for Buckling Strength - R H Leicester
21-2-2	Beam-Column Formulae for Design Codes - R H Leicester
21-15-1	Rectangular Section Deep Beam - Columns with Continuous Lateral Restraint - H J Burgess
21-15-2	Buckling Modes and Permissible Axial Loads for Continuously Braced Columns - H J Burgess
21-15-3	Simple Approaches for Column Bracing Calculations - H J Burgess
21-15-4	Calculations for Discrete Column Restraints - H J Burgess
22-2-1	Buckling and Reliability Checking of Timber Columns - S Huang, P M Yu and J Y Hong
22-2-2	Proposal for the Design of Compressed Timber Members by Adopting the Second-Order Stress Theory - P Kaiser
30-2-1	Beam-Column Formula for Specific Truss Applications - W Lau, F Lam and J D Barrett
31-2-1	Deformation and Stability of Columns of Viscoelastic Material Wood - P Becker and K Rautenstrauch
34-2-1	Long-Term Experiments with Columns: Results and Possible Consequences on Column Design – W Moorkamp, W Schelling, P Becker, K Rautenstrauch
34-2-2	Proposal for Compressive Member Design Based on Long-Term Simulation Studies – P Becker, K Rautenstrauch
35-2-1	Computer Simulations on the Reliability of Timber Columns Regarding Hygrothermal Effects- R Hartnack, K-U Schober, K Rautenstrauch
36-2-1	The Reliability of Timber Columns Based on Stochastical Principles - K Rautenstrauch, R Hartnack
38-2-1	Long-term Load Bearing of Wooden Columns Influenced by Climate – View on Code - R Hartnack, K Rautenstrauch

SYMBOLS

3-3-1	Symbols for Structural Timber Design - J Kuipers and B Norén
4-3-1	Symbols for Timber Structure Design - J Kuipers and B Norén
28-3-1	Symbols for Timber and Wood-Based Materials - J Kuipers and B Noren
1	Symbols for Use in Structural Timber Design

PLYWOOD

20-4-1	Considerations of Reliability - Based Design for Structural Composite Products - M R O'Halloran, J A Johnson, E G Elias and T P Cunningham
21-4-1	Modelling for Prediction of Strength of Veneer Having Knots - Y Hirashima
22-4-1	Scientific Research into Plywood and Plywood Building Constructions the Results and Findings of which are Incorporated into Construction Standard Specifications of the USSR - I M Guskov
22-4-2	Evaluation of Characteristic values for Wood-Based Sheet Materials - E G Elias
24-4-1	APA Structural-Use Design Values: An Update to Panel Design Capacities - A L Kuchar, E G Elias, B Yeh and M R O'Halloran

STRESS GRADING

1-5-1	Quality Specifications for Sawn Timber and Precision Timber - Norwegian Standard NS 3080
1-5-2	Specification for Timber Grades for Structural Use - British Standard BS 4978
4-5-1	Draft Proposal for an International Standard for Stress Grading Coniferous Sawn Softwood - ECE Timber Committee
16-5-1	Grading Errors in Practice - B Thunell
16-5-2	On the Effect of Measurement Errors when Grading Structural Timber- L Nordberg and B Thunell
19-5-1	Stress-Grading by ECE Standards of Italian-Grown Douglas-Fir Dimension Lumber from Young Thinnings - L Uzielli
19-5-2	Structural Softwood from Afforestation Regions in Western Norway - R Lackner
21-5-1	Non-Destructive Test by Frequency of Full Size Timber for Grading - T Nakai
22-5-1	Fundamental Vibration Frequency as a Parameter for Grading Sawn Timber - T Nakai, T Tanaka and H Nagao
24-5-1	Influence of Stress Grading System on Length Effect Factors for Lumber Loaded in Compression - A Campos and I Smith
26-5-1	Structural Properties of French Grown Timber According to Various Grading Methods - F Rouger, C De Lafond and A El Quadrani
28-5-1	Grading Methods for Structural Timber - Principles for Approval - S Ohlsson
28-5-2	Relationship of Moduli of Elasticity in Tension and in Bending of Solid Timber - N Burger and P Glos
29-5-1	The Effect of Edge Knots on the Strength of SPF MSR Lumber - T Courchene, F Lam and J D Barrett
29-5-2	Determination of Moment Configuration Factors using Grading Machine Readings - T D G Canisius and T Isaksson
31-5-1	Influence of Varying Growth Characteristics on Stiffness Grading of Structural Timber - S Ormarsson, H Petersson, O Dahlblom and K Persson
31-5-2	A Comparison of In-Grade Test Procedures - R H Leicester, H Breitinger and H Fordham
32-5-1	Actual Possibilities of the Machine Grading of Timber - K Frühwald and A Bernasconi
32-5-2	Detection of Severe Timber Defects by Machine Grading - A Bernasconi, L Boström and B Schacht
34-5-1	Influence of Proof Loading on the Reliability of Members – F Lam, S Abayakoon, S Svensson, C Gyamfi
36-5-1	Settings for Strength Grading Machines – Evaluation of the Procedure according to prEN 14081, part 2 - C Bengtsson, M Fonselius

STRESSES FOR SOLID TIMBER

12-6-1	Strength Classifications for Timber Engineering Codes - R H Leicester and W G Keating
12-6-2	Strength Classes for British Standard BS 5268 - J R Tory
13-6-1	Strength Classes for the CIB Code - J R Tory
13-6-2	Consideration of Size Effects and Longitudinal Shear Strength for Uncracked Beams - R O Foschi and J D Barrett
13-6-3	Consideration of Shear Strength on End-Cracked Beams - J D Barrett and R O Foschi
15-6-1	Characteristic Strength Values for the ECE Standard for Timber - J G Sunley
16-6-1	Size Factors for Timber Bending and Tension Stresses - A R Fewell
16-6-2	Strength Classes for International Codes - A R Fewell and J G Sunley
17-6-1	The Determination of Grade Stresses from Characteristic Stresses for BS 5268: Part 2 - A R Fewell
17-6-2	The Determination of Softwood Strength Properties for Grades, Strength Classes and Laminated Timber for BS 5268: Part 2 - A R Fewell
18-6-1	Comment on Papers: 18-6-2 and 18-6-3 - R H Leicester
18-6-2	Configuration Factors for the Bending Strength of Timber - R H Leicester
18-6-3	Notes on Sampling Factors for Characteristic Values - R H Leicester
18-6-4	Size Effects in Timber Explained by a Modified Weakest Link Theory- B Madsen and A H Buchanan
18-6-5	Placement and Selection of Growth Defects in Test Specimens - H Riberholt
18-6-6	Partial Safety-Coefficients for the Load-Carrying Capacity of Timber Structures - B Norén and J-0 Nylander
19-6-1	Effect of Age and/or Load on Timber Strength - J Kuipers
19-6-2	Confidence in Estimates of Characteristic Values - R H Leicester
19-6-3	Fracture Toughness of Wood - Mode I - K Wright and M Fonselius
19-6-4	Fracture Toughness of Pine - Mode II - K Wright
19-6-5	Drying Stresses in Round Timber - A Ranta-Maunus
19-6-6	A Dynamic Method for Determining Elastic Properties of Wood - R Görlacher
20-6-1	A Comparative Investigation of the Engineering Properties of "Whitewoods" Imported to Israel from Various Origins - U Korin
20-6-2	Effects of Yield Class, Tree Section, Forest and Size on Strength of Home Grown Sitka Spruce - V Picardo
20-6-3	Determination of Shear Strength and Strength Perpendicular to Grain - H J Larsen
21-6-1	Draft Australian Standard: Methods for Evaluation of Strength and Stiffness of Graded Timber - R H Leicester
21-6-2	The Determination of Characteristic Strength Values for Stress Grades of Structural Timber. Part 1 - A R Fewell and P Glos
21-6-3	Shear Strength in Bending of Timber - U Korin
22-6-1	Size Effects and Property Relationships for Canadian 2-inch Dimension Lumber - J D Barrett and H Griffin
22-6-2	Moisture Content Adjustements for In-Grade Data - J D Barrett and W Lau
22-6-3	A Discussion of Lumber Property Relationships in Eurocode 5 - D W Green and D E Kretschmann
22-6-4	Effect of Wood Preservatives on the Strength Properties of Wood - F Ronai

23-6-1 Timber in Compression Perpendicular to Grain - U Korin

24-6-1 Discussion of the Failure Criterion for Combined Bending and Compression - T A C M van der Put

24-6-3 Effect of Within Member Variability on Bending Strength of Structural Timber - I Czmoch, S Thelandersson and H J Larsen

24-6-4 Protection of Structural Timber Against Fungal Attack Requirements and Testing- K Jaworska, M Rylko and W Nozynski

24-6-5 Derivation of the Characteristic Bending Strength of Solid Timber According to CEN-Document prEN 384 - A J M Leijten

25-6-1 Moment Configuration Factors for Simple Beams- T D G Canisius

25-6-3 Bearing Capacity of Timber - U Korin

25-6-4 On Design Criteria for Tension Perpendicular to Grain - H Petersson

25-6-5 Size Effects in Visually Graded Softwood Structural Lumber - J D Barrett, F Lam and W Lau

26-6-1 Discussion and Proposal of a General Failure Criterion for Wood - T A C M van der Put

27-6-1 Development of the "Critical Bearing": Design Clause in CSA-086.1 - C Lum and E Karacabeyli

27-6-2 Size Effects in Timber: Novelty Never Ends - F Rouger and T Fewell

27-6-3 Comparison of Full-Size Sugi (Cryptomeria japonica D.Don) Structural Performance in Bending of Round Timber, Two Surfaces Sawn Timber and Square Sawn Timber - T Nakai, H Nagao and T Tanaka

28-6-1 Shear Strength of Canadian Softwood Structural Lumber - F Lam, H Yee and J D Barrett

28-6-2 Shear Strength of Douglas Fir Timbers - B Madsen

28-6-3 On the Influence of the Loading Head Profiles on Determined Bending Strength - L Muszyñsky and R Szukala

28-6-4 Effect of Test Standard, Length and Load Configuration on Bending Strength of Structural Timber- T Isaksson and S Thelandersson

28-6-5 Grading Machine Readings and their Use in the Calculation of Moment Configuration Factors - T Canisius, T Isaksson and S Thelandersson

28-6-6 End Conditions for Tension Testing of Solid Timber Perpendicular to Grain - T Canisius

29-6-1 Effect of Size on Tensile Strength of Timber - N Burger and P Glos

29-6-2 Equivalence of In-Grade Testing Standards - R H Leicester, H O Breitinger and H F Fordham

30-6-1 Strength Relationships in Structural Timber Subjected to Bending and Tension - N Burger and P Glos

30-6-2 Characteristic Design Stresses in Tension for Radiata Pine Grown in Canterbury - A Tsehaye, J C F Walker and A H Buchanan

30-6-3 Timber as a Natural Composite: Explanation of Some Peculiarities in the Mechanical Behaviour - E Gehri

31-6-1 Length and Moment Configuration Factors - T Isaksson

31-6-2 Tensile Strength Perpendicular to Grain According to EN 1193 - H J Blaß and M Schmid

31-6-3 Strength of Small Diameter Round Timber - A Ranta-Maunus, U Saarelainen and H Boren

31-6-4	Compression Strength Perpendicular to Grain of Structural Timber and Glulam - L Damkilde, P Hoffmeyer and T N Pedersen

31-6-5	Bearing Strength of Timber Beams - R H Leicester, H Fordham and H Breitinger

32-6-1	Development of High-Resistance Glued Robinia Products and an Attempt to Assign Such Products to the European System of Strength Classes - G Schickhofer and B Obermayr

32-6-2	Length and Load Configuration Effects in the Code Format - T Isaksson

32-6-3	Length Effect on the Tensile Strength of Truss Chord Members - F Lam

32-6-4	Tensile Strength Perpendicular to Grain of Glued Laminated Timber - H J Blaß and M Schmid

32-6-5	On the Reliability-based Strength Adjustment Factors for Timber Design - T D G Canisius

34-6-1	Material Strength Properties for Canadian Species Used in Japanese Post and Beam Construction - J D Barrett, F Lam, S Nakajima

35-6-1	Evaluation of Different Size Effect Models for Tension Perpendicular to Grain Design - S Aicher, G Dill-Langer

35-6-2	Tensile Strength of Glulam Perpendicular to Grain - Effects of Moisture Gradients - J Jönsson, S Thelandersson

36-6-1	Characteristic Shear Strength Values Based on Tests According to EN 1193 - P Glos, J Denzler

37-6-1	Tensile Strength of Nordic Birch - K H Solli

37-6-2	Effect of Test Piece Orientation on Characteristic Bending Strength of Structural Timber - P Glos, J K Denzler

37-6-3	Strength and Stiffness Behaviour of Beech Laminations for High Strength Glulam - P Glos, J K Denzler, P W Linsenmann

37-6-4	A Review of Existing Standards Related to Calculation of Characteristic Values of Timber - F Rouger

37-6-5	Influence of the Rolling-Shear Modulus on the Strength and Stiffness of Structural Bonded Timber Elements - P Fellmoser, H J Blass

38-6-1	Design Specifications for Notched Beams in AS:1720 - R H Leicester

38-6-2	Characteristic Bending Strength of Beech Glulam - H J Blaß, M Frese

38-6-3	Shear Strength of Glued Laminated Timber - H Klapp, H Brüninghoff

39-6-1	Allocation of Central European hardwoods into EN 1912 - P Glos, J K Denzler

39-6-2	Revisiting EN 338 and EN 384 Basics and Procedures - R Steiger, M Arnold, M Fontana

40-6-1	Bearing Strength Perpendicular to the Grain of Locally Loaded Timber Blocks - A J M Leijten, J C M Schoenmakers

40-6-2	Experimental Study of Compression and Shear Strength of Spruce Timber - M Poussa, P Tukiainen, A Ranta-Maunus

40-6-3	Analysis of Tension and Bending strength of Graded Spruce Timber - A Hanhijärvi, A Ranta-Maunus, H Sarkama, M Kohsaku, M Poussa, J Puttonen

41-6-1	Design of Inclined Glulam Members with an End Notch on the Tension Face - A Asiz, I Smith

41-6-2	A New Design Approach for End-notched Beams - View on Code - K Rautenstrauch, B Franke, S Franke, K U Schober

41-6-3	The Design Rules in Eurocode 5 for Compression Perpendicular to the Grain - Continuous Supported Beams - H J Larsen, T A C M van der Put, A J M Leijten

41-6-4	Size Effects in Bending – J K Denzler, P Glos

42-6-1 Variability of Strength of European Spruce - A Ranta-Maunus, J K Denzler

42-6-2 Impact Loaded Structural Timber Elements Made from Swiss Grown Norway Spruce - R Widmann, R Steiger

42-6-3 Modelling the Bending Strength of Timber Components –Implications to Test Standards - J Köhler, M Sandomeer, T Isaksson, B Källsner

43-6-1 The Bearing Strength of Timber Beams on Discrete Supports - A Jorissen, B de Leijer, A Leijten

44-6-1 Impact of Material Properties on the Fracture Mechanics Design Approach for Notched Beams in Eurocode 5 - R Jockwer, R Steiger, A Frangi, J Köhler

44-6-2 Interaction of Shear Stresses and Stresses Perpendicular to the Grain - R Steiger, E Gehri

TIMBER JOINTS AND FASTENERS

1-7-1 Mechanical Fasteners and Fastenings in Timber Structures - E G Stern

4-7-1 Proposal for a Basic Test Method for the Evaluation of Structural Timber Joints with Mechanical Fasteners and Connectors - RILEM 3TT Committee

4-7-2 Test Methods for Wood Fasteners - K Möhler

5-7-1 Influence of Loading Procedure on Strength and Slip-Behaviour in Testing Timber Joints - K Möhler

5-7-2 Recommendations for Testing Methods for Joints with Mechanical Fasteners and Connectors in Load-Bearing Timber Structures - RILEM 3 TT Committee

5-7-3 CIB-Recommendations for the Evaluation of Results of Tests on Joints with Mechanical Fasteners and Connectors used in Load-Bearing Timber Structures - J Kuipers

6-7-1 Recommendations for Testing Methods for Joints with Mechanical Fasteners and Connectors in Load-Bearing Timber Structures (seventh draft) - RILEM 3 TT Committee

6-7-2 Proposal for Testing Integral Nail Plates as Timber Joints - K Möhler

6-7-3 Rules for Evaluation of Values of Strength and Deformation from Test Results - Mechanical Timber Joints - M Johansen, J Kuipers, B Norén

6-7-4 Comments to Rules for Testing Timber Joints and Derivation of Characteristic Values for Rigidity and Strength - B Norén

7-7-1 Testing of Integral Nail Plates as Timber Joints - K Möhler

7-7-2 Long Duration Tests on Timber Joints - J Kuipers

7-7-3 Tests with Mechanically Jointed Beams with a Varying Spacing of Fasteners - K Möhler

7-100-1 CIB-Timber Code Chapter 5.3 Mechanical Fasteners;CIB-Timber Standard 06 and 07 - H J Larsen

9-7-1 Design of Truss Plate Joints - F J Keenan

9-7-2 Staples - K Möhler

11-7-1 A Draft Proposal for International Standard: ISO Document ISO/TC 165N 38E

12-7-1 Load-Carrying Capacity and Deformation Characteristics of Nailed Joints - J Ehlbeck

12-7-2 Design of Bolted Joints - H J Larsen

12-7-3 Design of Joints with Nail Plates - B Norén

13-7-1 Polish Standard BN-80/7159-04: Parts 00-01-02-03-04-05. "Structures from Wood and Wood-based Materials. Methods of Test and Strength Criteria for Joints with Mechanical Fasteners"

13-7-2	Investigation of the Effect of Number of Nails in a Joint on its Load Carrying Ability - W Nozynski
13-7-3	International Acceptance of Manufacture, Marking and Control of Finger-jointed Structural Timber - B Norén
13-7-4	Design of Joints with Nail Plates - Calculation of Slip - B Norén
13-7-5	Design of Joints with Nail Plates - The Heel Joint - B Källsner
13-7-6	Nail Deflection Data for Design - H J Burgess
13-7-7	Test on Bolted Joints - P Vermeyden
13-7-8	Comments to paper CIB-W18/12-7-3 "Design of Joints with Nail Plates"- B Norén
13-7-9	Strength of Finger Joints - H J Larsen
13-100-4	CIB Structural Timber Design Code. Proposal for Section 6.1.5 Nail Plates - N I Bovim
14-7-1	Design of Joints with Nail Plates (second edition) - B Norén
14-7-2	Method of Testing Nails in Wood (second draft, August 1980) - B Norén
14-7-3	Load-Slip Relationship of Nailed Joints - J Ehlbeck and H J Larsen
14-7-4	Wood Failure in Joints with Nail Plates - B Norén
14-7-5	The Effect of Support Eccentricity on the Design of W- and WW-Trussed with Nail Plate Connectors - B Källsner
14-7-6	Derivation of the Allowable Load in Case of Nail Plate Joints Perpendicular to Grain - K Möhler
14-7-7	Comments on CIB-W18/14-7-1 - T A C M van der Put
15-7-1	Final Recommendation TT-1A: Testing Methods for Joints with Mechanical Fasteners in Load-Bearing Timber Structures. Annex A Punched Metal Plate Fasteners - Joint Committee RILEM/CIB-3TT
16-7-1	Load Carrying Capacity of Dowels - E Gehri
16-7-2	Bolted Timber Joints: A Literature Survey - N Harding
16-7-3	Bolted Timber Joints: Practical Aspects of Construction and Design; a Survey - N Harding
16-7-4	Bolted Timber Joints: Draft Experimental Work Plan - Building Research Association of New Zealand
17-7-1	Mechanical Properties of Nails and their Influence on Mechanical Properties of Nailed Timber Joints Subjected to Lateral Loads - I Smith, L R J Whale, C Anderson and L Held
17-7-2	Notes on the Effective Number of Dowels and Nails in Timber Joints - G Steck
18-7-1	Model Specification for Driven Fasteners for Assembly of Pallets and Related Structures - E G Stern and W B Wallin
18-7-2	The Influence of the Orientation of Mechanical Joints on their Mechanical Properties - I Smith and L R J Whale
18-7-3	Influence of Number of Rows of Fasteners or Connectors upon the Ultimate Capacity of Axially Loaded Timber Joints - I Smith and G Steck
18-7-4	A Detailed Testing Method for Nailplate Joints - J Kangas
18-7-5	Principles for Design Values of Nailplates in Finland - J Kangas
18-7-6	The Strength of Nailplates - N I Bovim and E Aasheim
19-7-1	Behaviour of Nailed and Bolted Joints under Short-Term Lateral Load - Conclusions from Some Recent Research - L R J Whale, I Smith and B O Hilson

19-7-2 Glued Bolts in Glulam - H Riberholt

19-7-3 Effectiveness of Multiple Fastener Joints According to National Codes and Eurocode 5 (Draft) - G Steck

19-7-4 The Prediction of the Long-Term Load Carrying Capacity of Joints in Wood Structures - Y M Ivanov and Y Y Slavic

19-7-5 Slip in Joints under Long-Term Loading - T Feldborg and M Johansen

19-7-6 The Derivation of Design Clauses for Nailed and Bolted Joints in Eurocode 5 - L R J Whale and I Smith

19-7-7 Design of Joints with Nail Plates - Principles - B Norén

19-7-8 Shear Tests for Nail Plates - B Norén

19-7-9 Advances in Technology of Joints for Laminated Timber - Analyses of the Structural Behaviour - M Piazza and G Turrini

19-15-1 Connections Deformability in Timber Structures: A Theoretical Evaluation of its Influence on Seismic Effects - A Ceccotti and A Vignoli

20-7-1 Design of Nailed and Bolted Joints-Proposals for the Revision of Existing Formulae in Draft Eurocode 5 and the CIB Code - L R J Whale, I Smith and H J Larsen

20-7-2 Slip in Joints under Long Term Loading - T Feldborg and M Johansen

20-7-3 Ultimate Properties of Bolted Joints in Glued-Laminated Timber - M Yasumura, T Murota and H Sakai

20-7-4 Modelling the Load-Deformation Behaviour of Connections with Pin-Type Fasteners under Combined Moment, Thrust and Shear Forces - I Smith

21-7-1 Nails under Long-Term Withdrawal Loading - T Feldborg and M Johansen

21-7-2 Glued Bolts in Glulam-Proposals for CIB Code - H Riberholt

21-7-3 Nail Plate Joint Behaviour under Shear Loading - T Poutanen

21-7-4 Design of Joints with Laterally Loaded Dowels. Proposals for Improving the Design Rules in the CIB Code and the Draft Eurocode 5 - J Ehlbeck and H Werner

21-7-5 Axially Loaded Nails: Proposals for a Supplement to the CIB Code - J Ehlbeck and W Siebert

22-7-1 End Grain Connections with Laterally Loaded Steel Bolts A draft proposal for design rules in the CIB Code - J Ehlbeck and M Gerold

22-7-2 Determination of Perpendicular-to-Grain Tensile Stresses in Joints with Dowel-Type Fasteners - A draft proposal for design rules - J Ehlbeck, R Görlacher and H Werner

22-7-3 Design of Double-Shear Joints with Non-Metallic Dowels A proposal for a supplement of the design concept - J Ehlbeck and O Eberhart

22-7-4 The Effect of Load on Strength of Timber Joints at high Working Load Level - A J M Leijten

22-7-5 Plasticity Requirements for Portal Frame Corners - R Gunnewijk and A J M Leijten

22-7-6 Background Information on Design of Glulam Rivet Connections in CSA/CAN3-086.1-M89 - A proposal for a supplement of the design concept - E Karacabeyli and D P Janssens

22-7-7 Mechanical Properties of Joints in Glued-Laminated Beams under Reversed Cyclic Loading - M Yasumura

22-7-8 Strength of Glued Lap Timber Joints - P Glos and H Horstmann

22-7-9 Toothed Rings Type Bistyp 075 at the Joints of Fir Wood - J Kerste

22-7-10 Calculation of Joints and Fastenings as Compared with the International State - K Zimmer and K Lissner

22-7-11 Joints on Glued-in Steel Bars Present Relatively New and Progressive Solution in Terms of Timber Structure Design - G N Zubarev, F A Boitemirov and V M Golovina

22-7-12 The Development of Design Codes for Timber Structures made of Compositive Bars with Plate Joints based on Cyclindrical Nails - Y V Piskunov

22-7-13 Designing of Glued Wood Structures Joints on Glued-in Bars - S B Turkovsky

23-7-1 Proposal for a Design Code for Nail Plates - E Aasheim and K H Solli

23-7-2 Load Distribution in Nailed Joints - H J Blass

24-7-1 Theoretical and Experimental Tension and Shear Capacity of Nail Plate Connections - B Källsner and J Kangas

24-7-2 Testing Method and Determination of Basic Working Loads for Timber Joints with Mechanical Fasteners - Y Hirashima and F Kamiya

24-7-3 Anchorage Capacity of Nail Plate - J Kangas

25-7-2 Softwood and Hardwood Embedding Strength for Dowel type Fasteners - J Ehlbeck and H Werner

25-7-4 A Guide for Application of Quality Indexes for Driven Fasteners Used in Connections in Wood Structures - E G Stern

25-7-5 35 Years of Experience with Certain Types of Connectors and Connector Plates Used for the Assembly of Wood Structures and their Components- E G Stern

25-7-6 Characteristic Strength of Split-ring and Shear-plate Connections - H J Blass, J Ehlbeck and M Schlager

25-7-7 Characteristic Strength of Tooth-plate Connector Joints - H J Blass, J Ehlbeck and M Schlager

25-7-8 Extending Yield Theory to Screw Connections - T E McLain

25-7-9 Determination of k_{def} for Nailed Joints - J W G van de Kuilen

25-7-10 Characteristic Strength of UK Timber Connectors - A V Page and C J Mettem

25-7-11 Multiple-fastener Dowel-type Joints, a Selected Review of Research and Codes - C J Mettem and A V Page

25-7-12 Load Distributions in Multiple-fastener Bolted Joints in European Whitewood Glulam, with Steel Side Plates - C J Mettem and A V Page

26-7-1 Proposed Test Method for Dynamic Properties of Connections Assembled with Mechanical Fasteners - J D Dolan

26-7-2 Validatory Tests and Proposed Design Formulae for the Load-Carrying Capacity of Toothed-Plate Connectored Joints - C J Mettem, A V Page and G Davis

26-7-3 Definitions of Terms and Multi-Language Terminology Pertaining to Metal Connector Plates - E G Stern

26-7-4 Design of Joints Based on in V-Shape Glued-in Rods - J Kangas

26-7-5 Tests on Timber Concrete Composite Structural Elements (TCCs) - A U Meierhofer

27-7-1 Glulam Arch Bridge and Design of it's Moment-Resisting Joints - K Komatsu and S Usuku

27-7-2 Characteristic Load - Carrying Capacity of Joints with Dowel - type Fasteners in Regard to the System Properties - H Werner

27-7-3 Steel Failure Design in Truss Plate Joints - T Poutanen

28-7-1	Expanded Tube Joint in Locally DP Reinforced Timber - A J M Leijten, P Ragupathy and K S Virdi
28-7-2	A Strength and Stiffness Model for the Expanded Tube Joint - A J M Leijten
28-7-3	Load-carrying Capacity of Steel-to Timber Joints with Annular Ring Shanked Nails. A Comparison with the EC5 Design Method - R Görlacher
28-7-4	Dynamic Effects on Metal-Plate Connected Wood Truss Joints - S Kent, R Gupta and T Miller
28-7-5	Failure of the Timber Bolted Joints Subjected to Lateral Load Perpendicular to Grain - M Yasumura and L Daudeville
28-7-6	Design Procedure for Locally Reinforced Joints with Dowel-type Fasteners - H Werner
28-7-7	Variability and Effects of Moisture Content on the Withdrawal Characteristics for Lumber as Opposed to Clear Wood - J D Dolan and J W Stelmokas
28-7-8	Nail Plate Capacity in Joint Line - A Kevarinmäki and J Kangas
28-7-9	Axial Strength of Glued-In Bolts - Calculation Model Based on Non-Linear Fracture Mechanics - A Preliminary Study - C J Johansson, E Serrano, P J Gustafsson and B Enquist
28-7-10	Cyclic Lateral Dowel Connection Tests for seismic and Wind Evaluation - J D Dolan
29-7-1	A Simple Method for Lateral Load-Carrying Capacity of Dowel-Type Fasteners - J Kangas and J Kurkela
29-7-2	Nail Plate Joint Behaviour at Low Versus High Load Level - T Poutanen
29-7-3	The Moment Resistance of Tee and Butt - Joint Nail Plate Test Specimens - A Comparison with Current Design Methods - A Reffold, L R J Whale and B S Choo
29-7-4	A Critical Review of the Moment Rotation Test Method Proposed in prEN 1075 - M Bettison, B S Choo and L R J Whale
29-7-5	Explanation of the Translation and Rotation Behaviour of Prestressed Moment Timber Joints - A J M Leijten
29-7-6	Design of Joints and Frame Corners using Dowel-Type Fasteners - E Gehri
29-7-7	Quasi-Static Reversed-Cyclic Testing of Nailed Joints - E Karacabeyli and A Ceccotti
29-7-8	Failure of Bolted Joints Loaded Parallel to the Grain: Experiment and Simulation - L Davenne, L Daudeville and M Yasumura
30-7-1	Flexural Behaviour of GLT Beams End-Jointed by Glued-in Hardwood Dowels - K Komatsu, A Koizumi, J Jensen, T Sasaki and Y Iijima
30-7-2	Modelling of the Block Tearing Failure in Nailed Steel-to-Timber Joints - J Kangas, K Aalto and A Kevarinmäki
30-7-3	Cyclic Testing of Joints with Dowels and Slotted-in Steel Plates - E Aasheim
30-7-4	A Steel-to-Timber Dowelled Joint of High Performance in Combination with a High Strength Wood Composite (Parallam) - E Gehri
30-7-5	Multiple Fastener Timber Connections with Dowel Type Fasteners - A Jorissen
30-7-6	Influence of Ductility on Load-Carrying Capacity of Joints with Dowel-Type Fasteners - A Mischler
31-7-1	Mechanical Properties of Dowel Type Joints under Reversed Cyclic Lateral Loading - M Yasumura
31-7-2	Design of Joints with Laterally Loaded Dowels - A Mischler

31-7-3 Flexural Behaviour of Glulam Beams Edge-Jointed by Lagscrews with Steel Splice Plates - K Komatsu

31-7-4 Design on Timber Capacity in Nailed Steel-to-Timber Joints - J Kangas and J Vesa

31-7-5 Timber Contact in Chord Splices of Nail Plate Structures - A Kevarinmäki

31-7-6 The Fastener Yield Strength in Bending - A Jorissen and H J Blaß

31-7-7 A Proposal for Simplification of Johansen`s Formulae, Dealing With the Design of Dowelled-Type Fasteners - F Rouger

31-7-8 Simplified Design of Connections with Dowel-type fasteners - H J Blaß and J Ehlbeck

32-7-1 Behaviour of Wood-Steel-Wood Bolted Glulam Connections - M Mohammad and J H P Quenneville

32-7-2 A new set of experimental tests on beams loaded perpendicular-to-grain by dowel-type joints- M Ballerini

32-7-3 Design and Analysis of Bolted Timber Joints under Lateral Force Perpendicular to Grain - M Yasumura and L Daudeville

32-7-4 Predicting Capacities of Joints with Laterally Loaded Nails - I Smith and P Quenneville

32-7-5 Strength Reduction Rules for Multiple Fastener Joints - A Mischler and E Gehri

32-7-6 The Stiffness of Multiple Bolted Connections - A Jorissen

32-7-7 Concentric Loading Tests on Girder Truss Components - T N Reynolds, A Reffold, V Enjily and L Whale

32-7-8 Dowel Type Connections with Slotted-In Steel Plates - M U Pedersen, C O Clorius, L Damkilde, P Hoffmeyer and L Esklidsen

32-7-9 Creep of Nail Plate Reinforced Bolt Joints - J Vesa and A Kevarinmäki

32-7-10 The Behaviour of Timber Joints with Ring Connectors - E Gehri and A Mischler

32-7-11 Non-Metallic, Adhesiveless Joints for Timber Structures - R D Drake, M P Ansell, C J Mettem and R Bainbridge

32-7-12 Effect of Spacing and Edge Distance on the Axial Strength of Glued-in Rods - H J Blaß and B Laskewitz

32-7-13 Evaluation of Material Combinations for Bonded in Rods to Achieve Improved Timber Connections - C J Mettem, R J Bainbridge, K Harvey, M P Ansell, J G Broughton and A R Hutchinson

33-7-1 Determination of Yield Strength and Ultimate Strength of Dowel-Type Timber Joints – M Yasumura and K Sawata

33-7-2 Lateral Shear Capacity of Nailed Joints – U Korin

33-7-3 Height-Adjustable Connector for Composite Beams – Y V Piskunov and E G Stern

33-7-4 Engineering Ductility Assessment for a Nailed Slotted-In Steel Connection in Glulam– L Stehn and H Johansson

33-7-5 Effective Bending Capacity of Dowel-Type Fasteners - H J Blaß, A Bienhaus and V Krämer

33-7-6 Load-Carrying Capacity of Joints with Dowel-Type Fasteners and Interlayers - H J Blaß and B Laskewitz

33-7-7 Evaluation of Perpendicular to Grain Failure of Beams caused by Concentrated Loads of Joints – A J M Leijten and T A C M van der Put

33-7-8 Test Methods for Glued-In Rods for Timber Structures – C Bengtsson and C J Johansson

33-7-9 Stiffness Analysis of Nail Plates – P Ellegaard

33-7-10	Capacity, Fire Resistance and Gluing Pattern of the Rods in V-Connections – J Kangas
33-7-11	Bonded-In Pultrusions for Moment-Resisting Timber Connections – K Harvey, M P Ansell, C J Mettem, R J Bainbridge and N Alexandre
33-7-12	Fatigue Performance of Bonded-In Rods in Glulam, Using Three Adhesive Types - R J Bainbridge, K Harvey, C J Mettem and M P Ansell
34-7-1	Splitting Strength of Beams Loaded by Connections Perpendicular to Grain, Model Validation – A J M Leijten, A Jorissen
34-7-2	Numerical LEFM analyses for the evaluation of failure loads of beams loaded perpendicular-to-grain by single-dowel connections – M Ballerini, R Bezzi
34-7-3	Dowel joints loaded perpendicular to grain - H J Larsen, P J Gustafsson
34-7-4	Quality Control of Connections based on in V-shape glued-in Steel Rods – J Kangas, A Kevarinmäki
34-7-5	Testing Connector Types for Laminated-Timber-Concrete Composite Elements – M Grosse, S Lehmann, K Rautenstrauch
34-7-6	Behaviour of Axially Loaded Glued-in Rods - Requirements and Resistance, Especially for Spruce Timber Perpendicular to the Grain Direction – A Bernasconi
34-7-7	Embedding characteristics on fibre reinforcement and densified timber joints - P Haller, J Wehsener, T Birk
34-7-8	GIROD – Glued-in Rods for Timber Structures – C Bengtsson, C-J Johansson
34-7-9	Criteria for Damage and Failure of Dowel-Type Joints Subjected to Force Perpendicular to the Grain – M Yasumura
34-7-10	Interaction Between Splitting and Block Shear Failure of Joints – A J M Leijten, A Jorissen, J Kuipers
34-7-11	Limit states design of dowel-fastener joints – Placement of modification factors and partial factors, and calculation of variability in resistance – I Smith, G Foliente
34-7-12	Design and Modelling of Knee Joints - J Nielsen, P Ellegaard
34-7-13	Timber-Steel Shot Fired Nail Connections at Ultimate Limit States - R J Bainbridge, P Larsen, C J Mettem, P Alam, M P Ansell
35-7-1	New Estimating Method of Bolted Cross-lapped Joints with Timber Side Members - M Noguchi, K Komatsu
35-7-2	Analysis on Multiple Lag Screwed Timber Joints with Timber Side Members - K Komatsu, S Takino, M Nakatani, H Tateishi
35-7-3	Joints with Inclined Screws - A Kevarinmäki
35-7-4	Joints with Inclined Screws - I Bejtka, H J Blaß
35-7-5	Effect of distances, Spacing and Number of Dowels in a Row an the Load Carrying Capacity of Connections with Dowels failing by Splitting - M Schmid, R Frasson, H J Blaß
35-7 6	Effect of Row Spacing on the Capacity of Bolted Timber Connections Loaded Perpendicular-to-grain - P Quenneville, M Kasim
35-7-7	Splitting Strength of Beams Loaded by Connections, Model Comparison - A J M Leijten
35-7-8	Load-Carrying Capacity of Perpendicular to the Grain Loaded Timber Joints with Multiple Fasteners - O Borth, K U Schober, K Rautenstrauch
35-7-9	Determination of fracture parameter for dowel-type joints loaded perpendicular to wooden grain and its application - M Yasumura
35-7-10	Analysis and Design of Modified Attic Trusses with Punched Metal Plate Fasteners - P Ellegaard
35-7-11	Joint Properties of Plybamboo Sheets in Prefabricated Housing - G E Gonzalez

35-7-12	Fiber-Reinforced Beam-to-Column Connections for Seismic Applications - B Kasal, A Heiduschke, P Haller
36-7-1	Shear Tests in Timber-LWAC with Screw-Type Connections - L Jorge, H Cruz, S Lopes
36-7-2	Plug Shear Failure in Nailed Timber Connections: Experimental Studies - H Johnsson
36-7-3	Nail-Laminated Timber Elements in Natural Surface-Composite with Mineral Bound Layer - S Lehmann, K Rautenstrauch
36-7-4	Mechanical Properties of Timber-Concrete Joints Made With Steel Dowels - A Dias, J W G van de Kuilen, H Cruz
36-7-5	Comparison of Hysteresis Responses of Different Sheating to Framing Joints - B Dujič, R Zarnić
36-7- 6	Evaluation and Estimation of the Performance of the Nail Joints and Shear Walls under Dry/Humid Cyclic Climate - S Nakajima
36-7-7	Beams Transversally Loaded by Dowel-Type Joints: Influence on Splitting Strength of Beam Thickness and Dowel Size - M Ballerini, A Giovanella
36-7-8	Splitting Strength of Beams Loaded by Connections - J L Jensen
36-7-9	A Tensile Fracture Model for Joints with Rods or Dowels loaded Perpendicular-to-Grain - J L Jensen, P J Gustafsson, H J Larsen
36-7-10	A Numerical Model to Simulate the Load-Displacement Time-History of Mutiple-Bolt Connections Subjected to Various Loadings - C P Heine, J D Dolan
36-7-11	Reliability of Timber Structures, Theory and Dowel-Type Connection Failures - A Ranta-Maunus, A Kevarinmäki
37-7-1	Development of the "Displaced Volume Model" to Predict Failure for Multiple-Bolt Timber Joints - D M Carradine, J D Dolan, C P Heine
37-7-2	Mechanical Models of the Knee Joints with Cross-Lapped Glued Joints and Glued in Steel Rods - M Noguchi, K Komatsu
37-7-3	Simplification of the Neural Network Model for Predicting the Load-Carrying Capacity of Dowel-Type Connections - A Cointe, F Rouger
37-7-4	Bolted Wood Connections Loaded Perpendicular-to-Grain- A Proposed Design Approach - M C G Lehoux, J H P Quenneville
37-7-5	A New Prediction Formula for the Splitting Strength of Beams Loaded by Dowel Type Connections - M Ballerini
37-7-6	Plug Shear Failure: The Tensile Failure Mode and the Effect of Spacing - H Johnsson
37-7-7	Block Shear Failure Test with Dowel-Type Connection in Diagonal LVL Structure - M Kairi
37-7-8	Glued-in Steel Rods: A Design Approach for Axially Loaded Single Rods Set Parallel to the Grain - R Steiger, E Gehri, R Widmann
37-7-9	Glued in Rods in Load Bearing Timber Structures - Status regarding European Standards for Test Procedures - B Källander
37-7-10	French Data Concerning Glued-in Rods - C Faye, L Le Magorou, P Morlier, J Surleau
37-7-11	Enhancement of Dowel-Type Fasteners by Glued Connectors - C O Clorius, A Højman
37-7-12	Review of Probability Data for Timber Connections with Dowel-Type Fasteners - A J M Leijten, J Köhler, A Jorissen
37-7-13	Behaviour of Fasteners and Glued-in Rods Produced From Stainless Steel - A Kevarinmäki
37-7-14	Dowel joints in Engineered Wood Products: Assessment of Simple Fracture Mechanics Models - M Snow, I Smith, A Asiz

37-7-15	Numerical Modelling of Timber and Connection Elements Used in Timber-Concrete-Composite Constructions - M Grosse, K Rautenstrauch
38-7-1	A Numerical Investigation on the Splitting Strength of Beams Loaded Perpendicular-to-grain by Multiple-dowel Connections – M Ballerini, M Rizzi
38-7-2	A Probabilistic Framework for the Reliability Assessment of Connections with Dowel Type Fasteners - J Köhler
38-7-3	Load Carrying Capacity of Curved Glulam Beams Reinforced with self-tapping Screws - J Jönsson, S Thelandersson
38-7-4	Self-tapping Screws as Reinforcements in Connections with Dowel-Type Fasteners- I Bejtka, H J Blaß
38-7-5	The Yield Capacity of Dowel Type Fasteners - A Jorissen, A Leijten
38-7-6	Nails in Spruce - Splitting Sensitivity, End Grain Joints and Withdrawal Strength - A Kevarinmäki
38-7-7	Design of Timber Connections with Slotted-in Steel Plates and Small Diameter Steel Tube Fasteners - B Murty, I Smith, A Asiz
39-7-1	Effective in-row Capacity of Multiple-Fastener Connections - P Quenneville, M Bickerdike
39-7-2	Self-tapping Screws as Reinforcements in Beam Supports - I Bejtka, H J Blaß
39-7-3	Connectors for Timber-concrete Composite-Bridges - A Döhrer, K Rautenstrauch
39-7-4	Block Shear Failure at Dowelled Double Shear Steel-to-timber Connections - A Hanhijärvi, A Kevarinmäki, R Yli-Koski
39-7-5	Load Carrying Capacity of Joints with Dowel Type Fasteners in Solid Wood Panels - T Uibel, H J Blaß
39-7-6	Generalised Canadian Approach for Design of Connections with Dowel Fasteners - P Quenneville, I Smith, A Asiz, M Snow, Y H Chui
40-7-1	Predicting the Strength of Bolted Timber Connections Subjected to Fire - M Fragiacomo, A Buchanan, D Carshalton, P Moss, C Austruy
40-7-2	Edge Joints with Dowel Type Fasteners in Cross Laminated Timber - H J Blaß, T Uibel
40-7-3	Design Method against Timber Failure Mechanisms of Dowelled Steel-to-Timber Connections - A Hanhijärvi, A Kevarinmäki
40-7-4	A EYM Based Simplified Design Formula for the Load-carrying Capacity of Dowel-type Connections - M Ballerini
40-7-5	Evaluation of the Slip Modulus for Ultimate Limit State Verifications of Timber-Concrete Composite Structures - E Lukaszewska, M Fragiacomo, A Frangi
40-7-6	Models for the Predictions of the Ductile and Brittle Failure Modes (Parallel-to-Grain) of Timber Rivet Connections - M Marjerrison, P Quenneville
40-7-7	Creep of Timber and Timber-Concrete Joints. - J W G van de Kuilen, A M P G Dias
40-7-8	Lag Screwed Timber Joints with Timber Side Members- K Komatsu, S Takino, H Tateishi
41-7-1	Applicability of Existing Design Approaches to Mechanical Joints in Structural Composite Lumber - M Snow, I Smith, A Asiz, M Ballerini
41-7-2	Validation of the Canadian Bolted Connection Design Proposal - P Quenneville, J Jensen
41-7-3	Ductility of Moment Resisting Dowelled Joints in Heavy Timber Structures - A Polastri, R Tomasi, M Piazza, I Smith
41-7-4	Mechanical Behaviour of Traditional Timber Connections: Proposals for Design, Based on Experimental and Numerical Investigations. Part I: Birdsmouth - C Faye, P Garcia, L Le Magorou, F Rouger

41-7-5 Embedding Strength of European Hardwoods - U Hübner, T Bogensperger, G Schickhofer

42-7-1 Base Parameters of Self-tapping Screws - G Pirnbacher, R Brandner, G Schickhofer

42-7-2 Joints with Inclined Screws and Steel Plates as Outer Members - H Krenn, G Schickhofer

42-7-3 Models for the Calculation of the Withdrawal Capacity of Self-tapping Screws - M Frese, H J Blaß

42-7-4 Embedding Strength of New Zealand Timber and Recommendation for the NZ Standard - S Franke, P Quenneville

42-7-5 Load Carrying Capacity of Timber-Wood Fiber Insulation Board – Joints with Dowel Type Fasteners - G Gebhardt, H J Blaß

42-7-6 Prediction of the Fatigue Resistance of Timber-Concrete-Composite Connections - U Kuhlmann, P Aldi

42-7-7 Using Screws for Structural Applications in Laminated Veneer Lumber - D M Carradine, M P Newcombe, A H Buchanan

42-7-8 Influence of Fastener Spacings on Joint Performance - Experimental Results and Codification - E Gehri

42-7-9 Connections with Glued-in Hardwood Rods Subjected to Combined Bending and Shear Actions - J L Jensen, P Quenneville

43-7-1 Probabilistic Capacity Prediction of Timber Joints under Brittle Failure Modes - T Tannert, T Vallée, and F Lam

43-7-2 Ductility in Timber Structures - A Jorissen, M Fragiacomo

43-7-3 Design of Mechanically Jointed Concrete-Timber Beams Taking into Account the Plastic Behaviour of the Fasteners - H J Larsen, H Riberholt, A Ceccotti

43-7-4 Design of Timber-Concrete Composite Beams with Notched Connections - M Fragiacomo, D Yeoh

43-7-5 Development of Design Procedures for Timber Concrete Composite Floors in Australia and New Zealand - K Crews, C Gerber

43-7-6 Failure Behaviour and Resistance of Dowel-Type Connections Loaded Perpendicular to Grain - B Franke, P Quenneville

43-7-7 Predicting Time Dependent Effects in Unbonded Post-Tensioned Timber Beams and Frames - S Giorgini, A Neale, A Palermo, D Carradine, S Pampanin, A H Buchanan

43-7-8 Simplified Design of Post-tensioned Timber Frames - M Newcombe, M Cusiel, S Pampanin, A Palermo, A H Buchanan

44-7-1 Pull-through Capacity in Plywood and OSB - J Munch-Andersen, J D Sørensen

44-7-2 Design Concept for CLT - Reinforced with Self-Tapping Screws - P Mestek, H Kreuzinger, S Winter

44-7-3 Fatigue Behaviour of the Stud Connector Used for Timber-Concrete Composite Bridges – K Rautenstrauch, J Mueller

44-7-4 The Stiffness of Beam to Column Connections in Post-Tensioned Timber Frames – T Smith, W van Beerschoten, A Palermo, S Pampanin, F C Ponzo

44-7-5 Design Approach for the Splitting Failure of Dowel-Type Connections Loaded Perpendicular to Grain - Bettina Franke, Pierre Quenneville

LOAD SHARING

3-8-1 Load Sharing - An Investigation on the State of Research and Development of Design Criteria - E Levin

4-8-1 A Review of Load-Sharing in Theory and Practice - E Levin

DURATION OF LOAD

19-1-1 Duration of Load Effects and Reliability Based Design (Single Member) - R O Foschi and Z C Yao

19-6-1 Effect of Age and/or Load on Timber Strength - J Kuipers

19-7-4 The Prediction of the Long-Term Load Carrying Capacity of Joints in Wood Structures - Y M Ivanov and Y Y Slavic

19-7-5 Slip in Joints under Long-Term Loading - T Feldborg and M Johansen

20-7-2 Slip in Joints under Long-Term Loading - T Feldborg and M Johansen

22-9-1 Long-Term Tests with Glued Laminated Timber Girders - M Badstube, W Rug and W Schöne

22-9-2 Strength of One-Layer solid and Lengthways Glued Elements of Wood Structures and its Alteration from Sustained Load - L M Kovaltchuk, I N Boitemirova and G B Uspenskaya

24-9-1 Long Term Bending Creep of Wood - T Toratti

24-9-2 Collection of Creep Data of Timber - A Ranta-Maunus

24-9-3 Deformation Modification Factors for Calculating Built-up Wood-Based Structures - I R Kliger

25-9-2 DVM Analysis of Wood. Lifetime, Residual Strength and Quality - L F Nielsen

26-9-1 Long Term Deformations in Wood Based Panels under Natural Climate Conditions. A Comparative Study - S Thelandersson, J Nordh, T Nordh and S Sandahl

28-9-1 Evaluation of Creep Behavior of Structural Lumber in Natural Environment - R Gupta and R Shen

30-9-1 DOL Effect in Tension Perpendicular to the Grain of Glulam Depending on Service Classes and Volume - S Aicher and G Dill-Langer

30-9-2 Damage Modelling of Glulam in Tension Perpendicular to Grain in Variable Climate - G Dill-Langer and S Aicher

31-9-1 Duration of Load Effect in Tension Perpendicular to Grain in Curved Glulam - A Ranta-Maunus

32-9-1 Bending-Stress-Redistribution Caused by Different Creep in Tension and Compression and Resulting DOL-Effect - P Becker and K Rautenstrauch

32-9-2 The Long Term Performance of Ply-Web Beams - R Grantham and V Enjily

36-9-1 Load Duration Factors for Instantaneous Loads - A J M Leijten, B Jansson

39-9-1 Simplified Approach for the Long-Term Behaviour of Timber-Concrete Composite Beams According to the Eurocode 5 Provisions - M Fragiacomo, A Ceccotti

TIMBER BEAMS

4-10-1 The Design of Simple Beams - H J Burgess

4-10-2 Calculation of Timber Beams Subjected to Bending and Normal Force - H J Larsen

5-10-1 The Design of Timber Beams - H J Larsen

9-10-1 The Distribution of Shear Stresses in Timber Beams - F J Keenan

9-10-2 Beams Notched at the Ends - K Möhler

11-10-1 Tapered Timber Beams - H Riberholt

13-6-2 Consideration of Size Effects in Longitudinal Shear Strength for Uncracked Beams - R O Foschi and J D Barrett

13-6-3	Consideration of Shear Strength on End-Cracked Beams - J D Barrett and R O Foschi
18-10-1	Submission to the CIB-W18 Committee on the Design of Ply Web Beams by Consideration of the Type of Stress in the Flanges - J A Baird
18-10-2	Longitudinal Shear Design of Glued Laminated Beams - R O Foschi
19-10-1	Possible Code Approaches to Lateral Buckling in Beams - H J Burgess
19-2-1	Creep Buckling Strength of Timber Beams and Columns - R H Leicester
20-2-1	Lateral Buckling Theory for Rectangular Section Deep Beam-Columns - H J Burgess
20-10-1	Draft Clause for CIB Code for Beams with Initial Imperfections - H J Burgess
20-10-2	Space Joists in Irish Timber - W J Robinson
20-10-3	Composite Structure of Timber Joists and Concrete Slab - T Poutanen
21-10-1	A Study of Strength of Notched Beams - P J Gustafsson
22-10-1	Design of Endnotched Beams - H J Larsen and P J Gustafsson
22-10-2	Dimensions of Wooden Flexural Members under Constant Loads - A Pozgai
22-10-3	Thin-Walled Wood-Based Flanges in Composite Beams - J König
22-10-4	The Calculation of Wooden Bars with flexible Joints in Accordance with the Polish Standart Code and Strict Theoretical Methods - Z Mielczarek
23-10-1	Tension Perpendicular to the Grain at Notches and Joints - T A C M van der Put
23-10-2	Dimensioning of Beams with Cracks, Notches and Holes. An Application of Fracture Mechanics - K Riipola
23-10-3	Size Factors for the Bending and Tension Strength of Structural Timber - J D Barret and A R Fewell
23-12-1	Bending Strength of Glulam Beams, a Design Proposal - J Ehlbeck and F Colling
23-12-3	Glulam Beams, Bending Strength in Relation to the Bending Strength of the Finger Joints - H Riberholt
24-10-1	Shear Strength of Continuous Beams - R H Leicester and F G Young
25-10-1	The Strength of Norwegian Glued Laminated Beams - K Solli, E Aasheim and R H Falk
25-10-2	The Influence of the Elastic Modulus on the Simulated Bending Strength of Hyperstatic Timber Beams - T D G Canisius
27-10-1	Determination of Shear Modulus - R Görlacher and J Kürth
29-10-1	Time Dependent Lateral Buckling of Timber Beams - F Rouger
29-10-2	Determination of Modulus of Elasticity in Bending According to EN 408 - K H Solli
29-10-3	On Determination of Modulus of Elasticity in Bending - L Boström, S Ormarsson and O Dahlblom
29-10-4	Relation of Moduli of Elasticity in Flatwise and Edgewise Bending of Solid Timber - C J Johansson, A Steffen and E W Wormuth
30-10-1	Nondestructive Evaluation of Wood-based Members and Structures with the Help of Modal Analysis - P Kuklik
30-10-2	Measurement of Modulus of Elasticity in Bending - L Boström
30-10-3	A Weak Zone Model for Timber in Bending - B Källsner, K Salmela and O Ditlevsen

30-10-4 Load Carrying Capacity of Timber Beams with Narrow Moment Peaks - T Isaksson and J Freysoldt

37-10-1 Design of Rim Boards for Use with I-Joists Framing Systems - B Yeh, T G Williamson

40-10- 1 Extension of EC5 Annex B Formulas for the Design of Timber-concrete Composite Structures - J Schänzlin, M Fragiacomo

40-10-2 Simplified Design Method for Mechanically Jointed Beams - U A Girhammar

41-10-1 Composite Action of I-Joist Floor Systems - T G Williamson, B Yeh

41-10-2 Evaluation of the Prestressing Losses in Timber Members Prestressed with Unbonded Tendons - M Fragiacomo, M Davies

41-10-3 Relationship Between Global and Local MOE – J K Denzler, P Stapel, P Glos

42-10-1 Relationships Between Local, Global and Dynamic Modulus of Elasticity for Soft- and Hardwoods – G J P Ravenshorst, J W G van de Kuilen

ENVIRONMENTAL CONDITIONS

5-11-1 Climate Grading for the Code of Practice - B Norén

6-11-1 Climate Grading (2) - B Norén

9-11-1 Climate Classes for Timber Design - F J Keenan

19-11-1 Experimental Analysis on Ancient Downgraded Timber Structures - B Leggeri and L Paolini

19-6-5 Drying Stresses in Round Timber - A Ranta-Maunus

22-11-1 Corrosion and Adaptation Factors for Chemically Aggressive Media with Timber Structures - K Erler

29-11-1 Load Duration Effect on Structural Beams under Varying Climate Influence of Size and Shape - P Galimard and P Morlier

30-11-1 Probabilistic Design Models for the Durability of Timber Constructions - R H Leicester

36-11-1 Structural Durability of Timber in Ground Contact – R H Leicester, C H Wang, M N Nguyen, G C Foliente, C McKenzie

38-11-1 Design Specifications for the Durability of Timber – R H Leicester, C-H Wang, M Nguyen, G C Foliente

38-11-2 Consideration of Moisture Exposure of Timber Structures as an Action - M Häglund, S Thelandersson

LAMINATED MEMBERS

6-12-1 Directives for the Fabrication of Load-Bearing Structures of Glued Timber - A van der Velden and J Kuipers

8-12-1 Testing of Big Glulam Timber Beams - H Kolb and P Frech

8-12-2 Instruction for the Reinforcement of Apertures in Glulam Beams - H Kolb and P Frech

8-12-3 Glulam Standard Part 1: Glued Timber Structures; Requirements for Timber (Second Draft)

9-12-1 Experiments to Provide for Elevated Forces at the Supports of Wooden Beams with Particular Regard to Shearing Stresses and Long-Term Loadings - F Wassipaul and R Lackner

9-12-2 Two Laminated Timber Arch Railway Bridges Built in Perth in 1849 - L G Booth

9-6-4	Consideration of Combined Stresses for Lumber and Glued Laminated Timber - K Möhler
11-6-3	Consideration of Combined Stresses for Lumber and Glued Laminated Timber (addition to Paper CIB-W18/9-6-4) - K Möhler
12-12-1	Glulam Standard Part 2: Glued Timber Structures; Rating (3rd draft)
12-12-2	Glulam Standard Part 3: Glued Timber Structures; Performance (3 rd draft)
13-12-1	Glulam Standard Part 3: Glued Timber Structures; Performance (4th draft)
14-12-1	Proposals for CEI-Bois/CIB-W18 Glulam Standards - H J Larsen
14-12-2	Guidelines for the Manufacturing of Glued Load-Bearing Timber Structures - Stevin Laboratory
14-12-3	Double Tapered Curved Glulam Beams - H Riberholt
14-12-4	Comment on CIB-W18/14-12-3 - E Gehri
18-12-1	Report on European Glulam Control and Production Standard - H Riberholt
18-10-2	Longitudinal Shear Design of Glued Laminated Beams - R O Foschi
19-12-1	Strength of Glued Laminated Timber - J Ehlbeck and F Colling
19-12-2	Strength Model for Glulam Columns - H J Blaß
19-12-3	Influence of Volume and Stress Distribution on the Shear Strength and Tensile Strength Perpendicular to Grain - F Colling
19-12-4	Time-Dependent Behaviour of Glued-Laminated Beams - F Zaupa
21-12-1	Modulus of Rupture of Glulam Beam Composed of Arbitrary Laminae - K Komatsu and N Kawamoto
21-12-2	An Appraisal of the Young's Modulus Values Specified for Glulam in Eurocode 5- L R J Whale, B O Hilson and P D Rodd
21-12-3	The Strength of Glued Laminated Timber (Glulam): Influence of Lamination Qualities and Strength of Finger Joints - J Ehlbeck and F Colling
21-12-4	Comparison of a Shear Strength Design Method in Eurocode 5 and a More Traditional One - H Riberholt
22-12-1	The Dependence of the Bending Strength on the Glued Laminated Timber Girder Depth - M Badstube, W Rug and W Schöne
22-12-2	Acid Deterioration of Glulam Beams in Buildings from the Early Half of the 1960s - Prelimination summary of the research project; Overhead pictures - B A Hedlund
22-12-3	Experimental Investigation of normal Stress Distribution in Glue Laminated Wooden Arches - Z Mielczarek and W Chanaj
22-12-4	Ultimate Strength of Wooden Beams with Tension Reinforcement as a Function of Random Material Properties - R Candowicz and T Dziuba
23-12-1	Bending Strength of Glulam Beams, a Design Proposal - J Ehlbeck and F Colling
23-12-2	Probability Based Design Method for Glued Laminated Timber - M F Stone
23-12-3	Glulam Beams, Bending Strength in Relation to the Bending Strength of the Finger Joints - H Riberholt
23-12-4	Glued Laminated Timber - Strength Classes and Determination of Characteristic Properties - H Riberholt, J Ehlbeck and A Fewell
24-12-1	Contribution to the Determination of the Bending Strength of Glulam Beams - F Colling, J Ehlbeck and R Görlacher
24-12-2	Influence of Perpendicular-to-Grain Stressed Volume on the Load-Carrying Capacity of Curved and Tapered Glulam Beams - J Ehlbeck and J Kürth

25-12-1 Determination of Characteristic Bending Values of Glued Laminated Timber. EN-Approach and Reality - E Gehri

26-12-1 Norwegian Bending Tests with Glued Laminated Beams-Comparative Calculations with the "Karlsruhe Calculation Model" - E Aasheim, K Solli, F Colling, R H Falk, J Ehlbeck and R Görlacher

26-12-2 Simulation Analysis of Norwegian Spruce Glued-Laminated Timber - R Hernandez and R H Falk

26-12-3 Investigation of Laminating Effects in Glued-Laminated Timber - F Colling and R H Falk

26-12-4 Comparing Design Results for Glulam Beams According to Eurocode 5 and to the French Working Stress Design Code (CB71) - F Rouger

27-12-1 State of the Art Report: Glulam Timber Bridge Design in the U.S. - M A Ritter and T G Williamson

27-12-2 Common Design Practice for Timber Bridges in the United Kingdom - C J Mettem, J P Marcroft and G Davis

27-12-3 Influence of Weak Zones on Stress Distribution in Glulam Beams - E Serrano and H J Larsen

28-12-1 Determination of Characteristic Bending Strength of Glued Laminated Timber - E Gehri

28-12-2 Size Factor of Norwegian Glued Laminated Beams - E Aasheim and K H Solli

28-12-3 Design of Glulam Beams with Holes - K Riipola

28-12-4 Compression Resistance of Glued Laminated Timber Short Columns- U Korin

29-12-1 Development of Efficient Glued Laminated Timber - G Schickhofer

30-12-1 Experimental Investigation and Analysis of Reinforced Glulam Beams - K Oiger

31-12-1 Depth Factor for Glued Laminated Timber-Discussion of the Eurocode 5 Approach - B Källsner, O Carling and C J Johansson

32-12-1 The bending stiffness of nail-laminated timber elements in transverse direction- T Wolf and O Schäfer

33-12-1 Internal Stresses in the Cross-Grain Direction of Wood Induced by Climate Variation – J Jönsson and S Svensson

34-12-1 High-Strength I-Joist Compatible Glulam Manufactured with LVL Tension Laminations – B Yeh, T G Williamson

34-12-2 Evaluation of Glulam Shear Strength Using A Full-Size Four-Point Test Method – B Yeh, T G Williamson

34-12-3 Design Model for FRP Reinforced Glulam Beams – M Romani, H J Blaß

34-12-4 Moisture induced stresses in glulam cross sections – J Jönsson

34-12-5 Load Carrying Capacity of Nail-Laminated Timber under Concentrated Loads – V Krämer, H J Blaß

34-12-6 Determination of Shear Strength Values for GLT Using Visual and Machine Graded Spruce Laminations – G Schickhofer

34-12-7 Mechanically Jointed Beams: Possibilities of Analysis and some special Problems – H Kreuzinger

35-12-1 Glulam Beams with Round Holes – a Comparison of Different Design Approaches vs. Test Data - S Aicher L Höfflin

36-12-1 Problems with Shear and Bearing Strength of LVL in Highly Loaded Structures - H Bier

36-12-2 Weibull Based Design of Round Holes in Glulam - L Höfflin, S Aicher

37-12-1 Development of Structural LVL from Tropical Wood and Evaluation of Their Performance for the Structural Components of Wooden Houses. Part-1. Application of Tropical LVL to a Roof Truss - K Komatsu, Y Idris, S Yuwasdiki, B Subiyakto, A Firmanti

37-12-2 Reinforcement of LVL Beams With Bonded-in Plates and Rods - Effect of Placement of Steel and FRP Reinforcements on Beam Strength and Stiffness - P Alam, M P Ansell, D Smedley

39-12-1 Recommended Procedures for Determination of Distribution Widths in the Design of Stress Laminated Timber Plate Decks - K Crews

39-12-2 In-situ Strengthening of Timber Structures with CFRP - K U Schober, S Franke, K Rautenstrauch

39-12-3 Effect of Checking and Non-Glued Edge Joints on the Shear Strength of Structural Glued Laminated Timber Beams - B Yeh, T G Williamson, Z A Martin

39-12-4 A Contribution to the Design and System Effect of Cross Laminated Timber (CLT) - R Jöbstl, T Moosbrugger, T Bogensperger, G Schickhofer

39-12-5 Behaviour of Glulam in Compression Perpendicular to Grain in Different Strength Grades and Load Configurations - M Augustin, A Ruli, R Brandner, G Schickhofer

40-12-1 Development of New Constructions of Glulam Beams in Canada - F Lam, N Mohadevan

40-12-2 Determination of Modulus of Shear and Elasticity of Glued Laminated Timber and Related Examination - R Brandner, E Gehri, T Bogensperger, G Schickhofer

40-12-3 Comparative Examination of Creep of GTL and CLT-Slabs in Bending - R A Jöbstl, G Schickhofer,

40-12-4 Standard Practice for the Derivation of Design Properties of Structural Glued Laminated Timber in the United States - T G Williamson, B Yeh

40-12-5 Creep and Creep-Rupture Behaviour of Structural Composite Lumber Evaluated in Accordance with ASTM D 6815 - B Yeh, T G Williamson.

40-12-6 Bending Strength of Combined Beech-Spruce Glulam - M Frese, H J Blaß

40-12-7 Quality Control of Glulam: Shear Tests of Glue Lines - R Steiger, E Gehri

41-12-1 Paper withdrawn by the author

41-12-2 Bending Strength of Spruce Glulam: New Models for the Characteristic Bending Strength - M Frese, H J Blass,

41-12-3 In-Plane Shear Strength of Cross Laminated Timber - R A Joebstl, T Bogensperger, G Schickhofer

41-12-4 Strength of Glulam Beams with Holes - Tests of Quadratic Holes and Literature Test Results Compilation - H Danielsson, P J Gustafsson

42-12-1 Glulam Beams with Holes Reinforced by Steel Bars – S Aicher, L Höfflin

42-12-2 Analysis of X-lam Panel-to-Panel Connections under Monotonic and Cyclic Loading - C Sandhaas, L Boukes, J W G van de Kuilen, A Ceccotti

42-12-3 Laminating Lumber and End Joint Properties for FRP-Reinforced Glulam Beams - T G Williamson, B Yeh

43-12-4 Validity of Bending Tests on Strip-Shaped Specimens to Derive Bending Strength and Stiffness Properties of Cross-Laminated Solid Timber (CLT) - R Steiger, A Gülzow

42-12-5 Mechanical Properties of Stress Laminated Timber Decks - Experimental Study - K Karlsson, R Crocetti, R Kliger

43-12-1 Fatigue Behaviour of Finger Jointed Lumber - S Aicher, G Stapf

43-12-2 Experimental and Numercial Investigation on the Shear Strength of Glulam - R Crocetti, P J Gustafsson, H Danielsson, A Emilsson, S Ormarsson

43-12-3 System Effects in Glued Laminated Timber in Tension and Bending - M Frese, H J Blaß

43-12-4 Experimental Investigations on Mechanical Behaviour of Glued Solid timber - C Faye, F Rouger, P Garcia

44-12-1 Properties of CLT-Panels Exposed to Compression Perpendicular to their Plane- T Bogensperger, M Augustin, G Schickhofer

44-12-2 Strength of Spruce Glulam Subjected to Longitudinal Compression – M Frese, M Enders-Comberg, H J Blaß, P Glos

44-12-3 Glued Laminated Timber: A proposal for New Beam Layups - F Rouger, P Garcia

44-12-4 Glulam Beams with Internally and Externally Reinforced Holes – Test, Detailing and Design – S Aicher

44-12-5 Size Effect of Bending Strength in Glulam Beam - F Lam

PARTICLE AND FIBRE BUILDING BOARDS

7-13-1 Fibre Building Boards for CIB Timber Code (First Draft)- O Brynildsen

9-13-1 Determination of the Bearing Strength and the Load-Deformation Characteristics of Particleboard - K Möhler, T Budianto and J Ehlbeck

9-13-2 The Structural Use of Tempered Hardboard - W W L Chan

11-13-1 Tests on Laminated Beams from Hardboard under Short- and Longterm Load - W Nozynski

11-13-2 Determination of Deformation of Special Densified Hardboard under Long-term Load and Varying Temperature and Humidity Conditions - W Halfar

11-13-3 Determination of Deformation of Hardboard under Long-term Load in Changing Climate - W Halfar

14-4-1 An Introduction to Performance Standards for Wood-Base Panel Products - D H Brown

14-4-2 Proposal for Presenting Data on the Properties of Structural Panels - T Schmidt

16-13-1 Effect of Test Piece Size on Panel Bending Properties - P W Post

20-4-1 Considerations of Reliability - Based Design for Structural Composite Products - M R O'Halloran, J A Johnson, E G Elias and T P Cunningham

20-13-1 Classification Systems for Structural Wood-Based Sheet Materials - V C Kearley and A R Abbott

21-13-1 Design Values for Nailed Chipboard - Timber Joints - A R Abbott

25-13-1 Bending Strength and Stiffness of Izopanel Plates - Z Mielczarek

28-13-1 Background Information for "Design Rated Oriented Strand Board (OSB)" in CSA Standards - Summary of Short-term Test Results - E Karacabeyli, P Lau, C R Henderson, F V Meakes and W Deacon

28-13-2 Torsional Stiffness of Wood-Hardboard Composed I-Beam - P Olejniczak

TRUSSED RAFTERS

4-9-1 Long-term Loading of Trussed Rafters with Different Connection Systems - T Feldborg and M Johansen

6-9-3 Deflection of Trussed Rafters under Alternating Loading During a Year - T Feldborg and M Johansen

7-2-1 Lateral Bracing of Timber Struts - J A Simon

9-14-1 Timber Trusses - Code Related Problems - T F Williams

9-7-1 Design of Truss Plate Joints - F J Keenan

10-14-1 Design of Roof Bracing - The State of the Art in South Africa - P A V Bryant and J A Simon

11-14-1 Design of Metal Plate Connected Wood Trusses - A R Egerup

12-14-1 A Simple Design Method for Standard Trusses - A R Egerup

13-14-1 Truss Design Method for CIB Timber Code - A R Egerup

13-14-2 Trussed Rafters, Static Models - H Riberholt

13-14-3 Comparison of 3 Truss Models Designed by Different Assumptions for Slip and E-Modulus - K Möhler

14-14-1 Wood Trussed Rafter Design - T Feldborg and M Johansen

14-14-2 Truss-Plate Modelling in the Analysis of Trusses - R O Foschi

14-14-3 Cantilevered Timber Trusses - A R Egerup

14-7-5 The Effect of Support Eccentricity on the Design of W- and WW-Trusses with Nail Plate Connectors - B Källsner

15-14-1 Guidelines for Static Models of Trussed Rafters - H Riberholt

15-14-2 The Influence of Various Factors on the Accuracy of the Structural Analysis of Timber Roof Trusses - F R P Pienaar

15-14-3 Bracing Calculations for Trussed Rafter Roofs - H J Burgess

15-14-4 The Design of Continuous Members in Timber Trussed Rafters with Punched Metal Connector Plates - P O Reece

15-14-5 A Rafter Design Method Matching U.K. Test Results for Trussed Rafters - H J Burgess

16-14-1 Full-Scale Tests on Timber Fink Trusses Made from Irish Grown Sitka Spruce - V Picardo

17-14-1 Data from Full Scale Tests on Prefabricated Trussed Rafters - V Picardo

17-14-2 Simplified Static Analysis and Dimensioning of Trussed Rafters - H Riberholt

17-14-3 Simplified Calculation Method for W-Trusses - B Källsner

18-14-1 Simplified Calculation Method for W-Trusses (Part 2) - B Källsner

18-14-2 Model for Trussed Rafter Design - T Poutanen

19-14-1 Annex on Simplified Design of W-Trusses - H J Larsen

19-14-2 Simplified Static Analysis and Dimensioning of Trussed Rafters - Part 2 - H Riberholt

19-14-3 Joint Eccentricity in Trussed Rafters - T Poutanen

20-14-1 Some Notes about Testing Nail Plates Subjected to Moment Load - T Poutanen

20-14-2 Moment Distribution in Trussed Rafters - T Poutanen

20-14-3 Practical Design Methods for Trussed Rafters - A R Egerup

22-14-1 Guidelines for Design of Timber Trussed Rafters - H Riberholt

23-14-1 Analyses of Timber Trussed Rafters of the W-Type - H Riberholt

23-14-2 Proposal for Eurocode 5 Text on Timber Trussed Rafters - H Riberholt

24-14-1 Capacity of Support Areas Reinforced with Nail Plates in Trussed Rafters - A Kevarinmäki

25-14-1 Moment Anchorage Capacity of Nail Plates in Shear Tests - A Kevarinmaki and J. Kangas

25-14-2 Design Values of Anchorage Strength of Nail Plate Joints by 2-curve Method and Interpolation - J Kangas and A Kevarinmaki

26-14-1	Test of Nail Plates Subjected to Moment - E Aasheim
26-14-2	Moment Anchorage Capacity of Nail Plates - A Kevarinmäki and J Kangas
26-14-3	Rotational Stiffness of Nail Plates in Moment Anchorage - A Kevarinmäki and J Kangas
26-14-4	Solution of Plastic Moment Anchorage Stress in Nail Plates - A Kevarinmäki
26-14-5	Testing of Metal-Plate-Connected Wood-Truss Joints - R Gupta
26-14-6	Simulated Accidental Events on a Trussed Rafter Roofed Building - C J Mettem and J P Marcroft
30-14-1	The Stability Behaviour of Timber Trussed Rafter Roofs - Studies Based on Eurocode 5 and Full Scale Testing - R J Bainbridge, C J Mettern, A Reffold and T Studer
32-14-1	Analysis of Timber Reinforced with Punched Metal Plate Fasteners- J Nielsen
33-14-1	Moment Capacity of Timber Beams Loaded in Four-Point Bending and Reinforced with Punched Metal Plate Fasteners – J Nielsen
36-14-1	Effect of Chord Splice Joints on Force Distribution in Trusses with Punched Metal Plate Fasteners - P Ellegaard
36-14-2	Monte Carlo Simulation and Reliability Analysis of Roof Trusses with Punched Metal Plate Fasteners - M Hansson, P Ellegaard
36-14-3	Truss Trouble – R H Leicester, J Goldfinch, P Paevere, G C Foliente
40-14-1	Timber Trusses with Punched Metal Plate Fasteners - Design for Transport and Erection - H J Blaß

STRUCTURAL STABILITY

8-15-1	Laterally Loaded Timber Columns: Tests and Theory - H J Larsen
13-15-1	Timber and Wood-Based Products Structures. Panels for Roof Coverings. Methods of Testing and Strength Assessment Criteria. Polish Standard BN-78/7159-03
16-15-1	Determination of Bracing Structures for Compression Members and Beams - H Brüninghoff
17-15-1	Proposal for Chapter 7.4 Bracing - H Brüninghoff
17-15-2	Seismic Design of Small Wood Framed Houses - K F Hansen
18-15-1	Full-Scale Structures in Glued Laminated Timber, Dynamic Tests: Theoretical and Experimental Studies - A Ceccotti and A Vignoli
18-15-2	Stabilizing Bracings - H Brüninghoff
19-15-1	Connections Deformability in Timber Structures: a Theoretical Evaluation of its Influence on Seismic Effects - A Ceccotti and A Vignoli
19-15-2	The Bracing of Trussed Beams - M H Kessel and J Natterer
19-15-3	Racking Resistance of Wooden Frame Walls with Various Openings - M Yasumura
19-15-4	Some Experiences of Restoration of Timber Structures for Country Buildings - G Cardinale and P Spinelli
19-15-5	Non-Destructive Vibration Tests on Existing Wooden Dwellings - Y Hirashima
20-15-1	Behaviour Factor of Timber Structures in Seismic Zones. - A Ceccotti and A Vignoli
21-15-1	Rectangular Section Deep Beam - Columns with Continuous Lateral Restraint - H J Burgess

21-15-2 Buckling Modes and Permissible Axial Loads for Continuously Braced Columns- H J Burgess

21-15-3 Simple Approaches for Column Bracing Calculations - H J Burgess

21-15-4 Calculations for Discrete Column Restraints - H J Burgess

21-15-5 Behaviour Factor of Timber Structures in Seismic Zones (Part Two) - A Ceccotti and A Vignoli

22-15-1 Suggested Changes in Code Bracing Recommendations for Beams and Columns - H J Burgess

22-15-2 Research and Development of Timber Frame Structures for Agriculture in Poland- S Kus and J Kerste

22-15-3 Ensuring of Three-Dimensional Stiffness of Buildings with Wood Structures - A K Shenghelia

22-15-5 Seismic Behavior of Arched Frames in Timber Construction - M Yasumura

22-15-6 The Robustness of Timber Structures - C J Mettem and J P Marcroft

22-15-7 Influence of Geometrical and Structural Imperfections on the Limit Load of Wood Columns - P Dutko

23-15-1 Calculation of a Wind Girder Loaded also by Discretely Spaced Braces for Roof Members - H J Burgess

23-15-2 Stability Design and Code Rules for Straight Timber Beams - T A C M van der Put

23-15-3 A Brief Description of Formula of Beam-Columns in China Code - S Y Huang

23-15-4 Seismic Behavior of Braced Frames in Timber Construction - M Yasumara

23-15-5 On a Better Evaluation of the Seismic Behavior Factor of Low-Dissipative Timber Structures - A Ceccotti and A Vignoli

23-15-6 Disproportionate Collapse of Timber Structures - C J Mettem and J P Marcroft

23-15-7 Performance of Timber Frame Structures During the Loma Prieta California Earthquake - M R O'Halloran and E G Elias

24-15-2 Discussion About the Description of Timber Beam-Column Formula - S Y Huang

24-15-3 Seismic Behavior of Wood-Framed Shear Walls - M Yasumura

25-15-1 Structural Assessment of Timber Framed Building Systems - U Korin

25-15-3 Mechanical Properties of Wood-framed Shear Walls Subjected to Reversed Cyclic Lateral Loading - M Yasumura

26-15-1 Bracing Requirements to Prevent Lateral Buckling in Trussed Rafters - C J Mettem and P J Moss

26-15-2 Eurocode 8 - Part 1.3 - Chapter 5 - Specific Rules for Timber Buildings in Seismic Regions - K Becker, A Ceccotti, H Charlier, E Katsaragakis, H J Larsen and H Zeitter

26-15-3 Hurricane Andrew - Structural Performance of Buildings in South Florida - M R O'Halloran, E L Keith, J D Rose and T P Cunningham

29-15-1 Lateral Resistance of Wood Based Shear Walls with Oversized Sheathing Panels - F Lam, H G L Prion and M He

29-15-2 Damage of Wooden Buildings Caused by the 1995 Hyogo-Ken Nanbu Earthquake - M Yasumura, N Kawai, N Yamaguchi and S Nakajima

29-15-3 The Racking Resistance of Timber Frame Walls: Design by Test and Calculation - D R Griffiths, C J Mettem, V Enjily, P J Steer

29-15-4 Current Developments in Medium-Rise Timber Frame Buildings in the UK - C J Mettem, G C Pitts, P J Steer, V Enjily

29-15-5 Natural Frequency Prediction for Timber Floors - R J Bainbridge, and C J Mettem

30-15-1 Cyclic Performance of Perforated Wood Shear Walls with Oversize Oriented Strand Board Panels - Ming He, H Magnusson, F Lam, and H G L Prion

30-15-2 A Numerical Analysis of Shear Walls Structural Performances - L Davenne, L Daudeville, N Kawai and M Yasumura

30-15-3 Seismic Force Modification Factors for the Design of Multi-Storey Wood-Frame Platform Construction - E Karacabeyli and A Ceccotti

30-15-4 Evaluation of Wood Framed Shear Walls Subjected to Lateral Load - M Yasumura and N Kawai

31-15-1 Seismic Performance Testing On Wood-Framed Shear Wall - N Kawai

31-15-2 Robustness Principles in the Design of Medium-Rise Timber-Framed Buildings - C J Mettem, M W Milner, R J Bainbridge and V. Enjily

31-15-3 Numerical Simulation of Pseudo-Dynamic Tests Performed to Shear Walls - L Daudeville, L Davenne, N Richard, N Kawai and M Yasumura

31-15-4 Force Modification Factors for Braced Timber Frames - H G L Prion, M Popovski and E Karacabeyli

32-15-1 Three-Dimensional Interaction in Stabilisation of Multi-Storey Timber Frame Buildings - S Andreasson

32-15-2 Application of Capacity Spectrum Method to Timber Houses - N Kawai

32-15-3 Design Methods for Shear Walls with Openings - C Ni, E Karacabeyli and A Ceccotti

32-15-4 Static Cyclic Lateral Loading Tests on Nailed Plywood Shear Walls - K Komatsu, K H Hwang and Y Itou

33-15-1 Lateral Load Capacities of Horizontally Sheathed Unblocked Shear Walls – C Ni, E Karacabeyli and A Ceccotti

33-15-2 Prediction of Earthquake Response of Timber Houses Considering Shear Deformation of Horizontal Frames – N Kawai

33-15-3 Eurocode 5 Rules for Bracing – H J Larsen

34-15-1 A simplified plastic model for design of partially anchored wood-framed shear walls – B Källsner, U A Girhammar, Liping Wu

34-15-2 The Effect of the Moisture Content on the Performance of the Shear Walls – S Nakajima

34-15-3 Evaluation of Damping Capacity of Timber Structures for Seismic Design – M Yasumura

35-15-1 On test methods for determining racking strength and stiffness of wood-framed shear walls - B Källsner, U A Girhammar, L Wu

35-15-2 A Plastic Design Model for Partially Anchored Wood-framed Shear Walls with Openings - U A Girhammar, L Wu, B Källsner

35-15-3 Evaluation and Estimation of the Performance of the Shear Walls in Humid Climate - S Nakajima

35-15-4 Influence of Vertical Load on Lateral Resistance of Timber Frame Walls - B Dujič, R Žarnić

35-15-5 Cyclic and Seismic Performances of a Timber-Concrete System - Local and Full Scale Experimental Results - E Fournely, P Racher

35-15-6 Design of timber-concrete composite structures according to EC5 - 2002 version - A Ceccotti, M Fragiacomo, R M Gutkowski

35-15-7 Design of timber structures in seismic zones according to EC8- 2002 version - A Ceccotti, T Toratti, B Dujič

35-15-8	Design Methods to Prevent Premature Failure of Joints at Shear Wall Corners - N Kawai, H Okiura
36-15-1	Monitoring Light-Frame Timber Buildings: Environmental Loads and Load Paths – I Smith et al.
36-15-2	Applicability of Design Methods to Prevent Premature Failure of Joints at Shear Wall Corners in Case of Post and Beam Construction - N Kawai, H Isoda
36-15-3	Effects of Screw Spacing and Edge Boards on the Cyclic Performance of Timber Frame and Structural Insulated Panel Roof Systems - D M Carradine, J D Dolan, F E Woeste
36-15-4	Pseudo-Dynamic Tests on Conventional Timber Structures with Shear Walls - M Yasumura
36-15-5	Experimental Investigation of Laminated Timber Frames with Fiber-reinforced Connections under Earthquake Loads - B Kasal, P Haller, S Pospisil, I Jirovsky, A Heiduschke, M Drdacky
36-15-6	Effect of Test Configurations and Protocols on the Performance of Shear Walls - F Lam, D Jossen, J Gu, N Yamaguchi, H G L Prion
36-15-7	Comparison of Monotonic and Cyclic Performance of Light-Frame Shear Walls - J D Dolan, A J Toothman
37-15-1	Estimating 3D Behavior of Conventional Timber Structures with Shear Walls by Pseudodynamic Tests - M Yasumura, M Uesugi, L Davenne
37-15-2	Testing of Racking Behavior of Massive Wooden Wall Panels - B Dujič, J Pucelj, R Žarnić
37-15-3	Influence of Framing Joints on Plastic Capacity of Partially Anchored Wood-Framed Shear Walls - B Källsner, U A Girhammar
37-15-4	Bracing of Timber Members in Compression - J Munch-Andersen
37-15-5	Acceptance Criteria for the Use of Structural Insulated Panels in High Risk Seismic Areas - B Yeh, T D Skaggs, T G Williamson Z A Martin
37-15-6	Predicting Load Paths in Shearwalls - Hongyong Mi, Ying-Hei Chui, I Smith, M Mohammad
38-15-1	Background Information on ISO STANDARD 16670 for Cyclic Testing of Connections - E Karacabeyli, M Yasumura, G C Foliente, A Ceccotti
38-15-2	Testing & Product Standards – a Comparison of EN to ASTM, AS/NZ and ISO Standards – A Ranta-Maunus, V Enjily
38-15-3	Framework for Lateral Load Design Provisions for Engineered Wood Structures in Canada - M Popovski, E Karacabeyli
38-15-4	Design of Shear Walls without Hold-Downs - Chun Ni, E Karacabeyli
38-15-5	Plastic design of partially anchored wood-framed wall diaphragms with and without openings - B Källsner, U A Girhammar
38-15-6	Racking of Wooden Walls Exposed to Different Boundary Conditions - B Dujič, S Aicher, R Žarnić
38-15-7	A Portal Frame Design for Raised Wood Floor Applications - T G Williamson, Z A Martin, B Yeh
38-15-8	Linear Elastic Design Method for Timber Framed Ceiling, Floor and Wall Diaphragms - Jarmo Leskelä
38-15-9	A Unified Design Method for the Racking Resistance of Timber Framed Walls for Inclusion in EUROCODE 5 - R Griffiths, B Källsner, H J Blass, V Enjily
39-15-1	Effect of Transverse Walls on Capacity of Wood-Framed Wall Diaphragms - U A Girhammar, B Källsner

39-15-2 Which Seismic Behaviour Factor for Multi-Storey Buildings made of Cross-Laminated Wooden Panels? - M Follesa, M P Lauriola, C Minowa, N Kawai, C Sandhaas, M Yasumura, A Ceccotti

39-15-3 Laminated Timber Frames under dynamic Loadings - A Heiduschke, B Kasal, P Haller

39-15-4 Code Provisions for Seismic Design of Multi-storey Post-tensioned Timber Buildings - S Pampanin, A Palermo, A Buchanan, M Fragiacomo, B Deam

40-15-1 Design of Safe Timber Structures – How Can we Learn from Structural Failures? - S Thelandersson, E Frühwald

40-15-2 Effect of Transverse Walls on Capacity of Wood-Framed Wall Diaphragms—Part 2 - U A Girhammar, B Källsner

40-15-3 Midply Wood Shear Wall System: Concept, Performance and Code Implementation - Chun Ni, M Popovski, E Karacabeyli, E Varoglu, S Stiemer

40-15-4 Seismic Behaviour of Tall Wood-Frame Walls - M Popovski, A Peterson, E Karacabeyli

40-15-5 International Standard Development of Lateral Load Test Method for Shear Walls - M Yasumura, E Karacabeyli

40-15-6 Influence of Openings on Shear Capacity of Wooden Walls - B Dujič, S Klobcar, R Žarnić

41-15-1 Need for a Harmonized Approach for Calculations of Ductility of Timber Assemblies - W Muñoz, M Mohammad, A Salenikovich, P Quenneville

41-15-2 Plastic Design of Wood Frame Wall Diaphragms in Low and Medium Rise Buildings - B Källsner, U A Girhammar

41 15-3 Failure Analysis of Light Wood Frame Structures under Wind Load - A Asiz, Y H Chui, I Smith

41-15-4 Combined Shear and Wind Uplift Resistance of Wood Structural Panel Shearwalls B Yeh, T G Williamson

41-15-5 Behaviour of Prefabricated Timber Wall Elements under Static and Cyclic Loading – P Schädle, H J Blass

42-15-1 Design Aspects on Anchoring the Bottom Rail in Partially Anchored Wood-Framed Shear Walls - U A Girhammar, B Källsner

42-15-2 New Seismic Design Provisions for Shearwalls and Diaphragms in the Canadian Standard for Engineering Design in Wood - M Popovski, E Karacabeyli, Chun Ni, P Lepper, G Doudak

42-15-3 Stability Capacity and Lateral Bracing Force of Metal Plate Connected Wood Truss Assemblies - Xiaobin Song, F Lam, Hao Huang, Minjuan He

42-15-4 Improved Method for Determining Braced Wall Requirements for Conventional Wood-Frame Buildings - Chun Ni, H Rainer, E Karacabeyli

43-15-1 Influence of the Boundary Conditions on the Racking Strength of Shear Walls with an Opening - M Yasumura

43-15-2 Influence of Different Standards on the Determination of Earthquake Properties of Timber Shear Wall Systems - P Schädle, H J Blaß

43-15-3 Full-Scale Shear Wall Tests for Force Transfer Around Openings - T Skaggs, B Yeh, F Lam

43-15-4 Optimized Anchor-Bolt Spacing for Structural Panel Shearwalls Subjected to Combined Shear and Wind Uplift Forces - B Yeh, E Keith, T Skaggs

44-15-1 A Proposal for Revision of the Current Timber Part (Section 8) of Eurocode 8 Part 1 - M Follesa, M Fragiacomo, M P Lauriola

44-15-2 Influence of Vertical Loads on Lateral Resistance and Deflections of Light-Frame Shear Walls - M Payeur, A Salenikovich, W Muñoz

FIRE

STATISTICS AND DATA ANALYSIS

GLUED JOINTS

FRACTURE MECHANICS

23-19-2 The Fracture Energy of Wood in Tension Perpendicular to the Grain. Results from a Joint Testing Project - H J Larsen and P J Gustafsson

23-19-3 Application of Fracture Mechanics to Timber Structures - A Ranta-Maunus

24-19-1 The Fracture Energy of Wood in Tension Perpendicular to the Grain - H J Larsen and P J Gustafsson

28-19-1 Fracture of Wood in Tension Perpendicular to the Grain: Experiment and Numerical Simulation by Damage Mechanics - L Daudeville, M Yasumura and J D Lanvin

28-19-2 A New Method of Determining Fracture Energy in Forward Shear along the Grain - H D Mansfield-Williams

28-19-3 Fracture Design Analysis of Wooden Beams with Holes and Notches. Finite Element Analysis based on Energy Release Rate Approach - H Petersson

28-19-4 Design of Timber Beams with Holes by Means of Fracture Mechanics - S Aicher, J Schmidt and S Brunold

30-19-1 Failure Analysis of Single-Bolt Joints - L Daudeville, L Davenne and M Yasumura

37 - 19 - 1 Determination of Fracture Mechanics Parameters for Wood with the Help of Close Range Photogrammetry - S Franke, B Franke, K Rautenstrauch

39-19-1 First Evaluation Steps of Design Rules in the European and German codes of Transverse Tension Areas - S Franke, B Franke, K Rautenstrauch

SERVICEABILITY

27-20-1 Codification of Serviceability Criteria - R H Leicester

27-20-2 On the Experimental Determination of Factor k_{def} and Slip Modulus k_{ser} from Short- and Long-Term Tests on a Timber-Concrete Composite (TCC) Beam - S Capretti and A Ceccotti

27-20-3 Serviceability Limit States: A Proposal for Updating Eurocode 5 with Respect to Eurocode 1 - P Racher and F Rouger

27-20-4 Creep Behavior of Timber under External Conditions - C Le Govic, F Rouger, T Toratti and P Morlier

30-20-1 Design Principles for Timber in Compression Perpendicular to Grain - S Thelandersson and A Mårtensson

30-20-2 Serviceability Performance of Timber Floors - Eurocode 5 and Full Scale Testing - R J Bainbridge and C J Mettem

32-20-1 Floor Vibrations - B Mohr

37 - 20 - 1 A New Design Method to Control Vibrations Induced by Foot Steps in Timber Floors - Lin J Hu, Y H Chui

37 - 20 - 2 Serviceability Limit States of Wooden Footbridges. Vibrations Caused by Pedestrians - P Hamm

43-20-1 The Long Term Instrumentation of a Timber Building in Nelson NZ - the Need for Standardisation - H W Morris, S R Uma, K Gledhill, P Omenzetter, M Worth

TEST METHODS

31-21-1 Development of an Optimised Test Configuration to Determine Shear Strength of Glued Laminated Timber - G Schickhofer and B Obermayr

31-21-2 An Impact Strength Test Method for Structural Timber. The Theory and a Preliminary Study - T D G Canisius

35-21-1	Full-Scale Edgewise Shear Tests for Laminated Veneer Lumber- B Yeh, T G Williamson
39-21-1	Timber Density Restrictions for Timber Connection Tests According to EN28970/ISO8970 - A Leijten, J Köhler, A Jorissen
39-21-2	The Mechanical Inconsistence in the Evaluation of the Modulus of Elasticity According to EN384 - T Bogensperger, H Unterwieser, G Schickhofer
40 - 21 - 1	ASTM D198 - Interlaboratory Study for Modulus of Elasticity of Lumber in Bending - A Salenikovich
40 - 21 - 2	New Test Configuration for CLT-Wall-Elements under Shear Load - T Bogensperger, T Moosbrugger, G Schickhofer
41-21-1	Determination of Shear Modulus by Means of Standardized Four-Point Bending Tests - R Brandner, B Freytag, G Schickhofer
43-21-1	Estimation of Load-Bearing Capacity of Timber Connections - J Munch-Andersen, J D Sørensen, F Sørensen
43-21-2	A New Method to Determine Suitable Spacings and Distances for Self-tapping Screws - T Uibel, H J Blaß

CIB TIMBER CODE

2-100-1	A Framework for the Production of an International Code of Practice for the Structural Use of Timber - W T Curry
5-100-1	Design of Solid Timber Columns (First Draft) - H J Larsen
5-100-2	A Draft Outline of a Code for Timber Structures - L G Booth
6-100-1	Comments on Document 5-100-1; Design of Solid Timber Columns - H J Larsen and E Theilgaard
6-100-2	CIB Timber Code: CIB Timber Standards - H J Larsen and E Theilgaard
7-100-1	CIB Timber Code Chapter 5.3 Mechanical Fasteners; CIB Timber Standard 06 and 07 - H J Larsen
8-100-1	CIB Timber Code - List of Contents (Second Draft) - H J Larsen
9-100-1	The CIB Timber Code (Second Draft)
11-100-1	CIB Structural Timber Design Code (Third Draft)
11-100-2	Comments Received on the CIB Code - U Saarelainen; Y M Ivanov, R H Leicester, W Nozynski, W R A Meyer, P Beckmann; R Marsh
11-100-3	CIB Structural Timber Design Code; Chapter 3 - H J Larsen
12-100-1	Comment on the CIB Code - Sous-Commission Glulam
12-100-2	Comment on the CIB Code - R H Leicester
12-100-3	CIB Structural Timber Design Code (Fourth Draft)
13-100-1	Agreed Changes to CIB Structural Timber Design Code
13-100-2	CIB Structural Timber Design Code. Chapter 9: Performance in Fire
13-100-3a	Comments on CIB Structural Timber Design Code
13-100-3b	Comments on CIB Structural Timber Design Code - W R A Meyer
13-100-3c	Comments on CIB Structural Timber Design Code - British Standards Institution
13-100-4	CIB Structural Timber Design Code. Proposal for Section 6.1.5 Nail Plates - N I Bovim
14-103-2	Comments on the CIB Structural Timber Design Code - R H Leicester
15-103-1	Resolutions of TC 165-meeting in Athens 1981-10-12/13

21-100-1 CIB Structural Timber Design Code. Proposed Changes of Sections on Lateral Instability, Columns and Nails - H J Larsen

22-100-1 Proposal for Including an Updated Design Method for Bearing Stresses in CIB W18 - Structural Timber Design Code - B Madsen

22-100-2 Proposal for Including Size Effects in CIB W18A Timber Design Code - B Madsen

22-100-3 CIB Structural Timber Design Code - Proposed Changes of Section on Thin-Flanged Beams - J König

22-100-4 Modification Factor for "Aggressive Media" - a Proposal for a Supplement to the CIB Model Code - K Erler and W Rug

22-100-5 Timber Design Code in Czechoslovakia and Comparison with CIB Model Code - P Dutko and B Kozelouh

LOADING CODES

4-101-1 Loading Regulations - Nordic Committee for Building Regulations

4-101-2 Comments on the Loading Regulations - Nordic Committee for Building Regulations

37-101-1 Action Combination Processing for the Eurocodes Basis of Software to Assist the Engineer - Y Robert, A V Page, R Thépaut, C J Mettem

43-101-1 Dependant Versus Independent Loads in Structural Design - T Poutanen

STRUCTURAL DESIGN CODES

1-102-1 Survey of Status of Building Codes, Specifications etc., in USA - E G Stern

1-102-2 Australian Codes for Use of Timber in Structures - R H Leicester

1-102-3 Contemporary Concepts for Structural Timber Codes - R H Leicester

1-102-4 Revision of CP 112 - First Draft, July 1972 - British Standards Institution

4-102-1 Comparsion of Codes and Safety Requirements for Timber Structures in EEC Countries - Timber Research and Development Association

4-102-2 Nordic Proposals for Safety Code for Structures and Loading Code for Design of Structures - O A Brynildsen

4-102-3 Proposal for Safety Codes for Load-Carrying Structures - Nordic Committee for Building Regulations

4-102-4 Comments to Proposal for Safety Codes for Load-Carrying Structures - Nordic Committee for Building Regulations

4-102-5 Extract from Norwegian Standard NS 3470 "Timber Structures"

4-102-6 Draft for Revision of CP 112 "The Structural Use of Timber" - W T Curry

8-102-1 Polish Standard PN-73/B-03150: Timber Structures; Statistical Calculations and Designing

8-102-2 The Russian Timber Code: Summary of Contents

9-102-1 Svensk Byggnorm 1975 (2nd Edition); Chapter 27: Timber Construction

11-102-1 Eurocodes - H J Larsen

13-102-1 Program of Standardisation Work Involving Timber Structures and Wood-Based Products in Poland

17-102-1 Safety Principles - H J Larsen and H Riberholt

17-102-2 Partial Coefficients Limit States Design Codes for Structural Timberwork - I Smith

18-102-1	Antiseismic Rules for Timber Structures: an Italian Proposal - G Augusti and A Ceccotti
18-1-2	Eurocode 5, Timber Structures - H J Larsen
19-102-1	Eurocode 5 - Requirements to Timber - Drafting Panel Eurocode 5
19-102-2	Eurocode 5 and CIB Structural Timber Design Code - H J Larsen
19-102-3	Comments on the Format of Eurocode 5 - A R Fewell
19-102-4	New Developments of Limit States Design for the New GDR Timber Design Code - W Rug and M Badstube
19-7-3	Effectiveness of Multiple Fastener Joints According to National Codes and Eurocode 5 (Draft) - G Steck
19-7-6	The Derivation of Design Clauses for Nailed and Bolted Joints in Eurocode5 - L R J Whale and I Smith
19-14-1	Annex on Simplified Design of W-Trusses - H J Larsen
20-102-1	Development of a GDR Limit States Design Code for Timber Structures - W Rug and M Badstube
21-102-1	Research Activities Towards a New GDR Timber Design Code Based on Limit States Design - W Rug and M Badstube
22-102-1	New GDR Timber Design Code, State and Development - W Rug, M Badstube and W Kofent
22-102-2	Timber Strength Parameters for the New USSR Design Code and its Comparison with International Code - Y Y Slavik, N D Denesh and E B Ryumina
22-102-3	Norwegian Timber Design Code - Extract from a New Version - E Aasheim and K H Solli
23-7-1	Proposal for a Design Code for Nail Plates - E Aasheim and K H Solli
24-102-2	Timber Footbridges: A Comparison Between Static and Dynamic Design Criteria - A Ceccotti and N de Robertis
25-102-1	Latest Development of Eurocode 5 - H J Larsen
25-102-1A	Annex to Paper CIB-W18/25-102-1. Eurocode 5 - Design of Notched Beams - H J Larsen, H Riberholt and P J Gustafsson
25-102-2	Control of Deflections in Timber Structures with Reference to Eurocode 5 - A Martensson and S Thelandersson
28-102-1	Eurocode 5 - Design of Timber Structures - Part 2: Bridges - D Bajolet, E Gehri, J König, H Kreuzinger, H J Larsen, R Mäkipuro and C Mettem
28-102-2	Racking Strength of Wall Diaphragms - Discussion of the Eurocode 5 Approach - B Källsner
29-102-1	Model Code for the Probabilistic Design of Timber Structures - H J Larsen, T Isaksson and S Thelandersson
30-102-1	Concepts for Drafting International Codes and Standards for Timber Constructions - R H Leicester
33-102-1	International Standards for Bamboo – J J A Janssen
35-102-1	Design Characteristics and Results According to EUROCODE 5 and SNiP Procedures - L Ozola, T Keskküla
35-102-2	Model Code for the Reliability-Based Design of Timber Structures - H J Larsen
36-102-1	Predicted Reliability of Elements and Classification of Timber Structures - L Ozola, T Keskküla
36-102-2	Calibration of Reliability-Based Timber Design Codes: Choosing a Fatigue Model - I Smith

38-102-1 A New Generation of Timber Design Practices and Code Provisions Linking System and Connection Design - A Asiz, I Smith

38-102-2 Uncertainties Involved in Structural Timber Design by Different Code Formats - L Ozola, T Keskküla

38-102-3 Comparison of the Eurocode 5 and Actual Croatian Codes for Wood Classification and Design With the Proposal for More Objective Way of Classification - V Rajcic A Bjelanovic

39-102-1 Calibration of Partial Factors in the Danish Timber Code - H Riberholt

41 - 102 - 1 Consequences of EC 5 for Danish Best Practise - J Munch-Andersen

41 - 102 - 2 Development of New Swiss standards for the Assessment of Existing Load Bearing Structures – R Steiger, J Köhler

41 – 102 - 3 Measuring the CO2 Footprint of Timber Buildings – A Buchanan, S John

INTERNATIONAL STANDARDS ORGANISATION

3-103-1 Method for the Preparation of Standards Concerning the Safety of Structures (ISO/DIS 3250) - International Standards Organisation ISO/TC98

4-103-1 A Proposal for Undertaking the Preparation of an International Standard on Timber Structures - International Standards Organisation

5-103-1 Comments on the Report of the Consultion with Member Bodies Concerning ISO/TC/P129 - Timber Structures - Dansk Ingeniorforening

7-103-1 ISO Technical Committees and Membership of ISO/TC 165

8-103-1 Draft Resolutions of ISO/TC 165

12-103-1 ISO/TC 165 Ottawa, September 1979

13-103-1 Report from ISO/TC 165 - A Sorensen

14-103-1 Comments on ISO/TC 165 N52 "Timber Structures; Solid Timber in Structural Sizes; Determination of Some Physical and Mechanical Properties"

14-103-2 Comments on the CIB Structural Timber Design Code - R H Leicester

21-103-1 Concept of a Complete Set of Standards - R H Leicester

JOINT COMMITTEE ON STRUCTURAL SAFETY

3-104-1 International System on Unified Standard Codes of Practice for Structures - Comité Européen du Béton (CEB)

7-104-1 Volume 1: Common Unified Rules for Different Types of Construction and Material - CEB

37-104-1 Proposal for a Probabilistic Model Code for Design of Timber Structures - J Köhler, H Faber

CIB PROGRAMME, POLICY AND MEETINGS

1-105-1 A Note on International Organisations Active in the Field of Utilisation of Timber - P Sonnemans

5-105-1 The Work and Objectives of CIB-W18-Timber Structures - J G Sunley

10-105-1 The Work of CIB-W18 Timber Structures - J G Sunley

15-105-1 Terms of Reference for Timber - Framed Housing Sub-Group of CIB-W18

19-105-1 Tropical and Hardwood Timbers Structures - R H Leicester

21-105-1 First Conference of CIB-W18B, Tropical and Hardwood Timber Structures Singapore, 26 - 28 October 1987 - R H Leicester

INTERNATIONAL UNION OF FORESTRY RESEARCH ORGANISATIONS

7-106-1 Time and Moisture Effects - CIB W18/IUFRO 55.02-03 Working Party

CIB-W18/44-5-1

INTERNATIONAL COUNCIL FOR RESEARCH AND INNOVATION IN BUILDING AND CONSTRUCTION

WORKING COMMISSION W18 - TIMBER STRUCTURES

ASSESSMENT OF DIFFERENT KNOT-INDICATORS TO PREDICT STRENGTH AND STIFFNESS PROPERTIES OF TIMBER BOARDS

G Fink

M Deublein

J Köhler

ETH Zürich

SWITZERLAND

MEETING FORTY FOUR

ALGHERO

ITALY

AUGUST 2011

Presented by G Fink

H Blass commented that P Glos did similar work and asked if there was any comparison with Glos' results. He also asked about the length of the knot section under consideration. G Fink responded that comparison with Glos' results has not yet been done and the length of the knot section was 150 mm.

R Harris asked and received clarification that in addition to knot parameters and stiffness additional indicators included MOE_F, MOE_{ws} and density etc.

P Stapel and G Fink discussed suggestion on possible changes in grading practice.

F Lam commented that there commercial machines such as Continuous lumber tester and Cook Bolinders are available to measure the bending stiffness along member length. It would be useful to consider such system for obtaining MOE rather than using a predictive approach.

JW Van de Kuilen received clarification that the six strain measurements within a measurement zone were averaged for the calculation of localized MOE.

R Harris commented on the influence of juvenile wood could be significant as the current paper did not consider material with pith presence. His experience with UK Douglas fir indicated that variation in stiffness when considering juvenile wood seemed to be significant.

Assessment of different knot-indicators to predict strength and stiffness properties of timber boards

Gerhard Fink

Markus Deublein

Jochen Kohler

ETH Zurich, Switzerland

1 Introduction

Timber is a natural grown material which has, compared to other building materials, a large variation in its load bearing behaviour. This variation can be observed between different growth regions, between different boards within the same growth region and even within one particular timber board. In the past, numerous models have been developed to describe the variability of the load bearing behaviour; e.g. for ultimate bending capacity (Isaksson 1999), for ultimate tensile-capacity and bending-stiffness (Taylor & Bender 1991), for bending stiffness (Kline et al. 1986) and for tension-stiffness (Fink & Kohler 2011). The variability of the load bearing behaviour within timber boards is highly dependent on morphological characteristics of the tree, especially on knots and their arrangement. Accordingly, numerous studies have been conducted to identify knot related indicators that are capable to describe the influence of knots on the load bearing behaviour of timber boards relevant for the design of timber structures. In general, the developed indicators can be categorised into two groups: group 1 represents knot indicators that are assessed based on visible knot pattern (measureable at the surface of the board), group 2 represents knot indicators, which are assessed based on cross section area of the knots. In Table 1 the most relevant indicators of group 2 are described.

The interrelation between the knot indicators described in Table 1 and the load bearing behaviour is assumed to be known. In Denzler (2007), Isaksson (1999) and Boatright & Garrett (1979) the interrelation between the ultimate bending capacity and different knot indicators is analysed. In the study of Isaksson (1999) the correlation coefficient between the bending capacity and the two knot indicators tKAR and mKAR is addressed and a correlation coefficient of $\rho = 0.40$ has been identified. Additionally, Isaksson (1999) has developed knot indicators for the prediction of component ultimate bending capacity that are based on the visible knot pattern with similar correlation. Denzler (2007) has identified significantly larger correlation coefficients between the ultimate bending capacity and the knot indicators ($\rho = -0.59$ for tKAR and $\rho = -0.63$ for mKAR). Furthermore, Denzler (2007) has developed alternative knot indicators containing the perpendicular distance of a knot to the neutral axis. However, the implementation of this feature has not yielded any increase of the correlation ($-0.43 < \rho < -0.34$). Denzler (2007) also has analysed the correlation of knot indicators based on the visible knot pattern according to DIN 4074-1 (2008) which show even lower correlation coefficients than the group 2 knot indicators ($-0.56 < \rho < -0.41$). Boatright & Garrett (1979) have analysed the influence of the knot ratio on the percentage reduction of the bending capacity of clear specimens ($\rho = 0.39$).

Table 1. Overview of relevant knot indicators.

tKAR	**t**otal **k**not **a**rea **r**atio (Isaksson 1999)	• Ratio between the projected knot area within a length of 150 mm and the cross section area. • Overlapping knots are counted only once.
mKAR	**m**arginal **k**not **a**rea **r**atio (Isaksson 1999)	• Ratio between the projected knot area within a length of 150 mm and the cross section area. • Calculated at the outer quarter of the cross section area. • Overlapping knots are counted only once. • Developed for bending.
CWAR	**c**lear **w**ood **a**rea **r**atio (Mitsuhashi et al. 2008)	• The CWAR is the complement of the knot area ratio (for a length of 100 mm)
ARF	**a**rea **r**eduction **f**actor (Mitsuhashi et al. 2008)	• The ARF is the complement of knot area ratio (for a length of 100 mm), including a local area reduction factor based on Hankinson's formula: $f_{t,\theta} = \frac{0.1}{\sin^{1.4}\theta + 0.1 \cdot \cos^{1.4}\theta} \cdot f_{t,0}$

Courchene et al. (1996) have analysed the interrelation between tKAR and bending capacity as well as between tKAR and ultimate tension capacity. In both cases, the relationship is illustrated qualitatively and no significant correlation can be observed. Mitsuhashi et al. (2008) have compared two knot indicators (ARF and CWAR) with the ultimate tension capacity. For two different samples the knot indicator CWAR leads to a correlation coefficient of $\rho = 0.33$ and $\rho = 0.14$. The knot indicator ARF shows a higher correlation $\rho = 0.44$ and $\rho = 0.26$, respectively.

The interrelation between the stiffness and the knot area properties are analysed in Samson & Blanchet (1992) and Fink & Kohler (2011). Samson & Blanchet (1992) have analysed the influence of single centre knots on the bending stiffness. The results show that the influence of a central knot on the bending stiffness is quite small; e.g. a knot with a projected area of 1/3 of the cross section leads to a reduction of the bending stiffness of 10%. Furthermore no significant differences have been detected between live and dead knots. Fink & Kohler (2011) have analysed the interrelation between the tension stiffness of knot sections and the tKAR for timber specimens of one specific strength class (L25) and have observed an correlation coefficient of $\rho = 0.46$.

In the following the influence of different knot indicators, such as knot size, knot position or the area of local grain deviating around knots, on the strength and stiffness related properties are analysed. Based on the results knot indicators are developed.

2 Experimental analysis

1.1 Material

The stiffness related section behaviour is analysed based on two samples, each of 30 randomly selected specimens; the species is Norway spruce (Picea abies) from a South-German provenience. The boards are graded into the strength classes L25 and L40 according to the European standard EN 14081-4 (2009b). The dimension is 126×44×4000 mm. According to EN 14081-4 (2009b) the strength classes L25 and L40 require a minimum characteristic tension capacity of 14.5 MPa and 26.0 MPa, respectively. Timber boards of this strength grade are used to produce glued laminated timber (glulam) GL24 and GL36 EN 14080 (2008). The grading of the boards is performed by the GoldenEye 706 grading device manufactured by MiCROTEC (Brixen, IT).

The tension capacity is analysed individually for three samples, each of 150 randomly selected Swiss grown Norway spruce specimens. The dimensions of these reference samples are 90×45×4000 mm, 110×45×4000 mm and 230×45×4000 mm, respectively.

For all timber boards the dimensions and the position of every knot with a diameter larger than 10 mm is assessed and recorded. Furthermore, destructive tension test to estimate the ultimate tension capacity and non-destructive tension tests to estimate the tension-stiffness are performed. In order to ensure comparability of the test results, all tension tests are performed with standard moisture content according to EN 408 (2009a); i.e. equilibrium moisture content of the specimen in standard climate: (20 ± 2)°C and (65 ± 5)% relative humidity.

2.1 Non-destructive tension tests

The stiffness properties are measured with an infrared camera system during a non-destructive tension test. The boards are subdivided into 1) sections containing knot clusters or large single knots (denoted as knot sections, KS) and 2) sections between the knot sections (denoted as clear wood sections, CWS). At the beginning and the end of each section and at the edge of the total measured area (optical range of the infrared camera) three high frequent infrared light emitting diodes (LEDs) are mounted (Figure 1). The boards are loaded with an axial tension force, which represents 45% of the estimated maximum tension capacity. The maximum tension capacity has been estimated based on the measurements of the GoldenEye 706 grading device. Over the entire time of the test performance the LEDs send light impulses with a frequency of 20 Hz and based on this their positions are measured with the infrared camera system (Figure 3). Each board is measured twice (at the top and bottom side).

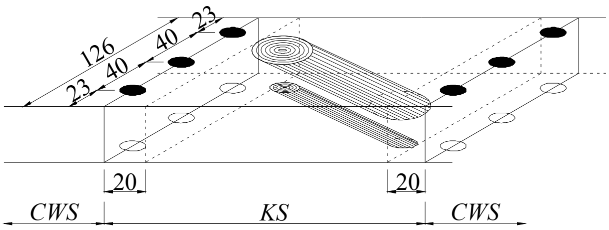

Figure 1. Illustration of the LED-arrangement around a knot cluster.

For the estimation of the modulus of elasticity (MOE) the strains over the board axis (calculated with the relative LED displacement of both sides) are used. The local strains within the KS are not considered separately. The assessment of the MOE is made by means of a linear regression model of the stress strain estimates according to EN 408 (2009a); i.e. with strains between 10% and 40% of the estimated maximum tension capacity. For all assessed MOE estimations the coefficient of determination R^2 was larger than 0.96. However, it has to be noted that some configurations for the determination of the MOE are not completely conform with the requirements according to EN 408; i.e. according to EN 408 the calculation of the MOE by means of linear regression requires a coefficient of determination larger than 0.99 and the length for the MOE estimation has to be 5 times the width. For the investigated test specimens this requirement would equal to a range for the stain measurement of 630 mm. In the present study the average length of the strain measurement ranges of corresponds to the average length of KS being equal to 94 mm. The mean MOE over the total measured area is estimated based on the measured strain between the outmost LEDs.

The properties of the KS depend on parameters, such as size of the knots and/or the knot arrangement. Thus, the probabilistic characteristics of the properties of the KS are difficult to describe. A weak section (WS) with a fixed length c = 150 mm is introduced. The MOE of the KS (MOE_{KS}) is converted into the MOE of a WS (MOE_{WS}) according to Equation 1. In this equation the MOE of the WS is calculated utilizing the estimated MOE of the KS and the MOEs of the two adjacent sections. In Figure 2 the estimated MOE of each section and the estimated mean MOE are illustrated for one board. For a more detailed description of the test procedure see Fink & Kohler (2011).

$$\frac{1}{MOE_{j,WS}} = \frac{1}{c}\left(\frac{l_{j,KS}}{MOE_{j,KS}} + \frac{c-l_{j,KS}}{2MOE_{j-1,CWS}} + \frac{c-l_{j,KS}}{2MOE_{j+1,CWS}}\right) \quad \mathit{for}\ l_{j,KS} \leq 150mm$$

$$MOE_{j,WS} = MOE_{j,KS} \quad \mathit{for}\ l_{j,KS} > 150mm \tag{1}$$

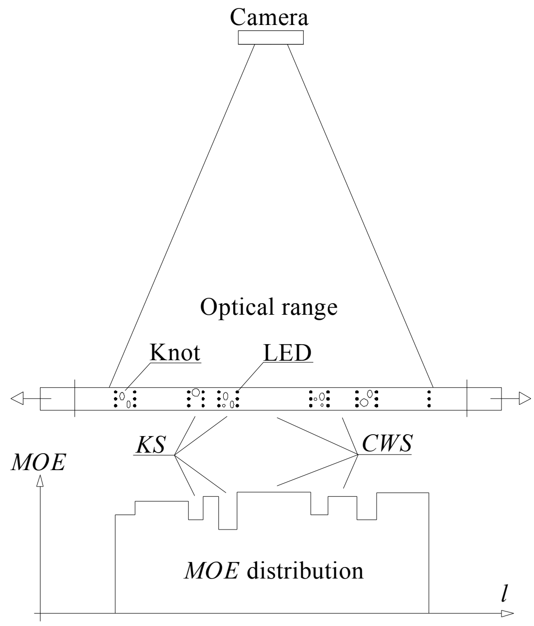

Figure 3. Illustration of the experimental set-up.

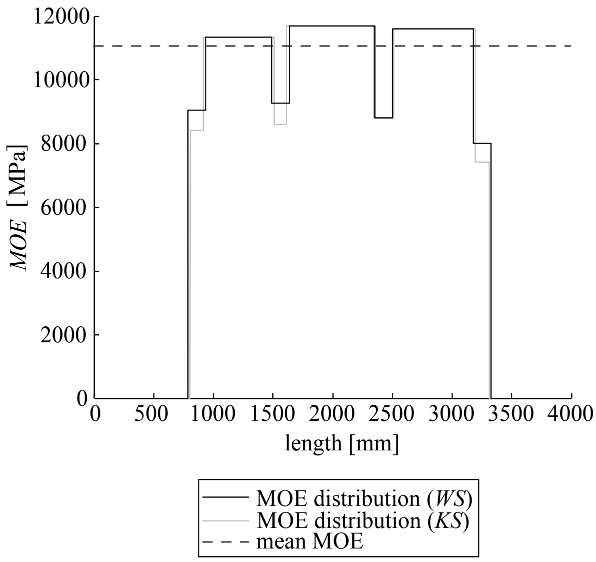

Figure 2. Example of the MOE distribution.

2.3 Destructive tension test

The reference boards were tested destructively in tension with the same tension machine as described in Section 2.2. The tests have been performed according to EN 408 (2009a) which requires a testing range of at least 9 times the width of the boards and a range for the strain measurement of 5 times the width. In order to collect as much information as possible about the individual boards the test range was maximized over the whole testable range of the boards just being limited by the clamping jaws of the tension test device at both ends of the boards. The resulting testing range corresponds to 3’360 mm.

2.4 Additional tests

In addition to the tension tests and the knot measurement the ultrasonic runtime, the Eigenfrequency, the dimensions, the weight and the moisture content were measured. Based on the ultrasonic runtime and the Eigenfrequency the corresponding dynamic MOEs of each board were calculated according to Equation 2 and 3 (Görlacher 1984, Steiger 1996). The dynamic MOEs have to be considered as average values over the entire length of the board. The assessed values of the MOEs are corrected to a reference moisture content according to EN 384 (2004).

$$MOE_{US} = \rho \, v^2 \tag{2}$$

$$MOE_F = (2 \, l \, f_0)^2 \, \rho \tag{3}$$

3 Variation of strength and stiffness properties

Timber which is loaded on tension transmits the load by its tensioned fibres in longitudinal direction. Based on the fact that timber is a natural grown material the grain orientation of commercial timber boards might deviate from being exactly parallel to the board's longitudinal axis. Two reasons for this might be distinguished; global deviation due to spiral grain and local deviation due to knots and knot clusters. The spiral orientation of the fibres in log is described by the so called spiral grain angle (Harris 1989). For Norway spruce specimens the magnitude of the spiral grain angles has been found to vary in general between zero and five degrees. The MOE in tension is about 15% lower for a board with a spiral grain angle of four degrees compared to a board with no spiral grain angle (Gerhards 1988, Ormarsson et al. 1998). In addition to the spiral grain orientation the strength and the stiffness of a timber board depends on physio-morphological parameters such as the annual ring width, the density or the distance to the pith. All these parameters are causing variability in the timber material properties within one board and between different boards.

Within board variations are assumed to be highly related to the occurrence of knots or knot clusters. In a hypothetical defect-free specimen the grains would be located perfectly parallel to each other in the longitudinal direction of the log. The load bearing capacity would be maximized. However, as soon as knots are involved the grains are forced to detour around these knots. This leads to changes in the grain angle and a reduction of the load bearing capacity. An overview of different models that describe the distribution of the grain orientation around knots is given in Foley (2001).

For timber elements loaded in tension parallel to the grain direction the change of the grain orientation may lead to partly stress redistributions from tension parallel to the grain to tension perpendicular to grain. These redistributions may lead to a local weakening of the timber board due to the fact that strength and stiffness related properties perpendicular to the grain are significantly lower than parallel to the grain.

Nordic spruce timber specimens are commonly characterized by a sequence of knot clusters divided by sections without any disturbance of knots. The knot clusters are distributed over the length of the board with rather regular longitudinal distances. Considering the trunk of a tree the average distance between the clusters is directly related to the yearly primary growth of the tree. Within one cluster, knots are growing horizontally in radial direction. Every knot has its origin in the pith. As described above, the change of the grain orientation appears in the areas around the knots. In Figure 4a the knots (black area) and the ambient area with disturbed grain orientation (grey area) within one cross section of the tree are illustrated. Since the individual boards are cut out of the natural shape of the timber log during the sawing process the well-structured natural arrangement of the knots becomes decomposed due to different sawing patterns. As a result, numerous different knot arrangements within the timber boards are occurring (Figure 4b,c). The sawing process additionally cuts parts of the grains as illustrated in Figure 4d. For timber loaded in tension the forces within these cut grains have to be transferred by shear forces to the adjacent grains which results in an additional local weakening.

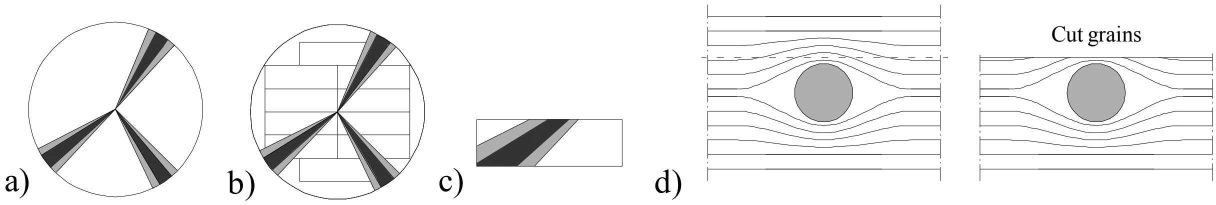

Figure 4. a) knot arrangement within the cross section of a tree trunk b) influence of the sawing pattern on the knot distribution within the sawn timber boards and c) resulting knot area within the cross section of one board d) schematic illustration of the cutting grains by the sawing process.

4 Influence of knots on the stiffness

As described above the within member variation of stiffness properties is highly related to knots and their arrangement. In the following the influence of different indicators on the stiffness of the KS/WS is analysed. To simplify the model only boards without pith are used. All indicators are analysed for every KS/WS within a section length of 150mm. Every knot in the board is assumed to have cylindrical shape. The position of the pith (always beyond the cross section of the boards) is estimated based on the intersection point of the two outer edges of each knot cylinder as sketched in Figure 5b. The position of the pith is only used for the calculation of indicator 2 and 3. For splay knots a constant knot diameter of 20mm is assumed. The influence of the knot indicators, described above, is analysed on the:

1. MOE_{WS} MOE of the WS
2. $\Delta MOE_{mean-WS}$ Difference between the mean MOE of the entire board and the MOE of the WS
3. ΔMOE_{CWS-WS} Difference between the mean MOE of the CWS of the entire board and the MOE of the WS.
4. MOE_{KS} MOE of the KS
5. $\Delta MOE_{mean-KS}$ Difference between the mean MOE of the entire board and the MOE of the KS.
6. ΔMOE_{CWS-KS} Difference between the mean MOE of the CWS of the entire board and the MOE of the KS.

Table 2. Description of knot indicators.

Nr.	Description
1	Projected knot area – overlapping areas are counted once (Figure 5a).
2	Projected area with local deviation of the grain orientation. It is assumed, that these area is the area within the double aperture angle than the knot (Figure 5b).
3	Projected area of cut grains. It was assumed that all grains have the same thickness within the area with local deviation of the grain orientation (Figure 5c).
4	Number of knots within a KS/WS.
5	Mean falling gradient of the knot axis (Figure 5d).
6	Mean distance of the knots to the board axis – measured on the horizontal board axis a_i (Figure 5e).
7	Mean distance between the knots perpendicular to the board axis b_i (Figure 5f).
8	Mean distance between the knots longitudinal to the board axis c_i (Figure 5f).
9	Mean distance between the knots d_i (Figure 5f).
10	Live or dead knots. Therefore a mean value for the entire boards is used. 0 denote that the majority of the knots are live knots; 1 denotes that the majority of the knots are live knots only on one board side; 2 denote that the majority of the knots are dead knots.
11	Maximal visual knot diameter f_{max} (Figure 5g).
12	Maximal visual knot diameter – perpendicular to the board axis e_{max} (Figure 5g).
13	Sum of all maximal visual knot diameter – within one KS/WS Σ f (Figure 5g).
14	Sum of all visual knot diameter – perpendicular to the board axis Σ e (Figure 5g).
15	Sum of all knot diameter on the board axis g_i (Figure 5e).

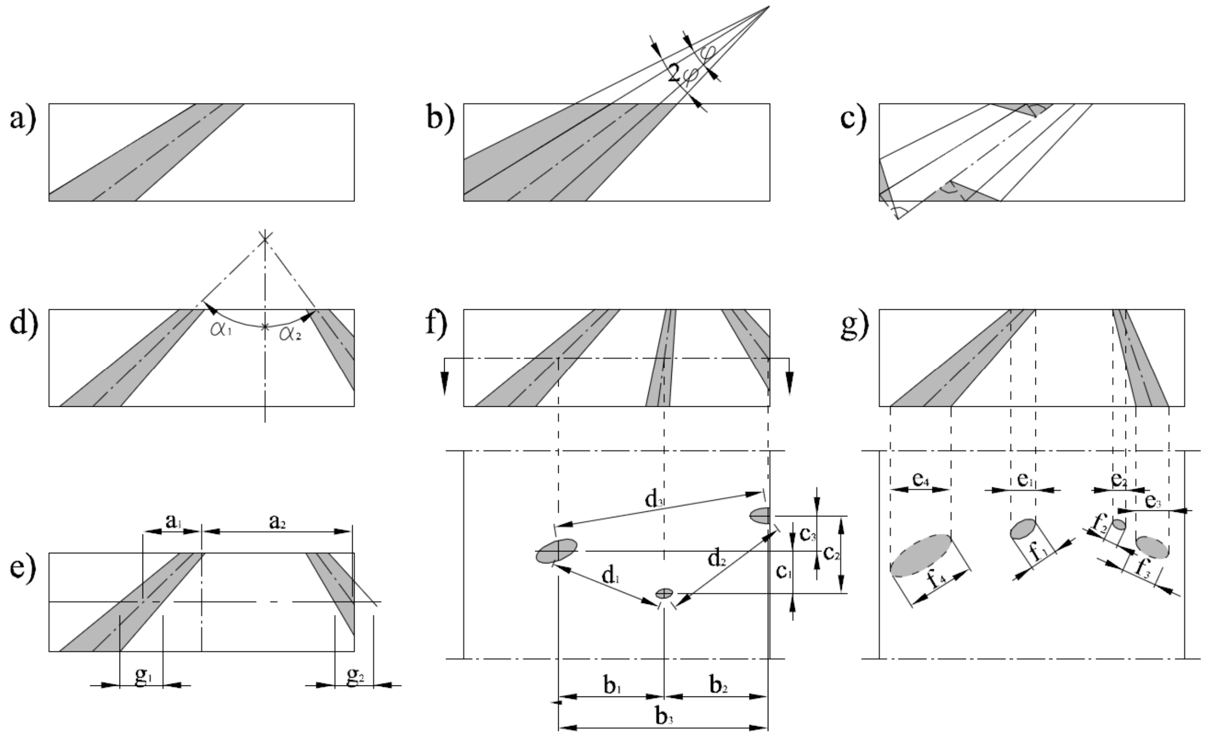

Figure 5. a) projected knot area b) projected area with local deviation of the grain orientation c) projected area of cut grains d) falling gradient of the knot axis e) distance of the knots to the board axis f) distance between the knots g) knot diameter.

Table 3. Correlation coefficient ρ between the knot indicators and the MOEs and the Δ MOEs.

	1	2	3	4	5	6	7	8	9	10	11	12	13	14	15
MOE_{WS}	-0.39	-0.35	-0.36	-0.08	0.05	0.09	0.10	-0.20	0.05	0.17	-0.27	-0.27	-0.32	-0.31	0.01
$\Delta MOE_{mean-WS}$	0.61	0.59	0.53	0.33	-0.08	-0.08	0.19	0.20	0.21	-0.08	0.35	0.33	0.49	0.50	0.18
ΔMOE_{CWS-WS}	0.56	0.53	0.52	0.22	-0.02	-0.07	0.11	0.09	0.11	-0.20	0.40	0.37	0.44	0.43	0.16
MOE_{KS}	-0.38	-0.34	-0.40	0.00	0.01	0.07	0.10	-0.05	0.08	0.21	-0.29	-0.30	-0.28	-0.28	0.01
$\Delta MOE_{mean-KS}$	0.44	0.42	0.46	0.12	-0.01	-0.04	0.14	-0.08	0.11	-0.12	0.29	0.29	0.30	0.31	0.13
ΔMOE_{CWS-KS}	0.41	0.39	0.45	0.05	0.02	-0.03	0.08	-0.12	0.04	-0.20	0.33	0.32	0.28	0.27	0.12

Table 4. Correlation matrix between the knot indicators.

	1	2	3	4	5	6	7	8	9	10	11	12	13	14	15
1	1.00	0.96	0.78	0.57	-0.33	-0.31	0.19	0.40	0.26	-0.13	0.37	0.37	0.77	0.78	0.19
2	0.96	1.00	0.70	0.65	-0.36	-0.23	0.37	0.39	0.42	-0.12	0.45	0.47	0.84	0.85	0.37
3	0.78	0.70	1.00	0.30	-0.14	-0.18	0.16	0.16	0.18	-0.13	0.37	0.37	0.66	0.66	0.13
4	0.57	0.65	0.30	1.00	-0.38	-0.16	0.62	0.56	0.69	0.04	0.23	0.24	0.75	0.77	0.50
5	-0.33	-0.36	-0.14	-0.38	1.00	0.71	-0.25	-0.23	-0.29	-0.04	0.10	0.10	-0.27	-0.27	-0.05
6	-0.31	-0.23	-0.18	-0.16	0.71	1.00	0.05	-0.17	0.01	-0.01	0.27	0.29	-0.07	-0.08	0.28
7	0.19	0.37	0.16	0.62	-0.25	0.05	1.00	0.20	0.97	0.06	0.28	0.32	0.57	0.55	0.69
8	0.40	0.39	0.16	0.56	-0.23	-0.17	0.20	1.00	0.41	0.03	0.08	0.08	0.43	0.46	0.15
9	0.26	0.42	0.18	0.69	-0.29	0.01	0.97	0.41	1.00	0.06	0.29	0.32	0.62	0.61	0.68
10	-0.13	-0.12	-0.13	0.04	-0.04	-0.01	0.06	0.03	0.06	1.00	-0.19	-0.22	-0.09	-0.09	-0.04
11	0.37	0.45	0.37	0.23	0.10	0.27	0.28	0.08	0.29	-0.19	1.00	0.95	0.62	0.61	0.51
12	0.37	0.47	0.37	0.24	0.10	0.29	0.32	0.08	0.32	-0.22	0.95	1.00	0.61	0.63	0.53
13	0.77	0.84	0.66	0.75	-0.27	-0.07	0.57	0.43	0.62	-0.09	0.62	0.61	1.00	0.98	0.57
14	0.78	0.85	0.66	0.77	-0.27	-0.08	0.55	0.46	0.61	-0.09	0.61	0.63	0.98	1.00	0.55
15	0.19	0.37	0.13	0.50	-0.05	0.28	0.69	0.15	0.68	-0.04	0.51	0.53	0.57	0.55	1.00

The correlation coefficient ρ between the indicators and the $MOEs$ / $\Delta MOEs$ are provided in Table 3. The correlations between the different knot indicators are illustrated in Table 4. In the following some findings of the study are listed:

- In general the results in Table 3 are revealing higher correlations between the knot indicators and the WS rather than the KS.
- The correlation with the MOEs and ΔMOEs is enhanced by applying the sum of indicator 1 and 3 ($\rho_{MOE,WS} = 0.402$, $\rho_{\Delta MOE,mean-WS} = 0.621$, $\rho_{\Delta MOE,CWS-WS} = 0.580$, $\rho_{MOE,KS} = 0.404$, $\rho_{\Delta MOE,mean-KS} = 0.464$, $\rho_{\Delta MOE,CWS-KS} = 0.440$). The difference is, however, too small to legitimate the additional effort.
- Additional to the knot indicators described above the projected knot area is calculated for every type of knot. Side knots, edge knots, splay knots and narrow side knots are differentiated. The four independent projected knot areas are put in a linear regression model. Based on this approach the coefficient of correlation is advanced to $\rho_{\Delta MOE,mean-WS} = 0.621$. This suggests that the influence of the knot position might have a miner influence on the stiffness of a KS/WS.
- The results show that only a very small proportion of the projected knot areas are overlapping each other. Accordingly, the interrelationships between the projected knot areas and the stiffness properties are assumed to remain the same when the overlapping projections are counted single or multiple.

In order to enhance the correlation of the individual knot indicators with the stiffness properties as given in Table 3 the indicators were combined in different configurations. Therefore a linear regression model (Equation 4) was used, where Y is the predicted MOE or the predicted ΔMOE, β are the regression coefficients, X are the input variables and ε is the error term. The most promising knot indicator combinations are described in more detail in the following section.

$$Y = \beta_0 + \beta_1 X_1 ..... + \beta_i X_i + \varepsilon \tag{4}$$

4.1 Correlation to the MOE

As described above timber boards from two different grading classes are analysed. The results show that the majority of the weak sections (WS) of the grading class L40 have greater MOE than the clear wood section (CWS) of the lower grading class. On this reason a direct relation between knots and MOE can never fit well without an additional indicator which describes the material properties of the entire board. To clarify this, the interrelation between the projected knot area (knot indicators 1) and the MOE_{WS} is illustrated in Figure 6.

To predict the MOE_{KS} and MOE_{WS} a linear regression model was developed which includes only knot indicators which are straightforward to measure (Model I). Therefore, equation 4 is used with the following input variables: X_1 Density [kg/m^3], X_2 Knot indicator 4 [-], X_3 Knot indicator 14 [mm].

The different stiffness properties (MOE_{KS} and MOE_{WS}) are used as response variables for the regression analysis. The regression coefficients are estimated by means of the maximum likelihood method. The error term is assumed to be normal distributed with $\mu_\varepsilon = 0$ and a standard deviation σ_ε. The results of the regression analysis are shown in Table 5 in terms of the expected values and variances of the regression coefficients. Additionally the values for the correlations and the standard deviation of the error term are enlisted.

Table 5. Estimated parameters, their variations, the correlatio n coefficient and the standard deviation of the error term of Model I.

	MOE_{WS}		MOE_{KS}	
	$E[\beta_i]$	$Var(\beta_i)$	$E[\beta_i]$	$Var(\beta_i)$
β_0	$-6.52\cdot10^3$	$6.04\cdot10^5$	$-5.75\cdot10^3$	$8.43\cdot10^5$
β_1	38.9	2.41	33.9	3.37
β_2	$1.20\cdot10^3$	$2.29\cdot10^4$	$1.63\cdot10^3$	$3.19\cdot10^4$
β_3	-49.5	14.4	-54.6	20.1
$\rho_{MOE,WS/KS}$	0.863		0.800	
σ_ε	1243		1468	

The results show that especially the MOE of the WS can be predicted quite well based on the results of the regression analysis. When the estimated dynamic MOE based on Eigenfrequency measurement $\left(MOE_F[N/mm^2]\right)$ is used instead of the density the model shows a correlation coefficient equal to ρ= 0.909 for the prediction of the MOE_{WS} (with $\beta_0 = 869$, $\beta_1 = 0.800$, $\beta_2 = 391$ and $\beta_3 = -31.5$) and ρ= 0.832 for the prediction of the MOE_{KS} (with $\beta_0 = 775$, $\beta_1 = 0.689$, $\beta_2 = 930$ and $\beta_3 = -39.1$).

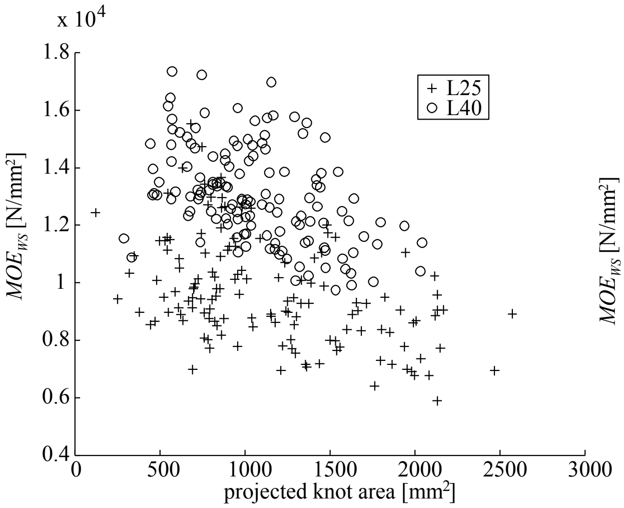

Figure 6. Correlation between projected knot area and MOE of the WS.

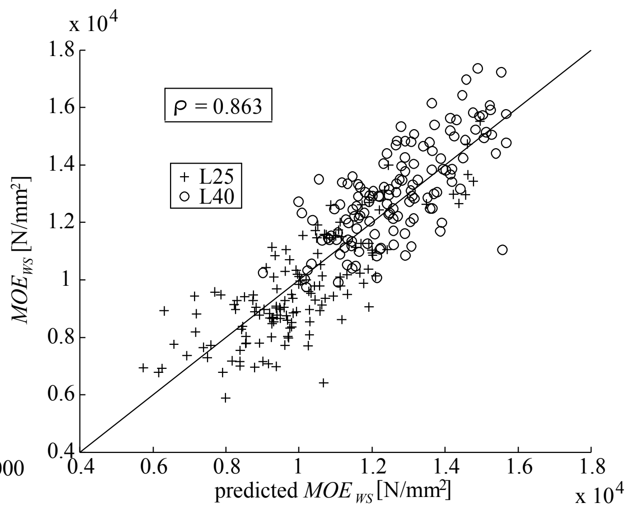

Figure 7. Correlation between the predicted and the estimated MOE of the WS based on the Model I.

4.2 Correlation to the delta MOE

An alternative way to describe the stiffness within a KS/WS is to identify the local decrease of the stiffness within a timber board based on knot clusters and their arrangements. For this purpose, two different approaches can be used. The first one describes the local stiffness decrease based on the measurements of the clear wood sections and the latter describes the local stiffness decrease based on the mean stiffness of the entire board. From a practical perspective it is more efficient to use the second approach since well-established non-destructive measurement procedures are existing which are capable to detect the mean stiffness of timber boards over their entire length; e.g. ultrasonic runtime, Eigenfrequency and density. The combination of all stiffness indicating measurements results in a rather small increase of the correlation coefficient ($\rho_{\Delta MOE,mean-WS}$= 0.651, $\rho_{\Delta MOE,CWS-WS}$= 0.653, $\rho_{\Delta MOE,mean-KS}$= 0.585, $\rho_{\Delta MOE,CWS-KS}$= 0.599). Furthermore a large number of regression parameters (knot indicators) is needed for this approach. Thus, a model is developed which includes only the projected knot area as an indicators (Model II). Therefore, equation 4 is used with the following input variable: X_1 projected knot area (knot indicator 1) [mm²].

Table 6. Estimated parameters, their variations, the correlation coefficient and the standard deviation of the error term of Model II.

	$\Delta MOE_{mean-WS}$		$\Delta MOE_{mean-KS}$	
	$E[\beta_i]$	$Var(\beta_i)$	$E[\beta_i]$	$Var(\beta_i)$
β_0	48.6	$2.05 \cdot 10^4$	1328	$4.73 \cdot 10^4$
β_1	1.54	$1.43 \cdot 10^{-2}$	1.48	$3.30 \cdot 10^{-2}$
$\rho_{\Delta MOE,mean-WS/KS}$	0.614		0.442	
σ_ε	916		1392	

In the following the developed regression models will be adapted with the estimated MOE_F. Therefore every ΔMOE (calculated with the regression model described above) is subtracted from the associated estimated MOE_F. The derived prediction of the MOE is compared with the MOE_{WS} and the MOE_{KS}. The results show that the MOE can be predicted quite well (ρ= 0.918 for MOE_{WS} and ρ= 0.830 for MOE_{KS}). The results even show a higher correlation coefficient than with the model described above. However, therefore an additional linear regression model, with $\beta_0 = 344$ and $\beta_1 = 0.841$ is essential.

5 Influence of knots on the tension capacity

Just as for the variation of stiffness properties the variation of strength properties within one board is highly related to knots and their arrangement. The influence of the same knot indicators as introduced above are analysed, without knot indicator 10 and 13.

All knot indicators are estimated for every KS/WS within the testing range of the boards. The knot indicators are only estimated for boards without pith. The tension capacities are measured for three different cross sectional dimensions. For this purpose, the first four knot indicators are divided by the particular cross sectional area. Knot indicators 14 and 15 are divided by the perimeter of the cross sectional area. It is assumed that the KS with the highest values of knot indicator 1 or 14 within one board correspond to the KS with the lowest tension capacity. In approximately 50% of the boards the two different knot indicators detect the same KS (123 of 244). However, the correlation coefficients between the identified KS and the tension capacity are similar (Table 7) for both knot indicators. It can may be concluded that several KS within one timber beam are similar efficient for the prediction of the tension capacity.

Table 7. Correlation coefficients ρ between the knot indicators, the MOE_F (F), the MOE_{US} (US) and the density (D) with the tension capacity.

		F	US	D	1	2	3	4	5	6	7	8	9	11	12	14	15
14	$f_{t,0,1}$	0.77	0.65	0.47	-0.53	-0.53	-0.43	-0.25	0.03	-0.05	-0.13	-0.06	-0.13	-0.30	-0.32	-0.52	-0.21
1	$f_{t,0,1}$				-0.55	-0.53	-0.46	-0.24	-0.02	0.08	-0.14	-0.12	-0.14	0.06	-0.41	-0.55	-0.20

The results show a correlation between the MOE_F and MOE_{US} and the tension capacity of $\rho = 0.77$ and $\rho = 0.65$, respectively. This is representing only boards without pith. The correlations of all boards show similar values of $\rho = 0.78$ and $\rho = 0.66$, respectively: i.e. in this study, boards with pith have similar correlations between MOE_F and MOE_{US} and the tension capacity as those without pith.

To predict the tension capacity a multivariate linear regression model is established which includes only knot indicators which are straightforward to be measured. For the identification of KS the maximal value of knot indicator 14 is used. Equation 4 is used with the following input variables: X_1 MOE_F [N/mm^2], X_2 Knot indicator 4 [1/mm], X_3 Knot indicator 14 [-].

Table 8. Estimated parameters, their variations, the correlation coefficient.

	β_0	β_1	β_2	β_3
$E[\beta_i]$	-6.54	$3.30 \cdot 10^{-3}$	$1.13 \cdot 10^{4}$	-37.6
$Var(\beta_i)$	11.1	$4.49 \cdot 10^{-8}$	$9.32 \cdot 10^{6}$	35.6

The model results in a correlation coefficient $\rho = 0.803$ and standard deviation of the error term $\sigma_\varepsilon = 7.19$, which is only a small improvement of the correlation by additional explanatory knot indicators. Furthermore, it has to be mentioned that the standard deviation of the error term being equal to $\sigma_\varepsilon = 7\text{MPa}$ is rather high. However, a correlation coefficient of $\rho = 0.803$ for the prediction of the tension capacity of timber boards is achieved.

In addition the weakest section of one board is combined with 1) the adjacent weak sections and 2) the second weakest section of the board. For both, no significant improvement of the strength prediction could be detected ($\rho = 0.804$ and $\rho = 0.807$, respectively).

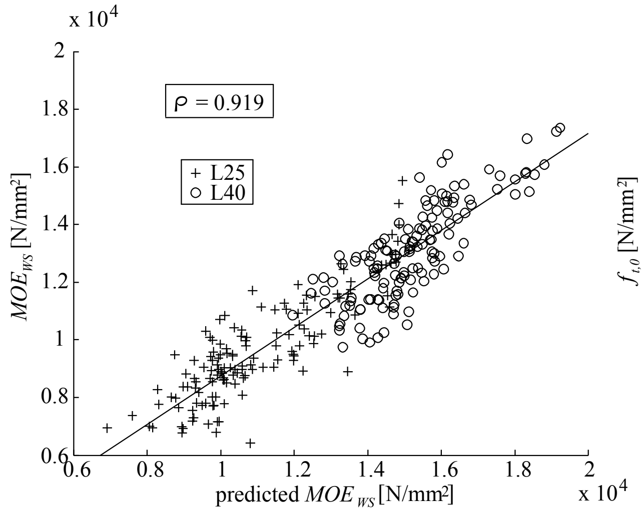

Figure 8. Correlation between the predicted MOE and the estimated MOE of the WS based on the Model II.

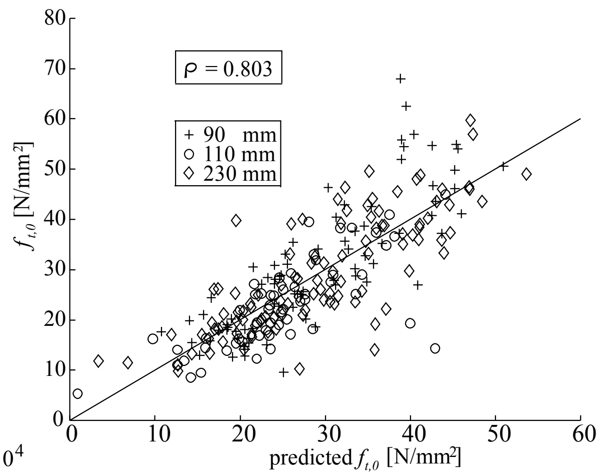

Figure 9. Correlation between the predicted and the estimated tension capacity.

6 Conclusions and outlook

In the present study the influence of different knot indicators on the strength and stiffness related properties are analysed and the interrelation between indicators is documented. Based on the results 2 models for the prediction of the local stiffness of areas with knots or knot clusters are developed. The first model predicts the absolute value of the stiffness and the second model predicts the weakening of the stiffness to the estimated mean MOE. Both models show a correlation between the predicted and the estimated stiffness of $\rho > 0.9$. Additionaly a model for ultimate tension capacity prediction with a correlation coefficient $\rho > 0.8$ is developed. The main findings of this study are summarized as follows:

- A direct interrelation between knot indicators and stiffness properties of sections containing knots cannot described well without an additional indicator that describes average material properties of the board.
- The knot position might have a low influence on the stiffness of sections containing knots.
- Only a very small proportion of the projected knot areas are overlapping each other. Accordingly, the prediction of the strength and stiffness related properties using the project-

ed knot area ratio (tKAR) are similar when the overlapping projections are counted single or multiple.

- The sum of all visual knots – perpendicular to the board axis divided by the perimeter of the cross sectional area and the tKAR are similar efficient to detect the weakest point within the beam.
- The prediction of the tension capacity based on the weakest section is only marginally improved through including their adjacent weak section.

The presented study has analysed only timber boards without pith. The models should be adapted with timber boards containing pith in further studies. Additionally the model can be adapted with the position of the pith and a more detailed consideration of the knot conditions (e.g. live or dead knot).

7 References

Boatright, S. W. J. & Garrett, G. G. 1979. The Effect of Knots on the Fracture Strength of Wood - II. A Comparative Study of Methods of Assessment, and Comments on the Application of Fracture Mechanics to Structural Timber, *Holzforschung*, 33 (3), pp. 72-77.

CEN 2004. DIN EN 384 - Determination of characteristic values of mechanical properties and density; German version EN 384:2004, Brussels, European Committee for Standardization.

CEN 2008. DIN prEN 14080 - Timber structures - Glued laminated timber and glued laminated solid timber - Requirements; German version, Brussels, European Committee for Standardization.

CEN 2009a. DIN EN 408 - Timber structures - Structural timber and glued laminated timber - Determination of some physical and mechanical properties; German version prEN 408:2009, Brussels, European Committee for Standardization.

CEN 2009b. DIN EN 14081-4 - Timber structures - Strength graded structural timber with rectangular crosssection - Part 4: Machine grading - Grading machine settings for machine controlled systems; German version, Brussels, European Committee for Standardization.

Courchene, T., Lam, F. & Barrett., J. D. 1996. The effects of edge knots on the strength of SPF MSR lumber, Proceedings of CIB-W18, Bordeaux, France.

Denzler, J. K. 2007. Modellierung des Grösseneffektes bei biegebeanspruchtem Fichtenschnittholz, TU-München.

DIN 2008. DIN 4074-1 Sortierung von Holz nach der Tragfähigkeit - Teil 1: Nadelschnittholz, Berlin, Normenausschuss Bauwesen (NABau) im DIN (Deutsches Institut für Normung e.V.).

Fink, G. & Kohler, J. 2011. Multiscale Vaiability of Stiffness Properties of Timber Boards, ICASP Applications of Statistics and Probability in Civil Engineering, Zurich.

Foley, C. 2001. A three-dimensional paradigm of fiber orientation in timber, *Wood Science and Technology*, 35 (5), pp. 453-465.

Gerhards, C. C. 1988. Effect of slope of grain on tensile strength, *Forest Products Journal*, 38 (7/8), pp. 39f.

Görlacher, R. 1984. Ein neues Messverfahren zur Bestimmung des Elastizitätsmoduls von Holz, *Holz als Roh- und Werkstoff*, 42, pp. 219-222.

Harris, J. M. 1989. *Spiral Grain and Wave Phenomena in Wood Formation*. Berlin Heidelberg, Springer.

Isaksson, T. 1999. Modelling the Variability of Bending Strength in Structural Timber, Report TVBK-1015, Lund Institute of Technology, PhD.

Kline, D. E., Woeste, F. E. & Bendtsen, B. A. 1986. Stochastic model for modulus of elasticity of lumber, *Wood and Fiber Science*, 18, pp. 228-238.

Mitsuhashi, K., Poussa, M. & Puttonen, J. 2008. Method for predicting tension capacity of sawn timber considering slope of grain around knots, *Journal of wood science*, 54 (3), pp. 189-195.

Ormarsson, S., Dahlblom, O. & Persson, K. 1998. Influence of varying growth characteristics of stiffness grading of structural timber, Proceedings of CIB-W18, Savonlinna, Finland.

Samson, M. & Blanchet, L. 1992. Effect of knots on the flatwise bending stiffness of lumber members, *European Journal of Wood and Wood Products*, 50 (4), pp. 148-152.

Steiger, R. 1996. Mechanische Eigenschaften von Schweizer Fichten-Bauholz bei Biege-, Zug-, Druckund kombinierter M/N-Beanspruchung - Sortierung von Rund- und Schnittholz mittels Ultraschall, IBK Bericht Nr. 221, Zurich, ETH Zurich.

Taylor, S. E. & Bender, D. A. 1991. Stochastic Model for Localized Tensile Strength and Modulus of Elasticity in Lumber *Wood and Fiber Science*, Volume 23 (Number 4), pp. 501-519.

CIB-W18/44-5-2

INTERNATIONAL COUNCIL FOR RESEARCH AND INNOVATION IN BUILDING AND CONSTRUCTION

WORKING COMMISSION W18 - TIMBER STRUCTURES

ADAPTIVE PRODUCTION SETTINGS METHOD FOR STRENGTH GRADING

G Turk
University of Ljubljana

SLOVENIA

A Ranta-Maunus
VTT

FINLAND

MEETING FORTY FOUR

ALGHERO

ITALY

AUGUST 2011

Presented by A Ranta-Maunus

JW Van de Kuilen commented that the interest is to minimize the number of rejects. The problem here was that it was far too optimized as we would have to ask whether it would be acceptable that 20% of the material did not meet the requirement.

F Rouger commented that the impact of the method was less than 0.5%. There were discussions on the accuracy of the simulation method. As Table 12 was based on simulated results and showed 20% of the samples did not meet requirements why there was not corresponding influence on yield. A Ranta-Maunus responded that although there were a number of rejects but yield could go up or down between grades.

P Stapel agreed that there were movements between grades. S Aicher agreed that the results seemed logical.

J Köhler commented that references were not complete and there was a need to move from counting pieces to consider structural design issues; extend the work to consider what would be the influence on the capacity of the structural elements. He commented also that method should be based on robust IP.

Adaptive production settings method for strength grading

Goran Turk
University of Ljubljana, Slovenia

Alpo Ranta-Maunus
VTT, Finland

1 Introduction

The grading method which is presently used in Europe is based on standard EN 14081-2. In order to determine machine settings a sample of at least 900 boards needs to be prepared, graded and tested. Based on these at least 900 boards, the machine settings are obtained which are to be used in actual grading. However, the grading practice shows that the shifts in material properties may have an important influence on the properties of the graded material and as a consequence grading results. The initial sample which is usually used to determine the machine settings is too small to include the influence of quality shifts. As a result the present grading method may be too conservative for higher strength material and too generous for lower strength material. See Bacher (2009) and Ranta-Maunus and Denzler (2009).

In order to overcome this drawback the adaptive settings method is presented here. The basic idea of this method is the utilization of measured indicating properties (IP), such as modulus of elasticity, density, knot area ratio (KAR), etc. The continuously recorded IP's are used for automatic settings adjustments.

The method was tested on a sample of approximately 200 000 spruce boards for which the IP's were recorded. The grade determinig properties were simulated by a computer programme so that the mean values, variances and correlations corresponded to the previously obtained laboratory data.

2 Available data set

The data from the grading machine GoldenEye-706 at two saw mills in Nordic countries were available. The grading machine uses X-Ray radiation to determine sizes, knots and density of a board via grey scale image, and combines this information to a frequency measurement to determine the dynamic modulus of elasticity E_{dyn}. Using this information the machine estimates the bending strength of each board by calculating its indicating property IP-MOR = $f_{m,mod}$ for bending strength with an equation based on multi linear regression. Also IP-MOE and IP-density are used as grading parameters.

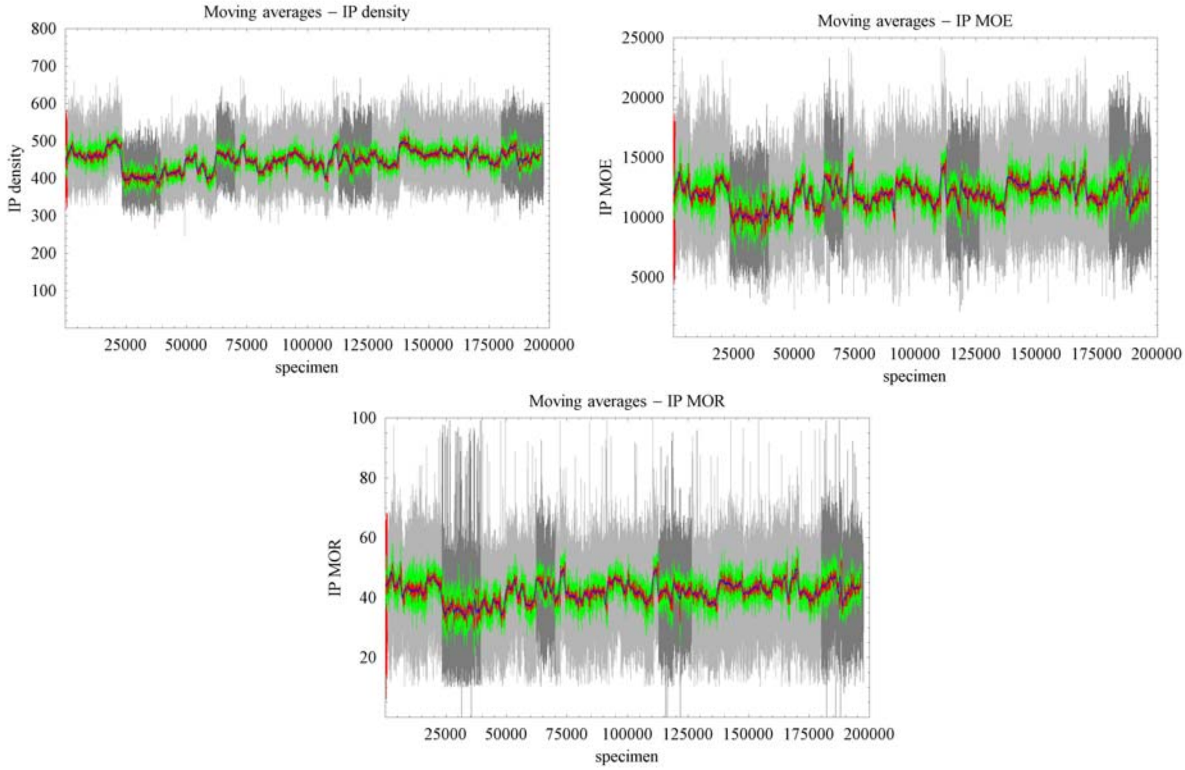

Figure 1: Moving averages of indicating properties in order of production

The different shades of grey are showing all the IP values of nearly 200 000 boards of different sizes in Figure 1. The green, red and blue lines are showing the moving averages of these IP values with window sizes of 10, 100 and 1000, respectively.

We can observe that quality shifts often occur with the change of specimen size. Specifically, the values for larger boards (225 and 200 mm) exhibit lower values of all IP's. However, this effect is not the size/height effect known by engineers, but related to timber quality. In addition, there are some considerable shifts in the same size batch, too. These shifts could be due to different growth conditions, forestry management practices, dimensions of the specimens, sawing patterns and other parameters.

In total, 196 570 boards of spruce ran through the machine. The dimensions varied between w = 75 mm and w = 225 mm in width and t = 40 mm to t = 50 mm in thickness. Sample sizes and average properties are given in Table 1.

Table 1: Average properties of graded material

Sample	n	w mm	ρ_{mean} kg/m³	E_{mean} N/mm²	$f_{m,mod,mean}$ N/mm²
SE 100-200	22 503	100-200	470	12396	44.0
FI 225	16 065	225	401	10104	35.6
FI 200	22 900	200	423	11159	39.2
FI 175	7 867	175	461	12685	43.8
FI 150	42 609	150	447	12019	42.3
FI 125	13 829	125	449	11934	41.7
FI 100	53 473	100	460	12188	42.6
FI 75	17 334	75	461	12207	43.4
all	196 580				

Besides the moving averages which show how the properties of material change in time, it is interesting to observe how the coefficients of variation and correlation coefficients change. The first explains the changes in variability of material, the later explains the changes in linear dependence of the indicating properties. These statistical properties are shown in Figure 2.

We can see that the variability as well as linear dependence does not change as vigorously as the average values of the properties. Only a few, relatively smaller shifts in the coefficient of variation and the correlation coefficients are noticeable, e.g. in the case of the largest width of 225 mm. This is an important characteristic of the data set which enables us to assume that the important changes of the properties are only in absolute value whereas the variability and dependence between properties remain constant. This assumption is the basis for the simulation technique which will be explained later.

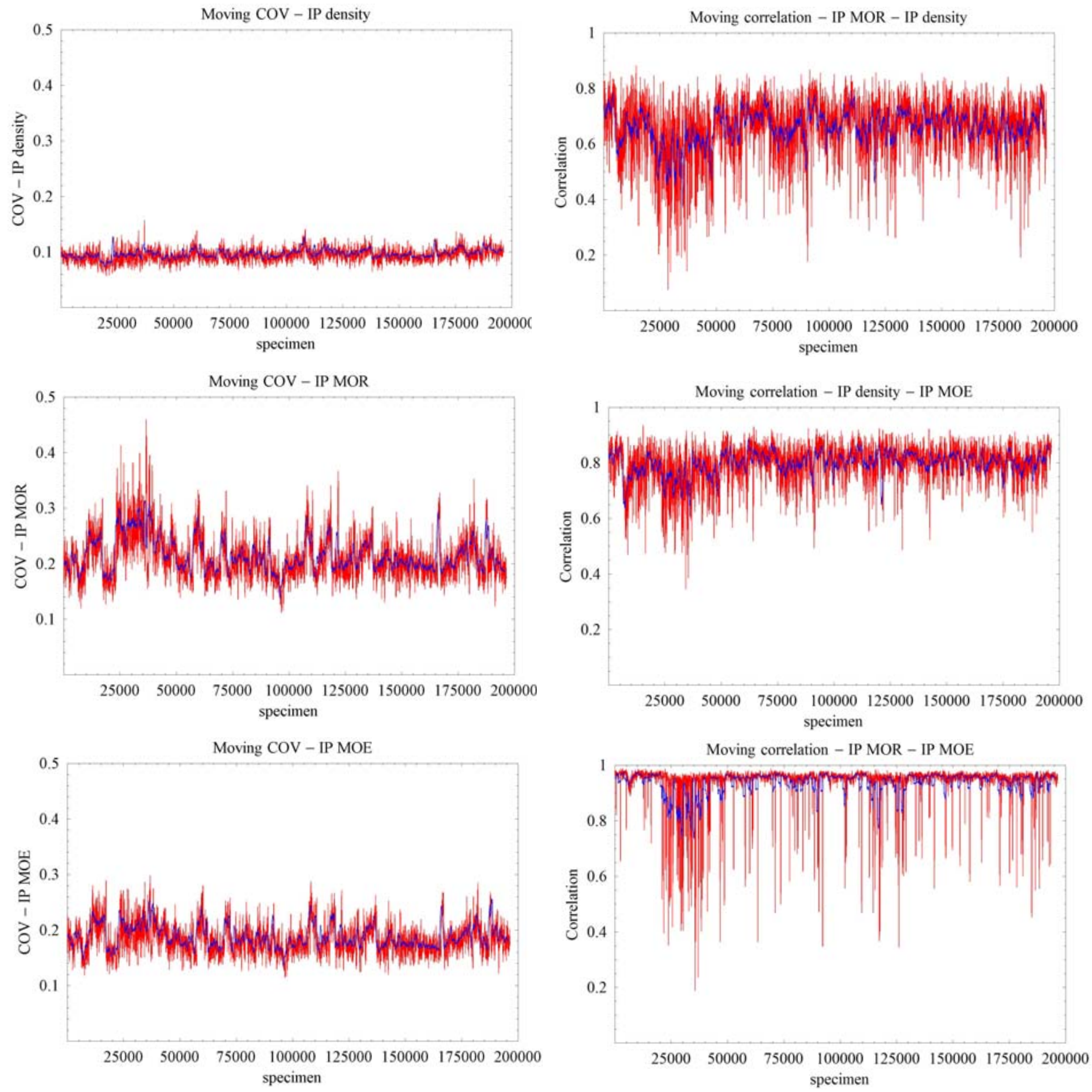

Figure 2: Moving coefficients of variation and moving correlation coefficients

3 Computer simulation

In order to estimate the efficiency and correctness of the grading method a very large sample needs to be examined. The experiments on a very large sample require time and financial means which are usually not available. Therefore, synthetic data obtained by computer simulation are commonly used.

The first and most important step in the computer simulation is random sample generation. Since computers are not random machines, only pseudo-random data can be generated. This fact and the fact that is very difficult to generate a sample with all the statistical properties of the actual population, raise a question of the correctness of the simulation analyses.

This drawback is partially overcome by the proposed method in which the actual data from the grading machine are used and only those values which are impossible or too expensive to obtain by experimets were generated by the computer.

A generation method is developed which uses the actual data for IP's and generates only grade determining properties so that the means, variances and correlations are the same as obtained by previously gathered experimental data. The method is based on condensation of the Cholesky decomposition of variance-covariance matrix. The details of the procedure are described in Ranta-Maunus and Turk (2010).

4 The adaptive settings determination

The basic idea of the method is that the machine settings are changed from the initial settings based on the average of IP's of the last n_w boards graded to the specific grade

$$f_{\mathrm{mod},th} = f_{\mathrm{mod},th,ini} + \alpha\left(f_{\mathrm{mod,mean},ref} - f_{\mathrm{mod,mean},nw}\right)$$

where $f_{\mathrm{mod},th}$ means settings (thresholds), $f_{\mathrm{mod,mean},nw}$ is the average of the last n_w values graded to the grade by using initial settings, $f_{\mathrm{mod,mean},ref}$ is the average value in the reference sample used for the determination of initial settings, and α is the parameter which determines the power of the adjustment.

In this paper we use

$$\alpha = 1.75 - 0.03C$$

where C means C-class (i.e. C=24 for C24). The last equation is based on the slopes of regression lines (Ranta-Maunus and Turk, 2010). In this paper we analyse a grading method which uses three parallel IP's, and the same adaptive settings determination is applied to all settings.

4.1 Initial settings

Initial settings $f_{\mathrm{mod},th,ini}$ have an important role in the proposed method. There are several possibilites for the initial settings determination. One of them was presented by Ranta-Maunus and Turk (2010). Here, the settings given by the standard EN 14081-4 are used as initial settings.

4.2 Reference values

Reference mean values $f_{\mathrm{mod,mean},ref}$ are determined along with the initial settings determination. The reference values for Nordic spruce based on material used for the determination of the standard settings of GoldenEye-706 are given in Table 3.

Table 2: Initial settings – EN 14081-4 settings

Grade (combination)	$f_{\mathrm{mod},th}$ N/mm^2	$E_{\mathrm{mod},th}$ N/mm^2	$\rho_{\mathrm{mod},th}$ kg/m^3
C40	49.6	12000	410
C30(C40/C30)	36.1	10000	370
C18(C40/C30/C18)	15.3	5500	310
C24(C40/C24)	15.3	5500	320

Table 3: Reference values

Grade (combination)	$f_{\mathrm{mod,mean},ref}$ N/mm^2	$E_{\mathrm{mod,mean},ref}$ N/mm^2	$\rho_{\mathrm{mod,mean},ref}$ kg/m^3
C40	55.1	14800	475
C30(C40/C30)	43.6	11800	435
C18(C40/C30/C18)	31.6	8900	395
C24(C40/C24)	39.6	10800	422

Table 4: Requirements

		C40	C30	C24	C18
f_{05}	N/mm^2	40.0	26.8	21.4	16.1
f_{005}	N/mm^2	26.7	17.9	14.3	10.7
E_{mean}	N/mm^2	13300	11400	10450	8550
ρ_{05}	kg/m^3	420	380	350	320

Table 4 gives European norm requirements for grades (k_v-factor for strength and 0.95 factor for MOE are applied). In addition, the requirement applied in this analysis to 0.5 percentile of strength, $f_{005} > 0.67 f_{05}$ is shown.

5 Results

The measured IP data of 195 071 boards are included in verification. This sample is divided into a sequence of 98 sub-samples of size 2000. For each sub-sample, the grading according to the EN 14081-4 settings and adaptive production settings is done. In all cases the yield to every strength class is determined, and a test if the graded material fulfils the requirements from Table 4 is performed.

The grade combination C40/C30/C18 and C40/C24 are analysed.

Firstly, the effect of window size n_w is explored. The window sizes between 100 and 500 are tried. The results of the yields in different grades and the percentage of the subsamples for which the requirements from Table 4 were not fulfilled are presented in Tables 5-8.

Table 5: Yields obtained to C40, C30, C18 and reject for 195 071 boards

EN 14081-4 settings					
	C40	C30	C18	Rejects	Total
	0.199	0.515	0.279	0.006	1.000
Adaptive settings method					
window size	C40	C30	C18	Rejects	Total
100	0.191	0.507	0.290	0.011	1.000
300	0.192	0.508	0.290	0.010	1.000
500	0.192	0.509	0.289	0.010	1.000

Table 6: Percentage of sub-samples when requirements from Table 4 were not fulfilled

EN 14081-4 settings			
	C40	C30	C18
	10.2%	6.1%	0.0%
Adaptive settings method			
window size	C40	C30	C18
100	3.1%	3.1%	0.0%
300	3.1%	1.0%	0.0%
500	3.1%	0.0%	0.0%

Table 7: Yields obtained to C40, C24 and reject for 195 071 boards

EN 14081-4 settings				
	C40	C24	Rejects	Total
	0.199	0.793	0.007	1.00
Adaptive settings method				
window size	C40	C24	Rejects	Total
100	0.191	0.783	0.026	1.000
300	0.192	0.785	0.023	1.000
500	0.192	0.787	0.022	1.000

Table 8: Percentage of sub-samples when requirements from Table 4 were not fulfilled

EN 14081-4 settings		
	C40	C24
	10.2%	20.4%
Adaptive settings method		
window size	C40	C24
100	3.1%	16.3%
300	3.1%	14.3%
500	3.1%	12.2%

The parameter α seems to be a very important one since it determines the power of the settings adjustment. The proposed values stem from the relations between characteristic strength of in-grade timber and average IP-MOR of the same sample (see Ranta-Maunus and Turk, 2010).

In order to verify if the proposed values of α are adequate, the analyses for scaled values of α are performed. I.e., the values of α are multiplied by the factors α_{ref} between 0.7 and 1.2. The results for yields and percentage of subsamples which don't fulfil the requirements from Table 4 are given in Tables 9-12. The window size $n_w = 300$ is used in these analyses. The typical reason why requirements are not fulfilled is too low density ρ_{05} for C40 and C30 but can be any of the criteria for C24, stiffness E_{mean} and characteristic strength f_{05} being most common.

Table 9: Yields obtained to C40, C30, C18 and reject for 195 071 boards

EN 14081-4 settings					
	C40	C30	C18	Rejects	Total
	0.199	0.515	0.279	0.006	1.000
Adaptive settings method					
α_{ref}	C40	C30	C18	Rejects	Total
0.7	0.194	0.511	0.286	0.008	1.000
0.8	0.194	0.510	0.287	0.009	1.000
0.9	0.193	0.509	0.288	0.009	1.000
1.0	0.192	0.508	0.290	0.010	1.000
1.1	0.191	0.507	0.291	0.011	1.000
1.2	0.190	0.506	0.292	0.012	1.000

Table 10: Percentage of sub-samples when requirements from Table 4 were not fulfilled

EN 14081-4 settings			
	C40	C30	C18
	10.2%	6.1%	0.0%
Adaptive settings method			
α_{ref}	C40	C30	C18
0.7	4.1%	0.0%	0.0%
0.8	4.1%	0.0%	0.0%
0.9	3.1%	1.0%	0.0%
1.0	3.1%	1.0%	0.0%
1.1	2.0%	1.0%	0.0%
1.2	1.0%	1.0%	0.0%

Table 11: Yields obtained to C40, C24 and reject for 195 071 boards

EN 14081-4 settings				
	C40	C24	Rejects	Total
	0.199	0.793	0.007	1.00
Adaptive settings method				
α_{ref}	C40	C24	Rejects	Total
0.7	0.194	0.789	0.016	1.000
0.8	0.193	0.788	0.018	1.000
0.9	0.193	0.787	0.021	1.000
1.0	0.192	0.785	0.023	1.000
1.1	0.191	0.783	0.026	1.000
1.2	0.190	0.781	0.028	1.000

Table 12: Percentage of sub-samples when requirements from Table 4 were not fulfilled

EN 14081-4 settings		
	C40	C24
	10.2%	20.4%
Adaptive settings method		
α_{ref}	C40	C24
0.7	4.1%	17.3%
0.8	4.1%	16.3%
0.9	3.1%	13.3%
1.0	3.1%	14.3%
1.1	2.0%	14.3%
1.2	1.0%	15.3%

6 Conclusions

Some experience with the adaptive settings method was gained by the presented research.

In this paper the adaptive settings method is presented as an extension to the presently used standard method. The settings from the standard are used as the initial settings, and the averages from the samples from which the standard settings were determined are used as reference mean values.

There is only one free parameter in the adaptive settings method which needs to be presumed. This is the parameter α. Firstly, the values of α for different grades is determined based on previous results (see Ranta-Maunus and Turk, 2010). These values were then scaled by a factor which ranged between 0.7 and 1.2. The results are quite surprising since it seems that the sensitivity of results with respect to factor α is very low – different values of α give almost the same results. This is one very important good characteristic of the proposed adaptive settings method.

In comparison to European standard method from EN 14081-4, number of samples which do not fulfill requirements decreases considerably when adaptive settings method is used. However, a problem remains in case of grade C24, in which the percentage of not fulfilling samples remains around 15%. Increase of initial settings is needed if higher reliability is wanted.

In this paper adaptive settings method has been shown to work as nicely as intended for Nordic grown spruce when an advanced strength grading method is used which has high coefficient of determination between strength and IP ($r^2 > 0.6$). When less accurate methods are used the applicability of the method is not obvious. A limitation of the proposed method is that regression line between strength and IP must not vary too much in the production when same initial settings are used. Variation of regression lines is known to be caused by different growth conditions, but it may also be caused by inaccuracy of grading method itself.

7 Acknowledgement

Stora Enso Timber and MiCROTEC are the owners of the strength grading data of sawmills and they kindly forwarded the data to be analysed.

8 References

Bacher M. (2009). GoldenEye-706 Quality shifts. Cost Action E53, Topic 4: Quality control in production of wood and wood based material. Meeting in Bled, Slovenia. 5p.

CEN: EN 14081-2: 2005 Timber structures – Strength graded structural timber with rectangular cross section – Part 2: Machine grading; additional requirements for initial type testing. European Committee for Standardization. 69 p., 2005.

CEN: EN 338: 2009 Structural timber – Strength classes, European Committee for Standardization, 2009.

CEN: EN 14081-4:2009 Timber structures – Strength graded structural timber with rectangular cross section – Part 4: Machine grading – Grading machine settings for machine controlled systems". European Committee for Standardization. 69 p., 2009.

Ranta-Maunus A. and Denzler J.K.: Variability of strength of European spruce. CIB-W18 Meeting 2009, paper 42-6-1.

Ranta-Maunus A., Turk G.: Approach of dynamic production settings for machine strength grading, WCTE 2010.

CIB-W18/44-5-3

INTERNATIONAL COUNCIL FOR RESEARCH AND INNOVATION IN BUILDING AND CONSTRUCTION

WORKING COMMISSION W18 - TIMBER STRUCTURES

INITIAL SETTINGS FOR MACHINE STRENGTH GRADED STRUCTURAL TIMBER

R Ziethén

SP Trätek, Borås

C Bengtsson

SP Trätek, Borås,

Linnaeus University, Växjö

SWEDEN

MEETING FORTY FOUR

ALGHERO

ITALY

AUGUST 2011

Presented by R Ziethén

V Enjily asked why C16 was not considered. R Ziethén responded that the principles would be the same regardless of grade or grade combinations. Further C16 is not common in Sweden. A Ranta-Maunus commented that he did not like the example where the material was graded to C18 alone. R Ziethén responded that this topic is frequently discussed and may be hard for the producers to change.

P Stapel and R Ziethén had discussion about the common practice of always grading to the highest grade and the question why characteristic values and yield were compared. R Ziethén confirmed that not more than two settings per combination for each location were recommended even though strength settings depended on the grade combinations.

Initial settings for machine strength graded structural timber

Rune Ziethén
SP Trätek, Box 857, SE-501 15 Borås, Sweden

Charlotte Bengtsson
SP Trätek, Box 857, SE-501 15 Borås, Sweden,
School of Engineering, Linnaeus University, SE-351 95 Växjö, Sweden

1 Introduction

The results presented in this paper come from the European research project GRADEWOOD. The main objective of the GRADEWOOD project is to enhance the use and to improve the reliability of wood as a structural material. One of the tasks in the project is to evaluate the European standard EN 14081 part 1 to 4 and to suggest possible improvements of the standard. The Standard EN 14081 consists of four parts:

14081-1	General requirements for strength grading
14081-2	Derivation and supervision of settings using the machine control method
14081-3	Derivation and supervision of settings using the output control method
14081-4	Approved settings for existing grading machines

This paper describes an alternative to the procedure described in EN 14081 part 2, the so called "Cost matrix method", see Rouger (1997).

2 Background

2.1 Complexity

The method described in EN 14081-2 is complicated and it is also an issue of several interpretations of the text written. Because of this a special task group, TG1, was established to interpret the standard and to assess reports with settings for strength grading machines based on these interpretations.

Still today, almost 15 years after the first discussions about the present method there is an ongoing change of requested information and provisions for sampling and calculations. Today it is not possible for anyone to have settings approved based on a report in accordance with the valid standard.

The present standard has a number of major weaknesses:

- Several different settings for the same grade

- The reference, “optimum grading” in the standard is only clearly defined for single grades
- The method is sensitive to very small deviations and outliers within a sub sample
- The method is sensitive to very small deviations between the sub samples

Weaknesses with the present standard EN 14081 was also presented by Bengtsson and Fonselius (2003).

2.2 Settings based on the 5th-percentile

The requirements in EN 338 for the grade determining properties are based on 5th-percentile calculated by ranking for strength and for density and on the mean value for MOE. The determination of settings in EN 14081-4 follows this and the calculations are based on the 5th-percentile of the strength for each grade in each grade combination. A result of this is several settings for each grade. Since the latest revision of EN 14081-4, in 2009 approximately 60 new so called ITT-reports, each containing one or more new tables with settings, have been issued. The published EN 14081-4 contains 63 tables with settings. As an example, spruce from the Nordic countries has 7 different settings for C18, the settings vary from 15,5 MPa up to 23,1 MPa, depending on grade combination. This leads to confusion. It is difficult to explain for producers and users of graded timber that different settings can be used depending on if the strongest material is included or if it is graded to a higher grade.

Another problem connected to the use of the 5th-percentile as grading criteria occurs for low strength grades. The 5th-percentiles for ungraded material from some European countries are shown below in Table 1 (test results from GRADEWOOD).

Table 1 5th percentile for the strength of material from five European countries.

Source country	**5th-percentile**	**Comment**
Sweden	23,0 MPa	Pine
Poland	20,0 MPa	Spruce
Finland	26,9 MPa	Pine, calculated from tension tests
Slovenia	21,1 MPa	Spruce
France	23,8 MPa	Spruce

The calculated 5th-percentile for these samples are all above the required strength for grade C22, 19,6 MPa. It means that all pieces will be accepted as C22 or lower and almost all pieces as C24. Without additional requirements there is almost no grading and even very weak pieces will be accepted.

A third disadvantage of the use of the 5th-percentile is connected to the determination of percentile values. When the number of observations decrease in the sample from which the 5th-percentile is calculated the result is more and more unreliable. When settings are determined for a grade combination it is often difficult to get enough of pieces in some grades to obtain reliable percentile values. Even with large data sets with more than 1000 tested pieces it is common to have less than 40 pieces in a grade in a grade combination, such as for example grade combination C18 – C24. In Figure 1 it is shown some examples of how the calculated percentile varies when the number of pieces is decreased. The data sets used in the calculations are ranked with respect to MOE and the corresponding strength values are used in the determination of the percentile.

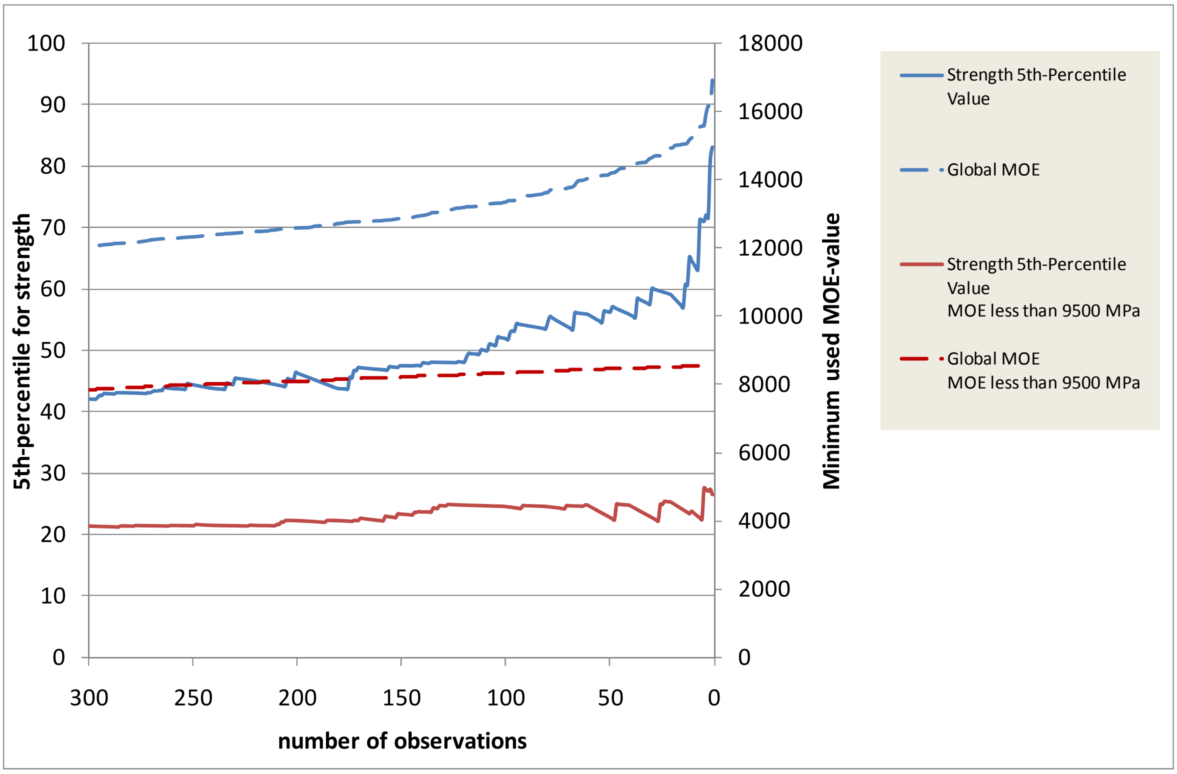

Figure 1 Variation of calculated percentile value as a function of the number of used pieces, blue lines show the results when all pieces have been used for the calculation of percentiles. Red lines show results when only pieces with MOE less than 9500 MPa have been used.

It can be seen that the reliability of the calculated percentile decreases when the number of used pieces is less than 100 when all pieces are used in the calculations. If only pieces with a MOE less than 9500 MPa is used, which simulates a grading of a combination of two grades the reliability of the calculated percentile decreases. So there is a severe problem with the 5th-percentiles that are used as a basis for the determination of settings.

2.3 Optimum grading as a grading reference

The optimum grading in EN 14081-2 is based on destructive bending or tension tests according to the European standards EN 408 and EN 384 and it serves as a "key" for the cost matrix analysis which is central for the determination of settings. The optimum grading is defined to be "the highest grade, of those for which settings are required, to which a piece of timber can be assigned, such that the grade determining properties of the graded sample will meet the values required for the grade". This definition is unambiguous only if one grade and rejects are graded. When a combination of grades is graded a higher number of pieces in the highest grade also results in a higher number of rejects. In Table 2 the results from optimum grading based on two different approaches can be seen. In the first approach as many pieces as possible was put into the highest grade, grade 1. In the second approach the number of rejects were minimised. Which of these two approaches that fits best to the definition or if both are in line with the intention can of course be discussed.

Table 2 Optimum grading using two different approaches. The first approach maximising the yield in the highest grade and the second approach minimising the rejects.

Grade	Number of specimens	
	First approach	Second approach
Grade 1	704	305
Grade 2	25	644
Reject	432	212

So far the optimum grading has been interpreted to be optimised from the highest grade and a higher number of rejects has been accepted although the yield from this grading has not been in line with the demands from the producers. This interpretation will have a significant effect on the results from the cost-matrix analysis and thus a major effect on the determined settings.

2.4 Sensitivity

As presented in Table 1 the 5th-percentile for the ungraded material can be close to or above the required strength. For these cases an additional requirement in EN 14081-2 is that at least 0,5% or 5 pieces from the used sample must be rejected in each grade combination. For the most common commercial grades, C16, C18 and C24, this is generally the used determining requirement. For these grades more than 99% of the tested material is not at all used for the determination of the settings. Settings determined by this requirement suffer from a not negligible effect from both outliers and random effects on the very low tail of the distribution.

Also for other grades the settings are highly depending on a few observations. One example (based on real data) shows that a change in density of 2 to 4 kg/m^3 for 7 out of 700 pieces in a sample can change the settings more than 5% and change the yield when grading with almost 10%. The economic effect of this change is large and can be the difference on the market between a competitive and a useless grading machine.

This high sensitivity of the method in EN 14081-2 also increases the problems to define the requirements when a sub sample is representative for the graded area. Not only the descriptive statistics, mean value, standard deviation and correlation between variables, but also the presence of single outliers is important.

2.5 Selection of sub samples

The method is sensitive to the selection of sub samples and the effects of adding and/or substituting sub samples are not always easy to predict. As example some test results from the GRADEWOOD project will be used. Four sub samples from Slovenia, containing almost 1200 pieces and two sub samples from Slovakia and Romania containing 300 pieces are chosen. Although the samples come from a limited area in Europe there seems to be a systematic difference between the material from Slovenia and the material from Slovakia and Romania. Both the strength distribution and the relation between stiffness, strength and density differs. Taking these differences into account the settings for Slovakia and Romania ought to be more conservative than the settings from Slovenia. In Table 3 the settings for Slovenia are presented and in Table 4 the settings when two sub samples from the Slovenian material containing approximately 300 pieces have been replaced by the two sub samples from Slovakia and Romania.

Table 3 Settings for some grades and grade combinations determined from four sub samples from Slovenia, red settings are lower than the minimum allowed setting blue settings are raised due to cost matrix requirements.

Grade	C40-C24	C30-C18	C27-C18	C24	C18
C40	30,8				
C30		23,7			
C27			21,6		
C24	**19,5**			15,9/18,0	
C18		15,9/18,0	20,2		15,9/18,0

Table 4 Settings for some grades and grade combinations determined from four sub samples from Slovenia, Slovakia and Romania, red settings are lower than the minimum allowed setting, blue settings are raised due to cost matrix requirements.

Grade	C40-C24	C30-C18	C27-C18	C24	C18
C40	31,3				
C30		26,5			
C27			23,7		
C24	**21,1**			17,5	
C18		15,8/17,5	17,6		15,7/17,5

From the settings derived above the following remarks can be made:

- The settings for the grades C27, C30 and C40 are just as expected highest for the sample containing pieces from Slovakia and Romania.
- The settings for the lower grades are lower for the sample containing pieces from Slovakia and Romania because the weaker material permits to use a lower minimum setting (0,5% reject from the samples).
- The setting for C18 in combination with C27 is considerably lower for the sample containing pieces from Slovakia and Romania because a higher setting is required for C27.

So, by adding weaker sub samples from Slovakia and Romania, that used by their own would result in higher settings, the settings for both Slovenia, Slovakia and Romania can be less conservative for the most common commercial grades.

The standard has no requirements when the sub samples no longer can be combined. With additional tests from different areas of Europe we can expect that these cases will increase as producers want to have common settings covering larger and larger parts of Europe.

3 The proposed new method

3.1 General

The examples above show some severe shortcomings of the present standard. An alternative to the method described in the standard is needed, a method that uses more of the information given by the test material used for deriving the settings. One alternative is linear regression, see Figure 2. Linear regression is a simple well defined statistical tool, see for example Jørgensen (1993). Some requirements that must be fulfilled by a new standard method is:

- Robust settings, different machines using the same principles should have the same settings providing a fair competition between machine types.
- The settings must produce reliable structural timber that fulfils the requirements.
- Easily understood. According to the harmonised standard the responsibility for the initial testing and determination of settings is the producers. The standard must support this.
- Transparent, the notified bodies who are responsible for the supervision of grading machines must be able to evaluate the determination of settings.

3.2 Linear regression

Depending on the assumed distribution of the variables the regression can be used on linear or logarithmic values. Linear values imply a constant standard deviation for the variables and logarithmic values imply a constant coefficient of variation for the variables. It has been found that the best fit with tested values is a constant coefficient of variation for strength and modulus of elasticity and a constant standard deviation for density. The principles and equations are the same in both cases and the result can be written in the form given by

Equation (1): $y_i = \hat{\beta}_0 + \hat{\beta}_1 x_i$ (1)

The method was presented Ziethén and Bengtsson (2009 and 2010) and it is only repeated shortly here.

3.3 Randomly distributed errors

The fitness of the regression model is often described by the coefficient of determination, r². A more informative method is to study the residual errors, the residual error, $e_{i,}$ is given by Equation (2): $e_i = Y_i - \left\lfloor \hat{\beta}_0 + \hat{\beta}_1 x_i \right\rfloor$ (2)

These errors can have a number of different causes, as example:

- Measurement errors in any of the two variables
- Imperfection of the model
- Not determined variables with an effect on the measured variables

The errors can be assumed to be normally distributed around the regression line, see Figure 2.

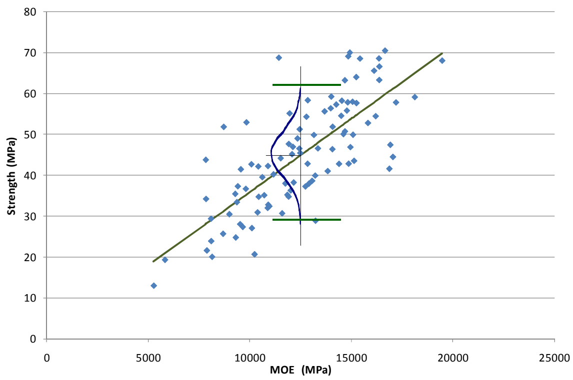

Figure 2 Linear regression with normally distributed residual errors.

The differences between the observed values and the values calculated according to the regression model, the residual error, give also a certain uncertainty to the regression model. The regression gives only the model that fit best to the observed values within the sample. So for both the constant and the scale factor there is an interval that can be calculated based on the errors. With an increasing number of observations the estimation of the model is better and better and the confidence interval for the regression is decreasing.

3.4 Expanded prediction interval

Grading of timber consists of another type of statistical challenge: to predict a future not yet observed observation. We will never know the true value but with increased sample size we can estimate the value with higher precision. The variance for the predicted value can be determined from the residual errors. From the variance we can calculate an interval for the predicted value. The prediction interval shows big similarities with the confidence interval but it is expanded with a constant 1 under the root sign. If the number of the observations used for the regression is large the equation for the prediction interval is given by Equation (3).

$$y^*(x) = \hat{\beta}_0 + \hat{\beta}_1 x \pm \hat{\sigma} \cdot t \qquad (3)$$

Where:

σ is describing the residual errors
t is the Student's t-factor

The expanded prediction interval together with the confidence interval is shown in Figure 3.

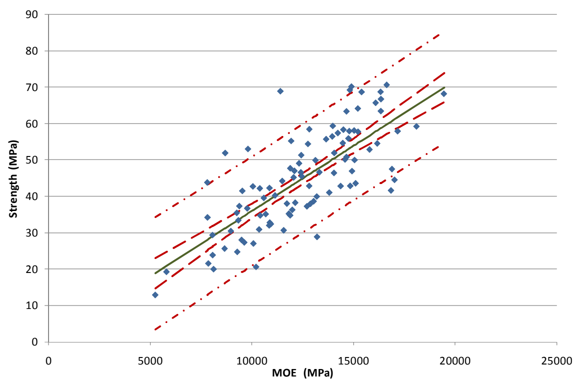

Figure 3 Regression line with confidence interval and the expanded prediction interval for calculations based on linear values.

4 Analysis of the new method

4.1 General

An analysis of the prediction limit method was presented by Ziethén and Bengtsson (2009 and 2010). The method was shown to be independent of mean values of the samples and to give more conservative values for grading results with weak correlation to grade determining properties.

4.2 Determination of the prediction limit level

In EN 338 the characteristic values for the grades are given as 5th-percentiles (strength, density) or mean value (stiffness). The prediction limit is related to a single observation and not to percentiles of a sample. It will therefore be necessary to find a level for the prediction limit where the 5th-percentile fulfills the requirements in EN 338. Based on the results from timber from Slovenia, tested within GRADEWOOD, the sliding 5th-percentile has been compared to different prediction limit levels. In Figure 4 the comparison between the sliding 5th-percentile and the 10% prediction limit is presented.

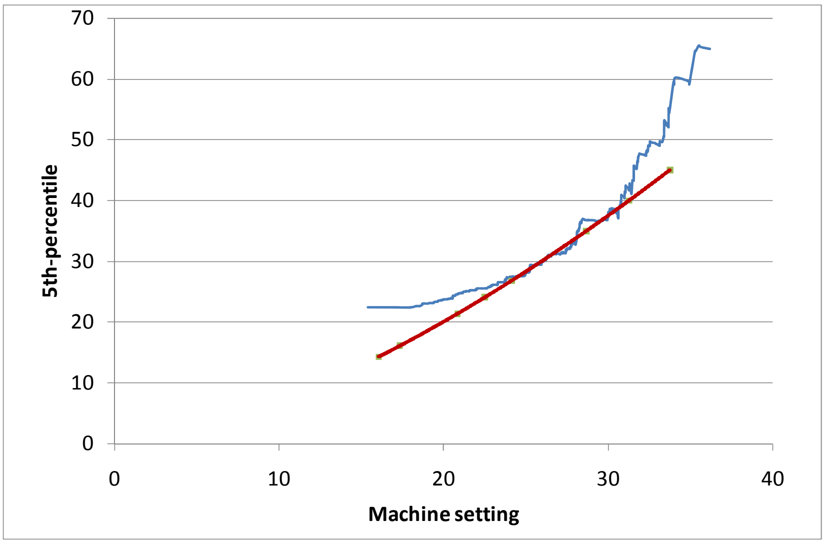

Figure 4 The sliding 5th-percentile for bending strength of Slovenian spruce (blue line) and the 10% prediction limit line calculated from the same material (red line).

For single grades, the 10% prediction limit fits well to the percentile values. For grades C24 and lower as well as for grades C35 and higher the prediction limit is increasingly conservative. For these grades, most important the lower, it will be necessary to adjust the settings in some way. This could be done by choosing a different prediction limit level for these grades, to divide the linear regression models into parts or by making a manual adjustment of the prediction limit. For the lowest grade in grade combinations it will be necessary to choose a more conservative prediction limit level to fulfil the required percentile values. The 5% prediction limit has shown to give reasonable results. The problems with the low and high grades remain and must be solved in the same way as for single grades. The same method as shown above for grading machines using one indicating property can be used for machines using multiple indicating properties. With different indicating properties for strength, MOE and density the combined grading result must be compared to the requirements, the prediction limit level for each of the IPs must then be less conservative. If not, the percentile values will be higher than required and these grading machines that should be more accurate in the grading process will be discriminated with a too low yield.

4.3 Settings for Slovenia, Slovakia and Romania derived by the prediction limit method

In Table 3 and Table 4 it was shown how the settings changed when two sub samples from Slovenia was substituted by two sub samples from Slovakia and Romania. The same material was used for calculations of settings using the prediction limit method. In Table 5 and Table 6 the results from these calculations are presented.

Table 5 Settings derived by prediction limit calculations for Slovenia.

	Setting for a single grade or the high grade in a combination	Setting for the low grade in a combination
C40	30,9	
C30	24,1	
C24	20,9	22,1
C18	17,3	18,4

Table 6 Settings for some grades and grade combinations derived by prediction limit calculations with four sub samples from Slovenia, Slovakia and Romania.

	Setting for a single grade or the high grade in a combination	Setting for the low grade in a combination
C40	32,2	
C30	25,8	
C24	21,1	22,8
C18	17,6	18,7

It can be seen that due to the difference in the relation between machine readings and required properties in the standard between Slovenia and Slovakia/Romania the settings are higher for the combined area. Differences in the correlation between properties have an influence on the settings. In this case the differences are logical and therefore easier to understand and foresee. The differences have an effect on all grades in the same direction but they have a larger impact on the high strength grades.

4.4 Requirements on data sets combined to derive settings

The data used in the calculation will have a common influence on the settings, pieces with lower strength for the same indication property will if they are mixed with pieces with a higher strength result in settings that are too unconservative. Therefore there must be requirement for the sub samples that are allowed to be used together to determine settings. If the difference between the models is too big they simply do not belong to a common population and shall therefore not be used to determine common settings.

5 Suggestions for a revised grading standard

The present standard, EN 14081, has shown to suffer from a number of severe shortcomings that result in settings that are too strongly influenced of random effects. There is a need for another method to determine settings and one suitable method is the prediction limit method. The prediction limit method can deal only with machines using a mathematical model between machine reading (IP) and the grade determining properties. This is a weakness compared to the present standard. However, today no machines based on systems without a model are in use but the item has to be taken into account. The main advantage with the method is that it is based on linear regression and therefore the effect of outliers will decrease and the settings will be far more robust and provide a fair competition between grading machine producers.

This proposal is so far a result from the research project GRADEWOOD and a number of questions have to be solved during a standardisation process. However, the answers to many of these questions can be found in the results from the GRADEWOOD project.
Some questions that have to be solved:

- The 5^{th}-percentile of different grades can be fulfilled with a correct choice of prediction limit level. The 10% prediction limit for single grades or for the highest grade in a combination and the 5% prediction limit for lower grades in a combination have so far shown to be good solutions.
- Other (less conservative) levels for the prediction limit will be necessary for grading devices with multiple machine readings (IPs).
- Requirements on sample sizes and regression models will be needed when samples are combined.
- Too conservative settings for low and maybe also for high grades must be dealt with.
- Restrictions may be needed for the choice of grade combinations. A reasonable restriction is to have a difference of more than 5 MPa between the required strength of the different grades.

The prediction limit method for derivation of initial settings is, with advantage, combined with continuous monitoring of the settings during the grading process in the sawmill. In this way the settings can be changed adaptively according to variations in incoming raw material that are graded, see Turk and Ranta-Maunus (2011).

6 Acknowledgement

This work was mainly carried out within the GRADEWOOD project, WoodWisdom-Net Project 112006B and Vinnova Dnr 2007-0126. In addition financial support is given by SP´s strategic competence funds. The financial support is gratefully acknowledged.

7 References

Bengtsson C., Fonselius M.: Settings for strength grading machines – evaluation of the procedure according to prEN14081, part 2, proceedings paper 36-5-1, Colorado, USA, 2003.

EN 384:2010 Structural timber - Determination of characteristic values of mechanical properties and density

EN 408:2010 Timber structures - Structural timber and glued laminated timber - Determination of some physical and mechanical properties

EN 338:2009 Structural timber - Strength classes

EN 14081-1:2005+A1:2011 Timber structures - Strength graded structural timber with rectangular cross section - Part 1: General requirements

EN 14081-2:2010 Timber structures - Strength graded structural timber with rectangular cross section - Part 2: Machine grading; additional requirements for initial type testing

EN 14081-3:2005 Timber structures - Strength graded structural timber with rectangular cross section - Part 3: Machine grading; additional requirements for factory production control

EN 14081-4:2009 Timber structures - Strength graded structural timber with rectangular cross section - Part 4: Machine grading - Grading machine settings for machine controlled systems

Jørgensen, B.: The theory of linear models, CRC Press, 1993.

Rouger, F.: A new statistical method for the establishment of machine settings, CIB W18, proceedings paper 30-17-1, Vancouver, Canada, 1997.

Turk, G., Ranta-Maunus, A.: Adaptive production settings method for strength grading, CIB W18, proceedings paper 44-5-2, Alghero, Italy, 2011

Ziethén, R., Bengtsson C.: Machine Strength Grading – a New Method for Derivation of Settings, CIB W18, proceedings paper 42-5-1, Dübendorf, Switzerland, 2009

Ziethén, R., Bengtsson C.: Machine strength grading – prediction limits – evaluation of a new method for derivation of settings, WCTE, Riva de Garda, 2010

Ziethén, R., Bengtsson C.: Machine strength grading – prediction limits – evaluation of a new method for derivation of settings, Cost E53, Edinburgh 2010

CIB-W18/44-6-1

INTERNATIONAL COUNCIL FOR RESEARCH AND INNOVATION IN BUILDING AND CONSTRUCTION

WORKING COMMISSION W18 - TIMBER STRUCTURES

IMPACT OF MATERIAL PROPERTIES ON THE FRACTURE MECHANICS DESIGN APPROACH FOR NOTCHED BEAMS IN EUROCODE 5

R Jockwer

R Steiger

EMPA, Dübendorf

A Frangi

J Köhler

ETH Zürich, Institute of Structural Engineering IBK

SWITZERLAND

MEETING FORTY FOUR

ALGHERO

ITALY

AUGUST 2011

Presented by R Jockwer

H Blass commented that different size of specimens may influence findings and asked if size effects were considered. R Jockwer responded that it was not yet studied. I Smith added that member thickness could influence fracture energy and commented that although the Canadian approach appeared to look like shear strength design, in effect it was just the format of the equation. I Smith also commented that in service behaviour would also be important not just short term behaviour.

Impact of material properties on the fracture mechanics design approach for notched beams in Eurocode 5

Robert Jockwer[1,2)]

René Steiger[1)]

Andrea Frangi[2)]

Jochen Köhler[2)]

[1)] EMPA, Swiss Federal Laboratories of Materials Science and Technology, Wood Laboratory, Dübendorf, Switzerland

[2)] ETH Zürich, Institute of Structural Engineering IBK, Zürich, Switzerland

1 Introduction

At notch corners stress concentrations occur due to the sudden change in cross section. Shear stresses and tensile stresses perpendicular to grain are leading to brittle failure of the notch. Therefore special design considerations are needed to guarantee structural safety.

Generally notches should be avoided. If this is not possible they should be reinforced in an adequate way to prevent failure. Within a small range of geometrical properties the design of unreinforced notched beams is possible if the decrease in strength is taken into account. This decrease in strength due to notches has been known for long time. Hence, several design approaches were published, leading to, however, different results. The present paper therefore aims at analysing the impact of material properties on the variation in strength of notches.

1.1 Design approaches for notched beams

In 1935 Scholten [1] developed an empirical design approach with a reduction of the strength proportional to the notch ratio α (Figure 1). A bilinear reduction of strength was determined by Mistler [2] in 1979 from experimental tests and from a study on a stochastic model. Leicester studied the theoretical stress distribution at notches [3] at the beginning of the 1970's. This led to the approach in the Australian Standard AS 1720 [4], which takes into account also size effects.

At the end of the 1980's Gustafsson developed a design approach for notched beams based on fracture energy [5]. The application of the fracture mechanic concept in timber engineering [6] was studied and later Gustafssons approach was implemented in Eurocode 5 (EC5) [7].

1.2 Development of the EC5 design approach

Gustafsson described the equlibrium of energy at a notched beam during crack growth. By rearranging the equation the average shear stresses were separated from a term including material properties and geometric parameters (Equation (1)).

$$\frac{V}{b\alpha h} = \frac{\sqrt{\frac{G_f}{d}}}{\sqrt{0.6\left(\alpha-\alpha^2\right)\frac{1}{G_{xy}} + \beta\sqrt{6\left(\frac{1}{\alpha}-\alpha^2\right)\frac{1}{E_x}}}} \qquad (1)$$

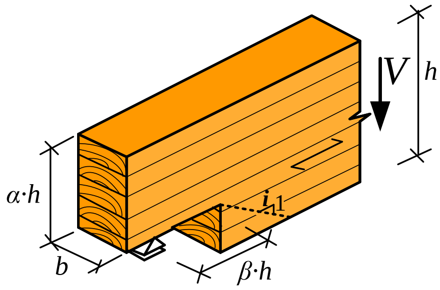

Figure 1: Notched glulam beam

The beam's height h, its notch ratio α and notch length ratio β, as specified in Figure 1, are the geometric parameters in the model. Fracture energy G_f, modulus of elasticity (MOE) E_x and shear modulus G_{xy} reflect the material properties.

Fracture energy is the only strength related material property in Equation (1). Gustafsson proposed that it is sufficient to take into account only the part of opening of the crack flanges (mode 1), since crack opening is the main failure mode ocurring at the notch. Hence, the general fracture energy G_f depending on the stress state at the crack tip was replaced by the fracture energy of mode 1 $G_{f,1}$ for crack opening only.

On the left hand side of Equation (1) the action effect and on the right hand side the resistance during crack growth can be identified. The resistance of the notch on the right hand side of Equation (1) increases for large notch ratios α. For a notch ratio of 1 the resistance approaches infinity since no notch exists in that case. However, the resistance is limited by the shear capacity of the beam. Hence, Equation (1) was extended by the shear strength f_v and the resulting reduction factor k_v was limited to an upper value of 1 (Equation (2)). The material property values can be summarised in two material constants A and B (Equation (3)). Riberholt, Enquist et al. [8] determined an additional term in a large test series taking into account notch taper i.

$$\tau = 1.5\frac{V}{b\alpha h} = f_v\, k_v \quad \text{with} \quad k_v = \min\left[1; \frac{A\left(1+\frac{1.1 i^{1.5}}{\sqrt{h}}\right)}{\sqrt{h}\left(\sqrt{\alpha-\alpha^2} + B\beta\sqrt{\frac{1}{\alpha}-\alpha^2}\right)}\right] \qquad (2)$$

and $$A = 1.5\sqrt{\frac{G_{f,1}E_x}{f_v^2}}\sqrt{\frac{G_{xy}}{0.6E_x}} \quad , \quad B = \sqrt{10\frac{G_{xy}}{E_x}} \qquad (3)$$

In standards specifying material properties as e.g. EN 338 [9] and EN 1194 [10] all material properties except fracture energy are given to apply Equation (2) for the relevant strength classes of timber. For the implementation of Equation (2) in EC5 Larsen and Gustafsson collected the values of fracture energy derived from experimental tests on different wood species and timber grades [11]. For densities in a range of $300\ \text{kg/m}^3 \le \rho \le 450\ \text{kg/m}^3$ Larsen et al. [12] suggested an approximation based on a linear regression of the results [11]:

$$G_{f,1} = 0.65\rho\,. \qquad (4)$$

Using this relationship and further test results on notched beams from literature the material constants were found to be $A = 5$ for solid timber and $A = 6.5$ for glulam and $B = 0.8$ for both solid timber and glulam [12]. In EC5 the material constant A is denoted k_n.

1.3 Test results from literature

The material constants found by Larsen et al. are used in different standards and handbooks for the design of timber structures like EC5 [7], DIN 1052 [13] and SIA 265 [14]. However, all these standards assume different material property values, especially different values of shear strength. Furthermore the characteristic (fifth percentile) values of shear strength were subject of permanent modifications in the recent years. In Table 1 characteristic values of shear strength are summarized for common European strength grades of solid timber and glulam. In Figure 2 the resulting estimated load bearing capacities are compared with capacities determined in experimental tests by Franke [15] and Rautenstrauch et al. [16].

Table 1: Charakteristic values of shear strength $f_{v,k}$ in different standards.

Standard		$f_{v,k}$ [N/mm^2]	
		C24	GL24h
EC5	EN 338 [9]	4	-
	EN 1194 [10]	-	2.7
	prEN 14080 [17]	-	3.5
DIN 1052 [13]		2	2.5
SIA 265 [14]		2.5	2.7

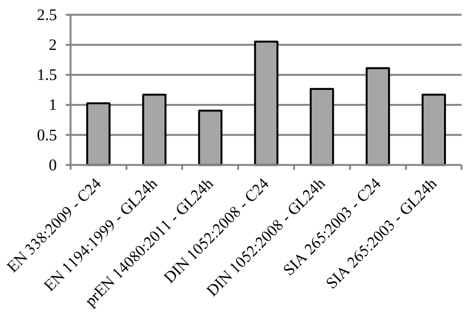

Figure 2: Ratio of mean notch capacity from tests [15] (n= 40) and [16] (n= 32) to calculated characteristic (fifth percentile) notch capacity according to different standards.

The ratios between mean experimental results and estimated notch capacity on the characteristic level in the order of 1 for EC5 are clearly too small and, hence, the notch capacity is overestimated. The ratios determined according to the German and Swiss standards DIN 1052 and SIA 265 are higher than according to EC5. However, it is not clear if the targed safety is complied by the estimated capacities.

Hence, it is to be identified to what extend the material properties take an impact on the notch capacity according to Equation (2) and if the material constants need to be updated to guarantee the desired safety level the standards are based on.

2 Impact of material properties on the EC5 design approach

For the application of Equation (2) in the design of structures according to EC5 material property values for shear strength f_v, MOE E_0 and shear modulus G are specified in material standards (for solid timber in EN 338 [9], for glulam in EN 1194 [10] and in the preliminary standard prEN 14080 [17]). Besides the given values material properties can be determined from experimental tests as specified in EN 408 [18]. Information about suitable distribution functions of the material properties can be found in part 3.5 of the JCSS Probabilistic Model Code [19]. However, fracture energy values are not specified in all these standards.

When evaluating the sensitivity of Equation (2) regarding the influence of any material property, mean values and variations of these properties have to be estimated and appropriate distribution functions have to be chosen.

2.1 Specification of material properties in standards and codes

Solid timber and glulam are assigned to strength classes as given in EN 338, EN 1194 and prEN 14080 according to the basic material properties bending strength (MOR), bending modulus of elasticity (MOE) and density. Other property values are not directly determined but rather are derived from these three properties using prescribed relationships.

- **MOE**: JCSS assigns MOE to be lognormal distributed with a coefficient of variation COV = 13% for both solid timber and glulam. This corresponds to the ratio between fifth percentile and mean value of MOE in grain direction $E_{0,g,0.05}$ / $E_{0,g,mean}$ = 0.81 given for glulam in EN 1194 assuming lognormal distribution. The ratio of 0.67 for solid timber in EN 384 leads to a higher COV = 23%.
- **Density**: Mean values of density in the range of ρ_{mean} = 390-480 kg/m^3 are given for common strength classes between C20 and C35 in EN 338. JCSS assumes density to be normal distributed with COV = 10% which is in line with the ratio of mean and fifth percentile values given in EN 338. The mean and fifth percentile values of density with ρ_{mean} = 370-500 kg/m^3 for strength classes GL20h to GL32h according to prEN 14080 result in COV = 5-7%, which is lower than the variation stated by JCSS.
- **Shear strength**: For glulam in EN 1194 and for solid timber in the 2004 version of EN 384 [20] a relationship between the characteristic values of shear strength and tensile strength of the lamella is stated. Glos and Denzler could not confirm this relationship [21, 22]. In prEN 14080 and in the current version of EN 384 [23] constant values therefore are given for shear strength of glulam and solid timber respectively. Relationships between mean and characteristic values of shear strength are not given in the cited standards. JCSS assumes a lognormal distribution with a coefficient of variation COV = 25% for solid timber and COV = 15% for glulam [19].
- **Shear modulus**: The shear modulus is correlated to MOE. In EN 384 and EN 1194 a ratio between MOE and shear modulus of 16 is specified. In prEN 14080 a constant value of shear modulus $G_{g,mean}$ = 650 N/mm^2 is assumed. This leads to ratios $E_{0,g,mean}$ / $G_{g,mean}$ between 12.3 and 21.5 since MOE is increasing for higher strength classes. JCSS assumes the same distribution and variation for MOE and shear modulus. With the lognormal distribution the ratio $G_{g,0.05}$ /$G_{g,mean}$ = 5/6 given in prEN 14080 leads to a COV = 11%.
- **Correlations between material properties**: For the correlation of all these material properties a medium correlation (0.6) is postulated in [19] except for the correlation between MOE and shear strength. Here only low correlation (0.4) is assumed.

Table 2: PDF and COV of material properties.

Material property	Distribution function [19]	Solid Timber		Glulam	
		COV [19]	COV EN	COV [19]	COV EN
MOE	Lognormal	13%	23%	13%	13%$^{1)}$ 11%$^{2)}$
Density	Normal	10%	10%	10%	5-7%$^{2)}$
Shear strength	Lognormal	25%	-	15%	-
Shear modulus	Lognormal	13%	-	13%	11%$^{2)}$

$^{1)}$ EN 1194:1999 $^{2)}$ prEN14080:2011

Table 3: Correlation of material properties.

Property	E_0	ρ	f_v	G
MOE	-	0.6	0.4	0.6
Density	0.6	-	0.6	0.6
Shear strength	0.4	0.6	-	0.6
Shear modulus	0.6	0.6	0.6	-

2.2 Fracture energy

Different test methods exist to determine fracture mechanical properties of timber. Tests on compact tension (CT) specimens, double cantilever beams (DCB) or a tension specimen with a slit are used to measure fracture toughness or energy release rates [24-26]. A simple method for determining fracture energy is making use of a single edge notched beam (SENB) specified in a Draft Standard of CIB-W18 in Annex B of [11] and [27], also known as Nordtest method. Fracture energy can be calculated from load displacement curves without the need for detailed information about elastic properties.

2.2.1 Results from tests on SENB according to the Draft Standard CIB-W18

Results from tests on SENB according to the Draft Standard CIB-W18 [11] are summarized in Table 4. Values were selected based on mean densities in the range of ρ_{mean} = 369-506 kg/m^3 reflecting the densities given in the material standards cited above.

A correlation between density and fracture energy can be found. However, this correlation is low for the observed range of densities being of relevance for structural applications [11, 28]: The standard deviation of the linear regression of the data in Figure 3 (σ_ε = 54 N/m) is nearly identical to the standard deviation calculated for the whole data without regression (σ_ε = 55 N/m). Hence, no correlation of fracture energy and density is assumed in the further parts of the present study.

Other authors found values different from those given in Table 4. Smith explains his values ($G_{f,1,mean}$ = 435 N/m with ρ_{mean} = 362 kg/m^3 at a moisture content (MC) of 12%), being rather high compared to other values, with the impact of the careful drying from green wood [29]: Fast kiln drying can produce cracks and reduces the values of fracture energy. This could explain the low values of fracture energy determined by Franke [15] ($G_{f,1,mean}$ = 171 N/m) and Daudeville [30] ($G_{f,1,mean}$ = 205 N/m) for commercial timber.

However, no clear effect of MC can be identified. Smith [29] found highest fracture energy values for MC = 18%, whereas Rug [31] found decreasing values for MCs higher than 12%. However, MCs lower than 12% provoke low values in fracture energy, since cracks arise during storage at low r.H. [11] or during cylic climate at low level [29].

Other parameters with impact on fracture energy are knots and the growth ring orientation. Knots severly increase fracture energy, due to their dowling effect [8]. Hence, most tests were done at carefully selected clear wood. For fracture surfaces tangentially to the growth rings higher values were determined than radialy to the growth rings [24, 30].

2.2.2 Mean value, distribution and variance of fracture energy

Parameters for distribution functions fitted to the fracture energy values of individual data from Table 4 are summarized in Table 5 . A lognormal distribution with a mean value of $G_{f,I,mean}$ = 300 N/m and a COV = 20% is used for the further study, the fifth percentile value then being $G_{f,I,0.05}$ = 216 N/m. A 3-parametric Weibull distribution in line with the study [28] describes the data well. However, it is not used here since it inhibits fracture energy values lower than the location parameter and hence is not adequate for the prediction.

For a mean density of $\rho_{g,mean}$ = 420 kg/m^3 the regression of mean values of fracture energy by Larsen and Gustafsson leads to a similar result of $G_{f,I,mean}$ = 291 N/m as in Table 5 whereas for lower or higher densities the mean values deviate considerably. The proposed simplification for characteristic values in Equation (3) for densities in the range of $\rho_{g,c}$ = 300 – 450 kg/m^3 is not adequate to describe the fracture energy: For a density as asked for C24 considerably higher fracture energies are resulting. A correlation of fracture energy with other material parameters could not be found in literature. However, a coefficient of correlation of 0.2 (very low correlation) can be assumed which is lower than that of tensile strength perpendicular to the grain and all these other properties [19].

Table 4: Values of fracture energy $G_{f,I,mean}$ from literature.

Reference:		***n* [-]**	**ρ_{mean} (COV) [kg/m³]**	**$G_{f,I,mean}$ (COV) [N/m]**
Larsen and Gustafsson [11]	Annex 1	37	426 (10.3%)	323 (14.9%)
	A. 4.3	6	369 (1.5%)	291 (12.1%)
	A. 8	62	458 (8.15%)	286 (20.3%)
	A. 10	29	506 (10.3%)	337 (15.3%)
	A. 11	12	503 (10.8%)	263 (15.9%)
Riberholt et al. [8]	Solid Timber	88	415 (7.9%)	290 (17.5%)
	Glulam	43	436 (8.6%)	311 (18%)
Gustafsson [5]		14	467 (11%)	294 (17.5%)
Jockwer [32]		48	478 (9.5%)	343 (18.2%)
Aicher et al. [28]		83	457 (5.3%)	277 (27.2%)
Gustafsson et al. [33]		-	475 (8.8%)	272 (15.4%)

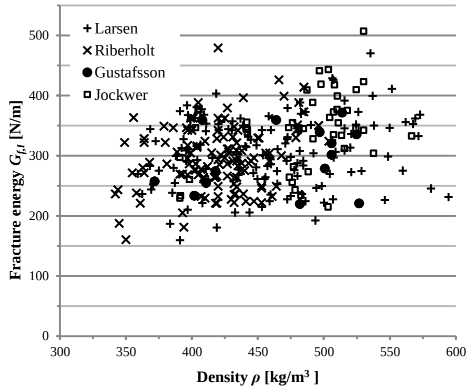

Figure 3: Fracture energy $G_{f,I}$ in dependency of density ρ from test results [5, 8, 11, 32] listed in Table 4.

Table 5: Distribution parameters for fracture energy.

	Individual data from Table 4			**Aicher [28]**
	Normal	**Logn.**	**2p-Weibull**	**3p-Weibull**
$G_{f,I,mean}$ [N/m]	306	**306**	305	283
Std [N/m]	58.1	**60.2**	62.7	74.9
COV	19%	**19.6%**	20.5%	26.5%
$G_{f,I,0.05}$ [N/m]	210	**218**	195	176

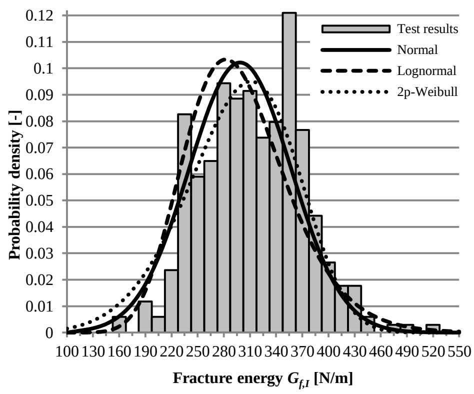

Figure 4: Distribution of fracture energy $G_{f,I}$ from test results [5, 8, 11, 32] listed in Table 4 and PDFs from Table 5.

2.3 Impact of varying material properties on the EC5 design approach

The sensitivity of material properties in Equation (2) was analysed by means of the structural reliability software COMREL [34] using the values and distributions listed in Table 6. The impact of MOE and shear modulus depends on the ratios α and β as can be seen in the denominator of Equation (1). The minimal notch length necessary for preventing compression failure perpendicular to the grain is in the range of $\beta = 0.1$ - 0.5 (GL24h) and $\beta = 0.2$ - 0.7 (C24), respectively. Larger notch length should be prevented since notch capacity is reduced considerably. Suitable notch ratios are not less than $\alpha = 0.5$ for solid timber and higher for glulam. Depending on the structure smaller notch ratios lead to uneconomical design due to the considerable decrease in beams capacity.

In the sensitivity analysis weighting factors α_i are determined, giving information about the relative impact of the respective parameter on the variation of notch capacity when calculated according to Equation (2) and on the related reliability. Fracture energy is the material property with the most impact on notch capacity as can be seen in Figure 5 and Figure 6. The impact of variations in both MOE and shear modulus is almost constant for different notch ratios α and notch length ratios β. However, depending on the values α and

β the impact is differently distributed in between MOE and shear modulus: the impact of shear modulus increases for larger α and smaller β, respectively. In the practical range of notch ratios $0.5 \leq \alpha \leq 1.0$ the influence of shear modulus and MOE is mostly depending on notch length ratio β.

It has to be taken into account that shear strength originally was not part of Equation (1). Equation (2) contains shear strength both in nummerator and denominator. That is why shear strength has no influence on the estimated notch capacity.

The ratio of MOE and shear modulus has only minor effect on the notch capactiy as estimated according to equation (2).

Table 6: Mean values and distributions of material properties in the sensitivity analysis.

Material property	Solid timber (C24)			Glulam (GL24h)		
	Mean	Distribution	COV	Mean	Distribution	COV
Fracture energy [N/m]	300	Lognormal	20%	300	Lognormal	20%
MOE [N/mm^2]	11000	Lognormal	13%	11600	Lognormal	13%
Shear modulus [N/mm^2]	690	Lognormal	13%	760	Lognormal	13%
Shear strength [N/mm^2]	6.2	Lognormal	25%	3.5	Lognormal	15%

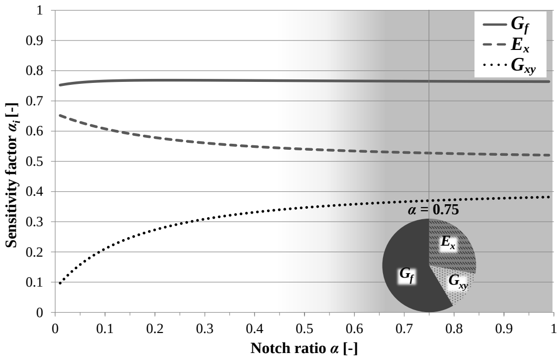

Figure 5: Impact of selected material properties on Equation (2) for notch length ratio β = 0.25 in glulam, range of suitable notch ratio α in grey.

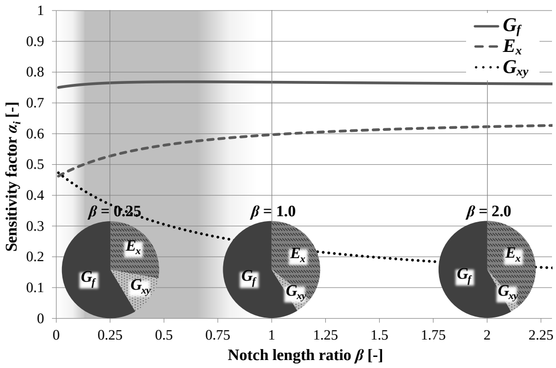

Figure 6: Impact of selected material properties on Equation (2) for notch ratio α = 0.75 in glulam, range of suitable notch length ratio β in grey.

3 Revisiting material parameters in the EC5 design approach

Material constants A and B in Equation (3) can be calculated using the material property values given in material standards EN 338 and EN 1194 or by analysing the results of experimental tests on notched beams. For the use in structural design and for their implementation in design codes these material parameters have to be set on a reliable and safe base. Hence, a reliability analysis is required.

3.1 Evaluation of experimental data from tests on notched beams

To compare the results from experimental tests with different geometrical configurations it is necessary to normalize the parameters. From the sensitivity analysis in chapter 2.3 fracture energy is found to be the key parameter with most impact on variation of notch capacity. The overall impact of both MOE and shear modulus is almost constant for notch ratios and notch length ratios in the common range in practise. For reasons of simplification and for a better comparison a constant ratio of MOE to shear modulus of

E_x / G_{xy} = 16 in line with the ratios given in EN 384 and EN 1194 and Larsen et al. [12] is assumed which leads to a parameter B = 0.8. Equation (2) can be solved for the remaining material properties:

$$1.5\frac{V_f}{b\alpha h}\cdot\frac{\sqrt{h}\left(\sqrt{\alpha-\alpha^2}+0.8\beta\sqrt{\frac{1}{\alpha}-\alpha^2}\right)}{\left(1+\frac{1.1i^{1.5}}{h}\right)}=f_v\,X\cdot 1.5\sqrt{\frac{G_{f,I}E_x}{f_v^2}\frac{1}{0.6\cdot 16}}=f_v\,A=A' \quad (5)$$

The model uncertainty of Equation (5) is covered by including an additional parameter X. The parameter A' neither depends on the geometrical parameters nor on the shear strength and can therefore be determined independently from the values given in different standards. It has the same unit [$Nmm^{-3/2}$] as stress intensity factors (SIF) K have and hence A' can be seen as the fracture toughness of the notch and can therefore be called notch strength. The corresponding critical SIF of mode 1 $K_{I,c}$ for the assumed crack opening is related to the energy release rate $G_{c,I}$ as follows:

$$K_{I,c}=\sqrt{G_{c,I}E_I} \qquad \text{with} \qquad E_I=\sqrt{2E_xE_y}\left(\sqrt{\frac{E_x}{E_y}}+\frac{E_x}{2G}-\nu\right)^{-\frac{1}{2}} \quad (6)$$

This corresponds to the material property part of A' neglecting the constant factors 1.5 and 0.6 and assuming that the energy release rate $G_{c,I}$ is equal to the fracture energy $G_{f,I}$. Using the ratios E_x / G_{xy} = 16 and E_x / E_y = 30 from EN 384 and EN 1194 and assuming a Poissons ratio ν = 0.4 a good agreement between the material property part of Equation (5) and $K_{I,c} = (G_{f,I}\cdot E_x/14)^{1/2}$ is found despite the fact that orthotropic material behaviour was not considered in Equation (1).

Table 7: Values of notch strength A' [$Nmm^{-3/2}$] for glulam from experimental results

	A'_{mean} **(COV)**
Riberholt et al. [8]	25.5 (21.0%)
Rautenstrauch et al. [16]	20.2 (24.4%)
Gustafsson et al. [33]	26.2 (26.2%)
Möhler, Mistler [35]	30.5 (26%)
All	25.7 (27.6%)

Table 8: Distribution parameters to describe the notch strength A' [$Nmm^{-3/2}$]

	A'_{mean} **(COV)**	$A'_{0.05}$
Normal	25.7 (27.6%)	14.0
Lognormal	**25.7 (28.2%)**	**15.7**
2p-Weibull	25.6 (29.8%)	12.8

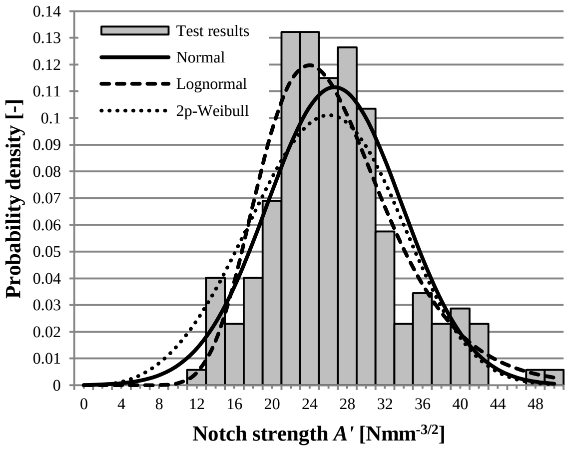

Figure 7: Distribution of notch strength A' from test results for glulam and PDFs as specified in Table 8

The notch strength parameter A' can be determined by analysing experimental data from tests on notched beams. In Table 7 results from tests on glulam beams are summarized and in Figure 7 the distribution of the notch strength parameter A' is given. A lognormal distribution with a mean value of A'_{mean} = 25.7 $Nmm^{-3/2}$ and COV = 28.2% fits the test data well.

3.2 Evaluation of theoretical distributions of material properties

The notch strength parameter *A'* depends only on fracture energy and shear modulus or MOE and ratio of MOE to shear modulus, respectively. Hence, the estimated notch strength can be determined by using the values and distributions as given in Table 6.

As can be seen in figure Figure 8 the mean value of the estimated strength is considerably higher and its variation lower compared to the analysed test results if no model uncertainty is assumed ($X = 1$). By chosing the model uncertainty to be lognormal distributed with $X_{mean} = 0.82$ and COV = 24% the notch strength is well representing the experimental data. The reason for considering this model uncertainty can be attributed to the assumption by Gustafsson that mode 1 failure of the notch is dominating the notch failure [5]. The fracture energy analysed in chapter 2.2 is pure mode 1 fracture energy. However, both fracture modes 1 and 2 take impact on the notch strength as has been described in different studies [15, 36]. In numerical studies and experimental tests Franke found that the sum of the occurring fracture energies is constant. For Norway spruce a mean sum of fracture energies from mode 1 and 2 fractures of

$$\left(G_{f,1} + G_{f,2}\right) = 210\ N/m \tag{7}$$

was determined, which corresponds to 65% of the fracture energy as assumed by Larsen et al. in Equation (4) [12]. If the model uncertainty *X* is implemented in the fracture energy by using equation (7), its coefficient of variation increases to COV ≈ 50%. Such high COV of fracture energies were also observed by Franke [15] by means of Close Range Photogrametry at notches.

Table 9: Distribution parameter to describe notch strength *A'* according to Equation (5) [Nmm$^{-3/2}$].

	A'_{mean} (COV)	$A'_{0.05}$	X_{mean} (COV)
Solid Timber	17.9 (28.7%)	12.4	0.66 (22.7%)
Glulam	22.8 (30.6%)	15.6	0.82 (24.4%)

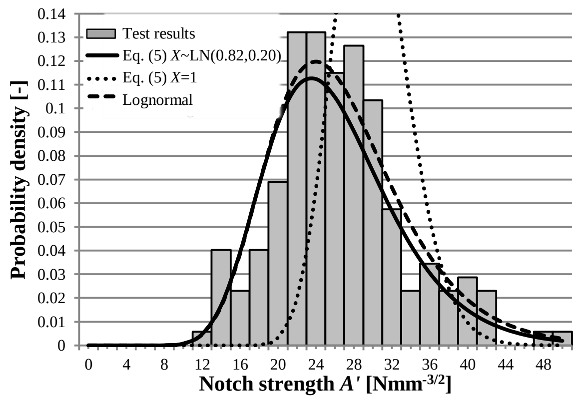

Figure 8: Distribution of notch strength *A'* from test results for glulam and notch strength according to Equation (5) with model uncertainty *X*.

3.3 Reliability of the EC5 design approach

Adequate material constants for the EC5 design approach can be derived by means of a reliability analysis. By taking into account the partial factors defined in EC5, the material constants can be adapted to assure the reliability of the design approach.

The design equation can be expressed for a simplified case with characteristic values of permanent (G_k) and variable (Q_k) action effects and characteristic value of the resistance R_k as follows [37]:

$$\frac{z\,R_k}{\gamma_m} - \gamma_G G_k - \gamma_Q Q_k = 0 \tag{8}$$

Both action effects and resistance are factored by partial factors γ_i. The characteristic value of the resistance R_k, depending on model uncertainties and dimensional variations between test and practice, is reduced by the partial factor γ_m in order to assure a certain reliability. In this study the modification factor to account for duration of load and moisture content was set to $k_{mod} = 1$ which corresponds to short term loading and service class 1. The variable z takes into account the individual geometric properties and configurations for a certain design and depends amongst others on the partial factors used: $z = f(\gamma_m, \gamma_G, \gamma_Q)$.

The ultimate limit state function g can be set up:

$$g = z\,\boldsymbol{R} - \boldsymbol{G} - \boldsymbol{Q} \tag{9}$$

Partial factors γ are to be chosen that way that the limit state function (Equation (9)) does not exceed a certain probability (here 10^{-5}) according to Equation (10) [19] for a given value of z and the distributed parameters resistance $\boldsymbol{R}$ and action effects $\boldsymbol{G}$ and $\boldsymbol{Q}$.

$$P_f\,(g \le 0) = P_f\,(z\,\boldsymbol{R} - \boldsymbol{G} - \boldsymbol{Q} \le 0) \le 10^{-5} \tag{10}$$

In EN 1990 [38] the partial factor is $\gamma_G = 1.35$ for permanent action effects and $\gamma_Q = 1.5$ for variable action effects. Regarding the partial factor γ_m a general value of 1.3 is recommended for solid timber and of 1.25 for glulam independently of the design situation [7]. These values were determined for the verification of strength of beams subjected to bending [39]. For other types of stresses like shear or tension, different γ_m values may be obtained. If these values are larger than those recommended in EC5 the desired failure probability is exceeded by applying the partial factors from EC5. If they are smaller failure probability is below the target level but uneconomical design is the consequence.

For the combined design approach in Equation (2) both partial factors for shear and notch capacities are to be considered. Since shear design shall not be affected by the partial factor for notch design, $\gamma_m = 1.3$ is set for the shear strength f_v. For the material constant A a partial factor γ_{Notch} is determined in order to verify that the failure probability is below the target probability for the notch capacity. However, the design value of the material constant A should be implemented in the design approach to not confuse the user with different partial factors. In the reliability analysis only the failure mode associated with the notch capacity of k_v is taken into account (the reliability of the system of failure modes (shear and notch related capacity) of k_v in Equation (2) is not studied). Therefore Equation (2) is rearranged to receive a design equation according to the format of Equation (8):

$$\frac{f_{v,k}}{\gamma_m}\cdot\frac{A_k}{\gamma_{Notch}}\cdot\underbrace{\frac{1.5\,b\,\alpha\,h\left(1+\dfrac{1.1 i^{1.5}}{h}\right)}{\sqrt{h}\left(\sqrt{\alpha-\alpha^2}+0.8\beta\sqrt{\dfrac{1}{\alpha}-\alpha^2}\right)}}_{z} - \gamma_G\,G_k - \gamma_Q\,Q_k = 0 \tag{11}$$

The product of characteristic values of shear strength $f_{v,k}$ and material constant A_k can be expressed by the fifth percentile value of notch strength $A'_{0.05}$ according to Equation (5) and Table 9. The corresponding limit state function according to Equation (9) is as follows:

$$g = z\,\boldsymbol{f}_v\left(\boldsymbol{X}\cdot 1.5\sqrt{\frac{\boldsymbol{G}_{f,I}\boldsymbol{E}_x}{\boldsymbol{f}_v^2\,0.6\cdot 16}}\right) - \boldsymbol{G} - \boldsymbol{Q} \tag{12}$$

In this limit state function all the properties shear strength $\boldsymbol{f_v}$, model uncertainty $\boldsymbol{X}$, fracture energy $\boldsymbol{G_{f,I}}$ and MOE $\boldsymbol{E_x}$ are distributed with parameters according to Table 6 and Table 9.

A ratio of $G_{mean} / Q_{mean} = 0.25$ of self weight and live loads is assumed. Wind and snow loads are neglected. The distribution parameter of $\boldsymbol{G}$ and $\boldsymbol{Q}$ are as given in Table 10 following JCSS recommendations [19].

The resulting notch strengths A', partial factors γ_{Notch} and material constants A for solid timber and glulam are summarized in Table 11. The relationship between partial factors and characteristic and mean values are shown in Figure 9.

Table 10: Distribution characteristics for load types according to JCSS [19] and partial factors.

Load type	Distr.	COV	char. level	γ
Self weight	Normal	10%	50%	1.35
Live Loads	Gamma	53%	98%	1.5

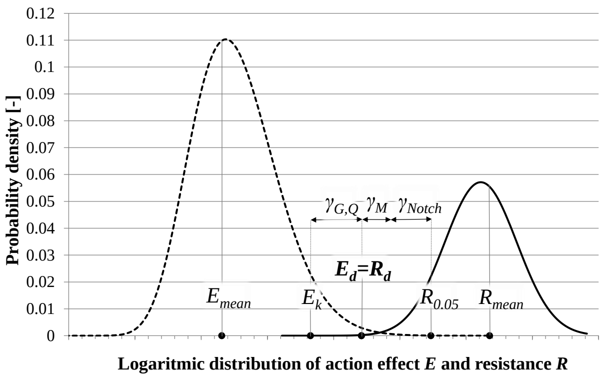

Figure 9: Illustration of mean-, characteristic-, fifth percentile- and design values of action effect *E* and restiance *R*.

Table 11: Resistances, partial factor and proposed material factors from reliability analysis.

	Solid Timber	**Glulam**
$\boldsymbol{A'_{mean}}$ **[Nmm$^{-3/2}$]**	17.9	22.8
$\boldsymbol{A'_{0.05}}$ **[Nmm$^{-3/2}$]**	12.4	15.6
$\boldsymbol{A'_d = f_{v,d}A_d}$ **[Nmm$^{-3/2}$]**	**9.1**	**10.9**
$\boldsymbol{\gamma_m}$	1.3	1.25
$\boldsymbol{\gamma_{Notch} = A'_{0.05} / (\gamma_m A'_d)}$	1.05	1.15
$\boldsymbol{A_d = A'_d / f_{v,d}}$ **[mm$^{1/2}$]**	**2.96** [1]	**3.17** [2] **3.89** [3]

[1] EN 338:2009

[2] EN 1194:1999

[3] prEN 14080:2011

The notch strength A'_d is independent from the shear strength value and can be used for different strength classes, similarly to the specified reaction force strength in the Canadian standard CSA 083.1-94 [40]. It is particularly suitable to be applied in design codes, when the material constants given for the design approaches should be independent of the shear strength values in product standards as it is the case for EC5 and the corresponding material standards EN 338, EN 1194 and prEN 14080, respectively. For the implementation of material constant A_d as factor k_n in EC5, the notch strength A'_d is divided by the corresponding shear strength values $f_{v,d}$ from valid material standards. If different shear strength values are assigned to the strength classes the highest value is to be used to determine the material factor to also provide the desired reliability for strength classes with lower shear strength values. E.g. in the calculation of the material constant A_d for glulam according to EN 1194 a characteristic value of shear strength $f_{v,k} = 4.3$ N/mm^2 assigned to GL32h is to be used.

Table 12: Suggested new values for material constant $\boldsymbol{k_n}$ for EC5 [7]

	Solid Timber	**Glulam**	
	EN 338:2009	**EN 1194:1999**	**prEN 14080:2011**
New value k_n	3	3.2	3.9
Current value k_n	5	6.5	

The suggested new values for the material constant k_n in Table 12 are up to two times smaller than the existing values in the final version of EC5 (EN 1995-1-1:2004) [7]. Other standards [40] and studies [41] declare similar values.

Conclusions

The impact of material properties on the fracture mechanical design approach for end notched beams as given in EC5 was studied. Values and distributions of elastic material properties included in the theoretical basis of the design approach are specified in standards and codes whereas fracture energy can only be found in literature. In the sensitivity analysis fracture energy is found to be the material property with the most impact on notch capacity. A comparison of the theoretical distribution of the notch capacity with data from experimental tests on notched beams shows a considerable model uncertainty when taking into account only mode 1 fracture instead of both mode 1 and 2 fractures. Values of notch strength A'_d were determined in a reliability analysis. They are particularly suitable for being implemented in design codes due to their independency towards shear strength. The revised design values of the material constants A_d, denoted k_n in EC5, were determined as well. Depending on the shear strength value used these adapted values to be implementated in EC5 are up to two times smaller than the existing values in the final 2004 version of EC5.

Literatur

1. Scholten, *Rounding notches makes stronger joists*, American Lumberman, January 19, 1935, p. 46.
2. Mistler, H.-L., *Die Tragfähigkeit des am Endauflager unten rechtwinklig ausgeklinkten Brettschichtträgers*, 1979, Lehrstuhl Ingenieurholzbau und Baukonstruktionen, Technischen Hochschule Karlsruhe, Karlsruhe.
3. Leicester, R.H., *Some aspects of stress fields at sharp notches in orthotropic material, 1. Plane stress*, Division of forest products technological paper no. 57, 1971, Commonwealth scientific and industrial research organization, Melbourne, Australia.
4. Standards Australia International, *AS 1720.1-1997: Australian Standard™ - Timber Structures - Part 1: Design methods*, 1997, Standards Australia International Ltd, Sydney, Australia.
5. Gustafsson, P.J., *A study of strength of notched beams*, CIB-W18 Meeting 21, 1988, Parksville, Canada, 21-10-1.
6. Valentin, G.H., et al., *Application of fracture mechanics to timber structures RILEM state-of-the-art report*, Research notes 1262, 1991, Technical research centre of Finland (VTT), Espoo, Finland.
7. European Committee for Standardization CEN, *EN 1995-1-1: Eurocode 5: Design of timber structures - Part 1-1: General - Common rules and rules for buildings*, 2004, CEN, Bruxelles, Belgium.
8. Riberholt, H., et al., *Timber beams notched at the support*, 1991, Afdelingen for Baerende Konstruktioner, Lyngby, Denmark.
9. European Committee for Standardization CEN, *EN 338: Structural timber - Strength classes*, 2009, CEN, Bruxelles, Belgium.
10. European Committee for Standardization CEN, *EN 1194: Timber structures - Glued laminated timber - Strength classes and determination of characteristic values*, 1999, CEN, Bruxelles, Belgium.
11. Larsen, H.J. and P.J. Gustafsson, *The fracture energy of wood in tension perpendicular to the grain*, CIB-W18 Meeting 23, 1990, Lissabon, Portugal, 23-19-2.
12. Larsen, H.J., H. Riberholt, and P.J. Gustafsson, *Annex to paper CIB-W18/25-102-1: Eurocode 5 - Design of notched beams*, CIB-W18 Meeting 25, 1992, Ahus, Sweden, 25-102-1A.
13. DIN Deutsches Institut für Normung e.V., *DIN 1052 (2008-12): Entwurf, Berechnung und Bemessung von Holzbauwerken - Allgemeine Bemessungsregeln und Bemessungsregeln für den Hochbau*, 2008, Beuth Verlag GmbH, Berlin, Germany.
14. Swiss Society of Engineers and Architects SIA, *Standard SIA 265 - Timber Structures*, 2003, SIA,, Zurich, Switzerland.

15. Franke, B., *Zur Bewertung der Tragfähigkeit von Trägerausklinkungen in Nadelholz*, 2008, Fakultät für Bauingenieurwesen, Bauhaus-Universität, Weimar.
16. Rautenstrauch, K., et al., *Beanspruchungsanalyse von Bauteilen aus Voll- und Brettschichtholz durch Industriephotogrammetrie am Beispiel von Ausklinkungen und Durchbrüchen. Schlussbericht*, Reihe Holzbauforschung Band 5, 2008, Fraunhofer IRB Verlag, Stuttgart, Germany.
17. European Committee for Standardization CEN, *prEN 14080: Timber structures - Glued laminated timber and glued solid timber - Requirement*, 2011, CEN, Bruxelles, Belgium.
18. European Committee for Standardization CEN, *EN 408: Timber structures - Structural timber and glued laminated timber - Determination of some physical and mechanical properties*, 2010, CEN, Bruxelles, Belgium.
19. JCSS, *Probabilistic Model Code*, 2007; Available from: www.jcss.ethz.ch.
20. European Committee for Standardization CEN, *EN 384: Structural timber - Determination of characteristic values of mechanical properties and density*, 2004, CEN, Bruxelles, Belgium.
21. Glos, P. and J. Denzler, *Characteristic Shear Strength Values Based on Tests According to EN 1193*, CIB-W18 Meeting 36, 2003, Colorado, USA, 36-6-1.
22. Denzler, J.K. and P. Glos, *Determination of shear strength values according to EN 408*, Materials and Structures, 2007, 40(1): 79-86.
23. European Committee for Standardization CEN, *EN 384: Structural timber - Determination of characteristic values of mechanical properties and density*, 2010, CEN, Bruxelles, Belgium.
24. Pizio, S., *Die Anwendung der Bruchmechanik zur Bemessung von Holzbauteilen, untersucht am durchbrochenen und am ausgeklinkten Träger*, Publikation Nr. 91-1, 1991, Institut für Baustatik und Stahlbau, ETH Zürich, Zurich, Switzerland.
25. Petterson, R.W. and J. Bodig, *Prediction of fracture-toughness of conifers*, Wood and Fiber Science, 1983, 15(4): 302-316.
26. Jensen, J.L., *Quasi-non-linear fracture mechanics analysis of the double cantilever beam specimen*, Journal of Wood Science, 2005, 51(6): 566-571.
27. Nordtest Method, *Wood: Fracture energy in tension perpendicular to the grain*, in *NT Build 422*, 1993, Nordtest, Espoo, Finland.
28. Aicher, S., *Bruchenergien, kritische Energiefreisetzungsraten und Bruchzähigkeiten von Fichte bei Zugbeanspruchung senkrecht zur Faserrichtung*, Holz als Roh- und Werkstoff, 1994, 52(6): 361-370.
29. Smith, I. and Y.H. Chui, *Factors affecting mode I fracture energy of plantation-grown red pine*, Wood Science and Technology, 1994, 28(2): 147-157.
30. Daudeville, L., M. Yasumura, and J.D. Lanvin, *Fracture of wood in tension perpendicular to the grain: experiment and numerical simulation by damage mechanics*, CIB-W18, 1995, Copenhagen, Denmark, 28-19-1.
31. Rug, W., M. Badstube, and W. Schöne, *Determination of the fracture energie of wood for tension perpendicular to the grain*, CIB-W18A Meeting 23, 1990, Portugal, 23-19-1.
32. Jockwer, R., *A study on fracture energy of glulam*, 2011, ETH Zurich, unpublished work
33. Gustafsson, P.J., P. Hoffmeyer, and G. Valentin, *DOL behaviour of end-notched beams-Zeitstandfestigkeit keilverzinkter Träger*, Holz als Roh- und Werkstoff, 1998, 56(5): 307-317.
34. Reliability Consulting Programs (RCP), *STRUREL, a Structural Reliability Analysis Program-System, COMREL & SYSREL*, 1997, RCP Consult, Munich.
35. Möhler, K. and H.-L. Mistler, *Untersuchungen über den Einfluss von Ausklinkungen im Auflagerbereich von Holzbiegeträgern auf die Tragfestigkeit*, 1978, Lehrstuhl für Ingenieurholzbau und Baukonstruktionen, Karlsruhe, Germany.
36. Riipola, K., *Dimensioning of beams with cracks, notches and holes. An application of fracture mechanics*, CIB-W18 Meeting 23, 1990, Lisbon, Portugal, 23-10-2.
37. Köhler, J., J.D. Sørensen, and M.H. Faber, *Probabilistic modeling of timber structures*, Structural Safety, 2007, 29(4): 255-267.
38. European Committee for Standardization CEN, *EN 1990/A1: Eurocode - Basis of structural design*, 2005, CEN, Bruxelles, Belgium.
39. Sørensen, J.D., *Calibration of Partial Safety Factors in Danish Structural Codes*, Proceedings of JCSS Workshop on Reliability Based Code Calibration, 2002, Zurich, Switzerland.
40. CSA, *O86.1-94: Engineering Design in Wood (Limit States Design)*, 1994, Canadian Standards Association, Etobicoke, Ontario, Canada.
41. Aicher, S. and L. Höfflin, *Glulam Beams with round holes- a comparision of different design approaches vs. test data*, CIB-W18 Meeting 35, 2002, Kyoto, Japan, 35-12-1.

CIB-W18/44-6-2

INTERNATIONAL COUNCIL FOR RESEARCH AND INNOVATION
IN BUILDING AND CONSTRUCTION

WORKING COMMISSION W18 - TIMBER STRUCTURES

INTERACTION OF SHEAR STRESSES AND STRESSES PERPENDICULAR TO THE GRAIN

R Steiger
Empa, Swiss Federal Laboratories for Materials Science and Technology
Dübendorf

E Gehri
Prof. emeritus ETH Zurich
Rüschlikon

SWITZERLAND

MEETING FORTY FOUR
ALGHERO
ITALY
AUGUST 2011

Presented by R Steiger
G Hochreiner commented that TU Wien work on this area should be considered. R Steiger agreed and commented that they are aware of the work; however, there is no design provision in codes except the Swiss code and the German approach is not continuous. There were discussions that the compression strength perpendicular to grain depends on the actual deformation allowed and therefore not real material properties.
S. Aicher and R Steiger discussed the merits of tensor polynomial approach in comparison to the Swiss approach.

Interaction of shear stresses and stresses perpendicular to the grain

R Steiger

Empa, Swiss Federal Laboratories for Materials Science and Technology

Dübendorf

E Gehri

Prof. emeritus ETH Zurich

Rüschlikon

SWITZERLAND

1 Abstract / Introduction

In timber structural elements, pure shear stresses occur in very rare cases only. Mostly, shear stresses interact with stresses perpendicular to the grain. Even shear tests according to the European standard EN 408:2010 [1] do not subject the specimen to pure shear, but due to the oblique load-to-grain angle of 14° this “shear testing” rather represents a combination of shear and compression perpendicular to the grain loading.

The beneficial influence of compression stresses perpendicular to the grain acting simultaneously with shear stresses has been known for decades (e.g. [2]) and has been found in recent experiments again (e.g. [3]) Most standards for the design of timber structures as e.g. Eurocode 5 (EC 5, EN 1995-1-1:2004) [4] thus allow for neglecting or reducing compression single forces acting at the upper face of beams close to their supports when verifying the shear strength. The contrary effect of shear strength being considerably reduced when acting in combination with tensile stresses perpendicular to the grain has mainly been described in the course of fracture mechanical studies and related experiments on wood (e.g. [5]).

A design model to account for combined shear stresses and stresses perpendicular to the grain was part of working draft versions of EC 5 (ENV 1995-1-1) in 1998. However, the final version EN 1995-1-1:2004 lacked of such a design model. In the Swiss timber design code SN 505265 (SIA 265) [6] published in 2003, a quantitative design approach was given, being valid over the whole range of perpendicular to the grain stresses (compression and tension). The respective elliptic model shows a good agreement with test results on small-sized specimens performed by Mistler in 1979 [7] and by Spengler in 1982 [8]. In 2009 Gehri [9] carried out single shear tests on large sized specimens in different configurations and proved the SIA 265 approach to fit the experimental data well.

The authors of the standard SIA 265 intended to provide a design formula being valid for as many different cases as possible (e.g. various wood species) and allowing for taking into account influences of moisture and size (stressed volume) by adjusting the single design values of perpendicular to the grain and shear strengths accordingly. Hence, the SIA 265 design approach bases on ratios between occurring stresses and respective strength values.

2 Situations where combined stresses occur

In structures combined shear and perpendicular stresses e.g. occur in step joints (Figure 1), in rigid frame corners (Figure 2) and in beams with notches (Figure 3) or holes (Figure 4).

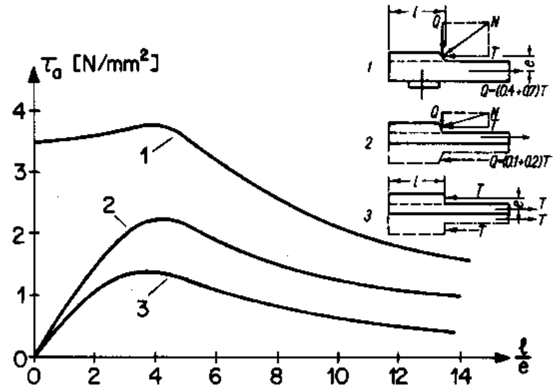

Figure 1: Influence of compression stresses perpendicular to the grain on the shear strength of step joints (original drawing, [2]).

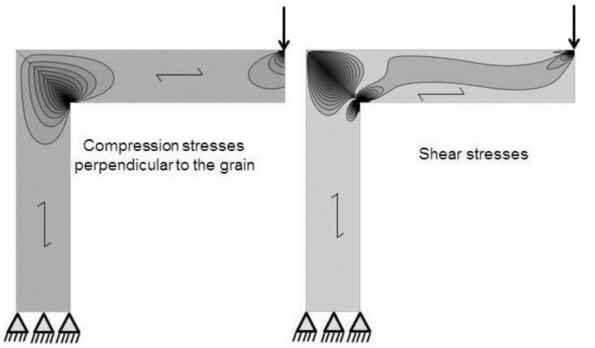

Figure 2: Distribution of shear stresses (right) and tensile stresses perpendicular to the grain (left) in a rigid frame corner subjected to a negative bending moment.

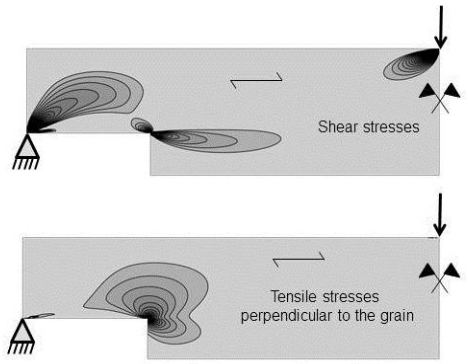

Figure 3: Stresses at notches.

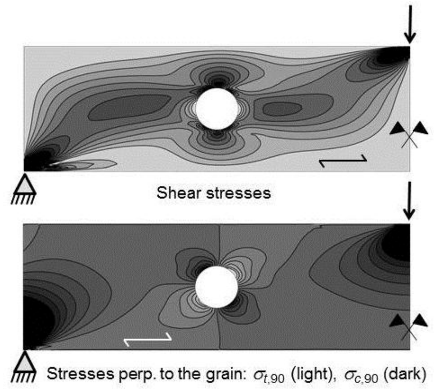

Figure 4: Stresses at holes.

The influence of perpendicular stresses on the shear strength was also found to be important when carrying out shear tests on beams (Figure 5) or on block-type specimens in order to e.g. assess the shear strength of bond lines (Figure 6).

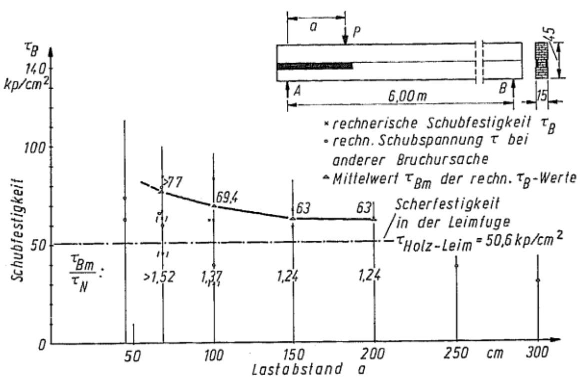

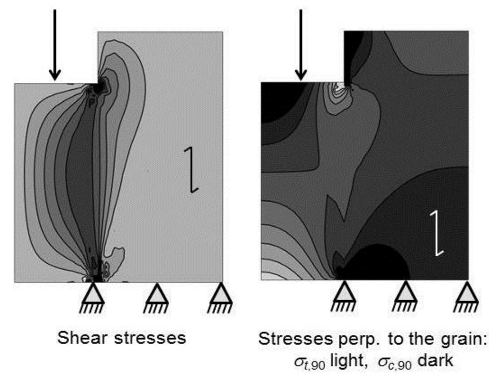

Figure 5: Influence of the distance a between load and support on the shear strength τ_B of glulam beams (original drawing, [10]).

Figure 6: Distribution of shear stresses (left) and transverse stresses (right) in ASTM D143 block shear tests [11].

3 Review of existing failure criteria and design approaches

3.1 Failure criteria as used in fracture mechanics

When evaluating the load-bearing capacity of timber elements by applying linear elastic fracture mechanics (LEFM), failure modes 1 (due to tensile stresses perpendicular to the crack) and 2 (shear failure) together with mixed mode failures (combinations of modes 1 and 2) have to be analysed (e.g. [12]). In the latter case often a universal failure criterion (Equation (1)) [13] is used to compare the occurring stress intensity factors (SIF) K_i with the respective critical SIF K_{ic}, the so-called fracture toughness. The exponents e_i in Equation (1) have to be empirically set based on test results, whereby values between 1 and 2 are reported in literature. Based on extensive tests with thin plates of balsa wood, Wu [14] found $e_1 = 1{,}03$ and $e_2 = 1{,}88$. Hence, he approximated the failure criterion for mixed mode fractures as presented in Equation (2):

$$\left(\frac{K_1}{K_{1c}}\right)^{e_1} + \left(\frac{K_2}{K_{2c}}\right)^{e_2} = 1 \qquad (1) \qquad\qquad \frac{K_1}{K_{1c}} + \left(\frac{K_2}{K_{2c}}\right)^{2} = 1 \qquad (2)$$

The Wu failure criterion has proved to be suitable to assess the load carrying capacity of softwood members subjected to combined perp. to the crack tensile and shear stresses (e.g. [15] and [12]). Concerning combined shear stresses and compression stresses acting perpendicular to the crack, much less information can be found in literature. Wu [14] indicated that his failure criterion (Equation (2)) might be valid for such cases also (Figure 7). An according verification/confirmation later on was given by Leicester [16] (Figure 8).

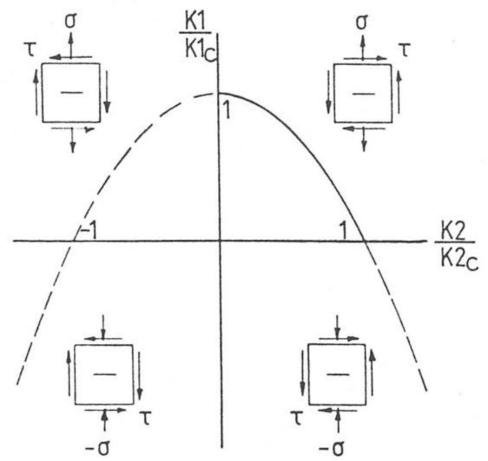

Figure 7: Interaction models according to Wu (original drawing, [14]).

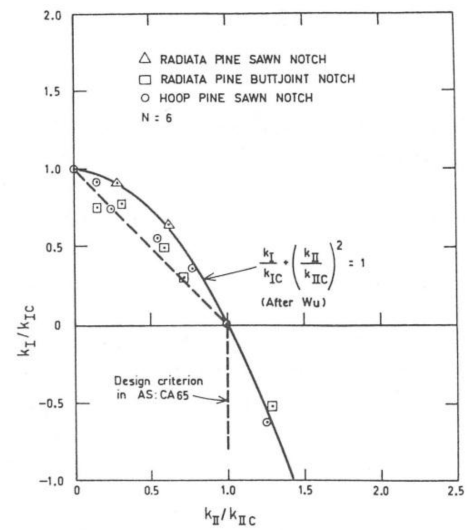

Figure 8: Wu failure criterion compared to experiments by Leicester (orig. drawing, [16]).

Hence, Logemann in his study on notched beams and beams with holes [12] suggested an elliptical failure criterion (Figure 9), for the following reasons:

- Due to its distinctive failure stress limit in each point, a closed (convex) failure curve appears as being logic from the physical point of view.
- The ellipse represents such a closed curve and has a distinctive maximum, which fits experimental data well e.g. of experiments performed by Spengler (see 4.1.2).
- If $b >> a$, then the differences between the Wu criterion and the elliptical model in the first quadrant are small (Figure 10).

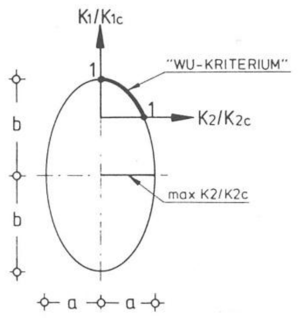

$$\frac{\left[\frac{K_1}{K_{1c}}+(b-1)\right]^2}{b^2}+\frac{\left(\frac{K_2}{K_{2c}}\right)^2}{a^2}\geq 1$$

b = 3,5 and a = 1,43 (according to tests by Spengler [8]).

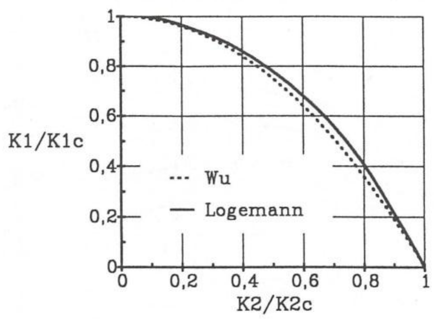

Figure 9: Elliptical failure criterion as used by Logemann (original drawing, [12]).

Figure 10: Wu failure criterion and elliptical approach by Logemann (original drawing, [12]).

A similar model was also used by Mandery when analysing the relationship between perpendicular to the grain compressive stresses and shear strength of wood [17]. Mandery based the failure modelling on the strength of an orthotropic material in a two-dimensional stress system. The strength model was derived from the energy distortion theory developed from the analytical work of Huber, von Mises and Hencky with the principal assumption of the material being isotropic and the failure being associated only with the energy absorbed in changing shape [18]. Mandery used the assumption postulated by Norris [19] that orthotropic materials were composed of an isotropic material with regularly spaced voids, this leading to the following Equation (3). For combined action of shear and perpendicular stresses the formula reduces to Equation (4):

$$\frac{f_1^2}{F_1^2}+\frac{f_2^2}{F_2^2}+\frac{f_{12}^2}{F_{12}^2}+\frac{f_1 f_2}{F_1 F_2}=1 \qquad (3)$$

$$\frac{f_2^2}{F_2^2}+\frac{f_{12}^2}{F_{12}^2}=1 \qquad (4)$$

f_1 , F_1 longitudinal (maximum) stress , longitudinal strength

f_2 , F_2 perpendicular to the grain (maximum) stresses , respective strength

f_{12} , F_{12} (maximum) shear stresses , respective strength.

Among the variety of failure criteria (see e.g. [20]), concerning the present study, the Norris criterion (Equation (4)) is of primary interest since it exhibits a quadratic formulation.

3.2 1998 working draft version of EC 5

The 1998 working draft version of EC 5 (ENV 1995-1-1) [4], contained in paragraph 6.2.6 a design approach to account for simultaneously acting shear and compression stresses perpendicular to the grain (Equation (5)). In paragraph 6.2.5 one could find a respective design equation for situations with simultaneous shear and tension stresses perpendicular to the grain (Equation (6)):

$$\frac{\tau_d}{f_{v,d}}-0{,}25\frac{\sigma_{c,90,d}}{f_{c,90,d}}\leq 1 \qquad (5)$$

$$\frac{\tau_d}{f_{v,d}}+k_{vol}\frac{\sigma_{t,90,d}}{f_{t,90,d}}\leq 1 \qquad (6)$$

$k_{vol}=1{,}0$ (solid timber), $k_{vol}\leq\left(\frac{V}{V_0}\right)^{0,2}$ (glulam). The reference volume V_0 is 0,01 m^3.

When graphing these design models in Figure 11, the reduction factor k_{vol} has been calculated for reference volumes of 0 to 1 m^3. In practical situations, reduction factors up to $k_{vol}=0{,}4$ occur. In order to simplify the design process a constant value of $k_{vol}=0{,}5$ could have been chosen.

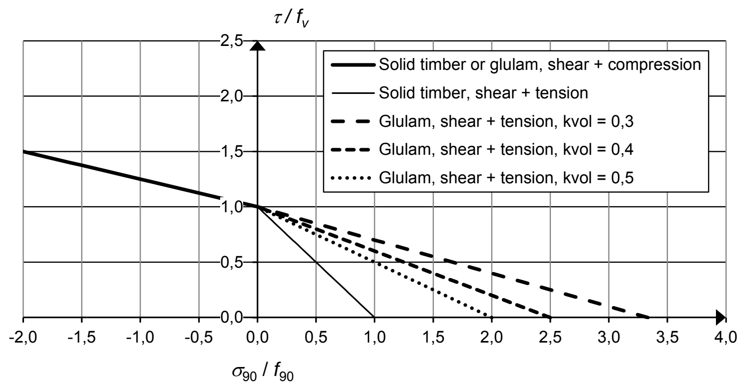

Figure 11: Design model in the 1998 working draft version of EC 5 to account for simultaneously acting shear stresses and stresses perpendicular to the grain.

The draft EC 5 design approach had the advantage of being very simple. However, in situations with either very small tension or compression stresses perpendicular to the grain, the design model does not progress continuously, which in reality cannot be true.

3.3 2003 edition of the Swiss standard SIA 265

3.3.1 Basic assumptions

The design model for combined shear stresses and stresses perpendicular to the grain in the Swiss standard for the design of timber structures SIA 265:2003 [6] is based on the following assumptions [21]:

- If the stresses perpendicular to the grain equal zero, the applicable shear stress is equal to the shear strength.
- In case of tension stresses perpendicular to the grain, the shear strength is reduced and reaches a value of zero if the perpendicular tension stress is equal to the respective strength value.
- Compression stresses simultaneously acting in perpendicular direction make shear stresses above the usual strength level possible. The maximum applicable shear stress is reached when the compression stress is equal to the respective strength value. If the load is increased further, failure due to perpendicular to the grain crushing occurs.
- The failure criterion should exhibit a continuous progression.

3.3.2 Analytical development

The design Equation (13) is based on an elliptical failure criterion (Eq. (7)) (Figure 12):

$$\frac{x^2}{a^2}+\frac{y^2}{b^2}=1 \tag{7}$$

the origin O_1 being located in the centre of the ellipse. The origin O_2 represents the point where there is neither perpendicular to the grain nor shear stress. The major radius a equals the sum of the perpendicular to the grain strengths in tension and in compression $a = f_{c,90} + f_{t,90}$ and the minor radius b has to be derived from Equation (7) assuming that in P_1 the perpendicular to the grain stresses σ_{90} equal 0 and the shear stress τ equals the shear strength f_v, $P_1(x_1 = f_{c,90}; y_1 = f_v)$:

$$\frac{f_{c,90}{}^2}{\left(f_{c,90}+f_{t,90}\right)^2}+\frac{f_v{}^2}{b^2}=1 \tag{8}$$

$$b^2=\frac{f_v{}^2\left(f_{c,90}+f_{t,90}\right)^2}{f_{t,90}^2+2f_{c,90}f_{t,90}} \tag{9}$$

For simultaneously acting shear and compression stresses perpendicular to the grain (in e.g. point P_3 with $x_3 = f_{c,90} - \sigma_{90,3}$ and $y_3 = \tau_3$) and for simultaneously acting shear and tensile stresses perpendicular to the grain (in e.g. point P_4 of the ellipse with $x_4 = f_{c,90} + \sigma_{90,4}$ and $y_4 = \tau_4$) the failure criterion can be expressed as:

$$\frac{\beta^2}{\left(f_{c,90}+f_{t,90}\right)^2}+\frac{\tau^2}{f_v^2}\cdot\frac{f_{t,90}^2+2f_{c,90}f_{t,90}}{\left(f_{c,90}+f_{t,90}\right)^2}\leq 1 \qquad (10) \qquad \text{with} \qquad \beta=\begin{matrix} f_{c,90}-\sigma_{c,90} \text{ in } P_3 \\ f_{c,90}+\sigma_{t,90} \text{ in } P_4 \end{matrix} \qquad (11)$$

In the range of $-f_{c,90} \leq \sigma_{90} \leq f_{t,90}$, the notation of the failure criterion can be optimised by assigning $\sigma_{90} = -\sigma_{c,90}$ (in case of compression) and $\sigma_{90} = \sigma_{t,90}$ (in case of tension) and by taking into account that $f_{t,90}^2 + 2f_{c,90}f_{t,90} = \left(f_{c,90}+f_{t,90}\right)^2 - f_{c,90}^2$:

$$\frac{\left(f_{c,90}+\sigma_{90}\right)^2}{\left(f_{c,90}+f_{t,90}\right)^2}+\frac{\tau^2}{f_v^2}\cdot\left[1-\left(\frac{f_{c,90}}{f_{c,90}+f_{t,90}}\right)^2\right]\leq 1 \qquad (12).$$

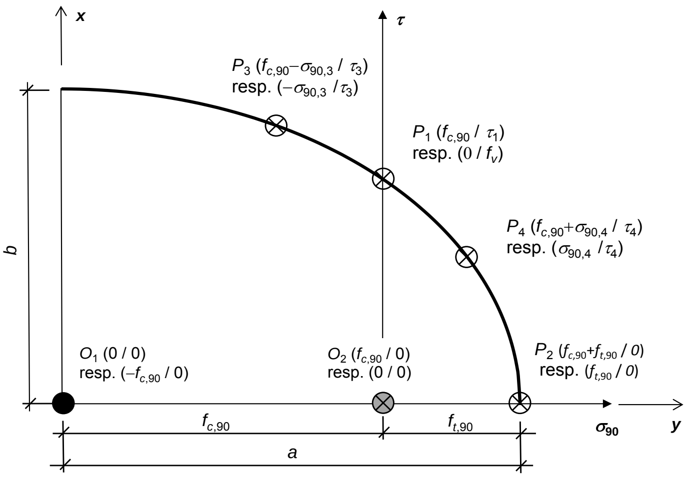

Figure 12: Basic assumptions of the design model for combined shear and perpendicular to the grain stresses according to the 2003 edition of the Swiss standard SIA 265 [6].

3.3.3 Resulting design equation

Based on design values of shear stress τ_d / shear strength $f_{v,d}$ and perpendicular to the grain stresses $\sigma_{90,d}$ / strengths $f_{c,90,d}$ and $f_{t,90,d}$, the design equation to account for simultaneously acting stresses in the range of $-f_{c,90,d} \leq \sigma_{90,d} \leq f_{t,90,d}$ results in

$$\left(\frac{f_{c,90,d}+\sigma_{90,d}}{f_{c,90,d}+f_{t,90,d}}\right)^2+\left(\frac{\tau_d}{f_{v,d}}\right)^2\left[1-\left(\frac{f_{c,90,d}}{f_{c,90,d}+f_{t,90,d}}\right)^2\right]\leq 1 \qquad (13)$$

where $\sigma_{90,d} = \sigma_{t,90,d}$ in case of tension and $\sigma_{90,d} = -\sigma_{c,90,d}$ in case of compression.

4 Verification of the 2003 SIA 265 design approach

4.1 Test results reported in literature

4.1.1 Experiments by Mistler at the Karlsruhe Institute of Technology in 1979

In 1979 Mistler performed tests on the load carrying capacity of end-notched beams with rectangular notches on the bottom side of the beam [7]. In the course of these tests he assessed failure strengths under combined shear and perpendicular to the crack (and grain) tensile stresses on specimens with dimensions as shown in Figure 13.

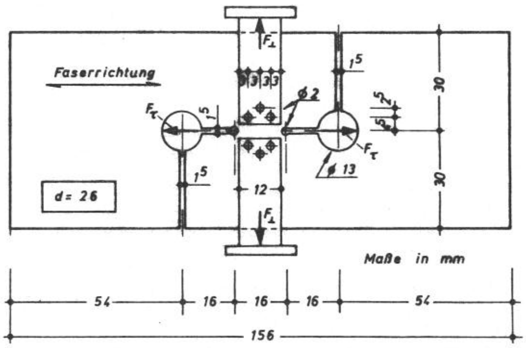

Figure 13: Test set-up as used by Mistler (original drawing, [7]).

The test results are graphed in Figure 14 together with a model according to Equation 14 given by Mistler to fit the data based on the probability of survival u_z on the mean and on both the 5%- and 95% level. The shear stresses are normalized by dividing them by the mean value of the test results for pure shear loading $\tau_{u,0}$.

$$\ln\left(\frac{1}{u_z}\right) = \left(\frac{\sigma_\perp}{1{,}8}\right)^{4{,}0} + \left(\frac{0{,}9298}{1-0{,}13\sigma_\perp}\cdot\frac{\tau}{\tau_{u,0}}\right)^{6{,}25} \qquad (14).$$

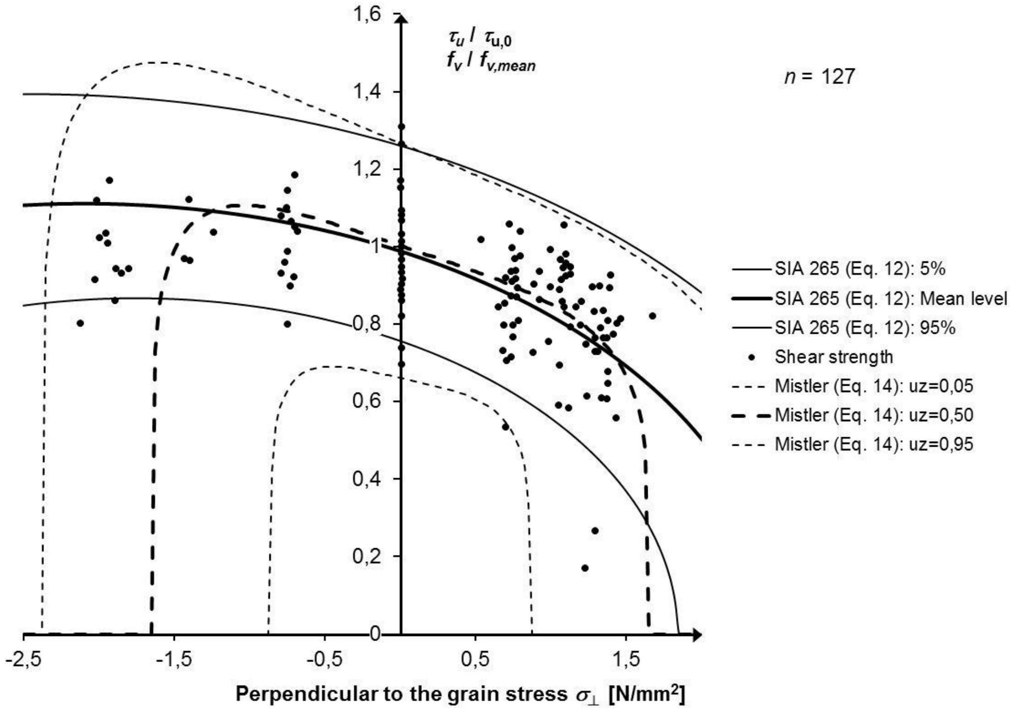

Figure 14: SIA 265 failure criterion for combined shear and perpendicular to the grain loading benchmarked to test results taken from a study by Mistler in 1979 [7].

From Figure 14 it can be concluded that when assigning the parameters in the SIA 265 failure criterion (Equation (12)) as listed in Table 1 the model fits Mistler's test data well.

Table 1: Parameters when fitting the SIA 265 failure criterion to data by Mistler [7]

	$f_v / f_{v,mean}$ 1) 2)	$f_{c,90}$ 3)	$f_{t,90}$ 1)	Remarks
Mean level	0,99 4)	2,1 N/mm² 4)	2,5 N/mm² 4)	1) Lognormal distribution, $n = \infty$
CoV	16% 4)	10% 5)	18% 4)	2) Normalized shear stress
5%-level	0,74	1,9 N/mm²	1,8 N/mm²	3) Normal distribution, $n = \infty$
95%-level	1,24	3,1 N/mm²	3,2 N/mm²	4) Test results [7] 5) JCSS, PMC [22]

4.1.2 Experiments by Spengler at the Technical University of Munich in 1982

In 1982 Spengler published a study [8] (the results of which were similar to those found by Keenan/Jaeger [23]) on the shear strength of Norway spruce glulam specimens subjected to combined shear stresses and stresses perpendicular to the grain. The specimens (length 220 mm, width 80 mm to 140 mm, thickness 22 mm to 32 mm) were adhesively bonded to steel plates (Figure 15) in order to guarantee a continuous load transfer. 15 mm wide holes and grooves at the specimens' ends helped to reduce stress peaks due to uneven stress distributions. In total Spengler carried out more than 740 tests. In the present paper only the series with specimens which had been stored in climate 20°C / 65% relative humidity until reaching equilibrium moisture content (MC) of approximately 12% are evaluated.

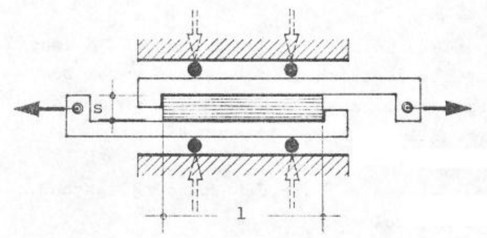

Figure 15: Set-up as used by Spengler (original drawing, [8]) when testing Norway spruce glulam specimens under combined shear and perpendicular to the grain compression loading.

In Figure 16 the test results are compared with the failure criterion provided by SIA 265:2003, graphed on the mean and both on the 5%- and 95% level. For the numerical values given in Table 2 the SIA 265 failure criterion again fits well to the test data.

Table 2: Parameters in the SIA 265 failure criterion when fitted to data by Spengler [8]

	$f_{v,mean}$ 1)	$f_{c,90}$ 2)	$f_{t,90}$ 1)	Remarks
Mean level	5,2 N/mm² 3)	4.5 N/mm² 3)	2,2 N/mm² 3)	1) Lognormal distribution, $n = \infty$ 2) Normal distribution, $n = \infty$ 3) Test results [8] 4) JCSS, PMC [22]
CoV	15% 3)	10% 4)	25% 4)	
5%-level	4.0 N/mm²	3.8 N/mm²	1,3 N/mm²	
95%-level	6.5 N/mm²	5.2 N/mm²	3,1 N/mm²	

In the course of studying possibilities to improve the shear resistance of glulam beams by means of screws and steel rods, Krüger [24] fitted a multiple regression model at the mean level to Spengler's data. This model, as shown in Figure 16 fits Spengler's data well. However, extrapolation especially in the range of small shear stresses and high perpendicular to the grain stresses (where the model of course was not made for nor needed!) would lead to wrong results.

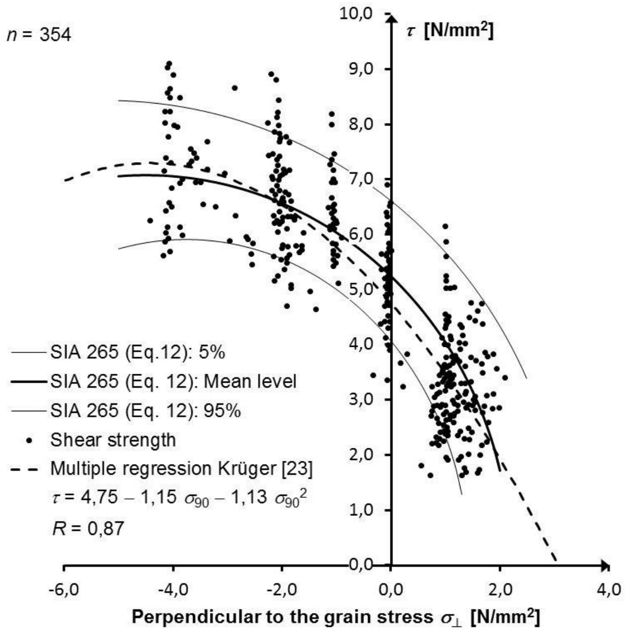

Figure 16: SIA 265 failure criterion for combined shear and perpendicular to the grain loading benchmarked to test results taken from a study by Spengler in 1982 [8].

4.1.3 Experiments by Eberhardsteiner

The study by Eberhardsteiner [25] consists of numerous experiments on Norway spruce specimens subjected to biaxial normal stresses with orthogonal stress components and varying load to grain angle. Some of the test results can be used for bench-marking the SIA 265 failure criterion. However, the use of the data would ask for calculating shear and perp to the grain stress components from the respective inclined principle stresses.

4.2 Own experiments

Being aware of the fact that shear strength and perpendicular to the grain tensile strength are strongly influenced by the size of the stressed volume, Gehri [9] carried out shear tests on Norway spruce glulam beams in structural sizes with two different loading configurations (Figure 17). These tests were not specifically focused on the verification of the SIA 265 design model being subject of this paper, but rather intended to derive shear modulus and shear strength of glulam beams in structural sizes. Obviously the acting shear forces in both configurations are the same. However, due to different perpendicular to the grain stress situations the ZZ-specimens compared to the DD-specimens in average showed approximately 20% lower shear strength values (Test results: see Table 3).

4.2.1 Test material and test set up

The 4 specimens in each sample were made from GL 28h Norway spruce glulam ($E_{0,g,mean}$ = 12’000 N/mm^2; $E_{90,g,mean}$ = 300 N/mm^2 [6]) and had cross-sectional sizes of 140 mm x 480 mm (DD-type specimens) and 120 mm x 480 mm respectively (ZZ-type specimens). The loads at loading points and supports were transferred into the specimens by means of vertically glued-in steel rods of diameter 16 mm with a metric thread M16 which enabled a field of uniform shear stress of sufficient size in order to be able to reliably measure occurring deformations in quadratic zones of 200 mm length (Figure 18).

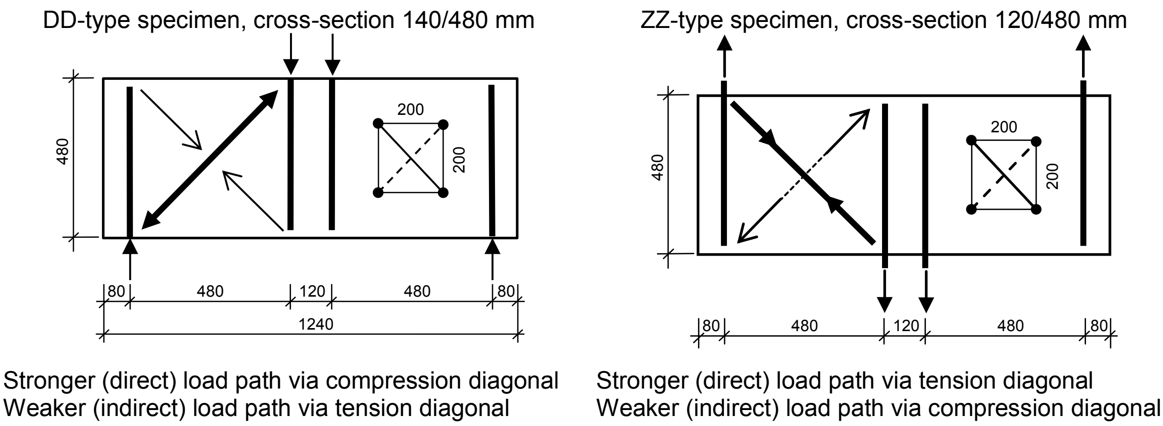

Figure 17: Shear tests on glulam beams in two different loading configurations [9]. High loads can be transferred to into the specimens by means of bonded-in steel rods.

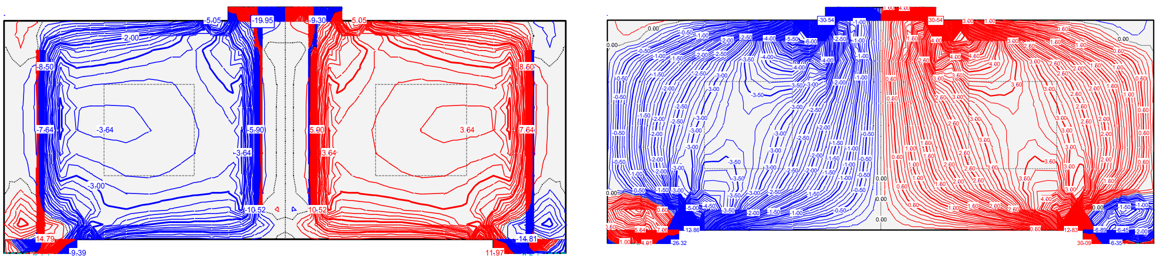

Figure 18: When transferring the loads into the specimen by means of glued-in steel rods, up to the elastic limit fields with uniform shear stress distribution of sufficient size occur (left), whereas they do not when directly transferring the loads to the timber beam (right).

4.2.2 Test results

The test results are compiled in Table 3. If the influence due to difference in shear stressed volume or in shear stressed area respectively is taken into account by a factor of $(\text{Ratio of sheared areas})^{-0,25} = (120/140)^{-0,25} = 1{,}04$ [26-29], the mean shear strength of the DD-specimens results in 4,92 N/mm^2 and hence the difference in shear strength between the two loading situations amounts to 20%.

Table 3: Test results: Ultimate loads F_u and shear strengths f_v [9]

Sample	Specimen	F_u [kN]	f_v [N/mm^2]	Mean values	CoV
ZZ	ZZ-1	164	4,27	$f_{v,mean}$ = 4,09 N/mm^2 $F_{u,mean}$ = 157 kN	5%
	ZZ-2	152	3,96		
	ZZ-3	149	3,88		
	ZZ-4	163	4,25		
DD	DD-1	210	4,69	$f_{v,mean}$ = 4,73 N/mm^2 $F_{u,mean}$ = 218 kN	6%
	DD-2	223	4,98		
	DD-3	196	4,38		
	DD-4	218	4,87		

4.2.3 Estimation of the stresses perpendicular to the grain

When tested in ZZ-configuration, the deformations in the tension diagonal of the measuring set up are increased by the 45° component of the deformation occurring in the load transfer zone. In case of using the DD-set up, the 45° component of the load transfer zone leads to a decrease in diagonal deformation (Figure 19).

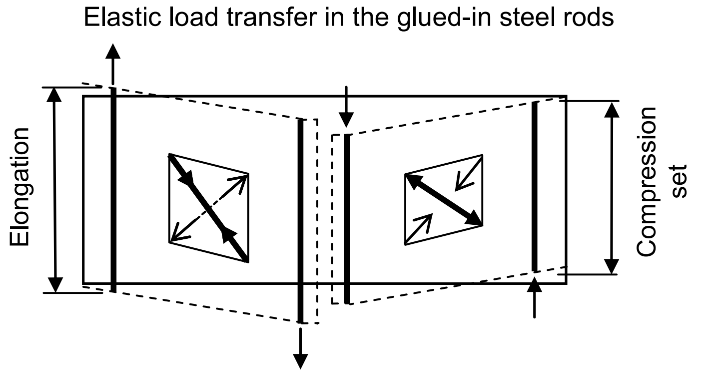

Figure 19: The deformations in ZZ-configuration (left) differ from those in DD-configuration (right) due to different deformation in the load transfer at the support.

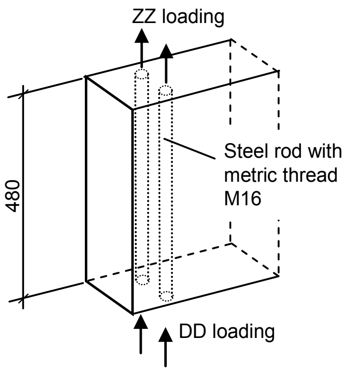

Figure 20: Load transfer zone at the support.

For the calculation of the respective deformations and resulting stresses, the following assumptions were made:

- The loads are transferred in the specimens evenly distributed over the beam's height by a pair of steel rods with metric thread M16 (Figure 20). The ratio of load being transferred by the surrounding timber was estimated to be about 10%.
- The average specific deformation of the timber was assumed to be equal to the one of the steel rod at mid-height.
- In order to account for the load duration in the shear test of approximately 1 hour (due to on-going measurements), the MOE perpendicular to the grain $E_{90,g,mean}$ (for short-term loading being equal to 300 N/mm^2 [6], [30, 31]) has been reduced to 200 N/mm^2.

For the mean values of the failure loads (Table 3) the stresses of the steel rods σ_{steel} (at mid-height) and the stresses in the timber σ_{timber} (in the middle zone of the beam) can therefore be evaluated as follows:

$$\sigma_{steel} = \frac{F_{u,mean}}{2 \cdot 1{,}1 \cdot A_{steel}} \qquad (15) \qquad \sigma_{timber} = \frac{2/3 \cdot E_{90,g,mean}}{E_{steel}} \cdot \sigma_{steel} \qquad (16)$$

$$\text{ZZ:} \quad \sigma_{steel} = \frac{157 \cdot 10^3}{2 \cdot 1{,}1 \cdot 314} = 227\,\text{N/mm}^2 \quad (17) \qquad \sigma_{timber} = \frac{200}{210 \cdot 10^3} \cdot 227 = 0{,}22\,\text{N/mm}^2 \quad (18)$$

$$\text{DD:} \quad \sigma_{steel} = \frac{218 \cdot 10^3}{2 \cdot 1{,}1 \cdot 314} = 316\,\text{N/mm}^2 \quad (19) \qquad \sigma_{timber} = \frac{200}{210 \cdot 10^3} \cdot 316 = 0{,}30\,\text{N/mm}^2 \quad (20).$$

These assumptions were verified to be correct by means of FEM calculations (Figure 18, left) and by ARAMIS optical 3D deformation analysis [32, 33].

4.2.4 Benchmarking of the SIA 265 design model to the test results

The experimental data can be well assessed by the SIA 265 design approach (Figure 21). For the tested material (glulam GL28h) the numerical values of the strengths perpendicular to the grain $f_{c,90,mean}$ and $f_{t,90,mean}$ are set 3,2 N/mm^2 [30, 31, 34] and 0,8 N/mm^2. (Note: These strength values depend on the size of the stressed volume!). If calculated from the EN 1194 characteristic values [35] by taking into account the distribution types and coefficients of variation in the JCSS probabilistic model code [22] the values result in 4 N/mm^2 and 0,8 N/mm^2 respectively. The mean shear strength is taken as derived from the tests (Table 3; interpolated and corrected to a width of 120 mm).

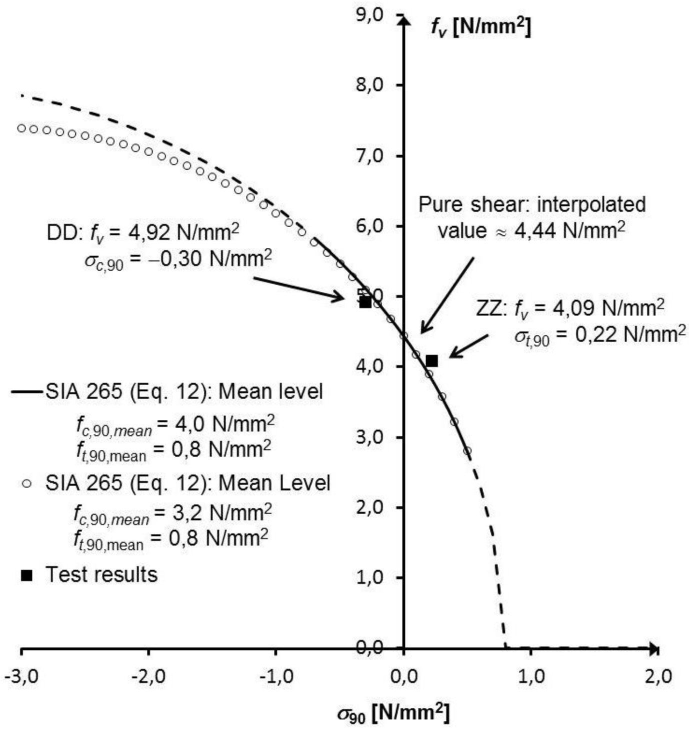

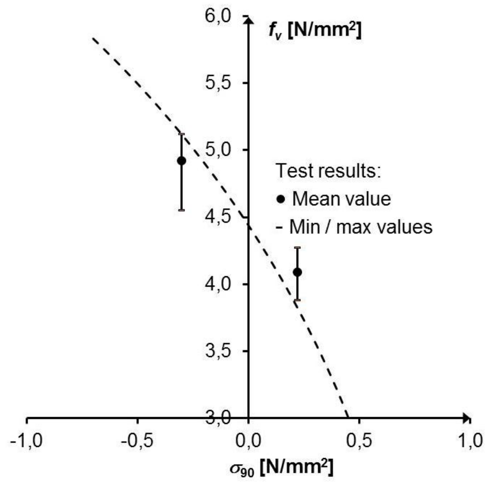

Figure 21: SIA 265 failure criterion for combined shear and perpendicular to the grain loading benchmarked to test results by Gehri [9].

5 Conclusions

From the above described theoretical considerations and experimental verification it can be concluded that the SIA 265 design model to account for combined shear and perpendicular to the grain stresses fits experimental data well. Due to its formulation in stress/strength ratios the design model allows for using it for different wood species and for adjusting the design values so that they reflect influences of stressed volume and moisture for each property accordingly. However, additional tests on specimens in structural sizes (preferably in other test configurations also) should be carried out in order to get more experimental data, especially with higher acting perpendicular to the grain stresses.

6 Acknowledgements

The providing of test specimens and test facilities by Neue Holzbau Lungern (www.neueholzbau.ch) and the assistance by Peter Haas in carrying out experiments and by Robert Jockwer in graphing the test results are gratefully acknowledged by the authors.

7 References

1. European Committee for Standardization, 2010: EN 408: Timber structures – Structural timber and glued laminated timber – Determination of some physical and mechanical properties. CEN, Bruxelles, Belgium.
2. Karlsen G.G., Goodman W.L., 1967: Wooden structures. Mir, Moscow, Russia.
3. Aicher S., Ohnesorge D., 2011: Shear strength of glued laminated timber made from European beech timber. European Journal of Wood and Wood Products 69(1): 143-154.
4. European Committee for Standardization, 2004: EN 1995-1-1 (Eurocode 5-1-1): Design of timber structures – Part 1-1: General – Common Rules and rules for buildings. CEN, Bruxelles, Belgium.
5. Valentin G.H., et al., 1991: Application of fracture mechanics to timber structures – RILEM state-of-the-art report. VTT Technical Research Centre of Finland, Research Notes. Vol. 1262. Espoo, Finland.
6. Swiss Society of Engineers and Architects SIA, 2003: Swiss Standard SN 505 265 (SIA 265): Timber Structures. SIA, Zurich, Switzerland.
7. Mistler H.L., 1979: Die Tragfähigkeit des am Endauflager unten rechtwinklig ausgeklinkten Brettschichtträgers. Lehrstuhl für Ingenieurholzbau und Baukonstruktionen, Technische Hochschule Karlsruhe, Germany.
8. Spengler R., 1982: Festigkeitsverhalten von Brettschichtholz unter zweiachsiger Beanspruchung, Teil 1: Ermittlung des Festigkeitsverhaltens von Brettelementen aus Fichte durch Versuche. Laboratorium für den konstruktiven Ingenieurbau LKI, Sonderforschungsbereich 96, Technische Universität München, Germany.
9. Gehri E., Haas P., 2009: Zur Schubfestigkeit von Brettschichtholz: Bedeutung der Prüfkonfiguration. Interner Versuchsbericht. Rüschlikon, Switzerland.
10. Baumeister A., et al., 1972: Neuere Karlsruher Forschungsarbeiten und Versuche im Ingenieurholzbau. bauen mit holz 74(6): 298-317.
11. Sretenovic A., et al., 2004: New shear assay for the simultaneous determination of shear strength and shear modulus in solid wood: Finite element modelling and experimental results. Wood and Fiber Science 36(3): 303-310.
12. Logemann M., 1991: Abschätzung der Tragfähigkeit von Holzbauteilen mit Ausklinkungen und Durchbrüchen. VDI Verlag, Düsseldorf, Germany.
13. Sähn S., Göldner H., Nickel J., 1993: Bruch- und Beurteilungskriterien in der Festigkeitslehre. Fachbuchverlag, Leipzig, Germany.
14. Wu E.M., 1963: Application of fracture mechanics to orthotropic plates. Naval Research Laboratory, University of Illinois, Urbana, USA.
15. Mall S.B., Murphy J.F., Shottafer J.E., 1983: Criterion for mixed mode fracture in wood. Engineering Mechanics 109(3): 680-690.
16. Leicester R.H., 1974: Fracture strength of wood. In: Proceedings of the First Australian Conference on Engineering Materials, August 26 – 29, 1974. University of New South Wales, Sydney, Australia.
17. Mandery W.L., 1969: Relationship between perpendicular compressive stress and shear strength of wood. Wood Science 1(3): 177-182.
18. Seely F.B., Smith J.O., 1952: Advanced mechanics of materials. John Wiley and Sons Inc. New York, USA.

19. Norris C.B., 1962: Strength of orthotropic materials subjected to combinded stresses. FPL Report No. 1816, F.P. Laboratory, Madison, Wisconsin, USA.
20. Aicher S., Klöck W., 2001: Linear versus quadratic failure criteria for in-plane loaded wood based panels. Otto-Graf Journal 12: 187-199.
21. Gehri E., Mischler, A., 1995: Holztragwerke: Entwurfs- und Konstruktionsregeln. Lignatec 2/1995. Lignum - Holzwirtschaft Schweiz, Zürich, Switzerland.
22. Joint Committee on Structural Safety JCSS, 2006: Probabilistic Model Code – Part 3.05: Resistance Models: Timber. www.jcss.ethz.ch/publications/publications.html .
23. Keenan F.J., Jaeger T.A., 1978: Effect of transverse stress on the shear strength and failure mechanism of douglas-fir. Proceedings of the First International Conference on Wood Fracture, August 14 – 16, 1978. Forintek Canada Corp., Western Forest Products Laboratory, Banff, Alberta, USA.
24. Krüger O., 2010: Schubverstärkung von Holz mit Holzschrauben und Gewindestangen. Proceedings des 16. Internationalen Holzbau-Forums IHF 2010 "Aus der Praxis – Für die Praxis", December 1 – 3, 2010. Garmisch-Partenkirchen, Germany.
25. Eberhardsteiner J., 2002: Mechanisches Verhalten von Fichtenholz – Experimentelle Bestimmung der biaxialen Festigkeitseigenschaften. Springer, Wien, New York.
26. Gehri E., 2010: Shear problems in timber engineering – Analysis and solutions. Proceedings of the 11th World Conference on Timber Engineering WCTE 2010, June 20 – 24, 2010. Riva del Garda, Italy. Paper No. 614.
27. Keenan F.J., 1974: Shear strength of wood beams. Forest Products Journal 24(9): 63-70.
28. Longworth J., 1977: Longitudinal shear strength of timber beams. Forest Products Journal 27(8): 19-23.
29. Soltis L.A., Rammer D.R., 1994: Shear strength of unckecked glued-laminated beams. Forest Products Journal 44(1): 51-57.
30. Augustin M., et al., 2006: Behaviour of glulam in compression perpendicular to grain in different strength grades and load configurations. Proceedings of CIB-W18 Meeting Thirty-Nine, 2006, Florence, Italy. Paper CIB-W18 39-12-5.
31. Blass H.J., Görlacher R., 2004: Compression perpendicular to the grain. Proceedings of the 8th World Conference on Timber Engineering WCTE 2004. June 14 – 17, 2004. Lahti, Finland. Vol. 2: 435-440.
32. Büeler M., 2011: Schubverhalten von Brettschichtholzträgern aus Buche und Esche. Master Thesis. Institute of Strcutural Engineering – Steel, Timber and Composite Structures, ETH Zürich, Switzerland.
33. http://www.gom.com/metrology-systems/system-overview/aramis.html.
34. Gehri E., 1997: Timber in compression perpendicular to the grain. Proceedings of the International Conference of IUFRO S 5.02 Timber Engineering. June 16 – 17, 1997. Copenhagen, Denmark. 355 – 374.
35. European Committee for Standardization, 2004: EN 1194: Timber structures – Glued laminated timber – Strength classes and determination of characteristic values. CEN, Bruxelles, Belgium.

CIB-W18/44-7-1

INTERNATIONAL COUNCIL FOR RESEARCH AND INNOVATION IN BUILDING AND CONSTRUCTION

WORKING COMMISSION W18 - TIMBER STRUCTURES

PULL-THROUGH CAPACITY IN PLYWOOD AND OSB

J Munch-Andersen
Danish Timber Information

J D Sørensen
Aalborg University

DENMARK

MEETING FORTY FOUR

ALGHERO

ITALY

AUGUST 2011

Presented by J Munch Andersen

F Lam commented that the statement that density of the panel did not influence pull through capacity was too strong. J Munch-Andersen responded that the analysis did not find any correlation. F Lam stated since the analysis considered reported data from different sources with a range of connectors and panel material, the influence of density was masked. If one were to consider a single connector type with panels of density, one would find density influence.

G Hochreiner and J Munch-Anderson discussed the issue that failure mode considerations may be important and modelling approach would be useful.

H Blass commented that KIT has additional results and questioned whether the head diameter of 18 mm is valid.

S. Aicher followed up on F Lam's point and commented that the range of applicability of plywood made from hardwood may not be valid. J Munch Andersen responded that that the results would be lower bound.

Pull-through capacity in plywood and OSB

Jørgen Munch-Andersen
Danish Timber Information, Denmark

John Dalsgaard Sørensen
Aalborg University, Denmark

Introduction

The characteristic pull-through capacity of heads of nails and screws is needed to determine the rope effect for laterally loaded fasteners used to fix sheathing to timber-frames. There is no values given in EN 1995 (Eurocode 5) but data for the pull through capacity of nail and screw heads has been found in four different references. All fasteners and panels are North American. A fairly general and accurate model is found and the characteristic values according to EN 1990 are determined.

Data

The data used originates from the following four references:

1 Herzog & Yeh (2006)
8d box nails in plywood and OSB of different thickness. About 40 repetitions for each type of panel, conditioned at 20 °C and 65 % RH. The diameter of the head d_{head} and panel thickness t in inches is also given in APA (2007). These values are used here as they seem to be more accurate than the values in mm stated in the paper.

2 Chow et al. (1998)
6d common nails in one type of plywood and two grades of OSB. 50 repetitions for each type of panel, conditioned at 20 °C and 65 % RH. d_{head} is not stated but according to the standard specification for 6 d common nails it is 17/64 inch or 6,75 mm.

3 Chui & Craft (2002)
Different types of round-headed screws (gauge 8 and 14), common nails (2" and 3") and power nails with full but eccentric head and with clipped (D-shaped) head. 30 repetitions for each type of panel, conditioned at 20 °C and 80 % RH. Measured values of d_{head} is reported and given in Table 1. For the power driven nails the heads are not circular but both max and min diameter are given. d_{head} in Table 1 is taken as the square root of the product of max and min diameter. This is likely to underestimate the area of the head for the clipped head nails slightly.

4 Forintek (n.a.)
Wood screw gauge 10 in thin plywood and OSB with thickness up to 18 mm. 10 repetitions for each type of panel. Conditioning, densities and d_{head} are not reported. According to American Standard B18.6.1 - 1961 the diameter for flat headed wood screws should be in the range 0,34 - 0,385 inch or 8,6 - 9,8 mm. According to a manufacturers brochures round-headed wood screws should be expected to be 5-10 % smaller. It is chosen to use d_{head} = 9,3 mm (the upper limit is the safe choice).

In all cases the mean value ($F_{head,obs}$) and the coefficient of variation (V_{obs}) (or standard deviation) are reported. All the data are assembled in Table 1. They represent plywood and OSB panels from many different manufactures and different thicknesses, even though most panels are about ½ inch thick. All thicknesses are nominal. The fastener types comprise round-headed wood screws, flat headed nails and power driven nails with eccentric head. Unfortunately no data for flat headed screws are found.

Model

In Herzog & Yeh (2006) and Forintek (n.a.) it is demonstrated for a specific type of fastener that the relationship between the pull-through capacity and the thickness of the panel is:

- linear,
- the same for plywood and OSB, and
- independent of density.

It appears that a quite good model for the mean value is

$$F_{head,model} = b\,t\,d_{head}$$

where b is a constant with dimension force/length^2, t is the nominal thickness of the panel and d_{head} is the diameter of the head, in principle the real diameter but otherwise the most informed guess. This is a physically reasonable model as the area of the rupture surface is proportional to $t\,d_{head}$ if a cone shaped rupture surface is anticipated.

EN 1990 offers in section D8 a method to estimate the characteristic load-carrying capacity when such a model is applied. The following is based on that method, modified to be used for data where only the mean value and the coefficient of variation are known for repetitions of the same test. The modifications are given in Annex A together with some quite accurate approximations that apply for practical use in general. These approximations are also given in Munch-Andersen et al. (2010).

The slope should be estimated from Eq. (D.7) in EN 1990 as

$$b = \frac{\Sigma F_{head,obs}\,t\,d_{head}}{\Sigma (t\,d_{head})^2}$$

where each value of $F_{head,obs}$ is repeated n_i times according to the number of repetitions it represents. In Table 2 the estimated values are given. It is seen that b is almost identical for plywood and OSB. Figure 1 shows the observed mean values of the capacities plotted against the value estimated by the model. The estimation method for b ensures that the deviation from the ideal line with slope 1 is minimized. It should be noted theat the above model for b is a generalisation of the model in Eq. (D.7) in EN 1990 which ensures that the bias becomes one).

Table 1. Data for pull-through capacity for nails and screws in plywood and OSB.

Fastener type	d_{head} mm	t mm	ρ kg/m3	n_i	$F_{head,obs}$ N	V_{obs}	$F_{head,model}$ N	$\overline{\Delta}_i$	Ref.
Plywood									
Clipped 2 3/8 pw.n.	6,9	11,1	400	30	1095	0,12	1437	-0,27	3
Clipped 3" pw. nail	6,2	11,1	400	30	1121	0,13	1291	-0,14	3
Wood screw #14	11,7	11,1	400	30	2215	0,13	2420	-0,09	3
Wood screw #8	7,2	11,1	400	30	1406	0,16	1492	-0,06	3
6d common nail	6,8	12,7	525	50	1526	0,15	1603	-0,05	2
2" common nail	6,2	11,1	400	30	1242	0,18	1288	-0,04	3
Wood screw #10	9,3	7,9	-	10	1342	0,09	1380	-0,03	4
8d box nail	7,5	9,5	519	40	1353	0,20	1343	0,01	1
Full 2 3/8 pw.nail	7,1	11,1	400	30	1503	0,10	1470	0,02	3
8d box nail	7,5	12,7	559	40	1909	0,12	1790	0,06	1
Full 3" power nail	6,0	11,1	400	30	1349	0,15	1249	0,08	3
3" common nail	8,1	11,1	400	30	1939	0,13	1683	0,14	3
OSB									
Clipped 2 3/8 pw.n.	6,9	11,1	590	30	1131	0,39	1440	-0,24	3
Wood screw #10	9,3	11,1	-	10	1648	0,27	1936	-0,16	4
6d common nail	6,8	12,7	685	50	1477	0,15	1606	-0,08	2
Wood screw #14	11,7	11,1	590	30	2241	0,20	2426	-0,08	3
Wood screw #10	9,3	18,3	-	10	2968	0,21	3181	-0,07	4
Full 2 3/8 pw. nail	7,1	11,1	590	30	1387	0,38	1473	-0,06	3
Clipped 3" pw. nail	6,2	11,1	590	30	1219	0,46	1294	-0,06	3
6d common nail	6,8	12,7	699	50	1526	0,18	1606	-0,05	2
6d common nail	6,8	11,1	659	50	1348	0,19	1405	-0,04	2
8d box nail	7,5	11,1	588	40	1566	0,19	1570	0,00	1
8d box nail	7,5	9,5	627	40	1353	0,27	1346	0,01	1
6d common nail	6,8	11,1	707	50	1428	0,20	1405	0,02	2
8d box nail	7,5	11,9	598	40	1749	0,17	1682	0,04	1
2" common nail	6,2	11,1	590	30	1399	0,20	1291	0,08	3
Wood screw #8	7,2	11,1	590	30	1628	0,20	1495	0,09	3
3" common nail	8,1	11,1	590	30	1862	0,26	1686	0,10	3
Full 3" power nail	6,0	11,1	590	30	1510	0,32	1252	0,19	3
Wood screw #10	9,3	15,1	-	10	3214	0,13	2628	0,20	4

The observations with power nails with clipped head (D-shaped) are not included in the analysis because the measurements reveal a significantly smaller capacity than predicted by the model for the other types of fasteners. Besides the size of the head is underestimated when the equivalent head diameter is calculated as it is done here. Further the coefficient of variation for OSB is extremely large (30 % – 50 %), see Table 1.

Table 2. Estimated parameters.

	b, N/mm^2	V_δ	"b_k", N/mm^2
Plywood and OSB	18,72	0,21	13,0
Only plywood	18,70	0,16	14,2
Only OSB	18,74	0,23	12,4

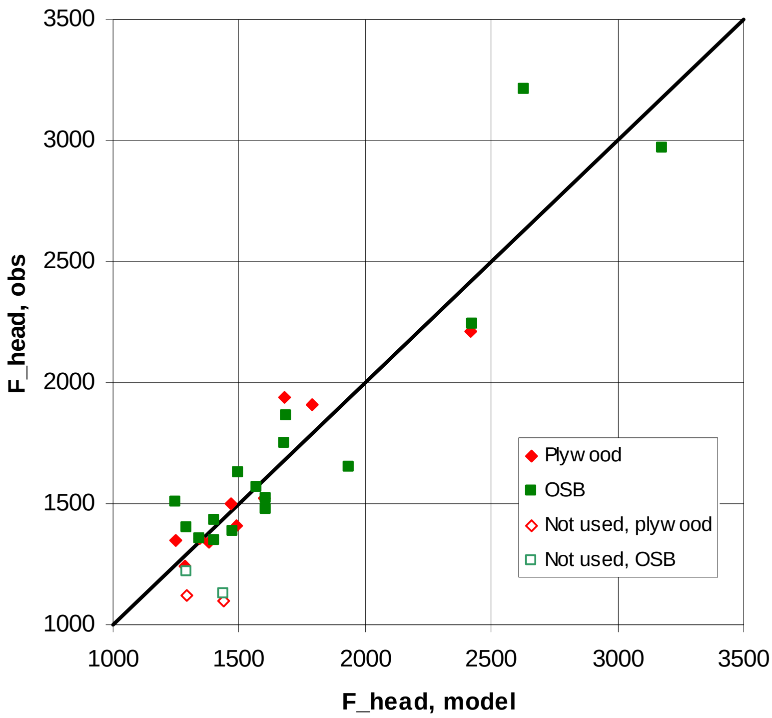

Figure 1. The observed mean pull-through capacities versus the capacities estimated from the model.

The coeffient of variation V_δ of the model is estimated from Eq (7) in Annex A with $s_{\Delta_i} = V_{obs}$ and $\overline{\Delta}_i = \ln(F_{head,obs,i} / F_{head,model,i})$. In Table 2 it is seen that the coefficient of variation is significantly smaller for plywood than for OSB implying that the characteristic value for plywood will be higher than for OSB, even though the model for the mean value is identical.

A large V_δ indicates a bad model. Attempts to include the density in the model or to use a power on t and d_{head} give no real improvement. For plywood it is somewhat surprising that the density does not matter.

When calculating the characteristic capacity using the procedure in EN 1990, Annex D the uncertainty of the basic variables should be added to the model uncertainty V_δ. But since there is no dependency on the density and because the tests represent a broad range of panels and fasteners there are no other uncertainties of the basic variables than those reflected by the tests. The term V_x in EN 1990 can therefore be assumed to be nil. The ratio between the characteristic and the mean value can then be estimated from

$$\eta = \exp(-k_s V_\delta - 0,5V_\delta{}^2)$$

where k_s is a number depending on the number of tests and the last term is a correction due to LogNormal-distribution of the capacity. Since there are many tests, k_s = 1,64 can be used. In Table 2 is given values for $"b_k" = \eta b$.

Discussion and conclusions

Based on results from about 1000 pull-through tests with various types of fasteners in plywood and OSB is it found that the pull-through capacity is proportional to the nominal thickness t of the panel and the diameter d_{head} of the head of the fastener. The characteristic capacities can be estimated from

$$\text{Plywood}: F_{head,k} = 14\,\text{N/mm}^2\, t\, d_{head}$$
$$\text{OSB}: \quad F_{head,k} = 12\,\text{N/mm}^2\, t\, d_{head}$$

with the following limitations:

- 9 mm $\leq t \leq$ 18 mm
- $d_{head} < t$
- For plywood the capacity should be reduced by 30% when applied to power nails with clipped head and screws with flat head.
- For OSB the estimate is not applicable to power nails with clipped head and screws with flat head.

The limits on t and d_{head} reflect the range of parameters represented in the tests. For t > 18 mm the value for t = 18 mm can be used.

Flat headed screws are not included in the test and power nails with clipped head gives quite low values.

For clipped heads in plywood the 30% reduction should be safe as the observations are 27% and 14% below the model and the coefficient of variation V_{obs} is similar to other types of fasteners. For OSB the very large coefficient of variation makes it impossible to estimate a value based on the few tests.

The large variation in general for OSB might be due to larger inhomogeneities in the material. The average density is higher than for plywood which might explain why the mean capacity becomes the same as for plywood. The particular large coefficient of variation and small mean value for clipped heads might be because those nails damage the surface more than the other types.

For flat headed screws the capacity might be smaller. For the more homogeneous plywood it is unlikely to be a great reduction, so 30 % will be a conservative guess. For OSB the surface will be damaged in an unpredictable way.

The density has no significant influence on the capacity.

References

Herzog, B & Yeh, B (2006). Nail Withdrawal and Pull-Through Strength of Structural-Use Panels. Proc. 9th World Conference on Timber Engineering, Portland, OR.

APA (2007) Nailhead pull-through strength of wood structural panels. TT-070A. APA - The Engineered Wood Association.

Chow, P, McNatt, JD, Lambrecths, SJ & Gertner, GZ (1988). Direct withdrawal and head pull-through performance of nails and stables in structural wood-based panel materials. Forrest Product J., vol 38 no 6.

Chui, Y H & Craft, S (2002). Fastener head pull-through resistance of plywood and oriented strand board. Canadian Jour. of Civil Enginerring, vol 29 pp 384-388.

Forintek (n.a.). Derivation of code requirement to prevent head pull-through failure of wood screws.

Munch-Andersen, J, Sørensen, J D & Sørensen, F (2010). Estimation of load-bearing capacity of timber connections. Proc. Of CIB-W18 Timber Structures. Nelson, New Zealand.

Annex A
Estimation of CoV of model error from data from literature

When a model of the type

$$x = bt \tag{1}$$

is used to describe the relation between the independent (input) variable t and the dependent (output) variable x the factor b should be estimated from test results.

When n levels of t are used the independent variables can be named t_i , $i = 1 \,.\,.\, n$. If the test is repeated n_i times for level i the dependent variables can be named x_{ij} , $j = 1 \,.\,.\, n_i$. The total number of tests is

$$N = \sum_{i=1}^{n} n_i$$

According to section D8 in EN 1990 the variation of the model error is determined from the standard deviation of

$$\Delta_{ij} = \ln \frac{x_{ij}}{bt_i} \tag{2}$$

The coefficient of variation of the error becomes approximately

$$V_\delta^2 \approx s_\Delta^2 = \frac{1}{N-1} \sum_{i=1}^{n} \sum_{j=1}^{n_i} \left(\Delta_{ij} - \overline{\Delta} \right)^2 \tag{3}$$

where

$$\overline{\Delta} = \frac{1}{N} \sum_{i=1}^{N} \Delta_{ij} \tag{4}$$

When data are found in the literature usually only t_i, the mean values $\overline{x}_i$ and the coefficient of variations V_{x_i} is reported. In the following it is shown how V_δ can be estimated based on these information. With the definitions

$$\overline{\Delta}_i = \frac{1}{n_i} \sum_{j=1}^{n_i} \Delta_{ij} \qquad \text{and} \tag{5}$$

$$s_{\Delta_i}^2 = \frac{1}{n_i - 1} \sum_{j=1}^{n_i} \left(\Delta_{ij} - \overline{\Delta}_i \right)^2 \tag{6}$$

Eq (3) can be rewritten

$$V_\delta^2 \approx s_\Delta^2 = \frac{1}{N-1} \sum_{i=1}^{n} \left[\left(n_i - 1 \right) s_{\Delta_i}^2 + n_i \left(\overline{\Delta}_i - \overline{\Delta} \right)^2 \right] \tag{7}$$

In Eq. (4) $\overline{\Delta} = 0$ will be a very accurate estimate, even for not very good models.

Eq (5) can for normal cases with good accuracy be substituted by

$$\overline{\Delta}_i \approx \ln \frac{\overline{x}_i}{bt_i} \tag{8}$$

where the mean of the logarithms is replaced by the logarithm of the mean.

In Eq. (6) the last term can be then rewritten

$$\Delta_{ij} - \overline{\Delta}_i = \ln \frac{x_{ij}}{bt_i} - \ln \frac{\overline{x}_i}{bt_i} = \ln x_{ij} - \ln \overline{x}_i$$

so

$$s_{\Delta_i}^2 = \frac{1}{n_i - 1} \sum_{j=1}^{n_i} \left(\ln x_{ij} - \ln \overline{x}_i \right)^2$$

which is seen to be equal to the standard deviation of ln(x_i). This can with good accuracy can be substituted by V_{x_i} . Therefore

$$s_{\Delta_i}^2 \approx V_{x_i}^2 \tag{9}$$

Hereby good estimates for all terms in Eq. (7) are available.

Note: When the factor b is estimated from the mean values $\overline{x}_i$ these should be weighted by n_i if the number is not the same for all levels of t_i. The easiest way is to repeat each $\overline{x}_i$ n_i times in the estimation.

Example

In Table A1 is given an example with constructed data chosen such that b = 10 and the coefficient of variation for each level of t is approximately constant. Figure 1 shows a plot of x_{ij} versus bt_i.

It is seen that $n = 4$ and all $n_i = 5$ so $N = 20$. From Eqs. (3) and (4) are found

$s_\Delta = 0{,}0775$ and $\overline{\Delta} = 0{,}0006 \approx 0$.

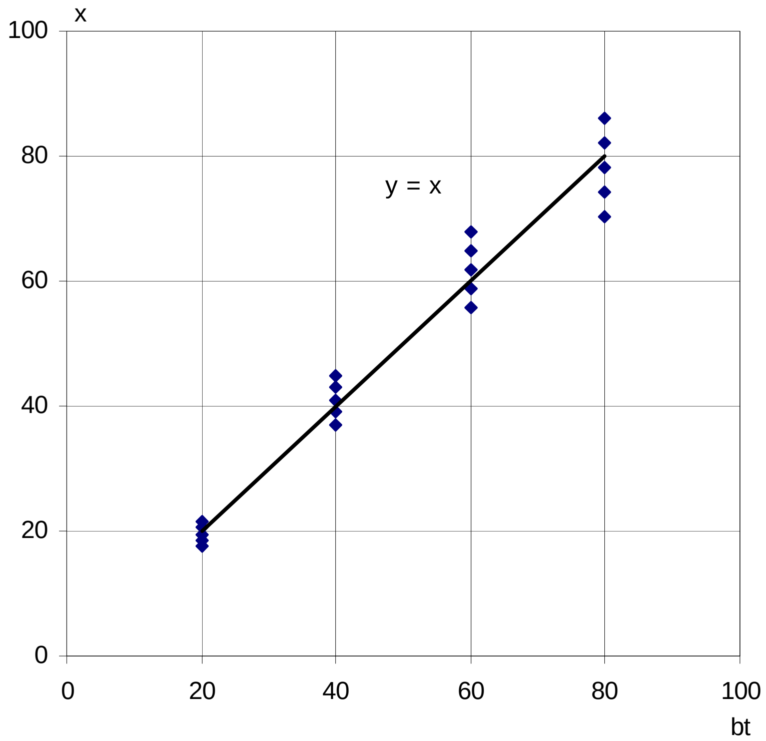

Figure A1. The observed values versus the estimated for b = 10. b should be chosen such that the slope of the best linear regression line becomes 1.

Table A1. Data and calculations when all data are available.

i	j	t_i	x_{ij}	bt_i (1)	Δ_{ij} (2)	$\overline{\Delta}_i$ (5)	s_{Δ_i} (6)
1	1	2	17,5	20	-0,134		
1	2	2	18,5	20	-0,078		
1	3	2	19,5	20	-0,025		
1	4	2	20,5	20	0,025		
1	5	2	21,5	20	0,072	-0,0280	0,0814
2	1	4	37,0	40	-0,078		
2	2	4	39,0	40	-0,025		
2	3	4	41,0	40	0,025		
2	4	4	43,0	40	0,072		
2	5	4	45,0	40	0,118	0,0223	0,0774
3	1	6	55,9	60	-0,071		
3	2	6	58,9	60	-0,019		
3	3	6	61,9	60	0,031		
3	4	6	64,9	60	0,079		
3	5	6	67,9	60	0,124	0,0288	0,0769
4	1	8	70,2	80	-0,131		
4	2	8	74,2	80	-0,075		
4	3	8	78,2	80	-0,023		
4	4	8	82,2	80	0,027		
4	5	8	86,2	80	0,075	-0,0254	0,0812

If only $\overline{x_i}$ and V_{x_i} are known the data will be as in Table A2. From Eq. (7) is found $s_\Delta = 0{,}0773$. It is seen to be very accurate for this example.

Table A2. Data and calculations when only mean values and coefficient of variation is known.

i	n_i	t_i	$\overline{x_i}$	bt_i (1)	V_{x_i}	$\overline{\Delta}_i$ (8)	s_{Δ_i} (9)
1	5	2	19,5	20	0,0811	-0,025	0,0811
2	5	4	41	40	0,0771	0,025	0,0771
3	5	6	61,9	60	0,0766	0,031	0,0766
4	5	8	78,2	80	0,0809	-0,023	0,0809

CIB-W18/44-7-2

INTERNATIONAL COUNCIL FOR RESEARCH AND INNOVATION IN BUILDING AND CONSTRUCTION

WORKING COMMISSION W18 - TIMBER STRUCTURES

DESIGN CONCEPT FOR CLT - REINFORCED WITH SELFTAPPING SCREWS

P Mestek

H Kreuzinger

S Winter

Lehrstuhl für Holzbau und Baukonstruktion

TU München

GERMANY

MEETING FORTY FOUR

ALGHERO

ITALY

AUGUST 2011

Presented by P Mestek

H Blass commented that considering the average k_{R90} behaviour for comparison between test and model would be okay. For final design considerations, would it be possible to consider characteristic values by shifting the whole line. P Mestek agreed.

H Blass commented about the stiffness of screws in relationship to the rolling shear load path and asked whether screw withdrawal was observed. P Mestek responded mostly screw tension failures were observed and only one case of withdrawal was seen. H Blass asked how one would know that the screws were loaded to their capacity. P Mestek responded that this was a simplification for the practical design concept.

F Lam commented reporting r^2 values with two data clouds as shown in Figures 6 and 7 is not appropriate.

U Kuhlmann received explanations about that the effective width was based on elastic theory.

Design concept for CLT - reinforced with self-tapping screws

P. Mestek, H. Kreuzinger, S. Winter

Lehrstuhl für Holzbau und Baukonstruktion

TU München

Abstract: Concentrated loads on Cross Laminated Timber elements (CLT) in areas of point supports or load applications cause high local shear stresses. Inclined self-tapping screws with continuous threads have turned out to be an effective reinforcement. As neither the German design standard DIN 1052 [1] nor technical approvals cover this construction method a research project funded by the AiF [2] was conducted to gather basic information for its application. These basics include the determination of shear stresses next to concentrated loads, the interaction of compression perpendicular to the grain and rolling shear stresses as well as theoretical and experimental examinations of the load bearing behaviour of reinforced CLT-elements. This paper presents the main research results. A design concept validated by means of the test results is proposed [3].

1 Introduction

Ceilings of CLT are generally simply supported on two sides so that uniaxial load transfer is activated parallel to the lamellas of the top layers. Due to the composition of the CLT-elements, with an orthogonally alternating orientation of neighbouring board layers, the slabs are also suitable for constructions with point supports. These systems profit from the biaxial load transfer and the possibility of the prefabrication of large-scale elements.

Concentrated loading causes high shear stresses in these areas (Fig. 1). Since the rolling shear capacity of timber is considerably lower than its shear capacity parallel to the grain shear-fracture appears in the cross layers of CLT elements. First tests within the scope of pilot projects revealed that reinforcements with inclined self-tapping screws noticeably enhance the shear capacity of the CLT-elements [4]. As these reinforcements are not covered by the current design standards a research project funded by the AiF [2] was conducted to gather basic information for their application.

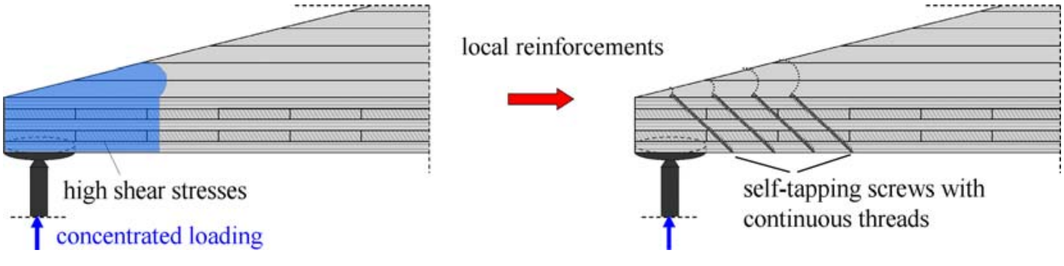

Fig. 1 Local reinforcements by self-tapping screws with continuous threads

2 Experimental tests

Within the scope of the project various experimental tests were carried out. Some small-scale tests were necessary to determine material and system parameters for the FEM-simulations carried out in parallel. Tests with CLT-elements supplied basic information for the interaction of rolling shear and compression perpendicular to the grain as well as for the load bearing behaviour and the strengthening effect of CLT-elements reinforced by self-tapping screws.

2.1 Material und fabrication

The cross section of the test specimens consisted of seven layers, the total thickness of the elements was 119 mm (7 x 17 mm) respectively 189 mm (7 x 27 mm). The base plates were built up of spruce boards of grade S10 (visual grading according to DIN 4074-1 [5]) that were not glued along their edges. The density of the boards for the cross layers ranged between 440 kg/m^3 and 480 kg/m^3. Due to the fabrication process by vacuum gluing, the lamellas of the test series “Type 119” and “Type 189” had relief grooves parallel to the grain as shown in Figure 2.

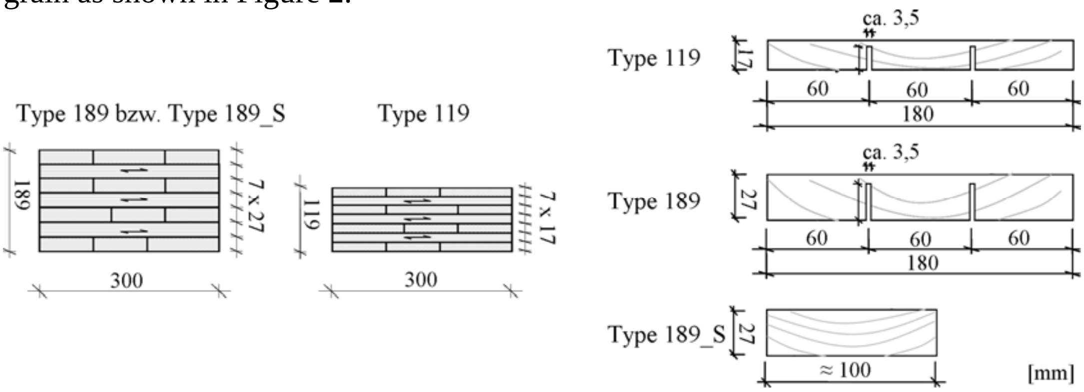

Fig. 2 Cross sections and dimensions of the single boards

2.2 Interaction of rolling shear stresses and compression perpendicular to the grain

Concentrated loading in CLT elements causes a combination of high shear stresses and compression perpendicular to the grain (Fig. 3). The positive effect of compression on the shear capacity parallel to the grain is an established fact and has been object of various investigations [6], [7]. However, comparable evaluations concerning the interaction of rolling shear strength and compression perpendicular to the grain are not yet available. Hence experimental tests were carried out to gather first information on the increase in rolling shear capacity due to this stress interaction. Therefore shear elements inclined against the vertical by 10° were stressed by a shear force. The shear force was induced into the layers parallel to the primary direction (Fig. 4). The initiation of the compression was developed by lateral steel profiles (HEA 100) coupled with exterior rods. The rods in combination

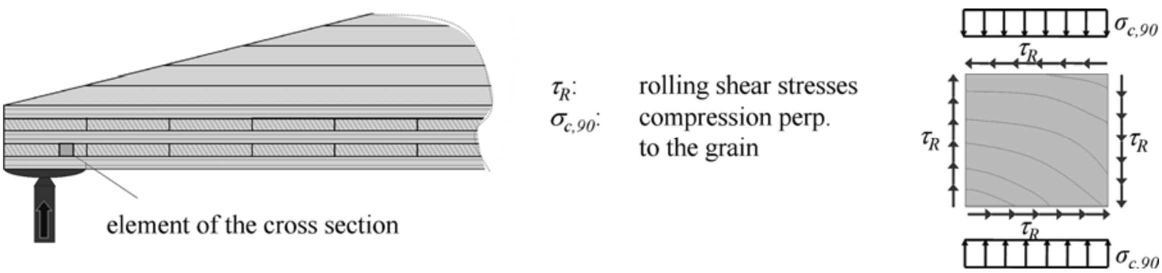

Fig. 3 Interaction of rolling shear and compression perp. to the grain caused by concentrated loading

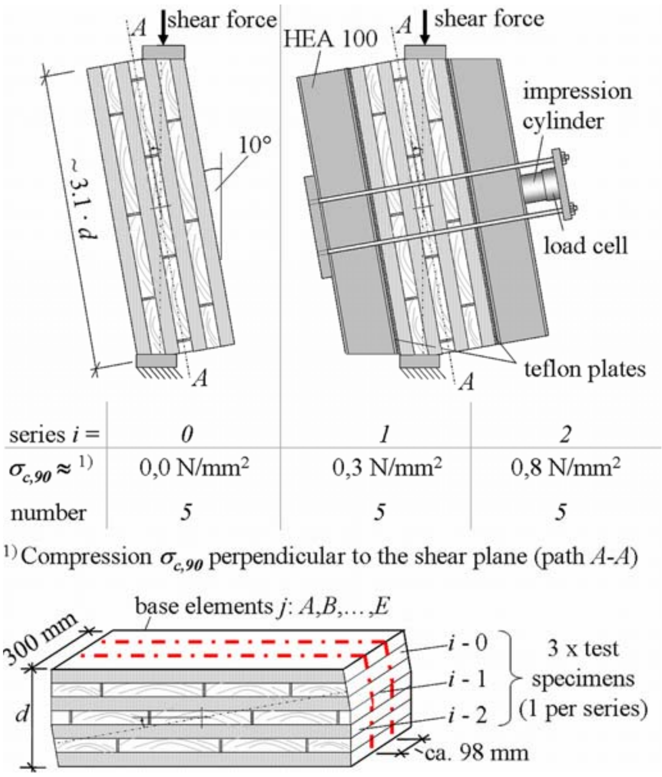

Fig. 4: Test configuration

with the head plates and the impression cylinder enabled the initiation of a specific compression that could be controlled by the load cell. Fraction minimizing teflon plates between the test specimens and the steel profiles avoided any transfer of shear forces by the framework and guaranteed free shear deformation of the test samples. The base elements had a width of 300 mm. As shown in Fig. 4 five base elements of each section type were separated into three test specimens. To minimize the variation of the results one test specimen per base element was assigned to each test series. In order to determine a reference value one series (i = 0) of each section type was tested without external pre-stressing.

The simulation of the test configuration by using an FEM-shell-model [8] shows that due to the inclined load initiation compression perpendicular to the shear plane is mainly located in the boundary region (Fig. 5). Because of its rapid decrease it was neglected in the course of further evaluations. The force component parallel to the shear plane causes an almost constant distribution of rolling shear stresses. So the rolling shear capacity was calculated on the assumption of a constant stress distribution. The mean values in table 1 indicate, that not only the material but essentially the geometric relations of the board dimensions respectively the arrangements of the relief grooves influence the level of resistance. It appeared that the smaller the ratio of the distance between the gaps or relief grooves to the thickness of the layers, the smaller the rolling shear capacity.

Table 1: Mean values of the rolling shear capacity

Elements		Type 119-i		Type 189-i		Type 189_S-i	
Series i	$\sigma_{c,90}$ [N/mm²]	$f_{R,mean,i}$ [N/mm²]	COV [-]	$f_{R,mean,i}$ [N/mm²]	COV [-]	$f_{R,mean,i}$ [N/mm²]	COV [-]
$i = 0$	0,00	1,47	0,08	0,90	0,09	1,42	0,06
$i = 1$	≈ 0,30	1,52	0,07	1,10	0,09	1,61	0,04
$i = 2$	≈ 0,80	1,84	0,07	1,27	0,06	1,83	0,04

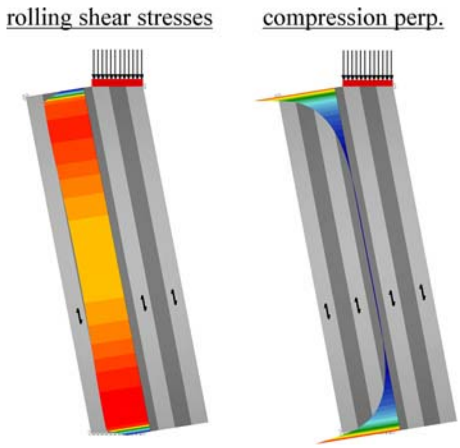

Fig. 5: Distribution of stresses

The main focus was directed to the increase of the strength and not on the value of the rolling shear strength itself. As reference values served the results of the series without external pre-stressing. The increase in the rolling shear capacity can be described by the parameter $k_{R,90}$ according to equation (1). The evaluation was carried out separately for each base element to minimize the influence of the material properties.

$$k_{R,90} = \frac{f_{R,i,j}}{f_{R,i=0,j}} \qquad \text{with} \quad i = 1, 2 \text{ and } j = A, \ldots, E \qquad (1)$$

The chart in Fig. 6 illustrates the evaluation of the parameter $k_{R,90}$ according to equation (1) and the corresponding regression curves of each element type. It appears that the ratio of the distance between the gaps to the thickness of the layer affects the parameter $k_{R,90}$ as well. Nevertheless it does not seem useful to consider this geometrical ratio within a practical design concept, since the influence of the ratio on the resistance is already taken into account by the characteristic rolling shear capacity in the technical approvals. In addition the designing engineer does generally not know the exact dimension of the boards and even less the arrangement of the relief grooves. So the final proposal for the parameter $k_{R,90}$ was derived on the basis of a regression curve including all results without differentiation of the element types (Fig. 7). It represents a conservative criterion for the stress interaction that allows an increase of maximal 20 % of the rolling shear capacity. The parameter $k_{R,90}$ should be applied within the stress verification as shown in the following equations:

$$\tau_{R,d} \leq k_{R,90} \cdot f_{R,d} \qquad \text{with} \qquad k_{R,90} = \min\begin{cases} 1 + 0{,}35 \cdot \sigma_{c,90} \\ 1{,}20 \end{cases} [-] \quad \text{and} \quad \sigma_{c,90} \text{ in N/mm}^2 \qquad (2) \text{ and } (3)$$

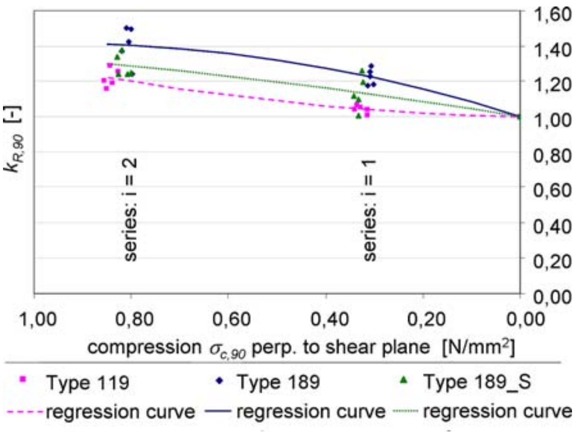

Fig. 6 Evaluation of $k_{R,90}$ for each element type

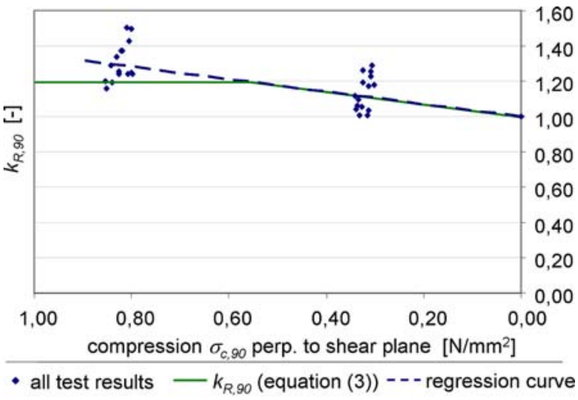

Fig. 7 Proposal for the calculation of $k_{R,90}$

2.3 Reinforcements – uniaxial load transfer

The load bearing behaviour of reinforced CLT elements was analysed by means of various test configurations. Tests with shear elements that were inclined against the vertical by 10° (analogue to Fig. 4, without pre-stressing) are described and evaluated in [2]. In addition the following four-point-bending tests according to CUAP 03.04/06 [9] were carried out. The test configuration and main dimensions are shown in Fig. 8. First one unreinforced series of each element type was tested to determine a reference value of the rolling shear capacity. Table 2 contains the calculated mean and characteristic values. Then the elements of the remaining series were reinforced with self-tapping screws with continuous threads (Spax-S [10], diameter d = 8,0 mm). The primary criterion to describe the influence of the reinforcements on the structural behaviour is the strengthening factor $\eta_{mean,i}$. It is defined by the ratio of the proof loads of the

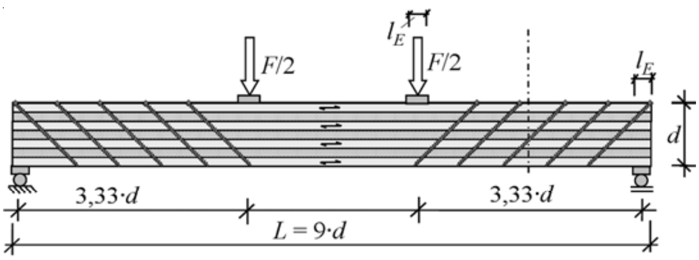

	d	L	l_E	width b	
Type 119	119	1070	50	300	[mm]
Type 189 / 189_S	189	1700	80	300	[mm]

Fig. 8 Configuration of four-point-bending tests

Table 2: Rolling shear capacity of the unreinforced elements

Element Type	Type 119	Type 189	Type 189_S	
$f_{R,mean,0}$	1,35	0,97	1,34	[N/mm^2]
$f_{R,k,0}$	1,13	0,77	1,08	[N/mm^2]
$f_{R,k}$ (acc. to abZ)	0,70	0,70	0,70	[N/mm^2]

reinforced elements to the proof loads of the unreinforced reference series:

$$\eta_{mean,i} = \frac{F_{mean,i}}{F_{mean,0}} \qquad \left(= \frac{F_{mean,\,reinforced\ specimens}}{F_{mean,\,unreinforced\ specimens}} \right) \tag{4}$$

Tables 3 to 5 give a general view of the tested arrangements of screws for each element type and also contain the strengthening factor $\eta_{mean,i}$, calculated on the basis of the test results. Each series consisted of five test specimens. The results reveal that the application of screws increases the load-carrying capacity by up to 64 %. Even comparatively few screws cause an increase of more than 25 %. So the structural behaviour is affected positively by a growing number of screws. Consequently the failure mode changes and the elements partially fail by bending and not by shear fracture.

Table 3: Type 119 – strengthening factor $\eta_{mean,i}$

Arrangement of the screws (d = 8,0 mm) in mm	Type	$\eta_{mean,i}$ [-]	COV [-]
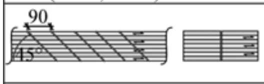	119-1	**1,25**	0,03
	119-2	**1,30**	0,09

Table 4: Type 189 – strengthening factor $\eta_{mean,i}$

Arrangement of the screws (d = 8,0 mm) in mm	Type	$\eta_{mean,i}$ [-]	COV [-]
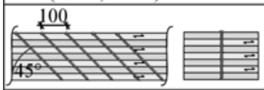	189-1	**1,31**	0,05
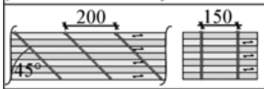	189-2	**1,38**	0,06
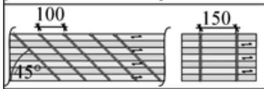	189-3	**1,64**	0,08
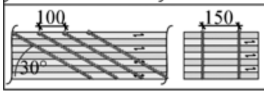	189-4	**1,59**	0,04

Table 5: Type 189_S – strengthening factor $\eta_{mean,i}$

Arrangement of the screws (d = 8,0 mm) in mm	Type	$\eta_{mean,i}$ [-]	COV [-]
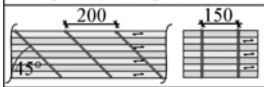	189_S-2	**1,34**	0,02
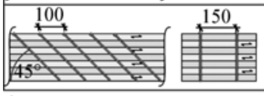	189_S-3	**1,46***	0,10*

*partially bending failure

2.4 Reinforcements – biaxial load transfer

Shear tests with plate elements were carried out to gain preliminary experience with reinforcements by self-tapping screws under biaxial load transfer. Plate elements supported along all sides and stressed by concentrated loading as well as elements with point supports in the corner regions were used according to the configurations shown in Fig. 10. A first test revealed intense indentations in the area of loading (Fig. 9). As a consequence self-tapping screws under the steel plates of the load application respectively the point supports were applied vertically to serve as reinforcements. Further information on this kind of reinforcement is given in [11].

Fig. 9 Intense indentations in the area of the load application

One unreinforced series of each configuration was tested to determine the reference values of the shear capacity. Then the series of reinforced elements shown in Fig. 10 were carried out. The series “Type 189_E-2” consisted of two, all others of three test specimens. Table 6 shows the strengthening factors $\eta_{mean,i}$ calculated by means of the proof loads according to equation (1) analogous to the tests on beam elements. The increase in load-carrying capacity ranged between 26 % and 49 %.

Table 6: Mean values of proof loads and strengthening factor $\eta_{mean,i}$

test configuration	central load Type 189_P-i		point support in corner region Type 189_E-i		
series i =	0 (unreinforced)	1 (reinforced)	0 (unreinforced)	1 (reinforced)	2 (reinforced)
mean value of proof loads $F_{mean,i}$ [kN]	381,1	479,4	304,9	409,7	455,6
COV [-]	0,05	0,02	0,04	0,05	0,01
strengthening factor $\eta_{mean,i}$ [-]	-	**1,26**	-	**1,34**	**1,49**

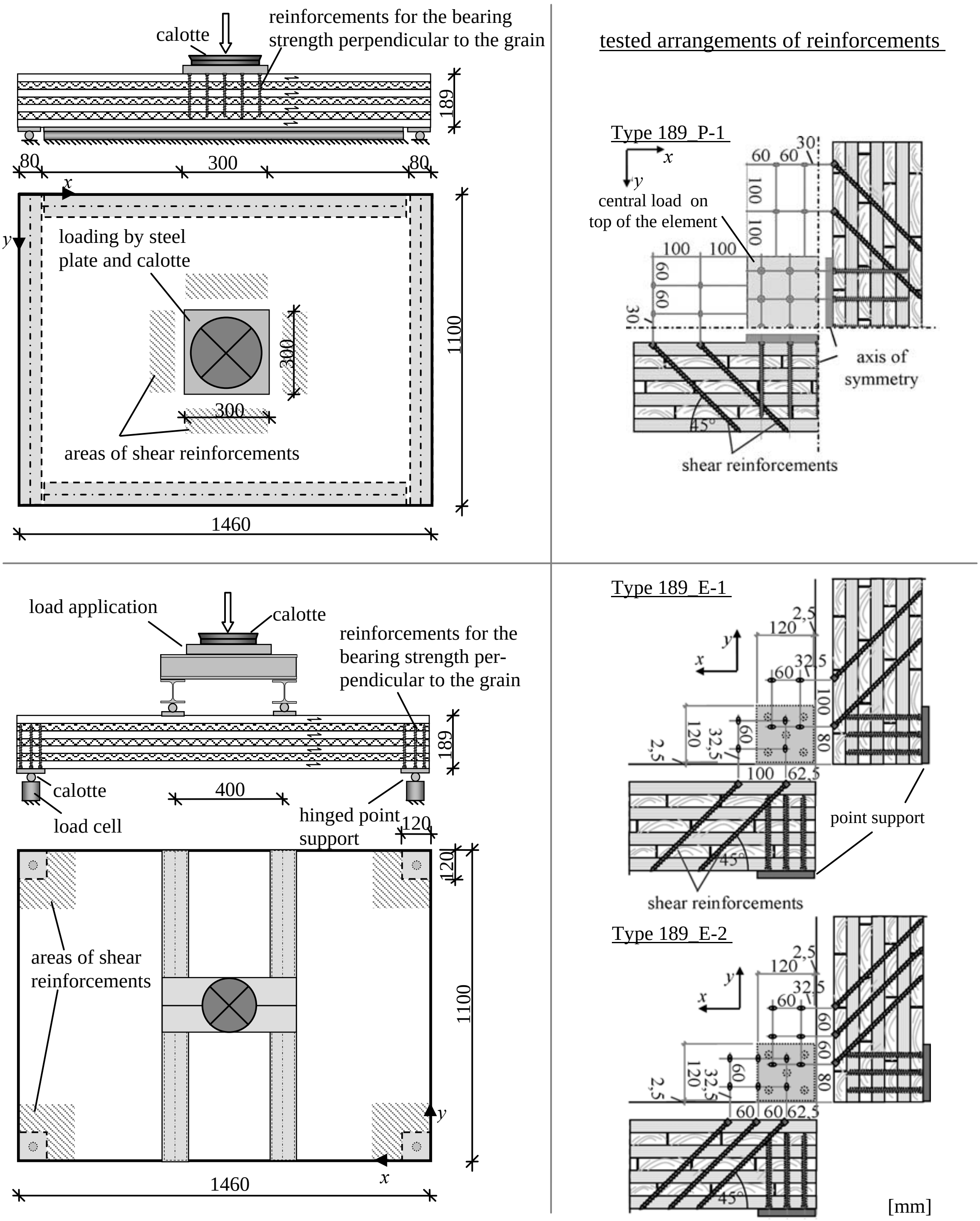

Fig. 10 Test configurations and arrangements of reinforcements

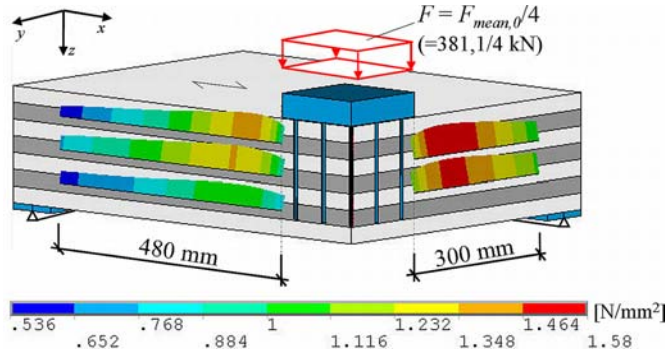

Fig. 11 Distribution of rolling shear stresses of the series “Type 189_P-0” (unreinforced element)

Due to the biaxial load transfer it is not possible to analytically calculate the rolling shear capacity by means of the proof loads. FEM-simulations were necessary to evaluate the rolling shear stresses at the time of failure. The simulations were done with the program ANSYS [12] using a solid model taking into account the symmetrical conditions (Fig. 11). The rolling shear stresses determined by the simulations exceed the rolling shear capacity according to the four-point-bending tests by up to 70 %. Further examinations revealed that this cannot be explained only by the stress interaction. Hence it may be assumed, that in case of biaxial load transfer additional effects like dispersion and redistribution of stresses or dowelling effects caused by less stressed areas get activated and thus lead to these comparatively high strength values.

3 Calculation of internal forces and stresses

In contrast to simply supported CLT slabs with uniformly distributed loads there are no calculation toolkits or design charts for constructions with point supports or concentrated loads available that guarantee a cost-effective and safe design. In the case of shear-design it is first of all necessary to evaluate the distribution of shear forces in primary and secondary supporting direction to be able to calculate the decisive shear stresses. Hence different influencing factors concerning the distribution of shear forces were examined by means of a parameter study in order to find an approach for the simple estimation of shear stressing. The calculations of this study were carried out using girder-grid-models in order to avoid stress peaks caused by concentrated loads and to minimize the computational effort. The required stiffnesses were calculated according to annex D.3 of the German design code DIN 1052 [1] using the material constants of boards of the strength class C 24.

Different influencing variables concerning the distribution of shear forces were evaluated. Detailed descriptions can be found in [2] and [3]. The significant variables and considered limits were:

- Thickness d of the elements: $0{,}10\text{ m} < d < 0{,}22\text{ m}$
- Ratio of the spans l/b: $1 < l/b < 3$
- Number of layers n: $5 < n < 11$
- Quadratic support (Fig. 13/14) $b_{A,x} = b_{A,y}$

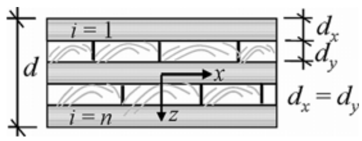

Fig. 12 Examined section type

The following structural systems were analysed:

- Central point support respectively concentrated loading
- Point support in the corner region

The results reveal that in the analysed systems the distribution of shear forces is predominantly influenced by the number of layers. Other parameters, like the ratio l/b of the element dimensions or its thickness can be neglected. So the shear force in primary direction can be calculated by applying the following equations and the shear force in secondary direction by the equilibrium of the forces.

- Central point support / concentrated loading (Fig. 13): $V_{xz} \approx 0{,}33 \cdot n^{-0{,}1} \cdot F_k$ (5)
- Point support in the corner region (Fig. 14): $V_{xz} \approx 0{,}67 \cdot n^{-0{,}1} \cdot F_k$ (6)

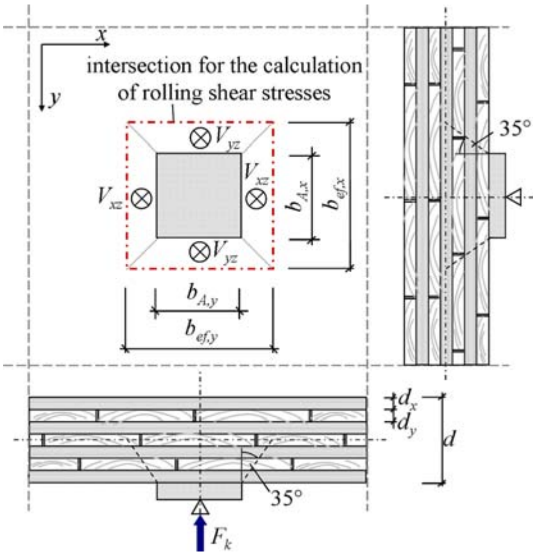

Fig. 13 Central point support / concentr. loading

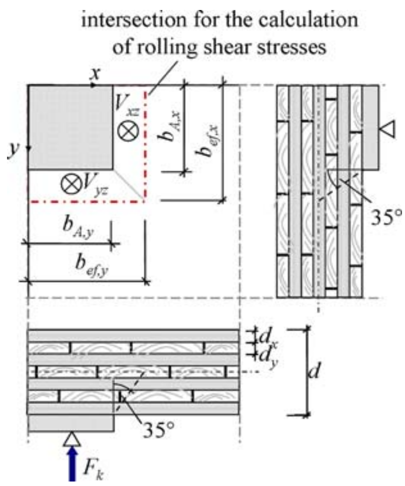

Fig. 14 Point support in the corner region

The calculation of the rolling shear stresses along the edges of the support leads to conservative but inefficient results. Hence different approaches of the load distribution were analysed by FEM-simulations using solid models [3]. It appeared that for the analysed systems and conditions the load distribution can be assumed at an angle of 35° to the centre line of the CLT elements. So the governing rolling shear stresses can be calculated by using the effective width shown in Fig. 13 and Fig. 14.

In addition the simulations show that there is a relatively constant distribution of shear stresses along the edges of central point supports. In contrast to this an increase of shear stresses in direction of the edges can be observed along the support edges of point supports in the corner regions (Fig. 15). This increase is according to the calculations in [3] more distinctive with growing ratio of the width of the supports to the thickness of the element. But the analyses of the effective width were based on the assumption that there is a constant distribution of shear stresses. Therefore it was necessary to determine a parameter k_A that considers the increase mentioned. Taking all results into account the rolling shear stresses can be calculated by the following simplified equations:

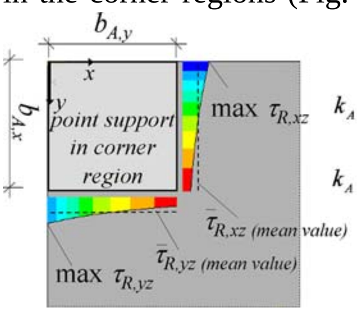

$$k_A = \frac{\max \tau_{R,xz}}{\bar{\tau}_{R,xz}} \quad (7)$$

$$k_A = \frac{\max \tau_{R,yz}}{\bar{\tau}_{R,yz}} \quad (8)$$

Fig. 15 Distribution of stresses

$$\tau_{R,xz} = \frac{V_{xz} / b_{ef,x}}{k_{R,x} \cdot (d_x + d_y)} \cdot k_A \qquad \text{and} \qquad \tau_{R,yz} = \frac{V_{yz} / b_{ef,y}}{k_{R,y} \cdot (d_x + d_y)} \cdot k_A \qquad (9) \text{ and } (10)$$

Table 7: Parameter $k_{R,x}$ and $k_{R,y}$ [-]

number of layers n	5	7	9	11
$k_{R,x}$	2,00	2,50	3,33	3,89
$k_{R,y}$	1,00	2,00	2,50	3,33

Table 8: Parameter k_A [-]

ratio of $b_{A,x}/d$ or $b_{A,y}/d$		≤ 1,0	≤ 1,5	≤ 2,0
point support in corner region	k_A=	1,35	1,50	1,65
central point support / concentrated loading	k_A=	1,00		

The equations can also be used for beam elements under uniaxial load transfer. In this case the effective width corresponds with the width of the beam and k_A is k_A = 1,0.

Note: In the equations (9) and (10) there is no differentiation of the shear forces of plane A and B according to the shear analogy (annex D.3 of DIN 1052 [1]), because this simplified assumption was taken as basis within the determination of the effective width.

4 Design concept

The FEM-models described in [2] and [3] on the basis of shell or volume elements are mainly suited for academic research or the analysis of special constructional details. But these simulations are comparatively complex and error-prone because of the great number of input parameters. For a general design concept it makes more sense to use a strut and tie model, which describes the structural behaviour of the composite section of CLT and self-tapping screws in a simplified manner. So it needs considerably fewer input parameters.

The following conditions respectively limits of application were defined to guarantee the verification by the results of the experimental tests and to realize a practical design concept.

- Symmetrical cross section
- Inclination of 45° of the screws
- Arrangements of the screws according to Fig. 16

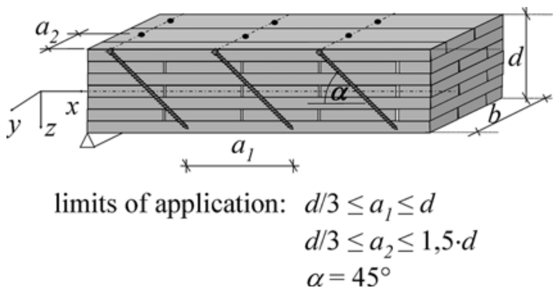

Fig. 16 Arrangements of the screws

4.1 Uniaxial load transfer

According to this design concept the load-carrying capacity under shear stresses of reinforced CLT elements is composed of the rolling shear capacity of the cross layer itself and the proportionate load-carrying capacity of the screws. The assumption of this simultaneous effect is justified, because the experimental tests show that despite the small shear deformation of the CLT elements tension forces are activated in the screws. For the calculation of the proportionate load-carrying capacity of the screws the model shown in Fig 17 can be used. The screws, symbolised by the diagonal struts, bear forces parallel to the shear plane. Due to the fact, that it is mainly a shear model the influence of bending is neglected. The screws in tension additionally cause compression perpendicular to the shear plane which affects the rolling shear capacity positively. In Fig. 17 springs symbolize the transfer of the compression forces. The influence of the stress interaction is considered by the parameter $k_{R,90}$ determined in chapter 2.2.

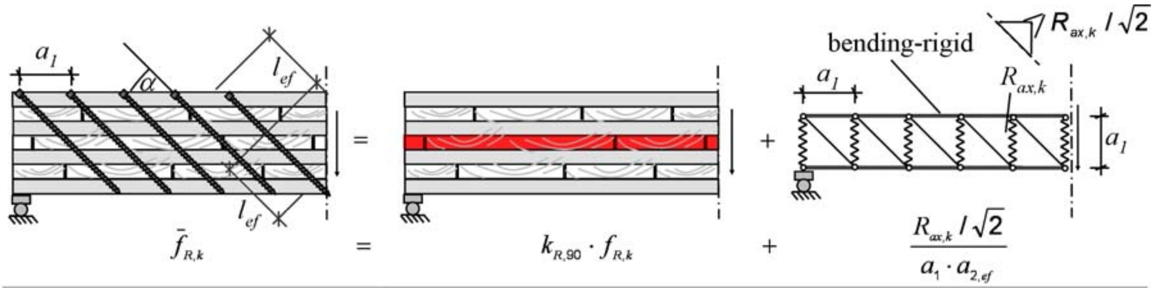

$\bar{f}_{R,k}$	charact. load-carrying capacity of the reinforced CLT under shear stresses	[N/mm²]
$f_{R,k}$	charact. rolling shear capacity (according to technical approvals)	[N/mm²]
$R_{ax,k}$	charact. load-carrying capacity of a screw parallel to its axis	[N]
a_1	distance of the screws parallel to the load bearing direction	[mm]
$a_{2,ef}$	effective distance of the screws perpendicular to the load bearing direction	[mm]
l_{ef}	effective embedment length of the screws for the calculation of $R_{ax,k}$	[mm]
$k_{R,90}$	parameter for the consideration of the stress interaction	[-]

Fig. 17 Design concept on the basis of a strut and tie model

In this case the capacity of the screws is essentially dependent on their withdrawal strength. Universal equations for its calculation are currently not available for an inclination of 45°. However, the investigations within this research project revealed that on the basis of the result of BLAß & UIBEL [13] the withdrawal strength $R_{ax,k}$ of the screws can be calculated approximately according to equation (11).

$$R_{ax,k} = \min\begin{cases} 24{,}8 \cdot d^{0,8} \cdot \ell_{ef}^{0,9} \\ R_{t,u,k} \end{cases} \quad [\mathrm{N}] \tag{11}$$

d diameter of the screws in mm

l_{ef} effective embedment length of the screws in mm

$R_{t,u,k}$ tensile capacity (according to technical approvals)

The effective embedment length l_{ef} according to equation (12) is dependent on the position of the layer. It results from the minimal penetration length of the screws, based on the centre line of the decisive layer. Fig. 18 shows typical geometric relations.

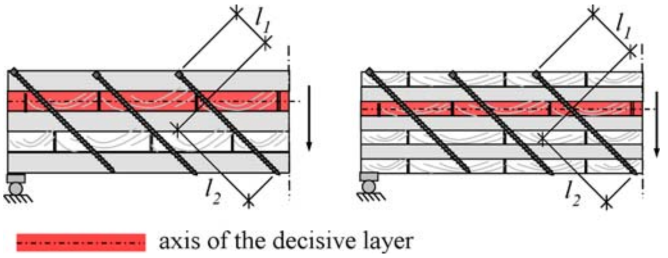

$$l_{ef} = \min\begin{cases} l_1 \\ l_2 \end{cases} \tag{12}$$

Fig. 18 Definition of the effective embedment length l_{ef} of the screws

The compression perpendicular to the grain should be determined by the vertical force component of the screws and the distances between them. Equation (14) delivers the effective distance $a_{2,ef}$, which is the minimum of the real distance a_2 and the quotient of the element width b and the number of screw lines $n_\perp$ perpendicular to the load bearing direction.

$$\sigma_{c,90} = \frac{R_{ax,k} / \sqrt{2}}{a_1 \cdot a_{2,ef}} \qquad \text{with} \qquad a_{2,ef} = \max\begin{cases} a_2 \\ b / n_\perp \end{cases} \qquad (13) \text{ and } (14)$$

The influence of the stress interaction should be considered by the parameter $k_{R,90}$:

$$k_{R,90} = \min\begin{cases} 1 + 0{,}35 \cdot \sigma_{c,90} \\ 1{,}20 \end{cases} \quad [-] \qquad \text{with } \sigma_{c,90} \text{ in N/mm}^2 \tag{15}$$

This finally leads to the following shear verification for reinforced CLT according to the design model shown in Fig. 17.

$$\tau_{R,d} \le k_{\mathrm{mod}} \cdot \frac{\bar{f}_{R,k}}{\gamma_M} \qquad \text{with} \qquad \bar{f}_{R,k} = k_{R,90} \cdot f_{R,k} + \frac{R_{ax,k} / \sqrt{2}}{a_1 \cdot a_{2,ef}} \qquad (16) \text{ and } (17)$$

4.2 Biaxial load transfer

Even unreinforced CLT elements show high compressive stresses perpendicular to the grain in areas of point supports or concentrated loading. So the positive influence of the stress interaction on the rolling shear capacity should be considered in the shear design of CLT elements without reinforcements. The compression $\sigma_{c,90}$ perpendicular to the grain and the governing rolling shear stress $\tau_{R,d}$ have to be determined by capable computation

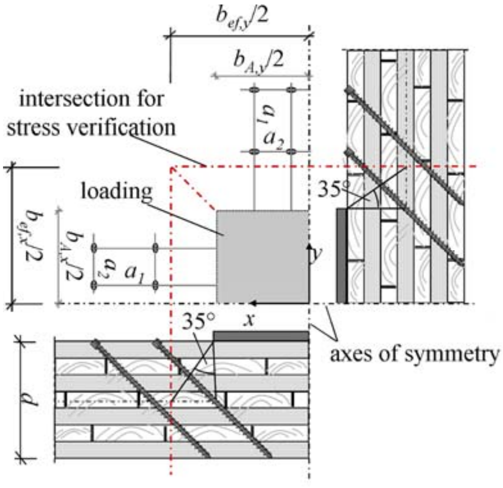

Fig. 19 Central point support / concentr. loading

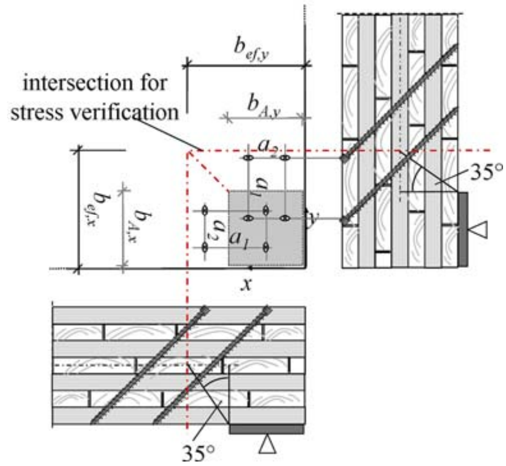

Fig. 20 Point support in the corner region

programs. In standard cases the stresses can also be estimated by the effective width $b_{ef,x}$ and $b_{ef,y}$, which result from the load distribution at an angle of 35° to the centre line of the elements (Fig. 19 and Fig. 20).

$$\sigma_{c,90} = \frac{F_k}{b_{ef,x} \cdot b_{ef,y}} \qquad \text{with} \quad F_k\text{:} \quad \text{charact. support force or concentrated load} \tag{18}$$

Again in the course of the stress verification the influence of the stress interaction ought to be considered by the parameter $k_{R,90}$ according to equation (15):

$$\tau_{R,d} \le k_{\text{mod}} \cdot \frac{k_{R,90} \cdot f_{R,k}}{\gamma_M} \tag{19}$$

The design concept for reinforced CLT elements under biaxial load transfer is also generally based on the strut and tie model for beam elements shown in Fig. 17. However, in this case there is no clearly definable element width. So instead of the beam width b the effective width $b_{ef,x}$ or $b_{ef,y}$ has to be used to determine the effective distance of the screw lines $a_{2,ef}$ perpendicular to the load bearing direction. In primary direction $a_{2,ef}$ is:

$$a_{2,ef} = \max \begin{cases} a_2 \\ b_{ef,x} / n_{\perp} \end{cases} \tag{20}$$

with $n_{\perp}$: number of screw lines $n_{\perp}$ perpendicular to the load bearing direction

The total compression $\sigma_{c,90}$ perpendicular to the grain, needed for the determination of the parameter $k_{R,90}$, is the result of the superposition of the compression components caused by the concentrated loading and vertical force component of the screws:

$$\sigma_{c,90} = \frac{F_k}{b_{ef,x} \cdot b_{ef,y}} + \frac{R_{ax,k} / \sqrt{2}}{a_1 \cdot a_{2,ef}} \tag{21}$$

In the course of the shear verification in equation (22) the shear stress $\tau_{R,d}$, determined on the basis of an unreinforced cross section, has to be compared with the load-carrying capacity of the reinforced elements according to the strut and tie model. Again the rolling shear stresses have to be calculated by capable computation programs or can be estimated by the simplified method using an effective width as described in chapter 3.

$$\tau_{R,d} \le k_{\text{mod}} \cdot \frac{\bar{f}_{R,k}}{\gamma_M} \qquad \text{with} \quad \bar{f}_{R,k} = k_{R,90} \cdot f_{R,k} + \frac{R_{ax,k} / \sqrt{2}}{a_1 \cdot a_{2,ef}} \qquad \text{(22) and (23)}$$

4.3 Verification of the design concept

In order to verify the proposal of the design concept the charts in Fig. 21 contain the characteristic load-carrying capacity according to the strut and tie model as well as the proof loads, the mean values and the 5%-quantile values of the four-point-bending test.

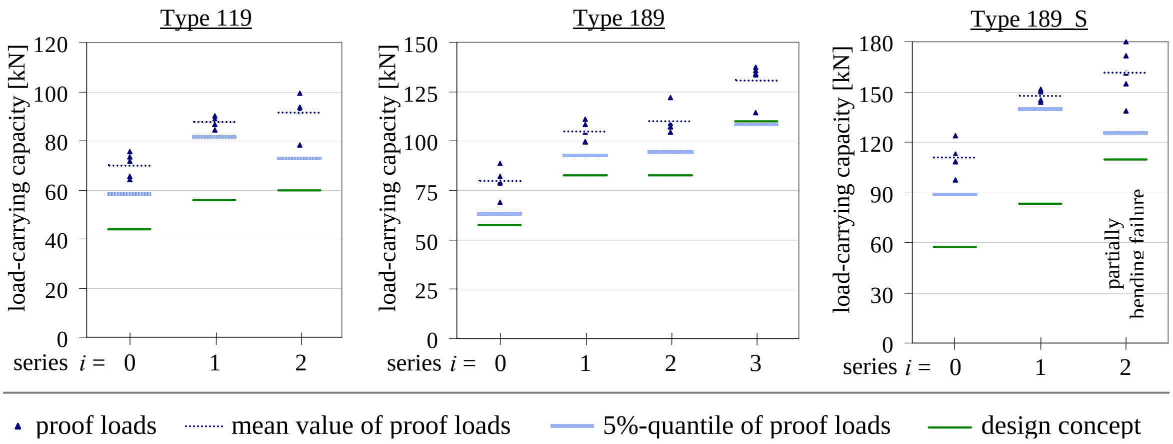

Fig. 21 Comparison of the test results (four-point-bending test) with the design concept

The charts in Fig. 22 show the analogical comparison of the design concept with the results of tests on biaxial load transfer. This time the design concept delivers two components of the load-carrying capacity. Hence the values $F_{max,x,i}$ and $F_{max,y,i}$ indicate the load-carrying capacity according to the strut and tie model in primary and secondary direction. The stresses were calculated according to the simplified method described in chapter 3.

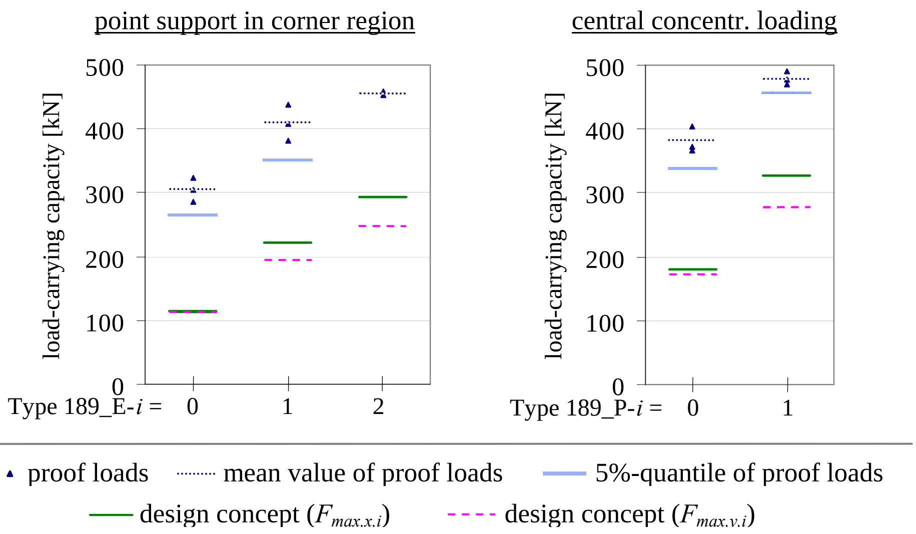

Fig. 22 Comparison of the test results with the design concept – biaxial load transfer

The comparisons verify that the proposed design model represents a conservative approach for the shear design of reinforced CLT. The difference between the values of the design concept and the mean values remains for each element type quite constant. This signifies that the increase in load-carrying capacity as a result of the reinforcements is covered fairly well by the design concept. But especially under biaxial load transfer the base level, which means the design value of the unreinforced series, is considerably underestimated. This corresponds to the results of the FEM-simulations, which also delivered for the unreinforced series considerably higher rolling shear stresses than the rolling shear capacity determined by tests on beam elements under uniaxial load transfer.

5 Conclusion

The results presented in this paper allow the shear design of CLT under concentrated loading considering reinforcements by inclined self-tapping screws with continuous threads. The main conclusions delivered by the described research project are:

- Concentrated loading in CLT elements causes a combination of high shear stresses and compression perpendicular to the grain. By means of experimental tests the positive effect of this stress interaction on the rolling shear capacity was verified and a design concept is proposed.
- Self-tapping screws with continuous threads are a simple and efficient reinforcement. They allow a cost-effective shear design of CLT structures, as they can be applied systematically in localised areas with high shear stresses. Thus they increase the load-carrying capacity in the decisive areas. A simplified design concept validated by means of test results is recommended. It is based upon a strut and tie model and can be used for beam elements as well as plate elements under concentrated loading.
- In the case of a biaxial load transfer additional effects are activated, leading to an increase in the rolling shear capacity compared to that of beam elements. For economic reasons it should be analysed how far the redundant structural behaviour may be considered for the shear verification. One approach might be the use of increased values for the rolling shear capacity in cases of biaxial load transfer.

Acknowledgement

The research project was kindly supported by the German Society of Wood Research (DGfH) and the International Association for Technical Issues related to Wood (iVTH). Special gratitude is extended to the German Federation of Industrial Research Associations (AiF) for funding the project with financial means of the German Federal Ministry of Economics and Technology (BMWi).

Literature

[1] DIN 1052:2008-12: Entwurf, Berechnung und Bemessung von Holzbauwerken. Allgemeine Bemessungsregeln und Bemessungsregeln für den Hochbau.

[2] Mestek, P.; Winter, S.: Konzentrierte Lasteinleitung in Brettsperrholzkonstruktionen - Verstärkungsmaßnahmen. Schlussbericht zum AiF-Forschungsvorhaben Nr. 15892, TU München, 2011.

[3] Mestek, P: Punktgestützte Flächentragwerke aus Brettsperrholz (BSP) - Schubbemessung unter Berücksichtigung von Schubverstärkungen. Dissertation, TU München, expected for 10/2011.

[4] Colling, F.; Bedö, S.: Prüfbericht Nr.: H06-01/1-ZE-PB; Kompetenzzentrum Konstruktiver Ingenieurbau, Abteilung Holzbau, Fachhochschule Augsburg, unpublished, 2007.

[5] DIN 4074-1:2008-12: Sortierung von Holz nach der Tragfähigkeit – Teil 1: Nadelschnittholz.

[6] Spengler, R.: Festigkeitsverhalten von Brettschichtholz unter zweiachsiger Beanspruchung, Teil 1 - Ermittlung des Festigkeitsverhaltens von Brettelementen aus Fichte durch Versuche. Hrsg.: Laboratorium für den Konstruktiven Ingenieurbau (LKI), Berichte zur Zuverlässigkeitstheorie der Bauwerke H.62/1982.

[7] Hemmer, K.: Versagensarten des Holzes der Weißtanne (Abies Alba) unter mehrachsiger Beanspruchung. Dissertation, TH Karlsruhe, 1984.

[8] Sofistik 2010 Statik. Sofistik AG, Oberschleißheim, 2009.

[9] Common Understanding of Assessment Procedure: “Solid wood slab element to be used as a structural element in buildings”; ETA request No 03.04/06, Austria, 2005.

[10] abZ. Nr. Z-9.1-519 vom 07. Mai 2007; SPAX-S Schrauben mit Vollgewinde als Holzverbindungsmittel; ABC Verbindungstechnik GmbH & Co. KG, Ennepetal, Deutschland; Deutsches Institut für Bautechnik, Berlin, 2007.

[11] Bejtka, I.: Verstärkungen von Bauteilen aus Holz mit Vollgewindeschrauben. Dissertation erschienen in: Karlsruher Berichte zum Ingenieurholzbau 2, Universitätsverlag Karlsruhe, 2005.

[12] ANSYS, Finite Elemente Programm, Release 12.0.

[13] Blaß, H.J.: Uibel, T.: Bemessungsvorschläge für Verbindungsmittel in Brettsperrholz. Bauen mit Holz, Heft 2, 2009.

INTERNATIONAL COUNCIL FOR RESEARCH AND INNOVATION IN BUILDING AND CONSTRUCTION

WORKING COMMISSION W18 - TIMBER STRUCTURES

FATIGUE BEHAVIOUR OF THE STUD CONNECTOR USED FOR TIMBER-CONCRETE COMPOSITE BRIDGES

J Mueller

K Rautenstrauch

Department of Timber and Masonry Engineering, Bauhaus University Weimar

GERMANY

MEETING FORTY FOUR

ALGHERO

ITALY

AUGUST 2011

Presented by J Müller

G Hochreiner questioned the choice of frequency as different frequencies would influence the results. He also asked about the shear area for design.

H Müller responded that the choice of frequency was based on standard/typical procedures from literature as they are logistics limitations. Also there were discussions that compression perpendicular to grain stresses existed from the test set up and they wanted to simulate the possibility of such load in the structure. However they could not say how much the level of such load would be.

A Ceccotti commented that references from Finnish colleagues should be considered from structural engineering literature.

K Crews asked and received confirmation that the span of the bridge of interest was 15 mm. K Crews commented that the system would not be suitable for span over 30 m. Based on the span one should consider frequency of 8 to 10 Hz or higher.

R Harris commented that the volume wood used in the bridge seemed to be large and questioned why concrete composite. J Müller responded that it was for stiffness consideration. R Harris stated that then fatigue should not be an issue of concern.

U Kuhlmann stated that there is a fundamental difference between dynamic loading and behaviour under cyclical loading where there is a strength change. She commented that the low run out level did not give a real S/N curve and one should increase the load level to get real fatigue failure to draw the S/N line. J Müller responded that work would be continued at higher load level.

I Smith commented the whether such isolated test could be applied to actual structure.

M Fragiacomo stated that there was information from Colorado State University in this area and suggested exchange of information.

Fatigue Behaviour of the Stud Connector Used for Timber-Concrete Composite Bridges

J Mueller, K Rautenstrauch

Department of Timber and Masonry Engineering, Bauhaus University Weimar, Germany

1 Introduction

The first timber-concrete composite (TCC) road bridge in Germany was realised with the construction of the Birkberg-Bridge near Wippra ([1] and [2]). Therefore a suitable connector, which can transfer the occurring shear forces between the concrete deck and the log-glued laminated timber main girders, had been developed at the Department of Timber and Masonry Engineering of the Bauhaus University Weimar. The so called stud connector consists of a 3 cm thick steel plate with welded shear studs on the concrete side. At the beginning of 2011 work started for a further building as timber-concrete composite construction with the application of the stud connector. The so called Heinzenberg-Bridge across a highway with two lanes in each direction in North Rhine-Westphalia (Germany) serves as a wildlife crossing.

The paper presents first results of a current research project that focuses on the fatigue behaviour of the stud connector. Due to a new test setup and a modified design of the shear joint, at first short-time tests were accomplished. Afterwards dynamic investigations were realised on the basis of these tests.

2 Experimental tests

2.1 Short-time shear tests

2.1.1 Test specimen, experimental setup and load history

With the current research project eleven short-time shear tests have been accomplished to investigate the load bearing- and deformation behaviour of the stud connector. In this context, the specimen were divided into three different test series depending on the design of the joint. The build-up of the samples of series E-K-A (Fig. 2) and E-K-B – each with three specimens – is based on the geometry of the stud connector of a further research project ([3] and [4]), in which the most important result was the development of a preferred geometry for the connector with a depth of the step joint of 3 cm. This configuration was also used for the construction of the Birkberg-Bridge Wippra (Fig. 1). In that way, the new results can also be compared with the outcomes of extensive investigations of a further research project [3]. The only difference between the series E-K-

A and E-K-B consists of the width of the steel stud connector in direction of the shear force (175 mm for series E-K-A and 200 mm for series E-K-B). The test specimen consisting of glued laminated timber (strength class GL32h) with dimensions 200 x 200 x 800 mm have a length of timber in front of the step joint of 500 mm.

Fig. 1: Log-glued timber main girder with stud connectors (Birkberg-Bridge)

Fig. 2: Specimen of series E-K-A with accurately fitting milled notch and stud connector

There was investigated a new modified design of the joint with the arrangement of a 1.25 cm thick layer consisting of polymer resin compounded concrete (PC) between stud connector and timber. Therefore five specimen were tested in series E-K-PC (Fig. 5). PC is an end product with general technical approval composed of a matrix of mineral additives and a polymeric resin system as binder. It offers also high compression stability because of its compound.

Fig. 4: Test setup and measuring equipment for short-time- and dynamic shear tests

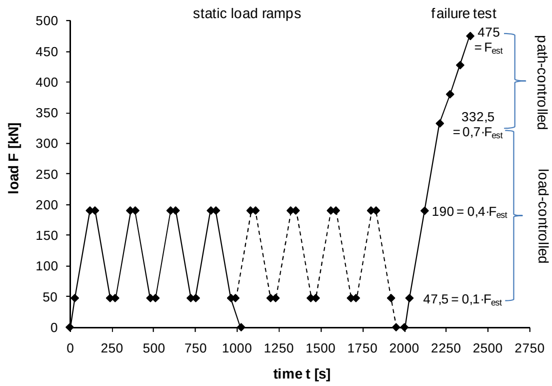

Fig. 3: Load history of the short-time shear tests

Fig. 5: Specimen of series E-K-PC with a layer consisting of PC in the facing area

The primal intention of the current research project only contains the investigation of the transmission of the shear force from the stud connector into the timber cross section. For this reason, the test setup was simplified compared to the further research project, because the concrete was substituted for steel profiles, which can be handled more easily. However, the basic test setup of the so-called push-out-test remains. The test setup was fitted into a servo-hydraulic testing facility with a capacity of 1.000 kN, which was used for the static as well as for the dynamic tests (Fig. 4). The ultimate load of about 475 kN per specimen could be estimated for the load history (Fig. 3) based on preliminary calculations and the measured loads at rupture of the further project [3]. Corresponding to DIN EN 26891 [5], the load history consists of static load ramps for the determination of an initial slip modulus. Afterwards the failure tests were conducted.

2.1.2 Results

Four static load ramps were arranged according to the load history. In case of series E-K-A and E-K-B eight ramps were enforced and the initial slip modulus of the joint was determined. The load-displacement curves of the static load ramps for specimen E-K-B-1 are shown as an example (Fig. 6). The relative displacement between timber and stud connector was recorded with four dial indicators placed in the middle of the front and the back side of each joint (Fig. 4). On the abscissa, the relative displacement as average value of the deformation of the four vertical dial indicators is plotted. According to DIN EN 26891 [5] the recorded relative displacement in the area between 10 and 40 % of the established ultimate load serves as the basis for evaluation of the slip modulus of the connection. All specimen were analysed in that way.

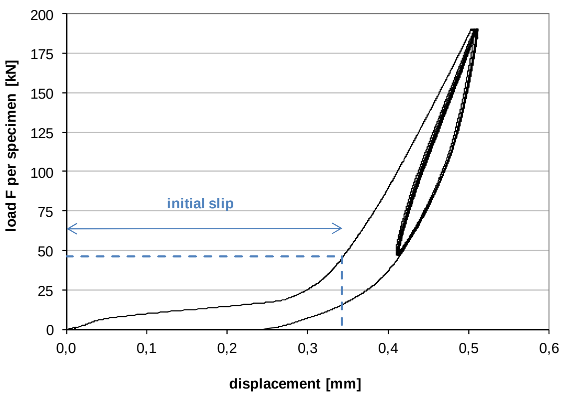

Fig. 6: Load-displacement curve of specimen E-K-B-1 (static load ramps)

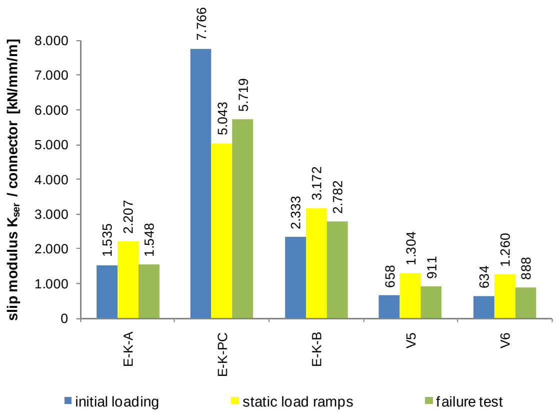

Fig. 7: Averaged values of slip modulus K_{ser} for all test series

Due to the initial loading, the stud connector fits over the whole surface on the timber. Therefore a significant increase of the stiffness of the joint is remarkable. This effect, the so called initial slip, appears in different intensities with all specimen of series E-K-A and E-K-B. After overcoming the initial slip, the load-displacement curves of the following load ramps are nearly congruent and show a monotone distribution of the slip modulus.

The force was raised until the failure of the shear joint directly after the statical load ramps. The specimen E-K-B-1 (Fig. 8) shows representatively a characteristical progression of the load-displacement curve for a multitude of test items. After a linear part with very high stiffness the curve passes over by nearly 2/3 of the ultimate load into a non-linear, planer progression. The successive failure of the joint was attented by partly occurred little local load drops. Due to shearing of timber in front of the joint, the brittle failure occurs as expected in most cases only in one shear joint (Fig. 9, left shear joint).

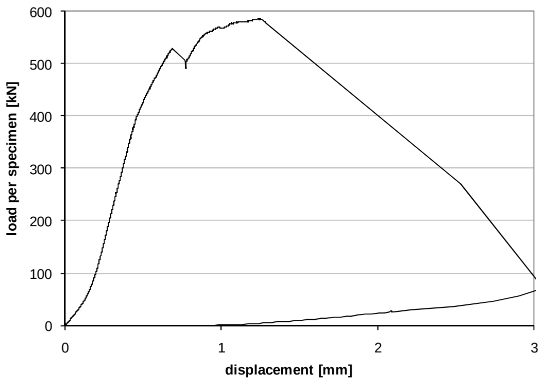

Fig. 8: Load-displacement curve of specimen E-K-B-1 (failure test)

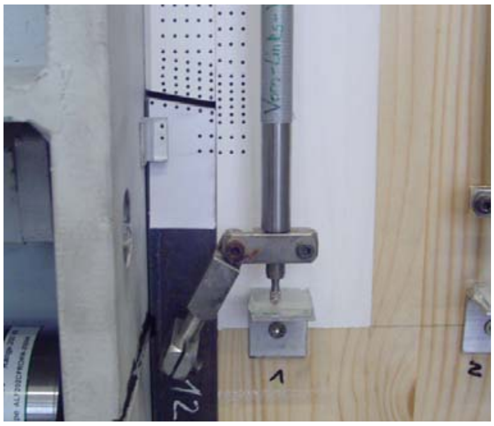

Fig. 9: Failure of specimen E-K-B-1 due to shearing of timber in front of the joint

The comparison of the investigated slip modulus demonstrated obviously (Fig. 7), that the arrangement of a PC-layer (series E-K-PC) between stud connector and timber, which equalises all tolerances due to manufacturing, causes a duplication up to a triplication of the stiffness of the joint compared to the series with direct contact between timber and steel (series E-K-A and E-K-B). That shows explicitly the positive effect of a consistent introduction of the shear forces over the whole surface via the polymer concrete into the timber. This impact is enforced additionally by the filling (impregnation) of the truncated timber cells with the resin from the polymer concrete. Furthermore the stud connector can be embed accurately fitting into the milled notch, so that the initial slip is almost eliminated. This is very important, because the initial slip has a huge influence on the slip modulus of the shear connection, especially in the case of very low relative displacements between stud connector and timber. The determined slip modulus of the series E-K-A and E-K-B have approximately similar dimensions. The stiffness of the joint, which was used for the calculation of the Birkberg-Bridge (series V5 and V6 [3]), is listed additionally in the chart above to get an overview (Fig. 7).

The length of timber in front of the step joint failured through brittle shearing due to transgression of the average shear strength in the joint in all eleven specimen which were tested in the three series. But plastic strains in the load transferring area between stud connector and timber could be established before the global failure in the test occured. That indicated a local compressive failure under the angle of 10° to the grain in the contact area. A load drop caused by a local constricted failure mode in the joint appeared with eight of the eleven specimen before the final shear failure. Afterwards there could be noticed a flat increase in each case in the load-displacement curve (Fig. 8). The comparison of the ultimate loads among each other shows that all failure loads are on a similar level – except series E-K-A with lower values (Fig. 10). Therefore no enhancement of shear strength in the joint developed in view of the insert of PC. Only the measured displacements in the state of failure are considerably lower because of the very good fitting and the elimination of the initial slip in series E-K-PC.

2.2 Fatigue tests

2.2.1 Intention, extent of tests and load history

The aim of the dynamic investigations consists of the determination of S-N-lines for the stud connector to implement reliable information about the dynamic behaviour of the connection. Based on the results of the short-time shear tests, altogether 18 tests were arranged so far. Both kinds of design of the joint – with and without a PC layer in the force transferring area – were analyzed with nine tests each. The initial point for the dynamic experiments is the average value of the ultimate load of the arranged short-time shear test series E-K-A and E-K-PC, which was established with 460 kN per specimen (Fig. 10). Altogether three different load levels with 40, 50 and 60 % of this average value were investigated as maximum load.

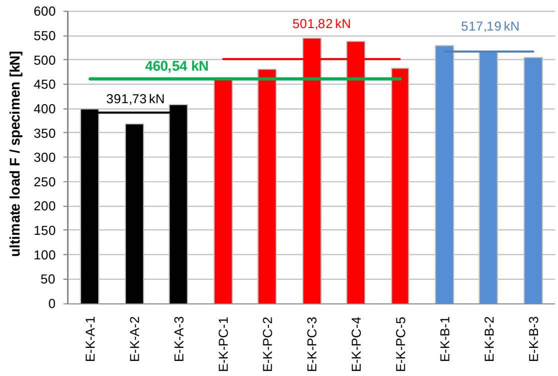

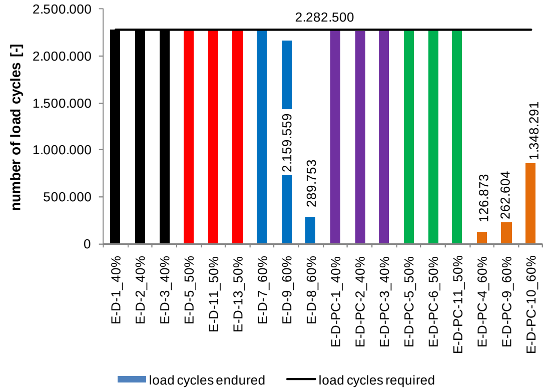

Fig. 10: Ultimate loads of the specimen of all series (short-time shear tests)

Fig. 11: Scheme of fatigue tests

All supplemental boundary conditions for the load history (Fig. 12) were determined based on an extensive literature evaluation.

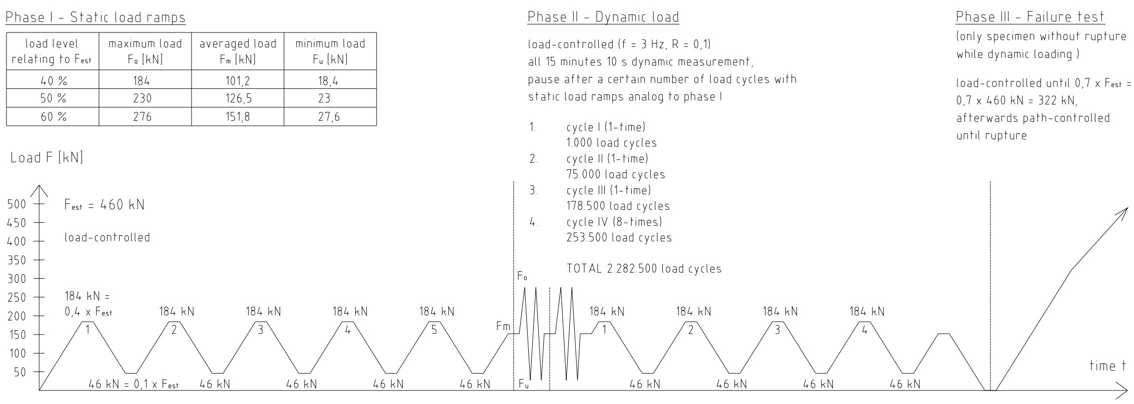

Fig. 12: Load history of fatigue tests according to DIN 50100 [6]

The minimum number of load cycles a specimen has to achieve obligatory to be classified as a fatigue-tested specimen without rupture was configured appropriate to the DIN technical report 101 [7] on two million load cycles. The investigations of Simon [4], Molina [8], Aldi [9], Bathon [10] and Aicher [11] emanate from a frequency of 3 hertz which was also used in this project. The stress ratio which defines the relation between minimum and maximum load is arranged with 0.1 and represents consequently the highest load amplitudes which can be expected in bridge construction. Based on these boundary conditions, the entire test period for one fatigue tested specimen without rupture amounts to a little more then ten days.

2.2.2 Results

The test results will be explained with the help of one representative of each series for the load level of 50 %. Corresponding to the load history, the specimen passed a total of 2.282.500 dynamic load cycles with 12 statical intermediate measurements and following failure test – in case they did not fracture during the dynamic loading. The slip modulus K_{ser} was determined analogue to the procedure of short-time shear tests for each statical measurement. The comparison of the series with and without PC (Fig. 13) shows clearly the influence of the initial slip and the involved lower slip modulus of the series without PC. Whereas these specimen has to overcome the initial slip first, the design of the joint with PC can transfer the load immediately due to the elimination of the initial slip.

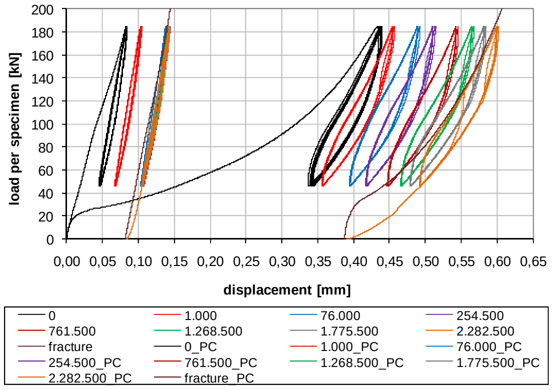

Fig. 13: Averaged load-displacement curves of specimen E-D-5 and E-D-PC-5

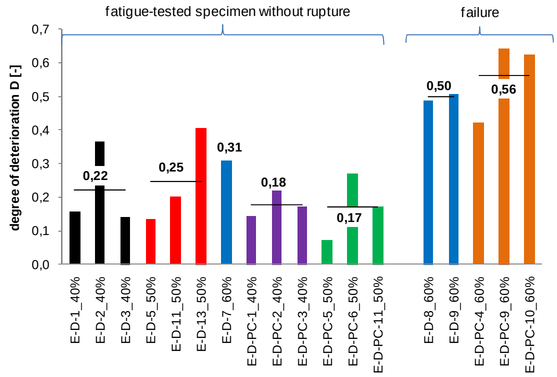

Fig. 14: Degree of deterioration of all specimen depending on the load level

Afterwards a compression of the grain in the facing area occurred in both series because of the dynamic loading. Due to the pulsating load over lots of cycles the timber structure is continuously damaged. The development of macrocracks especially in the shear joint is a result of the earlier appearance of microfissures. This development leads to the decrease of slip modulus and a deformation increase. It was found out for both types of the joint that the length of timber in front of the step joint shear off abruptly and besides the development of cracks without previous indication by a grade of damage between 50 and 60 %. The level of damage is depending proportionally on the load class. The grade of deterioration according to Hult [12] is defined as the ratio of considered stiffness after a certain number of load cycles to the maximum slip modulus:

$$D^n = 1 - \frac{\sigma}{\varepsilon \cdot E_{max}} = 1 - \frac{\varepsilon \cdot E^n}{\varepsilon \cdot E_{max}} = 1 - \frac{E^n}{E_{max}} = 1 - \frac{K^n_{ser}}{K_{ser,max}} \qquad (1).$$

A totally intact specimen has the value “0” for the level of damage while the grade of damage “1” describes a totally destroyed test sample. The values in between specify the attenuated rigidity properties of the material as a result of the deterioration. The upper chart (Fig. 14) determines the damage for a run-out after tolerated 2.282.500 cycles while the levels of damage for the failures (D = 1) were defined at the moment of the last possible statical measurement.

The comparison of the presented designs of the joint shows a lower decrease of the slip modulus at the load levels of 40 and 50 % at the series with PC than in the unreinforced tests. This is the effect of the accurate fitting of the connection whereby a direct and laminar introduction of the load with consistent loading impulses is possible. This pulsed load and the involved continuous expansion of existing initial cracks lead to a faster failure of the PC-specimen at the high load level (60 %), at which the whole PC-series fractured. In contrast there is a more grievous action-tolerance in specimen without PC due to the worst adaption of the stud connector. This gives the possibility for a higher dissipation of energy which entails a slower progression of material damage. The energy dissipation varies indeed with a high margin of deviation regarding to the results due to not predictable inaccuracies in installation. Therefore the specimen of PC-series have to be favoured in the final consequence because of the little deviation in results which allows a clear determination between run-outs and cases of rupture.

The following schematic diagrams (Fig. 15 and 16) contain the development of the averaged slip modulus as well as the degree of damage over the number of endured load cycles. Beside the confirmation of the statements on the grade of damage it can be determined, that the progression of damage of all series is signified by an intense increase within the first 500.000 cycles. After that, the development of the curve declines a little bit. At first there is a compressive failure under an angle to the grain in the facing area as a result of the advancing compression of the truncated fibres. The straight line decreases because a further compactation of the grain is not possible. So this progression describes the second failure mechanism, which is the shear failure of the timber in front of the step joint.

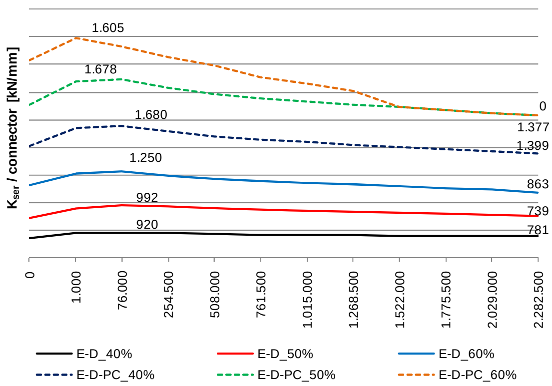

Fig. 15: Development of slip modulus

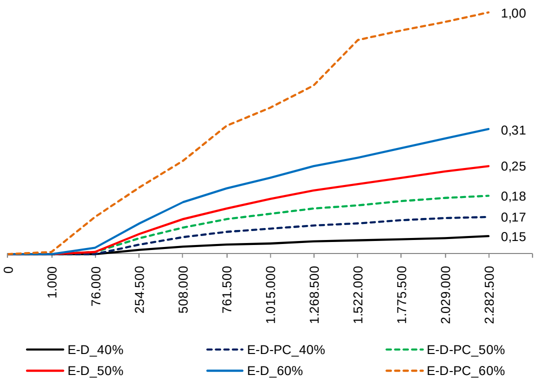

Fig. 16: Decrease of stiffness due to damage

3 Comparison according to the rules

3.1 Ultimate loads according to DIN EN 1995-1-1 resp. 1995-2

On the basis of the fatigue evidence regulated in DIN EN 1995-2 [13] the coefficient k_{fat}, which describes the decrease of statical strength due to fatigue stress, can be calculated with the following formula:

$$k_{fat} = 1 - \frac{1-R}{a \cdot (b-R)} \cdot \log(\beta \cdot N_{obs} \cdot t_L) \geq 0 \qquad (2).$$

The so-called stress ratio R between minimum and maximum load has been assumed according to experimental tests to 0.1, the coefficient β has been set to 3 because of substantial consequences in the case of failure. The product consisting of load cycles per anno N_{obs} and the intended service life t_L amounted as a minimum value to two million cycles [7]. Due to shear stress, the parameters regarding fatigue addicted to “a” = 6.7 and “b” = 1.3. The theoretical characteristic ultimate load for the failure mode shearing of timber in front of the joint $P_{t,v,k}$ can be calculated according to the proposal of a design concept presented in [1] and [2]. The extention of this equation about the fatigue coefficient k_{fat} makes it possible to estimate not only the ultimate load for short-time stress (k_{fat} = 1.0) but also after a certain number of cycles:

$$P_{t,v,k} = k_{fat} \cdot f_{v,k} \cdot b \cdot l_V \qquad (3).$$

It can be assumed that because of the additional load of the concrete deck onto the timber girder the activation of a lateral pressure raises up the shear strength of timber $f_{v,k}$ about 40 % (1,4 · $f_{v,k}$ = 1,4 · 2,5 N/mm² = 3,5 N/mm²). Concomitant the code DIN EN 1995-1 [14] limited the calculative length of timber in front of the joint to the eightfold depth of the step joint (8 · t_v = 240 mm) to prevent too high stress peaks in the bearing area. The comparison of theoretical and experimental load bearing capacities (Fig. 17) contains also the length of timber in front of the joint to consider the boundary conditions of the tests. The factor b is consistent with the used width of the groove of 200 mm.

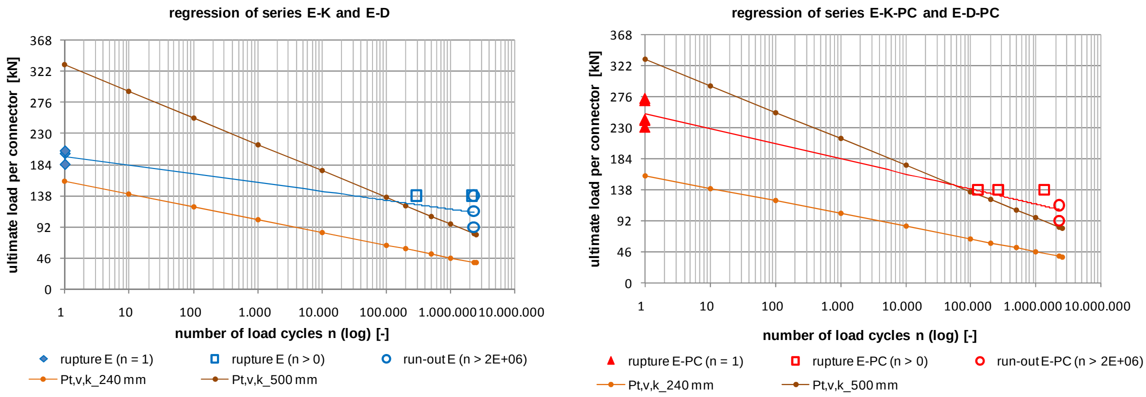

Fig. 17: Comparison of calculated and experimental ultimate loads of the shear joint for the different series

The comparison contains the achieved ultimate loads of the short-time tests with the assigned load cycle 1. Aside there are plotted the endured cycles with the respective load levels, which are consistent to maximum loads per connector of 92 kN (40 %), 115 kN (50 %) as well as 138 kN (60 %). The length of timber in front of the step joint according to the code amounts to 240 mm. Both series, the design with and as well as without polymer concrete in the joint, achieve the required load for this length. In contrast to that, no specimen of the short-time tests – independent of the design of the joint – reaches the theoretical load bearing capacity for a length of timber in front of the joint of 500 mm. On the other hand, the decrease of the strength corresponding to the code is very steep, so that the specimen which failed while the dynamic loading – nearly all test samples with a load level of 60 % – as well as the run-outs lay above this line. It can be recommended on the basis of analysis of short-time as well as fatigue tests to increase limitation of timber in front of the step joint due to the mechanism of shear failure in combination with lateral pressure. A length of the ninefold of the depth of the step joint is approved for the design of the joint with direct contact between stud connector and timber, a length of approximately 11,5 · t_V can be recommended for the configuration with polymer concrete.

3.2 S-N-line

The following graph (Fig. 18) contains the achieved ultimate loads of the short-time shear tests and the endured cycles associated with the respective load levels (40, 50 and 60 %). The ordinate in this chart shows the ratio $F_{existent}$ / F_{max}, whereas F_{max} is defined as the average value of the ultimate loads of the short-time tests of each series. The S-N-line for each series is determined by means of a regression analysis, whereas the highest approximation can be achieved with a logarithmical function with the form $y = a \cdot \ln(x) + b$. The k_{fat}-line according to the code [13] is shown additionally to allow a better classification of the results.

A result of the comparison between theoretical and experimental loads and mainly due to the widening of both lines is, that the shear strength corresponding to the code for an application of the stud connector can be appreciated as safe. Based on the present results, the fatigue strength (Fig. 19) for the series with direct contact between stud connector and timber amounts to nearly 59 % of the respective ultimate load (mean value) of the short-time tests. The fatigue resistance for the series with a PC-layer in the bearing area was determined to 46 % of the corresponding short-time load. It was in both series that only one specimen did not fail at the next higher load level (60 % = 70.46 % for series E-D and 55 % for series E-D-PC). This estimation is very safe, because all fatigue-tested specimen without rupture at the load level of 50 % count as failure for the development of the S-N-line. The specimen with polymer concrete show lower fatigue strength in spite of the higher loads in the short-time tests and the advanced values of slip modulus compared to the unreinforced series. Reasons for that are the low energy dissipation and the high stiffness of the joint, which leads to a rapid propagation of existent microcracks and therefore to a high damage of the material due to pulsed introduction of the load.

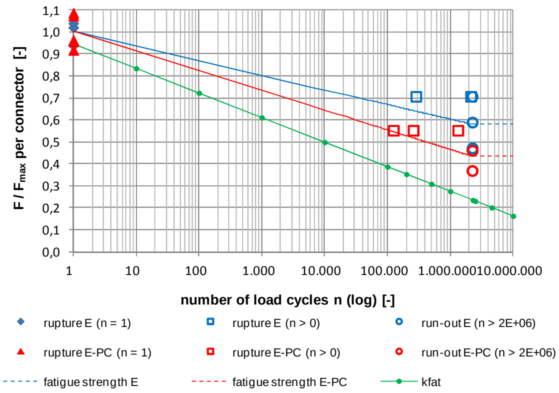

Fig. 18: S-N-line, regression of series E-K and E-D resp. E-K-PC and E-D-PC

load level relating to F_{est} = 460 kN per specimen	maximum load per connector while dynamic loading $F_{o,con}$ [kN]	averaged ultimate load per connector $F_{est,con}$ E-K-A: 195,86 kN E-K-PC: 250,91 kN $F_{o,con}$ / $F_{est,con}$	
		E-K-A	E-K-PC
40 %	92	46,97 %	36,67 %
50 %	**115**	**58,71 %**	**45,83 %**
60 %	138	70,46 %	55,00 %

Fig. 19: Proposal for the fatigue strength of the shear joint for series E-D and E-D-PC

The determined slopes of the S-N-lines of each series are equated with the k_{fat}-line according to the code for the calculation of the coefficient “a” for each series by a constant value of the factor “b”. In this way the concept of fatigue verification according to DIN EN 1995-2 [13] can be used for timber-concrete composite girders with stud connectors under shear stress. Based on the preliminary results of the investigations the coefficient “a” can be suggested with 11.25 for series E-D and 8.39 for series E-D-PC.

4 Conclusion

An intermediate result of the current research project is that the previous investigations show explicitly the advantages of the arrangement of a PC-layer in the load bearing area. The use of polymer concrete equalises all tolerances due to manufacturing so that the stud connector can be embed accurately fitting into the milled notch. Consequently, the initial slip can be eliminated which leads to a very high stiffness of the joint. Furhermore the fitting accuracy causes a consistent load distribution over the whole contact area of the groove. The variance of the experimental results are significant lower, compared to the design of the joint with direct contact between stud connector and timber, which leads to a higher safety.

Altogehter there have been accomplished 18 tests under pulsating stress for three different load levels (40, 50 and 60 % of average value of the ultimate loads of short-time tests as maximum load) so far. A first result is that the fatigue strength of the shear joint can be estimated to nearly 59 % of the corresponding ultimate load of the short-time tests for the series with direct contact between stud connector and timber. The series with a layer consisting of polymer concrete in the load bearing area offers a fatigue resistance of approximately 46 % of the corresponding short-time load. Both test series observe the requirements for the fatigue verification according to code with sufficient safety distance.

Acknowledgements

The presented results are elaborated in the line with the current research project “Trag-, Verformungs- und Ermüdungsverhalten spezieller Verbundelemente für Holz-Beton-Verbundstraßenbrücken“, which is financed by the German ministry for economy and technology via the *Arbeitsgemeinschaft industrieller Forschungsvereinigungen “Otto von Guericke” e. V. (AiF)* in collaboration with the International Association for Technical Issues related to Wood (iVTH). These institutions are gratefully acknowledged.

5 References

[1] Rautenstrauch, K.: Holz-Beton-Verbund-Bauweise bei Schwerlastbrücken – Zum Tragverhalten und einem gebauten Pilotprojekt, Tagungsband „Ingenieurholzbau; Karlsruher Tage 2009“; Bruderverlag, Universität Karlsruhe, Oktober 2009

[2] Rautenstrauch, K., Simon, A.; Mueller, J.: The First Timber-Concrete Composite Road Bridge in Germany. Proceedings of the 11th World Conference on Timber Engineering (WCTE), Riva del Garda, Italy, June 2010

[3] Rautenstrauch, K.; Simon, A.: Weiterentwicklung der Holz-Beton-Verbund-bauweise unter Einsatz von blockverleimten Brettschichtholzquerschnitten bei Straßenbrücken. Schlussbericht zum AiF-Forschungsvorhaben 14275 BR, Januar 2008, Bauhaus-Universität Weimar, 2008

[4] Simon, A.: Analyse zum Trag- und Verformungsverhalten von Straßenbrücken in Holz-Beton-Verbundbauweise. Dissertation, Bauhaus-Universität Weimar, 2008

[5] DIN EN 26891: 1991-07: Verbindungen mit mechanischen Verbindungsmitteln – Allgemeine Grundsätze für die Ermittlung der Tragfähigkeit und des Verformungsverhaltens (ISO 6891:1983). Deutsche Fassung EN 26891:1991.

[6] DIN 50100:1978-02. Dauerschwingversuch.

[7] DIN-Fachbericht 101: Einwirkungen auf Brücken, 2009-03

[8] Molina, J. C.: Analise do comportamento dinamico da ligacao formada por barras de aco coladas para tabuleiros mistos de madeira e concreto para pontes, PhD thesis, Escola de Engenharia de Sao Carlos da Universidade de Sao Paulo, 2008

[9] Kuhlmann, U.; Aldi, P.: Prediction of the Fatigue Resistance of Timber-Concrete-Composite Connections. Paper CIB-W18/42-7-11; 42nd CIB-W18-Meeting, Duebendorf, Switzerland, August 2009

[10] Bathon, L.; Bletz-Mühldorfer, O.: Ermüdungsbetrachtungen von hölzernen Straßenbrücken – Chancen und Möglichkeiten der Holz-Beton-Verbundbauweise. 1. Internationale Holzbrückentage, Bad Wörishofen, Deutschland, März 2010

[11] Aicher, S.; Stapf, G.: Dynamische Beanspruchbarkeit von keilgezinktem Vollholz aus Kiefer. Abschlussbericht zum Forschungsvorhaben, Materialprüfungsanstalt Universität Stuttgart, Otto-Graf-Institut, 2010

[12] Hult, J.: Introduction and general overview. In Continuum Damage Mechanics: Theory and Applications, Krajcinovic&Lemaitre (eds.): Springer-Verlag, 1987

[13] DIN EN 1995-2:2010-12: Eurocode 5: Bemessung und Konstruktion von Holzbauten – Teil 2: Brücken

[14] DIN EN 1995-1-1:2010-12: Eurocode 5: Bemessung und Konstruktion von Holzbauten – Teil 1-1: Allgemeines – Allg. Regeln und Regeln für den Hochbau

INTERNATIONAL COUNCIL FOR RESEARCH AND INNOVATION IN BUILDING AND CONSTRUCTION

WORKING COMMISSION W18 - TIMBER STRUCTURES

THE STIFFNESS OF BEAM TO COLUMN CONNECTIONS IN POST-TENSIONED TIMBER FRAMES

W van Beerschoten

T Smith

A Palermo

S Pampanin

University of Canterbury

NEW ZEALAND

F.C. Ponzo

University of Potenza

ITALY

MEETING FORTY FOUR

ALGHERO

ITALY

AUGUST 2011

Presented by T Smith

H Blass asked about the energy dissipation or q factor for such system. T Smith responded that they are looking at equivalent viscous damping values in the range of 12 % to 16%.

I Smith discussed the local failure influence on the behaviour of system. T Smith stated that the system can be designed and installed for other moment resisting systems and walls.

B Dujic asked what would be the level of damage in the joint and how could one evaluate the damage. T smith stated that damage could be evaluated from visual inspection if the energy dissipation devices were not hidden in the member. The damaged devices can then be replaced. Also instrumentations can be installed in the building to evaluate movement and hence damage. B Dujic and T Smith further discussed the practicality of such practice in real buildings.

M Fragiacomo and S Pampanin discussed further the applicability of the approach to other building systems.

B Dujic stated that one could design this as elastic case if the damage was so low.

A Ceccotti said that in real building how could one clad over this. T Smith responded it would be an issue for the architect.

M Yasumura asked about the control of the relaxation of the timber on post tensioning. He stated that based on the shown hysteresis curve, energy dissipation would be very low. T smith stated that the relaxation could be controlled by periodic re-tensioning. The amount of damping would not be an issue as it can be controlled by the size of the steel devices. It is more important that pinching effect is minimal.

M Popovski asked about the interest of application of such concept to CLT. S Pampanin responded that there are interests in New Zealand and F Lam in Canada will also be working on this issue.

The Stiffness of Beam to Column Connections in Post-Tensioned Timber Frames

W. van Beerschoten[1], T. Smith[1], A. Palermo[1], S. Pampanin[1], F.C. Ponzo[2]

[1] University of Canterbury, New Zealand

[2] University of Potenza, Italy

1 Introduction

Over the past five years Pres-Lam post-tensioned timber frames have been developed at the University of Canterbury [Buchanan *et al.*, 2011] in collaboration with the international research consortium Structural Timber Innovation Company, STIC Ltd. Engineered wood products, such as glulam and Laminated Veneer Lumber (LVL), make it possible to manufacture large timber sections, which can be used in combination with post-tensioning technology. Continuous unbonded post-tensioning cables, anchored at exterior columns, clamp beams and columns together, creating moment resisting connections.

The idea of unbonded post-tensioned timber frames was adapted from post-tensioned concrete systems. The technique has been developed during the PRESSS (PREcast Seismic Structural Systems) program at the University of California, San Diego [Priestley *et al.*, 1999]. A step-by-step general design procedure which described the frame response was presented [Pampanin *et al.*, 2001]. This design procedure included the Monolitic Beam Analogy (MBA) which was necessary to describe the complete moment-rotation behaviour of the connection. Further development of the design procedure lead to the Modified Monolitic Beam Analogy (MMBA) which included the pre-yield behaviour [Palermo, 2004] and is included in the New Zealand concrete design standard [Standards New Zealand, 2006]. Although originally developed as a seismic system, the use of unbonded post-tensioned concrete frames has also been extended to gravity dominated frames with the development of the Brooklyn system [Pampanin *et al.*, 2004].

A modified section analysis design procedure of post-tensioned seismic-resisting timber frames has been presented [Pampanin *et al.*, 2006]. More recently, design guidelines for the seismic design of post-tensioned timber frames, based on procedures for precast concrete systems (walls and frames) [Priestley, 2002] have been suggested by Newcombe *et al.* [2010]. The proposed design procedure is based on displacement based design and provides design formulae for the main contributions to interstorey drift; beam and column rotation, joint panel shear deformation and connection rotation.

New beam-column connection testing [Van Beerschoten *et al.*, 2011], [Smith *et al.*, 2011] with different post-tensioning arrangements has lead to a more comprehensive understanding of the connection behaviour. In this paper modifications to the design procedure are proposed.

2 Experimental testing

This section presents an overview of experimental testing on which the modifications to the design procedure are based. A differentiation is made between seismic frames, Figure 1a and 1c, where the design is governed by lateral loads and gravity frames, Figure 1b and 1d, where the design is governed by vertical loads. Figure 1 also gives the most important design equations for the design of post-tensioned rocking connections.

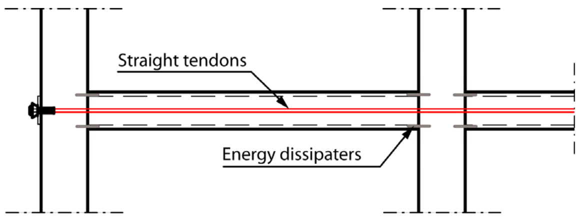

(a) Seismic Frame

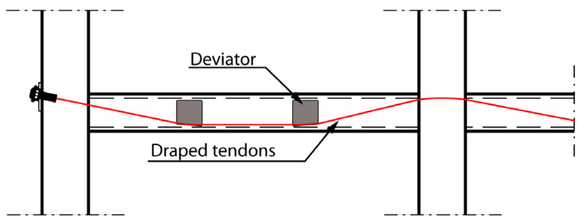

(b) Gravity Frame

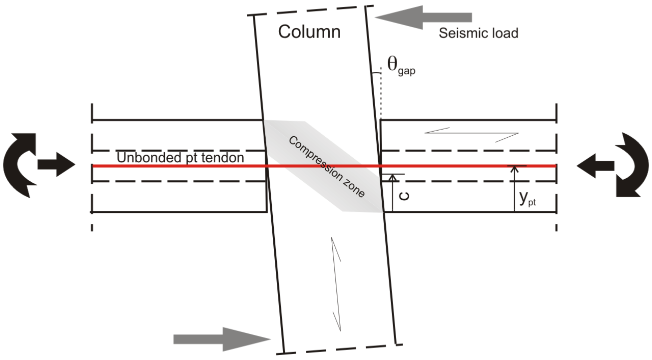

(c) Seismic Connection

$$\varepsilon_{pt} = \frac{\theta_{gap}\left(y_{PT} - c\right)}{l_{ub}} \qquad \textit{Eq. 1.1}$$

$$\varepsilon_t = c\left(3\frac{\theta_{gap}}{L_{cant}} + \phi_{dec}\right) \qquad \textit{Eq. 1.2}$$

$$C_t = 0.5\varepsilon_t E_{con} b_b h_b \qquad \textit{Eq. 1.3}$$

$$M_n = C_t\left(y_{PT} - c/3\right) \qquad \textit{Eq. 1.4}$$

Where:

ε_{pt} = Increase in strain in PT tendon
θ_{gap} = Imposed rotation of gap
y_{PT} = Distance from extreme beam fibre to centroid of post-tensioning
c = Height of compression zone
l_{ub} = Unbonded length of post tensioning
ε_t = Strain in outer timber fibre
L_{cant} = Distance from interface to point of contraflexure (zero moment point)
E_{con} = Connection E-modulus
b_b = Width of beam
h_b = Height of beam
ϕ_{dec} = Decompression curvature
C_t = Compressive force in timber

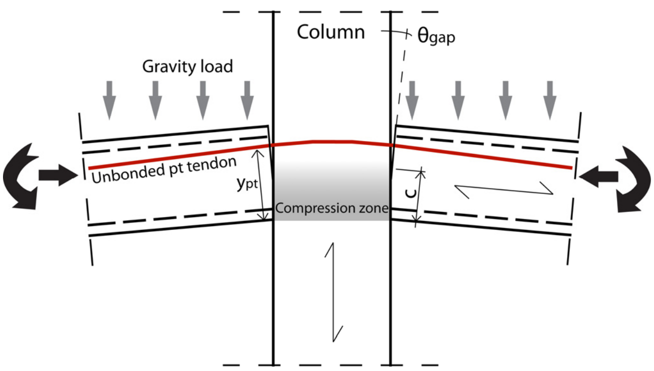

(d) Gravity Connection

Figure 1 – Comparison between seismic and gravity frame and connections

2.1 Test descriptions

In 2008 a full scale seismic connection test was performed on an external and internal beam-column joint at the University of Canterbury, New Zealand, see Figure 2a (PT1) [Iqbal *et al.*, 2010]. This testing was performed to investigate additional complexities arising in full scale specimens, such as high joint deformation and local damage mechanisms. The column was tested with different reinforcing techniques and at different levels of post-tensioning. In this paper the results of the external connection without mild-steel energy dissipaters will be evaluated in order to get a clear comparison.

In 2010 a full scale exteriour beam-column connection designed for gravity loading was tested at the University of Canterbury in New Zealand, see Figure 2b (PT2) [Van Beerschoten *et al.*, 2011]. The post-tensioning tendon was placed eccentrically to generate an uplift force in the beam at the location of the deviator. The experimental research focused on ways to minimise the joint rotation due to compression perpendicular to the grain in the column and thereby increasing the stiffness of the joint. Several methods of reinforcement using LVL and steel have been tested. In this paper only the results from the unreinforced column will be evaluated.

In 2011 a full scale seismic connection using glulam was tested in the structural laboratory of the University of Basilicata in Potenza, Italy, see Figure 2c (PT3) [Smith *et al.*, 2011]. The study evaluated the feasibility of applying jointed ductile post tensioning technology to glulam, which is a more widespread material globally. The aim of the project was to evaluate and improve the systems seismic performance and develop its use in multi-storey timber buildings. Testing focused on the development and application of additional systems of energy dissipation, though in this paper only the results of testing without energy dissipaters will be evaluated.

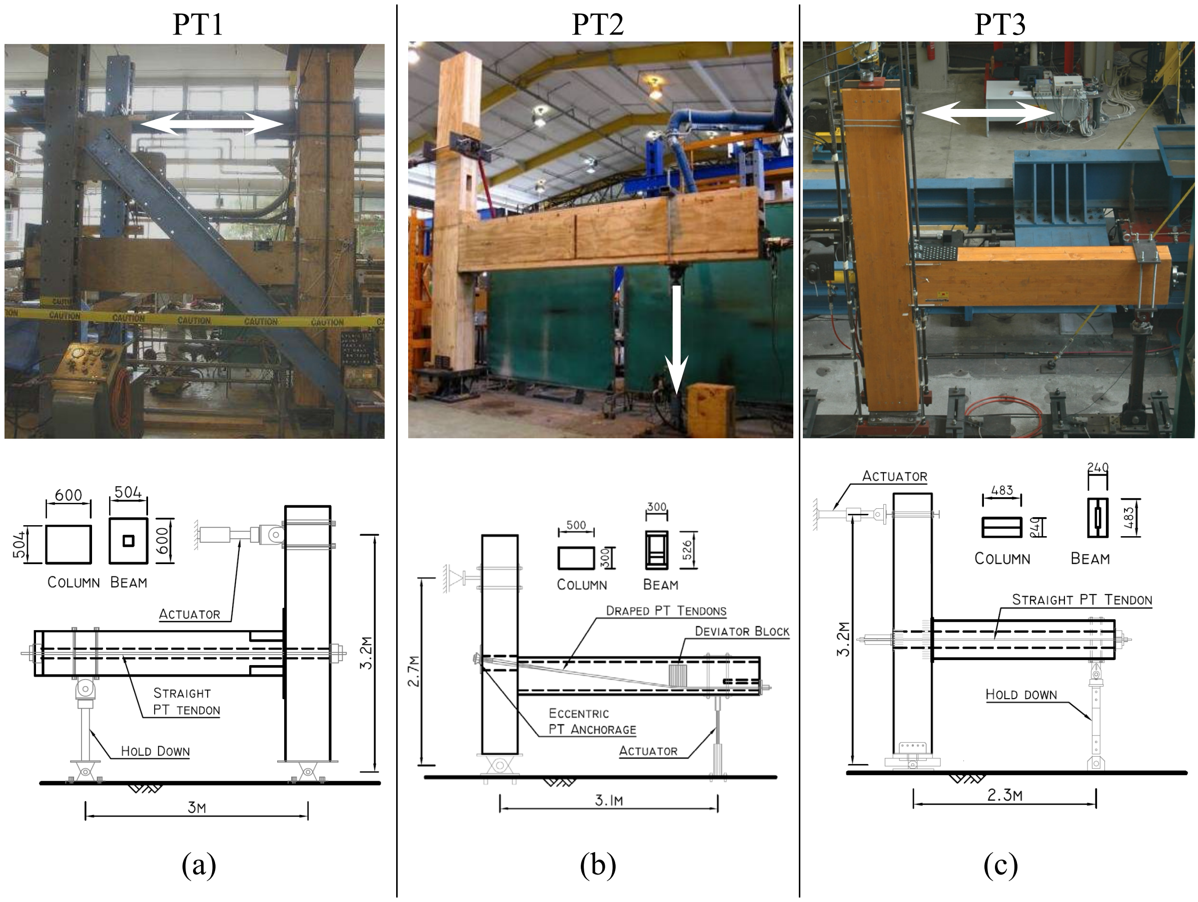

Figure 2 – Overview of test setup for (a) PT1, (b) PT2 and (c) PT3

Table 1 – Material properties and test data

Property	**Units**	**PT1**	**PT2**	**PT3**
Timber Grade	-	HySpan LVL	LVL11	GL32h
E Modulus Parallel to grain	$E_{t,par}$ (MPa)	13,200	10,700	13,700
E Modulus Perpendicular to grain	$E_{t,perp}$ (MPa)	660	600	420
Initial Post Tension Force	$F_{pt,i}$ (kN)	490 (25% f_y)	220 (35% f_y)	150 (65% f_y)
Initial Timber Stress	$\sigma_{t,c,i}$ (Mpa)	2.2	3.0	1.4
Decompression Moment	M_{dec} (kNm)	40	29	12

2.2 Test results

In the case of seismic testing, results are normally shown as lateral force versus drift graphs. For the analysis of the connection behaviour it is necessary to evaluate the connection moment-rotation graphs, as shown in Figure 3. The evaluation of this rotation (θ_{con}, more details in next paragraph and Figure 4) means that the elastic rotation components must be isolated from the beam (θ_b), column (θ_c) and joint panel (θ_j) rotations. From the graphs presented in Figure 3 a clear initial stiffness can be seen, followed by a reduction in stiffness when decompression occurs in the top fibre of the beam and gap opening starts.

The calculated connection response, based on the MMBA is shown as the short dashed lines in Figure 3. Also shown by the long dashed lines are the calculations based on the empirical formula proposed by Newcombe *et al.* [2010]. It can be seen that the MMBA does not include the initial stiffness, whereas the empirical formula improves this, but still cannot be considered sufficiently accurate for the analyzed tests. It must be noted that both calculation methods are not developed for eccentrically placed tendons and therefore the calculated tendon forces for test PT2 have been modified to fit the experimental results.

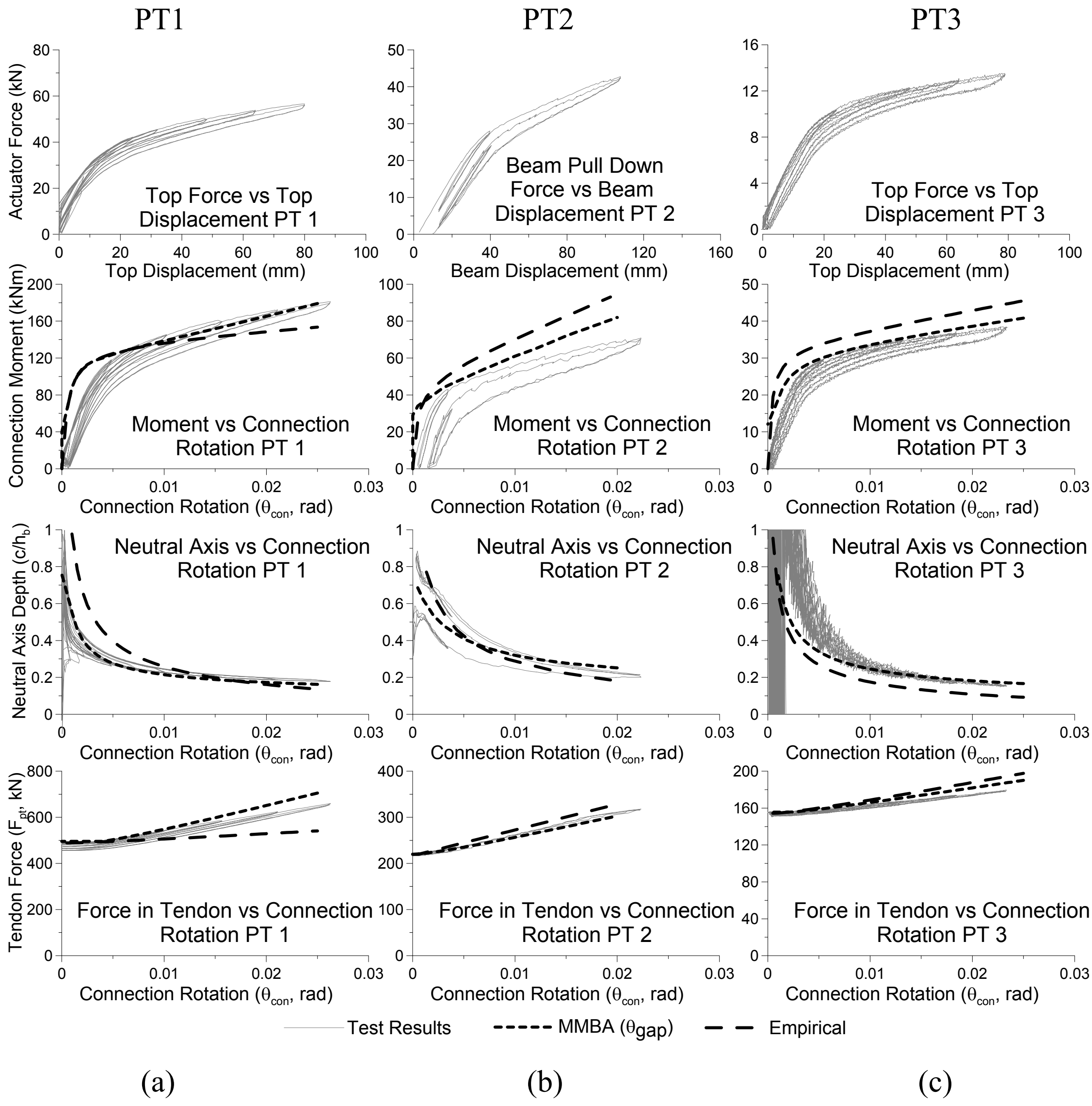

Figure 3 – Connection moment-rotation and Load-displacement graphs for (a) seismic LVL test (PT 1), (b) gravity LVL test (PT 2) and (c) seismic Glulam test (PT 3).

3 Deformation/stiffness components

The deformation of frames generally consists of three parts, the beam deformation (θ_b), the joint deformation (θ_{joint}) and the column deformation (θ_c) [Buchanan *et al.*, 1993]. In previous publications [Newcombe *et al.*, 2010] the joint deformation was split in the joint panel shear deformation (θ_j) and the connection deformation (θ_{con}), where the connection deformation was evaluated by an empirical relationship as it was suggested that the MMBA was inaccurate at small rotations. Evaluation of new test data lead to the conclusion that the connection deformation should be split into two parts; the gap opening (θ_{gap}), which can be described by the MMBA, and the interface compression deformation (θ_{int}), as is shown in Figure 4a.

The first three components shown in Figure 4c are calculated through the use of common elastic deformation formulas. These formulas are related directly to the moment at the interface as shown in Eq. 4.4. The interface compression deformation and gap opening are further described in this section.

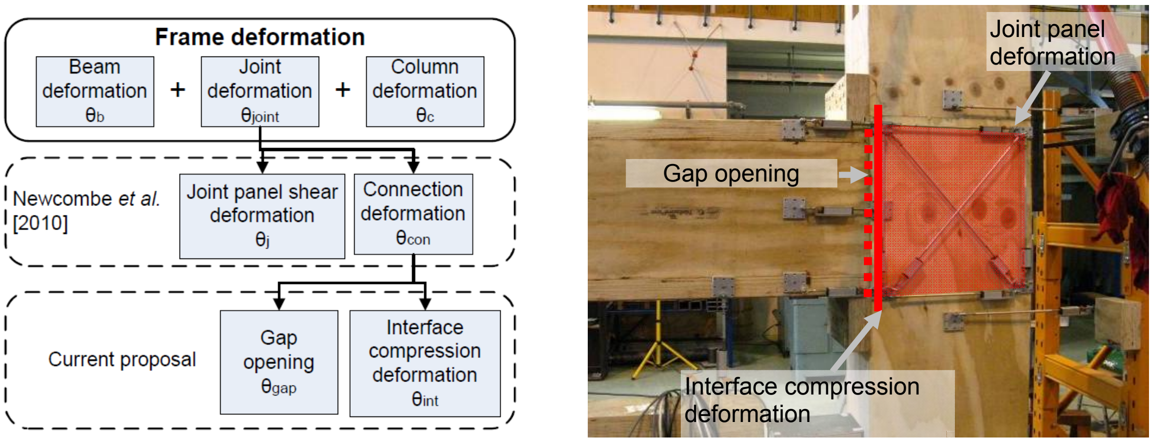

(a) (b)

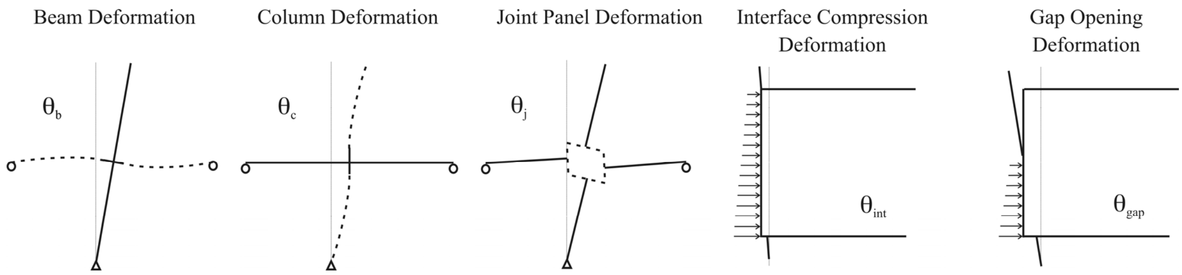

(c)

$$\theta_b = \frac{\phi_b}{L_b}\left(\frac{(L_b - h_c)^2}{6} + \frac{E_{t,perp}h_b^2}{4G_t}\right) \quad \theta_c = \frac{\phi_c}{H}\left(\frac{(H - h_b)^2}{6} + \frac{E_{t,perp}h_c^2}{4G_t}\right) \quad \theta_j = \gamma\left(1 - \frac{h_c}{L_b} - \frac{h_b}{H}\right) \quad k_{b,c,j} = \frac{M}{\theta_{b,c,j}}$$

Eq. *4.1* *Eq.4.2* *Eq. 4.3* *Eq.4.4*

(d)

Figure 4 – (a) Proposed separation of deformation components, (b) graphic of deformation components, (c) illustration of five different deformation components and (d) design equations (for lateral loading only) for beam, column and joint panel shear deformation.

3.1 Gap opening

As mentioned previously, a detailed design procedure for the moment calculation of a hybrid joint has been devised. This iterative procedure involves the imposing of a connection rotation and an initial estimation of the neutral axis depth which is then updated using force equilibrium. The strain values in the beam member (be it in concrete, steel or timber) are calculated using a comparable monolithic beam. Once force equilibrium is satisfied the moment capacity of the connection is calculated.

Traditionally in the application of this procedure to the design of post-tensioned timber the imposed connection rotation (θ_{imp}) has been equalled to the connection rotation (θ_{con}) which equals the total design rotation with all other elastic rotations (θ_c, θ_b, θ_j) removed.

It can be seen from Figure 3 that the MMBA captures the performance of the seismic post-tensioned only system reasonably well for the two seismic cases (PT1 and PT3) in terms of the moment resistance at the performance point of 0.025rad rotation (approximately 2.5% total drift). For gravity connections the MMBA calculations are not as accurate, this is because the MMBA has been developed for the design of seismic connections with centrally located straight tendons and needs minor modification in order to accurately predict the behaviour of post-tensioned connections with eccentrically placed tendons. Further developments in this area are ongoing.

A significant error in initial stiffness of the connection can be seen. This initial stiffness is essential for both seismic and gravity frames. For seismic frames the initial stiffness is crucial for two reasons: i) under serviceable load the nature of timber as a highly flexible material means interstorey displacements can be significant, if initial stiffness are not accurate predicted under a moderate event although structural damage will not occur the large displacements can damage non-structural elements, ii) under ultimate limit state loading the initial stiffness of the connection will control the activation of any form of dissipation applied to the connection, underestimation of gap opening will lead to these devices not being used to their full potential. In gravity frames the initial joint stiffness has a strong influence on beam deflections and moment distributions within the frame at the serviceability limit state design level.

3.2 Interface compression deformation

The experimental test results (Figure 3) show an initial connection stiffness before decompression, which is not captured by the MMBA. This initial stiffness is purely due to elastic deformation of the column interface caused by compression perpendicular to the grain. Therefore this deformation component (θ_{int}) has to be added to the connection design. The separation of the connection rotation into the gap opening (θ_{gap}) and the interface compression deformation (θ_{int}) makes it possible to use existing mechanical models to predict the connection behaviour.

A multi-spring model has been developed which is based on the compression stiffness of the timber column. It is assumed that the deformation of the interface can be described by a linear function, Eq. 6.1, which can be solved using the two equilibrium equations Eq. 6.3 and Eq. 6.4. The stiffness of the springs is given by integrating the strain profile over the depth of the column, as is shown by Eq. 6.5 and 6.6, and is previously described by Blass *et al.* [2004]. The spring stiffness includes the spreading of the compressive stress at a 45^0 angle, though it can be easily changed to one sided spreading or no spreading. Also compression reinforcement like timber parallel to the grain [Van Beerschoten *et al.*, 2011] or screws [Bejtka *et al.*, 2006] can be incorporated into the spring stiffness.

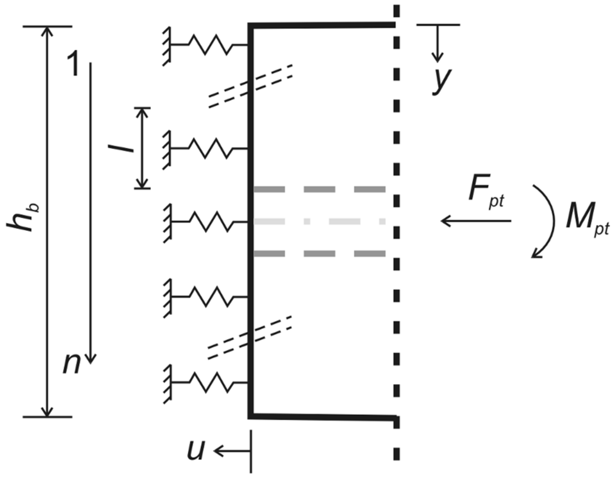

$$u_i(y) = a \cdot y_i + b \qquad \textit{Eq. 6.1}$$

$$F_i = k_i \cdot u_i \qquad \textit{Eq. 6.2}$$

$$F_{pt} = \sum F_i = a\sum_{i=1}^{n} k_i y_i + b\sum_{i=1}^{n} k_i \qquad \textit{Eq. 6.3}$$

$$M_{pt} + F_{pt} \cdot y_{pt} = a\sum_{i=1}^{n} k_i y_i^2 + b\sum_{i=1}^{n} k_i y_i \qquad \textit{Eq. 6.4}$$

Where:
a = Rotation of connection about centre of beam
b = Displacement in the column at top of beam
i = Spring number
n = Total number of springs
l = Tributary height of spring
k_i = Spring stiffness
y_i = Distance from top of beam to centre of spring

(a)

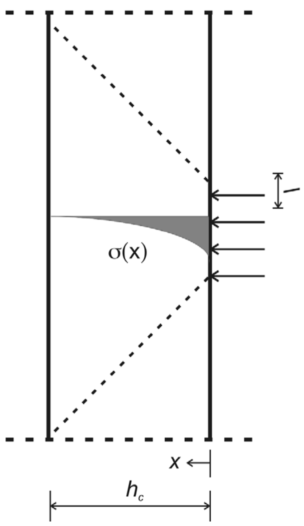

$$u = \int_0^{h_c} \frac{\sigma(x)}{E_{90}} dx = \frac{F}{E_{90} b l} \int_0^{h_c} \frac{1}{\left(2\frac{x}{l}+1\right)} dx = \frac{F}{2E_{90} b} \ln\left(2\frac{h_c}{l}+1\right) \qquad \textit{Eq. 6.5}$$

$$u_i = \frac{F_i}{k_i} \quad \rightarrow \quad k_i = \frac{2E_{90} b_i}{\ln\left(2\frac{h_c}{l_i}+1\right)} \qquad \textit{Eq. 6.6}$$

Where:
u = Spring displacement
h_c = Height of column
σ(x) = Stress over depth of column
E_{90} = Stiffness perpendicular to the grain
F = Force in the spring
b = Width of the part of beam in compression
l = Tributary height of spring

(b)

Figure 6 – (a) Multi-spring model of column compression deformation and (b) derivation of spring stiffness based on column compression perpendicular to the grain.

The interface compression deformation (θ_{int}) is the rotation of the beam into the column, which is given by the parameter *'a'* in Eq. 6.1. The interface rotational stiffness follows from the change in rotation when solving Eq.6.3 and 6.4 for different values of connection moment. Figure 7 shows testing results with the predicted gap opening (θ_{gap}) and the combination of gap opening and interface compression deformation (θ_{gap} + θ_{int},). It can be seen that this modification accurately captures the initial stiffness.

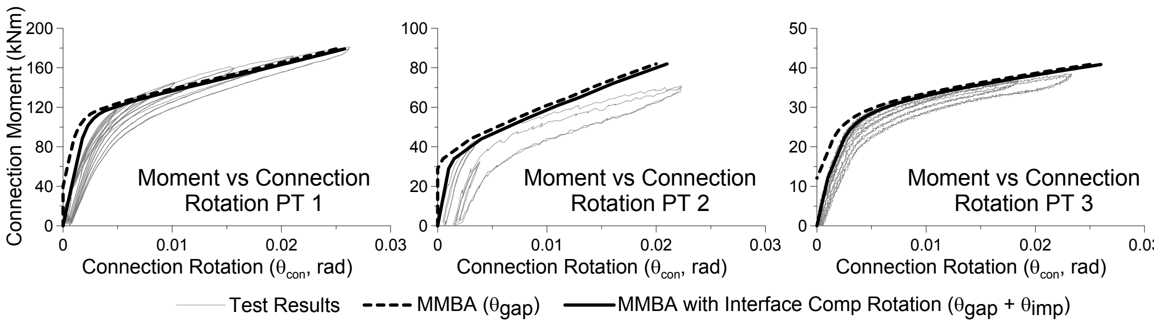

Figure 7 – Connection moment-rotation graphs with predictions from column compression deformation and gap opening (MMBA).

4 Incorporating the Initial Stiffness in Design Procedures

Combining the two rotation calculation procedures described above the moment rotation behaviour of a beam to column joint connection can be accurately defined. This is applicable for both seismic and gravity only connections. This section presents firstly the modification to the seismic design procedures, in order to incorporate the column compression deformation. Secondly it presents a way the connection rotations can be used in the gravity design of a post-tensioned timber frame.

4.1 Seismic Design

In seismic design firstly the decompression moment must be calculated and the corresponding rotation found from the procedure described in Section 3.2. This will provide the initial stiffness of the connection up until gap opening. Once this is completed the MMBA described in Section 3.1 is used to calculate the moment response. This is done taking the initial imposed rotation θ_{imp} as the gap rotation θ_{gap} (ie. when $\theta_{int} = \theta_{dec}$ and $\theta_{imp} = 0$). The MMBA is used to calculate the moment response up to compression yield of the timber elements.

In seismic design a target drift level is selected and moment demand is defined. As mentioned previously this moment response will depend on the rotation created by the gap opening, therefore in order to apply the MMBA all elastic rotations must be deducted to find the correct imposed rotation ($\theta_{imp} = \theta_{gap}$ in design). A small number of iterations in the design process may be necessary before convergence is found as the elastic rotations depend on the connection moment.

4.2 Gravity design

In gravity design the post-tensioning tendon can be represented by equivalent forces. These forces depend on the amount of gap opening and the beam deflections, both which results in tendon elongation. This elongation means an iterative procedure is needed as outlined in [Palermo *et al.*, 2010], although ignoring the tendon elongation will result in a conservative design as the increased tendon force reduces deflections and gap opening.

Table 2 gives the rotation and stiffness values for test PT2, which illustrates the importance of the interface deformation in the SLS design. The joint rotational stiffness (θ_{joint}) is different for internal and external connections as is illustrated in Table 2. A possible design choice would be to have decompression happening past the Serviceability Limit State (SLS) connection moment. In case of an internal beam-column connection the initial stiffness follows directly from the interface compression. In the Ultimate Limit State (ULS) design the full moment-rotation curve needs to be evaluated, as is shown in Figure 8 and Table 2. In the ULS design of an external beam-column connection the gap opening governs the design, whereas the column rotations become negligible due to their high stiffness.

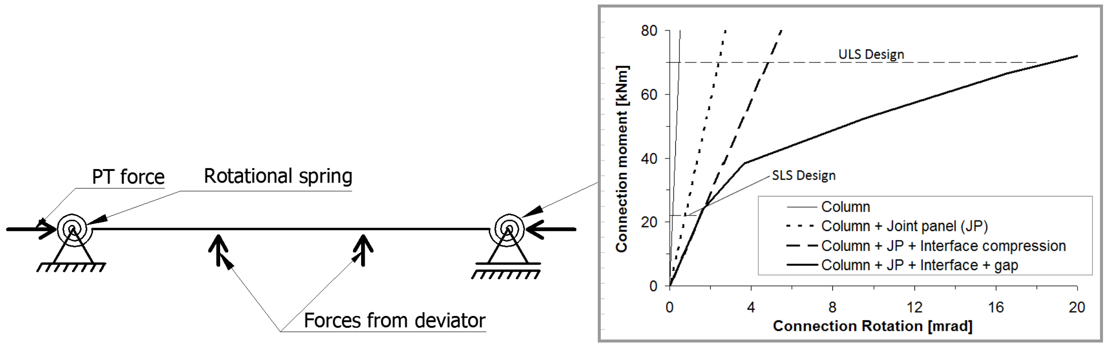

Figure 8 – Schematics of simplified gravity design for a post-tensioned timber frame

Table 2 – Rotation and stiffness values for SLS and ULS design of internal and external beam-column (bc) joints for gravity frames (PT2).

		SLS (M_{con} = 22kNm)				ULS (M_{con} = 70kNm)			
		Internal bc-joint		External bc-joint		Internal bc-joint		External bc-joint	
		Value	*% of total*	*Value*	*% of total*	*Value*	*% of total*	*Value*	*% of total*
Column[1]	θ_c (mrad)	-		0.14	10%	-		0.45	2%
	k_c (kNm/mrad)	-		155		-		155	
Joint panel[2]	θ_j (mrad)	-		0.61	40%	-		1.94	10%
	k_c (kNm/mrad)	-		36		-		36	
Interface[3]	θ_{int} (mrad)	0.76	100%	0.76	50%	2.41	14%	2.41	12%
	k_c (kNm/mrad)	29		29		29		29	
Gap[4] (effective stiffness)	θ_{gap} (mrad)	-		-		15	86%	15	76%
	k_c (kNm/mrad)	-		-		4.7		4.7	
Total	θ_{spring} (mrad)	0.76	100%	1.51	100%	17.41	100%	19.80	100%
	k_{spring} (kNm/mrad)	29.0		14.5		4.0		3.5	

[1] *= from analytical formula* [2] *= from test data* [3] *= from multi-spring model* [4] *= from MMBA*

5 Conclusions

A modification to the design of post-tensioned timber beam-column connections has been presented and it has been shown that this allows an accurate prediction of the full moment-rotation behaviour of the connection, whether it is a seismic or gravity connection. Elastic interface compression deformation can be modelled with a multi-spring model and results in accurate predictions of the initial joint stiffness. Combined with the MMBA the full connection behaviour is described by mechanical models.

In seismic design the accurate prediction of the initial stiffness of the joint is important as it will aid in the design of additional dissipative devices. These have a certain activation point which may not be reached at the desired drift if the initial stiffness value is ignored. In addition it will aid the accurate prediction of SLS drifts which can lead to non-structural damage. In gravity design the joint rotational stiffness, which is strongly influenced by the interface deformation, can be used to analyze beam deflections and bending moment distribution in the frame.

Acknowledgements

The authors wish to acknowledge STIC for their financial support. The LVL was kindly provided by Carter Holt Harvey limited and Nelson Pine Industries Ltd. Glulam manufacture was performed by HOLZBAU SUD in Calitri, Italy. The post-tensioning material was supplied by BBR Contech for the LVL and INPES S.p.A. for glulam testing.

References

Bejtka, I., and Blass, H. J. [2006]. *"Self-tapping screws as reinforcement in beam supports"*. CIB-W18, Florence, Italy.

Blass, H. J., and Görlacher, R. [2004]. *"Compression perpendicular to the grain"*. World Conference on Timber Engineering, Lahti, Finland.

Buchanan, A., and Fairweather, R. H. [1993]. *"Seismic design of glulam structures"*. Bulletin of the New Zealand National Society for Earthquake Engineering, Vol. 26, 4, 415-436 p.

Buchanan, A. H., Palermo, A., Carradine, D., and Pampanin, S. [2011]. *"Post-tensioned timber frame buildings"*. The Structural Engineer (in press).

Iqbal, A., Pampanin, S., and Buchanan, A. H. [2010]. *"Seismic Performance of Prestressed Timber Beam-Column Sub-Assemblies"*. New Zealand Society for Eearthquake Engineering Conference, Wellington, New Zealand.

Newcombe, M., Cursiel, M., Pampanin, S., Palermo, A., and Buchanan, A. [2010]. *"Simplified design of post-tensioned timber frames"*. CIB W18, Nelson, New Zealand.

Palermo, A. [2004]. *"Use of Controlled Rocking in the Seismic Design of Bridges"*. Doctate Thesis, Technical University of Milan, Technical Institute of Milan, Milan.

Palermo, A., Pampanin, S., Carradine, D., Buchanan, A., Lago, B., Dibenedetto, C., Giorgini, S., and Ronca, P. [2010]. *"Enhanced performance of longitudinally post-tensioned long-span LVL beams"*. 11th WCTE, Trentino, Italy.

Pampanin, S., Pagani, C., and Zambelli, S. [2004]. *"Cable-stayed and suspended post-tensioned solutions for precast concrete frames: the Brooklyn system"*. New Zealand Concrete Society Conference, Queenstown, New Zealand.

Pampanin, S., Palermo, A., Buchanan, A., Fragiacomo, M., and Deam, B. [2006]. *"Code Provisions for Seismic Design of Multi-Storey Post-Tensioned Timber Buildings"*. CIB W18/39, Florence, Italy.

Pampanin, S., Priestley, N., and Sritharan, S. [2001]. *"Analytical Modelling of the Seismic Behaviour of Precast Concrete Frames Designed with Ductile Connections"*. Journal of Earthquake Engineering, Vol. 5, 3, 329-367 p.

Priestley, M. J. N. [2002]. *"Direct Displacement-Based Design of Precast/Prestressed Concrete Buildings"*. PCI journal, Vol. 47, 6, pp. 66-79 p.

Priestley, M. J. N., Sritharan, S., Conley, J. R., and Pampanin, S. [1999]. *"Preliminary Results and Conclusions from the PRESSS Five-story Precast Concrete Test-Building"*. PCI journal, Vol. 44, 6, 42-67 p.

Smith, T., Pampanin, S., Carradine, D., Buchanan, A., Ponzo, F., Cesare, A., and Nigro, D. [2011]. *"Experimental Investigations into Post-Tensioned Timber Frames with Advanced Damping Systems."*. Il XIV Convegno di Ingegneria Sismica, Bari, Italy.

Standards New Zealand [2006]. *"Concrete structures standard"*. NZS3061:2006, Standards New Zealand, Wellington, New Zealand.

Van Beerschoten, W., Palermo, A., Carradine, D., Sarti, F., and Buchanan, A. [2011]. *"Experimental Investigation on the Stiffness of Beam-Column Connections in Post-Tensioned Timber Frames"*. Structural Engineering World Conference, Como, Italy.

CIB-W18/44-7-5

INTERNATIONAL COUNCIL FOR RESEARCH AND INNOVATION IN BUILDING AND CONSTRUCTION

WORKING COMMISSION W18 - TIMBER STRUCTURES

DESIGN APPROACH FOR THE SPLITTING FAILURE OF DOWELTYPE CONNECTIONS LOADED PERPENDICULAR TO GRAIN

B Franke

P Quenneville

University of Auckland

NEW ZEALAND

MEETING FORTY FOUR

ALGHERO

ITALY

AUGUST 2011

Presented by B Franke

A Jorissen commented that the fracture energy seemed to be dependent on connection lay out and geometry. B Franke responded that fracture energy was known for Mode I and II but not for combined stresses and fracture energy may be related to stress states in mix mode and this approach may be okay for practical reason. Furthermore curve of normalized fracture energy was used.

A Jorissen commented that there were significant developments of theoretical equations in the last decade. This study was based on experimental approach this be justified. B Franke responded that situation was configuration dependent and if analytical based approach was available, one could consider them.

A Jorissen asked whether the ductile and brittle failures in experimental separated. B Franke replied that no and they always used the combinations of both failure modes.

M Ballerini received clarifications about how the crack surfaces for mode I and II and how to calculate some of the parameters.

I Smith asked how the current approach compared with past results. B Franke stated that they try to consider the more complex cases to arrive at rational solutions.

S Winter commented that design approach based on fracture mechanics with unit-less factors would be difficult to justify in codes. B Franke responded that the factors in this study did not have such problems.

G Hochreiner asked about overlaying of shear stresses and B Franke responded that CIB W18 last year addressed the issue.

Design approach for the splitting failure of dowel-type connections loaded perpendicular to grain

Bettina Franke, Pierre Quenneville

University of Auckland, New Zealand

1 Introduction

For the prediction of the splitting failure of double shear dowel-type connections loaded perpendicular to grain, different design equations are available in various international standards. Current research results and publications show that there are disagreements between the experimental results and the international design standards, e.g. FRANKE & QUENNEVILLE [9], [10], SCHOENMAKERS [19], JENSEN [14], BALLERINI [3]. The current international design standards are based on one hand, on a strength criterion and on the other hand, on fracture mechanic. But important geometry parameters are partly or not at all respected in the design equations and therefore result in uncertain predictions or in conservative values.

The paper presents the investigation of the splitting failure behaviour of double shear dowel-type connections using numerical test series and fracture mechanics methods. These numerical test series are used for the determination of the failure criteria for dowel-type connections. The fracture values reached show that the geometry of the connection, the loaded edge distance and the depth of the beam influence the ratio between the fracture mode I and mode II. The fracture criteria found will be used for a design equation that takes into account the important parameters as well as the ratio between the fracture modes for tension and shear. The approach considers the dependency of the splitting load capacity on the geometry parameters of single and multiple dowel-type connections. The correlation between the design equation and experimental test results published confirms the method used and the failure criteria determined.

2 Analyses of the failure behaviour using fracture mechanic

2.1 Fracture mechanic

Fracture mechanic is a recent design method compared to the established stress based strength assessment theory. For cases with high stress singularities like connections, holes or notches, the methods of the fracture mechanics are useful for the description of the failure process, the splitting of the wood. In general, the crack process is classified in three different modes. The fracture mode I describes the symmetric separation under normal tension stress, mode II contains the in plane shear stress and mode III the out of plane shear stress. Dowel-type connections loaded perpendicular to grain, as shown in Figure 1, fail, considering the stress situation, in the fracture mode I and II, the so called mixed mode.

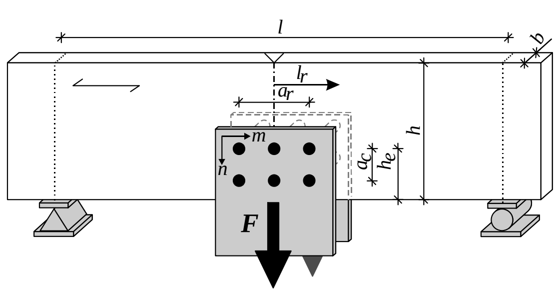

Figure 1: Sketch of dowel-type connections loaded perpendicular to grain with variables defined

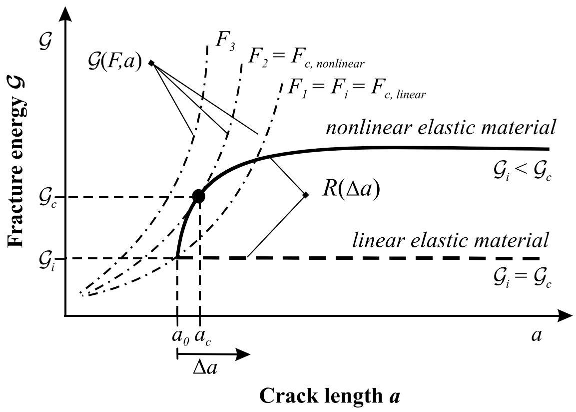

Figure 2: Crack resistances curves for linear and non-linear elastic material behaviours

The energy needed to create new crack surfaces or for the crack propagation is extracted from the mechanical energy of the complete system. The released energy of the system for the infinitesimal crack propagation is called energy release rate.

The linear elastic fracture mechanics use a constant, material related critical value. In this case, at the moment of crack initiation, the energy release rate is equal to the critical energy release rate. For any further crack propagation, the crack resistance is constant and the crack becomes unstable. For nonlinear elastic material: If the crack resistance increases more than the crack extension force under a constant load during crack propagation, then the crack growth is stable, cf. Equation (1). If the energy release rate exceeds the critical value, the crack will grow in an unstable manner and the system fails, cf. Equation (2).

$$\left.\frac{\partial \mathcal{G}}{\partial a}\right|_{F=const} < \frac{dR}{da} \tag{1}$$

$$\left.\frac{\partial \mathcal{G}}{\partial a}\right|_{F=const} \geq \frac{dR}{da} \tag{2}$$

Figure 2 shows the crack resistance curves for the cases of the material behaviours described and the corresponding critical fracture energy release rates. This method was used to determine the critical fracture energy of each connection layout investigated. Furthermore the critical fracture energies were split into the fracture mode I and mode II using the method of ISHIKAWA [13]. The fracture energies determined are not comparable with the fracture energies known for the pure fracture mode I or II, because they are caused by a realistic connection layout with the corresponding stress situation and do not relate to a test setup for the investigation of a single fracture mode. Therefore, in this paper, the fracture energies determined for dowel-type connections are called specific critical fracture energies, $\mathcal{G}^{I,II}_{spec,c}$.

2.2 Test series

Numerical test series are mainly used for the analyses of the failure behaviour using fracture mechanic methods. Various connections as single dowel-type connections with different loaded edge distances or multiple dowel-type connections with a different number of dowels per row or column as well as different spacing within the connection are included and summarized in Table 1. 30 specimens are simulated with uniformly probabilistically distributed material parameters for each numerical test series. Therefore the following results are presented as mean values.

Table 1: Numerical test series

Group - Description		Specimen				
		Sizes b / h / l [mm]	Dowel m x n	Loaded edge distance h_e/h	Connection width a_r	Connection height a_c
A -	Loaded edge distance h = (190/300/400/600/800) mm	80/h/610	1 x 1	0.2, 0.3, 0.4 0.5, 0.6, 0.7, 0.8	-	-
B -	Connection width h = 190 mm	80/190/4h + a_r	2 x 1	0.2, 0.3, 0.4, 0.5, 0.6, 0.7, 0.8	3d, 4d, 6d, 8d, 10d, 15d, 20d, 25d	-
C -	Connection width h = (300/400/600/800) mm	80/h/4h + a_r	2 x 1	0.3, 0.5, 0.7	3d, 6d, 8d, 10d, 20d	-
D -	Increasing number of columns	80/190/610	1,2,3,4,5,6 x 1	0.4, 0.6	(n-1) 3d	-
E -	Increasing number of columns	80/304/1320	1,2,3,4 x 1,2,3	0.44, 0.7	16.8d	-
F -	Increasing number of rows	80/304/1320	1,2,3,4 x 1,2,3	0.44, 0.7	16.8d	(m-1) 3d
G -	Increasing spacing between rows	80/304/1320	2,3 x 2	0.44, 0.7	16.8d	3d, 4.5d, 6d

Depending on the connection size and layout, the load deflection curves of dowel type connections describe very brittle failure behaviour or show the incidence of plastic deformations before the brittle failure occurs. The brittle failure occurs due to the splitting of the wood under tension perpendicular to grain and/or shear stress. The ductile failure which leads to plastic deformations depends on the embedment strength of the wood and the bending capacity of the dowel. The numerical model used simulates both the splitting failure of wood under tension perpendicular to grain and shear as well as the ductile failure of wood due to compression. However, since the focus is to investigate the brittle failure mechanism, the bending of the dowel is not included in the numerical model and the influence is neglected. This is acceptable if the dowel slenderness ratio is small and ductile behaviour due to dowel bending is minimized.

The numerical model was defined as a 2-dimensional model based on the purpose to especially investigate the splitting of the wood and is presented in [9], [11]. The numerical model includes the important realistic failure process and its adequacy has been proofed on comprehensive experimental test series from [15] and [18].

2.2 The specific fracture energy for dowel-type connections

For each dowel of the connection investigated, the crack resistance curves as well as the critical specific fracture energies were determined. For a 3 by 2 dowel type connection, in total 12 crack resistance curves for each fracture mode and 24 critical specific fracture energies were determined. Analysing the distribution of the critical fracture energies related to the connection layout shows that the dowels at the top corners trigger the unstable failure. For example, for the 3 by 2 dowel-type connection, the crack growth becomes unstable and leads to the failure of the complete connection if the failure criterion is reached for the top corner dowels 1.1 and 1.3 of the connection, as shown in Figure 3. The analyses of the energy lines show, that the cracks between the outer dowels (inner part of the connection) becomes also unstable and the wood between the dowels 1.1 and 1.3 is then completely separated. The failure load is in this case 60 kN. The outline of the connection layout is described by the loaded edge distance h_e and the connection width a_r for multiple dowel type connections and will be used for the design proposal to estimate the failure loads. The top sketches of Figure 3 show the critical area used for the design proposal for this 3 by 2 dowel type connection.

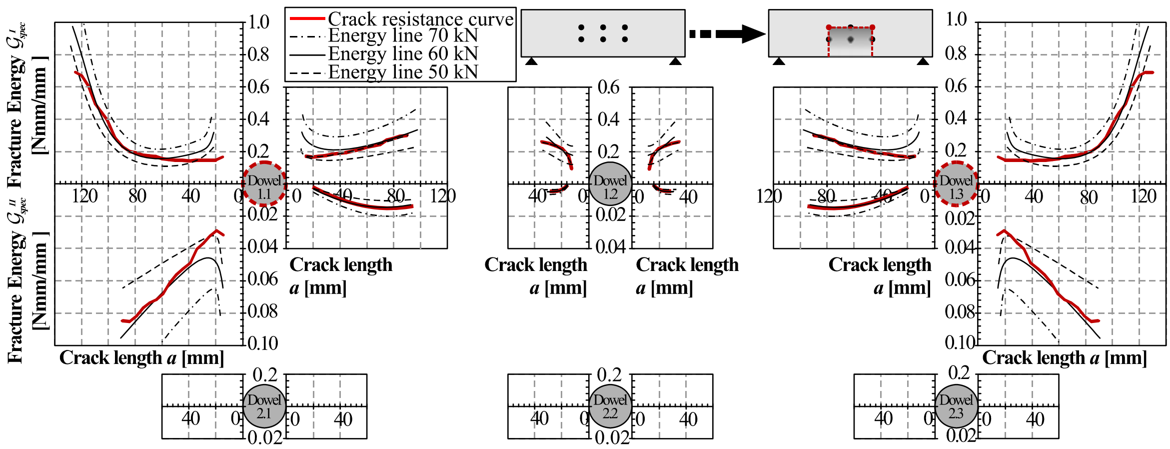

Figure 3: Distribution of the fracture energies for a m x n = 3 x 2 dowel type connection at failure load

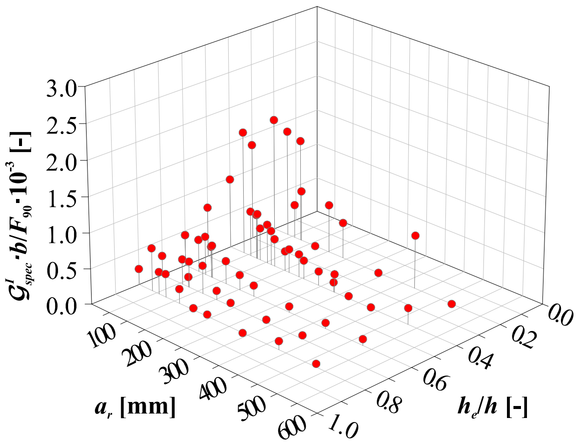

Figure 4: Distribution of the specific critical fracture energies for mode I for a member depth h = 190 mm

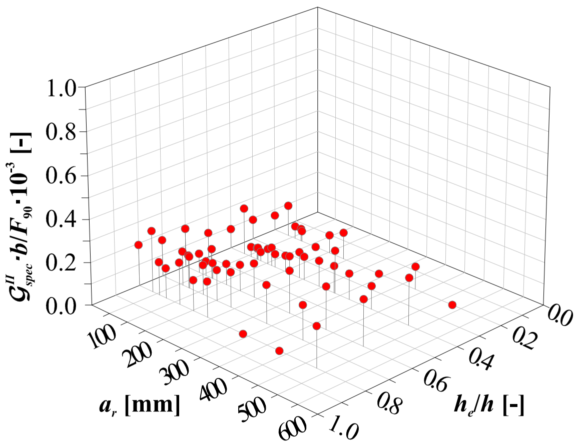

Figure 5: Distribution of the specific critical fracture energies for mode II for a member depth h = 190 mm

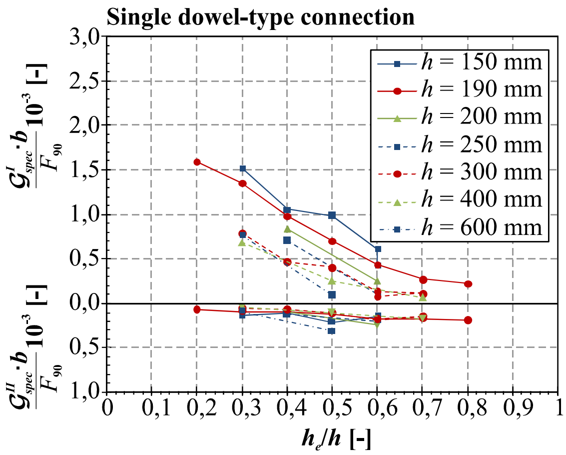

Figure 6: Distribution of the specific critical fracture energies over the member depth h for mode I and II

Applying the nonlinear fracture mechanic, the distribution of the specific critical fracture energies of the dowels at the edge of the top row determined shows a dependency on the loaded edge distance h_e, the connection width a_r and the depth of the member h. Figure 4 and Figure 5 summarize the results of all numerical test series with a member depth h = 190 mm and show the dependency on the loaded edge distance h_e/h and the connection width a_r. The differences for fracture mode I are higher than for mode II. Similar distributions could be observed for different depths of the member h.

The distribution of the specific critical fracture energies over the member depth shows an influence on the fracture mode I but not on mode II, as shown in Figure 6 for single dowel-type connections. Furthermore the results of a previous study show an increase of the load capacity with an increase of the number of rows parallel to the grain, [10]. Connections with more than one row lead to a reduction of the stress singularities at the dowels at the corner of the top row. The reduced stress situation leads to the increase of the load capacity.

3 Design proposal for double shear dowel-type connections loaded perpendicular to the grain

3.1 Failure criterion for connections

The splitting failure of dowel type connections described by critical specific fracture energies can be summarized using common failure criteria. The distribution of the numerical test series investigated shows that the quadratic failure criterion encloses mostly all failure case, as shown in Figure 7. In general, the fracture criteria are expressed with the fracture toughness K which is related to the fracture energy $\mathcal{G}$ as follow:

$$\mathcal{G} = \frac{1}{E^*} K^2 \tag{3}$$

where E^* is the specific modulus of elasticity.

The quadratic failure criterion will be used for the assessment of dowel-type connections. Because fracture mechanic methods for the design proposal are used, it has to be considered that the failure load includes small cracks in the cross section of the member. These small cracks resulting from the loading situation have to be distinguished from the main crack propagation which leads to the failure of the connection and/or the member.

3.3 Design proposal for connections

The load capacities of double shear dowel-type connections loaded perpendicular to grain depend on the number of dowels, the connection layout as well as the loaded edge distance and the member cross section. An influence on the position of the connection along the span of the beam could not be observed [9] and is therefore not considered in the design approach. Depending on the connection layout and its position over the member depth, the connection fails either in a ductile failure such as bending of the dowel or the embedment failure of the wood or in a splitting failure, the cracking of the wood. Therefore the following design proposal for the splitting failure of dowel-type connections loaded perpendicular to grain has to be used in combination with the European yield model for the prediction of the ductile failure behaviour as given in Eq. (4). The minimum of these failures gives the load carrying capacity of the connection.

$$F_{connection} = \min \begin{cases} F_{ductile}\left(\text{EYM}\right) \\ F_{splitting} = F_{90} \end{cases} \tag{4}$$

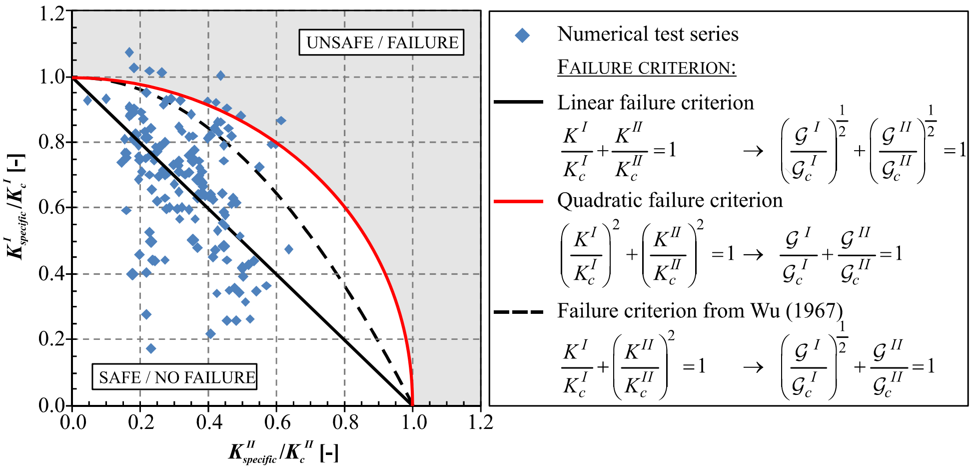

Figure 7: Failure criteria for dowel type connections loaded perpendicular to grain

For the design proposal for the splitting failure, the quadratic failure criterion determined will be used to consider different connection layouts and to get a comprehensive design approach. Substituting the individual critical specific fracture energies with the distribution of the normalized fracture energies, the splitting load F_{90} for dowel-type connections in wood becomes:

$$F_{90} = \frac{b \cdot 10^3}{\left(\frac{\mathcal{G}^{I}_{norm}}{\mathcal{G}^{I}_{c}} + \frac{\mathcal{G}^{II}_{norm}}{\mathcal{G}^{II}_{c}}\right)} \cdot k_r \tag{5}$$

where F_{90} in [N] is the load capacity depending on the splitting failure of the wood. $\mathcal{G}^{I}_{c}$ and $\mathcal{G}^{II}_{c}$ in [Nmm/mm²] are the critical material fracture energies for the fracture mode I or II for the material in the connection, as published in e.g. [16], [22]. The parameter b in [mm] is the width of the member.

The normalized fracture energies enclose all individual critical specific fracture energies of the connection considered. Therefore the critical specific fracture energy of each numerical test was normalized with the specimen width b and the splitting load F_{90}, see Eq. (6), as per [4]. In a further step, the distribution of all values were expressed with a 3-dimensional group of curves, which depends on the loaded edge distance h_e/h, the connection width a_r in [mm] and the member depth h, as shown in Eq. (7) and Eq. (8). Figure 8 shows as example the curve for the member depth h = 190 mm compared to the individual values of the numerical test series. The empirically determined Eq. (7) and Eq. (8) are based on more than 200 different connection layouts investigated.

$$\mathcal{G}^{I,II}_{norm} = \frac{\mathcal{G}^{I,II}_{spec} \cdot b}{F_{90}} \tag{6}$$

$$\mathcal{G}^{I}_{norm} = e^{\left(h^{-1}\left(200 - 10 h_e \cdot h^{-0.25} - a_r\right)\right)} \tag{7}$$

$$\mathcal{G}^{II}_{norm} = \left(0.05 + 0.12\frac{h_e}{h} + 1 \cdot 10^{-3} a_r\right) \tag{8}$$

The factor k_r encloses the effect of the number of rows parallel to grain n. The load capacity increases with increasing the number of rows, because of the more distributed stress situation than for connections with one row. For an increasing number of rows, the load capacity as well as the stress situation become constant, as shown in Figure 9. This behaviour could be summarized using the quadratic interaction of the areas of the tension stress perpendicular to grain and the shear stress besides the dowels at the corner of the top row, see Figure 10. The quadratic interaction of the stress compared to the distribution of the load capacities, shows the same behaviour, see Figure 9. These results lead to the following new approximation of the factor k_r:

$$k_r = \begin{cases} 1 & \text{for} \quad n = 1 \\ 0.1 + \left(\arctan(n)\right)^{0.6} & \text{for} \quad n > 1 \end{cases} \tag{9}$$

The distribution of the factor k_r, like in the German design standard DIN 1052:2008 [6] or the design approach by BALLERINI [3], could not be confirmed. The numerical test results of test group G, which enclose in addition to different number of rows, also different spacing between the rows, show that the load capacity does not increase with increasing the spacing. Therefore a dependency on the spacing between the rows is not included in the factor k_r.

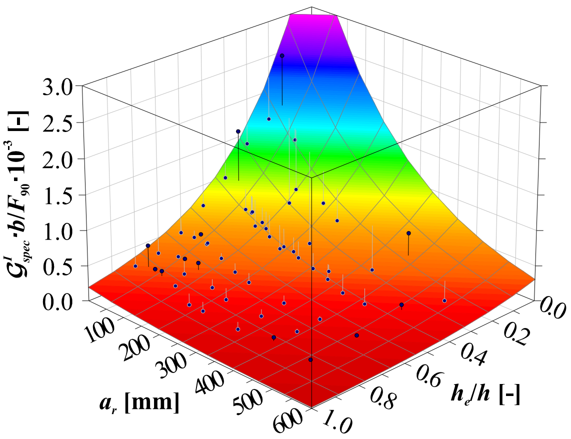

Figure 8: 3-dim. curve of the normalized fracture energies for mode I compared to the individual numerical test results, for a member depth h = 190 mm

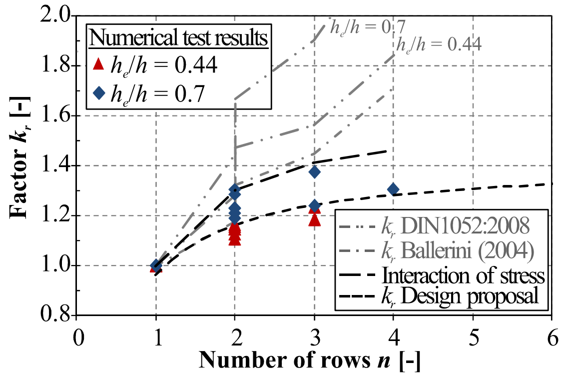

Figure 9: Factor k_r, depending on the numerical load capacities and stress situations determined according to DIN1052:2008 and BALLERINI [3]

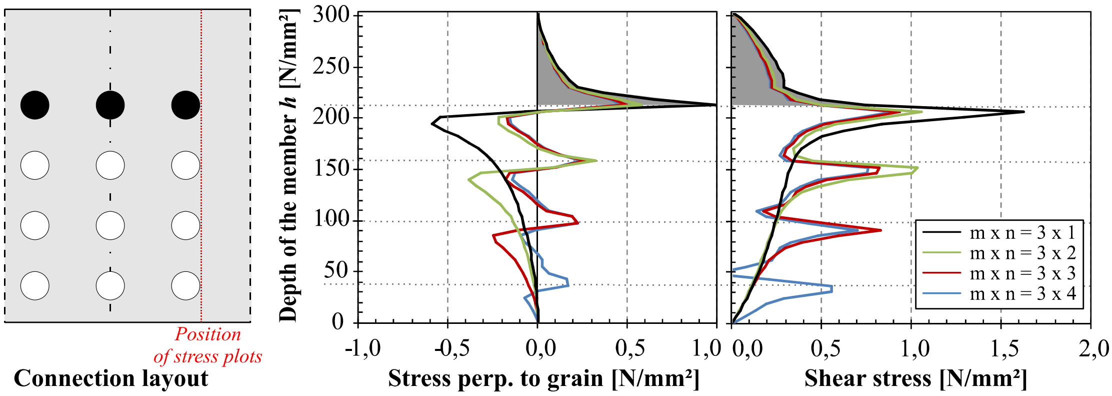

Figure 10: Stress distributions besides the dowel at the edge of the rows over the depth of the member, for different number of rows, and for a constant displacement of u = 1 mm

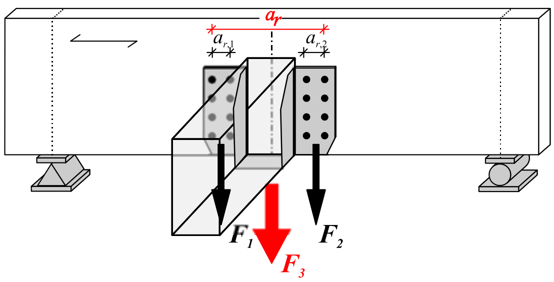

$$F_{90} = \min \begin{cases} F_1(a_{r,1}) + F_2(a_{r,2}) \\ F_3(a_r) \end{cases} \tag{10}$$

Figure 11: Design for nail plates or double dowel-type connections

For connections with more than two columns, e.g. nail plate connections as in Figure 11 or double dowel-type connections, the splitting load has to be determined on the one hand with the connection width a_r for the complete connection and also as single connections with the individual connection width $a_{r,i}$. The minimum of the load capacities of Eq. (10) is the governing splitting load capacity of the connection.

4 Discussion

4.2 Comparison to experimental test series published

The design proposal will be first compared to the comprehensive experimental test series with single and multiple dowel-type connections done by RESHKE [18], KASIM [15] and LEHOUX [17] with Canadian spruce glulam. The effect of the connection width a_r, the loaded edge distance h_e/h and the number of dowels from m x n = 1 x 1 up to 3 x 2 were observed in the experimental test series. The material values used for Canadian spruce glulam are equal to the material settings for the numerical simulation and are referenced in [12] and [22]. The critical fracture energies $\mathcal{G}_c^I = 0.225$ Nmm/mm^2 and $\mathcal{G}_c^{II} = 0.650$ Nmm/mm^2 were used. Figure 12 shows the comparison of the design proposal predictions and the experimental results as well as the numerical test series.

Furthermore, the design proposal predictions are also compared with the experimental test series from: BALLERINI [1], [2] who investigated mainly different depths of the member and different loaded edge distances; MÖHLER & LAUTENSCHLÄGER [7] who observed different number of rows, connection widths and loaded edge distances; and EHLBECK &

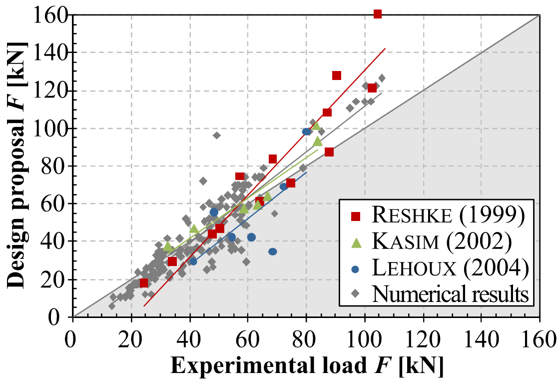

Figure 12: Experimental test series done by KASIM/ RESHKE/ LEHOUX [15], [17], [18] in Canadian spruce glulam

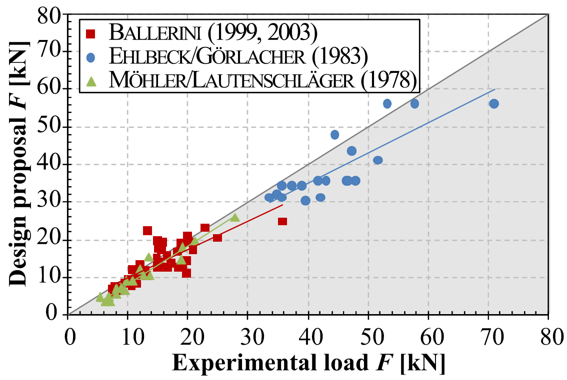

Figure 13: Experimental test series done by BALLERINI/ MÖHLER/ LAUTENSCHLÄGER/ EHLBECK/ GÖRLACHER [1], [2], [7] in European spruce

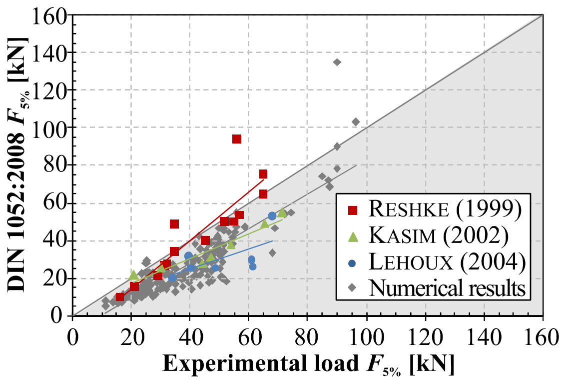

Figure 14: Experimental test series done by KASIM/ RESHKE/ LEHOUX [15], [17], [18] compared to DIN1052:2008

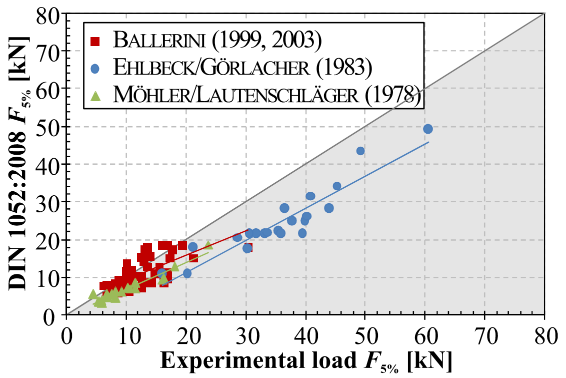

Figure 15: Experimental test series done by BALLERINI/ MÖHLER/ LAUTENSCHLÄGER/ EHLBECK/ GÖRLACHER [1], [2], [7] compared to DIN1052:2008

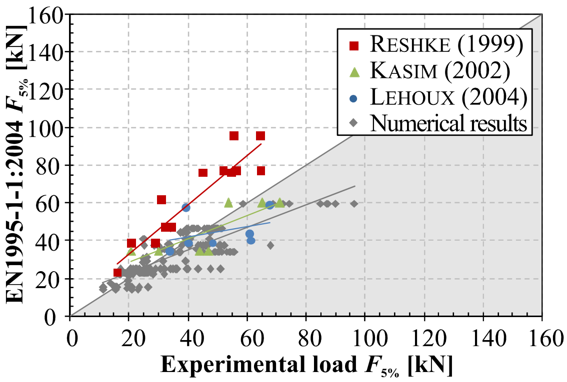

Figure 16: Experimental test series done by KASIM/ RESHKE/ LEHOUX [15], [17], [18] compared to EN1995-1-1:2004

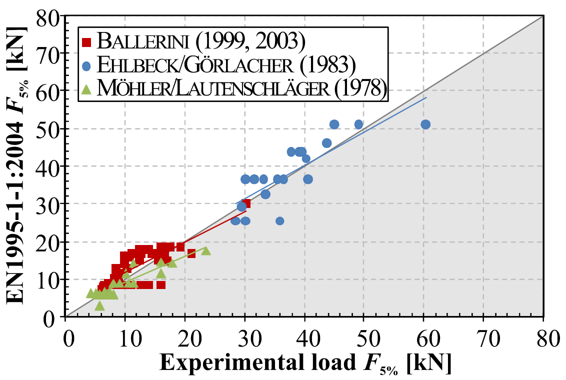

Figure 17: Experimental test series done by BALLERINI/ MÖHLER/ LAUTENSCHLÄGER/ EHLBECK/ GÖRLACHER [1],[2],[7] compared to EN1995-1-1:2004

GÖRLACHER [7] who did tests with nailed steel-to-wood connections. The test series are done in European spruce; for which the same material values, as used before, could be found in [16]. Figure 13 shows a close correlation in the comparison of the experimental test series and the design proposal.

4.1 Comparison to international design standards

For the comparison of the design proposal with the current two main international design standards, the same experimental and numerical test series were used. On the one hand, the concept of the European design standard EN 1995-1-1:2004 which is based on fracture mechanics methods and was introduced by V. D. PUT & LEIJTEN [21], and on the other hand, the concept of the German design standard DIN 1052:2008 which is based on a strength criterion and was introduced by EHLBECK, GÖRLACHER & WERNER [7] were compared. For these comparisons, the 5% percentile values of the material parameters, as given in [5], [6], [8], and experimental results are used. In the experimental test series, where the values are unknown, the average values were reduced by about 15%.

From Figures 14, 15, 16 and 17, one can observe that both the DIN 1052:2008 and the EN 1955-1-1:2004 design equations result in inconsistent predictions of the failure strength. The predictions using the DIN 1052:2008 equations are more consistent but can be overly conservative. The predictions using the EN 1995-1-1:2004 equations are inadequate, as one can observe, neglecting the effect of some of the connection configuration parameters.

5 Conclusion

A new design proposal is presented for double shear dowel-type connections which allows the design of the splitting failure of the wood due to connections loaded perpendicular to grain. The design approach based on fracture mechanics methods encloses important parameters which influence the load capacity of the connection. The comparison of the design results with comprehensive experimental test series done in Canadian and European spruce confirms the procedure of the design proposal. The good agreement in comparison with over 100 different experimental test configurations confirms also that the current international standards have to be proofed and/or improved.

The new design approach will be compared to comprehensive experimental test series done with laminated veneer lumber (LVL).

6 Acknowledgment

This research work is supported by the Structural Timber Innovation Company (STIC) of New Zealand.

7 References

[1] Ballerini, M. (1999): A new set of experimental tests on beams loaded perpendicular to grain by dowel-type joints, CIB-W18, paper 32-7-2, Austria.

[2] Ballerini, M. (2003): Beams transversally loaded by dowel-type joints: Influence on splitting strength of beam thickness and dowel size, CIB-W18, paper 36-7-8, USA.

[3] Ballerini, M. (2004): A new prediction formula for the splitting strength of beams loaded by dowel-type connections, CIB-W18, paper 37-7-5, United Kingdom.

[4] Borth, O. (2002): Abschätzung der Tragfähigkeit von Queranschlüssen an Trägern aus Voll- und Brettschichtholz im Rahmen der Linear-Elastischen Bruchmechanik. Doctoral thesis, Bauhaus University Weimar, Germany.

[5] Canadian Standards Association (2009): O86-09 Engineering design in wood. Mississauga, Canada.

[6] Deutsches Institut für Normung e. V. (2008): DIN 1052:2008 Entwurf, Berechnung und Bemessung von Holzbauwerken – Allgemeine Bemessungsregeln und Bemessungsregeln für den Hochbau. Berlin, Germany.

[7] Ehlbeck, J., Görlacher, R., Werner, H. (1989): Determination of perpendicular to grain tensile stresses in joints with dowel-type fasteners. In: International council for research and innovation in building and construction, CIB-W18, paper 22-7-2, Germany.

[8] European Committee for Standardization (CEN) (2004): EN 1995-1-1:2004 Design of Timber structures. Brussels, Belgium.

[9] Franke, B., Quenneville, P. (2010): Analyses of the failure behaviour of transversly loaded dowel type connections in wood. In: Proceedings of 11th World Conference on Timber Engineering, Italy.

[10] Franke, B., Quenneville, P. (2010): Failure behaviour and resistance of dowel-type connections loaded perpendicular to grain, CIB-W18, paper 43-7-6, New Zealand.

[11] Franke, B., Quenneville, P. (2011): Numerical modeling of the failure behavior of dowel connections in wood. In: ASCE, Journal of Engineering Mechanics 137, 186, 155-226.

[12] Forest Products Laboratory (1999): Wood Handbook - Wood as an Engineering Material. Gen. Tech. Rep. FPL-GTR-113, U.S. Department of Agriculture, Madison, USA.

[13] Ishikawa H., Kitagawa H., Okamura H. (1979): J Integral of a mixed mode crack and its application. In: Volume3, ICM 3, Cambridge, England.

[14] Jensen, J. L. (2005): Splitting strength of beams loaded perpendicular to grain by dowel joints, In: Journal of Wood Science 51, p. 480-485.

[15] Kasim, M. H. (2002): Bolted timber connections loaded perpendicular-to-grain - Effect of row spacing on resistance. Royal Military College of Canada, Kingston, Canada.

[16] Larsen, H. J., Gustafsson, P. J. (1990): The fracture energy of wood in tension perpendicular to grain – results from a joint testing project. In: International council for research and innovation in building and construction, CIB-W18, paper 23-19-2, Portugal.

[17] Lehoux, M. C. G. (2004): Bolted timber connections loaded perpendicular to grain. A proposed design approach. Royal Military College of Canada, Kingston, Canada.

[18] Reshke, R. (1999): Bolted timber connections loaded perpendicular-to-grain - Influence of joint configuration parameters on strength. Royal Military College of Canada, Kingston, Canada.

[19] Schoenmakers, J. C. M. (2010): Fracture and failure mechanisms in timber loaded perpendicular to the grain by mechanical connections, Doctoral thesis, University of Technology Eindhoven, Netherlands.

[20] Wu, E. M. (1967): Application of fracture mechanics to anisotropic plates. Journal of Applied Mechanics, Series E, 34(4), p. 967-974.

[21] Van der Put, T. A. C. M., Leijten, A. J. M. (2000): Evaluation of perpendicular to grain failure of beams caused by concentrated loads of joints. In: International council for research and innovation in building and construction, CIB-W18, paper 33-7-7, The Netherlands.

[22] Vasic, S. (2002): Applications of fracture mechanics to wood. The University of New Brunswick, New Brunswick, Canada.

CIB-W18/44-12-1

INTERNATIONAL COUNCIL FOR RESEARCH AND INNOVATION
IN BUILDING AND CONSTRUCTION

WORKING COMMISSION W18 - TIMBER STRUCTURES

PROPERTIES OF CLT-PANELS EXPOSED TO COMPRESSION PERPENDICULAR TO THEIR PLANE

T Bogensperger

M Augustin

holz.bau forschungs gmbh, Graz

G Schickhofer

Institute for Timber Engineering and Wood Technology, TU Graz

AUSTRIA

MEETING FORTY FOUR

ALGHERO

ITALY

AUGUST 2011

Presented by T Bogensperger

H Blass asked why reinforcement techniques were not considered. T Bogensperger responded that they were well aware of reinforcement techniques but wanted to consider basic properties first.

H Blass asked what the failure criteria were for FEM. T Bogensperger responded that failure criteria were based on deformation.

S Franke and T Bogensperger discussed the fact in some configuration one edge could not have bending of the fibres and the elasto-plastic behaviour. T Bogensperger stated that the next step would have to consider shear behaviour.

Properties of CLT-Panels Exposed to Compression Perpendicular to their Plane

Thomas Bogensperger*, Manfred Augustin*, Gerhard Schickhofer**
*) holz.bau forschungs gmbh, Inffeldgasse 24, A-8010 Graz, Austria
**) Institute for Timber Engineering and Wood Technology, TU Graz, A-8010 Graz, Austria

Mechanical properties of Cross Laminated Timber elements (CLT elements) compressed orthogonally to their plane are significantly better than those of comparable glulam. The reason for this can be found in the different lay-up of the CLT. Whereas glulam features only unidirectional layers (lamellas), CLT elements are built-up with layers orthogonal to each other. In this way adjacent layers of CLT elements support each other and act as an alternating "reinforcement", which leads to better mechanical properties than for timber or glulam.

This paper will present results for the stiffness and strength of cubic CLT specimens tested in accordance with EN 408 . The results for the mean value of the modulus perpendicular to plane $E_{c,90,clt,mean}=450$ *N/mm² and for the characteristic strength values perpendicular to plane* $f_{c,90,clt,k}=2.85$ *N/mm² are about 30% higher than those of comparable glulam specimens.*

In practice CLT elements are carried by linear or punctual supports (e. g. columns). For the design and verification $k_{c,90}-$*values are required and therefore tests for different loading situations ("central" - "longitudinal edge" - "crosswise edge" - "vertex") were carried out. Based on a characteristic strength values perpendicular to plane of* $f_{c,90,clt,k}=2.85$ *N/mm² and the loading situation* $k_{c,90,clt}-$*values (in accord. to EN 1995-1-1) between 1.4 and 1.9 can be proposed.*

1 Introduction and motivation

The use of Cross Laminated Timber (CLT) and the associated building system has become established as a new European solid timber construction technique. Within timber based building systems CLT is in competition with e. g. lightweight timber frame building systems. Naturally CLT also competes with different materials, e. g. building systems based on bricks and concrete. CLT plates are excellently applicable for single or multi-family houses as slabs acting uniaxially. In particular cases, which are illustrated in Figure 1, ceiling elements are subjected to biaxial load bearing behaviour due to the partially punctual support of the CLT plate.
Seen from an engineering point of view, this two-axial load bearing behaviour has to be verified according to the common plate theories derived by Kirchhof for plates without shear flexibility and by Reissner-Mindlin for general plates if shear effects are to be included. CLT is a strongly orthotropic structure in comparison to e. g. a steel plate and therefore the characteristic strength values and stiffness values are significantly lower in comparison to the values in the plane. This explains why especially the verification of punctual or line-shaped load introduction has such a high significance for CLT-plates.
This question is focused on in this paper and a proposal will be made for the verification of punctual load introduction by single columns perpendicular to the plane.

Figure 1: Solid timber building system with CLT, partially supported with columns

2 glulam: state of the art

2.1 *Characteristic strength values perpendicular to grain for glulam*

Quite a lot of research on the strength of glulam perpendicular to grain has been carried out which suggests that, it is more or less constant for all grading classes [1,4,8]. For a convenient comparison the strength values of international research of the last decade have been collected in Table 1.

Table 1: mechanical properties of glulam: compression perpendicular to grain ($f_{c,90,g,k}$)

Author	Series	Nr. of speci-men [-]	Gauge length [mm]	Density ρ_{12} [kg/m³]			MOE $E_{c,90}$ [N/mm²]			Strength $f_{c,90}$ [N/mm²]		
				$\rho_{12,mean}$	COV	$\rho_{12,k}$	$E_{c,90,g,mean}$	COV	$E_{c,90,g,k}$	$f_{c,90,g,mean}$	COV	$f_{c,90,g,k}$
Hoffmeyer, P.; et. al., 1999 [4]	-	120	200	466	4,8	433	274	13	215*	2,87	9,3	2,44‡‡
Augustin, et al., 2006 [1]	I/K1	19	200	490	5,02	449	299	19,86	201	3,10	22,10	1,99**
	I/K2	22	200	439	4,99	403	301	12,02	241	3,01	17,58	2,13**
	I/K3	21	200	418	11,98	335	320	22,91	200	3,12	18,01	2,18**
	II/1/MS10	41	200	417	7,71	364	265	21,24	172	3,35	19,62	2,33**
	II/1/ MS13	40	200	447	6,04	402	292	15,64	217	3,43	21,05	2,33**
	II/1/ MS17	41	200	493	6,04	444	318	16,81	230	3,16	17,58	2,30**
	All (weighted)	-	200	451	7,0	400	299	18,0	210	3,20	19,3	2,21**

Note:
* not given in the paper; calculated for a normal distribution
** characteristic value in accordance to EN 14358
‡‡ 5 % quantile value

According to the values given in Table 1, a characteristic strength value $f_{c,90,g,k}$ of 2.25 N/mm² can be proposed for glulam as a weighted mean value over all series.

2.2 *EN 1995-1-1:2009 and EN 1994:1999*

In EN 1995-1-1 [12] the verification of compression perpendicular to grain has to fulfill the following condition:

$$\sigma_{c,90,d} \leq k_{c,90} \cdot f_{c,90,d}$$

with:
$\sigma_{c,90,d}$ design stress perpendicular to grain
$f_{c,90,d}$ design strength perpendicular to grain
$k_{c,90}$ factor, taking into account partial compression situation

with the following definition of relevant stress perpendicular to grain:

$$\sigma_{c,90,d} = \frac{F_{c,90,d}}{A_{ef}}$$

with:
$F_{c,90,d}$ applied design load perpendicular to grain
A_{ef} associated effective area

This effective area is the contact area between the two parts, enlarged by maximum of 30 mm at each side in the grain direction. Additional rules, which can limit this increase of 30 mm, are given in detail in EN 1995-1-1 [12].

Values for the $k_{c,90}$ parameter are given in EN 1995-1-1 for glulam with

- $k_{c,90}$=1.50 for continuous support like swells and
- $k_{c,90}$=1.75 for single support like columns under beams

if specific geometric conditions are fulfilled.

For the resistance, the appropriate strength perpendicular to grain is found in EN 1194:1999 [15], where the following formula can be found:

$$f_{c,90,g,k} = 0.7 \cdot f_{t,0,l,k}^{0.5}$$

with:

$f_{c,90,g,k}$ characteristic strength perpendicular to grain for glulam (index '*g*')

$f_{t,0,l,k}$ characteristic tension strength of single lamella (index '*l*')

This formula leads to a characteristic strength value of $f_{c,90,g,k}$=2.70 N/mm², based on a tensile strength of $f_{t,0,l,k}$=14.5 N/mm² for widely used grading class GL24h. Increasing strength values of the boards lead to higher $f_{c,90,g,k}$ values of the glulam. The second factor, the so-called $k_{c,90}$ value, is given as a constant value − either 1.50 for continuous support or 1.75 for discrete support. Additional rules concerning some minimal length values are given in detail in EN 1995-1-1.

2.3 prEN 14080:2011

In this European standard [14], which is still a working document, a constant value of 2.5 N/mm² can be found for homogeneous and combined glulam.

2.4 Summary

In table 2 a summary of $f_{c,90,g,k}$ values is given for good comparison.

Table 2: Summary of $f_{c,90,g,k}$ strength values

	$f_{c,90,g,k}$	%	remark
research	2.25	*100*	based on [1, 4, 8]
EN 1194:1999 [15]	2.7	*120*	for glulam GL24h
prEN 14080:2011[14]	2.5	*111*	for all GLT strength classes

3 CLT perpendicular to plane – current research at TU Graz

3.1 Characteristic strength values for CLT

The basic strength value $f_{c,90,clt,k}$ has to be investigated similarly to glulam. Rules for the geometry of glulam test specimens are specified in EN 408 [13]. EN 408 demands cubes with a height of h_{ref}=200 mm and a minimum length of 100 mm in the fibre direction. The compressed area of the test specimens should be 25,000 mm², which leads to a size length of 160·160 mm². The tests conducted were analyzed according to EN 408 (limitation of remaining plastic strains perpendicular to grain to 1%, Fig. 2).

In order to achieve comparable results for CLT the same procedure and the same evaluation process was chosen for the CLT cubes. At Graz University of Technology two diploma thesis were carried out on this topic. The first one

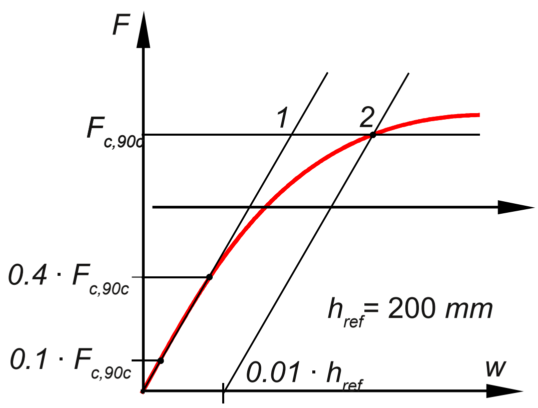

Figure 2: Evaluation of strength perp. to grain according to EN 408 [13]

was completed by Y. Halili [3] and the second one by C. Salzmann [9]. The results of these diploma thesis tie in well with results by E. Serrano et al. [1, 10].

Y. Halili investigated CLT produced under laboratory conditions. Therefore he was able to investigate effects due to following selected parameters: :

- Type of board (edge grained, flat grained boards) “Series I“
- Number of layers (3, 5, 7, 9 and 20 layers) “Series II“.
- Ratio of the thicknesses of adjacent layers. The number of layers investigated was 5 and 7. This ratio is given by the quotient of d_q/d_l “Series III“.

In contrast to this work Salzmann investigated 5-layered CLT test specimens with overall heights of 150, 161, 165 and 197 mm, which were produced by one single manufacturer. The type of board can only be classified as random as industrial CLT elements are predominantly edge grained but sometimes also flat grained and intermediate grained.

Series “I”

The parameters investigated in this series are the location of the boards in the original stem. Three different types of boards are focused on: flat-sawn timber, boards close to the pith and heartwood boards. These different boards are illustrated in Figure 3.

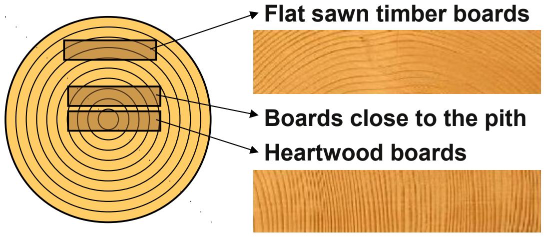

Figure 3: Different kinds of boards, investigated in series “I“[3]

Series “II”

The parameter investigated here is the number of layers. The numbers examined were 3, 5, 7, 9 and 20 (see Figure 4).

Series “III”

The parameter investigated here is the relative thickness of adjacent layers. This thickness relation is determined by the ratio of d_q to d_l. The values investigated for this parameter are d_q/d_l =1.0, d_q/d_l =2/3 and d_q/d_l =1/3. These tests were carried out with 5- and 7-layered CLT cubes. A typical picture of a 5-layered CLT cube can be seen in Figure 5.

Figure 4: Pictures of some test specimens of series “II“[3]

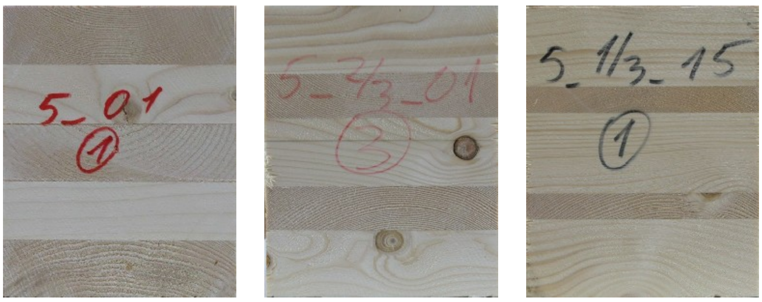

Figure 5: Pictures of some test specimens of series “III“[3]

Series based on cubes with origin in industrial production

In contrast to the series above the overall height of the CLT cubes tested in the diploma thesis of [9] varies between 150 mm, 161 mm, 165 mm and 197 mm. Some typical pictures of this industrially manufactured CLT cube series can be viewed in Figure 6.

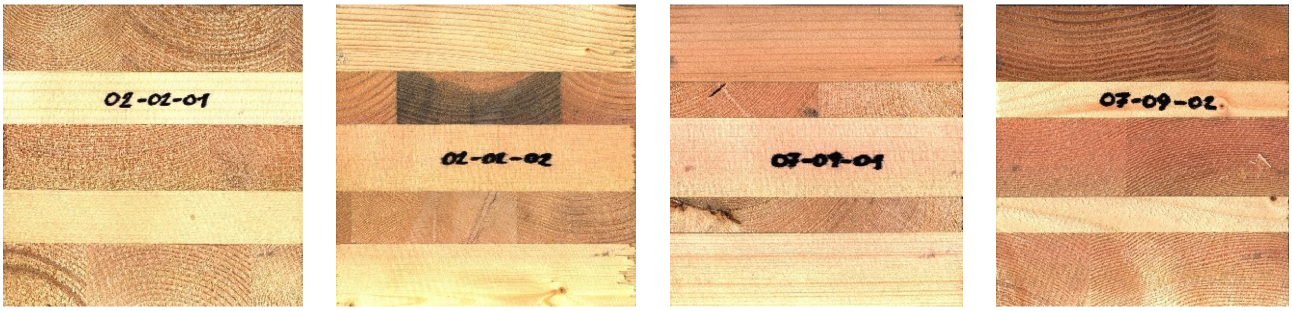

Figure 6: Pictures of some test specimens of industrially manufactured CLT [9]

Investigations of compression strength were also carried out by Al-douri, Hamodi [1] and Serrano and Enquist [10] in series "A". They tested industrially produced CLT cubes with three layers, a thickness of 120 mm and a base area of 200·200 mm².

An overview of the results of all studies mentioned above [2, 8, 9] can be found in Table 3. Box plots for compression strength are shown in Figure 7. Left box plot shows cubes with same thickness, right box plot those with unequal layer thicknesses. Same box plots for mean stiffness can be seen in Figure 8. Based on these strength values a mean strength value $f_{c,90,clt,k}$ for CLT elements is suggested with 2.85 N/mm², which is an increase of about 27% based on $f_{c,90,g,k}$=2.25 N/mm² for glulam (see Chapter 2.1). A comparison of stiffness parameters perpendicular to plane for CLT and perpendicular to grain for glulam based on the values given in tables 1 and 3 shows a mean value of $E_{c,90,g,mean}$≈300 N/mm² for glulam (Table 1) and $E_{c,90,clt,mean}$≈450 N/mm² as a mean value over all for CLT (Table 3). The increase in stiffness amounts to 50%.

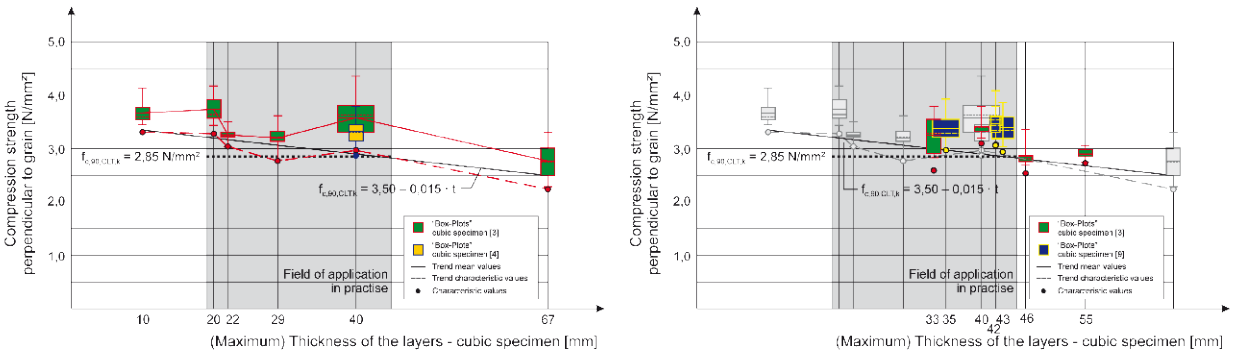

Figure 7: Box plots for compression strength perpendicular to plane

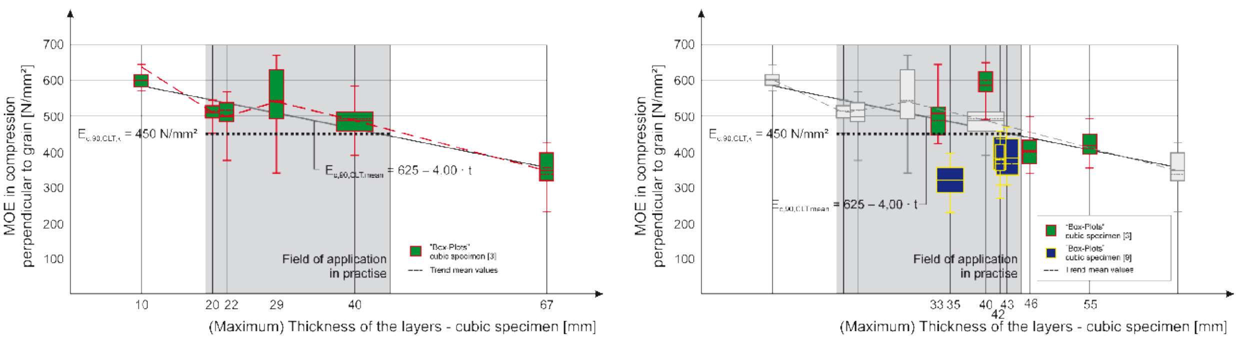

Figure 8: Box plots *for stiffness perpendicular to plane*

Table 3: mechanical properties of CLT: compression perpendicular to plane ($f_{c,90,clt,k}$)

Author	Series	Nr. of speci-men [-]	Gauge length [mm]	Density ρ_{12} [kg/m³]			MOE $E_{c,90,mean}$ [N/mm²]			Strength $f_{c,90}$ [N/mm²]		
				$\rho_{12,mean}$	COV	$\rho_{12,k}$	$E_{c,90,clt,mean}$	COV	$E_{c,90,clt,k}$	$f_{c,90,clt,mean}$	COV	$f_{c,90,clt,k}$ **
Halili Y., 2008 [3]	I_SW	16	200	449	5,1	411	532	7,5	466	3,22	3,5	3,00
	I_KN	16	200	427	4,1	398	482	4,7	444	3,36	4,1	3,10
	I_KW	16	200	419	3,0	399	426	10,5	352	4,28	4,7	3,89
	II_3	16	200	411	3,7	386	346	15,3	259	2,77	10,5	2,24
	II_5	41	200	421	4,3	391	487	9,6	410	3,58	9,9	2,97
	II_7	16	200	494	5,2	451	540	17,4	386	3,20	7,1	2,77
	II_9	16	200	452	3,1	429	499	10,8	411	3,26	3,6	3,04
	II_20	16	200	453	2,0	438	599	3,6	564	3,67	5,2	3,31
	III_5_1/3	16	200	452	2,3	435	402	10,5	332	2,86	6,2	2,54
	III_5_2/3	16	200	439	2,5	421	417	9,9	349	2,90	3,4	2,73
	III_7_1/3	16	200	436	4,9	401	507	15,5	377	3,25	11,1	2,59
	III_7_2/3	16	200	460	4,1	429	586	8,6	503	3,41	4,8	3,10
Salzmann C., 2010 [9]	"150"	15	150	462	4.9	425	440	13.0	346	3.52	7.8	3.01
	"161"	35	161	467	4.7	431	367	14.4	280	3.34	8.1	2.86
	"165"	27	165	442	3.8	414	435	13.5	338	3.33	10.0	2.69
	"197"	10	197	446	1.9	432	387	15.7	287	3.43	7.0	2.96
Al-douri, Hamodi [1] Serrano E., Enquist B., 2010 [10]	-	15*	120	430	2.9	410	-	-	-	3.33+	7.4	2.86+

Note:
** characteristic value in accordance to EN 14358
* specimen 200 x 200 mm
+ moisture content of specimen: mean u = 10,0 %

3.2 Load introduction in CLT plates – $k_{c,90,clt}$ factors

An increase factor $k_{c,90,clt}$, taking into account partly distributed loads similarly to glulam ($k_{c,90}$), has to be investigated for CLT. Four typical load arrangements (see Figure 9) can be detected to be most relevant for the actual problem [9]. The red area denotes the load introduction area with a size of 160·160 = 25600 mm².

Above test specimens with dimensions of 600·600 mm² basic area are made of the same CLT plates as the CLT cubes, which originate from the industrially manufactured CLT plates. Thickness h_{ref} of the particular CLT plates are 150 mm, 161 mm, 165 mm and 197 mm instead of h_{ref}=200 mm. Size of test specimens and test arrangement is illustrated in Figure 10.

Figure 11 shows some impressions of the deformed CLT plates under a condition, which is beyond the limits according to EN 408 [13].

Results of these tests are given in Table 4. The results include the 4 different CLT types, therefore results describe an average behaviour of CLT.

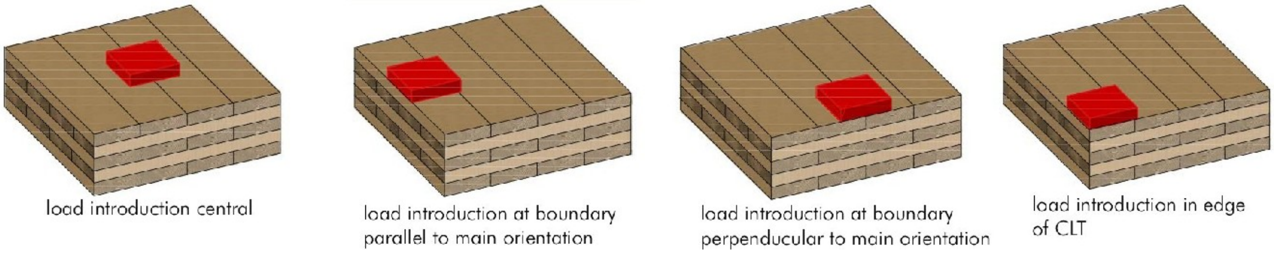

Figure 9: CLT with partly distributed loads – typical positions of loads for CLT plates [9]

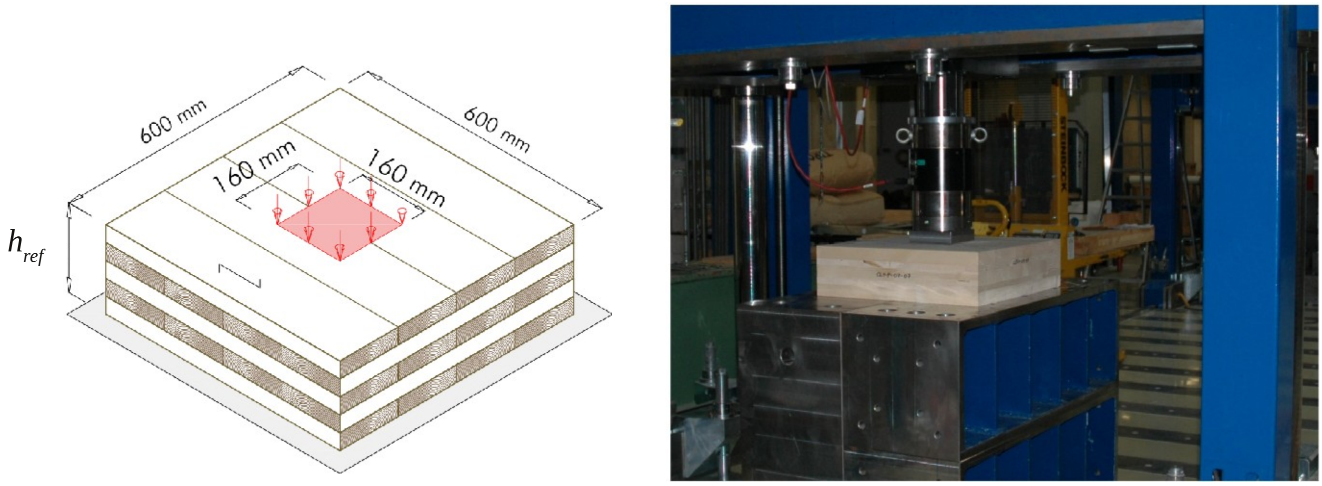

Figure 10: Test configuration and test arrangement for CLT with partly distributed loads [9]

Based on these test results, proper $k_{c,90,clt}$ factors can be derived based on a characteristic strength value $f_{c,90,clt,k}$ with 2.85 N/mm² ($k_{c,90,clt}$ see Table 5).

Remark: These $k_{c,90,\ clt}$ values do not make use of the additional enlargement in fibre direction of the load introduction area, as it is specified for glulam with a maximum value of 30 mm at each side. Characteristic load perpendicular to plane can be calculated now

$$F_{c,90,clt,k} = k_{c,90,clt} \cdot f_{c,90,clt,k} \cdot A$$

with:

$F_{c,90,clt,k}$	characteristic design load perpendicular to plane
$k_{c,90,clt}$	factor, according to Table 5
$f_{c,90,clt,k}$	characteristic strength value perp. to plane with $f_{c,90,clt,k}$=2.85 N/mm²
A	associated contact area, which transmits load into CLT

Figure 11: CLT plates with partly distributed loads – deformations [9]

Table 4: mechanical properties of CLT plates with partly distributed loads [3,9,10]

Author	Series	Nr. of speci-men [-]	Gauge length [mm]	Density ρ_{12} [kg/m³]			Apparent stiffness $K_{90,app}^{(+)}$ [N/mm²]			Strength $f_{c,90}$ [N/mm²]		
				$\rho_{12,mean}$	COV	$\rho_{12,k}$	Mean	COV	5 %	$f_{c,90,clt,mean}$	COV	$f_{c,90,clt,k}^{**}$
Halili Y., 2008 [3]	central	5	200	419	0,8	414	736	7,2	649	5,92	4,8	5,26
Salzmann C., 2010 [9]	central	3	150	488	0,9	480	632	9,2	536	6,37	7,6	5,02
		3	161	478	6,5	427	631	14,3	483	6,54	6,0	5,41
		5	165	454	1,0	446	649	16,3	475	5,72	11,1	4,33
		4	197	443	1,5	432	632	6,7	563	7,01	5,4	6,07
		15	***	463	2,2	445	636	11,9	512	6,36	7,9	5,15
	Longi-tudinal edge	3	150	488	0,9	480	572	12,7	453	5,08	16,2	2,94
		3	161	484	1,1	476	504	15,2	378	5,01	3,9	4,42
		5	165	448	2,9	426	555	17,2	398	5,50	11,3	4,14
		11	***	469	2,0	454	546	15,4	408	5,25	10,6	3,89
	Crosswise edge	3	150	488	0,9	480	578	7,1	510	4,97	4,1	4,37
		3	161	439	2,0	425	440	9,6	370	5,09	8,6	3,88
		5	165	442	2,6	423	493	13,0	388	5,47	11,4	4,05
		11	***	454	2,0	439	502	10,5	416	5,23	8,7	4,09
	vertex	3	150	465	5,7	421	435	14,9	328	4,45	12,8	2,99
		3	161	450	1,6	439	455	6,6	406	4,81	3,3	4,32
		5	165	438	1,9	425	514	4,8	473	5,03	10,6	3,83
		4	197	445	1,6	433	470	6,7	418	5,52	7,6	4,48
		15	***	448	2,5	429	475	7,7	416	5,00	8,8	3,93

Note:
* not given in the paper; calculated for a normal distribution
** characteristic value in accordance to EN 14358
*** all weighted
+ apparent stiffness $K_{90,app}$ due to load spreading in CLT plate, for details see [9]

Table 5: Proposal for $k_{c,90,clt}$ values depending on $f_{c,90,clt,k}$ for the different load introductions

Load introduction	# of tests	$f_{c,90,clt,k}$ *[N/mm²]*	$k_{c,90,clt}$ *[−]*
central	15	2.85	1.8
longitudinal edge	10		1.5
crosswise edge	10		1.5
vertex	15		1.4

4 Numerical analysis

4.1 Stiffness calculation of CLT and glulam cubes

Due to a good correlation between strength perpendicular and stiffness [3] numerical results regarding stiffness comparison between glulam and CLT will be shown here on basis of a linear elastic orthotopic material behaviour. The increase in stiffness could be a good orientation for the increase in strength. Mechanical behaviour strongly depends on the poisson ratios of the material parameters. The two models (glulam-cube, CLT-cube) with a basic area of 25600 mm² consists of 5 boards in each case. Two different heights are investigated: one height is 150 mm with lamella thickness of 30 mm, the second height is 200 mm with lamella thickness of 40 mm. Material parameters are taken from F. H. Neuhaus [6] and summarized in Table 6 for moisture content of 12%. Numbering and sequence of axis in table 6 is 1 for radial, 2 for tangential and 3 for longitudinal. Poisson values (μ_{rt}, μ_{rl}, μ_{tl}) of Table 6 are below the main diagonal of the compliance material matrix in notation of Voigt. Material orientation of each board is modeled in a zylindrical coordinate system. Heartwood boards are located in the middle of a stem and therefore the location of board in stem is 0 cm (Table 7). Flat sawn timber boards are those with a high distance from the stem. In Table 7 boards with a maximum distance of 25 cm are shown. A fixed deformation of 2 mm is applied to glulam and CLT cubes. Impressions to this fixed deformation is given in Figure 13. The increase of stiffness of CLT cube versus glulam cube depending on the type of board (heartwood – flat sawn) is given in Table 7.

Table 6: elastic orthotropic material parameters [6]

E_r	E_t	E_l	μ_{rt}	μ_{rl}	μ_{tl}	G_{rt}	G_{rl}	G_{tl}
820	420	12000	0.602	0.042	0.027	42.4	620	740

Table 7: calculated increase of stiffness −glulam versus CLT cube

	height of cube h=200 *mm*			height of cube h=150 *mm*		
location of board in stem	$E_{90,g}$	$E_{90,clt}$	$\Delta=\frac{E_{90,clt}-E_{90,g}}{E_{90,g}}\cdot 100$	$E_{90,g}$	$E_{90,clt}$	$\Delta=\frac{E_{90,clt}-E_{90,g}}{E_{90,g}}\cdot 100$
0 [*cm*]	367	434	18%	382	448	17%
5 [*cm*]	351	535	52%	370	535	45%
10 [*cm*]	505	653	29%	539	658	22%
15 [*cm*]	612	738	21%	646	748	16%
20 [*cm*]	678	792	17%	709	805	14%
25 [*cm*]	721	826	15%	747	840	12%

Based on these simulations an increase in stiffness for ordinary CLT cubes in relation to glulam cubes can be expected to be approximately 30% as an averaged value (see Figure 12).

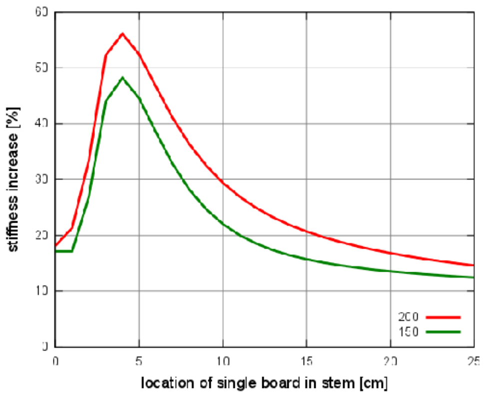

Figure 12: Difference of stiffness between glulam and CLT cube

4.2 Calculation of load bearing capacity of CLT plates and timber swells

For comparison purpose a finite element simulation was carried out, taking into account the non-linear ductile material behaviour of timber under pressure perpendicular to grain. Material formulation is purely linear orthotropic elastic in all directions. An elastic-plastic material formulation is introduced additionally parallel to load direction, that means perpendicular to plane. The elastic-plastic behaviouris handled according to the algorithms in [11]. A brief overview of the governing equations is given here for uniaxial behaviour.

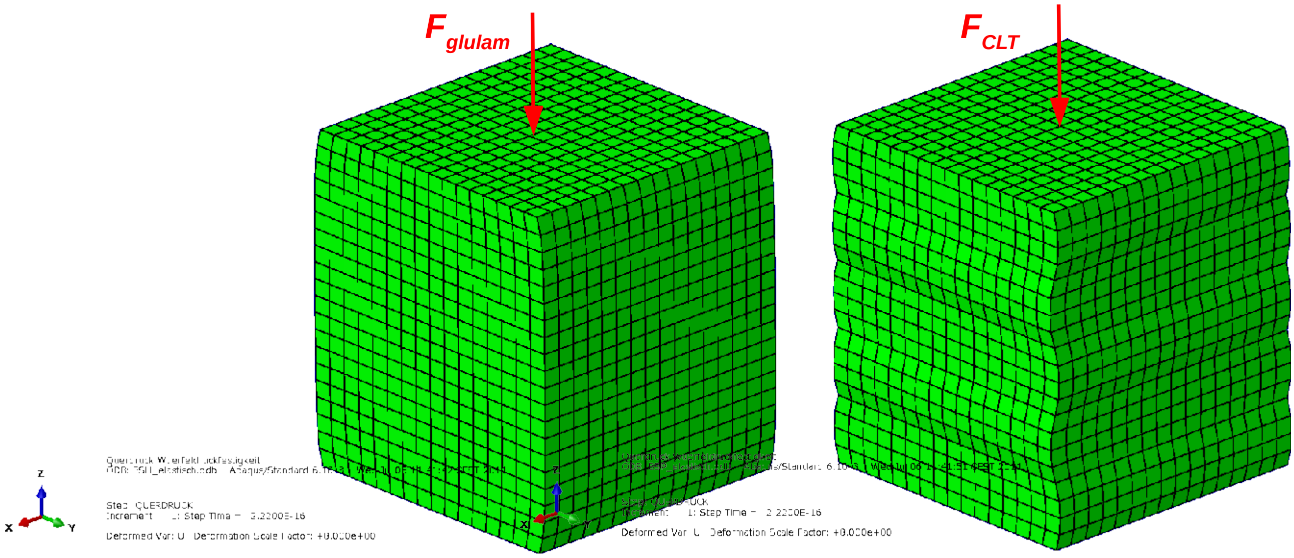

Figure 13: 200 mm high glulam cube (left) and CLT cube (right) under fixed deformation of 2 mm

Flow rule for simple one axial material behaviour is given by [11]

$$f(\sigma,q)=|\sigma|+q_{iso}-f_y=0$$

with:

$f(\sigma,q)$	flow rule equation	
σ	stress component	[N/mm²]
q_{iso}	isotropic hardening stress	[N/mm²]
f_y	strength or yield strength	[N/mm²]

Material law for stress component is formulated with the elastic strains ε_{el}. A linear additive decomposition of the total stain (ε) in an elastic part (ε_{el}) and a plastic (ε_{pl}) part is assumed. The material equations for the stress component σ and the hardening component q are given in terms of rates. Rates are written in dotted notation $\dot{()}=d()/dt$ (derivations to t).

$$\varepsilon=\varepsilon_{el}+\varepsilon_{pl}$$
$$\dot{\sigma}=E\cdot(\dot{\varepsilon}-\dot{\varepsilon}_{pl})$$
$$\dot{q}_{iso}=-H\cdot\dot{\alpha}$$

with:

ε	total strain	[-]
ε_{el}	elastic part of the strain [-]	
ε_{pl}	plastic part of the strain [-]	
E	modulus of elasticity	[N/mm²]
H	linear hardening modulus	[N/mm²]
α	variable, taking into account internal damage (energy dissipation) due to plastic flow	[-]

Two evolution equations are needed additionally, in order to solve these unknowns (ε_{pl}, α, σ, q_{iso}). Associated flow rule leads to the two equations, formulated also in terms of rates.

$$\dot{\varepsilon}_{pl}=\lambda\cdot\frac{\partial f(\sigma,q_{iso})}{\partial\sigma}=\lambda\cdot\mathrm{sign}(\sigma)\quad\text{with derivation of }\frac{\partial f(\sigma,q_{iso})}{\partial\sigma}=\mathrm{sign}(\sigma)$$
$$\alpha=\lambda\cdot\frac{\partial f(\sigma,q_{iso})}{\partial q}=\lambda\quad\text{with derivation of }\frac{\partial f(\sigma,q_{iso})}{\partial q}=1$$

with:

λ Lagrange Parameter, further unknown to be solved

Consequent extension to 3D linear elastic orthotropic has to be further accomplished under inclusion of elastic-plastic material behaviour in radial axis. Little linear hardening has been regarded here, because tests show good agreement with this assumption.

The integration algorithm of equations above is preferably the well known return-mapping algorithm for isotropic hardening, e.g. [11]. This linear orthotropic 3D elastic material model with elastic-plastic behaviour perpendicular to plane, a consistent elastic-plastic 3D material stiffness matrix and a local iterative implicit solution scheme is realized as a FORTRAN user subroutine for the general FE package ABAQUS. The chosen material parameter for the material are extracted from [9] and given in Table 8. Local orientation of the material was chosen, that the elastic-plastic behaviour appears in the radial direction, which is perpendicular to plane.

Table 8: material parameters for the user subroutine in ABAQUS

$E_{\|\|}$	E_T	E_R	μ_{tl}	μ_{rl}	μ_{rt}	G_{LT}	G_{LR}	G_{TR}
11600.0	300.0	300.0	0.02	0.02	0.40	650.0	650.0	65.0

An elastic-plastic behaviour is formulated in radial direction (E_R). The assumed yielding strength is 2.10 N/mm². Linear hardening is assumed, as the linearity of hardening is sufficient in the scope. Non linear hardening occurs later when higher compression strains have been developed. The linear hardening module H is assumed with a value of 3.0 N/mm². Using material parameters of Table 8, the elastic-plastic behaviour of the material in radial direction is shown in Figure 16. This approach realizes the main material behaviour directly in a mechanical model without using extension of the von Mises yield criterion to orthotropic materials (Hill's criteria). Failure due to shear and tension parallel to grain can be added in these models by cohesive planes, but these improved models are not presented in this paper.

Both timber swells (length=900 mm, width=160 mm, height=90/200/480 mm) and CLT plates (600 mm/600 mm/165 mm) under partial load introduction were investigated by the numeric model. In the following figure 14 some impressions of these timber swells in a deformed situation are given, whereas deformed CLT plates (only central and vertex loaded CLT plates) are shown in Figure 15.

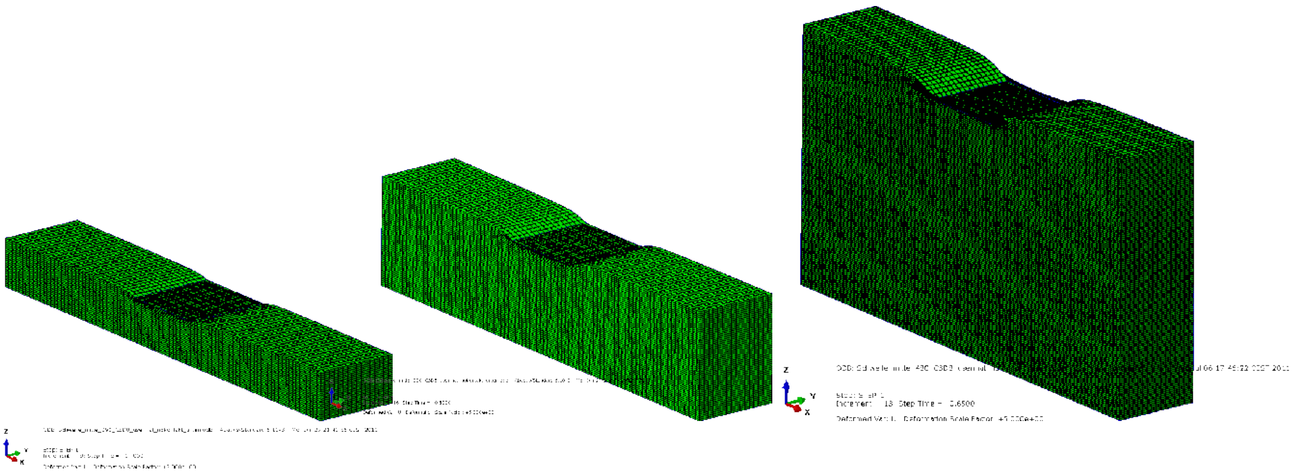

Figure 14: deformed timber swells (90/200/480 mm height)

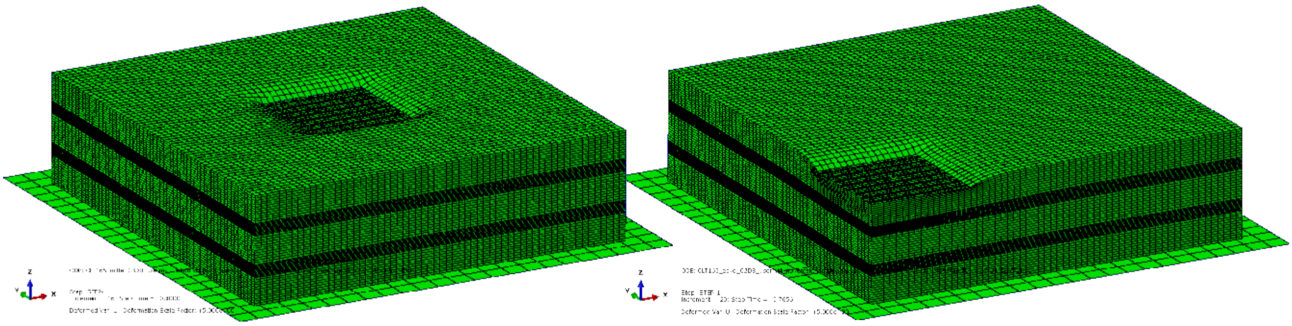

Figure 15: deformed CLT plates (height=165 mm, load position central/vertex)

Calculated load displacement curves are illustrated in Figure 17 for three swells (length=900 mm, width=160 mm, height=90/200/480 mm) and CLT-plates with four positions of loads (600 mm/600 mm/165 mm).

The following $k_{c,90}$ and $k_{c,90,\,clt}$ factors can be calculated, based on these load displacement curves, using the evaluation procedure according to EN 14358:2007. As the ultimate load perpendicular to plane is a product of the basic strength value $f_{c,90,k}$ and the associated $k_{c,90}$ factors, assumptions for the basic $f_{c,90,k}$ values have to be made. $f_{c,90,g,k}$ values for swells (glulam) are assumed with 2.25 N/mm², $f_{c,90,clt,k}$ values for CLT are assumed with 2.85 N/mm². Results of $k_{c,90}$ factors are summarized in Table 9.

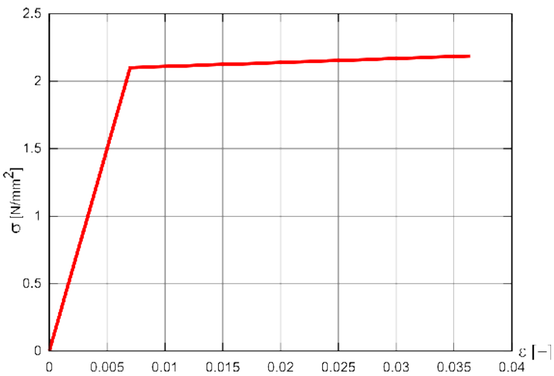

Figure 16: elastic-plastic behaviour in radial direction

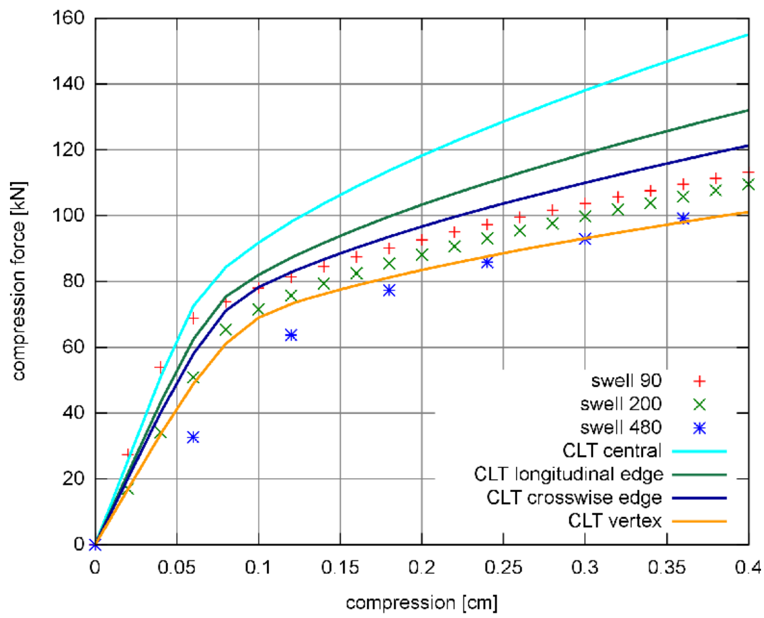

Figure 17: calculated load displacement curves for swells and CLT plates under punctual loads

By means of the numerical calculations, well known influence of height of structure on $k_{c,90,clt}$ factors can be studied. As the height for CLT differs only little, influence is expected to remain small. A comparison is given in Table 10, comparing CLT with height of 165 mm and 200 mm.

Table 9: $k_{c,90}$ and $k_{c,90,clt}$ factors, based on a numeric model for swells and CLT plates in comparison to experimental test results

	FEM simulations	empirical tests	
swells	$k_{c,90}$	$k_{c,90}$	source
swell height=90 *mm*	1.50	–	–
swell height=200 *mm*	1.77	1.9	Augustin et al. [1]
swell height=480 *mm*	2.32	2.5	
CLT plate	$k_{c,90,clt}$	$k_{c,90,clt}$ based on table 5	
load position “central”	1.83	1.8	Salzmann [9]
load position “longitudinal” edge”	1.58	1.5	
load position “crosswise edge”	1.47	1.5	
load position “vertex”	1.25	1.4	

Table 10: comparison of $k_{c,90,clt}$ factors for CLT with different height

	$k_{c,90,clt}$ (165)	$k_{c,90,clt}$ (200)
load position "central"	1.83	1.93
load position "longitudinal" edge"	1.58	1.66
load position "crosswise edge"	1.47	1.53
load position "vertex"	1.25	1.30

Influence of load introduction area is also studied by the FE-model. Two different load areas in comparison to the standard area with 160·160=25600 mm² are studied: a smaller one (50 % area reduction) is chosen with 113·113≈12800 mm² and a large one (50% increase) with 196·196≈38400 mm². Results of the FE study are given in Table 11 for a constant CLT height of 200 mm.

Table 11: comparison of $k_{c,90,clt}$ factors for CLT with variation of load introduction area

	relative area	$k_{c,90,clt}$ (h_{ref}=200 mm)
standard area 160·160 *mm²*	100%	1.93
enhanced area 196·196 *mm²*	150%	1.93·0.90
reduced area 113·113 *mm²*	50%	1.93·1.35

5 Discussion of results

5.1 Glulam

A proper compression strength perpendicular to grain, based on rules of EN 14358:2007, can be presented with a value of $f_{c,90,g,k}$=2.25 N/mm². This $f_{c,90,g,k}$ value can be considered as reliable, as a comparison and evaluation of a internal series [1] and another international series [4] shows in Chapter 2.1. A big difference can be observed to proposed values in actual codes with a value of $f_{c,90,g,k}$=2.7 N/mm² [15], which results in a remarkable difference of 20%. Especially partial load introduction is of particular interest in timber engineering and in such situation an additional factor, called as $k_{c,90}$, can be applied. Ultimate compression resistance perpendicular to grain is remarkable increased by this $k_{c,90}$ factor.

International discussion has been often controlled by the question, whether compression perpendicular to grain is a real ULS verification or is it only a SLS verification with loads at the ULS level. Discussion can be summarized also with the question whether compression strain perpendicular to grain leads to dangerous loss of strength or only to a reduction of serviceability.

Let us consider a continuous beam with two spans at the internal support, where a large hogging moment exists. Load introduction take place by resistance perpendicular to grain (see Figure 18). Two different heights of this glulam beam should be considered, one with 200 mm, the second with 480 mm height.

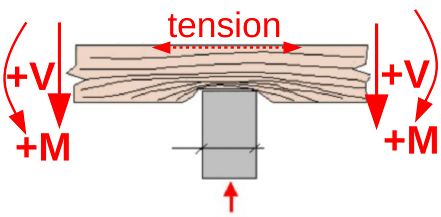

Figure 18: continuous beam with internal support

Based on FE investigations, relevant $k_{c,90}$ values for beams at internal support are marginally higher than comparable values for continuous support. Use of conventional $k_{c,90}$ factors for continuous support are therefore at the safe side.

T. A. C. M. van der Put [7] published reliable $k_{c,90}$ values, based on a stress equilibrium equations and the so called method of characteristics as mathematical solution technique for solution of differential equations. He published the simple formula

$$k_{c,90}=\sqrt{\frac{L}{s}}\leqslant 5 \text{ with } L=s+3\cdot H$$

with:

s length of load introduction

H height of swell

Limitations like small distance to end of swell (a) or second load near introduction (l_1) do not apply $k_{c,90}$ in this example [5]. A comparison for two heights of glulam beams (200 mm and 480 mm) are given in Table 12 and 13.

Table 12: comparison of compression strength of glulam beam (height=200 mm) at internal support

source of $k_{c,90}$	$k_{c,90}$	$f_{c,90,k}$	$f_{c,90,k}\cdot k_{c,90}$	Diff [%]
Augustin et al	1.90	2.25	4.28	[–]
FEM	1.77	2.25	3.98	-6.84%
van der Put	1.70	2.25	3.82	-10.76%

Table 13: comparison of compression strength of glulam beam (height=480 mm) at internal support

source of $k_{c,90}$	$k_{c,90}$	$f_{c,90,k}$	$f_{c,90,k}\cdot k_{c,90}$	Diff [%]
Augustin et al.	2.50	2.25	5.63	[–]
FEM	2.32	2.25	5.22	-7.20%
van der Put	2.35	2.25	5.28	-6.19%

Based on the characteristic compression strength perpendicular to grain, given in 2.1, differences of calculated strength for the partial load introduction in the glulam beam are in the range up to 10% (Table 12 and 13). It is noted in [5], that strains perpendicular to grain can be expected in the range of 10% for loads at ULS level, if a stress distribution of 1:1.5 is used. As $k_{c,90}$ factors in Table 12 and 13, calculated with formula of van der Put, agree well with those of Augustin et al., which are evaluated at 1% plastic compression strain limit, reason could be found in the lower characteristic strength $f_{c,90,k}$ of 2.25 N/mm².

EN 1995-1-1 delivers a $k_{c,90}$ value of $k_{c,90}$=1.75 for this situation. Together with the effective length of 2·30=60 *mm* and a characteristic strength of $f_{c,90,g,k}$=2.7 N/mm² a characteristic compression strength of $k_{c,90}\cdot f_{c,90,g,k}$=1.75·(220/160)·2.70=6.50 N/mm² can be calculated. A quick comparison shows, that load introduction in the small beam is overestimated by 52% for height 200 mm and 15.5% for 480 mm.

5.2 CLT

The situation for CLT is slightly different to glulam. A strong variation in height can not expected, CLT elements vary between 120 and 200 mm in standard case. A reliable compression strength perpendicular to plane can be presented with a value of $f_{c,90,clt,k}$=2.85 N/mm². Appendant $k_{c,90,clt}$ values are in the range of 1.3 up to 1.8, depending on the load introduction, as given in Chapter 3.1 and 4.2. A serious situation can occur in the internal domain at local support with columns, where hogging moments take place additionally. Here a $k_{c,90,clt}$ factor of 1.8 could mark a good choice, which prevents large deformations perpendicular to plane, which would leave to perpendicular overstraining due to the hogging moments in the plate. If a 30% overload over the characteristic strength in a CLT plate is assumed, a strain of about 3.12% (about 2.25% remain as plastic strain) can be calculated based on curve “CLT central” of Figure 17. This strain leads to a total deformation of about 5 mm for a CLT element with an overall height of 165 mm. Due to this reduction of cross section height, loss in bending height can be expected with about 6%, based on reduction of section modules.

Reinforcements in CLT plates for compression perpendicular to plane were not treated up to now. Several solutions exist and this topic could mark the next step of research at competence center for Timber Engineering and Wood Technology in Graz.

6 Summary

Characteristic strength values for CLT with $f_{c,90,clt,k}$=2.85 N/mm² has been proposed. Associated $k_{c,90,clt}$ values depend only marginally on geometric parameters like height (Table 10) and load introduction area (Table 11). Therefore a $k_{c,90,clt}$ of 1.9 for central loading can be proposed. Other load positions are summarized in Table 10. For simplification purpose a minimal $k_{c,90,clt}$ value of 1.4 for all non central load positions can be proposed. Further research work should be carried out on reliable functions for $k_{c,90,clt}$, taking into account influence of CLT height and load intoduction area.

Acknowledge

The research work within the project 1.1.2 is financed by the competence centre holz.bau forschungs gmbh and performed in collaboration with the Institute for Timber Engineering and Wood Technology of the Graz University of Technology and the partners from industry Haas-group, Mayr-Melnhof Kaufmann and Holzcluster Steiermark.

The project is fostered through the funds of the Federal Ministry of Economics, Family and Youth, the Federal Ministry of Transport, Innovation and Technology, the Styrian Business Promotion Agency Association and the province of Styria (A3 and A14).

References

[1] Al-douri H.K.H., Hamodi K.A.M.H.: *Compression Strength Perpendicular to Grain in Cross-Laminated Timber (CLT)*, Master's thesis, School of Technology and Design, Växjö Universitet, 2009

[2] Augustin M., Ruli A., Brandner R. Schickhofer G.: *Behavior of Glulam Perpendicular to grain in Different Strength Grades and Load Configurations*, Proceedings of CIB-W18. Paper 39-12-6, 2006, Florence, Italy.

[3] Halili Y.: *Versuchstechnische Ermittlung von Querdruckkenngrössen für Brettsperrholz.* Diploma thesis, Institute for Timber Engineering and Wood Technology, Graz University of Technology, 2008.

[4] Hoffmeyer P. , Damkilde L., Pedersen T. N.: *Structural timber and glulam in compression perpendicular to grain*, Holz als Roh- und Werkstoff 58, p. 73-80, Springer-Verlag 2000.

[5] Larsen H. J., Leijten A.J.M., T. A. C. M. van der Put: *The Design Rules in Eurocode 5 for Compression Perpendicular to the Grain - Continuous and semi continuous supported beams*, Proceedings of CIB-W18. Paper 41-6-3, 2008, St. Andrews, Canada.

[6] Neuhaus F. H.: *Elastizitätszahlen von Fichtenholz in Abhängigkeit von der Holzfeuchtigkeit*, PhD 1981, Institut für Konstruktiven Ingenieurbau, Ruhr-Universität Bochum, Germany.

[7] Van der Put T.A.C.M.: *Derivation of the bearing strength perpendicular to the grain of locally loaded timber blocks*, Holz als Roh- und Werkstoff 66, p. 409-417, Springer-V. 2008.

[8] Ruli A.: *Längs und quer zur Faserrichtung auf Druck beanspruchtes Brettschichtholz*, Diploma thesis, Institute for Timber Engineering and Wood Technology, Graz University of Technology, 2004.

[9] Salzmann Chr.: *Ermittlung von Querdruckkenngrössen für Brettsperrholz*, Master thesis, Inst. for Timber Engineering and Wood Technology, Graz University of Technology, 2010.

[10] Serrano E., Enquist B.: *Compression Strength perpendicular to grain in Cross-Laminated Timber (CLT)*, World Conferene on Timber Engineering (WCTE), Riva del Garda, 2010.

[11] Simo J. C., Hughes TJ.R.: *Computational Inelasticity*, ISBN 0-387-97520-9, Springer-Verlag New York, Inc., 1998.

[12] Eurocode EN 1995-1-1: *Design of timber struclures - and rules for buildings Part 1·1: General - Comman rules*, consolidated version, 2009-07-01.

[13] EN 408: *Timber Structures - Structural timber and glued laminated timber - Determination of some physical and mechanical properties*, 2007-06.

[14] EN 14080: *Timber structures - Glued laminated timber and glued solid timber*, 2011-03-01

[15] EN 1194: *Timber structures - Glued laminated timber - Strength classes and determination of characteristic values*, 1999-09-01

INTERNATIONAL COUNCIL FOR RESEARCH AND INNOVATION IN BUILDING AND CONSTRUCTION

WORKING COMMISSION W18 - TIMBER STRUCTURES

STRENGTH OF SPRUCE GLULAM SUBJECTED TO LONGITUDINAL COMPRESSION

M Frese

M Enders-Comberg

H J Blaß

KIT Holzbau und Baukonstruktionen

P Glos

TU München, Holzforschung München

GERMANY

MEETING FORTY FOUR

ALGHERO

ITALY

AUGUST 2011

Presented by M Frese

J Köhler and M Frese discussed the procedures used to consider the lengthwise correlation of material properties.

R Harris asked how one would know the specimens were of sufficient poor quality to be representative. M Frese responded that the comparisons of density should the material are representative and further comparisons between simulations and experiments showed good agreement. R Harris questioned the high influence of moisture content on compression strength parallel to grain and questioned again whether the tested material was at too high a quality. M Frese stated it might be good to perform tests on glulam with wider range of density and H Blass confirmed that the glulam material was not of particular good quality.

F Lam commented that compared to clear wood values the influence of moisture content on compression strength parallel to grain is of the same magnitude; however, the COV of the compression strength seemed to be low. M Frese responded that it could be explained by homogenisation of material via the lamination process. J Munch-Andersen commented that the variation of the simulation agreed with the experiments.

A Jorissen commented that the moisture content on compression strength of wood is well known and asked whether one sought another k_{mod} for compression. M Frese explained about the proposed model. Currently the same k_{mod} is used for service class 1 and 2. The work aimed to study the limit of the moisture to assess the influence.

A Frangi asked whether the results were compared to older results. M Frese responded no and they only used the test results from 50 specimens in the current study.

Strength of spruce glulam subjected to longitudinal compression

Matthias Frese, Markus Enders-Comberg, Hans Joachim Blaß
Karlsruher Institut für Technologie, Holzbau und Baukonstruktionen,

Peter Glos
Technische Universität München, Holzforschung München

1 Introduction

In present product standards for glulam, EN 1194 (1999) and E DIN EN 14080 (2009), the characteristic compressive strength ranges between 24 and 31 MPa. This applies to the glulam strength classes GL24h to GL36h. These characteristic values are derived from the tensile strength of the sawn timber used. In the draft European standard prEN 14080 (2009), it is suggested that the characteristic compressive strength is equal to the corresponding bending strength. By doing so, the compressive strength of the classes GL20h to GL32h, which are at present considered to be of relevance for the practical application, comes to 20 to 32 MPa.
However, the level of these strength values could be questioned. Table 1 shows estimated values for the compressive strength of glulam laminates and 95 % prediction limits [1]. The values were derived from tests on specimens representing boards of European spruce (*Picea abies*) for glulam. The length of the specimens was 180 mm parallel to the grain; its cross-section corresponded to the board width and depth. With this size, it was intended to model individual board elements composing glulam. The estimated values and the prediction limits are tabulated depending on the parameters oven-dry density (ρ_0) and knot area ratio (*KAR*). The reference moisture content (u) is 12 %. An approximate comparison between the estimated values considering the 95 % prediction limits and the strength values in the product standards and in the draft European standard prEN 14080 (2009), respectively, indicates that glulam particularly with small knots and above-average density may provide considerably higher compressive strength. Further, as the estimated values and the parameters ρ_0 and *KAR* refer to single board sections − not glued together − the lamination effect present in glulam may result in an additional strength increase.

Table 1 Estimated values for the compressive strength of glulam laminates [1], evaluation for u = 12 %

	ρ_0 [g/cm³] 0.350	0.400	0.450	0.500	0.550
KAR = 10 %					
Estimated value [MPa]	31.2	37.5	43.7	50.0	56.2
95 % prediction limits			+/-6.39		
KAR = 30 %					
Estimated value [MPa]	26.1	31.6	37.0	42.5	48.0
95 % prediction limits			+/-6.45		

This consideration constitutes the initial question for the work presented in this paper. The work, therefore, takes up the general idea of calculating the mechanical behaviour of glulam

[2]. In this sense, Glos [1] conducted tests and provided both a comprehensive experimental database and a variety of regression models to describe the mechanical behaviour of individual board elements. For direct applications of these models, see for example [3] regarding the bending strength of glulam or [4] in terms of the load-carrying capacity of glulam columns.
The objective of the present work is to provide a consistent strength model for the parallel-to-grain compressive strength of spruce glulam. In this sense, the compressive strength (f_c) is a function of the density and the *KAR*-value of the sawn timber used and the moisture content of the glulam. Eq. (1) constitutes the corresponding strength model in general terms while Eq. (2) is a simplified alternative without the parameter *KAR*. This alternative comes up to the fact that the compressive strength is mainly governed by the density and the moisture content.

$$f_c = f(\rho, KAR, u) \quad (1) \qquad\qquad f_c = f(\rho, u) \quad (2)$$

The three main steps of the present work are the following: A finite element model involving the stochastic character of the mechanical properties of timber is used to determine the glulam compressive strength. Tests from an ongoing research project serve as verification of the numerical approach. The specified strength models are finally derived through a regression analysis.

2 Methods

2.1 General

The present paper is based on a publication [5] and a previous CIB-W18 paper [6] where the parallel-to-grain tensile strength of glulam is numerically determined. Both report on the principle to simulate the load carrying capacity of axially loaded glulam using boards graded according to different methods; information on these methods and on further literature is given too. The following two sections are, therefore, restricted to the simulation of the compression specimens, its material and its strength. Section 2.4 deals with the verification of the simulation model used.

2.2 Simulation of the material and the specimens

In Table 2 nine grading methods are compiled that are used in the simulation. The values given are derived from test data. These methods provide a wide database with explanatory and response variables for the regression analysis. The mean oven-dry density ($\rho_{mean,0}$) and the corresponding standard deviation are the basis to calculate the mean ($\rho_{mean,12}$) and the characteristic density ($\rho_{k,12}$) at a moisture content of u = 12 %. The conversion is conducted with Eq. (3) stated in [7].

$$\rho_u = \rho_0 \frac{1+u}{1+0.84\rho_0 u} \quad (3)$$

The mean *KAR*-values (KAR_{mean}) tabulated in the last column of Table 2 are estimates to represent the knot sizes as explanatory variables.
The simulated specimen is a section with the length ℓ inside a long simulated glulam beam with the depth h (Fig. 1). The mechanical properties of the board and finger joint elements were simulated with regression models for compression properties in grain direction. They were derived on the basis of the experimental data described in [1]. For details of the equations, refer to [3].

Table 2 Grading methods used: density [g/cm³] and *KAR* of sawn timber

Grading	$\rho_{mean,0}$	s	$\rho_{mean,12}$	$\rho_{k,12}$	KAR_{mean}
VIS I (S10)	0.412	0.048	0.443	0.360	0.30
VIS II (S10/S13)	0.424	0.052	0.455	0.367	0.26
VIS III (S13)	0.447	0.050	0.479	0.394	0.19
DENS I	0.486	0.029	0.519	0.469	0.21
DENS II	0.504	0.027	0.537	0.492	0.20
EDYN I	0.481	0.037	0.514	0.452	0.22
EDYN II	0.492	0.034	0.525	0.467	0.22
EDYN III	0.505	0.035	0.538	0.480	0.20
EDYN IV	0.508	0.038	0.541	0.477	0.14

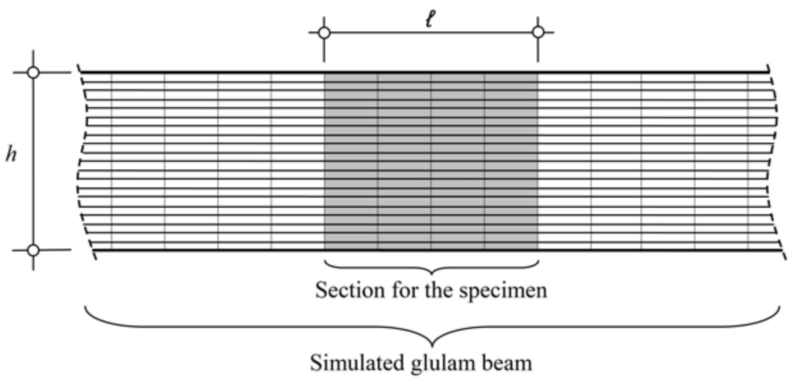

Fig. 1 Principle of the simulation: The simulated mechanical properties of the specimen are systematically taken from a short section (*grey zone*) of a simulated beam

2.3 Simulation of the glulam compressive strength

Fig. 2*a* shows the finite element model used for the simulation of the intended compression tests. The size of the simulated specimen follows EN 1194 (1999) and EN 408 (2003). Thus, the depth comes to 600 mm and, assuming a width (b) of 100 mm, the length and the gauge length (ℓ_g), respectively, comes to 600 mm too. The action line of the compressive force (F) coincides with the centre line. Due to hinged supports, the load introduction is free of bending moments. Both *grey zones* with infinite stiffness are used to model rigid steel plates, which results in plane cross-sections at the "end grain surfaces" of the simulated specimen.

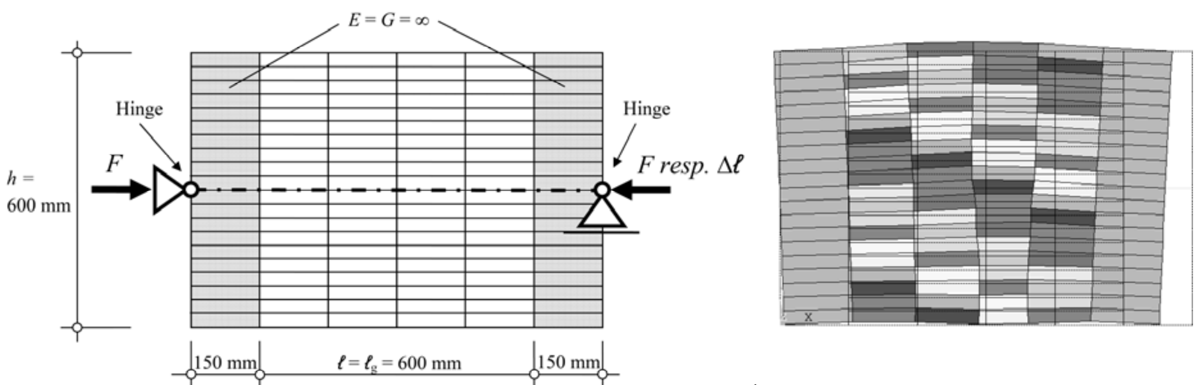

a b

Fig. 2 (*a*) Finite element model: hinged and bending-free load introduction in the structure; the *grey zones* indicate infinite stiffness, the *white* elements represent the modelled specimen. (*b*) The model after a simulated test ($|\varepsilon|$ = 0.5 %, scale factor = 20): The *shades of grey* of the modelled specimen stand for stochastic mechanical properties

The stress state is plane stress. In order to simplify the calculation, the material in each of the elements between the modelled steel plates is assumed to be ideal-elastic and ideal-plastic. The strain (ε) and the stress (σ) are calculated according to the Eq's (4) and (5). The displacement ($\Delta\ell$) refers to the centre line. Hence, both the strain and the stress are integral values. Fig. 2*b* shows a deformed shape after a simulation compared to the undeformed edge of the model.

$$\varepsilon = \frac{\Delta\ell}{\ell_g} \quad (4) \qquad\qquad \sigma = \frac{F}{b \cdot h} \quad (5)$$

2.4 Comparison between experimental and simulated data

2.4.1 Experimental results

50 compression tests on glulam specimens were conducted for another research project. These tests fit in with the objective of the present work because they are generally suitable to verify the finite element model used. Fig. 3 shows the test set-up by a photograph and a sketch. The upper three-dimensional hinge allows inclinations of the steel plate around two orthogonal axes. The size of the specimens is given through b = 80 mm, h = 200 mm (5 laminations) and ℓ = 480 mm. The mean displacement ($\Delta\ell$) was measured over the gauge length of ℓ_g = 320 mm. For this, displacement transducers were arranged on both narrow sides of the specimens.

a 

b 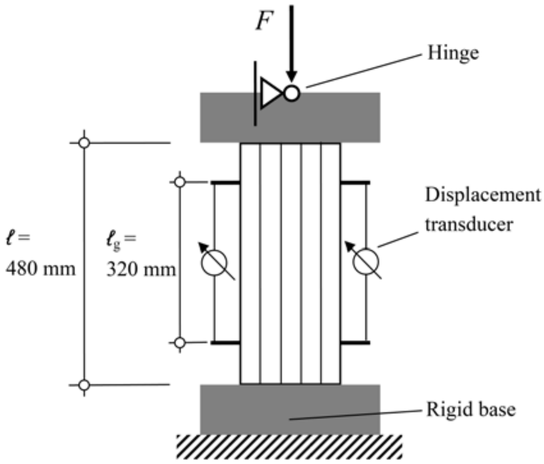

Fig. 3 Test set-up: (*a*) photograph and (*b*) schematic sketch

In general, the used glulam material nominally belongs to the strength class GL24h. The material's apparent density, referring to the entire specimen volume of 80 x 200 x 480 mm³, includes knots with local higher density. The mean apparent density comes to 0.457 g/cm³. As expected for glulam, the standard deviation is 0.021 g/cm³ only. The average moisture content referring to the entire specimens is 10.2 %.

The compressive stress and strain was calculated following Eq. (4) and (5), respectively. The stress-strain curves are shown in Fig. 4. By enlargement of the key area it becomes obvious that the maximum compressive stress (= compressive strength) is associated with an ultimate strain $|\varepsilon_u|$ between 0.25 % and 0.55 %. The mean of $|\varepsilon_u|$, normally distributed, is 0.404 %; the standard deviation amounts to 0.0526 %. The compressive MOE reflects the linear gradient of the stress-strain curves. The distributions of the compressive strength and the MOE are shown in Fig. 5. Both values are normally distributed. The mean compressive strength ($f_{c,mean}$) is 42.1 MPa and the 5th percentile ($f_{c,k}$) 36.4 MPa. The mean MOE (E_{mean}) amounts to 13,000 MPa.

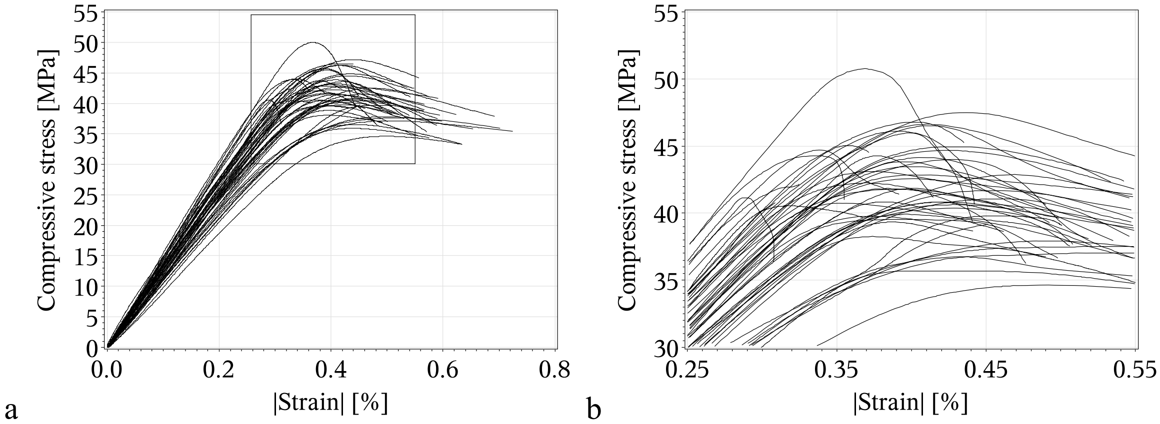

Fig. 4 Experimental stress-strain curves: (*a*) in total and (*b*) enlargement of the key area

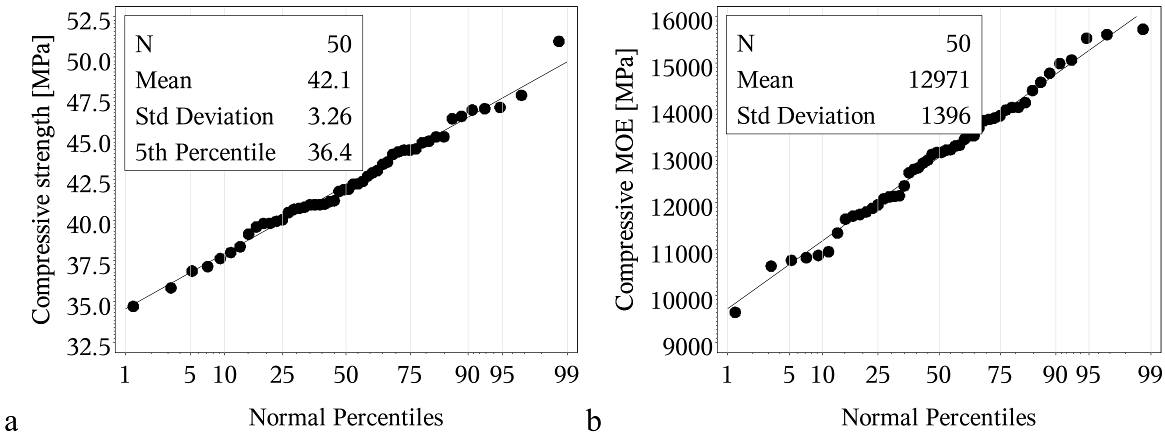

Fig. 5 Experimental mechanical properties: distribution of (*a*) strength and (*b*) MOE

2.4.2 Comparative simulation results

In this section, simulation results are described which constitute the counterpart of the experimental ones. A comparison between both − in the sense of a later verification, since experimental data were obtained first − follows in section 2.4.3.

The glulam material is simulated by the grading methods VIS I and VIS II (Table 2). They correspond to the visual grades "S10" and "S10 and better" according to DIN 4074-1 (2008) which are representative for glulam of strength class GL24h. Based on the density, it was not possible to identify one of the grading methods as most suitable for the verification. Consequently, it is conducted for both. Fig. 6*a* shows the adapted model to numerically reproduce the compression tests following the experimental configuration in Fig. 3. Due to the element length and depth (150 mm x 30 mm), the size of the simulated specimens agrees only approximately with the size of the tested specimens.

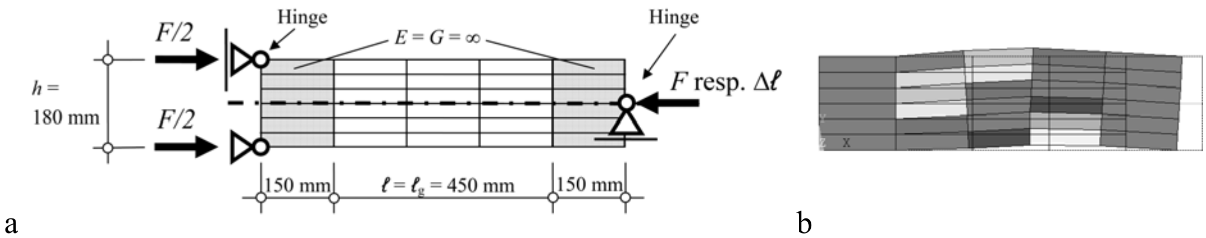

Fig. 6 (*a*) Finite element model for the verification and (*b*) example of a deformed specimen ($|\varepsilon_u|$ = 0.5 %, scale factor = 20)

The rigid lower steel base, shown in Fig. 3, is modelled with two supports on the specimen's left side. The mechanical properties were simulated for u = 10 % to correspond to the moisture content of the experimental specimens. The compressive strength is evaluated for $|\varepsilon_u|$ = 0.5 %. This strain constitutes the failure criterion for the simulations. Fig. 6*b* illustrates a picture of the specimen's deformed shape for $|\varepsilon_u|$ = 0.5 %. According to the boundary conditions on the left side no rotation of the modelled steel plate occurs.

500 simulations were performed for each grading method. The recorded stress-strain curves are shown in Fig. 7 to simplify matters for one fifth of the simulations only. Due to the assumption of ideal plasticity in each of the single elements of the model, the simulated curves do not reflect the experimental stress-strain curves, cf. Fig. 4: A negative gradient cannot occur. In reality, the ultimate strains (at maximum compressive stress) of the single elements scatter between 0.2 % and 0.8 % and the upper limit decreases with increasing moisture content [1]. In particular, simulations with stress-strain curves, showing a horizontal trend only beyond high strains, may lead to marginally higher strengths. This is due to single elements, of which the individual stress-strain relation has already a negative tangent modulus. This effect is discussed in [4] but is seen to be of minor influence for the actual simulations. Hence, the failure criterion $|\varepsilon_u|$ = 0.5 % is just a means to cover the maximum compressive stress, which is on average associated with $|\varepsilon_u| \approx$ 0.4 % as obtained in the tests. The curves in Fig. 7 do, therefore, not reflect the real compressive stress present at $|\varepsilon|$ = 0.5 %. The simulated mechanical properties are shown in Figs. 8 and 9: The mean values for VIS I are slightly lower than for VIS II. The 5th percentile of the strength is 38.7 compared to 40 MPa and the mean MOE comes to 12,600 in contrast to 13,100 MPa.

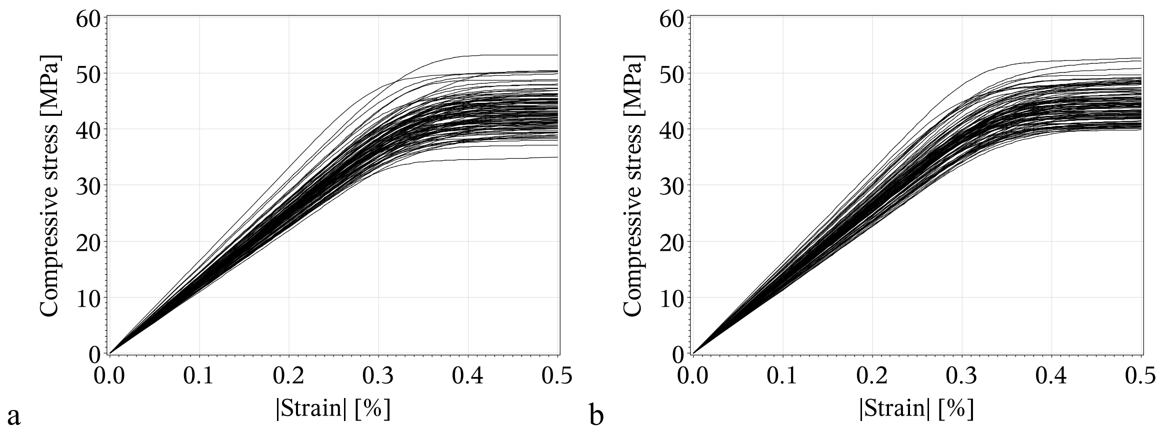

Fig. 7 Simulated stress-strain curves (100 of 500): (*a*) VIS I and (*b*) VIS II

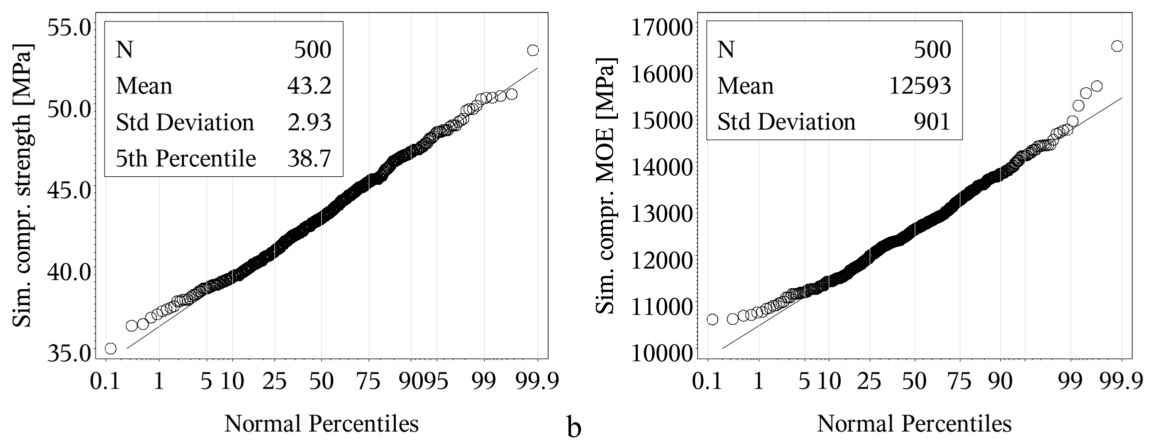

Fig. 8 VIS I: distribution of (*a*) strength and (*b*) MOE

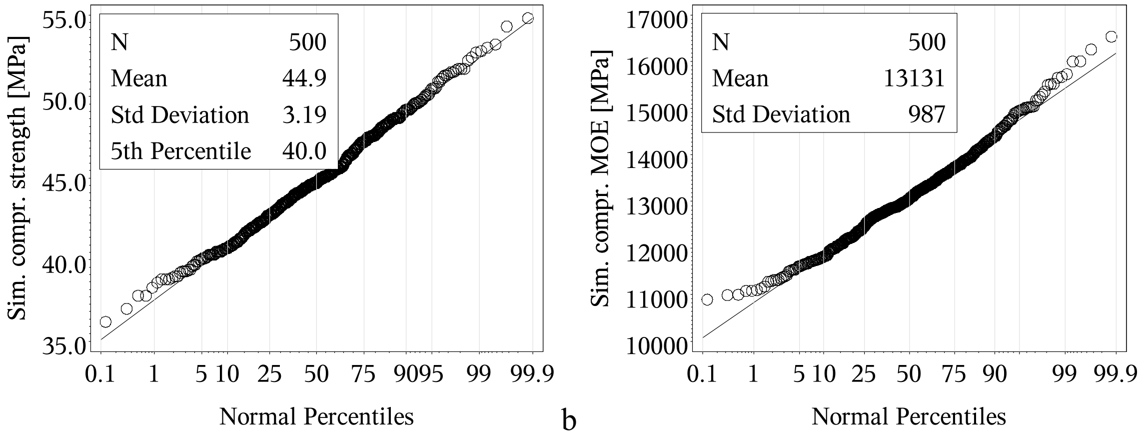

Fig. 9 VIS II: distribution of (*a*) strength and (*b*) MOE

2.4.3 Comparison

Table 3 contains the comparison between the simulated and the experimental data. The statistics refer to Figs. 5, 8 and 9. The simulated means of the compressive strength and of the MOE come to 103-107 % and 97-101 %, respectively, the simulated 5th percentiles to 106-110 % of the corresponding experimental values.

Consequently, the finite element model in part slightly overestimates the experimental values. Under consideration of the 95 % confidence limits (footnotes Table 3), the agreement may be even better or poorer. Reasons for an overestimation could be: First, the finite element model is restricted to a two-dimensional problem while the tests constitute a three-dimensional problem. Second, for strains shortly before and beyond the elastic limit, the ideal-elastic and ideal-plastic material behaviour in the single elements results in higher stresses compared to reality. A third reason concerns probable inaccuracies in relation to the modelling of the structural and physical material properties.

Relating to the standard deviations, the correlation is moderate in case of strength. In case of MOE, it is low since 25 % of the experimental values exceed 14,000 MPa in contrast to 5 % of the simulated ones only.

However, the agreement between the experimental and simulated strength values does not contradict the assumption that the finite element model is generally suitable to predict the parallel-to-grain compressive strength of glulam.

Table 3 Statistics of the simulated and experimental data [MPa]

	grading	$f_{c,mean}$	s	$f_{c,k}$[b]	E_{mean}	s
Simulation[a]	VIS I	43.2	2.93	38.7	12600	901
Simulation[a]	VIS II	44.9	3.19	40.0	13100	987
Experiment[a]	-	42.1[c]	3.26	36.4[d]	13000	1400
$\frac{\text{Sim.}}{\text{Exp.}}$	VIS I	1.03	0.90	1.06	0.97	0.64
$\frac{\text{Sim.}}{\text{Exp.}}$	VIS II	1.07	0.98	1.10	1.01	0.71

[a] u = 10 % for both experimental and simulated data; [b] parameter-free; [c] 95 % confidence limits: [41.2, 43.1]
[d] 95 % confidence limits: [35.1, 38.0]

3 Results

3.1 Simulated mechanical properties

The finite element model, as shown in Fig. 2*a*, was used to simulate compression tests. The test configuration corresponds to the test standard EN 408 (2003). For the moisture contents 12 % and 20 %, 500 simulations were conducted for each grading method. The moisture content of 16 % was examined with 200 simulations per method. The simulated mean ($f_{c,mean,sim}$) and characteristic strength values ($f_{c,k,sim}$) as well as the simulated mean MOE values ($E_{mean,sim}$) are compiled in Table 4 as a function of the grading methods and the moisture content. The mean or characteristic strength values and the moisture content in Table 4 constitute two variables for the regression analysis. Fig. 10 shows the cumulative frequencies of the strength values for the moisture content of 12 %. The 5th percentiles are highlighted by the intersection points between the horizontal reference lines and the distributions.

Table 4 Simulated mechanical properties [MPa] as a function of the moisture content [%]

	u	$f_{c,mean,sim}$	s	$f_{c,k,sim}$ [a]	$E_{mean,sim}$	s
VIS I	12	38.7	1.36	36.4	11600	400
VIS II		40.4	1.68	37.5	12100	470
VIS III		43.7	1.63	40.9	13000	450
DENS I		48.6	1.35	46.4	14300	370
DENS II		51.2	1.24	49.2	15100	350
EDYN I		48.4	1.37	46.2	14400	380
EDYN II		50.2	1.38	48.0	14900	360
EDYN III		53.1	1.39	50.9	15700	370
EDYN IV		53.4	1.38	51.0	15800	370
VIS I	16	31.5	1.25	29.4	10900	350
VIS II		32.8	1.35	30.4	11300	400
VIS III		35.6	1.31	33.4	12200	410
DENS I		39.4	1.03	37.6	13300	340
DENS II		41.6	0.98	39.9	14000	340
EDYN I		38.6	1.16	36.6	13100	360
EDYN II		40.1	1.12	38.4	13500	350
EDYN III		41.6	1.26	39.5	14000	380
EDYN IV		42.5	1.17	40.4	14300	350
VIS I	20	25.7	1.02	24.1	9960	330
VIS II		26.8	1.05	25.2	10400	370
VIS III		29.0	0.99	27.4	11100	340
DENS I		32.2	0.86	30.8	12100	320
DENS II		34.1	0.78	32.9	12700	310
EDYN I		31.6	0.96	30.1	11900	330
EDYN II		32.8	0.91	31.3	12300	330
EDYN III		34.1	0.98	32.5	12700	340
EDYN IV		34.8	1.00	33.1	13000	350

[a] parameter-free

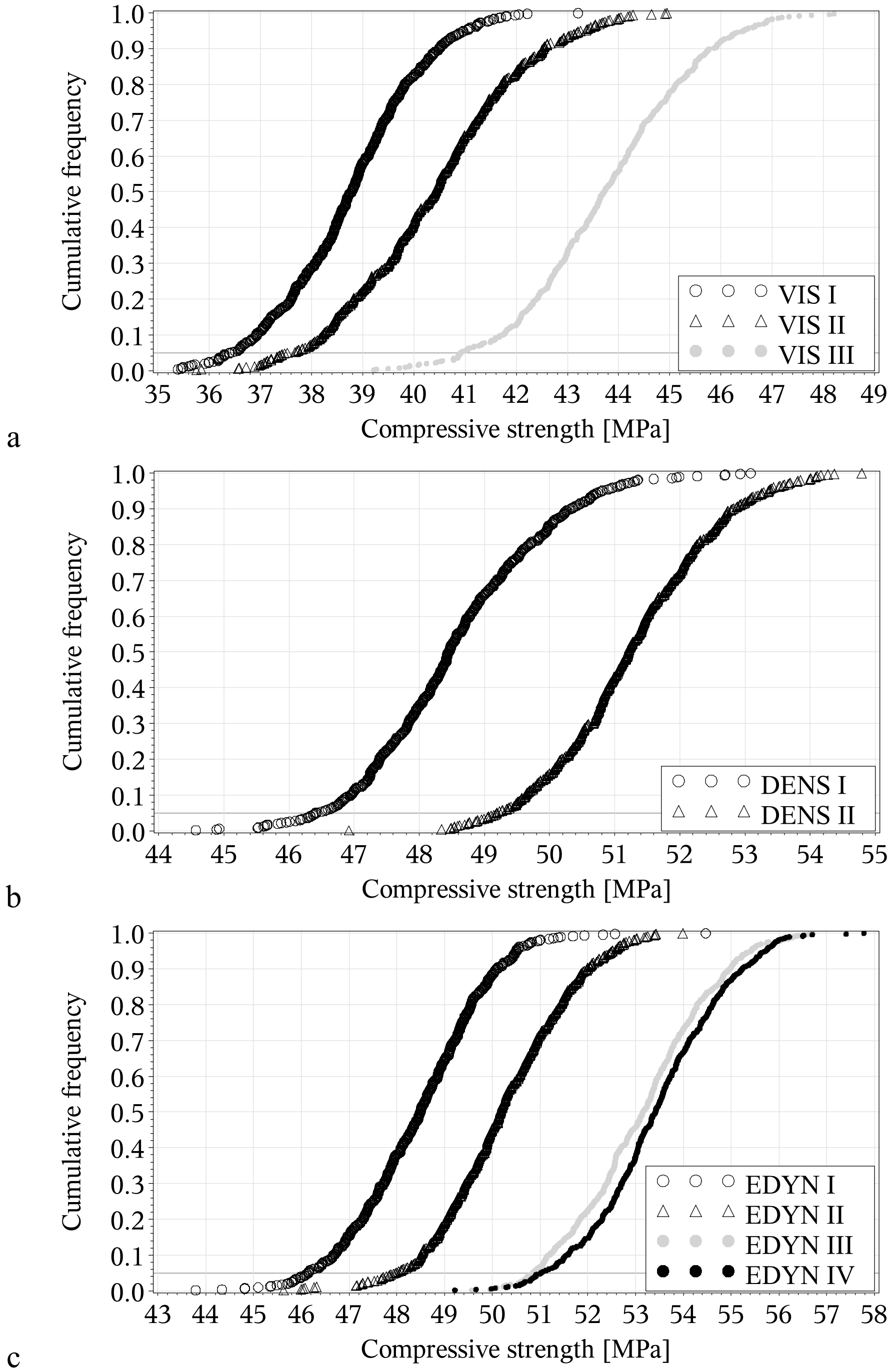

Fig. 10 Cumulative distributions of the compressive strength: (*a*) visual, (*b*) density-based and (*c*) MOE-based grading

3.2 Strength models

Fig. 11*a* shows the relationship between the simulated characteristic compressive strength – as response variable – and the characteristic density converted to u = 12 % ($\rho_{k,12}$ in Table 2) – as explanatory variable. The *stars*, *triangles* and *diamonds* represent the three moisture contents investigated. Due to the characteristic density as explanatory variable, this relation serves practical applications: The characteristic compressive strength can be directly predicted for any strength graded material. This applies either for material corresponding to strength classes or for individual material with known characteristic density. With the mean oven-dry density of the sawn timber ($\rho_{mean,0}$ in Table 2) – as explanatory variable – the relation in Fig. 11*b* is more accurate.

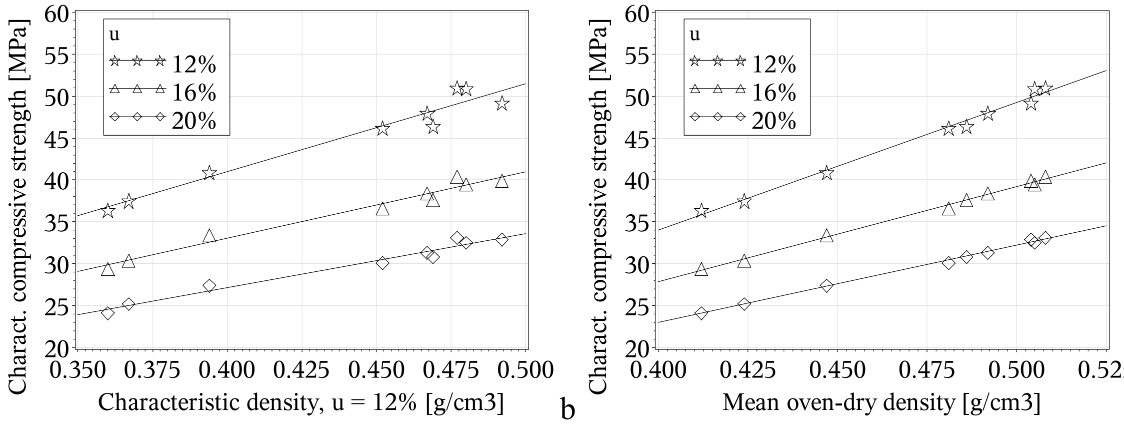

a b

Fig. 11 Prediction of characteristic compressive strength: dependent on (*a*) the characteristic density and (*b*) the oven-dry density

Eqs. (6) and (7), results of the regression analysis, constitute the specified strength models according to the Eqs. (1) and (2). For the analysis, the 27 datasets with the strength values and the moisture content (Table 4) and the corresponding densities (Table 2) were used and additionally the mean *KAR*-value (Table 2) for Eq. (6). The natural logarithm (log) slightly improves the models. *KAR* and *u* are inserted in the equation as ratio, not in percent, and ρ in g/cm³. A comparison between both equations shows that for practical applications it is dispensable to consider the knot area ratio since the decrease of the coefficient of determination (r^2) is insignificant.

$$\log(f_{\mathrm{c,k,sim}}) = 3.668 + 1.989\rho_{\mathrm{k,12}} - 0.5458KAR_{\mathrm{mean}} - 5.222u \quad \mathrm{n} = 27 \ \ \mathrm{r}^2 = 0.995 \tag{6}$$

$$\log(f_{\mathrm{c,k,sim}}) = 3.402 + 2.328\rho_{\mathrm{k,12}} - 5.222u \quad \mathrm{n} = 27 \ \ \mathrm{r}^2 = 0.989 \tag{7}$$

Eq. (8) is more or less a scientific form of Eq. (1): It is suitable to predict the mean compressive strength based on the mean oven-dry density, the mean *KAR*-value and the moisture content.

$$\log(f_{\mathrm{c,mean,sim}}) = 3.155 + 2.887\rho_{\mathrm{mean,0}} - 0.19KAR_{\mathrm{mean}} - 5.237u \quad \mathrm{n} = 27 \ \ \mathrm{r}^2 = 0.999 \tag{8}$$

For the independent variables $\rho_{\mathrm{mean,0}}$ = 0.40 and 0.55 g/cm³, KAR_{mean} = 0.30 and u = 0.12 the mean strength values amount to 37.5 and 57.8 MPa. These values are significantly higher than the estimated ones in Table 1, which are 31.6 and 48.0 MPa only. The corresponding ratios amount to 1.18:1 and 1.20:1. Even when taking into account model inaccuracies, there remains a pronounced strength increase. It is due to the lamination effect present in glulam subject to compression. First, it is comprehensible that knots in glulam do less affect the compressive strength than knots in single board sections. Second, the mean *KAR*-values from Table 2 refer to the largest *KAR*-values inside boards while the *KAR*-values from Table 1 stand for the mean present in the specimens used. Consequently, the large portion of clear sections in glulam contributes to the higher compressive strength too.

3.3 Discussion

Fig. 12 shows the characteristic compressive strength depending on the characteristic density of the sawn timber where Eq. (7) is evaluated for densities from 0.35 to 0.42 g/cm³ representing strength classes C24 to C40, and for moisture contents of 12 % and 20 %. The continuous and broken straight lines reflect the corresponding relations. Furthermore, the compressive strength values in EN 1194 (1999) are stated depending on the densities 0.35, 0.37, 0.39 and 0.41 g/cm³, quoted as indicative values in this standard. The connected *stars* show that this relation is similar to a straight line. Its inclination is greater compared to the two realisations of Eq. (7). The connection between the strength and density values, both of them proposed in prEN 14080 (2009-12), is shown by the connected *dots*. This graph is more or less comparable to the relation in EN 1194 (1999). But on closer examination, it is questionable, why it is sharply bended at the intersection point with a density of 0.37 g/cm³. In general, this is not in agreement with the behaviour of natural materials.

The experience shows that in service class 1 the moisture content will most likely not exceed 12 %. In service class 2, this threshold is estimated to be 20 %, cf. EN 1995-1-1 (2004). Consequently, it would be conceivable to define separated characteristic compressive strength values: Eq. (7), evaluated for u = 12 %, would optionally apply for service class 1. Evaluated with u = 20 %, Eq. (7) would necessarily apply for service classes 2 and 3 and to simplify matters for service class 1 too. Thereby, the modification factors (k_{mod}) in EN 1995-1-1 (2004) could still be used.

It is remarkable that the evaluation of Eq. (7) for u = 12 % leads to a compressive strength 50 % higher compared to an evaluation for u = 20 %. Therefore, the engineer's judgement on the moisture content which is likely to occur in a glulam member during service life could be given more weight. An individual estimation, considering important influences on the future moisture content, could be more precise than a rigid standard scheme. In this sense, Eq. (7) offers new possibilities too. For example, the compressive strength of particular glulam members in service class 2, having a moisture content far below 20 %, could be more exactly estimated.

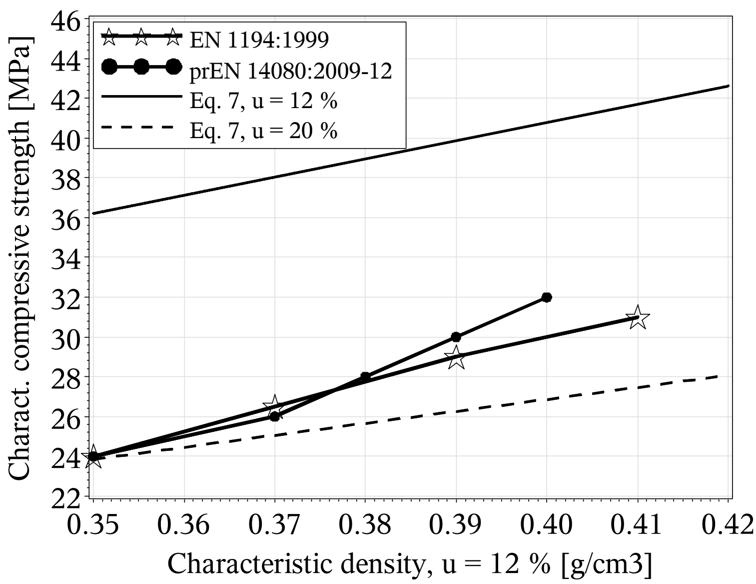

Fig. 12 Compressive strength as a function of density: comparison between relations in current product standards and Eq. (7), evaluated for two moisture contents

4 Summary

The aim of the work was to determine the parallel-to-grain compressive strength of spruce glulam. Based on compression tests, numerically reproduced, the influence of the density, the moisture content and the knot area ratio on the compressive strength was investigated. In agreement with previous findings in this area, both the density and the moisture content were

identified as decisive explanatory variables to predict the compressive strength. Hence, the knot area ratio of the used sawn timber contributes marginally to the strength prediction.
For practical applications, a strength model for the characteristic compressive strength was specified. Its variables are the characteristic density of the sawn timber used and the expected moisture content of the glulam. Comparisons between the model's strength prediction and stipulations in present product standards for glulam show: First, relating to service class 1 and 2, commonly considered (moisture content most likely below 20 %), the model leads to more minor nominal strength values in case of characteristic densities exceeding 350 kg/m³; for 350 kg/m³ (strength class C24), there is no difference. Second, relating to service class 1, solely considered (moisture content most likely below 12 %), the model's strength-density relation shows that present stipulations underestimate the compressive strength to a large extent.
The results of the work raise the question, how to consider the low moisture content of glulam members in service class 1, to make use of the available compressive strength. It is conceivable to use the model prediction, based on a moisture content of 20 %, for nominal values. Additionally, an option for 1.5 times nominal values may consider the higher strength in service class 1, if the maximum moisture content is below 12 %.

5 References

[1] Glos P (1978) Zur Bestimmung des Festigkeitsverhaltens von Brettschichtholz bei Druckbeanspruchung aus Werkstoff- und Einwirkungskenngrößen. Berichte zur Zuverlässigkeitstheorie der Bauwerke, Heft 35/78, Laboratorium für den konstruktiven Ingenieurbau, TU München

[2] Glos P, Maier W, Weigle U (1973) Bestimmung des Festigkeitsverhaltens von Fichtenbrettschichtholz als Grundlage für ein probabilistisches Bemessungsverfahren. Teil 1: Versuchseinrichtung für Kurzzeit-Druckversuche. Arbeitsberichte zur Sicherheitstheorie der Bauwerke, Heft 7/73, Laboratorium für den konstruktiven Ingenieurbau, TU München

[3] Ehlbeck J, Colling F, Görlacher R (1985) Einfluss keilgezinkter Lamellen auf die Biegefestigkeit von Brettschichtholzträgern. Holz als Roh- und Werkstoff 43:333-337, 369-373, 439-442

[4] Blaß HJ (1987) Tragfähigkeit von Druckstäben aus Brettschichtholz unter Berücksichtigung streuender Einflussgrößen. Karlsruhe, Universität (TH), Dissertation

[5] Frese M, Chen Y, Blaß HJ (2010) Tensile strength of spruce glulam. European Journal of Wood and Wood Products 68:257-265

[6] Frese M, Blaß HJ (2010) System effects in glued laminated timber in tension and bending. CIB-W18/43-12-3, Nelson, New Zealand

[7] Kollmann F (1982) Technologie des Holzes und der Holzwerkstoffe. 2. Aufl., Springer-Verlag, Berlin, Göttingen, Heidelberg

DIN 4074-1 (2008) Sortierung von Holz nach der Tragfähigkeit – Teil 1: Nadelschnittholz (Strength grading of wood – Part 1: Coniferous sawn timber)

E DIN EN 14080 (2009-02) Timber structures – Glued laminated timber and glued solid timber

EN 408 (2003) Timber structures – Structural timber and glued laminated timber – Determination of some physical and mechanical properties

EN 1194 (1999) Timber structures – Glued laminated timber – Strength classes and determination of characteristic values

EN 1995-1-1 (2004) Design of timber structures – Part 1-1: General – Common rules and rules for buildings

prEN 14080 (2009-12) Timber structures – Glued laminated timber and glued solid timber

CIB-W18/44-12-3

INTERNATIONAL COUNCIL FOR RESEARCH AND INNOVATION IN BUILDING AND CONSTRUCTION

WORKING COMMISSION W18 - TIMBER STRUCTURES

GLUED LAMINATED TIMBER: A PROPOSAL FOR NEW BEAM LAY-UPS

F Rouger

P Garcia

FCBA, Paris

FRANCE

MEETING FORTY FOUR

ALGHERO

ITALY

AUGUST 2011

Presented by F Rouger

R Harris commented that he was pleased to see the utilization of lower grade material. He commented that if one changed the requirement of the number of high grade lamina, one could create different grades of glulam material such that the product with 2 pieces of high grade lamina would be better than the product with one piece of high grade lamina. F Rouger responded that there would be a market for such product and the industry was demanding it.

P Stapel asked how one would make sure that the C14 is not a C24. R Rouger stated that they were machine graded with additional checks.

A Ranta-Maunus commented that this would be important for the industry.

G Hochreiner asked about the use of 80 mm thick laminae. R Rouger said that such thick laminae would not be used for glulam beams.

Glued Laminated Timber: A proposal for new beam lay-ups

By F Rouger, P Garcia

Abstract

In the current draft of EN 14080, beam lay-ups are proposed for combined glulam. At least two laminations of high strength on each outer zone of the beam are required in order to take benefit of the composite beam theory. In this paper, an investigation on extended allowances is reported. An experimental program has been carried out on 150 glulam beams for small depths (between 200 mm and 400 mm), combining different lay-ups (number of laminations in the outer zones, levels of strength classes). The test results have been compared with the theory. It demonstrates that beams with one lamination of high strength on each outer zone are still following the composite beams theory. A design proposal is included, that allows these beam lay-ups up to a certain depth.

Introduction

The draft European standard prEN 14080, currently under enquiry, has stated some rules for combined glulam, which have a strong limitation: the external zones of higher strength should comprise at least two lamellas.

The aim of this paper is to determine if this limitation could be ignored, and consequently if it was possible to make glulam beams with only one lamella of higher strength in each outer zone. The overall goal is to increase the use of secondary quality timber in structural elements.

In order to confirm this assumption, an experimental investigation has been carried out on different beam lay-ups, by varying strength classes and proportion of each zone.

For each beam lay-up, an average number of 15 beams have been tested. The characteristic values have been calculated according to EN 14358.

In addition to beams tests carried out at FCBA, finger joints tests have been performed within a company (Monnet-Sève) which made the glulam beams. These tests were performed for each strength class considered in the beams lay-ups (C30, TR26, and C14). The results have also been analyzed and included in the modelling according to the requirements of prEN 14080.

This paper presents and explains the results, and concludes with a proposal for prEN 14080.

Experimental investigation

Table 1 shows the beams lay-ups which have been tested. The number of beams within each lay-up varies from 13 to 18 (15 in average).

Most of the combinations are involving only one lamella of high strength in the outer zone. The number of internal lamellas varies from 3 to 8.

For three beams lay-ups (depth 240 mm, strength class combination TR26/C14 & C30/C14, depth 280 mm, combination C30/C14), the number of lamellas in each zone have been varied in order to check the influence of a decrease of external lamellas.

It should be noticed that the beams have a depth between 200 mm and 400 mm. This will influence the final recommendation.

Lot	Depth (mm)	Width (mm)	Length (mm)	Strength class Combination (external/internal)	Lamellas combination (ext./int./ext.)	Number of beams
L1	200	120	4000	TR26/C14	1/3/1	15
L2	240	120	4800	TR26/C14	1/4/1	13
L3					2/2/2	18
L4	240	120	4800	C30/C14	1/4/1	14
L5					2/2/2	14
L6	280	120	5600	C30/C14	1/5/1	15
L7					2/3/2	16
L8	320	120	6400	C30/C14	1/6/1	15
L9	400	120	8000	C30/C14	1/8/1	15

Table 1: Beams lay-ups

Test results.

Finger joints.

The results are summarized in Table 2 for each strength class.

Strength Class	*Mean bending strength (MPa)*	*Coefficient of variation*	*Characteristic value (MPa)*
C30	43,95	11,5%	34,96
TR26	45,34	21,76%	28,4
C14	38,57	15,30%	28,27

Table 2: Finger joints strength

The coefficients of variation are between 10% and 20%, which is usual.

The characteristic values (m_k) are calculated according to EN 14358, according to:

$$m_k = \exp\left(\bar{y} - k_s s_y\right) \tag{1}$$

where

$$\bar{y} = \frac{1}{n}\sum_{i=1}^{n}\ln\left(m_i\right) \tag{2}$$

and

$$s_y = \sqrt{\frac{1}{n-1}\sum_{i=1}^{n}\left(\ln\left(m_i\right) - \bar{y}\right)^2} \tag{3}$$

The coefficient k_s is determined according to $k_s = \frac{k}{\sqrt{n}}$ k is the α-percentile in a non-central t-distribution with (n-1) degrees of freedom and the non-centrality parameter $\lambda = u_{1-p}\sqrt{n}$. u_{1-p} is the (1 – p) percentile of the standardised normal distribution function.

The order of magnitude of k_s for a sample size between 10 and 20 varies from 2.10 to 1.93.

In addition, it has been checked that the strength of finger joints was within the limits required by prEN 14080:

$$1.4\, f_{t,0,l,k} \leq f_{m,j,k} \leq 12 + 1.4\, f_{t,0,l,k} \qquad (4)$$

where $f_{t,0,l,k}$ is the characteristic tensile strength of the lamellas and $f_{m,j,k}$ the characteristic bending strength of the finger joints.

Table 3 gives the lower and upper bounds of equation (4), as well as the characteristic bending strength of finger joints for each strength class. The last column gives the value which will have to be used in the calculation of the bending strength of glulam.

Strength Class	Lower bound (MPa)	Experimental characteristic value (MPa)	Upper bound (MPa)	Value to be used in the calculation (MPa)
C14	11,8	28,3	23,8	23,8
TR26	21,8	28,4	33,8	28,4
C30	25,2	35	37,2	35

Table 3: Values for finger joints to be used in the calculation

Glulam beams

Table 4 gives the characteristic values for the different combinations. 5% values have been calculated according to EN 14358.

Since MOE values have been calculated by using the global deflection, a correction has been applied to the test values to get “local values” (see last column). In absence of existing information, the correction given in EN 384 has been applied (E values are given in MPa in this equation):

$$E_{local} = 1.3E_{global} - 2690 \qquad (5)$$

Lot	Valeurs expérimentales					
	fm,mean (MPa)	CV	fmgk (MPa)	E global (GPa)	CV	E "local" (GPa)
L1	39,1	16,2%	27,9	10,4	6,3%	10,8
L2	38,5	14,0%	28,6	10,8	6,5%	11,4
L3	44,4	12,8%	34,4	11,4	4,8%	12,1
L4	40,7	16,2%	28,2	11,2	5,4%	11,9
L5	38,3	15,8%	27,8	11,1	4,4%	11,7
L6	37	18,6%	24,9	10,5	4,3%	11,0
L7	39,4	13,6%	29,5	11,4	5,6%	12,1
L8	37,5	16,2%	25,8	10,4	4,0%	10,8
L9	30,14	17,2%	21,15	10,4	5,8%	10,8

Table 4: Glulam beams test results

Calculation model for combined glulam

Each zone of the combined glulam beam is calculated according to the model defined in prEN 14080.

The characteristic bending strength is given by:

$$f_{m,g,k} = -2.2 + 2.5 f_{t,0,l,k}^{0.75} + 1.5\left(\frac{f_{m,j,k}}{1.4} - f_{t,0,l,k} + 6\right)^{0.65} \quad (6)$$

where $f_{t,0,l,k}$ is the characteristic tensile strength of the laminations and $f_{m,j,k}$ is the characteristic bending strength of the finger joints.

The mean modulus of elasticity is given by:

$$E_{0,g,mean} = 1.05 E_{t,0,l,mean} \quad (7)$$

where $E_{t,0,l,mean}$ is the mean modulus of elasticity of the laminations.

Stresses are calculated according to the theory of composite beams, developed by Timoshenko, and illustrated in Annex B of Eurocode 5. Stresses are calculated in each critical point of the cross-section, and the strength verification is carried out in each individual zone.

Analysis of the results

Table 5 gives the comparison between experimental and calculated values.

Experimental values have been corrected according the size effect equations:

$$f_{m,600} = k_h f_{m,h} \quad (8)$$

with:

$$k_h = Min\begin{cases} 1.1 \\ \left(\dfrac{h}{600}\right)^{0.1} \end{cases} \quad (9)$$

Lot	Depth (mm)	Beam lay-up		Strength (Mpa)		Stiffness (Gpa)	
		Strength classes	Number of lamellas	fmgk,600 (experimental)	fmgk (model)	Eg (experimental)	Eg (model)
L1	200	TR26/C14	1/3/1	**25,0**	**22,2**	**10,8**	**10,6**
L2	240	TR26/C14	1/4/1	**26,1**	**21,6**	**11,4**	**10,3**
L3	240		2/2/2	**31,4**	**23,8**	**12,1**	**11,4**
L4	240	C30/C14	1/4/1	**25,7**	**24,3**	**11,9**	**11,1**
L5	240		2/2/2	*25,4*	*27,1*	*11,7*	*12,4*
L6	280	C30/C14	1/5/1	*23,1*	*23,3*	**11,0**	**10,6**
L7	280		2/3/2	**27,3**	**26,6**	**12,1**	**12,2**
L8	320	C30/C14	1/6/1	**24,2**	**22,5**	**10,8**	**10,3**
L9	400	C30/C14	1/8/1	*20,3*	*21,7*	**10,8**	**9,9**

Table 5: Comparison between model and experiment
For bolded values: experiment > model
For italic values: experiment < model

Over 9 lots, 7 are totally acceptable.
Lot n°5 is slightly below in terms of both strength and stiffness.
Lot n°9 is slightly below in terms of strength only.

Over 6 lots with only one lamella in the outer zone, only one (lot n°9) is slightly below.

But these deviations are in our opinion quite acceptable, since they are due to inherent variability of glulam, which has an impact on the k_s factor (see equation (1)) for small sample sizes (less than 15).

This can be demonstrated as follows:

For lots n°5, 6 & 9, we looked at the minimum test values, which were then corrected by the size effect.

The results are the following:

- Lot n°5 : $f_{m,g,\min,600}$ = 27.2 MPa
- Lot n°6 : $f_{m,g,\min,600}$ = 23.5 MPa
- Lot n°5 : $f_{m,g,\min,600}$ = 22.4 MPa

In all cases, the minimum value corrected to the reference depth is larger than the required value.

Figures 1 and 2 illustrate the results.

Squared points correspond to lots with only one lamella in the outer zone, triangle points with two lamellas in the outer zone.

The solid line corresponds to the model given in prEN 14080.

The dotted line is a regression line going through the origin.

It should be noted that in average, experimental strength is 7% higher than given by the model, and experimental stiffness is more than 3% higher than the model.

Of course, combinations with only one lamella in the outer zones tend to give lower values, but this is correctly predicted by the model.

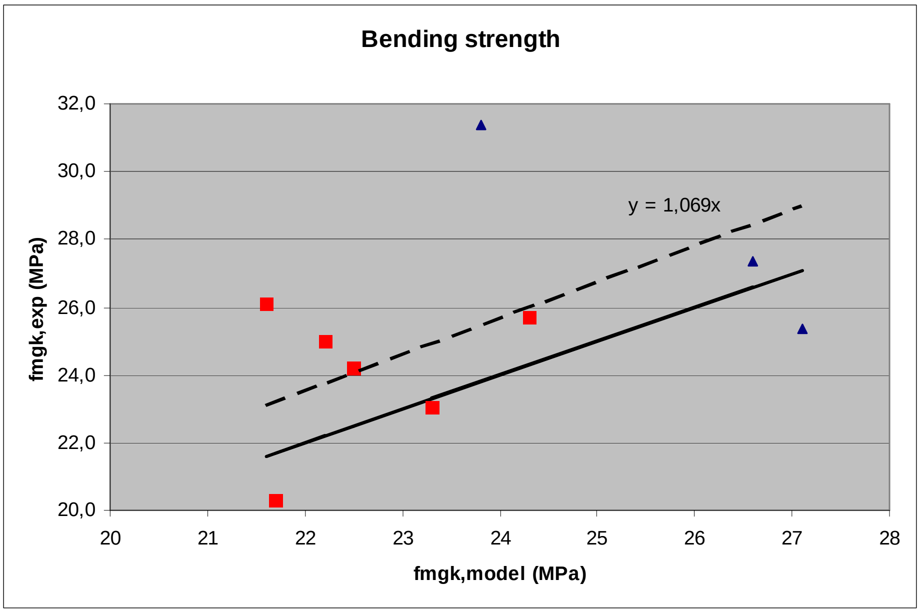

Figure 1: Experiment vs. model for strength

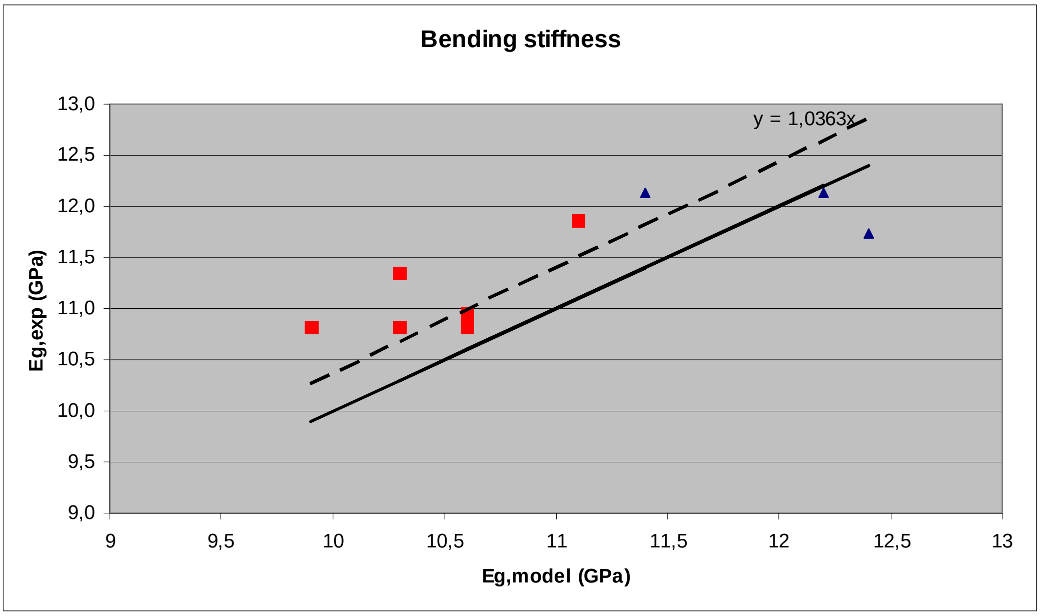

Figure 2: Experiment vs. model for stiffness

Design proposal

It is proposed to allow beam lay-ups with only one lamella in the outer zones. But this allowance should be limited in terms of maximum depth.

Our assumption is that the current requirement of two lamellas makes sense when the second lamella can undertake an extra stress due to failure of the first lamella. But this can happen only if the overstress is limited.

For small beams (e.g. less than 10 lamellas), the overstress will be larger than 25%, and it is not realistic to think that this stress transfer can happen.

Therefore, our proposal is to limit the allowance of only one lamella in the outer zone for beams up to 10 lamellas.

Conclusions

This project has demonstrated that it is possible to open the current version of prEN 14080 in order to allow combined glulam of small depth with only one lamella in the outer zones.

This allowance has a very strong impact for the economy of the sector, since it permits to use secondary quality timber in a larger proportion, and therefore make the best use of our material.

The authors would like to thank the company Monnet-Sève who gave financial support to this investigation.

References

EN 1995-1-1 Eurocode 5 - Design of timber structures - Part 1-1: General – Common rules and rules for buildings

EN384 - Structural timber - Determination of characteristic values of mechanical properties and density

prEN 14080 (2011) - Timber structures - Glued laminated timber and glued laminated solid timber - Requirements

EN 14358 - Timber structures - Calculation of characteristic 5-percentile values and acceptance criteria for a sample

CIB-W18/44-12-4

**INTERNATIONAL COUNCIL FOR RESEARCH AND INNOVATION
IN BUILDING AND CONSTRUCTION**

WORKING COMMISSION W18 - TIMBER STRUCTURES

GLULAM BEAMS WITH INTERNALLY AND EXTERNALLY REINFORCED HOLES – TESTS, DETAILING AND DESIGN

S Aicher

MPA University Stuttgart

GERMANY

MEETING FORTY FOUR

ALGHERO

ITALY

AUGUST 2011

Presented by S Aicher

A Buchanan asked what if the screws were installed in an inclined angle. S Aicher stated that it might create an issue in terms of placement of the screws that could not be matched with the high stress fields of both tension perpendicular to grain and shear. Although increases might be possible but not sure about how big an increase could be achieved.

BJ Yeh asked whether there could be an orientation effect for the reinforcing panel. S Aicher confirmed that panels were failing in tension but stated that the effect of orientation of the panel could be minimal.

F Lam received confirmation that 3-D FEM analysis was used with large number of nodes and elements.

S Franke asked whether softening behaviour from cracking considered. S Aicher responded no and pure elastic simple approach was used in the analysis and it would be interesting to see how far the internal cracks went.

Glulam beams with internally and externally reinforced holes – tests, detailing and design

S. Aicher
MPA University Stuttgart, Germany

1 Introduction

At present, the European timber design code does not contain design rules for holes in glulam or LVL, either unreinforced or reinforced. This represents a considerable draw back for the material timber vs. steel and reinforced concrete in specific, not unusual constructions. In contrary, the German National Annex to EC 5: Part 1-1 (DIN EN 1995-1-1/NA) incorporates a substantial set of design and construction rules for unreinforced and especially reinforced holes. Hereby different possibilities of non-visible internal and visible external reinforcements are included. In all cases, reinforcements are not permissible in beams where stresses perpendicular to grain occur in the construction component when holes are disregarded, e.g. in curved beams.

Firstly, the paper gives the design and construction rules for internal and external reinforcements specified in DIN EN 1995-1-1/NA. Second, several design rules are compared to results of finite element calculations. Third, results of recent tests on internal and external reinforcements are presented and discussed in view of the design rules.

2 Design of reinforced holes in DIN EN 1995-1-1/NA

2.1 General

The possible reinforcements according DIN EN 1995-1-1/NA:2010 comprise interior (invisible) strengthening methods by means of glued-in steel bars, re-bars and fully threaded wood screws, in general being self-tapping screws. The exterior reinforcements can be made by glued-on plywood panels acc. to EN 13986 and EN 636, glued-on LVL according i. a. to EN 14374 or EN 13986 and pressed-in nail plates. The latter reinforcement method, according to the standard, has to be handled analogously to glued-on panels. Employing usual rectangular nail plates this is by principle not possible as the plate does not follow the contour of the hole. This reinforcement method for holes is disregarded here. Figs. 1a, b shows the dimensional notations for reinforced holes. Table 1 specifies the permissible hole geometries and the dimensions and spacings for the different reinforcement types.

The basic idea of the reinforcement design consists in the assumption that the shear stresses respectively their resultant shear force, which can not be transferred in the reduced cross-section at the hole, are/is deviated by equivalent tension and compression forces $F_{t,90}$ and $F_{c,90}$ perpendicular to beam axis to the remaining cross-sections above and below the hole, respectively. The resultant tension force $F_{t,90}$ forms the basis of the design of beams with unreinforced and reinforced holes.

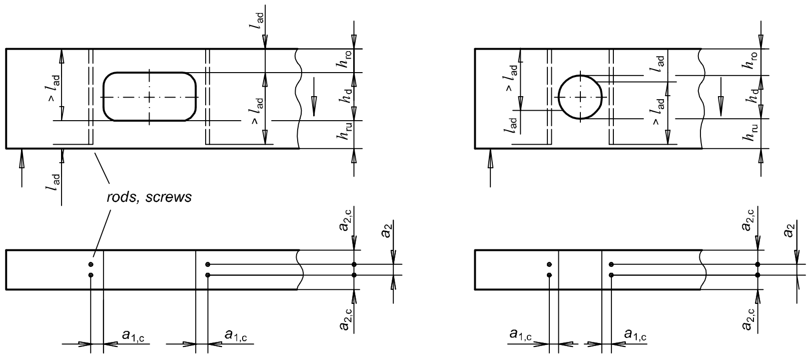

a)

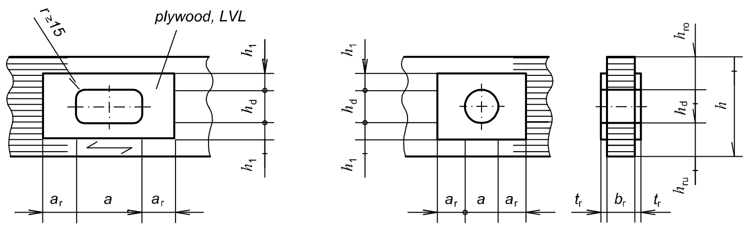

b)

Fig. 1a, b: Geometry and dimensional notations for glulam beams with holes, reinforced by
a) rods, screws b) glued-on plywood or LVL panels

reinforcement type	hole dimensions and edge distances				
	h_d/h	a/h_d	ℓ_v/h	ℓ_A/h	$h_{ro(ru)}/h$
rods, screws	$\leq 0{,}3$	$\leq 2{,}5$	≥ 1	$\geq 0{,}5$	$> 0{,}25$
panels	$\leq 0{,}4$				

Table 1: Permissible hole dimensions and edge distances

reinforcement type	edge distances, spacings, rod and panel dimensions
rods, screws	$2{,}5 \cdot d_r \leq a_{1,c} \leq 4 \cdot d_r$; $2{,}5 \cdot d_r < a_{2,c}$; $3 \cdot d_r < a_2$ $20\text{ mm} > d_r$; $2\ \ell_{ad} < \ell_{min}$
panels	$0{,}25 \cdot a \leq a_r \leq 0{,}3\ (h + h_d)$; $0{,}25 \cdot a \leq h_1$

Table 2: Permissible dimensions, edge distances and spacings for different reinforcement types

In case of reinforced holes it is assumed that the total tension force $F_{t,90}$ is transferred by the reinforcement. In case only a part of $F_{t,90}$ can be transferred by the reinforcement according to the simplified design equations, the design verification has to be performed with disregard to the contribution of the “insufficient” reinforcement. Force $F_{t,90}$ is composed of two additive parts where $F_{t,V}$ represents the - in general - dominating influence of the shear force V and $F_{t,M}$ is related to the influence of the moment M

$$F_{t,90,d} = F_{t,V,d} + F_{t,M,d} \qquad (1a)$$

where

$$F_{t,V,d} = V_d \frac{h_d}{4\,h}\left[3 - \frac{h_d^2}{h^2}\right], \quad F_{t,M,d} = M_d \frac{0{,}008}{h_r} \qquad \text{(1b,c)}$$

and

$h_r = \min\{h_{ro}; h_{ru}\}$ rectangular holes

$h_r = \min\{h_{ro} + 0{,}15\,h_d; \quad h_{ru} + 0{,}15\,h_d\}$ round holes

V_d, M_d design shear force and bending moment at the respective hole edge

In case of round holes quantity h_d in Eq. (1b) can be replaced by 0,7 h_d.

2.2 Interior Reinforcement with glued-in rods and screws

The standard specifies the equations for reinforcement with glued-in rods explicitly and states that the reinforcement with screws shall be performed accordingly (see Blass et. al., 2004). The design accounts essentially on the verification of the effective bond line shear stress τ_{ef}, assumed to be uniformly distributed at the rod periphery (d_r = nominal rod diameter) along effective bond length ℓ_{ad}

$$\frac{\tau_{ef,d}}{f_{k1,d}} \leq 1 \quad , \quad \tau_{ef,d} = \frac{F_{t,90,d}}{n \cdot d_r \cdot \pi \cdot \ell_{ad}} \qquad \text{(2a,b)}$$

where

n number of rods in width direction of beam at each side of the hole (note: in beam length direction the design shall account exclusively for one rod at the respective hole side)

$\ell_{ad} = h_{ru}$ or $\ell_{ad} = h_{ro}$ rectangular holes
$\ell_{ad} = h_{ru} + 0{,}15\,h_d$ or $\ell_{ad} = h_{ro} + 0{,}15\,h_d$ round holes
$f_{k1,d} = f_{k1,k} \cdot k_{mod} / \gamma_M$ design value of bond line shear strength

The characteristic value of the bond line shear strength $f_{k1,k}$ depends on the effective bond length ℓ_{ad} and is given in the standard, here Table 3, irrespective of the specific adhesive which must be approved for the purpose of glued-in rods.

ℓ_{ad} (in mm)	≤ 250	$250 < \ell_{ad} \leq 500$	$500 < \ell_{ad} \leq 1000$
$f_{k1,k}$ (in MPa)	4,0	$5{,}25 - 0{,}005 \cdot \ell_{ad}$	$3{,}5 - 0{,}0015 \cdot \ell_{ad}$

Table 3: Characteristic bond line shear strength for glued-in rods

Although not stated explicitly in the chapter on rod reinforcements in DIN EN 1995-1-1/NA it is evident that the tension capacity of the rod, R_{ax}, has to be verified too, as

$$\frac{F_{t,90,d}}{n \cdot R_{ax,d}} \leq 1, \qquad R_{ax,d} = f_{y,d} \cdot A_{ef} \qquad \text{(3a,b)}$$

where $f_{y,d}$ is the design yield strength of the rod and A_{ef} is the effective rod cross-section relevant for tension strength verification.

In case of rectangular holes the shear stress peaks at the hole corners shall be verified too, yet the standard does not give any design equations. However, it can be considered state of the art (i.a. Blass et al., 2004) to apply the solely known equation (Blass and Bejtka, 2003):

$$\tau_{corn,d} = \xi_{\tau,corn} \cdot \tau_{net,d} = \xi_{\tau,corn} \cdot 1{,}5 \frac{V_d}{b\,(h - h_d)} \tag{4a}$$

where

$$\xi_{\tau,corn} = 1{,}84 \left[1 + \left(\frac{a}{h}\right)\right] \left(\frac{h_d}{h}\right)^{0,2} \quad \text{for } 0{,}1 \le \frac{a}{h} < 1{,}0 \text{ and } 0{,}1 \le \frac{h_d}{h} \le 0{,}4. \tag{4b}$$

In fact the multiple regression solution for $\xi_{\tau,corn}$ specified by Eq. (4b) has been derived explicitly for the shear stress concentration at the corner of an unreinforced glulam beam with a rectangular hole. Nevertheless, according to the authors, the equation applies for holes reinforced with screws, too. This is due to the fact that screws, inserted perpendicular to the beam and fiber axis, do not contribute in significant manner to the bending and shear stiffness of the beam as compared to the unreinforced beam.

2.3 Exterior reinforcement with glued-on panels

The design comprises the verification of the glue line shear stress, outwardly assumed to be uniformly distributed

$$\frac{\tau_{ef,d}}{f_{k2,d}} \le 1 \quad , \quad \tau_{ef,d} = \frac{F_{t,90,d}}{2 \cdot a_r \cdot h_{ad}} \tag{5a,b}$$

where

$h_{ad} = h_1$	rectangular holes
$h_{ad} = h_1 + 0{,}15\ h_d$	round holes
$f_{k2,d} = f_{k2,k} \cdot k_{mod}/\gamma_M$	design value of bond line shear strength

The characteristic bond line shear strength value is specified as $f_{k2,k} = 0{,}75$ MPa associated to a non-uniform introduction of the shear stress between reinforcement panel and glulam beam (Note: this relativates the above comment on the uniform distribution of τ_{ef}). Secondly, a design verification of the tension stress in the reinforcement panel shall be performed as

$$k_k \frac{\sigma_{t,d}}{f_{t,d}} \le 1 \quad , \quad \sigma_{t,d} = \frac{F_{t,90,d}}{2 \cdot a_r \cdot t_r} \tag{6a,b}$$

where k_k accounts for the uneven normal stress distribution; a value of $k_k = 2$ may be assumed acc. to the standard unless a more detailed verification is provided, not given in literature today.

3 Verification of the reinforcement equations

In the following the design specifications and equations specified in DIN EN 1995-1-1/NA are checked for completeness and accuracy by means of finite element analysis (ANSYS, Release 13.0). The computations were throughout performed with a 3D model for the beams with holes and lateral reinforcements. All 3D models made use of the symmetry of the cross-sections vs. mid-width. The thickness of the plywood reinforcement and similarly halve of the glulam width were discretized by 6 elements each. The glue line was modelled explicitly by 4 elements throughout thickness, chosen as 0,5 mm, what is realistic for the applied bonding method, namely (screw-) gluing. The employed volume element type was solid 45.

The 3D computational results of the beams without lateral reinforcements, analyzed with regard to the assessment of $F_{t,90}$ acc. to the DIN EN 1995-1-1/NA-solution (in following abbreviated by DIN), were checked by a plane stress analysis, delivering almost identical results.

The employed stiffness values (in MPa) for the glulam beam (strength class GL 32 h) were $E_x = 13700$, $E_y = 460$, $G_{xy} = 850$, $G_{yz} = 50$, $v_{xy} = v_{yx} \cdot E_y/E_x = 0{,}015$. The stiffness values for the plywood reinforcements conformed to different strength (F) and MOE (E) classes of the plywood and varied from $E_x = 2500$ MPa, $E_y = 4000$ MPa to $E_x = 5000$ MPa, $E_y = 7000$ MPa; throughout $G_{xy} = 700$ MPa was assumed. The values related to thickness direction, being rather irrelevant in this context, were throughout chosen as $E_z = 370$ MPa and $G_{xz} = G_{zy} = 50$ MPa.

In a first step the accuracy of Eqs. (1a-c) for the resultant tension force $F_{t,90}$ perpendicular to grain, acting normal to the highest stressed area prone to cracking was checked. The potential crack area was always assumed to start at the hole periphery at a line marked by the intersection of the hole edge with the hole or corner radius at $\varphi = 45°$. In case of a prevailing shear force influence on $F_{t,90}$, denoted by $F_{t,V} > F_{t,M}$, there are actually two diagonally opposite crack planes starting at $\varphi = 45°$ and $45° + 180°$. It has to be stated that the maximum tension stress perpendicular to grain is not located exactly at $\varphi = 45°$ (+ 180°) but the differences with regard to the integral of the whole stress field are minor and can be disregarded in this context, at least for round holes (see Aicher and Höfflin, 2000; 2001). With regard to rectangular holes, it is obvious that the radius r of the corner has a tremendous effect on the peak stresses in the ultimate vicinity of the corner, however a significantly lower influence when considering a damage relevant Weibull stress (Höfflin and Aicher, 2003). The influence of the corner radius on the resultant tension force $F_{t,90}$ however is rather small, at least for sensible radii in the range of about 15 to 30 mm. Most of the computations were done with the minimum value of r = 15 mm as prescribed by the standard. The verifications of the $F_{t,90}$ equations were performed with a simply supported beam where the hole is placed in the constant shear force and hence linearly varying moment range.

The main results are given in Figs. 2a-c for the cases of a round hole, a square hole and for a rectangular hole with an aspect ratio of $a/h_d = 2$. In all graphs the ratio of the FE result vs. the DIN solution $F_{t,90,FE}$ / $F_{t,90,DIN}$ is plotted over the hole depth to beam depth ratio h_d/h for three different distances ℓ_A = 1h, 2h and 3h between the line of support and the closest edge of the hole. The chosen distances ℓ_A also denote moment vs. shear

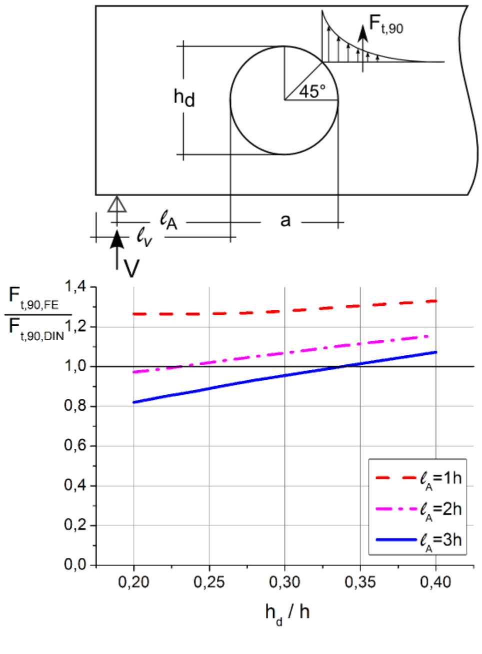

a)

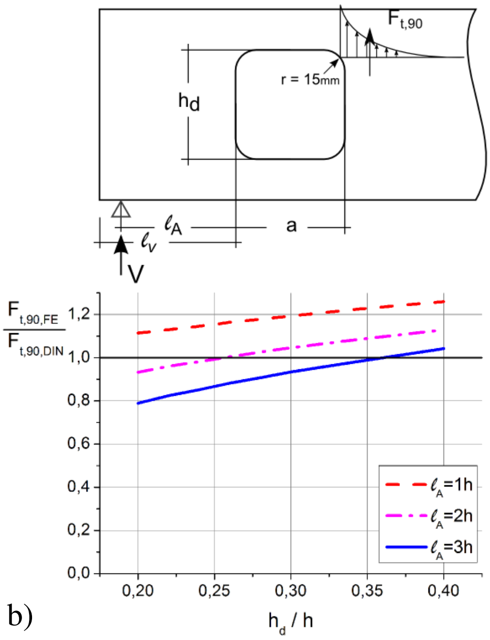

b)

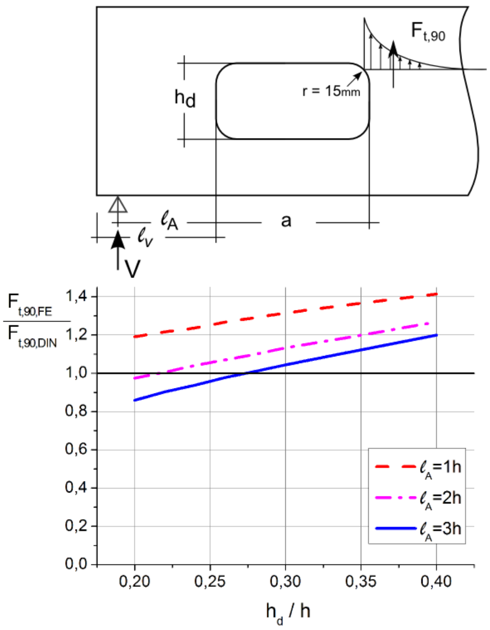

c)

Fig. 2 a – c: Comparison of the resultant maximum tension force $F_{t,90}$ acc. to FE analysis and DIN solution $F_{t,90,FE}/F_{t,90,DIN}$ depending on hole depth to beam depth ratio h_d/h and distance ℓ_A between support and closest hole edge for different hole geometries

a) round hole b) square hole

c) rectangular hole with aspect ratio $a/h_d = 2$

force ratios M/V = 1, 2 and 3 at the left hole edge. It can be seen that the $F_{t,90}$ ratio depends considerably on the hole to beam depth ratio h_d/h and further on the distance ℓ_A of the hole edge from the support, i.e. on the M/V ratio. For several configurations of h_d/h and ℓ_A/h the DIN solutions are conservative but especially for larger h_d/h ratios and ℓ_A/h-ratios of 1 to 2 the Eqs. (1a-c) deliver partly considerably smaller values than the FE-computations. Consequently, Eqs. (1b and c) have to adjusted accordingly whereby the principle build-up of Eq. (1b) for $F_{t,V}$ is mechanically plausible and should be preserved. In case of $F_{t,M}$ it was pointed out in earlier papers (i. a. Aicher and Höfflin, 2000) that Eq. (1c) is wrong in case of round holes and probably for rectangular holes, too. For replacement of Eq. (1c) the expression

$$F_{t,M,d} = 0{,}084\ \frac{M_d}{h}\left(\frac{h_d}{h}\right)^2 \qquad (7)$$

was derived for round holes from a FE parameter study (Aicher and Höfflin, 2001).

Regarding the design of internal reinforcements by screws and of lateral reinforcements by plywood or LVL, the design approach in DIN EN 1995-1-1/NA assumes that the total tension force $F_{t,90}$ is carried by the reinforcement. This is equivalent to the assumptions of a fully cracked cross-section, i. e. of a crack of the beam along full width of the beam with an extension of more than distance $a_{1,c}$ in case of an internal rod and along full panel strip width a_r in case of a lateral reinforcement.

On the other hand it is obvious that the glulam beam shares a considerable part of the force $F_{t,90}$ in the undamaged state and then gradually less in the increasingly cracked glulam beam state. The successive load transfer from the glulam beam to the reinforcement with increasing length of a crack in the glulam starting at the periphery of a round hole was revealed quantitatively by Aicher and Höfflin (2009) for the case of internal reinforcement by a screw or glued-in rod.

In case of lateral reinforcement, Figs. 3a,b reveal for a specific configuration of a square hole ($h_d/h = 0,4$), reinforced with significantly different sized panels, the distribution of $F_{t,90}$ between the glulam beam, $F_{t,90,g}$, and the lateral reinforcement, $F_{t,90,r}$, in the elastic, undamaged state. Hereby the influence of different panel MOE's and of the ratio $2t_r/b$ of total reinforcement thickness vs. beam width is shown. It is interesting to note, that the force in the panels, $F_{t,90,r}$, in case of sensible reinforcement ratios $2t_r/b \leq 0,4$ is less or maximally half of the total force $F_{t,90} = F_{t,90,g} + F_{t,90,r}$. The influence of the reinforcement dimension a_r, i.e. the width of the panel strip on each side of the hole has a less significant influence as anticipated. An increase of the width size by a factor of 2 (Fig. 3b vs. Fig. 3a) results in a rather small increase of $F_{t,90,r}$ of about 20 to 25 %. Further, it is interesting to note that the influence of the panel MOE $E_{r,y}$ perpendicular to beam axis, varied from 4000 MPa to 7000 MPa, on $F_{t,90,r}$ is considerably smaller then expected from the stiffness increase. These findings will be regarded further. However, already at this stage the modelling results back the experimental findings (see chap. 4), revealing a crack formation in the glulam cross-section at a rather/very low level of global shear force V, what results from the high $F_{t,90,g}$ / $F_{t,90,r}$ ratio.

The shear stress concentration at the corners of rectangular holes, which shall be verified in the design when internal reinforcements are used, is covered by Eqs. (4a) and (4b). The solutions, however, do not account explicitly for the obvious influence of the radius of curvature of the corners of the holes and this influence is also not immediately evident from Blass and Bejtka (2003). So, it is not clear for which radius the solution is conservative or not, especially with regard to the minimum radius of 15 mm prescribed by DIN EN 1995-1-1/NA. In order to assess this issue, exemplary calculations on rectangular holes were performed with explicit regard to the corner radius. The employed isoparametric elements allowed for curved edges, mirroring the respective corner radius with avoidance of any stress concentration or singularity problem. In a first step the largest permissible ratio of hole depth to beam depth h_d/h was analyzed for three different hole aspect ratios $a/h_d = 1$ (square hole), $a/h_d = 2$ and 2,5. These aspect ratios conform to parameters $a/h = 0,4$, 0,8 and 1,0, as employed in Eq. (4b).

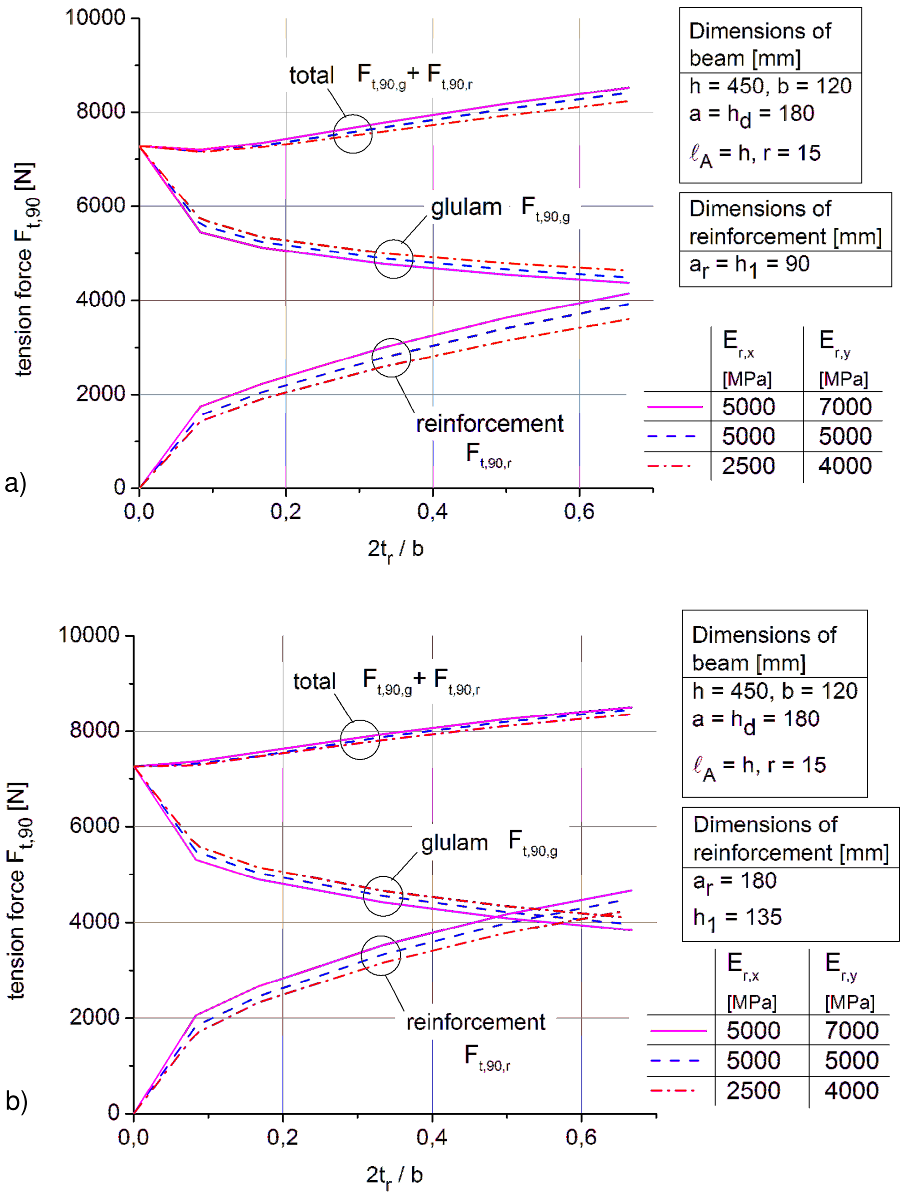

Fig. 3 a, b Distribution of $F_{t,90}$ between glulam and lateral plywood panel reinforcement in case of a square hole with a hole to beam depth ratio of $h_d/h = 0{,}4$ located in the constant shear force area close to the support at $\ell_A = h$, depending on reinforcement thickness vs. glulam width ratio $2t_r/b$ and different panel MOE configurations; shear force V = 36000 N

a) $a_r = h_1 = 90$ mm b) $a_r = 180$ mm, $h_1 = 135$ mm

The computational results for $\xi_{\tau,corn}$ vs. corner radius r are given in Fig. 4. The shear stress concentration factor $\xi_{\tau,corn}$ obtained from the FE calculations shows, as expected, a very distinct exponential relationship with decreasing corner radius r. Further, it can be seen that $\xi_{\tau,corn}$ depends considerably on the exact location of the stress evaluation at the corner periphery, whereby the evaluation of $\xi_{\tau,corn}$ at the location of the stress maximum delivers throughout considerably higher values as compared to the evaluation at an angle of 45° (note: the stress peak is located closer to the upper horizontal edge of the hole at about $\varphi = 60 - 70°$). It can be noticed that Eq. (4b) specifies for larger corner radii, dependant on the aspect ratio a/h_d, conservative solutions, whereas for small corner radii in the range of 15 mm to about 40 mm partially far too low values are predicted. It seems necessary to take the issue of the corner radius into account, either by a modified Eq. (4b) or by prescribing a larger corner radius.

For sake of an increased transparency to the design engineer it seems appropriate to relate the corner stress τ_{corn} to the shear stress in the gross cross-section instead to the net cross-section, as in the latter case this value has rather little physical relevance. The corner shear stress would then read (with $\xi_{\tau,corn}$ acc. to Eq. (4b)) different from Eq. (4a)

$$\tau_{corn,d} = \xi_{\tau,corn} \frac{h}{h-h_d} \cdot \tau_{gross,d} = \xi_{\tau,corn} \frac{h}{h-h_d} 1{,}5 \frac{V_d}{b \cdot h}. \tag{8}$$

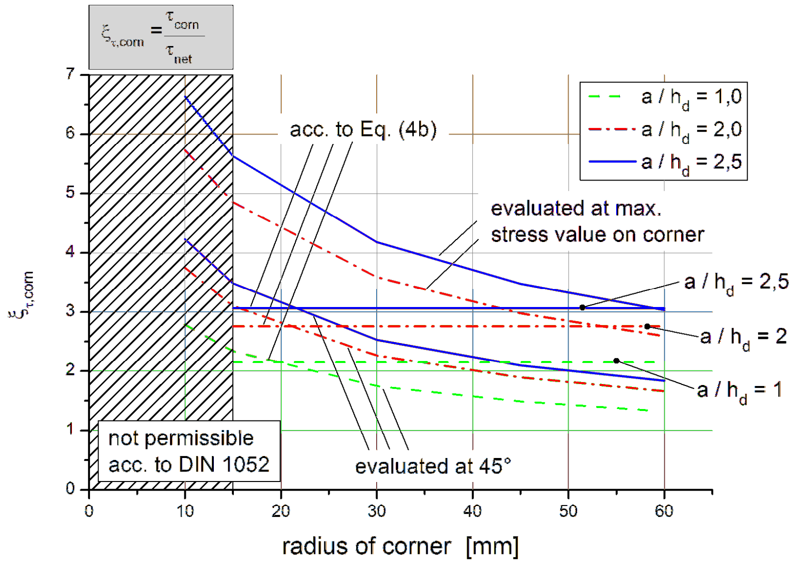

Fig. 4 Shear stress concentration factor $\xi_{\tau,corn}$ at the corner of a rectangular hole with three different aspect ratios a/h_d for a hole depth to beam depth ratio $h_d/h = 0{,}4$. The horizontal lines denote the solutions acc. to Eq. (4b).

4 Experimental investigations

4.1 General

The presented experimental investigations are part of a larger experimental campaign aiming to provide a consistent data base for the load capacities and failure mechanisms of glulam beams with round and rectangular holes reinforced by internal and external reinforcement alternatives. The lay-out of the experiments is closely related to the tests reported in Aicher and Höfflin (2009). This means that the glulam strength class (GL 32 h), the beam and hole sizes and the loading conditions (simply supported beam with two loads at mid-span) remained unchanged (see Fig. 5a). In case of the reinforcement with glued-in rods and self-tapping screws the same steel rods/screws and adhesive (in case of glued-in rods) as in the previous investigation were used; the changes in

the new tests with steel rods/screws concerned the number of bars and hence changed spacings and edge distances.
Figs. 5a-c show the geometry and dimensions of the specimens with exterior reinforcements of the round holes by plywood (the same beam and hole dimensions apply to the internally reinforced specimens). So far, five beams with significantly different sizes of plywood reinforcements were manufactured and tested. The employed plywood was spruce plywood with thicknesses of 15 mm (5 layer) and 21 mm (7 layer) of strength class F20/15 and MOE class E 45/25 acc. to EN 13986 and EN 636. According to the data sheets of the producer of the spruce plywood the characteristic in-plane tension strength and MOE values parallel to the grain direction of the face veneer (here orthogonal to beam axis) are $f_{t,0,k}$ = 9,6 MPa and $E_{t,0,mean}$ = 6400 MPa; the characteristic shear strength orthogonal to the panel plane is 3,5 MPa.

The fiber orientation of the outer veneer layer was glued perpendicular to beam axis (note: this issue is not prescribed in the standard yet recommended in Blass et al. (2004)). The gluing of the reinforcement panels onto the glulam was performed by so-called screw gluing with a gap-filling melamine-urea-formaldehyde (MUF) adhesive. The dimensions of the approved self-tapping screws were 4,0 mm x 70 mm. Some details on screw gluing are given in the draft of DIN 1052-10 (supplementing DIN EN 1995-1-1/NA) such as the minimum screw sizes, the maximum spacing ($a_{screw} \leq 15$ cm) and the maximum cramping influence area ($A_{screw} \leq 150$ cm^2) of the screws. These spacing and area provisions turned out to be far too large in order to achieve a good bond between the reinforcement panel and the glulam. This is also true for reduced dimensions of a_{screw} = 7,5 cm and A_{screw} = 90 cm^2. A fully satisfactory bond was achieved with a very small effective screwing area of about 20 cm^2.

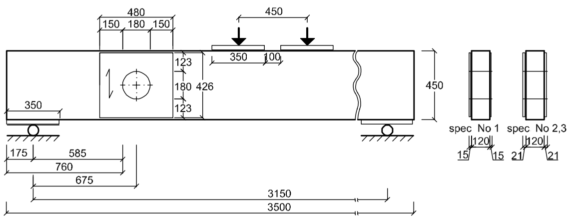

a)

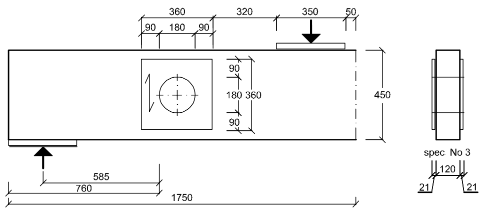

b)

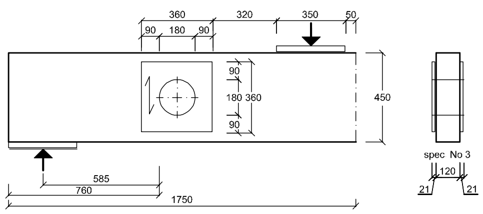

c)

Fig 5 a-c: Dimensions of investigated externally reinforced (glued-on spruce plywood) glulam beams with round holes (dimensions in mm)

a) $a_r = 150, h_1 = 123$ b) $a_r = h_1 = 90$ c) $a_r = h_1 = 45$

The nominal/outer diameter of the self-tapping screws and of the rods with metric thread of the internally reinforced specimens was d_r = 12 mm. The edge distances and spacings of the screws/bars (n = 2 per hole edge) were throughout $a_{1,c} = 3_{dr}$, $a_{2,c}$ = 2,5 d_r and $a_2 = 5d_r$.

4.2 Test results

Table 4 gives the primary test results. Given are the shear forces V_{init}, V_c and V_u at different damage resp. crack stages (for definitions see Aicher and Höfflin (2009)). Further, based on V_u the resultant tension force $F_{t,90,u} = V_u \cdot 0{,}2423$ acc. to Eqs. (1a-c) is evaluated and on the basis of this quantity the pull-out parameter $f_{1,u}$, the bond shear stress $\tau_{ef,u}$ and the tension stress in the plywood $\sigma_{t,u}$ are derived. The shear stress in the glulam at V_u is specified for the gross and net cross-section, b · h and b (h-h_d), respectively.

With regard to the failure occurrence it can be stated that the first crack formation always occurred at mid-width of the glulam cross-section at the hole periphery at an angle of about 45°. Irrespective of the type of reinforcement the first cracking always took place at the hole edge farther from the support, i.e. at the position of the higher moment. The load level of V_{init} is very roughly in the range of 1/3 to 1/2 of ultimate load. The ultimate brittle failure always occurred by crack formation starting at the hole edge closer to the support. In case of external plywood reinforcement the ultimate tension and shear failure in the plywood and in the glulam occurred at a load being roughly 10 % to 15 % higher than the shear force V_c, denoted by a crack fully developed along width of the glulam cross-section at the hole edge closer to the support.

reinforcement type	Specimen No	shear force at different crack/failure stages			resultant tension force at V_u	pull-out parameter (screws); effective bond shear stress at V_u	tension stress in plywood at V_u	peak tension stress with k_k = 2 at V_u	shear stress in glulam at V_u	
		V_{init}	V_c	V_u	$F_{t,90,u}$	$f_{1,u}$; $\tau_{ef,u}$	$\sigma_{t,u}$	$2 \cdot \sigma_{t,u}$	$\tau_{gross,u}$	$\tau_{net,u}$
-	-	kN	kN	kN	kN	N/mm²	N/mm²	N/mm²	N/mm²	N/mm²
self tapping screws	V2/1	26,5	55,5	100,4	24,33	6,26	-	-	2,79	4,65
	V2/2	43,6	54,5	81,1	19,65	5,05	-	-	2,25	3,75
glued-in rods	V4/1	26,4	61	110,4	26,75	2,19	-	-	3,07	5,11
	V4/2	38,5	48,6	85,8	20,79	1,70	-	-	2,38	3,97
glued-on plywood	1	51,3	64,7 [1)] 92,8 [2)]	106,96	25,92	0,576	5,76	11,52	2,97	4,95
	2	32,8	57,6 [1)] 82,5 [2)]	91,99 [3)]	22,29	0,495	3,54	7,08	2,56	4,26
	3	49,75	94,15	109,75	26,59	0,591	4,22	8,44	3,05	5,08
	4	30	45,51 [1)] 103,0 [2)]	113,58	27,52	1,31	7,28	14,56	3,16	5,26
	5	38,6	78,35	82,5	19,99	3,09	10,58	21,15	2,29	3,82

[1)] at lower left corner close to support (see Fig. 1a,b) [2)] at upper right corner (at ℓ_A + a)
[3)] imperfect gluing of the panel reinforcement due to insufficiently dense screw pattern

Table 4 : Compilation of test results of glulam beams with round holes (h_d/h = 0,4) strengthened with different internal and external reinforcements

In case of the specimens reinforced by screws or glued-in rods it is evident that the relevant material/interface resistances $f_{1,u}$ and $\tau_{ef,u}$ obtained at ultimate shear force V_u are significantly below the “intrinsic” material strength values $f_{1,k} = 80 \cdot 10^{-6} \cdot 430^2 = 14{,}8$ MPa and $f_{k1,k} = 4{,}0$ MPa. So, shear stress peaks interacting with tension stresses perpendicular to grain apparently manifest the failure load level. In case of exterior panel reinforcements it is obvious from the results of specimens No. 4 and No. 5 that the characteristic bond line strength $f_{k2,k} = 0{,}75$ MPa, as specified in the DIN standard, is far too conservative. It is further apparent by comparison of 2 $\sigma_{t,u}$ vs. tension strength $f_{t,0,k} = 9{,}6$ MPa of the panel that the application of a stress concentration factor of $k_k = 2$ for assessment of the uneven tension stress distribution in the panel is too conservative.

5 Conclusions

The investigations revealed the necessity to modify some aspects of the hole reinforcement design in DIN EN 1995-1-1/NA. Hereby, i. a. the influence of the shear stress interaction with tension stress perpendicular to beam axis has to be accounted for at reinforced (round) holes. Further, the issue of the corner radius at reinforced rectangular holes has to be addressed, as well as bond line strengths and manufacturing provisions in case of screw-gluing.

6 References

Aicher, S., Höfflin, L., (2000): A contribution to the analysis of glulam beams with round holes. Otto-Graf-Journal, Vol. 11, pp. 167 – 180, Otto-Graf-Institute, Materials Testing Institute of Stuttgart University

Aicher, S., Höfflin, L. (2001): Round holes in glulam members. Part 1: Analysis (In German). Bautechnik 78, (10), pp. 706 – 715

Aicher, S., Höfflin, L., Reinhardt, H. W. (2007): Round holes in members made of glued laminated timber. Part 2: Load capacity and design (In German). Bautechnik 84, (8), pp. 867 – 880

Aicher, S., Höfflin, L. (2009): Glulam beams with holes reinforced by steel bars, CIB W 18, Proceedings Meeting 42, Dübendorf, paper CIB-W 18/42-12-1

Blaß, H.J., Bejtka, I. (2003): Querzugverstärkungen in gefährdeten Bereichen mit selbstbohrenden Holzschrauben. Research Report, Versuchsanstalt für Stahl, Holz und Steine, Abt. Ingenieurholzbau, University Fridericiana Karlsruhe

Blaß, H.J., Ehlbeck, J., Kreuzinger, H., Steck, G. (2004): Erläuterungen zu DIN 1052:2004-08, Entwurf, Berechnung und Bemessungen von Holzbauwerken. 1. Auflage, DGfH Innovations- und Service GmbH, Munich

Höfflin, L., Aicher, S. (2003): Design of rectangular holes in glulam beams. Otto-Graf-Journal, Vol 14, pp. 211-229, Otto-Graf-Institute, Materials Testing Institute, University of Stuttgart

CIB-W18/44-12-5

INTERNATIONAL COUNCIL FOR RESEARCH AND INNOVATION IN BUILDING AND CONSTRUCTION

WORKING COMMISSION W18 - TIMBER STRUCTURES

SIZE EFFECT OF BENDING STRENGTH IN GLULAM BEAMS

F Lam

University of British Columbia

CANADA

MEETING FORTY FOUR

ALGHERO

ITALY

AUGUST 2011

Presented by F Lam

S Aicher received clarification that the tension strength of the T1 laminae was approximately 29 MPa and the characteristic bending strength of the glulam was similar.

J Köhler asked why the simulated results were not smooth for the strength to volume relationship. F Lam responded that the simulations considered the actual grades of the laminae in different layup. In some layups the percentage of the high grade laminae exceeded the minimum requirement.

I Smith asked whether the small beams failures were similar to the large beams. F Lam responded they failed the same way.

S Aicher and F Lam discussed the observation of failures in the interior laminae. S Aicher asked about the implication of the results for European consideration of glulam size effect. F Lam responded that the direct application of the results is limited to Canadian glulam. Nevertheless, in the case of European glulam, one should be careful with size effects consideration especially if the design of larger beam is governed by bending strength.

I Smith commented on dynamic failure mechanism and it might not be a Weibull based consideration.

SIZE EFFECT OF BENDING STRENGTH IN GLULAM BEAMS

Frank Lam
University of British Columbia, Canada

1 Introduction

Some strength properties of wood products are influenced by the volume of material under stress also known as size effect. In engineered wood products such as glue-laminated timber (glulam), size effect adjustment is of particular interest as members of large sizes can be produced by structurally end-joining individual laminae using finger joints to make longer members and then face bonding the members to make deep beams. Furthermore, one may be able to reduce the influence of size effect by controlling the quality of the laminae. Most modern design codes have provisions that consider the influence of size on the bending strength of glulam. The form of the size effect adjustment varies amongst the different codes. In the German DIN 1052 2004-2008 [1], size factor K_h is given by the equation $K_h = \min\left[1.1;\ \left(\frac{600}{h}\right)^{0.14}\right]$ where h is the height of the beam of interest in mm. The characteristic bending strength of beams with a height smaller than 600 mm can be increased by K_h but there is no requirement to decrease the characteristic bending strength of beams with height greater than 600 mm. In the US [2], a size factor is established as $K_Z = \left(\frac{b_o}{b} * \frac{d_o}{d} * \frac{L_o}{L}\right)^{\frac{1}{k}} \leq 1$ where b_o, d_o and L_o are the width, depth and length of a reference beam; b, d and L are the width, depth and length of the beam of interest. In US, the factor k is species dependent given as k=10 for Douglas fir and k=20 for Southern Yellow Pine and the reference beam size is 0.13 m x 0.30 m x 6.4 m. In the Canadian design code CAN/CSA-O86-09 Engineering Design in Wood [3], the size factor is defined as $K_Z = 1.03\left(bL\right)^{-0.18} \leq 1$ where b is the width of the widest building block used in the beam and L is the beam span. This size adjustment is used to reduce the specified bending strength of the beam of interest based on a reference beam size of 0.13 m x 0.61 m x 9.1 m. It is of interest that beam depth is not considered in the Canadian approach; the rationale being bending failures of glulam are controlled mainly by finger joints of the outermost tension layer. In North America, the bending strength of beams bigger than the reference size is decreased by the size factor while increases are not allowed for smaller beams.

Even though a consistent approach to size effect adjustment for different codes is not available, it should be noted that that these approaches were typically established based on engineering judgment supported by some empirical data. As testing program of large glulam beams is expensive, few experimental programs are available to establish size effect adjustment factor for glulam beams. Moody et al. [4] combined test results of many different studies with more than 500 Douglas fir and Southern Yellow Pine beams of different sizes and grades to establish the current form of K_z in the US code. It should be noted that k=20 for Southern Yellow Pine was derived from a different study.

Lam and Mohadeven [5] studied the properties of Canadian Douglas fir-Larch lamstock leading to the establishment of new grading rules and grades for laminae for 24f Douglas fir glulam which better fit the characteristics of the Canadian resource. During this research, a UBC computer program ULAG (Ultimate Load Analysis of Glulam), capable of predicting the bending strength properties of glulam beams, was calibrated and verified with the Douglas fir resource. As size effect is significantly influenced by the quality of wood and grading practices preliminary computer evaluations of large glulam beams using ULAG indicated that the size effect adjustment factor in the Canadian code may be overly conservative for the new Canadian glulam construction. This paper reports a combined experimental and computer approach to study the influence of size on the bending strength of glulam beam in the context of the Canadian code with the objectives to 1) find or confirm an appropriate form of the size effect reduction factor and 2) evaluate the feasibility of allowing smaller glulam beams to take advantage of size effect and be assigned higher design strengths.

2 Material

Full scale testing of large beams was conducted to verify the approach and develop new size effect adjustment provisions. The tests were carried out in three groups of beams with depths of 152 mm (B6 ½'), 610mm (B6 2'), and 914mm (B6 3'). Combining with the results of twenty-four 304 mm beams and twenty-four 610 mm beams reported by Lam and Mohadeven [5], the total number of beams under consideration was 102. Table 1 shows the details of the layup of the beams.

Table 1. Details of the layup of the tested beams

GRADE COMBINATION – UBC TEST BEAMS-DOUGLAS FIR/LARCH					
BEAM	B6	B12	B24	B36	
Lamina#	lumber grade	lumber grade	lumber grade	lumber grade	
1	T1 (1.9)	T1 (1.9)	T1 (1.9)	T1 (1.9)	Bottom
2	D	C (1.6)	B (1.8)	T1 (1.9)	
3	D	D	C (1.6)	B (1.8)	
4	CC (1.9)	D	C (1.6)	C (1.6)	
5		D	D	C (1.6)	
6		D	D	C (1.6)	
7		C (1.6)	D	D	
8		CC (1.9)	D	D	
9~12			D	D	
13			C (1.6)	D	
14			C (1.6)	D	
15			CC (1.9)	D	
16			CC (1.9)	D	
17				D	
18				D	
19~21				C (1.6)	
22~24				CC (1.9)	Top

3 Bending Test for Douglas Fir/Larch Glulam Beams

The modulus of elasticity (MOE) and modulus of rupture (MOR) values of the test beams were established following ASTM D198-05a [6]. The test machine was displacement controlled to achieve an average failure time of 10 minutes for each type of the beam. The details of the bending test configuration are shown in Table 2. The dimensions of each beam were measured at 3 locations along the length of the beams before testing. Moisture content was also checked. Prior to the destructive test, each beam was tested non-destructively for MOE.

Table 2. Details of the bending test configuration

Type of Beam	B6(1/2’)	B12 (1’)	B24 (2’)	B36 (3’)
Number of Lamina	4	8	16	24
Size (depth mm)	152	304	609	914
Span to depth ratio	18	21	18	18
Test Span (m)	2.74	6.38	10.96	16.45
Beam Length (m)	3.05	6.71	11.28	17.07
Loading rate (mm/min.)	7	10	13	22
Sample Size	30	24	36	12

3.1 Beam B6 Test

The specimens were tested in the UBC 110KN Bending Test Machine. Photo 1 shows a typical flexure test in progress. In the tests, each specimen was centered within the test span and mid-span deformation relative to the supports was monitored by using a yoke device and a linear voltage displacement transducer (DCDT). The DCDT’s were calibrated to permit measurement of deflection with an error not to exceed to ±0.5%. Load-deflection data were collected and stored for the calculation of MOE values. The apparent MOE (MOEapp) based on the relative deflection between the center of the specimen and the two supporting points was estimated from the geometry of the specimen and the slope of the load deformation relationship.

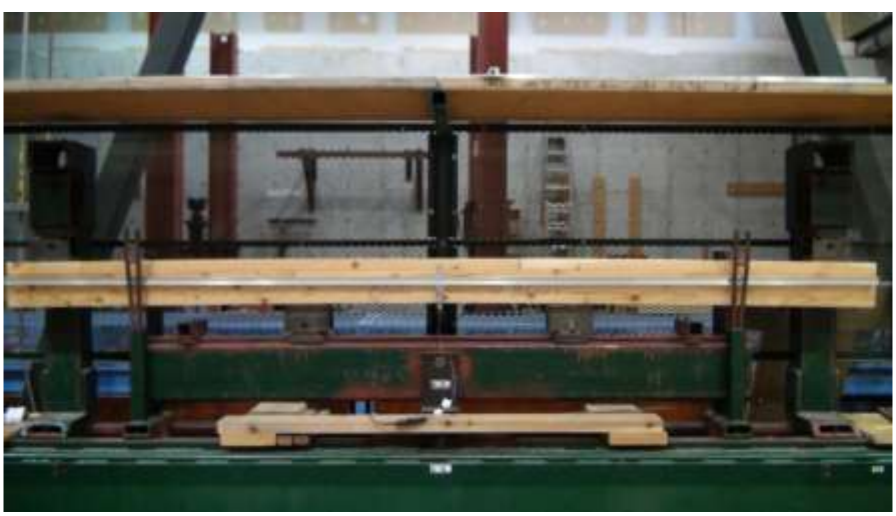

Photo 1. A B6 flexure test in progress

3.2 Beam B12, B24, and B36 Tests

The specimens were tested in the MTS Flextest GT structure test machine. Schematic view of the test assemblies is presented in Photo 2. Ten linear voltage displacement transducers were mounted onto each specimen, five on each side, to measure the deflection of the neutral axis of the beam at two loading points, center point, and two supporting points on each side of the beam. The MOEapp value was obtained from the test data.

Beams that have a depth-to-width ratio of five or greater is vulnerable to lateral instability during loading, thus requiring lateral supports. A total of five supports were used at center point, two load points, and two points located about halfway between a load point and a reaction at each end. Each support allowed vertical movement without frictional restraint but restricted lateral displacement.

Photo 2. B36 flexure test in progress

After the non-destructive test, the beams were loaded to failure in bending. The MOR values were obtained from the peak load and the specimen geometry. Descriptions of the failure mode were recorded for each beam. All the beam tests were videotaped by Sony color camcorder and a high speed camcorder.

4 Computer Analyses

4.1 ULAG Simulations

ULAG is a one dimensional linear stochastic finite element program developed to predict the statistics of the strength of a glulam beam. The key input strength parameters required are the tensile strength distributions of the lamina and finger joint and the corresponding MOE values. When simulating the structural performance of glulam beams, initial failure of a beam element is detected by the tensile fracture of the weakest element. Then the program adjusts the layups and keeps on simulating until successive beam element failures lead to the "collapse" of the beam. Based on a series of beam simulations, the strength properties statistics of the beam and their failure characteristics can be obtained.

The program ULAG was verified with the Douglas fir /Larch glulam beam test data. The bending simulations for nine types of the beams with depth of 152 mm (B6 ½'), 304 mm (B12 1'), 610 mm (B24 2'), 910 mm (B36 3'), 1.2 m (B48 4'), 1.5 m (B60 5'), 1.8 m (B72 6'), 2.1 m (B84 7'), 2.4 m (B96 8') and with different arrangement of beam layups (see Table 3) have been carried out with a 18 span-to-depth ratio. Table 4 shows a summary of simulation results. It should be noted that B6, B12, B24, B36 corresponded with the tested beams.

Table 3. Beams layups

Beam layup cases								
Top								B96 (8') L64
							B84 (7') L56	Cc
							Cc	Cc
						B72 (6') L48	Cc	Cc
						Cc	Cc	Cc
					B60 (5') L40	Cc	Cc	Cc
					Cc	Cc	Cc	Cc
					Cc	Cc	Cc	Cc
					Cc	Cc	Cc	Cc
				B48 (4') L32	Cc	Cc	C	C
				Cc	Cc	C	C	C
				Cc	C	C	C	C
				Cc	C	C	C	C
			B36 (3') L24	Cc	C	C	C	C
			Cc	C	C	C	C	C
			Cc	C	C	C	C	C
			Cc	C	D	D	D	C
			C	C	D	D	D	D
			C	D	D	D	D	D
			C	D	D	D	D	D
			D	…..	…..	…..	…..	…..
		B16 (2') L16	D	D	D	D	D	D
		Cc	D	D	D	D	D	C
		Cc	D	D	D	D	D	C
		C	D	D	D	D	C	C
		C	D	D	D	D	C	C
		D	D	D	D	C	C	C
		D	D	D	D	C	C	C
		D	D	D	C	C	C	C
	B12 (1') L8	D	D	D	C	C	C	C
	Cc	D	D	C	C	C	C	B
	C	D	D	C	C	C	B	B
	D	D	C	C	C	B	B	B
B6 (1/2') L4	D	D	C	C	B	B	B	B
Cc	D	C	C	B	B	B	T1	T1
D	D	C	B	B	T1	T1	T1	T1
D	C	B	T1	T1	T1	T1	T1	T1
T1	T1	T1	T1	T1	T1	T1	T1	T1

Table 4. Summary of the simulation results

ULAG Simulation	B6 (1/2')	B12 (1')	B24 (2')	B36 (3')	B48 (4')	B60 (5')	B72 (6')	B84 (7')	B96 (8')
Mean Failure Load (KN)	64.51	106.03	181.23	271.98	336.78	400.58	469.23	517.10	581.35
5th%tile Failure Load (KN)	46.18	82.16	142.84	219.00	272.15	310.50	374.25	416.93	458.28
COV (%)	16.73	13.21	11.95	10.23	10.53	12.22	11.08	11.27	11.63
MORmean (MPa)	58.76	48.29	41.27	41.20	38.35	36.49	35.62	33.91	33.10
MOR5th%tile (MPa)	42.07	37.42	32.53	33.18	30.99	28.28	28.41	27.55	26.09
MOE (GPa)	12.27	11.93	11.43	11.38	11.50	11.34	11.51	11.65	11.51
Number of Simulation	1000	1000	1000	1000	1000	1000	1000	1000	1000
Depth (mm)	152	304	609	914	1216	1520	1824	2120	2432

4.2 Comparison of the Results

A comparison between the ULAG predicted strength properties and bending test results is summarized in Table 5. The cumulative probability distributions of the predicted strength and test results from the aforementioned beams are shown Fig. 1. As shown in Table 5, ULAG predictions have a maximum error of 4.14% and 8.93% observed for the mean and 5th% tile MOR values, respectively. Very good prediction accuracy by ULAG was confirmed.

Table 5. Comparison between the ULAG prediction strength and bending test results

ULAG vs. Test results	B6(1/2')		B12 (1')		B24 (2')		B36 (3')	
	ULAG	Test	ULAG	Test	ULAG	Test	ULAG	Test
Mean Failure Load (kN)	64.51	63.26	106.03	88.57	181.23	187.90	271.98	274.58
5th%tile Failure Load (kN)	46.04	50.53	82.16	72.06	142.84	144.05	219.00	N/A
COV (%)	16.73	12.48	13.20	13.41	11.95	13.28	10.23	12.30
MORmean (MPa)	58.76	57.92	48.29	48.32	41.27	43.05	41.20	41.78
MOR5th%tile (MPa)	42.07	46.20	37.42	39.35	32.53	33.29	33.18	N/A
MOE (GPa)	12.27	12.68	11.93	13.33	11.43	12.89	11.38	12.98
Sample Size	1000	30	1000	24	1000	36	1000	12
Error-MORmean	1.45%		0.06%		4.14%		1.38%	
Error-MOR5th%tile	8.93%		4.89%		2.29%			

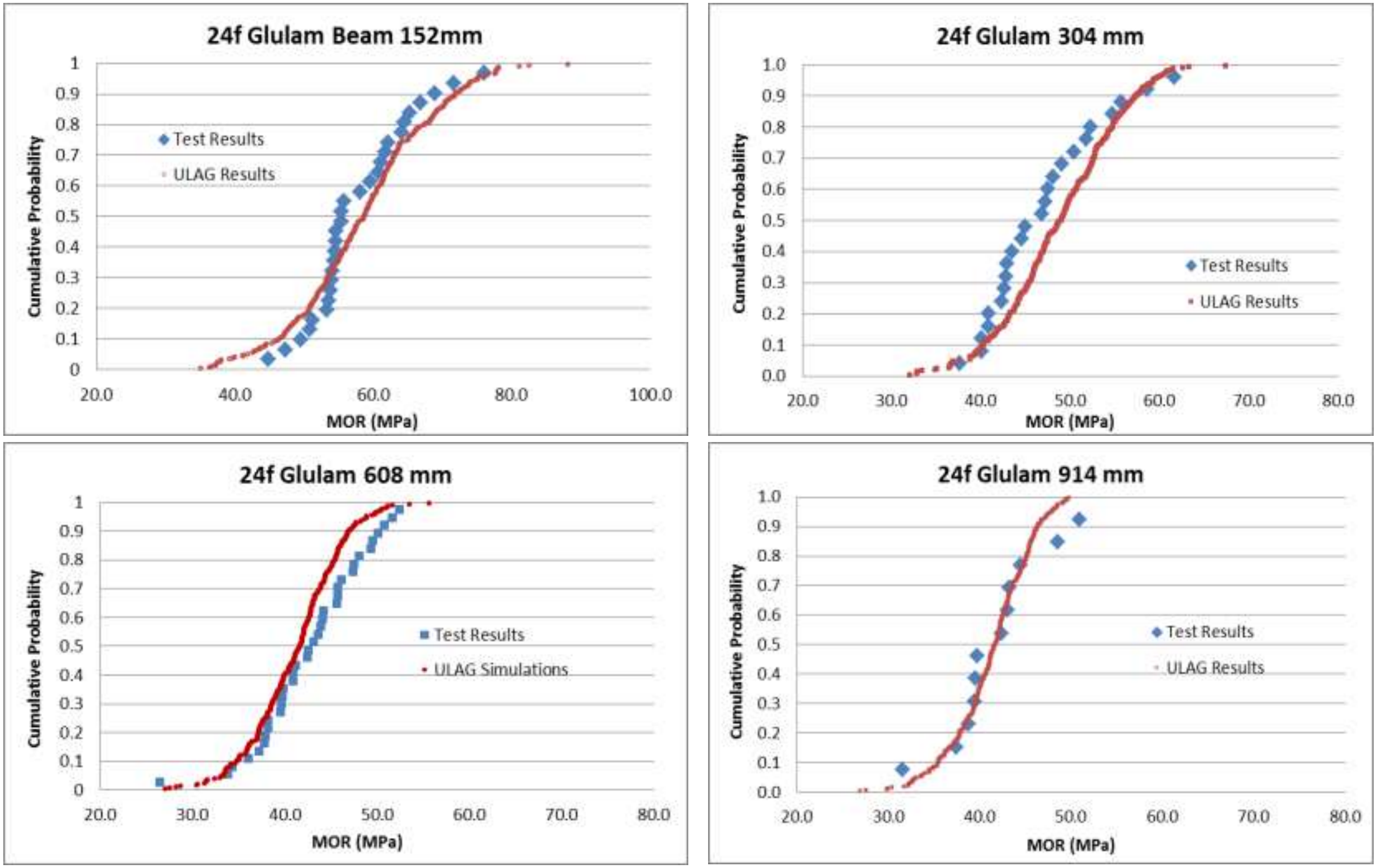

Fig. 1 Cumulative probability distributions of ULAG predicted strength and test results

5 Beam Size Effects in Bending

The simulated mean and fifth percentile strengths of the 610 mm deep beams were used as anchors to generate mean and fifth percentile strengths of different beam depths based on CSA and US (k=10), US (k=15) and US (k=20) procedures. Table 6 shows summary results of the size effect adjustment procedures. The relationship between the beam bending strengths with the beam volume is shown in Fig. 2.

Table 6. Summary results of the size effect adjustment procedures

Width	Depth	Length	Mean Load	Mean MOR	Volume	Adjustment Procedures based on			
						CSA	US	US'	US"
mm	mm	mm	(kN)	(MPa)	m^3	O86	k=10	k=15	k=20
130	152	2736	64.51	58.76	0.0541	41.27	54.47	49.66	47.41
130	304	5472	106.03	48.29	0.2163	41.27	47.42	45.28	44.24
130	609	10962	181.23	41.27	0.8679	41.27	41.27	41.27	41.27
130	914	16452	271.98	41.20	1.9548	38.36	38.05	39.10	39.63
130	1216	21888	336.78	38.35	3.4601	36.44	35.94	37.64	38.51
130	1520	27432.0	400.58	36.49	5.4206	34.99	34.36	36.53	37.66
130	1824	32918.4	469.23	35.62	7.8056	33.86	33.13	35.65	36.98
130	2120	38404.8	517.10	33.91	10.5844	32.93	32.14	34.93	36.42
130	2432	43891.2	581.35	33.10	13.8766	32.15	31.28	34.31	35.93
215	1219	21945.6			5.7516	33.27	34.16	36.38	37.55
215	1824	32918.4			12.9093	30.93	31.51	34.47	36.06
215	2128	38304.0			17.5248	30.10	30.56	33.78	35.51

Width	Depth	Length	5th%tile Load	5th%tile MOR	Volume	Adjustment Procedures based on			
						CSA	US	US'	US"
mm	mm	mm	(kN)	(MPa)	m^3	O86	k=10	k=15	k=20
130	152	2736	46.18	42.07	0.0541	32.53	42.94	39.14	37.37
130	304	5472	82.16	37.42	0.2163	32.53	37.38	35.69	34.87
130	609	10962	142.84	32.53	0.8679	32.53	32.53	32.53	32.53
130	914	16452	219.00	33.18	1.9548	30.24	29.99	30.82	31.24
130	1216	21888	272.15	30.99	3.4601	28.72	28.33	29.66	30.36
130	1520	27432.0	310.50	28.28	5.4206	27.58	27.08	28.79	29.68
130	1824	32918.4	374.25	28.41	7.8056	26.69	26.11	28.10	29.15
130	2120	38404.8	416.93	27.55	10.5844	25.96	25.33	27.53	28.71
130	2432	43891.2	458.28	26.09	13.8766	25.34	24.65	27.04	28.32
215	1219	21945.6			5.7516	26.22	26.92	28.68	29.59
215	1824	32918.4			12.9093	24.38	24.83	27.17	28.42
215	2128	38304.0			17.5248	23.72	24.09	26.62	27.99

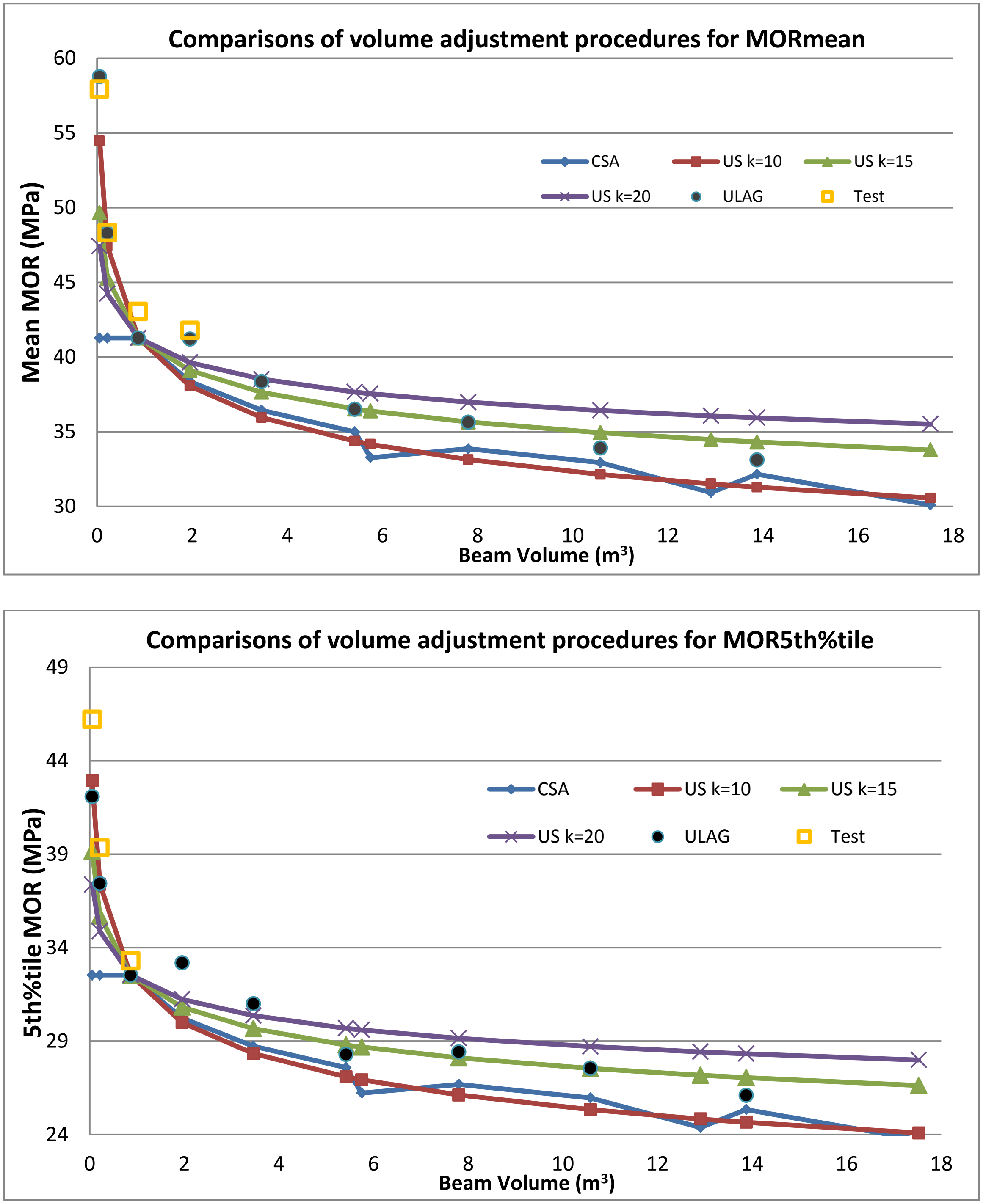

Fig. 2 Relationship between the bending strength with the beam volume factor

6 Recommendations for CSA O86

1) Allow beams smaller than the reference size to take advantage of size effect and be assigned higher design strengths;
2) Adopt the format of size effect adjustment to the US format;
3) The k factor can be conservatively kept at 1/10 pending the availability of more testing information and consider strategy of more conservative layups for deeper and wider beams or use a 1/15 factor for beams smaller than 1.8 m in depth (2x the deepest beam tested) and 1/10 for the bigger ones.

7 Acknowledgements

The authors express their sincere thanks to the Natural Resources of Canada Value to Wood program and the industrial partners, specially the Western Archrib-Structural Wood Systems and Structurlam Products for their financial and material support during the study. Authors also acknowledge Mr. Kent Fargey and Dr. Borjen Yeh for their technical supports during the study.

8 References

[1] DIN 1052 2004-2008, Design of timber structures-General rules and rules for building, Germany.

[2] ASTM. 2009. Practice for Establishing allowable properties for structural glued laminated timber (Glulam). Standard ASTM D 3737, American Society for Testing Materials, West Conshohocken, Pa.

[3] CAN/CSA-O86-09 Engineering Design in Wood, Canadian Standards Association, Rexdale, Ont.

[4] Moody, R., Falk, R., and Williamson, T. 1990. Strength of glulam beams-volume effects. Proc., the 1990 International timber engineering conference, Vol. 1: 176-182p, Tokyo, Japan.

[5] Lam, F., and Mohadevan, N. 2007. Development of New Construction of Glulam Beams in Canada. In Proc. Int'l Council for Building Research and Innovation in Building and Construction Working Commission W18-Timber Structures, Bled, Slovenia. CIB-W18/40-12-1. pp10.

[6] ASTM. 2009. Standard methods of static tests of timber in structural sizes. Standard ASTM D 198, American Society for Testing Materials, West Conshohocken, Pa.

CIB-W18/44-15-1

INTERNATIONAL COUNCIL FOR RESEARCH AND INNOVATION IN BUILDING AND CONSTRUCTION

WORKING COMMISSION W18 - TIMBER STRUCTURES

A PROPOSAL FOR REVISION OF THE CURRENT TIMBER PART (SECTION 8) OF EUROCODE 8 PART 1

M Follesa

Faculty of Civil Engineering, University of Cagliari

M Fragiacomo

Faculty of Architecture, University of Sassari

M P Lauriola

Faculty of Civil Engineering, University of Firenze

ITALY

MEETING FORTY FOUR

ALGHERO

ITALY

AUGUST 2011

Presented by M Follesa

V Enjily commented that this work just covered CLT but an important class of building products insulated panels consisting of I- beams were not considered. M Follesa replied that other building systems can be used provided that the ductility can be achieved.

A Ceccotti suggested that in EC8 there should be the possibility for designers to demonstrate the appropriate q factors for alternative systems. He expressed concern that the over strength factor of 1.6 for CLT may be too high based on his experience in the shake table test project in Japan where an engineered guess of 1.3 would be more reasonable. M Fragiacomo responded that based on single component test results it seemed that the over strength factor of 1.6 was appropriate. The work was still in progress.

A Buchanan provided explanation of the basis of the over strength factor of 2 used in New Zealand for nailed plywood connections in most timber structures. As there were difficulties in putting precise factors for different systems in the code, it would be more important to have the proper design philosophy recognized in the code. It would be important in codes to allow designers to come up with justifiable q factor.

S Pampanin further discussed the seismic design issues related drift values, yield displacements, stiffness, displacement based design and nonlinear design methods.

A proposal for revision of the current timber part (Section 8) of Eurocode 8 Part 1

Maurizio Follesa

Faculty of Civil Engineering, University of Cagliari, Italy

Massimo Fragiacomo

Faculty of Architecture, University of Sassari, Italy

Marco Pio Lauriola

Faculty of Civil Engineering, University of Firenze, Italy

Abstract

Section 8 of Eurocode 8 is very old (the first version was published in 1998) and quite short (6 pages in total). With regard to new building systems developed in Europe for the construction of multi-storey buildings, such as Cross Laminated Timber systems, there is a lack of design rules for the seismic design, and the few ones which may be applied are very conservative. Meanwhile important research projects have been completed, and the corresponding results can be used to propose new values for some important quantities for seismic design such as the behaviour factor. New detailing rules can also be suggested so as to ensure the energy dissipation corresponding to the overall target ductility is achieved. In this paper a first proposal for the revision of Section 8 of Eurocode 8 is presented. This proposal contains: (i) additional provisions for Capacity Based Design, including overstrength factors of ductile connections which are needed to avoid anticipated brittle failure mechanisms; (ii) more detailed description of the structural systems currently listed in the Eurocode 8 including other systems such as Log House buildings not currently considered; (iii) detailed verification of the current values of the behaviour factor according to the connection layout of each structural system; (iv) interstorey drift limits for performance-based design; (v) some provisions for the design of buildings with different lateral load resisting systems; and (vi) additional rules for shear walls and horizontal diaphragms.

1 Introduction

Eurocode 8 [1] deals with the design and construction of buildings and civil engineering works in seismic regions. Section 8 is the part related to the specific rules for timber buildings, which are considered as additional to those given in Eurocode 5 [2].

According to the general performance requirements and compliance criteria, all the structures should be designed to withstand the foreseen earthquake for that area. More specifically, in accordance with the so-called “no-collapse requirement”, the structure must be designed for the reference seismic action associated with a typical probability of exceedance of 10% in 50 years, corresponding to a reference return period of 475 years, so as it does not loose its structural integrity and it maintains a residual load carrying capacity after the earthquake. At the same time, the structure should also fulfil the “damage limitation requirements”, according to which the structure should survive an earthquake having a larger probability of exceedance (typically of 10% in 10 years, corresponding to a return period of 95 years) without the occurrence of damage and the associated limitations of use, the costs of which would be disproportionately high in comparison with the costs of the structure itself.

According to the performance-based design philosophy, the Limit States associated to the aforementioned conditions are the Ultimate Limit State and the Damage Limit State. In order to satisfy the Ultimate Limit State, structural systems shall be designed with an appropriate mixture of resistance and energy dissipation, which can be ensured only if ductile behaviour is achieved, and Capacity Based Design philosophy [3] is followed. In the definition given by Eurocode 8 [1], *"Capacity Based Design is the design method in which some elements of the structural system* (i.e. mechanical joints for the case of timber structures) *are chosen and suitably designed and detailed for energy dissipation under severe deformations while all other structural elements are provided with sufficient strength* (i.e. timber elements for the case of timber structures) *so that the chosen means of energy dissipation can be maintained"*.

As it is well explained in 2.2.2 2(P) of Eurocode 8 [1], "*The resistance and energy-dissipation capacity to be assigned to the structure are related to the extent to which its non-linear response is to be exploited. In operational terms such balance between resistance and energy-dissipation capacity is characterised by the values of the behaviour factor q and the associated ductility classification, which are given in the relevant Parts of EN 1998*". The behaviour factor q is defined as the "*factor used for design purposes to reduce the seismic actions in a linear static or modal analysis in order to account for the non-linear response of a structure, associated with the material, the structural system and the design procedures"* [1].

Therefore in order to ensure the achievement of the correct energy dissipation capacity assumed in the design, it should be verified that single structural elements and the structure as a whole are consistent with the chosen behaviour factor q. This condition may be regarded as fulfilled by applying the specific design rules and hierarchy of resistance criteria related to the various structural components for the different construction systems.

2.1 The current version of Section 8 of Eurocode 8

The current version of Section 8 of Eurocode 8 is divided into seven different parts, listed in the following:

General. Contains general information about this part of Eurocode 8, the specific terms related to timber structures and the design concepts.

Materials and properties of dissipative zones. In this part properties for materials and dissipative zones in seismic design are defined, particularly when using the concept of dissipative structural behaviour.

Ductility classes and behaviour factors. This is the most important part of the section, where the structural types permitted in seismic areas are listed and the relevant ductility class and behaviour factors defined in Table 8.1.

Structural analysis. In this section general information regarding the slip of joints, the Young modulus to be used in the analysis, and the detailing rules in order to consider horizontal diaphragms as rigid are given.

Detailing rules. Detailing rules for connections and horizontal diaphragms are given. Provisions for both carpentry and mechanical joints are also provided. However for horizontal diaphragms only light-frame floors are considered.

Table 8.1: Design concept, structural types and upper limit values of the behaviour factors for the three ductility classes.

Design concept and ductility class	**q**	**Examples of structures**
Low capacity to dissipate energy - DCL	1.5	Cantilevers; Beams; Arches with two or three pinned joints; Trusses joined with connectors.
Medium capacity to dissipate energy - DCM	2.0	Glued wall panels with glued diaphragms, connected with nails and bolts; Trusses with doweled and bolted joints; Mixed structures consisting of timber framing (resisting the horizontal forces) and non-load bearing infill.
	2.5	Hyperstatic portal frames with doweled and bolted joints (see **8.1.3(3)**P).
High capacity to dissipate energy - DCH	3.0	Nailed wall panels with glued diaphragms, connected with nails and bolts; Trusses with nailed joints.
	4.0	Hyperstatic portal frames with doweled and bolted joints (see **8.1.3(3)**P).
	5.0	Nailed wall panels with nailed diaphragms, connected with nails and bolts.

Safety verifications. In this part provisions for the k_{mod} and γ_M values to be used in the safety verifications are given for structures designed in accordance respectively with the concept of low dissipative and dissipative structural behaviour. In addition provisions are also given for the structural elements to which overstrength requirement applies in order to ensure the development of cyclic yielding in the dissipative zones, even though no value of the overstrength factor is given. Also detailing rules for carpentry joints to avoid brittle failure are given.

Control of design and construction. This latter section gives provisions on how the structural elements should be clearly detailed and identified in the design drawings and how they should be checked during the construction process.

2.2 What can be improved in Section 8 of Eurocode 8

The heading of Section 8 of Eurocode 8 is “Specific rules for timber buildings”, which should imply a clear definition and identification of the different structural systems for timber buildings. However, particularly for widely used structural systems such as cross-laminated (Xlam) and log house systems, it is sometimes hard to find the proper description in Table 8.1. This aspect is not irrelevant if we consider the importance of the correct choice of the ductility class and the relevant behaviour factor q according to the Capacity Based Design, which can be satisfied only by applying the specific design rules and hierarchy of resistance criteria provided for the specific construction system analysed. Moreover, for each structural system, it should be clearly stated the capacity design criteria and the specific design rules, as well as the overstrength factors.

Analysing the structural types listed in Table 8.1, it can be noticed that some of them are structural components of buildings, such as large span glulam roofs or timber buildings roofs (e.g. trusses with nailed, doweled or bolted joints); some other refer to structural systems used for old buildings (e.g. mixed structures consisting of timber framing and non-load bearing infill) but no longer used for new buildings; and only few of them clearly refer to residential buildings, which are the nowadays most commonly used type of construction.

Furthermore, some sentences should be corrected in order to avoid confusion or misunderstanding. For example in Table 8.1 the structural system "*Hyperstatic portal frames with doweled and bolted joints"* is mentioned twice, as a High Ductility Class with a q factor of 4.0 and as a Medium Ductility Class with a q factor of 2.5, depending on whether the specific requirements regarding the ductility capacity of connections given in 8.3.3(P) are or not satisfied, as specified in the subsequent Table 8.2. However, the structural system "*Nailed wall panels with nailed diaphragms*" is mentioned only once in Table 8.1 with the higher behaviour factor q, although the same ductility rule applies also for this system, thus generating possible confusion.

Also the ductility provisions given for the dissipative zones which limit the diameter of dowel type fasteners to 12 mm and the thickness of connected member to 10 times the fastener diameter in order to attain a ductile failure mechanism [4], appear to the Authors a limitation which could be superseded by requiring a failure mode characterized by the formation of one or two plastic hinges in the mechanical fastener, which can be easily checked using the Johanssen equations prescribed by the Eurocode 5 Part 1-1.

Finally some values of the behaviour factor q are considered by the Authors too high, especially in the lack of detailing rules and of Capacity Based Design criteria, such as the value of 4.0 for the behaviour factor q for "*Hyperstatic portal frames with doweled and bolted joints"*.

3 A proposal for a new Section 8 of Eurocode 8

The proposal consists of the following changes to the current version of Eurocode 8:

- Addition of a new section before the "Ductility classes and behaviour factors" entitled "Structural systems and capacity design rules" including detailed description of the main structural systems also using graphical sketches and definition of the overstrength factors for different types of connections.
- Correction of Table 8.1 and of some sentences in the "Ductility classes and behaviour factors" section.
- Some changes in the Detailing rules section including rules on structural systems with different lateral load resisting systems.
- Some changes in the Safety verification section including overstrength factors for Capacity Based Design and inter-storey drift limits for Performance based Design.

3.1 Structural systems for timber buildings and Capacity Based Design rules (New)

Timber buildings shall be classified into one of the following structural types according to their construction method:

- Cross laminated timber buildings
- Light-frame buildings
- Log House buildings

Other constructive systems used for the construction of timber buildings are:

- Mixed structures consisting of timber framing (resisting the horizontal forces) and non-load bearing infill
- Moment resisting frames
- Vertical cantilevers made of solid timber panels

Post and beam timber systems with vertical bracings made of timber or different materials (e.g. steel and reinforced concrete) can also be used, provided that the appropriate q factor associated with the reference type of bracing is assumed.

Mixed combinations of the above listed structural systems should be avoided in the same direction, however they are allowed in perpendicular directions. If different systems are used in the same direction, e.g. Light-frame buildings with XLam walls, non-linear static (push-over) or dynamic (time-history) analyses must be carried out to design the building.

Other structural systems used in seismic areas mostly for roof systems are:

- Arches with two or three pinned joints
- Beams and horizontal cantilevers
- Trusses with nailed joints
- Trusses with screwed, doweled and bolted joints

Different structural systems not listed above may be used provided that the properties of dissipative zones should be determined by tests either on single joints, on whole structures or on parts thereof in accordance with EN 12512 [5].

Cross laminated timber buildings

General Description

Cross laminated (Xlam) timber buildings are structures in which walls and floors are composed of cross laminated timber panels, i.e. panels made of an odd number (greater than 3) of layers of timber boards disposed alternatively at right angles and glued together.

The connection of the walls to the foundation should be made by means of mechanical fasteners (hold-down anchors, steel brackets, anchoring bolts, nails and screws) and should adequately restrain the wall against uplift and sliding. Uplift connections should be placed at wall ends and at opening ends, while sliding connections should be distributed uniformly along the wall length (Figure 1).

Walls shall have heights equal to the inter-storey height and may be made of a unique element up to the maximum transportable length or may be composed of more than one panel, of widths not greater than 2.6m, connected together by means of vertical joints made with mechanical fasteners (screws or nails). Perpendicular walls are connected by means of joints made with mechanical fasteners (usually screws).

Horizontal diaphragms are made of Xlam timber panels connected together by means of horizontal joints made with mechanical fasteners (screws or nails). The floor panels bear on the wall panels and are connected with mechanical fasteners (usually screws).

Other types of horizontal diaphragms may be used, provided that their in-plane rigidity is assured by means of sheathing material such as wood-based panels. Timber-concrete composite floors may be used provided that they are adequately connected to the lower and upper walls by means of mechanical fasteners. The concrete topping, in particular, shall be connected to the vertical panels to ensure the in-plane shear due to the diaphragm action is transferred to the walls and down to the foundations.

The upper walls will bear on the floor panels, and will be connected to the lower walls using mechanical fasteners similar to those used for the wall-foundation connection.

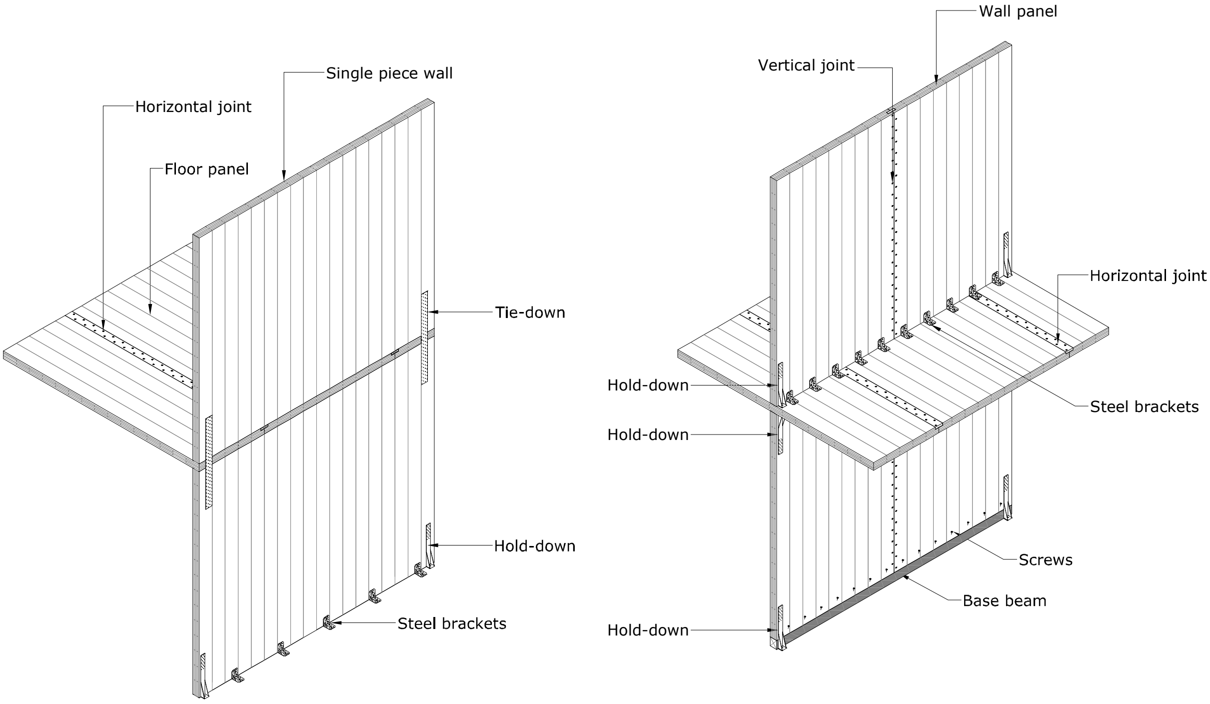

Figure 1: Walls and floors in Cross Laminated buildings

Capacity Design rules

Xlam timber buildings shall act at the greater possible extent as box-type structures. To achieve this, it is important to ensure that local failures which may compromise the box-type behaviour will not occur.

The connections devoted to the dissipative behaviour in a Xlam building are:

* vertical connection between wall panels in case of walls composed of more than one element;
* shear connection between upper and lower walls, and between walls and foundation;
* anchoring connections against uplift placed at wall ends and at wall openings.

In order to ensure the development of cyclic yielding in the dissipative zones, all other structural members and connections shall be designed with sufficient overstrength so as to avoid anticipated brittle failure. This overstrength requirement applies especially to (Fig.2):

* connections between adjacent floor panels in order to limit at the greater possible extent the relative slip and to assure a rigid in-plane behaviour;
* connection between floors and walls underneath thus assuring that at each storey there is a rigid floor to which the walls are rigidly connected;
* connection between perpendicular walls, particularly at the building corners, so that the stability of the walls itself and of the structural box is always assured;
* wall panels under in-plane vertical action due to the earthquake and floor panels under diaphragm action due to the earthquake.

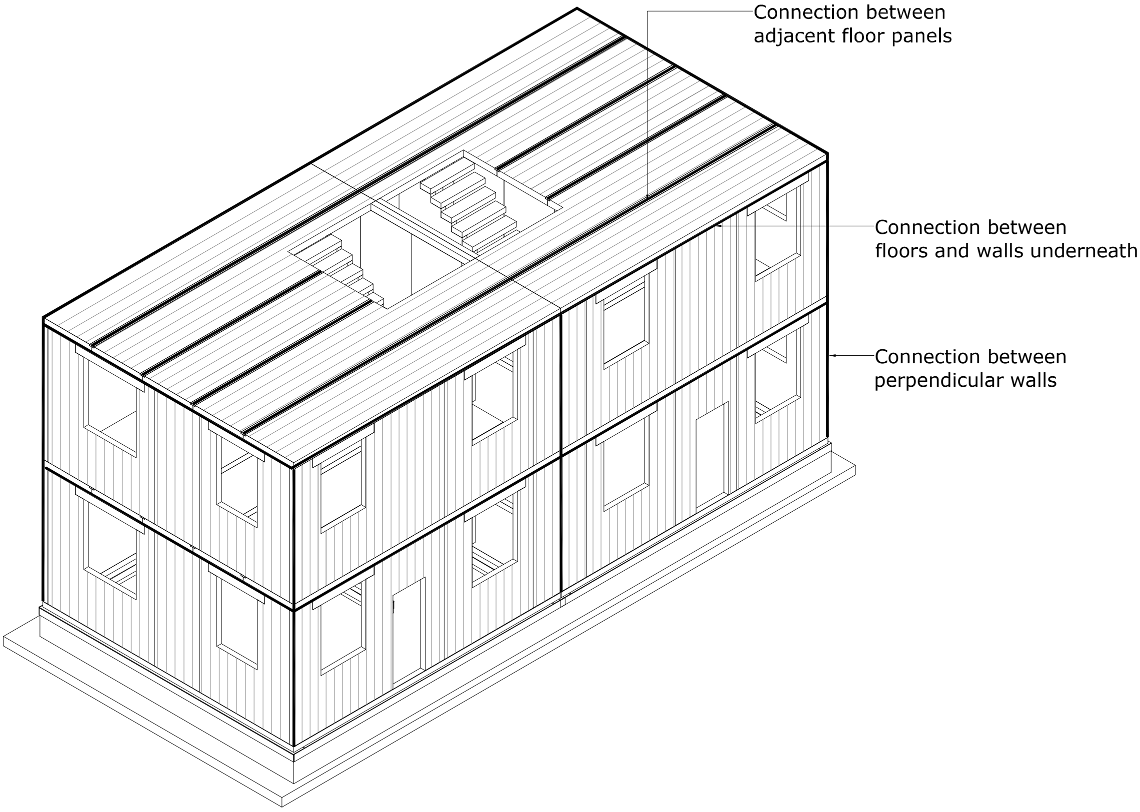

Figure 2: Connection to be designed with overstrength criteria in order to fulfil the capacity design criteria in Cross Laminated buildings [6].

The seismic resistance of shear walls should be higher at lower storeys and should decrease at higher storeys proportionally to the decrease of the storey seismic shear, thus leading to the simultaneous plasticization of the ductile connections in order to maximize the energy dissipation of the whole building.

Detailing rules

Nails other than smooth nails, as defined in EN 14592 [7], or screws should be used. Each single connection should be accurately detailed in order to avoid brittle failures. Special care should be used when designing the dissipative connections to ensure the attainment of a ductile failure mechanism characterized by the formation of one or two plastic hinges in the mechanical fastener [8]. A brittle failure mechanism in the weaker section of the steel plate should always be avoided in connections with steel brackets or hold-downs anchors connected to the wall panels by means of nails or screws.

Light-frame buildings

General Description

Light-frame buildings are structures in which walls, floors and roofs are made of timber frames to which a wood-based sheathing material (plywood or OSB) is connected by means of nails (Figure 3).

Shear walls are composed of a top and bottom plate and equally spaced vertical studs which the sheathing material is connected to on one or both sides.

Horizontal diaphragms are composed of equally spaced beams or joists and timber bridging in between, usually spaced at the same distance of wall studs, on top of which a wood-based sheathing material (plywood or OSB) is connected by means of nails. At each floor a perimeter edge beam should be provided to resist the tension forces which arise from the diaphragm action when the floor is loaded by horizontal forces acting in his plane.

The connection of the walls to the foundation should be made by means of mechanical fasteners (steel brackets, anchor bolts, nails and screws) and should adequately restrain the wall against overturning and sliding. Overturning connections should be placed at wall ends and at opening ends, while sliding connections should be distributed uniformly along the wall length.

Walls have heights equal to the inter-storey height. Perpendicular walls are connected by joining together two vertical studs with mechanical fasteners (usually nails or screws).

Other types of horizontal diaphragms may be used, such as cross laminated timber floors, provided that their in-plane rigidity is assured. Timber-concrete composite floors may be used provided that they are adequately connected to the lower and upper walls by means of mechanical fasteners. The concrete topping, in particular, shall be connected to the vertical panels to ensure the in-plane shear due to the diaphragm action is transferred to the walls and down to the foundations.

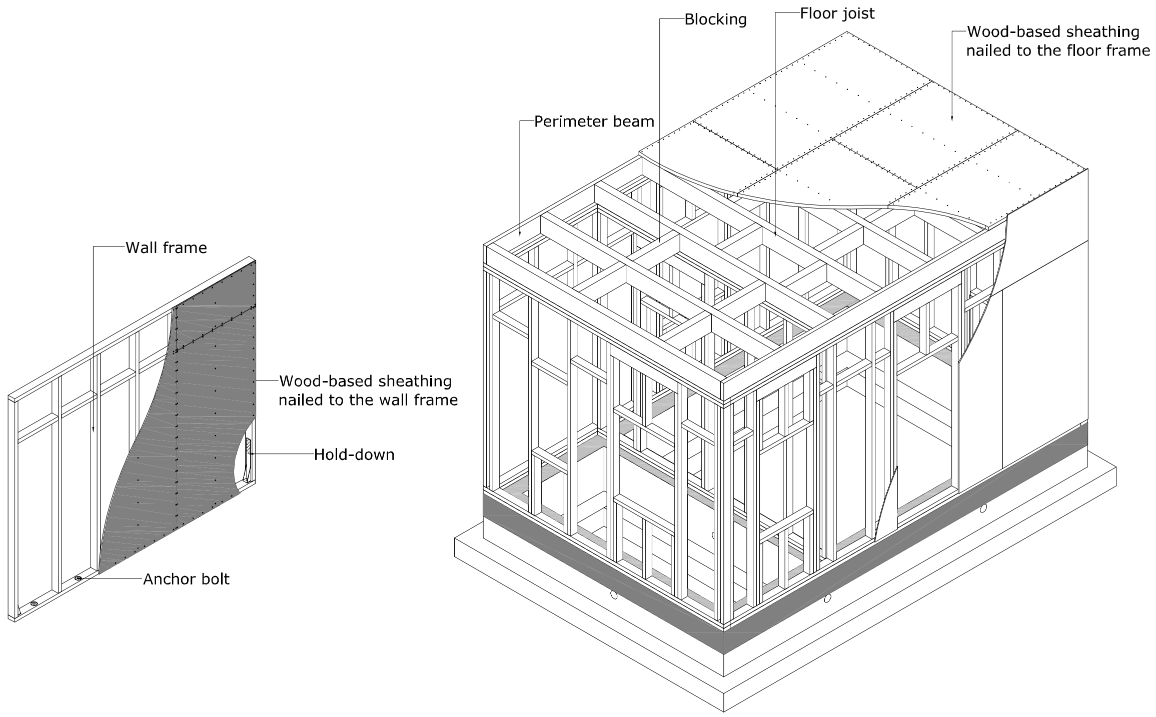

Figure 3: Walls and floors in light-frame buildings

Capacity Design rules

Light-frame buildings shall act at the greater possible extent as box-type structures. To achieve this it is important to ensure that local failures which may compromise the box-type behaviour will not occur.

The connections devoted to the dissipative behaviour in a light-frame building are nailed connection between sheathing material and timber frame in shear walls.

In order to ensure the development of cyclic yielding in the dissipative zones, all other structural members and connections shall be designed with sufficient overstrength so as to avoid anticipated brittle failure. This overstrength requirement applies especially to:

* nailed connections between sheathing and timber joists/beams at each floor;
* shear connections between upper and lower walls, and between walls and foundation;
* connections against uplift placed at wall ends and at wall openings;
* connection between floors and underneath walls thus assuring that at each storey there is a rigid floor to which the walls are rigidly connected;
* connection between perpendicular walls, particularly at the building corners, so that the stability of the walls itself and of the structural box is always assured;
* sheathing panels under in-plane shear induced by seismic actions;
* timber framing members (studs, plates, and joists) under axial forces induced by seismic actions.

The seismic resistance of shear walls should be higher at lower storeys and should decrease at higher storeys proportionally to the decrease of the storey seismic shear, thus leading to the simultaneous plasticization of the ductile connections in order to maximize the energy dissipation of the whole building.

Detailing rules

(omitted as this part will remained unchanged from the current version of EC8)

Log House buildings

General Description

Log House buildings are structures in which walls are made by the superposition of rectangular or round solid or glulam timber elements, prefabricated with upper and lower grooves in order to ease the overlapping and improve the stability of the wall, and connected together by means of steel tie-rods or screws (Figure 4).

The connection between perpendicular walls is made by means of carpentry joints obtained by notching the logs of the two walls or by means of screws.

Horizontal diaphragms are composed of equally spaced beams or joists and timber bridging in between, on top of which a wood-based sheathing made of plywood or OSB is connected with nails. At each floor a perimeter edge beam should be provided to resist the tension forces which arise from the diaphragm action when the floor is loaded by horizontal forces acting in his plane.

Other types of horizontal diaphragms may be used, such as cross laminated timber floors, provided that their in-plane rigidity is assured. Timber-concrete composite floors may be used provided that they are adequately connected to the lower and upper walls by means of mechanical fasteners. The concrete topping, in particular, shall be connected to the vertical panels to ensure the in-plane shear due to the diaphragm action is transferred to the walls and down to the foundations.

The connection of the walls to the foundation should be made by means of mechanical fasteners (tie rods, anchor bolts, nails and screws) and should adequately restrain the wall against overturning and sliding. Overturning connections should be placed at wall ends and at opening ends, while sliding connections should be distributed uniformly along the wall length.

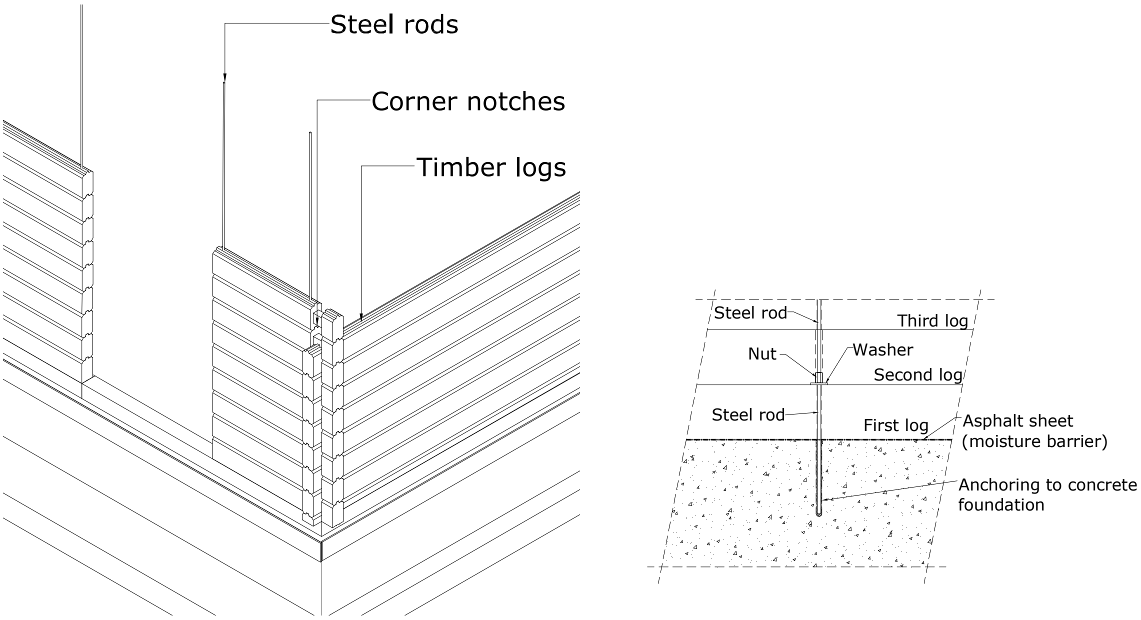

Figure 4: Perpendicular walls (left) and anchorage to foundation (right) details in Log House buildings

Capacity Design rules

Log house buildings shall act at the greater possible extent as box-type structures. To achieve this it is important to ensure that local failures which may compromise the box-type behaviour will not occur.

In order to ensure the development of the energy dissipation in the dissipative zones, all the connections to the foundation or between any massive sub-element should be designed with sufficient overstrength. To this regard also carpentry notching joints between perpendicular walls should be designed with sufficient overstrength.

The energy dissipation will be obtained due to friction between the logs.

Detailing rules

Carpentry joints between perpendicular logs which may fail due to deformations caused by load reversals, shall be designed in such a way that they are prevented from separating and remain in their original position.

Special care should be given to the design of wall openings in order to take into account shrinkage deformation due to moisture variations.

3.2 Ductility classes and behaviour factors (substituting the existing section)

Based on the previous capacity design criteria and design rules, the structural systems allowed in seismic areas are listed in Table 8.1, and the relevant ductility class and upper limit of the behaviour factors are given.

((2)and(3)P omitted as this part will remained unchanged from the current version of EC8)

(4) (*New*) The provisions of (3)P of this subclause and of 8.2(2) a) and 8.2(5) b) may be regarded as satisfied in the dissipative zones of all structural types except moment-resisting frames with high ductility joints and log house buildings if a ductile failure mechanism characterized by the formation of one or two plastic hinges in the mechanical fasteners is attained [8]. Referring to 8.2.2 of EN 1995-1-1 for timber-to-timber and panel-to-timber

connections, failure modes *a*, *b* and *c* for fasteners in single shear, and *g* and *h* for fasteners in double shear should be avoided. Referring to 8.2.3 of EN 1995-1-1 for steel-to-timber connections, failure modes *a*, *c* for fasteners in single shear, and *f*, *j* and *l* for fasteners in double shear should be avoided.

Table 8.1(New): Design concept, structural types and upper limit values of the behaviour factors for the three ductility classes.

Design concept and ductility class	**q**	**Examples of structures**
Low capacity to dissipate energy - DCL	1.5	Vertical cantilever walls. Beams and horizontal cantilevers. Arches with two or three pinned joints. Trusses joined with connectors (e.g. toothed metal plates). Moment resisting frames with glued joints
Medium capacity to dissipate energy - DCM	2.0	Cross laminated buildings with walls composed of a unique element without vertical joints. Log House Buildings. Trusses with screwed, doweled and bolted joints. Mixed structures consisting of timber framing (resisting the horizontal forces) and non-load bearing infill.
	2.5	Moment resisting frames with dowel-type fastener joints
High capacity to dissipate energy - DCH	3.0	Cross laminated buildings with walls composed of several panels connected with vertical joints made with mechanical fasteners (nails or screws) [6]. Trusses with nailed joints.
	4.0	Moment resisting frames with high ductility joints (e.g. densified veneer wood reinforced joints with expanded tube fasteners) [9]
	5.0	Light-frame buildings with nailed walls.

If the above requirement is not met, reduced upper limit values for the behaviour factor q, as given in Table 8.2, should be used.

Table 8.2 (New): Structural types and reduced upper limits of behaviour factors

Structural types	**Behaviour factor q**
Cross laminated buildings with walls composed of a unique element without vertical joints.	1.5
Trusses with screwed, doweled and bolted joints.	1.5
Mixed structures consisting of timber framing and non-load bearing infill.	1.5
Cross laminated buildings with walls composed of several panels connected with vertical joints made with mechanical fasteners (nails or screws).	2.0
Moment resisting frames with dowel-type fastener joints	2.0
Trusses with nailed joints.	2.0
Light-frame buildings.	3.0

In any case, special care should be used in dissipative structures to avoid brittle failure mechanisms such as shear plug, splitting and tearing of timber in the connection regions.

(5) (*New*) Moment-resisting frames with high-ductility joints are a special system which incorporate beam-column joints specifically designed to attain high ductility behaviour. An example is the use of densified veneer wood reinforced joints with expanded tube fasteners. The upper limit value of the behaviour factor listed in Table 8.1 can be used only if provision of (3)P for ductility class H structures is satisfied for the typical joint.

((6) omitted as this part will remain unchanged from the current version of EC8)

3.3 Safety verifications (additional)

All the structural members and connections which according to the reference Capacity Design rules are to be designed with sufficient overstrength so as to avoid anticipated brittle failure shall be dimensioned using the overstrength factors provided in Table 8.3. In the absence of any specific value within Table 8.3 for the dissipative connection used in the design, a conservative value of 1.6 shall be used for the overstrength factor.

Table 8.3 (New): Overstrength factors for typical structural types

Structural type	**Overstrength factor γ_{Rd}**
Trusses with doweled joints [10]	1.6*
Cross laminated timber buildings with walls composed of a unique element without vertical joints [8,11]	1.3**
Cross laminated timber buildings with walls composed of several wall panels connected with vertical joints made with mechanical fasteners (nails or screws) [11]	1.6**

*this value refers to the analytical prediction of the connection shear strength carried out using the formulas of connections with dowel-type fastener in the Eurocode 5 Part 1-1.
** this value refers to the experimental characteristic strength of the connection.

In order to meet the requirements for the Damage Limit State under a seismic action having a larger probability of occurrence than the design seismic action corresponding to the "no-collapse requirement" in accordance with 2.1(1)P and 3.2.1(3), the following limits applies:

a) for timber buildings having non-structural elements of brittle materials attached to the structure:

$d_r \nu \leq 0.005h$;

b) for timber buildings having ductile non-structural elements:

$d_r \nu \leq 0.010h$;

where

d_r is the design interstorey drift as defined in 4.4.2.2(2);
h is the storey height;
ν is the reduction factor which takes into account the lower return period of the seismic action associated with the damage limitation requirement.

4 Conclusions

A first proposal for revision of the current timber part (Section 8) of Eurocode 8 Part 1 is presented in this paper. The objective of this proposal is to start a discussion on the update of this part which is quite old, so as to reflect the current state of the art in timber construction and research in Europe. There is still some research that is needed to complete the proposal. Based on the current state-of-the-art of the research, only three structural types have their overstrength factors listed in Table 8.3, whereas values of the overstrength factor should be provided for all structural types with medium and high capacity to dissipate energy listed in Table 8.2. More information for capacity based design should be given, as well as additional design rules for the different structural systems such as moment resisting frames and cantilevered vertical walls which are being used more and more in modern timber buildings.

The proposal presented in this paper is based both on a large and long dating experience of some of the authors in the design of timber buildings in seismic areas in Europe, and on the results of important research projects undertaken in the last decade about the seismic behaviour of multi-storey timber buildings. It is mostly intended from the designer's benefit, trying to give as many indications as possible on the construction systems, the capacity design criteria and the detailing rules, and trying to avoid misunderstanding.

The concepts and principles contained in this paper may be considered as guidelines for proper design and detailing of timber buildings in seismic areas, leaving also the possibility for the designer to find new and appropriate solutions provided that their application is consistent with the Eurocode 8 general principles and criteria, according to the performance based design philosophy.

5 Acknowledgements

A very special thank to Prof. Ario Ceccotti of the Trees and Timber Institute of the Italian National Research Council (CNR-IVALSA), Sesto Fiorentino, Florence, for his fundamental contribution to this work. Thanks also to Eng. Davide Vassallo of Timber Engineering Associated, Florence for his precious contribution.

6 References

[1] European Committee for Standardization (CEN): "Eurocode 8: Design of structures for earthquake resistance – Part 1: General rules, seismic actions and rules for buildings." Brussels, Belgium, 2003.

[2] European Committee for Standardization (CEN): "Eurocode 5: Design of timber structures – Part 1-1: General rules and rules for buildings." Brussels, Belgium, 2004.

[3] T. Pauley, M.J.N. Priestley: "Seismic design of reinforced concrete and masonry buildings." Wiley Ed., 1992.

[4] A. Ceccotti, P. Touliatos "Detailing of timber structures in seismic areas." STEP Lecture D10, Timber Engineering STEP 2, 1995.

[5] European Committee for Standardization (CEN): "EN 12512: Timber structures - Test methods - Cyclic testing of joints made with mechanical fasteners." Brussels, Belgium, 2001.

[6] A. Ceccotti, M. Follesa, M.P. Lauriola "Which seismic behaviour factor for multi-storey buildings made of cross-laminated timber panels?" Proceedings of the 12th ANIDIS Conference, Pisa (Italy), June 14th–17th 2007 (in Italian).

[7] European Committee for Standardization (CEN): "EN 14592 - Timber structures - Dowel-type fasteners – Requirements." Brussels, Belgium, 2008.

[8] M. Fragiacomo, B. Dujic, I. Sustersic: "Elastic and ductile design of multi-storey crosslam massive wooden buildings under seismic actions." Engineering Structures, available online, doi:10.1016/j.engstruct.2011.05.020, 2011.

[9] A.J.M. Lejiten: "Densified veneer wood reinforced timber joints with expanded tube fasteners: the development of a new joint." Ph.D. Thesis, Delft University Press, the Netherlands, 1998.

[10] A. Jorissen, M. Fragiacomo: "General notes on ductility in timber structures." Engineering Structures, Special Issue on Timber Engineering, in print, 2011.

[11] I. Gavric, A. Ceccotti, M. Fragiacomo: "Experimental cyclic tests on cross-laminated timber panels and typical connections." Proceedings of the 14th ANIDIS Conference, Bari (Italy), September 18th-22nd 2011, CD.

CIB-W18/44-15-2

INTERNATIONAL COUNCIL FOR RESEARCH AND INNOVATION IN BUILDING AND CONSTRUCTION

WORKING COMMISSION W18 - TIMBER STRUCTURES

INFLUENCE OF VERTICAL LOADS ON LATERAL RESISTANCE AND DEFLECTIONS OF LIGHT-FRAME SHEAR WALLS

M. Payeur

Douglas Consultants inc,

A. Salenikovich

Université Laval

W. Muñoz

FPInnovations

CANADA

MEETING FORTY FOUR

ALGHERO

ITALY

AUGUST 2011

Presented by A Salenikovich

F Lam commented that given the seismic motions are three dimensional where upward accelerations can be expected, it might not be appropriate to rely on vertical loads for lateral resistance of wall systems. A Salenikovich agreed and commented that more discussions and studies on the topic would be needed.

B Dujic asked what force would be acting on the damaged stud as the information would be useful to gain understanding the rocking, uplift and shear mechanisms. A Salenikovich clarified that the forces in the damaged studs were not monitored.

Influence of vertical loads on lateral resistance and deflections of light-frame shear walls

M. Payeur[1], A. Salenikovich[2], W. Muñoz[3]

[1] Douglas Consultants inc, Canada

[2] Université Laval, Canada

[3] FPInnovations, Canada

Abstract

This experimental study is focused on the influence of vertical loads on the lateral resistance and deflections of light-frame walls. A total of 43 static and cyclic racking tests were performed on full-size walls with and without hold-downs with simultaneous application of uniformly distributed vertical load of different magnitudes. The wall specimens were 2.44×2.44 m and 2.44×4.88 m fully sheathed with OSB panels on one side. Control specimens were tested without vertical load according to relevant ASTM standards. Additional tests were performed on walls with hold-downs and vertical load. Lateral resistance values were predicted using European and North-American methods and compared with test results. Predictions of wall deflections were based on the formulas proposed in the Canadian timber design standard CSA-O86. This report includes discussion of the results and recommendations.

1 Introduction

Building structures must be designed to adequately resist the gravity loads (dead and live) and the lateral loads (wind and seismic). In the latter case, shear and overturning forces and deflections occur in the structure. In light-frame construction, it is diaphragms and shear walls that transfer these forces to the foundation through shear and hold-down restraint. The use of hold-down anchoring devices limits the overturning and therefore improves the lateral resistance of the system. However, these anchors are rarely used in the traditional light-frame construction and the resistance of such systems is largely unknown. One of the factors limiting the overturning of partially restrained bracing walls is the action of the gravity loads.

A few past studies focused on walls under combined vertical and lateral loads. In Canada, Ni and Karacabeyli [1] tested 2.44-m square walls under different magnitudes of vertical load. They showed that the rate of increase in lateral load capacity is a non-linear function of the applied vertical loads and they proposed two methods of prediction: empirical and mechanics-based. Later, Ni and Karacabeyli [2] also developed a mechanics-based model to predict the deflections of walls without hold-downs. Test results on 2.44-m square walls showed up to 67% higher deflections than predicted at the design level. The mechanical models have been adopted by the Canadian Wood Design Standard (CSA-O86) [3].

In the US, earlier study by Salenikovich [4] and subsequent development by the American Wood Council [5] were aimed at development of a mechanics-based design methodology for walls with and without hold-down restraint. In Europe, theoretical and experimental works by Källsner *et al*. [6], [7] led to the development of a Unified Design Method (Method C) for the racking resistance of timber framed walls for inclusion in Eurocode 5 [8].

Previously, Dujič and Žarnić [9] showed that shear walls are very sensitive to boundary conditions and to the method of applying the gravity load to the test specimens. However, the tests for combined racking and vertical loading are not standardized yet. In addition, the boundary conditions, i.e. transfer of the load to partially anchored walls, are not always realistic in current standards (e.g. [12], [13]). For example, the racking load is usually applied to the specimen through a rigid steel bar attached to the top plate of the wall. In this case, the performance of the specimen may be overestimated as it is augmented by the stiffness of the load distribution beam. When testing partially anchored walls, the rigid steel bar may also provide additional restraint against the wall uplift. A test facility eliminating this shortcoming was developed for this study with the goal to correlate properly the lateral resistance and the magnitude of the gravity load applied to the test specimen.

The objective of this study was to verify experimentally the predictions of the various models of light-frame wall performance under combined racking and vertical loads.

2 Predictions of the lateral resistance

In this section, four methods of calculation of the lateral resistance of partially anchored walls considering the vertical loads are presented. Using these methods one can calculate a reduction factor ($R \leq 1.0$) representing the ratio of the lateral resistances of a partially anchored wall and a fully anchored wall of the same configuration. Note that the notation used may differ from the original publications to facilitate the presentation and comparison.

Although three of these methods are mechanics-based, they produce different results due to different assumptions of the force distributions in the sheathing-to-framing connections, as shown in Figure 1. In these methods, it is assumed that all sheathing-to-bottom plate nails reach their ultimate shear capacity in either vertical (uplift) or horizontal (shear) directions or in combination of both.

2.1 Ni & Karacabeyli (empirical model)

The first one is the empirical approach developed by Ni and Karacabeyli [1] by fitting Equation 1 to their experimental results of racking test on 2.44-m square walls:

$$R = \frac{1}{1 + \frac{h}{l}\left(1 - \phi\right)^{3}} \tag{1}$$

where h = height of the wall, l = length of wall, and

$$\phi = \frac{P}{\upsilon h}$$

where P = vertical reaction at the end of the wall due to applied gravity loads (including the wall self weight), and υ = ultimate unit lateral resistance of a fully anchored wall.

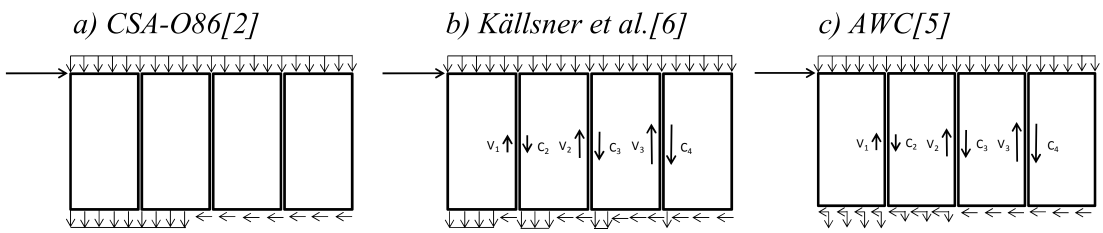

Figure 1. Force distributions in mechanics-based models.

2.2 CSA-O86

The mechanics-based method developed by Ni and Karacabeyli [1], is more conservative than their empirical approach and is relatively simple to use. It is why CSA-O86 [3] adopted this method in 2001 edition. In this simplified model, the wall is considered rigid, shear forces are transmitted between panels and no axial force is generated in the stud. As seen in Figure 1a, when the chord is not anchored to the foundation with a hold-down, a group of nails along some portion of the bottom plate will resist overturning leaving the rest of nails to resist the racking and base-shear forces. The reduction factor essentially accounts for the number of nails resisting the horizontal shear forces and is calculated as follows:

$$R = \sqrt{1 + 2\frac{P}{V_{hd}} + \left(\frac{h}{l}\right)^2} - \frac{h}{l} \tag{2}$$

where V_{hd} = ultimate lateral resistance of fully anchored wall.

2.3 Källsner et al.

The Unified Design Method (Method C) developed for Eurocode 5 is based on one of the mechanics-based models developed by Källsner *et al*. [6], [7], [8]. In this paper, the lower bound plastic method [6] is considered where the compressive forces are not transferred between sheathing panels. When two adjacent panels rotate and slide pass each other they transfer the axial forces to the studs through sheathing nails. The equilibrium of forces and moments is studied for each panel and, similar to the CSA-O86 model, some fasteners resist the overturning, and the other - the racking force (Figure 1b). The lateral resistance of the first panel is calculated using Equation 2 where the length of the wall (l) is replaced by the width of the sheathing panel (b). Starting with the second panel, each subsequent calculation must consider the effect of anchorage coming from the preceding panel:

$$C_i = V_{i-1} \tag{3}$$

where C_i = overturning restraint from the preceding panel and V_{i-1} = compressive force developed in the preceding panel.

Note that the overturning restraint cannot exceed the maximum shear capacity of the sheathing-to-stud connection ($C_i \leq \upsilon h$). The compressive force developed in a panel is calculated as follows:

$$V_i = G_i + \upsilon b(1 - R_i) + C_i \tag{4}$$

where G_i = sum of vertical loads applied on the top plate along the panel, b = width of sheathing panel and R_i = reduction factor of the i-th panel (Equation 5).

The formulation of this method considering only uniformly distributed vertical load is:

$$R_i = \sqrt{1 + 2\frac{C_i}{b\upsilon} + \frac{\omega}{\upsilon} + \left(\frac{h}{b}\right)^2} - \frac{h}{b} \tag{5}$$

where ω = uniformly distributed vertical load.

Once the reduction factors are calculated for each panel, the total reduction factor for the full length of the wall is taken as the average of all reduction factors.

2.4 AWC

The last model considered in this study is being developed by the American Wood Council [5] for inclusion in the NDS. Similar to the eariler Källsner's model, the lateral resistance is calculated for each panel. The difference is that all sheathing-to-bottom plate fasteners in one panel are considered resisting uniformly the horizontal shear and overturning until it is completely restrained. Therfore, the anchor effect of the preceding panel is different:

$$V_i = G_i + \upsilon b\sqrt{1 - R_i^2} + C_i \tag{6}$$

The general formulation considering uniformly distributed vertical load is relatively complex, so it is convenient to present the reduction factor as a root of quadratic equation:

$$R_i = \frac{-b + \sqrt{b^2 - 4ac}}{2a} \tag{7}$$

where

$$a = 1 + \left(\frac{2h}{b}\right)^2 \qquad b = -\frac{4h}{\upsilon b}\left(\frac{2C_i}{b} + \omega\right) \quad \text{and} \quad c = \frac{4C_i}{\upsilon^2 b}\left(\frac{C_i}{b} + \omega\right) + \left(\frac{\omega}{\upsilon}\right)^2 - 1$$

3 Prediction of wall deflection

The prediction of the lateral deflection of the top of the wall proposed by Ni and Karacabeyli [2] is included in the latest CSA-O86-09 edition [3] in the form of Equation 8, which consists of four terms: 1) deflection of the chords, 2) shear deformation of sheathing panels, 3) slip of sheathing nails, and 4) rotation of the wall due to the uplift movement of the tension chord.

$$\Delta_{sw} = \frac{2vh^3}{3EAl} + \frac{vh}{B_v} + 0.0025he_n + \frac{h}{l}d_a \tag{8}$$

where v = unit shear load at the top of the wall (N/mm), EA = axial stiffness of the chords (N), B_v = shear-through-thickness rigidity of the sheathing (N/mm), e_n = sheathing nail slip (mm), d_a = total vertical elongation of the wall anchorage system (mm).

For walls with hold-downs, d_a at design load is specified by the manufacturer and can be calculated in proportion to the reaction at the tension chord $R = (vh - P)$. For walls without hold-downs, d_a is calculated using the following equation:

$$d_a = 2.5 d_F K_m \left[\frac{(vh - P)\dfrac{s_n}{l}}{n_u} \right]^{1.7} \tag{9}$$

where d_F = sheathing nail diameter (mm), K_m = service creep factor, s_n = nail spacing around the panel edge (mm), and n_u = lateral resistance of the nails (N).

4 Test materials and methods

The shear wall test setup (Figure 2a) has been developed at Université Laval to allow application of uniformly distributed vertical load to the top plate simultaneously with the racking load and to minimize the influence of the load distribution bar on the specimen performance. Details of the setup and equipment are discussed in [10] and [11].

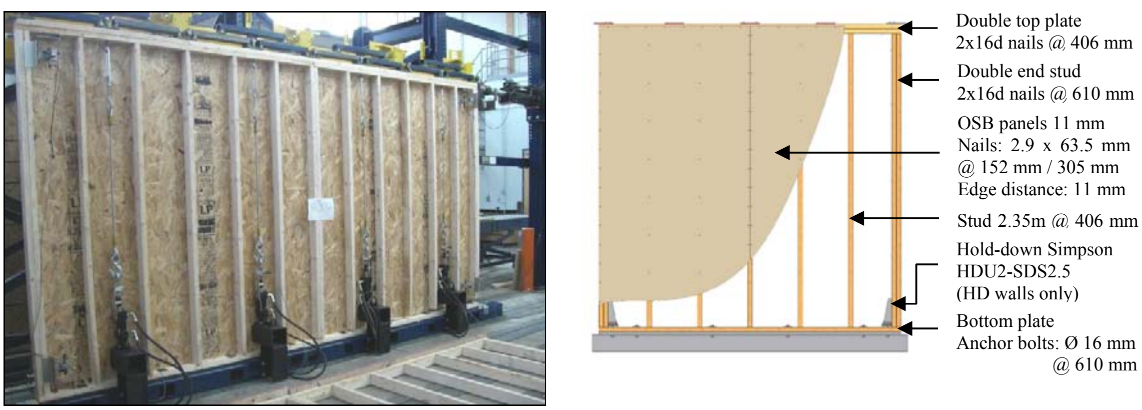

Figure 2. a) Test setup, b) Construction details of test specimens.

Test specimens were 2.44×2.44-m and 2.44×4.88-m walls. Control specimens (HD) were fully anchored to the base, i.e. attached with hold-downs and shear bolts; other specimens (NHD) were partially anchored, i.e., without hold-downs. Construction details of the specimens are shown in Figure 2b and discussed in [10] and [11]. The frames were built with 38x89-mm spruce-pine-fir (SPF) kiln-dry lumber, grade #2 & Better. In order to minimize variability of test data, all framing elements were sorted using E-computer in a way to maintain the average modulus of elasticity (MOE) of the framing members at the panel edges constant between specimens.

Half of the specimens were tested under static loading and another half - under cyclic loading. The static tests followed ASTM E564 [12] standard guidelines except that specimens were preloaded once to 25.4-mm displacement followed by a ramp loading at 15 mm/min. (Figure 3a). The cyclic tests followed ASTM E2126 [13] guidelines with Method C (CUREE basic loading protocol). The amplitude of cycles was determined by a ratio of a reference displacement, Δ (Figure 3b), corresponding to 60% of the displacement at failure of a static test specimen of the same configuration or to 2.5% of the panel height, whichever was less. A low frequency of excitation (0.1 Hz) was used to minimize inertial effects.

The following vertical loads acting on the wall were considered: a) self weight of the wall (0.35 kN/m), b) roof weight (1.0 kN/m), c) weight of one top storey and roof (3.5 kN/m), and d) load necessary to prevent the overturning. The first case represented standard testing conditions where no additional vertical load was applied to the specimen except for the weight of the test equipment (≈0.19 kN/m for 2.44-m long wall and ≈0.16 kN/m for 4.88-m long wall). The weight of the equipment was included in the estimations of the additional vertical loads in cases b), c) and d). To calculate the load necessary to prevent the overturning, the CSA-O86 method (Equation 2) was used, where V_{hd} was taken as the average lateral resistance of the fully anchored walls tested cyclically without additional vertical load. Not including the self weight of the wall, this distributed load was estimated at 8.0 kN/m for 4.88-m long wall and 16.3 kN/m for 2.44-m long wall.

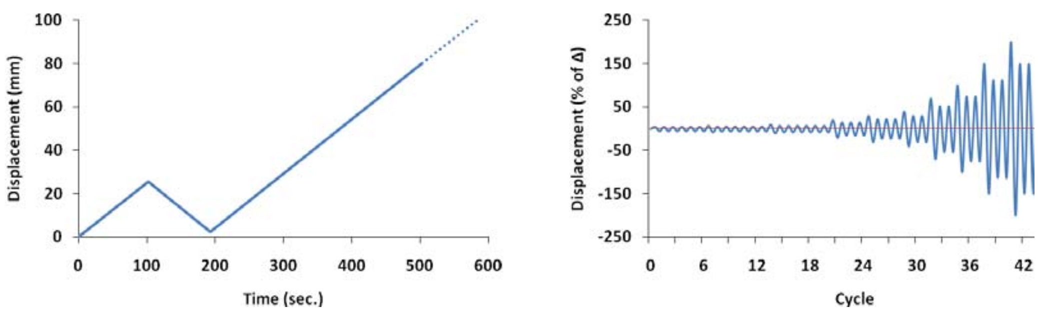

Figure 3. Displacement protocols: a) Static, b) Cyclic.

5 Results

The experimental program included 43 specimens with two replications per test configuration (except one 4.88-m HD static test with 3.85 kN/m gravity load). Figure 4 shows experimental load-deflection curves (average envelope curves in case of cyclic tests) along with the corresponding deflections calculated according to CSA-O86 (Equation 8) with the nail slip values taken from the prior tests by Muñoz [15] on similar materials. Table 1 shows the lateral resistance and reduction factors obtained from the experiments. These values are presented in Figure 4 along with the predictions of resistance according to the four methods.

It can be seen from the data that no significant differences were observed between the static and cyclic lateral resistance of the matched specimens (except one replication of static test 4.88-m NHD wall under 1.0 kN/m vertical load, which was about 13% lower than three other matched specimens). This low variation of results confirms proper matching of framing materials and consistent quality of the specimen assembly which assures confidence in the obtained results despite the low number of replications.

The additional gravity load (3.5 kN/m) did not add nor reduce the lateral capacity, stiffness or ductility of fully anchored walls. Similar conclusion was made by Dean and Shenton [16] who applied even greater vertical load to the walls with hold-downs.

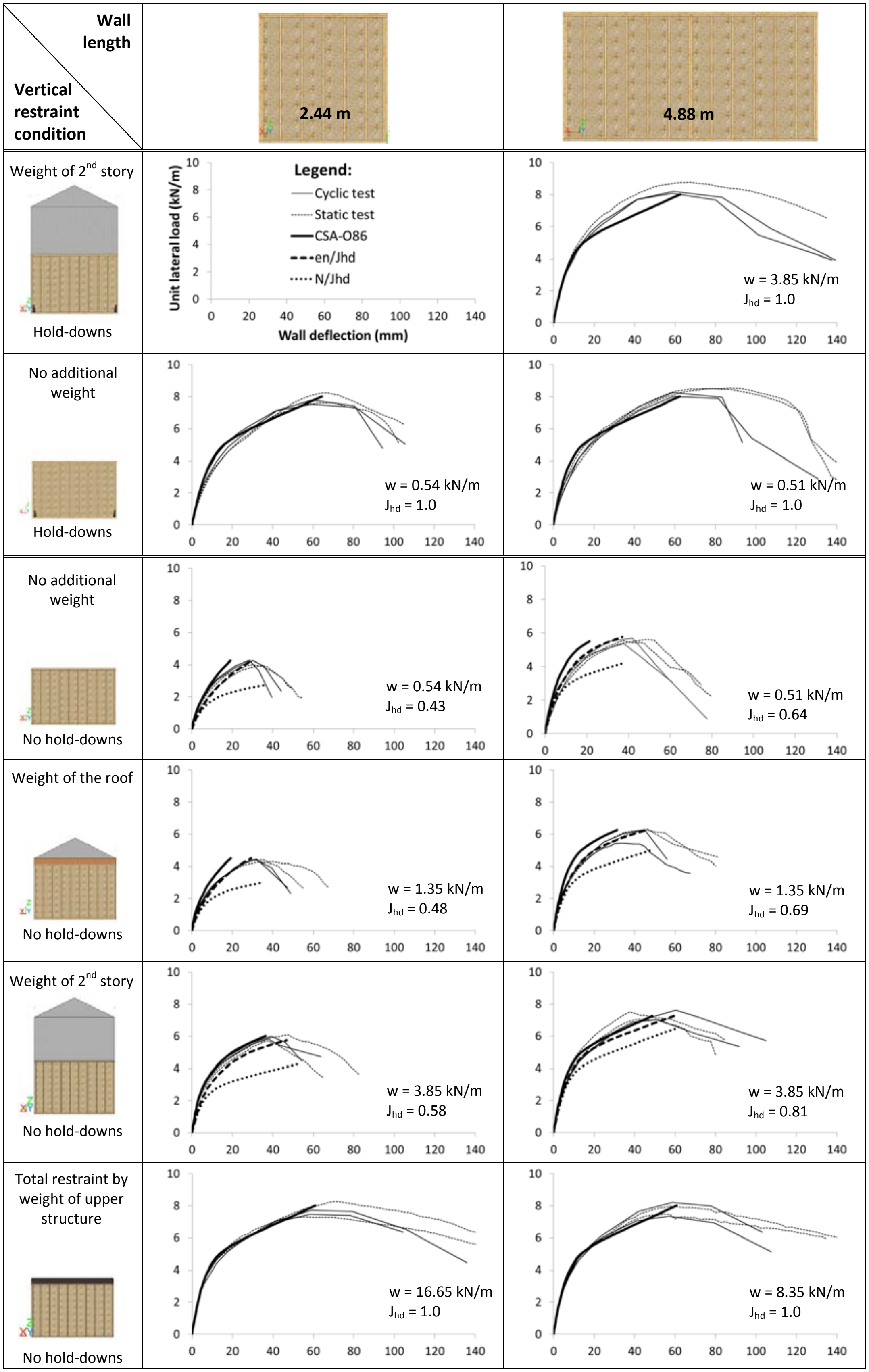

Figure 4. Experimental and predicted load-deflection curves.

Table 1: Lateral resistance of 2.44-m walls (left) and 4.88-m walls (right)

HD or NHD	Vertical load† (kN/m)	Cyclic tests		Static tests	
		Lateral load (kN)	*R*††	Lateral load (kN)	*R*††
HD	0.54	19.0	1.02	18.6	0.99
		18.4	0.98	20.2	1.08
NHD	0.54	10.4	0.56	9.8	0.52
		10.4	0.56	9.7	0.52
	1.35	10.7	0.57	10.4	0.56
		10.8	0.58	10.9	0.58
	3.85	14.1	0.75	14.7	0.79
		14.5	0.78	13.8	0.74
	16.65	17.8	0.95	16.9	0.90
		17.2	0.92	19.0	1.02

† Including the self-weigh of the wall and the test equipment.
†† Based on the average lateral load capacity of fully anchored walls tested cyclically without additional vertical load.

HD or NHD	Vertical load† (kN/m)	Cyclic tests		Static tests	
		Lateral load (kN)	*R*††	Lateral load (kN)	*R*††
HD	0.51	39.1	0.98	41.7	1.05
		40.2	1.01	41.6	1.05
	3.85	39.4	0.99	42.8	1.08
		40.0	1.01	-	-
NHD	0.51	27.7	0.70	26.7	0.67
		26.1	0.66	27.5	0.69
	1.35	30.8	0.78	30.4	0.77
		30.6	0.77	26.6	0.67
	3.85	34.3	0.86	34.7	0.87
		37.2	0.94	36.9	0.93
	8.35	35.8	0.90	36.9	0.93
		40.0	1.01	38.9	0.98

Comparing the predictions of the lateral resistance, it can be seen that the Källsner *et al.* [6] model in fact represents the lower bound solution whereas other models predict somewhat higher values. The CSA-O86 method yields the same predictions at lower vertical loads (up to 8 kN/m for 2.44-m walls, and up to 4 kN/m for 4.88-m walls), while the AWC method converges to the European model at higher vertical loads. The empirical method of Ni and Karacabeyli always predicts higher values in the cases studied.

Experimental results supported the empirical model of Ni and Karacabeyli for 2.44-m walls at light gravity loads (up to one top storey and roof) but it was not evident that the model would provide conservative estimate for higher loads and longer walls. The CSA-O86 mechanical model proved to provide conservative estimates for low-rise buildings, but it would overestimate the wall lateral capacity up to 10% at higher loads, as partially anchored walls showed a tendency not to render a 100% resistance of the fully anchored walls as predicted assuming the full contact between the sheathing panels. The Källsner *et al.* method [6] proved to be the lower bound estimate in all cases studied and its predictions were always on the conservative side. The AWC model being conservative at high vertical loads appeared somewhat less conservative in cases with minimum gravity loads.

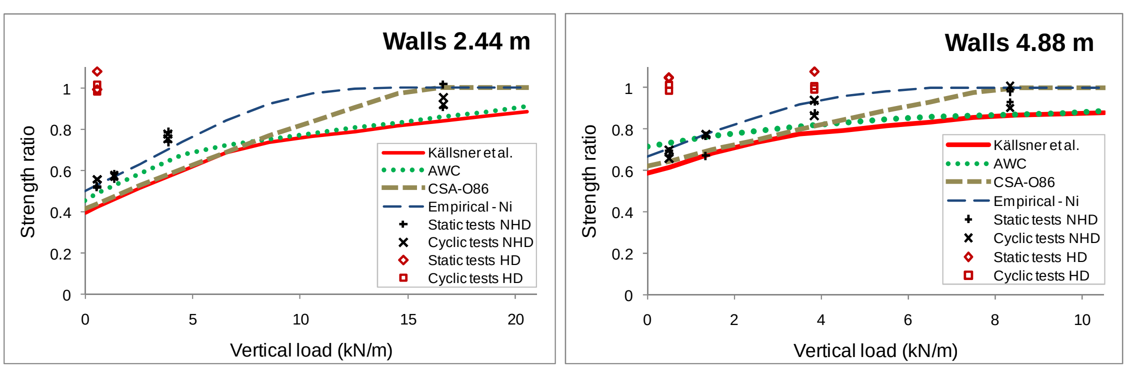

Figure 5. Comparison of four calculation methods with experimental results.

Figure 4 shows that the deflections can be predicted very well up to the maximum load using the CSA-O86 (Equation 8) for highly restrained walls ($J_{hd} \rightarrow 1.0$), while for poorly restrained walls the deflections appear to be underestimated. Ni and Karacabeyli [2] made the same observation and suggested that the nail slip was underestimated. We attempted to remediate this shortcoming in two alternative ways: a) by factoring the nail slip: e_n/J_{hd} or b) by factoring the force acting on the nails: N/J_{hd} when calculating e_n. Results are shown graphically in Figure 4 and comparisons of the wall deflections at the factored design load are shown in Table 2. The adjustments seem to improve the predictions for the walls without hold-downs; although, the latter adjustment (N/J_{hd}) appears excessive. Similar tendencies are observed if the experimental nail slip values are replaced by those from the standard [3] (see Appendix).

Table 2: Experimental and predicted deflections: 2.44-m walls (left) and 4.88-m walls (right)†

HD or NHD	Vertical load (kN/m)	Test average†† (mm)	Equation 8		
			e_n	e_n/J_{hd}	N/J_{hd}
HD	0.54	12.55	9.78	9.78	9.78
		1.00	0.78	0.78	0.78
NHD	0.54	4.96	4.05	6.48	8.93
		1.00	0.82	1.31	1.80
	1.35	5.54	4.05	6.48	8.93
		1.00	0.73	1.17	1.61
	3.85	3.90	3.65	5.67	7.68
		1.00	0.94	1.45	1.97
	16.65	9.38	8.09	8.09	8.09
		1.00	0.86	0.86	0.86

† Deflections are shown in mm. Grey cells show the ratio of the predicted deflection and the average test value.
†† Average deflection of all tested specimens at the factored design load (4.0 kN × J_{hd}).

HD or NHD	Vertical load (kN/m)	Test average†† (mm)	Equation 8		
			e_n	e_n/J_{hd}	N/J_{hd}
HD	0.51	11.62	8.77	8.77	8.77
		1.00	0.76	0.76	0.76
	3.85	9.06	8.77	8.77	8.77
		1.00	0.97	0.97	0.97
NHD	0.51	6.57	4.35	6.16	8.14
		1.00	0.66	0.94	1.24
	1.35	6.03	4.61	6.25	7.90
		1.00	0.76	1.04	1.31
	3.85	7.82	5.45	6.52	7.65
		1.00	0.70	0.83	0.98
	8.35	9.13	7.96	7.96	7.96
		1.00	0.87	0.87	0.87

6 Conclusions

A total of 43 light-frame 2.44×2.44-m and 2.44×4.88-m walls were tested under combined lateral and vertical loads of various magnitudes to compare their racking resistance and deflections with different prediction models.

No significant differences were observed between static and cyclic (CUREE basic protocol) test results. No adverse influence of additional vertical gravity load on the performance of fully anchored walls was noticed.

Comparisons of the lateral resistance showed the model by Källsner *et al*. [6] to be the most conservative and the empirical model (Ni and Karacabeyli) to be the least conservative with the CSA-O86 and AWC models in between. Comparison with test results shows that despite some differences, the methods considered in this study seem to provide overall reasonable estimates of the lateral capacity of light-frame walls under vertical loads in the practical range. It is a matter of preference by the code developing bodies to integrate one model or another in the engineering practice.

To improve prediction of the deflection of walls without hold-downs, the nail slip may be adjusted using the J_{hd} factor.

Acknowledgements

This research was made possible through the financial support of the Développement économique Canada pour les régions du Québec Projet Valeur ajoutée en génie du bois and the Natural Sciences and Engineering Research Council of Canada (NSERC) Discovery Grants Program. Hold-down anchors were provided by Simpson Strong-Tie free of charge. The research team would like to express their gratitude to Sylvain Auger, Éric Rousseau and Frédéric Nepton of Wood Research Centre at Université Laval for their assistance with the laboratory.

References

[1] Ni, C. and E. Karacabeyli: Capacity of shear wall segments without hold-downs. Wood Design Focus 12(2):10-17, 2002.

[2] Ni, C. and E. Karacabeyli: Deflections of nailed shearwalls and diaphragms. In: *Proceedings WCTE 2004*, Lahti, Finland, Vol. 3a: 259-262, 2004.

[3] Canadian Standards Association (CSA). CAN/CSA-O86-09. Engineering design in wood. Mississauga, Canada, 2010.

[4] Salenikovich, A. The Racking Performance of Light-Frame Shear Walls. PhD Dissertation. VP&SU, Blacksburg, VA, 2000.

[5] American Forest & Paper Association: Mechanicals-based design of wood shear walls with openings. Technical Report 13. Draft, 2009.

[6] Källsner, B., U. A. Girhammar, and L. Wu: A simplified plastic model for design of partially anchored wood-framed shear walls. In: *Proceedings CIB-W18/34-15-1*, Venice, Italy, 2001.

[7] Källsner, B., and U. A. Girhammar: A plastic lower bound method for design of wood-framed shear walls. In: *Proceedings WCTE 2004,* Lahti, Finland, 2004.

[8] Griffiths, B., V. Enjily, H. Blass and B. Källsner: A unified design method for the racking resistance of timber framed walls for inclusion in Eurocode 5. In: *Proceedings CIB-W18/38-15-9*, Karlsruhe, Germany, 2005.

[9] Dujič, B. and R. Žarnić: Influence of vertical load on lateral resistance of timber-framed walls. In: *Proceedings CIB-W18/35-15-4*, Kyoto, Japan, 2002.

[10] Salenikovich, A. and M. Payeur: Influence of vertical loads on lateral resistance of light-frame shear walls. In: *Proceedings WCTE 2010*, Riva del Garda, Italy, 2010.

[11] Payeur, M.: Influence des charges verticales sur les performances latérales des murs de refend en bois à ossature légère. MSc Thesis. Université Laval, 2011.

[12] American Society for Testing and Materials (ASTM): E564-06 Standard practice for static load test for shear resistance of framed walls for buildings, 2010.

[13] American Society for Testing and Materiels (ASTM): E2126-10 Standard test method for cyclic (reversed) load test for shear resistance of walls for buildings, 2010.

[14] American Forest & Paper Association: National design specification for wood construction. 2005 Edition.

[15] Muñoz, W.: Évaluation des systèmes de connexion pour les murs en bois en panneaux préfabriqués. PhD Dissertation. Université Laval, 2007.

[16] Dean, P. K. and H. W. Shenton: Experimental investigation of the effect of vertical load on the capacity of wood shear walls. J. of Structural Engineering, 131(7): 1104-1113, 2005.

Appendix. *Experimental and predicted load-deflection curves (e_n from CSA-O86).*

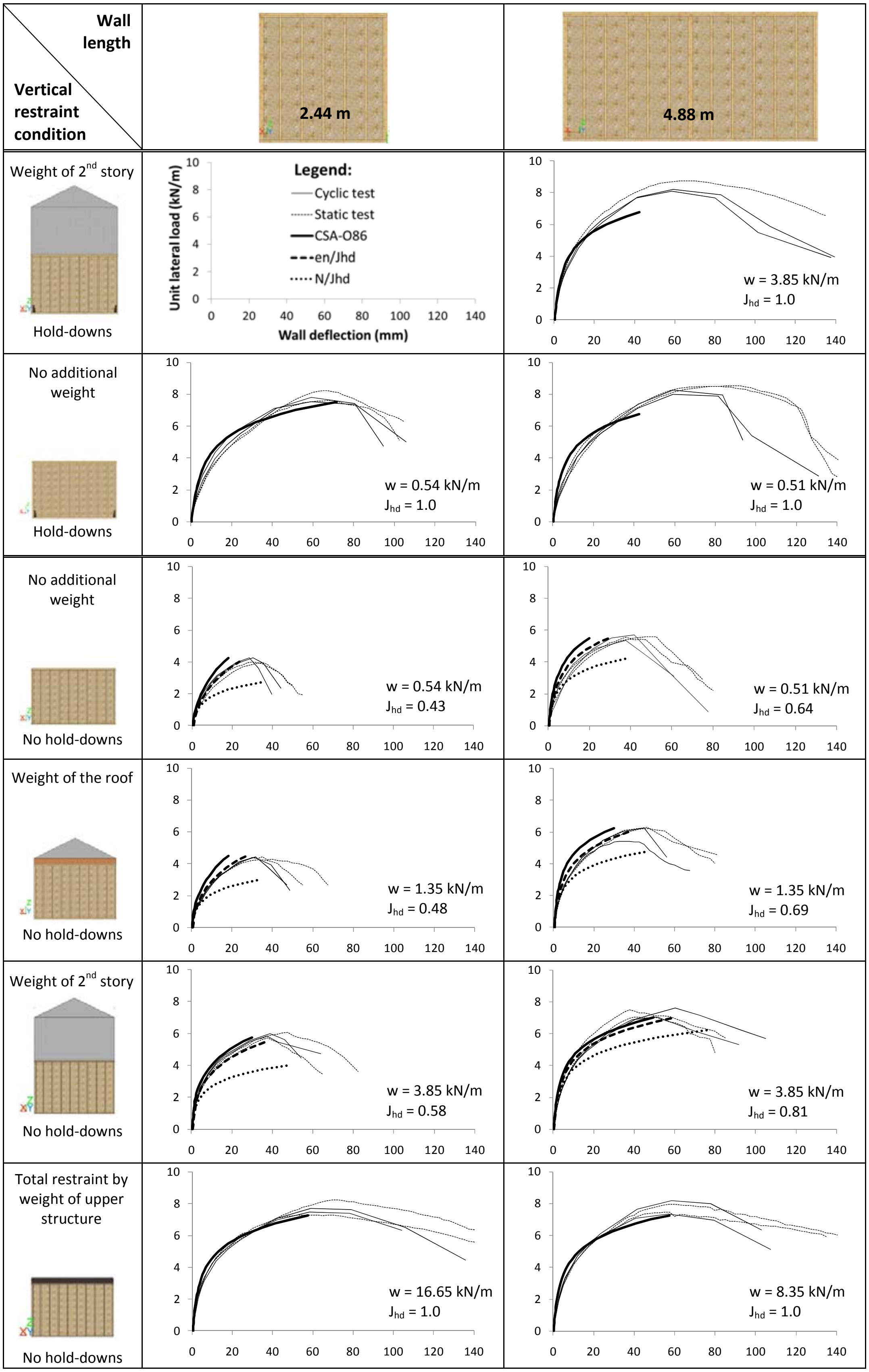

CIB-W18/44-15-3

INTERNATIONAL COUNCIL FOR RESEARCH AND INNOVATION
IN BUILDING AND CONSTRUCTION

WORKING COMMISSION W18 - TIMBER STRUCTURES

MODELLING FORCE TRANSFER AROUND OPENINGS OF FULL-SCALE SHEAR WALLS

T Skaggs

B Yeh

APA – The Engineered Wood Association

D Rammer

J Wacker

Forest Products Laboratory

U.S.A.

F Lam

Minghao Li

University of British Columbia

CANADA

MEETING FORTY FOUR

ALGHERO

ITALY

AUGUST 2011

Presented by T Skaggs

S Pampanin discussed the compression forces in the straps and the possibilities to make the straps work both in tension and compression. T Skaggs stated that flat straps would buckle in compression; alternative systems with rod would be possible; however the purpose of the bracket system used in the study was for experimental investigations only.

I Smith commented that there were full scale tests done in the US and asked what happened in full scale building system in relation to accuracy of the component evaluations. T Skaggs responded that the full scale building system test in US did not consider the force transfer around openings issues.

Modelling Force Transfer Around Openings of Full-Scale Shear Walls

Tom Skaggs and Borjen Yeh
APA – The Engineered Wood Association, U.S.A.
Frank Lam and Minghao Li
University of British Columbia, Canada
Doug Rammer and James Wacker
Forest Products Laboratory, U.S.A.

Abstract

Wood structural panel (WSP) sheathed shear walls and diaphragms are the primary lateral-load-resisting elements in wood-frame construction. The historical performance of light-frame structures in North America has been very good due, in part, to model building codes that are designed to preserve life safety. These model building codes have spawned continual improvement and refinement of engineering solutions. There is also an inherent redundancy of wood-frame construction using WSP shear walls and diaphragms. As wood-frame construction is continuously evolving, designers in many parts of North America are optimizing design solutions that require the understanding of force transfer between lateral load-resisting elements.

The design method for force transfer around openings (FTAO) has been a subject of interest by some engineering groups in the U.S., such as the Structural Engineers Association of California (SEAOC). Excellent examples of FTAO targeted to practitioners have been developed by a number of sources. However, very little test data are available to confirm design assumptions. The building code requirements for FTAO are vaguely written with the requirement that the methods must meet "rational analysis". Consequentially, countless techniques have been developed based on this performance-based notion. This paper discusses three methods which are generally accepted as meeting the rational analysis criterion. The drag strut, cantilever beam and Diekmann technique were examined in this study, which resulted in a wide range of predicted FTAO forces. This variation in predicted forces results in some structures being either over-built or less reliable than the intended performance objective.

This paper covers the two distinct portions of this research, the experimental study and the modelling analysis. Although the experimental study was partially reported by Skaggs et al. (2010), this paper is strictly focusing on the walls that were designed for force transfer around openings. Additional replications of the walls, and corrected strap force measurements are included in this paper. The modelling analysis includes simplified modelling using traditional engineering techniques, and more advanced modelling utilizing nonlinear finite element analysis. The various models were supported by 19 full-scale, 2.4 m x 3.6 m (8 ft x 12 ft) walls with various types and sizes of openings. Eight additional wall tests were conducted as part of this research program (Yeh, et al., 2011), however, these walls were not detailed for force transfer around openings, thus were not included in this paper.

This study was undertaken by a joint effort between APA – The Engineered Wood Association and the USDA Forest Products Laboratory (FPL), Madison, WI under a joint venture agreement funded by both organizations. The University of British Columbia, Vancouver, BC, provided the computer shear wall model simulation and analysis.

1. Introduction

Wood structural panel sheathed shear walls are important lateral force resisting components in wood-frame construction. These assemblies are effective in resisting seismic or wind loads. Wall openings for windows and doors, however, can greatly reduce the lateral resistance due to the discontinuity of load transfers as well as high force concentration around openings. The North American building codes provide three design alternatives for walls with openings. The first solution is to ignore the contribution of the wall segments above and below openings and only consider the full height segments in resisting lateral forces, often referred to as segmented shear wall method. This method could be considered the traditional shear wall method. The second approach, which is to account for the effects of openings in the walls using an empirical reduction factor, is known as the "perforated shear wall method". This method has tabulated empirical reduction factors and a number of limitations on the method. In addition, there are a number of special detailing requirements that are not required by the other two methods. The final method is codified and accepted as simply following "rational analysis". Much engineering consideration has been given to this topic (SEAOSC Seismology Committee, 2007) and excellent examples targeted to practitioners have been developed by a number of sources (SEAOC, 2007, Breyer et al. 2007, Diekmann, 1998). However, unlike the perforated shear wall method, very little test data has been collected to verify various rational analyses. The purpose of this study was to collect data on actual forces that are transferred around openings, and to compare, both simplified rational analysis as well as more rigorous finite element analysis.

2. Test Plan

In an effort to collect internal forces around openings of loaded walls, a series of twelve wall configurations were tested (Yeh et al, 2011). For this paper, a subset of eight assemblies will be discussed, as shown in Figure 1. The schematics in Figure 1 include the framing and sheathing plan, and the location of anchor bolts, hold downs and straps. This test series is based on the North American code permitted walls nailed with 10d common nails (3.75 mm diameter by 76 mm long or 0.131 in. diameter by 3 in. long) at a nail spacing of 51 mm (2 in.). The sheathing used in all cases was nominal 12 mm (15/32 in.) thick oriented strand board (OSB) APA STR I Rated Sheathing. All walls were 3.66 m 12 ft) long and 2.44 m (8 ft) tall. The lumber used for all of these tests was kiln-dried 38 x 89 mm (1-1/2 x 3-1/2 in.) Douglas-fir, purchased from the open market, and tested after conditioning to indoor laboratory environments (i.e. dry conditions). Additional framing information and boundary condition attachments are discussed in Yeh et al. (2011).

Walls 4, 5 and 6 have pier widths consistent with the narrowest segmented walls permitted by the code (height-to-width ratio of 3.5:1) when overturning restraint (hold-downs) is used on each end of the full height segments. The height of the window opening for Walls 4, 6 and 8 was 0.91 m (3 ft). Walls 5 and 9 had larger window heights of 1.52 m (5 ft). Wall 6 was common to Wall 4 with the exception that the typical 1.22 x 2.44 m (4 x 8 ft) sheathing was "wrapped around" the wall opening in "C" shaped pieces. This framing technique is commonly used in North America. It can be more time efficient to sheath over openings at first and then remove the sheathing in the openings area via a hand power saw or router.

Wall 8 has a pier height-to-width ratio of the full height segments of 2:1. Walls 10 and 11 contain very narrow wall segments for use in large openings such as garage fronts. The two walls are designed with openings on either side of pier and only on wall boundary, respectively. Finally, Wall 12 contains a wall with two asymmetric openings.

Most walls were tested with a cyclic loading protocol following ASTM E 2126, Method C, CUREE Basic Loading Protocol. The reference deformation, Δ, was set as 61 mm (2.4 in.). The term α was 0.5, resulting in maximum displacements applied to the wall of +/- 121 mm (4.8 in.). The displacement-based protocol was applied to the wall at 0.5 Hz with the exception of Wall 8b, which was loaded at 0.05 Hz. Two walls (Wall 4c and 5c) were tested following a monotonic test in accordance with ASTM E 564.

Finally, monotonic racking tests were conducted with the load being transferred directly into the top plate; thus no load head was utilized. The wall remained planar via structural tubes and low friction rub blocks directly bearing on face and back side of wall. For walls detailed as force transfer around openings, two Simpson Strong-Tie HTT22 hold-downs in line (facing seat-to-seat) were fastened through the sheathing and into the flat blocking. The hold-downs were intended to provide similar force transfer as the typically detailed flat strapping around openings. The hold-downs were connected via a 15.9 mm (5/8 in.) diameter calibrated tension bolt for measuring tension forces.

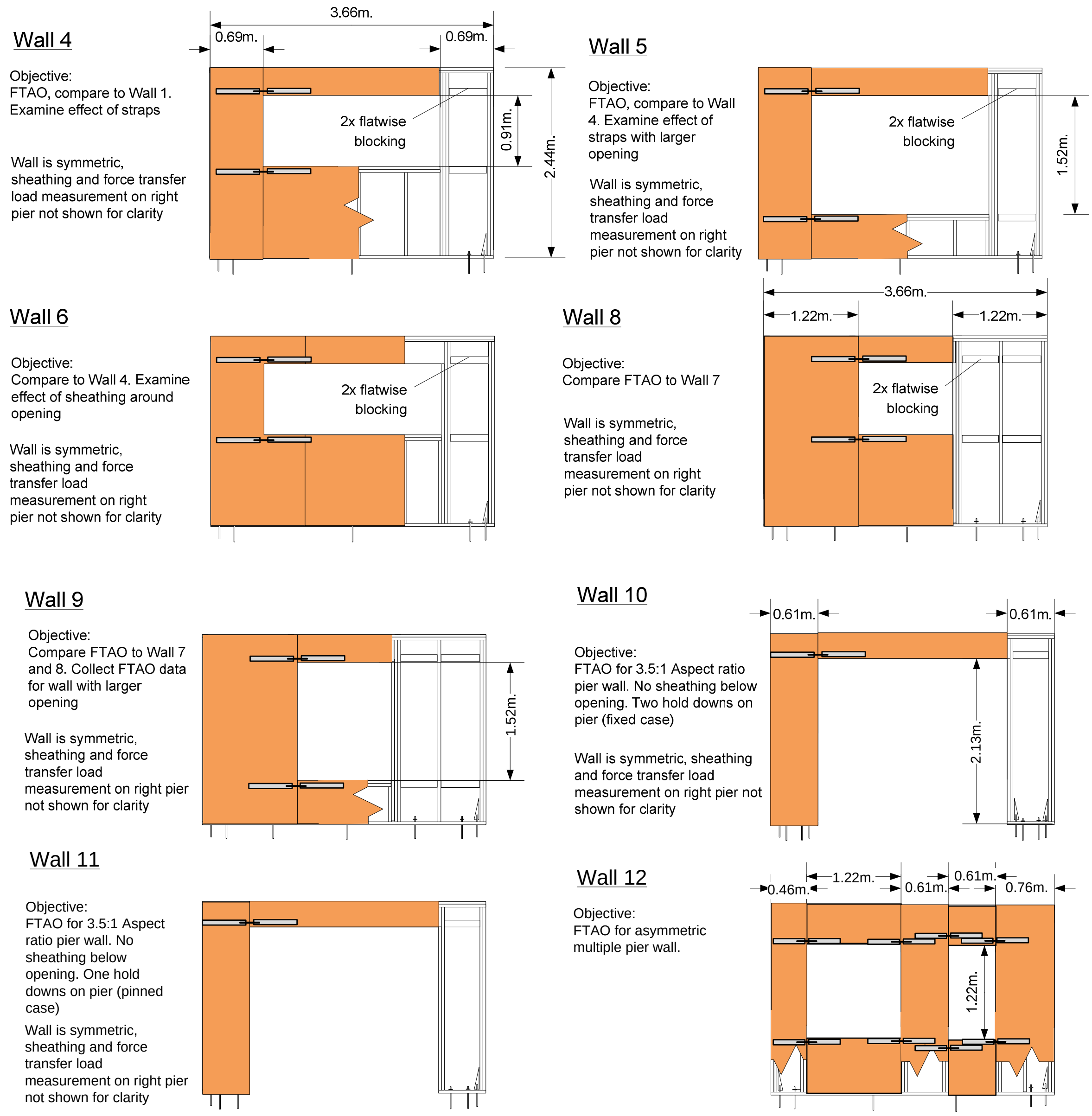

Figure 1. Test schematics for various force transfer around openings assemblies

3. Test Results

Table 1 presents the results of the global wall and calculated load factors. The allowable stress wall capacity is based on the code listed allowable unit shear multiplied by the effective length of the wall, as determined by the sum of the lengths of the full height piers. Table 1 also provides measured strap forces when the wall was subjected to the allowable stress wall capacity. Yeh et al. (2011) provides a comprehensive analysis of these wall tests.

Table 1. Global response of tested walls and strap forces.

Wall ID	Effective Wall Length [(1)]		Allowable Wall Capacity [(2)]		Average Maximum Load [(3)]		ASD Load Factor [(4)]	Measured Strap Forces [(5)]			
								Top		Bottom	
	(m)	(ft)	(kN)	(lbf)	(kN)	(lbf)		(kN)	(lbf)	(kN)	(lbf)
Wall 4a	1.37	4.5	17.4	3,915	66.4	14,930	3.81	3.05	687	6.61	1,490
Wall 4b	1.37	4.5	17.4	3,915	76.7	17,240	4.40	2.49	560	6.57	1,480
Wall 4c [(6)]	1.37	4.5	17.4	3,915	77.3	17,370	4.44	2.97	668	5.85	1,320
Wall 4d	1.37	4.5	17.4	3,915	68.2	15,330	3.92	4.47	1,010	7.41	1,670
Wall 5b	1.37	4.5	17.4	3,915	60.0	13,490	3.44	8.37	1,880	8.04	1,810
Wall 5c [(6)]	1.37	4.5	17.4	3,915	52.9	11,890	3.04	7.17	1,610	7.76	1,740
Wall 5d	1.37	4.5	17.4	3,915	52.0	11,680	2.98	7.26	1,630	10.26	2,310
Wall 6a	1.37	4.5	17.4	3,915	53.1	11,950	3.05	1.87	421	2.12	477
Wall 6b	1.37	4.5	17.4	3,915	60.4	13,580	3.47	2.71	609	2.73	614
Wall 8a	2.44	8.0	31.0	6,960	68.5	15,390	2.21	4.38	985	5.99	1,350
Wall 8b [(7)]	2.44	8.0	31.0	6,960	69.0	15,520	2.23	6.64	1,490	4.80	1,080
Wall 9a	2.44	8.0	31.0	6,960	67.8	15,250	2.19	7.45	1,670	7.35	1,650
Wall 9b	2.44	8.0	31.0	6,960	74.1	16,650	2.39	7.43	1,670	7.09	1,590
Wall 10a	1.22	4.0	15.5	3,480	33.2	7,470	2.15	7.03	1,580	n.a.	
Wall 10b	1.22	4.0	15.5	3,480	31.0	6,980	2.00	8.90	2,000	n.a.	
Wall 11a	1.22	4.0	15.5	3,480	28.8	6,480	1.86	10.97	2,470	n.a.	
Wall 11b	1.22	4.0	15.5	3,480	25.2	5,670	1.63	13.62	3,060	n.a.	
Wall 12a	1.83	6.0	23.5	5,220	71.3	16,030	3.07	3.59	807	5.17	1,160
Wall 12a	1.83	6.0	23.5	5,220	66.4	15,010	2.88	4.82	1,080	4.45	1,000

(1) Based on sum of the lengths of the full height segments of the wall.
(2) The shear capacity of the wall is the effective wall length times the allowable unit shear capacity, 12.70 kN/m (870 plf).
(3) The average of the absolute minimum negative and maximum positive applied forces.
(4) Average load applied to the wall divided by the wall capacity.
(5) Reported strap forces evaluated at the allowable wall capacity.
(6) Monotonic test.
(7) Loading duration increased by 10x.

4. Model Development

Typically walls that are designed for force transfer around openings attempt to reinforce the wall with openings such that the wall performs as if there was no opening. Generally increased nailing in the vertical and the horizontal directions as well as blocking and strapping are common methods being utilized for this reinforcement around openings. The authors are aware of at least three practical techniques which are generally accepted as rational analysis. The "drag strut" technique is a relatively simple rational analysis which treats the segments above and below the openings as "drag struts" (Martin, 2005). This analogy assumes that the shear loads in the full height segments are collected and concentrated into the sheathed segments above and below the openings. The second simple technique is referred to as "cantilever beam". This technique treats the forces above and below the openings as moment couples, which are sensitive to the height of the sheathed area above and below the openings. The mathematical development of these two techniques is presented by Martin (2005). Finally, the more rigorous mathematical technique is typically credited to a California structural engineer, Edward Diekmann, and well documented in the wood design textbook by Breyer et al. (2007). This technique assumes that the wall behaves as a monolith and internal forces are resolved by creating a series of free body diagrams. This is a common technique used by many west coast engineers in North America. Although the technique can be tedious for realistic walls with multiple openings, many design offices have developed spreadsheets based on either the Diekmann method or SEAOC (2007). The three aforementioned techniques could be considered practical rational analysis techniques.

For more advanced modelling, WALL2D was developed by the University of British Columbia, Vancouver, BC, Canada to model the behaviour of wood shear walls subjected to monotonic or cyclic loads (Li, et al. 2011a). This model consists of linear elastic beam elements for framing members, orthotropic plate elements for sheathing panels, linear springs for framing connections, and nonlinear oriented springs for panel-frame nailed connections. The model does not consider the rotational stiffness of framing connections. WALL2D accounts for the nonlinear behaviour of nailed connections as well as addresses the strength/stiffness degradation and pinching effects due to cyclic loading (Li, et al. 2011b). In this study, the nonlinearity in the tension-only strap connections around openings and hold-down connections was considered by nonlinear tension springs. Additionally, a type of asymmetric linear springs with higher compression stiffness but lower tension stiffness has also been introduced to consider the relatively high contact stiffness between header and blocking and wall studs when they are pushing against each other. Figure 2 illustrates the modified WALL2D model used in this study.

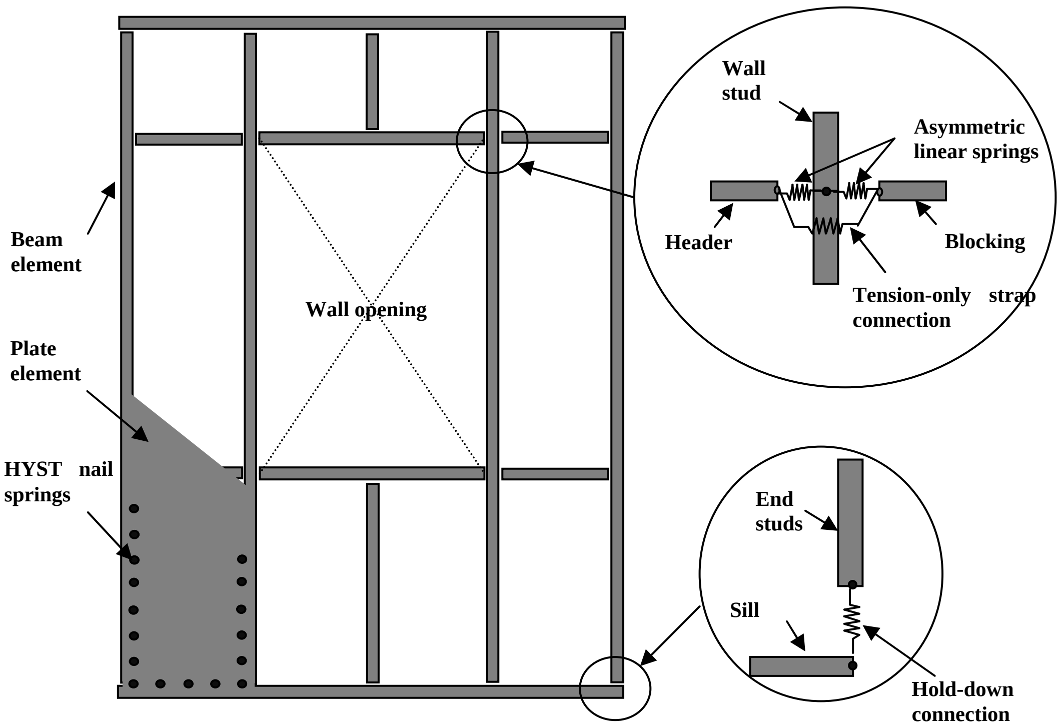

Figure 2. Schematics of WALL2D model for perforated wood-frame walls

Since nailed connections typically govern the shear behaviour of wood structural panel sheathed walls, nailed connection tests were conducted to calibrate the model, as shown in Figure 3. Additional explanation on these tests and calibration procedures and modelling parameters can be found in Li, et al. (2011a). Further discussion of the modelling assumptions of WALL2D is found in Li, et al. (2011b).

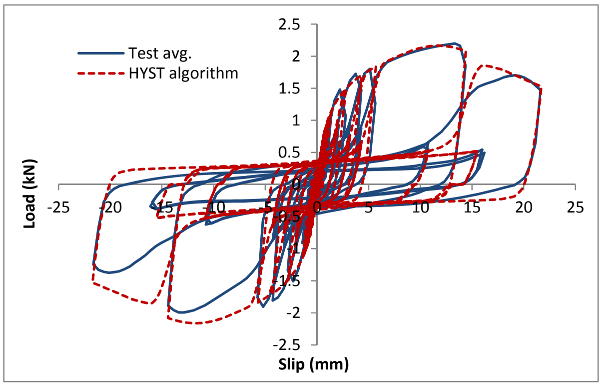

Figure 3. *Calibrated nail model vs average test data.*

5. Model Results

In the test program, the wall specimens were loaded so that maximum amplitudes of cycles in the CUREE basic protocol exceeded 100 mm (4 in.). The test results showed that, at a wall drift ratio of 2.5% (61 mm or 2.4 in.), these walls reached or approached their peak loads. In design practice, engineers are interested in evaluating the strap forces under the wall design load level which is normally significantly lower than the peak load. Therefore, in this study, the wall models were loaded until the maximum magnitudes of cycles reached 2.5% drift ratio. In general, the model predictions of eight wall configurations agreed well with the test results in terms of global load-drift responses and strap force responses, as illustrated in Figure 4 and 5, respectively.

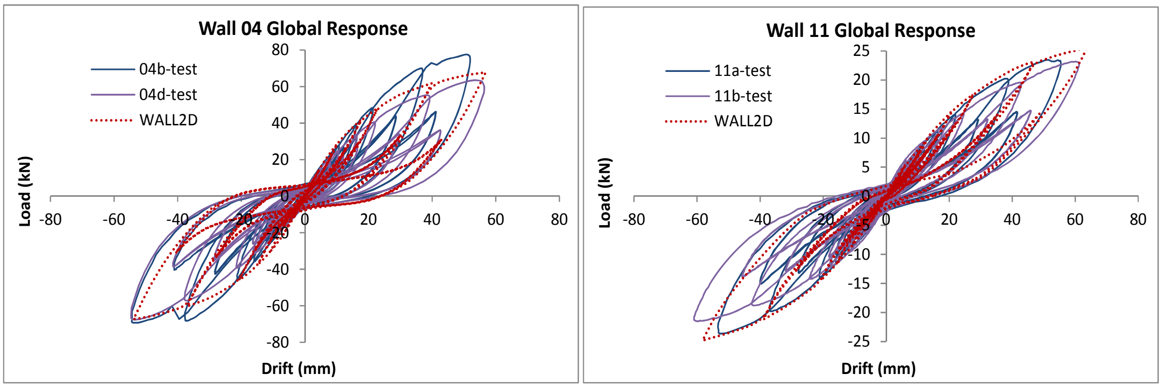

Figure 4. *Global response of WALL2D model as compared to cyclic test data*

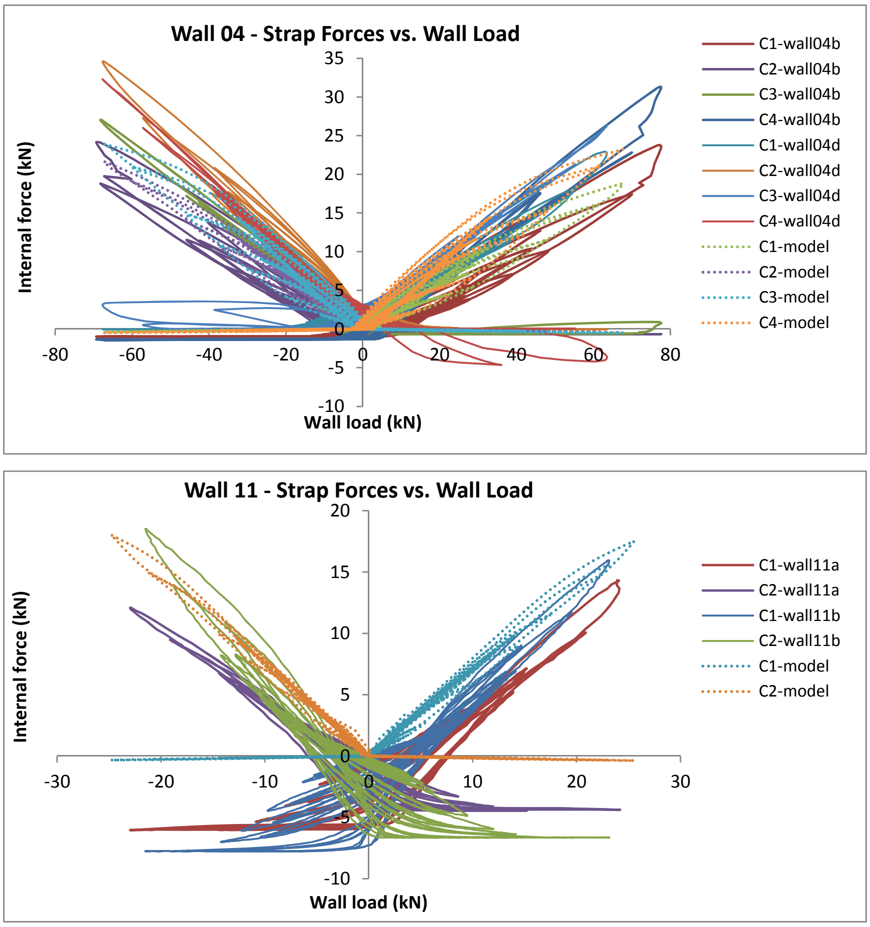

Figure 5. *WALL2D predicted FTAO strap forces vs. test results*

In order to design the strap connectors, it is important to evaluate the maximum forces transferred around openings under the design loads. In the U.S., 12.7 kN/m (870 plf) is a typical tabulated design load for wood-frame shear walls. Accordingly, the allowable wall capacity for a shear wall is calculated by multiplying the unit capacity with the total effective wall length (i.e., considering full-height wall segments). At the wall design load level, the predicted strap forces on the top corners (C1 and C2) and bottom corners (C3 and C4) of the opening were retrieved and compared with the test results. As expected, when the size of openings increased while the length of full-height piers remained the same, the strap forces increased. For all the wall configurations, the maximum prediction error from WALL2D was for Wall 6. Wall 6 was a special case in which "C"-shape sheathings were wrapped around the opening, resulting in an average prediction error of -15.2%. Note that additional discussion on individual walls, as well as modelled strap forces is provided by Li et al. (2011b).

Table 4 gives the maximum strap forces of four corners around the opening from the test data, WALL2D model, and three simplified design methods under the design loads. The prediction errors are given in parentheses. It can be seen that the WALL2D prediction error ranged from -15.4% to +4.3%. Drag strut method consistently underestimated strap forces except for Wall 6 with the "C"-shape sheathing panels. Cantilevered beam, and Diekmann's method, however, seemed to be very conservative. The Diekmann's method, the most sophisticated calculation method among the three practical design methods, seemed to provide reasonable predictions for the walls with window-type openings. One might consider including a correction factor of the Diekmann method on order of 1.2 to 1.3 if more accurate FTAO predictions are desired. However, many structural engineers are conservative by nature, and that decision would vary from office to office. It should be noted that the strap forces in Wall 6 with “C”-shape sheathing could not be reasonably predicted by any of three simplified methods even with the correction factor. Obviously the force load path around the openings is being transferred by the “C”-shaped sheathing. Perhaps a mechanics of material model considering either sheathing tensile strength or sheathing shear strength could be utilized to model the amount of the force transfer through the sheathing. The behaviour of walls with “C”-shaped sheathing is an interesting phenomenon which needs further studies.

Table 2. Maximum strap forces[(1)] (kN) predicted by WALL2D & simplified design methods

Wall No.	MEASURED	PREDICTED			
	Average force from wall tests [(2)]	WALL2D	Drag strut Technique	Cantilever Beam Technique	Diekmann Technique
4	6.61	6.23 (-5.7%)	5.44 (-17.7%)	19.90 (201.1%)	8.71 (31.8%)
5	8.69	9.07 (4.4%)	5.44 (-37.4%)	27.36 (214.8%)	14.51 (67.0%)
6	2.43	2.05 (-15.4%)	5.44 (124.1%)	19.90 (719.5%)	14.51 (497.5%)
8	5.51	5.75 (4.3%)	5.16 (-6.4%)	35.38 (542.0%)	8.26 (49.8%)
9	7.44	7.24 (-2.7%)	5.16 (-30.7%)	35.38 (375.5%)	13.76 (84.9%)
10	7.97	7.95 (-0.2%)	5.16 (-35.2%)	34.83 (337.0%)	n.a.
11	12.29	12.01 (-2.3%)	5.16 (-58.0%)	34.83 (183.4%)	n.a.
12	4.81	4.30 (-10.70%)	4.84 (0.6%)	21.28 (342.4%)	6.64 (38.0%).

(1) 1 lbf = 4.448 N

(2) Based on the maximum of the measured average top and average bottom strap forces.

6. Summary and Conclusion

This paper presents test data on a subset of twelve different wall assemblies more fully described in Yeh et al. (2011). The purpose of the analysis on this subset of 8 walls was to study the behaviour, both global and internal forces, of walls that were detailed to resist force transfer around opening. In general, the forces were transferred around openings utilizing straps except that Wall 6 also utilized sheathing for this load transfer mechanism. Several of these assemblies were tested with multiple replications, including variations in test method and loading duration. The replications showed good agreement between each other, even when walls were tested monotonically or cyclically, and when test duration was extended to ten times greater the original duration.

This paper also presented a study on force transfer around openings in perforated wood-frame shear walls using a finite element model called WALL2D, developed by the University of British Columbia. A total of eight wall configurations detailed for FTAO with different opening sizes and different lengths of full-height piers were modelled and analyzed. The model predicted wall load-drift hysteresis agreed well with the test results when the walls were loaded cyclically up to a drift ratio of 2.5%. At the wall design load level, the model predicted maximum strap forces around openings were also compared with the test results to check the model validity. It was also found that the model predictions agreed well with the test results compared with the three “rational” design methods commonly used by design engineers.

The current WALL2D model considers only the nonlinearities of panel-frame nail connections, hold-down connections, and strap connections around openings. It does not consider the nonlinearity or failure mechanism in sheathing panels and framing members. Therefore, it might over predict the wall response if those wall elements, in some situations, would also contribute significantly to wall nonlinearities. In fact, tearing failure of OSB sheathing panels was observed in some wall specimens when these walls had large deformations in the post-peak softening range. Furthermore, since framing members also play an important role in transferring loads among wall components in a perforated wall system, the model simulations would be more accurate if the properties of framing members, such as modulus of elasticity, were collected non-destructively before the walls were tested. Nevertheless, this model provides a useful tool to the study FTAO problem in perforated wood-frame walls. In future research, parametric studies can be further conducted to study the walls with different geometries, different opening sizes and different metal hardware for reinforcing corners of openings, providing more information for rational designs of perforated wood-frame walls.

Of the different models considered, one can conclude that the drag strut technique consistently underestimated the strap forces, and the cantilever beam technique consistently overestimated the strap forces. The Diekmann technique, the most computationally intensive of the practical methods, provided reasonable strap force predictions for the walls with window type openings. The more advanced nonlinear finite element model, WALL2D, provided a very accurate prediction for modelling the global wall results as well as the strap forces from FTAO. In the current form, WALL2D is likely too complicated for most engineering design offices; it is possible that this model could be used in the future for either developing simplified methods, or using the concepts in WALL2D to create a user friendly design tool.

7. Acknowledgements

This work is a joint research project of APA – The Engineered Wood Association, the University of British Columbia, and the USDA Forest Products Laboratory. This research was supported in part by funds provided by the Forest Products Laboratory, Forest Service, USDA.

8. References

1. ASTM International. 2009. *Standard test methods for cyclic (reversed) load test for shear resistance of vertical elements of the lateral force resisting systems for buildings. ASTM E2126-09,* West Conshohocken, PA.
2. ASTM International. 2009. *Standard practice for static load tests for shear resistance of framed walls for buildings, ASTM E 564 - 06.* West Conshohocken, PA.
3. Breyer, D. E., K. J. Fridley, K. E. Cobeen and D. G. Pollock. 2007. *Design of Wood Structures ASD/LRFD, 6th ed.,* McGraw Hill, New York, NY.
4. Diekmann, E. F. 1998. *Diaphragms and Shearwalls*, Wood Engineering and Construction Handbook, 3rd ed., K. F. Faherty and T. G. Williamson, eds, McGraw-Hill, New York, NY.
5. Li, M., R. O. Foschi, and F. Lam. 2011a. *Modeling hysteretic behavior of wood shear walls with a protocol-independent nail connection algorithm. Journal of Structural. Engineering*.
6. Li. M., F. Lam, B. Yeh and T. Skaggs. 2011b. *Modeling force transfer around openings in perforated wood-frame shear walls.* Submitted to Journal of Structural Engineering.

7. Martin, Z. A. 2005. *Design of wood structural panel shear walls with openings: A comparison of methods.* Wood Design Focus. 15 (1): 18 – 20.
8. Skaggs, T., B. Yeh, F. Lam, D. Rammer and J. Wacker. 2010. *Full-scale shear wall tests for force transfer around openings.* In: Proceedings of CIB-W18, paper 43-15-5.
9. Yeh, B, T. Skaggs. F. Lam, M. Li, D. Rammer, and J. Wacker, J. 2011. *Evaluations of force transfer around openings – experimental and analytical studies*. Final Report USDA Joint Venture Agreement 09-11111133-117, APA-The Engineered Wood Association, Tacoma, WA.
10. SEAOC. 2007. *2006 IBC Structural/Seismic design manual, volume 2: building design examples – light frame, masonry and tilt-up masonry*, Structural Engineers Association of California, Sacramento, CA.
11. SEAOC Seismology Committee. 2007. *Openings in wood frame shear walls, January 2007. The SEAOC blue book: seismic design recommendations.* Structural Engineers Association of California, Sacramento, CA.

CIB-W18/44-15-4

INTERNATIONAL COUNCIL FOR RESEARCH AND INNOVATION
IN BUILDING AND CONSTRUCTION

WORKING COMMISSION W18 - TIMBER STRUCTURES

DESIGN OF BOTTOM RAILS IN PARTIALLY ANCHORED SHEAR WALLS USING FRACTURE MECHANICS

E Serrano
A Olsson
Linnæus University, Växjö

J Vessby
Linnæus University and Tyréns AB, Växjö

U A Girhammar
Luleå University of Technology

B Källsner
Linnæus University, Växjö, and SP Stockholm

SWEDEN

MEETING FORTY FOUR
ALGHERO
ITALY
AUGUST 2011

Presented by E Serrano

V Enjily stated it would be more useful to have more details of the tests, for example, were bottom plates all cracked in the tests. E Serrano responded that for small washer size vertical sill plate cracks were observed and for large washer sizes horizontal sill plate cracks were observed.

S. Aicher commented about the why such construction was made. With a simple modification of construction detail/technique one could avoid such problem even though the analytical work is valid. E Serrano stated that the work was also curiosity driven.

Design of Bottom Rails in Partially Anchored Shear Walls Using Fracture Mechanics

Erik Serrano[1], Johan Vessby[2], Anders Olsson[1], Ulf Arne Girhammar[3], Bo Källsner[4]

[1]Linnæus University, Växjö, Sweden.
[2]Linnæus University, and Tyréns AB, Växjö, Sweden
[3]Luleå University of Technology, Sweden.
[4] Linnæus University, Växjö, and SP Technical Research Institute of Sweden, Stockholm, Sweden.

1. Introduction

A recent development in the design of medium-rise timber structures relates to the use of plastic design approaches that include three-dimensional effects e.g. Källsner and Girhammar (2006) and Källsner et.al. (2010). One of the greatest benefits with such an approach is that lateral walls connected to the stabilizing shear walls may be used as anchorage to counteract the considerable uplifting forces that may occur at times. On the one hand this design philosophy predicts an enhanced performance of the timber house. On the other hand it may introduce uplifting forces in the bottom rail, which is assumed to be anchored to the substrate. Thus the risk of splitting failure in the bottom rail must be assessed, since if such splitting of the rail occurs in a brittle manner, the plastic design philosophy may be put in question. The aim of the current study is to use the concept of fracture mechanics to establish and verify an analytical expression for the load bearing capacity of a bottom rail anchored to the substrate and exposed to an uplifting force through the sheathing. Such an expression makes it possible to predict the force at which splitting will occur. Bearing in mind that the failure modes are dominated by fracture perpendicular to the fiber direction, fracture mechanics is an appealing approach to use. Fracture mechanics has been successfully applied to other design situations in timber engineering, the best known example perhaps being the formulae of Eurocode 5 for the design of notched beams (Gustafsson 1988).

1.1 Geometry and loading conditions

A shear wall is connected to the substrate through the bottom rail or/and through hold down devices connecting the studs to the substrate. If the bottom rail is used for force transmission of horizontal forces to the substrate, the force is transmitted through dowel action in the anchor bolts and through friction between the rail and the substrate. The anchor bolts are, however, also at times necessary for holding down the rail, i.e. preventing it from lifting. An anchor bolt is placed in a predrilled hole in the wood, through a washer typically placed in the centre of the rail. This implies that an eccentricity is introduced between the uplifting forces from the sheet connected to the bottom rail and the hold down forces in the anchor bolt. If too large forces are introduced this eccentricity may cause a splitting failure in the rail. Two examples of such splitting failure are illustrated in Figure 1(a) for a vertical crack and (b) for a horizontal crack.

The example of the failure modes are shown to the left in the figure and a drawing that shows the geometrical parameters used for analyzing the structural performance of the rail is shown to the right. The failure modes illustrated in Figure 1(a) have been investigated experimentally (Girhammar and Källsner 2009) and an empirical design formula has been suggested

(Girhammar et al. 2010). The formula takes different washer sizes into account, and the failure mode has been studied for sheathing on one or both sides of the rail. However, the phenomenon has not been studied theoretically.

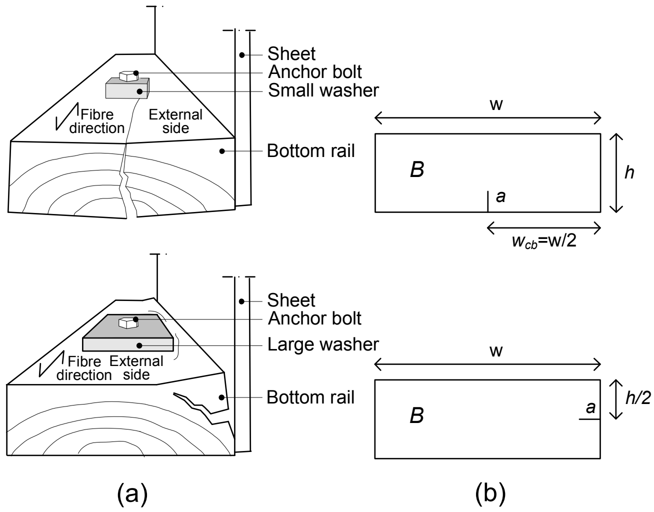

Figure 1. (a) Bottom rail at failure due to splitting. The rail is anchored to the substrate by means of an anchor bolt and a washer. (b) Parameters used in the current study for analyzing the rail.

The exact location of the crack may vary but two major types of failure, see Figure 1, were identified in Girhammar and Källsner (2009). In the current study, it is assumed that the crack initiates either from the bottom tensile edge, at half the width, w of the rail, or from half height of the rail, see Figure 1. The height of the rail is referred to as h, and the out of plane length of the rail, i.e. the "width" of the crack, will be referred to as B. Since the rail length B = 0.9 m was used in the experimental investigation by Girhammar and Källsner (2009), the same length will be used in the current study such that the results may be easily compared.

1.2 Material properties

In order to simplify the analyses of the rail all analyses are performed in two dimensions. It is likely, however, that using a two dimensional model, the predicted load-carrying capacity will be overestimated, since such a model does not take into account the variation in stress distribution in the longitudinal direction of the rail. Stress concentrations prior to fracture probably occur close to the anchor bolt. A three dimensional analysis could be used to evaluate the significance of this, and to suggest some factor that would compensate for it in a two dimensional model, but such an analysis is not presented in this paper. The rail is loaded perpendicular to its length direction, and thus the moduli perpendicular to this, E_R and E_T should be used in analyses performed in the radial-tangential plane (RT-plane). In design codes in general no distinction is made between the R- and T-directions and analyses based on analytical expressions suitable for hand-calculations should therefore preferably make use of only one in-plane modulus of elasticity (MOE). In addition, the shear stiffness in the RT-plane will influence the deformation pattern in the RT-plane. Index r in G_r represents *rolling shear* and the appropriate value to assign for G_r depends on the actual orientation of the annual rings. It is thus not a notation referring specifically to radial direction of the wood material. This rolling shear modulus is typically an order of magnitude lower than the RT-plane MOEs, and can therefore give rise to considerable deformation. In the present study the values of 600 and 500 MPa were chosen for E_R and E_T, respectively. For the cases where the Poisson effect is included, its value was set to ν_{RT} = 0.5. The strength of the timber in tension,

$f_{t,90}$ is set to 2.5 MPa and the critical energy release rate, G_{IC}, is assigned a value representative for pure mode I failure perpendicular to grain, in softwoods. This value was assumed to be constant, G_{IC} = 300 J/m^2, for any crack path in the RT-plane, which is an approximation. The values of the material parameters used herein are given in Table 1.

Table 1. Material data used in the performed analysis.

Material property	Value
E_R	600 MPa
E_T	500 MPa
G_r	50 MPa
ν_{RT}	0.5
$f_{t,90}$	2.5 MPa
G_{IC}	300 J/m^2

The material directions of the wood are assumed to be constant within the timber in the simple hand calculation approach. It is therefore not self-evident what value to use for the elastic parameters when comparing with the results from a 2D FE-model, where the cylindrical nature of the material is taken into account. In an orthotropic material, the effective modulus of elasticity and shear modulus, related to a fixed coordinate system, is shown in Figure 2. As can be seen, the effective values vary considerably with the angle of the material direction to the fixed global directions. In the present work, if nothing else is stated, the set of parameters corresponding to an annual ring orientation of zero degree angle (cf. Figure 2) is used for the hand calculation models. Thus, MOE was set to 500 MPa and rolling shear modulus to 50 MPa.

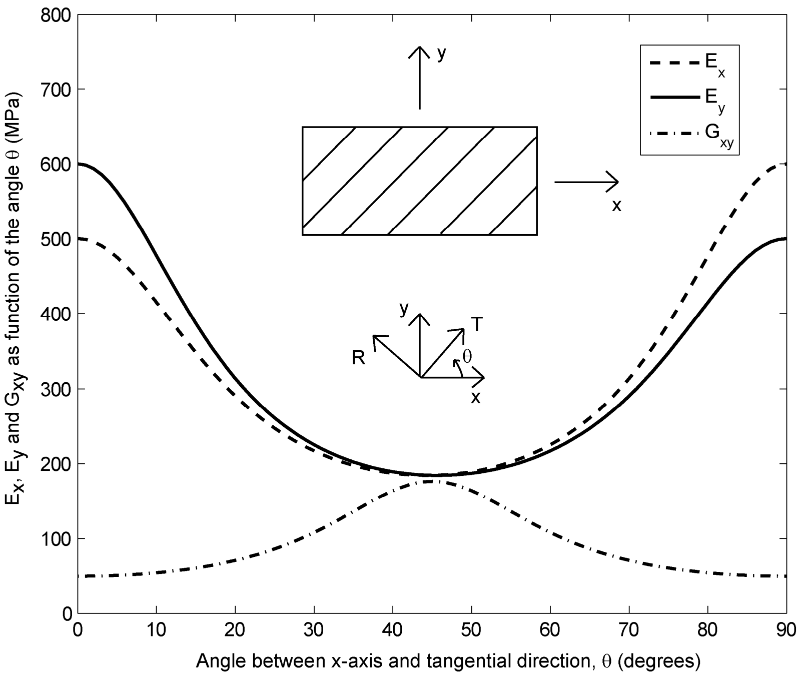

Figure 2. Influence of annual ring orientation on the effective moduli of elasticity and shear modulus referring to the global x-y-coordinate system.

2. Analysis methods

In this section linear elastic fracture mechanics (LEFM) theory leading to a suggested formula for calculating the load bearing capacity of a rail subjected to uplift forces and splitting is presented. In addition, a finite element model for assessing the compliance of the rail in more detail and a non-linear fracture mechanics (FCM) model for comparison are presented.

2.1 Basic LEFM theory – Energy release rate analysis

There are several approaches for analyzing a crack propagating in a material using LEFM. A crack is assumed to propagate when the energy release rate of the body equals the critical energy release rate of the material, G_C. By calculating the energy release rate for increasing crack length, the critical load (failure load) as a function of crack length can be obtained. Here, the so-called compliance method is used. The basis for this method is that, at crack propagation, the stiffness of the system is reduced, or equivalently, the compliance is increased. Details concerning such an approach can be found in e.g. Petersson (2002). For the case of a single point load, P^0, no body forces, and assuming quasi-static conditions, the change of potential energy $(-\Delta\Pi)$ of the system can be calculated

$$-\frac{\partial\Pi}{\partial a} = \frac{1}{2}P^0\frac{\partial u(P^0,a)}{\partial a} \tag{1}$$

where P^0 is a (constant) reference load acting on the system and a is the current crack length. The change of potential energy is in this case the driving "force" for crack propagation. At crack propagation we conclude that $-d\Pi/da = B \cdot G_C$, where B is the length of the studied rail and G_C is the critical energy release rate of the material.

If the notation P_c is used for the critical load and u_c for the corresponding displacement at the loading point (single point load case) the expression takes the form

$$\frac{P_c}{2}\frac{\partial u_c}{\partial a} = B \cdot G_C \tag{2}$$

With $C = u/P$ being equal to the compliance of the linear elastic structure, we obtain (assuming P being constant during crack propagation)

$$\frac{P_c^2}{2}\frac{\partial C}{\partial a} = B \cdot G_C \tag{3}$$

The value of G_C is strongly dependent on which mode of fracture is involved during crack propagation, and this mode of fracture will in general vary during loading, see Figure 2. For simplicity, here only mode I is taken into account so that $G_C = G_{IC}$. This simplification is practical and in general a safe approach, since $G_{IC} < G_{IIC}$.

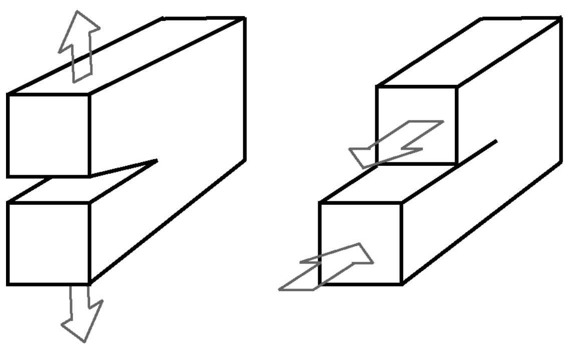

(a) (b)

Figure 3. Mode I (a) and mode II (b) loading.

As mentioned above, a further approximation made for simplicity is that the value of G_{IC} was set as independent of the crack direction in the RT-plane. More of the theory behind the energy release rate criterion may be found in e.g. Haller and Gustafsson (2002), Serrano and Gustafsson (2006) working specifically with wood or any standard text book on linear elastic fracture mechanics for a more general background.

2.2 Energy release rate – simplified hand calculations

Simple hand calculation formulae have been developed for two different assumptions of the position and direction of crack development: a vertical and a horizontal crack respectively.

2.2.1 Vertical crack

For commonly used rail- and washer dimensions the most frequently occurring failure mode is that a vertical crack develops. If the geometry of the studied bottom rail is simplified, the structure can be considered as a cantilever beam with the length w_{cb} and the height *(h-a), h* being the original height of the rail and *a* being the current crack length, see Figure 4.

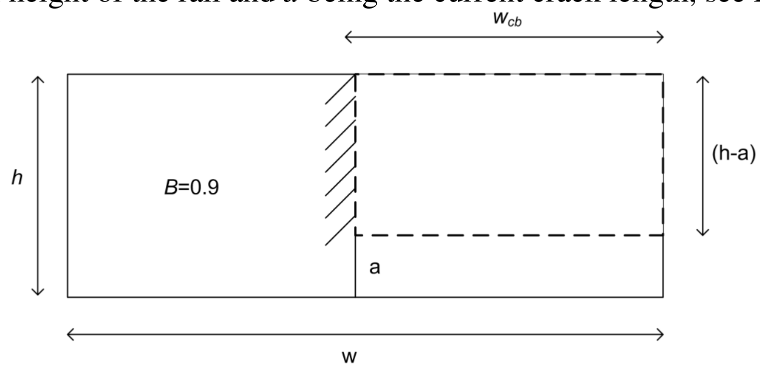

Figure 4. One end of the rail is considered a cantilever beam with the length w_{cb} and the height (h-a).

Once this simplification has been made the compliance of the cantilever beam can be expressed on basis of the bending and shear deformations of such a beam when subjected to a point load at the free end, i.e.

$$C(a) = \frac{4 \cdot w_{cb}^3}{E \cdot B \cdot (h-a)^3} + \frac{\beta \cdot w_{cb}}{G \cdot B \cdot (h-a)} \tag{4}$$

where E is a modulus of elasticity, G is the shear modulus and β is the shear correction factor, equal to 1.2 for a rectangular cross-section. The derivative of the compliance with respect to the crack length is obtained as

$$\frac{\partial C}{\partial a} = \frac{12 \cdot w_{cb}^3}{E \cdot B \cdot (h-a)^4} + \frac{\beta \cdot w_{cb}}{G \cdot B\ (h-a)^2} \tag{5}$$

The displacement, due to the load P, may be expressed as $u=P \cdot C$, and thus (3) may be reformulated to obtain an expression for the critical load. With $G_C = G_{IC}$, $E = E_{90}$ (stiffness in a direction perpendicular to grain, not necessarily coinciding with E_r or E_t) and $G = G_r$ we arrive at

$$P_c = \sqrt{\frac{2 \cdot B \cdot G_{IC}}{\frac{\partial C}{\partial a}}} = (h-a) \cdot B \cdot \sqrt{\frac{2 \cdot G_{IC}}{w_{cb}\left(\frac{12 \cdot w_{cb}^2}{E_{90} \cdot (h-a)^2} + \frac{\beta}{G_r}\right)}} \tag{6}$$

where P_c is the critical load. This equation thus represents the critical load as a function of the crack length, a. Although some approximations were introduced in the derivation of (6), the simple format is appealing. This closed-form solution based on a sound theoretical approach can be used to investigate the qualitative influence of various parameters. If necessary, (6) could also be calibrated to test results or more advanced analyses based on finite element results, by introducing additional parameters.

2.2.2 Horizontal crack

The second most common failure mode in the studied load case is that a crack develops horizontally from the position of the nails, commonly at half height of the rail. Such a crack would typically initially develop horizontally but would successively change direction so that it reaches the top side of the washer at a 45 degree angle, cf. Figure 1.

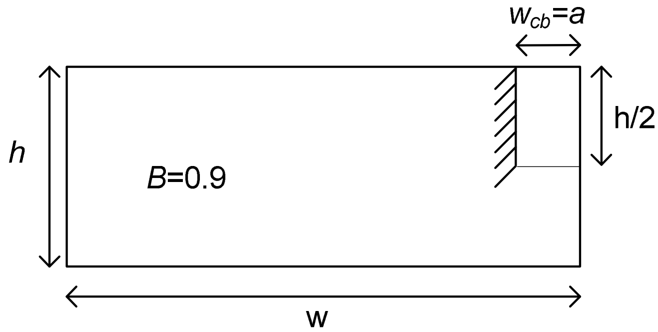

Figure 5. Simplified, one end of the rail may be seen as a cantilever beam with the length, w_{cb}, being equal to the length of the crack, a, and the height h/2.

In Figure 5 a simplified model for hand calculation for that case is suggested assuming a cantilever beam with the height $h/2$ and the length w_{cb} being equal to the length of the crack, a. Such approximation would be relevant for crack lengths less than about 15 mm since the direction of the crack would deviate to much from the suggested horizontal direction. Under these assumptions the compliance may be expressed as

$$C(a) = \frac{4 \cdot a^3}{E \cdot B \cdot \left(\frac{h}{2}\right)^3} + \frac{\beta a}{G_r \cdot B \cdot \left(\frac{h}{2}\right)} \tag{7}$$

using the same notations as was previously suggested for the vertical crack. The derivative of the compliance is obtained as

$$\partial C / \partial a = \frac{96 a^2}{E \cdot B \cdot h^3} + \frac{2\beta}{G_r \cdot B \cdot h} \tag{8}$$

Note that in the derivative of the compliance the shear contribution is constant, i.e. independent of the length of the crack while the contribution from the bending term depends in a quadratic manner on the length of the crack. Making use again of the general expression (3) we now obtain for the horizontal crack

$$P_c = B \cdot h \sqrt{\frac{G_{IC} \cdot G_r \cdot E \cdot h}{48 \cdot G_r \cdot a^2 + \beta \cdot h^2 \cdot E}} \tag{9}$$

For small crack lengths the bending term may be disregarded. Under such assumptions the critical load may be expressed as

$$P_c \approx B \cdot \sqrt{\frac{G_{IC} \cdot G_r \cdot h}{\beta}} \tag{10}$$

2.3 Energy release rate using the finite element method

The aim of the numerical analysis performed using the finite element method is to determine the compliance of the structure in order to calculate the critical load, see (3). This calculation is performed at different stages of the crack propagation. At each stage, the compliance is calculated by determining the displacement, $u_{0,i}$ under a constant load, and this is then repeated for different crack lengths a. The crack propagation length, Δa_i, is set to the side length of a finite element, so that for each propagation of the crack one node is released. For a stage in which node i has been released the corresponding physical crack length is set to

$$a \approx \frac{a_{i+1}+a_i}{2} \tag{11}$$

where a_i is the distance from the edge of the rail to node i and a_{i+1} is the distance from the bottom of the rail to node $i+1$. Thus the tip of the crack is assumed to be located at the mid-point of the edge of the newly released finite element.

A rail with h = 45 mm and w = 120 mm was loaded with the load P vertically in one degree of freedom at half the height of the right end of the rail. The boundary conditions were set so that the left bottom corner of the rail was pinned and the rest of the left bottom was prescribed to have zero vertical displacement. The boundary condition at the top of the rail was set so that displacement in vertical direction was restrained at the degree of freedom with the eccentricity e from the centre of the rail in order to give a simple condition corresponding to the effect of the washer. The length of the eccentricity of the top boundary condition was set to e_{bc} = 10 mm, a value that could easily be changed. Load, boundary conditions and notations used for width, w, height, h, eccentricity of the top boundary condition, e_{bc}, the distance from the vertical crack to the edge of the washer, e_0, the distance from the edge of the washer to the edge of the rail, e_{edge}, the length of the rail, B, and crack length, a, are all indicated in Figure 6 (a) and (b) respectively.

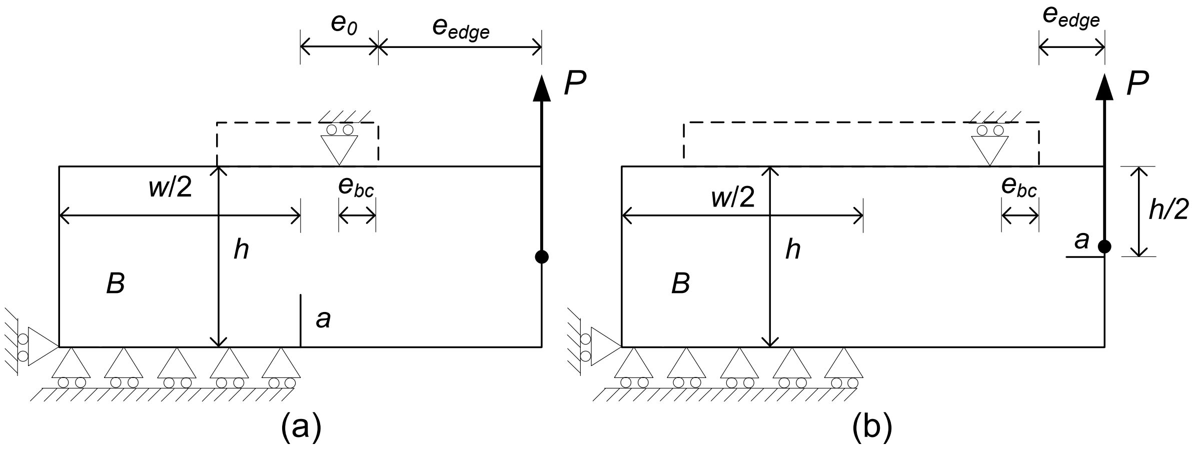

Figure 6. Geometry and applied load case for the studied rail with (a) a vertical crack and (b) a horizontal crack, each with the length a. The position of the washer (substituted by a boundary condition in the analyses) is indicated with dashed lines.

In the hand calculation models the length of the cantilever beam, w_{cb}, will be e_0+e_{edge} for the case with a vertical crack and a for the case of a horizontal crack. In the FEM model using LEFM by contrast, the distance from the edge of the rail to the location of the boundary condition at the top of the rail is e_{edge} +e_{bc} for both cases.

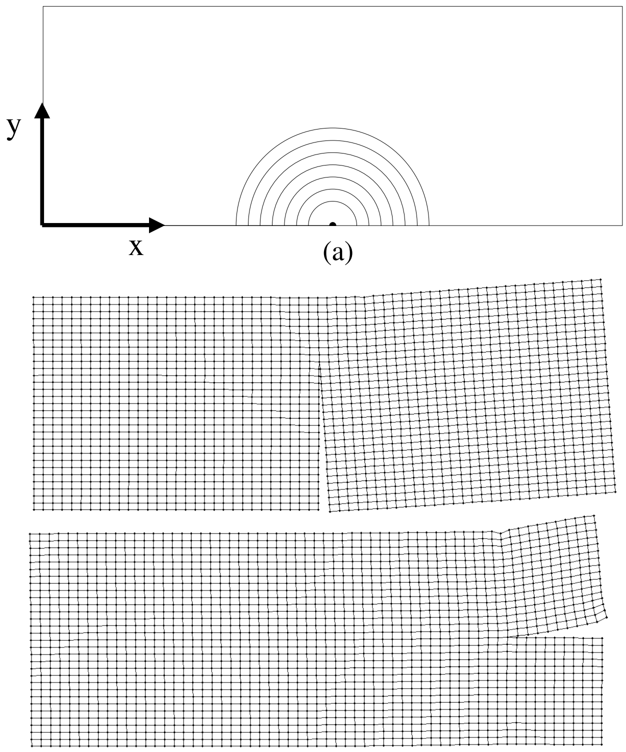

(a)

(b)

Figure 7. (a) The position of the pith was set to (x,y)= (60,0) mm. (b) The mesh used in the analyses with cracks that have propagated. Deformations are magnified 10 times.

The material was modeled using the orthotropic parameters introduced in Table 1. A cylindrical coordinate system was used to define the material orientation, the origin of this coordinate system being placed at the position (x,y)=(60,0), see Figure 7(a). Rectangular four node linear elements were used in the finite element model. The two-dimensional analyses were performed using the assumption of plane strain state with the length of the rail being 0.90 m. Examples of the meshes used for the analyses are shown in Figure 7(b) showing also the deformed rail, at a load of 1000 N with deformations being magnified 10 times. A total of 60 × 30 elements were used. For the shown states, the crack has propagated to about three quarters of the height of the rail and about 20 mm for the vertical and horizontal cracks, respectively.

2.4 Nonlinear fracture mechanics – fictitious crack model

A nonlinear fictitious crack model (FCM) was implemented as a complement to the hand calculations and the LEFM FE-model. The previously described crack propagation paths were used also in the nonlinear model. The material parameters of the wood material and the origin of the cylindrical coordinate system were set to the same as previously indicated. The characteristics of the crack were obtained assuming linear softening behavior from the strength perpendicular to the fibers, $f_{t,90}$, to the crack opening were no stresses are transmitted, w_c, cf. Figure 8. If the fracture energy and the strength perpendicular to the fibers according to Table 1 is used, the critical tip opening displacement, w_c, may be calculated to 0.24 mm. The same FCM was used for the two different cracks modeled.

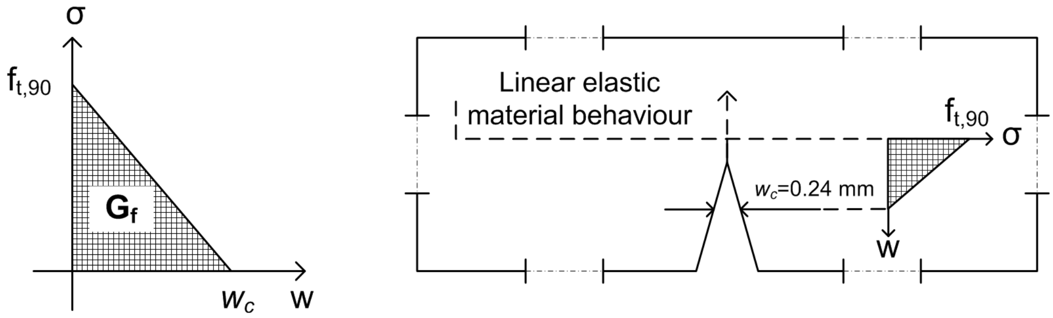

(a) (b)

Figure 8. (a) A linear softening behavior was assumed in the FCM, defining the critical opening displacement, w_c, where no stress can be transmitted. (b) Above the crack, i.e. above the position where the stress level is equal to $f_{t,90}$, the material behaves linearly elastically.

3. Results

In Figure 9 the critical load, P_c, obtained using the closed form expression (6) and the LEFM FE-model, respectively, is plotted as function of the crack length a in case of a vertical crack. The maximum load capacity calculated using the FCM is also indicated in Figure 9 but not as a function of the crack length, as this is not defined in the FCM analysis in a way comparable with the other calculations. On basis of the stress distribution it can be concluded, however, that the crack length is about 6 mm when the maximum load is reached according to the FCM analysis. In Figure 10 the complete course of loading for the FCM analysis is shown. The load is plotted versus the crack mouth opening displacement, CMOD, successively increasing for increasing displacements in the loading point and showing the strongly nonlinear behavior with softening after peak load. Assuming a 6 mm crack length the results from the closed form expression, the LEFM FE-model and the FCM FE-model are 12.4 kN, 12.3 kN and 13.9 kN, respectively. Considering the rough simplifications made there is thus a very good agreement between the different methods of analysis. It may also be noted that the agreement is acceptable between LEFM and the analytical model, i.e. the closed form expression, at least if crack lengths are smaller than 20 mm.

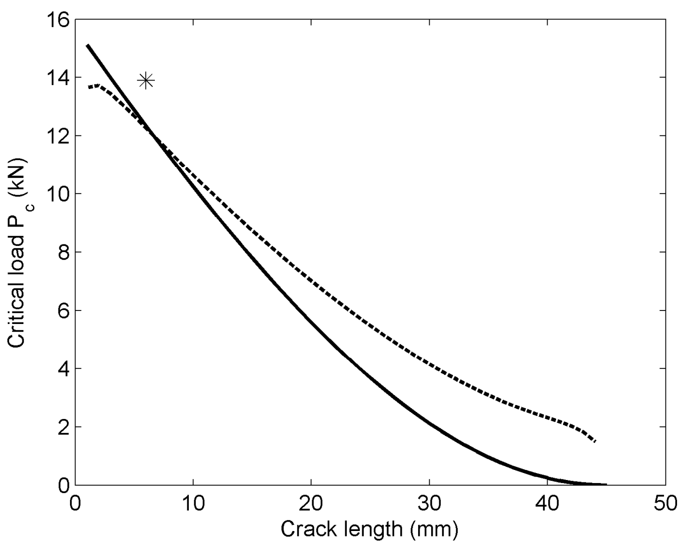

Figure 9. Critical load, P_c, as a function of crack length according to the closed form expression (solid line) and the LEFM FE simulation (dashed), both for the vertical crack. The asterisk indicates the critical load according to the FCM analysis, which appears at a state corresponding to a crack length of about 6 mm.

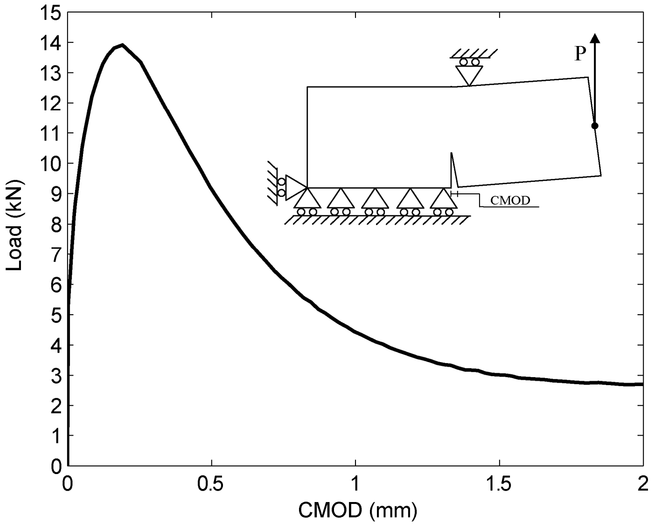

Figure 10. Load in the rail as a function of crack mouth opening displacement, CMOD for the vertical crack. The relation is obtained using the FCM.

In Figure 11 the critical load is shown for increasing crack lengths for the case of a horizontal crack. Similarly to the results from the vertical crack the results from the closed form expression, with and without consideration of bending, and the LEFM model, in this case for the horizontal crack are shown. As discussed earlier, see also Figure 1, the crack referred to as the horizontal crack is only horizontal for a limited crack length, around 15 mm, and thereafter deviates from the horizontal direction. This implies that the models should not be compared for lengths of the crack exceeding this value. In Figure 12 the complete course of loading for the FCM analysis is shown. The peak value, also shown in Figure 11, relates to the crack length 13 mm and the critical load $P_c = 21.1$ kN.

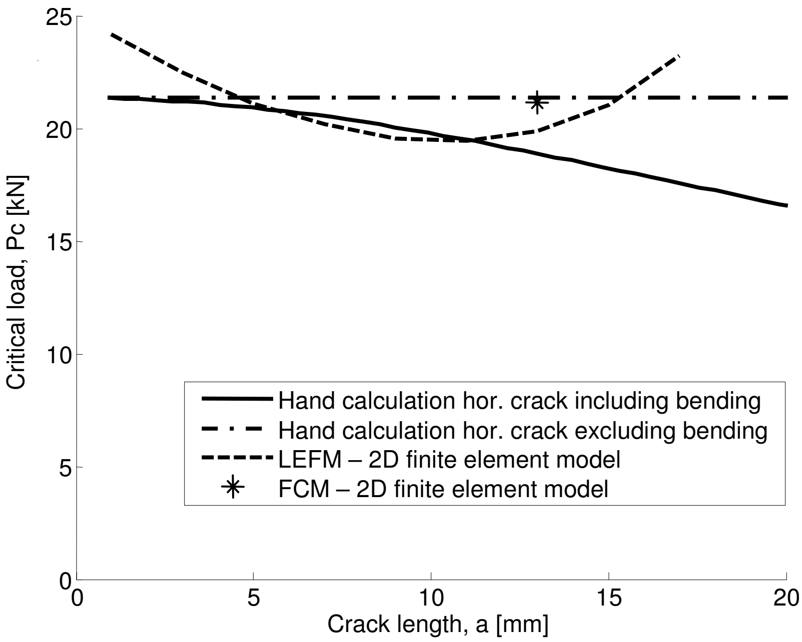

Figure 11. Critical load, P_c, as a function of crack length according to the closed form expression (solid line) and the LEFM FE simulation (dashed), both for the horizontal crack. The asterisk indicates the critical load according to the FCM analysis, which appears at a state corresponding to a crack length of about 13 mm.

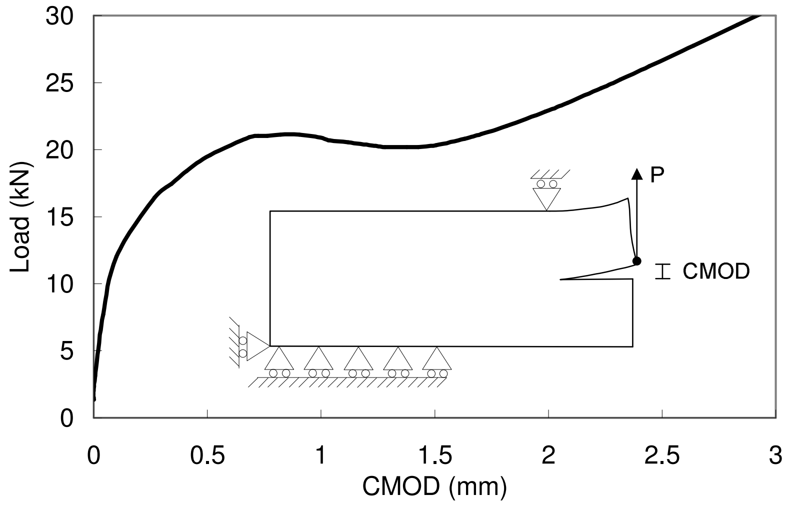

Figure 12. Load in the rail as a function of crack mouth opening displacement, CMOD for the horizontal crack. The relation is obtained using the FCM.

4. Discussion and comparison with experiments

The three different methods employed for analyzing the load capacity in the bottom rail for two different cracks give similar results, at least if the crack length, a, is not too large in relation to the in-plane dimensions of the rail. This is of course promising with respect to the usefulness of the simple, closed form expression developed above. However, the calculated results and the models employed should be compared and assessed by means of experimental results. Such experiments were performed (Girhammar et al. 2010) for different sizes and location of washers and for single and double sided sheathing on the rail. The critical failure load in the single-sided test with the smallest size of the washer, that being 40 mm wide, was found to be 12.1 kN for the vertical crack. This agrees rather well with the calculated values, see Figure 9.

Since the purpose was to establish a simple expression that could be used for hand calculation, some simplifications were made in the analytical model leading to the closed form expressions. One such simplification is the choice of the length of the cantilever in the model. This length could be considered a fitting parameter, taking into account a number of different factors such as the size and shape of the washer, the friction between the substrate and the rail, pretension of the anchor bolt and how the load P is introduced to the rail.

Another parameter to consider is the length of an assumed initial crack, a. Using $a=0$, the simplest possible way of expressing the critical load for the vertical crack would be

$$P_c = h \cdot B \cdot \sqrt{\frac{2 \cdot G_{IC}}{w_{cb}\left(\frac{12 \cdot w_{cb}^2}{E_{90} \cdot h^2} + \frac{\beta}{G_r}\right)}} \tag{12}$$

For the horizontal crack, $a=0$ would correspond to not considering the bending contribution, see eq. 10. Using $a=0$ would, however, lead to an overestimation of the critical load. Instead the choice of crack length to be used should preferably be estimated according to theoretical considerations related to the so-called initial crack method (Serrano and Gustafsson 2006). The proper crack length to use is (for pure mode I) according to this theory:

$$a_c = \frac{E_{90} \cdot G_{IC}}{\pi \cdot f_t^2} \tag{13}$$

In the present case, this would correspond to a crack length of 7.6 mm. The results from the FCM-analysis of the vertical crack indicated that the crack length at maximum load is about 6 mm, somewhat smaller than according to the suggested theory. Using (6) with an initial crack according to (13) would result in

$$P_c = \left(h - \frac{E_{90} \cdot G_{IC}}{\pi \cdot f_t^2}\right) \cdot B \cdot \sqrt{\frac{2 \cdot G_{IC}}{\left(\frac{12 \cdot w_{cb}^3}{E_{90} \cdot \left(h - \frac{E_{90} \cdot G_{IC}}{\pi \cdot f_t^2}\right)^2} + \frac{w_{cb}\beta}{G_r}\right)}} \tag{14}$$

which is a closed-form expression for the critical load with a theoretically sound basis. Note also that the approximate expression for the horizontal crack when disregarding the contribution from bending, see (10), is independent of the crack length.

In Girhammar et al. (2010) an *empirical* expression for the critical load as a function of the distance from the side of the washer to the edge of the rail is presented. Those results are compared with the expressions developed in the present work in Figure 13. The results from the analytical models in Figure 13 were obtained with E=400 MPa and G=70 MPa, which in turn corresponds to an average annual ring orientation of 10-15°, cf. Figure 2.

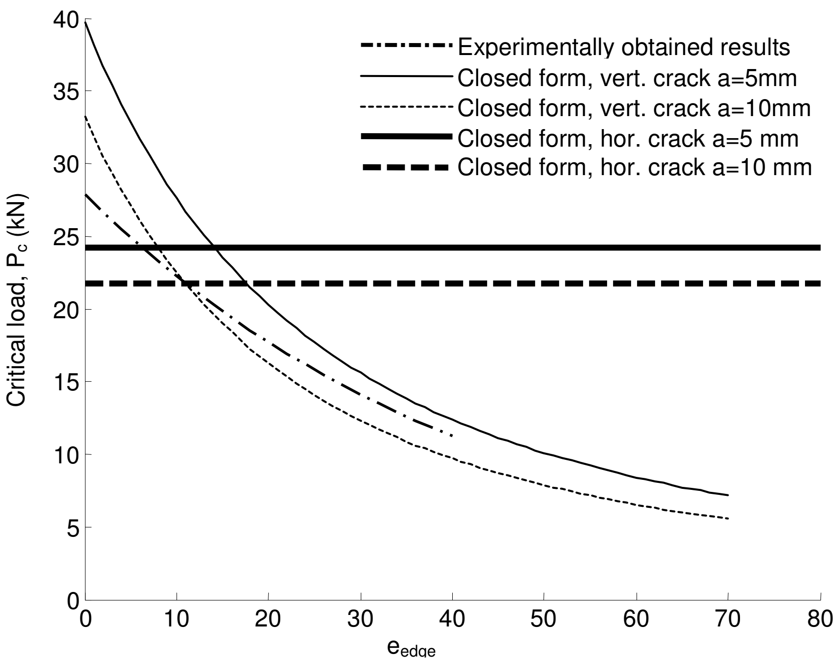

Figure 13. Comparison of results according to an empirical expression based on experiments and according to analytical models (eqs. 6 and 9). The curves show critical load versus length from washer edge to rail edge, e_{edge}. Washer size is here 40 mm. Horizontal curves correspond to a horizontal crack (eq.9.)

The agreement between the curves based on the analytical model and the curve based on experimental results is good. The larger the edge distance, the better the agreement with the assumption of a vertical crack, while shorter edge distances give a better agreement with model predictions based on the assumptions of a horizontal crack. Note that the results shown in Figure 13 were obtained without calibrating to the actual material parameters, nor to the annual ring orientations in the tests. In addition to such calibration, the length of the cantilever to be used in the analytical model could be used as a calibrating parameter.

5. Conclusions

The aim of the current study was to establish and verify a simple analytical expression that could be used to obtain the design load for vertically loaded rails fixed to the ground using washers. This was done by comparing analytical expressions to finite element models using LEFM and the FCM, respectively. The analytical expressions were also verified by a previously experimentally obtained expression. Good agreement could be found for the analytical expression in all cases indicating that they have potential for inclusion in the code. Some conclusions can be drawn from the study:

Although rather crude simplifications were used to establish the analytical expressions for the critical load, P_c , good agreement was found between the crack models and the two different fracture mechanic models, one linear and the other nonlinear, based on finite element modeling.

The length of the cantilever beam can be used as a fitting parameter, taking into account a broad range of parameters such as the geometry of the washer, the friction between rail and the substrate the pretension of the anchor bolt and the way that the load P is introduced.
The current study covers only one load case and should therefore not be generalized without further verification.

6. Acknowledgements

The authors express their sincere appreciation to The European Union's Structural Funds - The Regional Fund for their financial support.

7. References

Girhammar, U. A., Källsner, B. (2009). "Design aspects on anchoring the bottom rail in partially anchored wood-framed shear walls" *Proc. CIB-W18 meeting*, Duebendorf, Switzerland, paper 42-15-1.

Girhammar, U. A., Källsner, B., Daerga, P-A. (2010). "Recommendations for design of anchoring devices for bottom rails in partially anchored timber frame shear walls" *Proc. World conference on timber engineering,* Trentino, Italy.

Gustafsson, P. J. (1988). "A study of strength of notched beams" *Proc. CIB-W18 meeting*, Vancouver, Canada, paper 21-10-1.

Haller, P., Gustafsson, P.J. (2002). "An overview of fracture mechanics concepts." *Fracture mechanics models for strength analysis of timber beams with a hole or a notch – a report of RILEM TC-133*, P. J. Gustafsson, ed. TVSM-7134, Lund, Sweden.

Källsner, B., Girhammar, U. A. (2006) "A plastic design method for incompletely anchored wood-framed wall diaphragm" *Proc. World conference on timber engineering,* Portland, Oregon, USA.

Källsner, B., Girhammar, U. A., Vessby, J. (2010) "Some design aspects on anchoring of timber frame shear walls by transverse walls" *Proc World conference on timber engineering*, Riva del Garda, Italy.

Petersson, H. (2002). "Energy release rate analysis." Fracture mechanics models for strength analysis of timber beams with a hole or a notch – a report of RILEM TC-133, P. J. Gustafsson, ed., TVSM-7134, Lund, Sweden.

Serrano, E., Gustafsson, P. J. (2006) "Fracture mechanics in timber engineering – Strength analyses of components and joints", *Materials and Structures*, 40(1), 87-96.

CIB-W18/44-15-5

INTERNATIONAL COUNCIL FOR RESEARCH AND INNOVATION IN BUILDING AND CONSTRUCTION

WORKING COMMISSION W18 - TIMBER STRUCTURES

NOTES ON DEFORMATION AND DUCTILITY REQUIREMENTS IN TIMBER STRUCTURES

K A Malo,
P Ellingsbø
H C Stamatopoulos
The Norwegian University of Science and Technology, NTNU
Trondheim

NORWAY

MEETING FORTY FOUR

ALGHERO

ITALY

AUGUST 2011

Presented by K Malo

J W van de Kuilen and K Malo discussed about the time dependent deformations which would be partly recoverable were considered. This would be an important issue because part of the plastic deformation capacity would have been taken up by creep and one would only have the remaining deformation capacity available for the overload.

Notes on deformation and ductility requirements in timber structures

Kjell A. Malo, Pål Ellingsbø and Haris C. Stamatopoulos

Department of Structural Engineering
The Norwegian University of Science and Technology, NTNU
N-7491 Trondheim, Norway

1 Introduction

1.1 General

A majority of structural failures in larger timber structures can probably be related to improper design [1]. The situation is not very different for steel and concrete buildings, but the share of failures due to improper design seems to be less for steel and concrete structures. Causes may be that timber is a more complex material due to its strong anisotropic structure, or the designers are not so well educated in timber design, or the design guidelines and rules are not so well developed for timber structures in comparison to steel and concrete.

Possible consequences of a local structural failure may be limited to only local effects or, in turn, lead to fatal failures due to a progressive collapse mechanism. The term robustness (definition in [2]) is commonly used to characterize the ability of a structure to resist the possibility of a progressive collapse. Most codes and guidelines for timber design are concerned with the strength of components and connections. Apart from simple stiffness estimates of connectors, deformation properties of wooden structures are only implicitly handled, if taken into account at all. Deformations in connections are also rarely evaluated in praxis. Deformations in connections may govern the stress distribution in statically indeterminate structures and are important for impact resistance.

In EN 1990, Basis of Structural Design [3], the design principles state that potential damage due to impact or human errors shall not be disproportionate to the original cause and the potential effects shall be limited by robust design. Although the timber design code EN 1995 [4] complies with EN 1990, it offers very little help on how to fulfill these principles.

Increased robustness of timber structures can probably not be achieved without taking ductility, nonlinearity and deformation capacity of the connections into account, since most stress situation in wood lead to quite brittle behavior, see also [5] for further discussion on this topic. A common opinion in recent literature is that vulnerability with respect to progressive collapse due to wood brittleness can be decreased by utilization of plastic deformation of metallic fasteners. Numerous experimental results on timber connection behavior and metallic fasteners are reported, but the evaluation of these results in this context is sparse. In EN 1995, the required properties are not stated, nor is there any method available for design verification. In the paper some simple examples are studied and discussed in view of the need for ductility and deformation requirements in future design guidelines.

1.2 Robustness of structures

In US guidelines [6] progressive collapse is defined as *the spread of local damage, from an initiating event, from element to element resulting, eventually, in the collapse on an entire structure or a disproportionally larger part of it; also known as disproportionate collapse*.

Both Eurocode 1- Part 7 [2] and US guideline [6] outline overall strategies for mitigating the risk for progressive collapse in structures. A distinction can be made between design situations with identified accidental actions and the more unspecified design situations. Ideally all accidental situations should be avoided by various control schemes like event control, quality control, damage and deterioration assessment etc, but obviously a risk for accidents or intended damage will always be present. Furthermore, US NIST guideline [6] expresses a distinction between indirect methods and direct methods. The direct methods include the method of specific load resistance and the alternate load path method, while the indirect method covers prescriptive rules to provide a minimum level of integrity and connectivity in the structures without having to perform any specific analyses with respect to accidental loading.

For timber frame buildings of the type with platform floors and wall diaphragms both investigations and design guidelines to some extent exist, see e.g. test results in [7] and guidelines in [8]. For timber structures of the beam and post types and long spanning trusses and arches the availability of information seem to be less. In this paper we will make an attempt to address characteristics of beam type of structures.

2 Effects of end restraints on beams exposed to accidental loading

Herein we shall use simple beam models, either rotationally or axially restrained. The beam system may for example constitute a part of the floor of a multistory building or similar. It is assumed that the beam components are made out of wood in a conventional manner, either as solid wood or glulam. The overall design strategy usually assumes that wood behaves nearly linear elastic and that any nonlinearities will, or must, take place at possible connections. The scope here is to study the effect of the end restraints on beam systems exposed to a certain amount of unexpected additional loading Δq *in one of the bays*, in addition to the ordinary loading q. Moreover, it is assumed that the loading can be regarded as static. Preferably the beam system should withstand Δq without failure, and certainly not lead to a progressive collapse.

2.1 Beams with rotational end restraints

The basic relations for a rotationally restrained beam component, as depicted in Figure 1, are given by Eqs. (1) and (2). By use of the symbols in Figure 1, and assuming linear elastic response, the moment distribution due to uniform distributed loading is:

$$M(x) = \frac{ql^2}{12}\left[\frac{6\left(x/l\right)\left(K_2 - K_1\right) - 12 - 4K_2 + 2K_1}{12 + 4\left(K_1 + K_2\right) + K_1K_2} + 6\left(\frac{x}{l}\right)^2 - 6\left(\frac{x}{l}\right) + 1\right] \qquad (1)$$

The moment actions in the rotational springs become $M_1 = k_{r1}\theta_1$ and $M_2 = k_{r2}\theta_2$ .The rotational end stiffness is given relative to the bending stiffness of the beam, such that $K_i = k_{ri}l/EI$ where E is the modulus of elasticity and k_{ri} is the rotational stiffness of the end restraint.

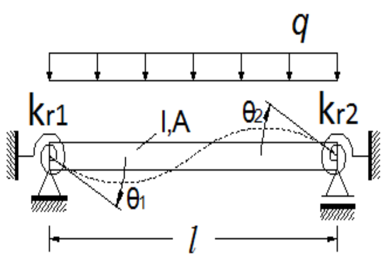

Figure 1 Rotationally restrained beam

The end rotations are given by Eq. (2) (positive clockwise, see Figure 1)

$$\theta_1 = \frac{ql^3}{12EI}\left[\frac{6 + K_2}{12 + 4\left(K_1 + K_2\right) + K_1K_2}\right] \quad \text{and} \quad \theta_2 = \frac{ql^3}{12EI}\left[\frac{-6 - K_1}{12 + 4\left(K_1 + K_2\right) + K_1K_2}\right] \qquad (2)$$

We will apply these relations on multiple span beam systems like the one depicted in Figure 2.

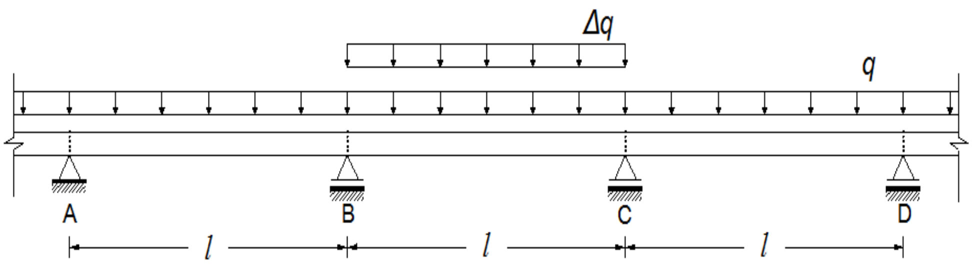

Figure 2 Multiple span beam system

The beam system is loaded by dead weight and live loading which, with sufficient accuracy, can be modeled as uniform distributed load q in all the bays. Assuming continuous beam, the moments at the supports will be close to $ql^2/12$ and the maximum moments in the spans become $M_s = ql^2/24$ due to the symmetry conditions. For symmetric cross-sections the design moments will hence be located at the supports.

However, there might also be some connections present, usually at the supports. Many types of connections in timber design show some initial slip behavior and this effect should be included in the evaluation of the moment distribution. Simplified this can be accounted for by performing the calculations in a stepwise manner by initially letting the calculation model be the one of a simply supported beam, where the end rotations might be estimated by use of Eq. (2) letting $K_1 = K_2 = 0$ until the end rotations of the beam, $\theta_1 = \theta_2 = ql^3/24EI$, have reached the level of the initial slip θ_i. For loading beyond this level, the stiffness of the end restraint should be introduced. The effect of initial slips at the supports will be a decrease of the moments at the supports and an increase of the maximum moments in the spans.

For an additional unexpected loading Δq in only one of the bays, e.g. span BC, the symmetry conditions do not apply. If we assume that the possible initial slip is either zero or the initial domain is passed due to the applied ordinary loading q, we can account for the end restraints here and apply Eq. (1), letting $q = \Delta q$. For a multiple span beam system, most cases will be covered by evaluation of internal and external bays as shown in Figure 3.

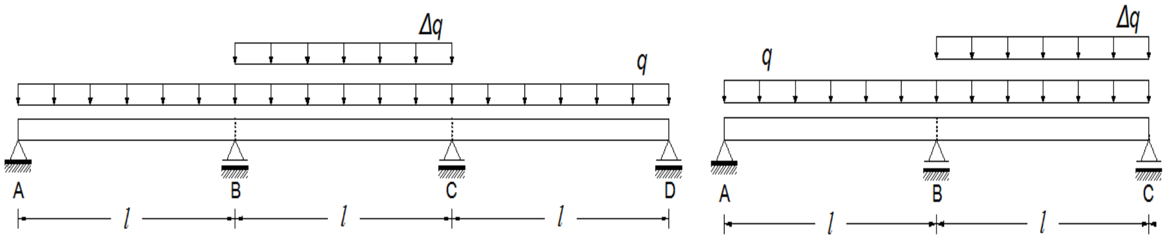

Figure 3 Rotationally restrained beam, left: internal bay, right: external bay.

For optimal design, the moment actions at the supports and in the span should be of the same size (linear elastic behavior and constant symmetric cross-section). For the internal bay BC to the left of Figure 3 exposed to the additional loading Δq, the requirements to the rotational restraints can be determined by letting $K_1 = K_2$ in Eq. (1) (symmetric condition) and equating the two moments determined from $x = 0$ and $x = l/2$.The result becomes $K_1 = K_2 = 6$ (or $k_{ri} = 6\,EI/l$) and $\Delta M_1 = \Delta M_2 = \Delta M_s = \Delta q\,l^2/16$. Similar for the external bay (BC to the right in Figure 3) we get $K_1 = 12(1+2\sqrt{2})/7 \approx 6.56$ and $\Delta M_1 = \Delta M_s \approx 1.03 \cdot \Delta q\,l^2/12$ (at $x = 0.586 \cdot l$).

For a continuous multiple bay system, like the one depicted in Figure 2, exposed to an additional (accidental) loading in a single bay, the rotational restraints from the neighboring bays (if any) will be of the order $K_1 = K_2 \approx 3$. Introduction of connections at the supports will most likely lower the rotational stiffness at the supports, also in cases where more members (e.g. columns) are connected at the supports. To avoid that an accidental load Δq will increase the moment in the span and thereby increase the possibility for brittle fracture, the stiffness must be considerable higher than $K_1 = K_2 = 7$ (or $k_{ri} = 7\,EI/l$). This will be very hard to achieve in a wooden beam system and most likely an accidental load in a single bay will increase the moment in the span relatively more than the moments at the supports and so increase the possibility of brittle fracture regardless of level of rotational end restraints. Assuming that end restraints have rotational stiffness $k_{ri} = 3\,EI/l$, the moment in the span will increase about 50% more than the moment(s) at the support(s), for both cases depicted in Figure 3. However, it is the sum of the load effects which will be governing, and the presence of rotational stiffness at the supports will certainly decrease the total moment action in the span.

2.2 Beams with axial restraints

One of the recommended actions in order to increase the robustness of structures is to tie the structural components together [2]. Again we will use a multiple bay beam systems as basis for some considerations. We assume that there are connections at each support with some rotational stiffness. Furthermore, ties are installed at the connections, or at the supports, or the neighboring beams might act as a tie, confer Figure 4. Moreover, we assume that the rotational stiffness at the supports is too small to influence the stress distribution significantly in the considered (central) beam and the structural model at the bottom of Figure 4 will be sufficient to model an accidental loading in a single bay.

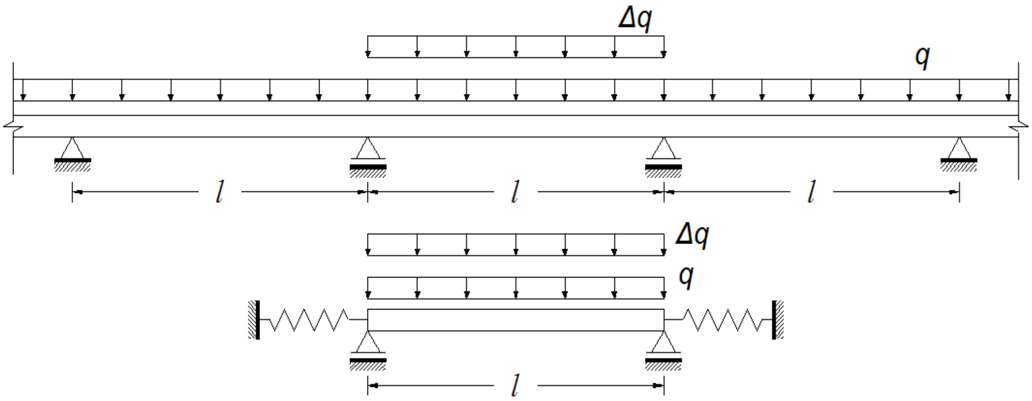

Figure 4 Axially restrained beams

The ties will have an axial stiffness probably not exceeding the axial stiffness of the beam itself, and as a simplified upper limit approach, we can use the simplified structural system shown in Figure 5. Here the axial stiffness of the tie itself is assumed to be infinite.

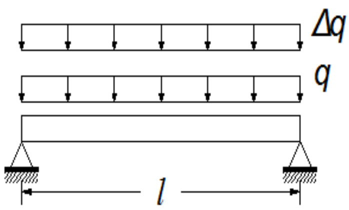

Figure 5 Axially fixed beam

By use of the principle of virtual work, an approximated simple expression can be derived assuming linear elastic material behavior. The load vs. deformation can be expressed by

$$q = \frac{384\,EI}{5\,l^4}\left(w_0 + \frac{12Aw_0^3}{35I}\right) \tag{3}$$

The symbol w_0 denotes the maximum deflection at mid-span. Equation (3) is nonlinear in w_0 and the principle of superposition does not apply. Consequently the total loading has to be used in the further considerations. Equation (3) can be expressed in dimensionless form by introducing:

$$\bar{q} = \frac{q+\Delta q}{h}\frac{5l^4}{384EI} \tag{4}$$

Moreover, we assume that the beam has a rectangular cross-section and let

$$A = b \cdot h \qquad I = bh^3/12 \qquad \beta = w_0/h \tag{5}$$

The result is

$$\bar{q} = \beta\left(1 + 144/35 \cdot \beta^2\right) \tag{6}$$

Solving for the dimensionless deflection β (deflection relative to the height of the beam h) we get

$$\beta = \frac{\alpha^{2/3} - 105}{36 \cdot \alpha^{1/3}} \qquad \text{where} \qquad \alpha = 5670 \cdot \bar{q} + 105\sqrt{105 + 2916 \cdot \bar{q}^2} \tag{7}$$

The load parameter $\bar{q}$ measure the load relative to the load and deflection on a simply supported beam, such that $\bar{q} = 1$ indicates that this load level on a similar simply supported beam would give mid-span deflection equal to the beam height h. Equation 7 is plotted on Figure 6.

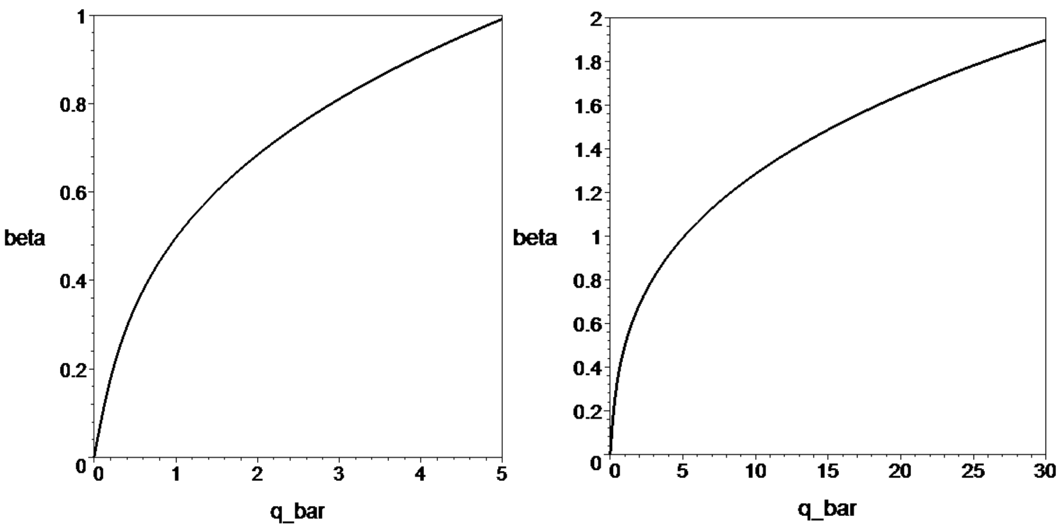

Figure 6 Relative deflection vs. transverse loading (dimensionless)

The latter terms in Eqs. (3) and (6) are due to the membrane action. Letting the membrane term in Eq. (6) also approach the value of unity, we see that the membrane action become more important than bending as $\beta > \sqrt{35/144} \approx 0.49$, or the deflection becomes larger than half of the beam height. For beams not fully restraint axially, more deflection is required to develop the membrane action. For simply supported beams with no axial restraints, the relation in Eq. (6) will be reduced to $\overline{q} = \beta$.

Maximum moment stress is evaluated directly from the shape function at mid-span and, in dimensionless form, we get:

$$m = \frac{M_s}{\frac{EI}{h/2}} = \frac{6}{\lambda^2}\beta \tag{8}$$

Here, we have introduced the slenderness ratio $\lambda = l/h$. The axial force in the beam is evaluated by calculating the average axial strain in the beam and the average axial stress then becomes (in dimensionless form):

$$n = \frac{N}{EA} = \frac{12}{5}\frac{\beta^2}{\lambda^2} \tag{9}$$

It is not clear to the authors which strength and stiffness values should be used for accidental (often impact) loading on timber structures. The additional loading should clearly be treated as instant loading. According [9] for earthquake design the elastic modulus should be increased by 10% relative to the short-term value, and it is assumed that the characteristic values are to be used. The characteristic 5% modulus of elasticity for structural solid wood is roughly 2/3 of the mean value, but the difference is smaller for glulam. Certainly all dynamic properties will be quite influenced of this choice, as the frequencies are stiffness dependent and will be quite out of range using characteristic values.

It is well known that at the strength of wood is considerably higher for instant loading; and numbers like 150% relative to the short term loading is mentioned in the literature. Furthermore, we have somewhat different strength values for tensile loading and moment action. Consequently these two failure modes have, in principle, to be treated separately. Possible interaction between these two capacities has also to be taken into account, but will be neglected here as the maximum moment occurs at mid-span, while the maximum axial force most likely will occur close to the supports.

We will compare the bending and axial stresses to the strength values, and the stress values can be evaluated from $\sigma_m = m \cdot E$ and $\sigma_t = n \cdot E$. However, it is more convenient to use dimensionless form of this comparison which becomes

$$m \leq \frac{f_m}{E_0} \qquad \text{and} \qquad n \leq \frac{f_t}{E_0} \tag{10}$$

since the dependency of the actual set of values (mean or characteristic, and time and size dependency) will be much smaller as the ratio between strength and stiffness is much less affected.

In Figure 7 the moment stress m from Eq. (8) is plotted as function of the dimensionless loading $\overline{q}$ for various values of the beam length/height ratios λ. The following ratios have been used: $\lambda = 10, 15, 20, 25, 30, 40, 60$. The smallest value of λ leads to the largest value of m for the same value of $\bar{q}$. Similar plots for the axial stress n (dimensionless) are given in Figure 8.

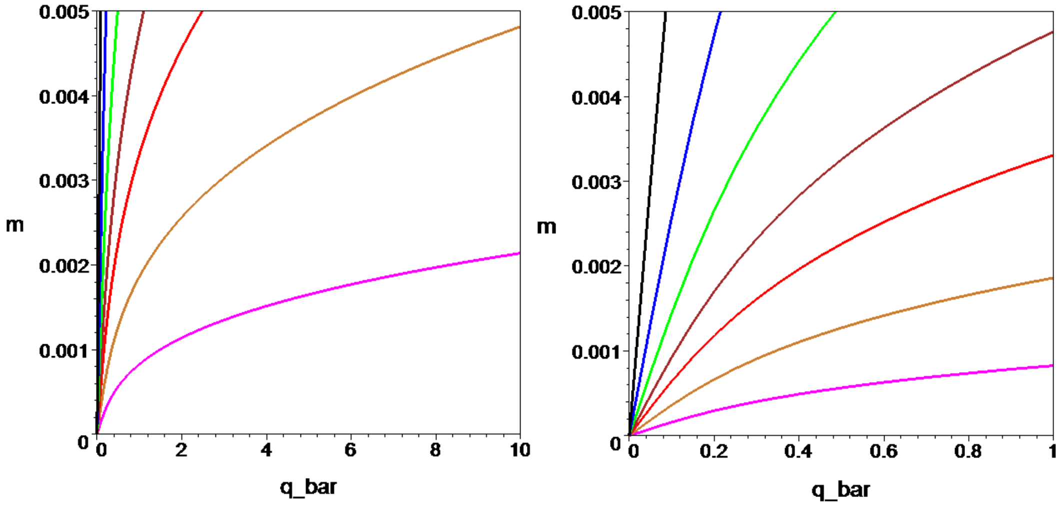

Figure 7 Moment stress *m* vs. $\bar{q}$ for $\lambda = 10, 15, 20, 25, 30, 40, 60$**.**

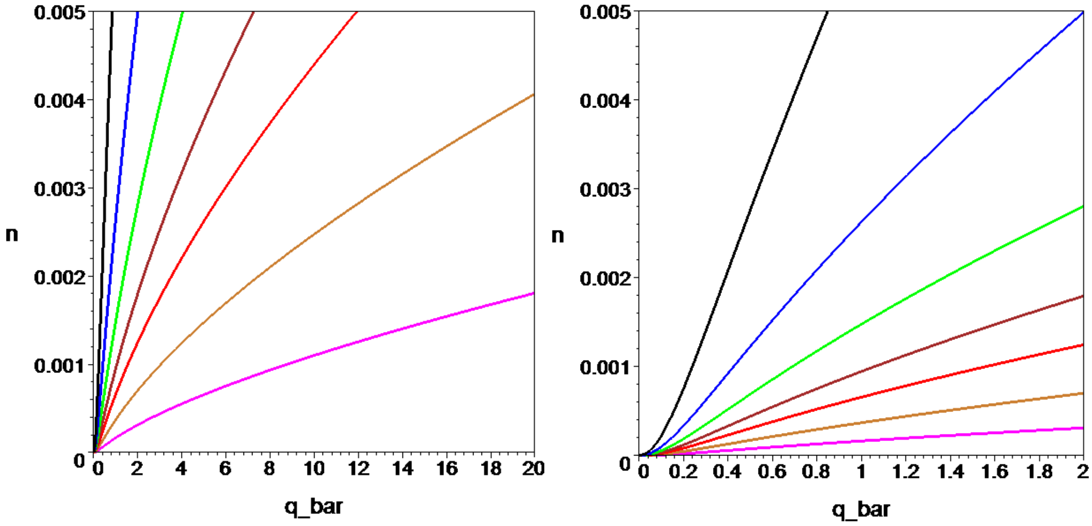

Figure 8 Axial stress *n* vs. $\bar{q}$ for $\lambda = 10, 15, 20, 25, 30, 40, 60$**.**

Using characteristic set of values for European softwood, the strength ranges for solid wood become $0.0030 < f_m/E_0 < 0.0043$ and $0.0017 < f_t/E_0 < 0.0026$, for bending and tension respectively. For glulam we find $0.0026 < f_m/E_0 < 0.0030$ and $0.0018 < f_t/E_0 < 0.0022$. Dimensionless strength ranges based on mean values for instantaneous loading are expected to be considerable larger. Based on the characteristic values above, we can roughly estimate that the moment/axial ratios *m/n* are close to 1.7 for solid wood, and 1.4 for glulam.

For a glulam beam with $\lambda = l/h = 20$ and a value of $m = 0.003$, we find e.g. from Figure 7 that the maximum load limited by bending will be $0.23 \cdot \bar{q}$. This is a 15% increase in load capacity relative to an axially unrestraint beam. For a slenderness value of $\lambda = l/h = 25$ the load bearing capacity will increase with 40% relative to pure bending, and for further increase of the slenderness a rapid increase of the load capacity occurs.

The axial tensile strength for glulam will be roughly 1.4 times less than for bending, say $n = 0.0030/1.4 = 0.0021$. By considering Figure 8 we estimate the limitation due to the axial stress to be about $\bar{q} = 1.45$, a considerable higher load level than obtained by the bending strength limitation. If we require that both the moment and axial capacity shall be fully utilized (with the assumption of $m = 0.003$ and $n = 0.0030/1.4 = 0.0021$) we find, by use of Eqs. (8) and (9), $\beta = 1.76$, $\bar{q} = 25$ and a corresponding slenderness ratio $\lambda = l/h = 60$. Usually beams have less slenderness and consequently bending will limit the potential strengthening by the use axial restraints. However, we see a significant potential for additional load bearing capacity by use of axial restraints in case of accidental loads.

3 Rate Effects

So far we have assumed that the rate of loading is too slow to create inertia effects and thereby influence the stress distribution in the structure. For accidental loading a rather high probability for rate effects is present. In this section we will just show an example on effects which might occur due to the rate of a failure process. The present example is no actual structure, but have similarities with the roof structure used in the Bad Reichenhall ice arena which failed in a fatal manner in 2006 [10]. The structural system consists of simply supported main glulam beams (*b* x *h* = 300 x 1900 mm), spanning 46 m and with spacing 7.5 m. The main beams are interconnected by a single transverse beam (200 x 600 mm) at mid span. Between the main beams a “roof skin” is assumed which is only connected to the main beams. The structural load carrying system is visualized in Figure 9. The objective is to study the effect of a possible failure in one of the main girders independent of the reason of the failure. To model failure of the middle beam the reaction forces at the supports are gradually decreased as a function of time. No other fracture or strength limitation is taken into account.

3.1 Numerical modeling

The modeling was done with a numerical code (ABAQUS) using beam elements, isotropic linear material behavior and implicit time domain solution procedure. The numerical model has only five main beams. The transverse bracing beam is continuous over all the main beams and is rigidly fixed (“glued”) to the main beams both with respect to rotations and translations. The transverse bracing beam has symmetry conditions at both ends. The beams are assumed to be of glulam quality, but since beam elements are used, only isotropic material properties are used. The elastic modulus of the main beam is kept constant at E=14000 MPa in all the analyses, while the stiffness of the bracing beam has been analyzed with four different modulus; 1000 MPa, 5000 MPa, 12000 MPa and 20000 MPa. This model feature takes into account the effect of various stiffness of the bracing beam as well as the effect of flexibility in the connections between the bracing beam and the main beams.

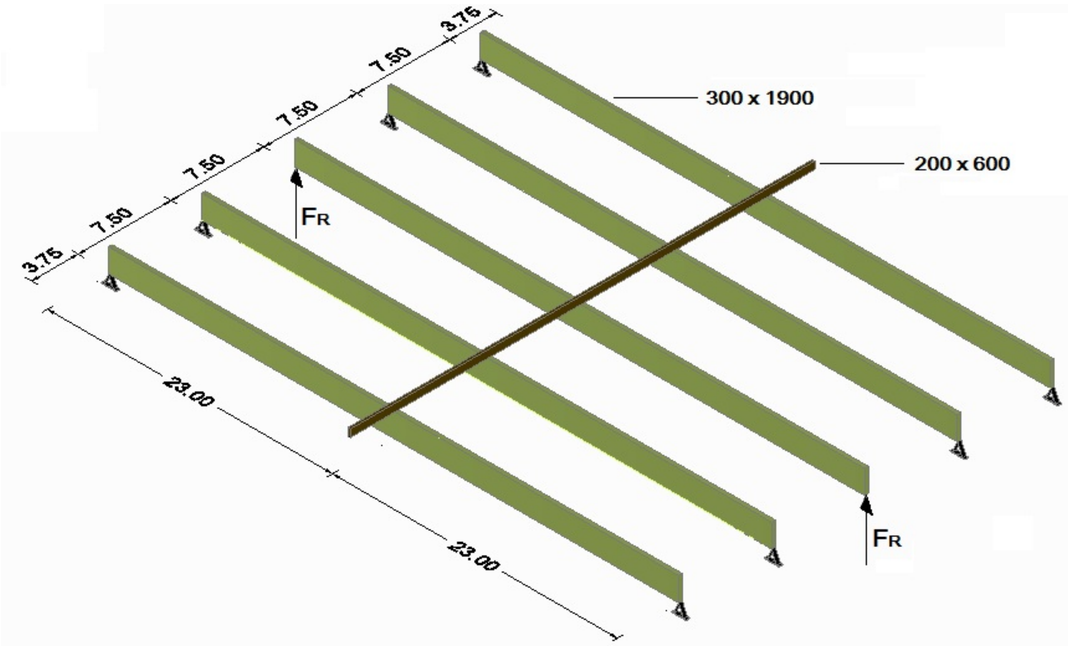

Figure 9: Roof beam system

The loading in the analyses consists of the self weight of the glulam parts plus a distributed live load of 3.5 kN/m^2. The live load is assumed uniformly distributed on the roof skin and modeled as a line load on the main beams. In case of failure of one of the main beams, the neighboring beams will get additional loading transferred by the transverse bracing beam in such a way that the total load on the roof is maintained.

The failure of the middle beam is modeled in a simplified manner by replacing the supports of the beam in the middle, by the reaction forces F_R obtained from an initial static step of the numerical simulation.

3.2 Loading and failure conditions

The system is loaded in three steps, first the distributed loads are applied linearly in a 10 second long static step, then the supports of the middle beam are replaced by the reaction forces F_R, see Figure 9. The loading is then kept constant for 10 new seconds in a dynamic step to ensure stability of the dynamic system. Finally, in the last step, failure is introduced in the middle main beam by decreasing the reaction forces F_R at the two supports. The following durations of the modeled failure was used: 0.1 second (called instant in the result section), 10 sec, 20 sec, 60 sec and 180 sec. The reduction of the reaction forces down to zero was linear over the period of failure.

3.3 Results from numerical simulations

After failure of the middle beam, the remaining beams have to carry additional loading. The additional loading is monitored for the second beam from right in Figure 9 by evaluating the interface force between the second beam and the transverse bracing beam. The interface forces are plotted in Figure 10 for close to instant failure (failure period of 0.1 s) and various stiffness of the transverse beam. The ratios between stiffness for the main beams and the transverse beam are in the order from 5 to almost 100. Numbers for the maximum forces are given in Table 1. The plots and the numbers are normalized by the present static forces prior to failure.

A small system effect occurs since the load in the static case would have been 1.5 instead of the obtained value of 1.43 (Table 1) due to the distributing effect of the transverse beam. The load increase in a pure static case is hence 43%. Considering the adjacent beams as single degree-of-freedom systems exposed to instant loading, we expect a dynamic amplification factor close to 2.0 for a linear system, and consequently a maximum dynamic force close to 1.86. However, conferring Table 1 and Figure 10, we see the interface force ratios are in the excess of 2.2, almost independent of the stiffness of the transverse coupling beam. In this case the system effect will also lead to increased dynamic amplifications at failure.

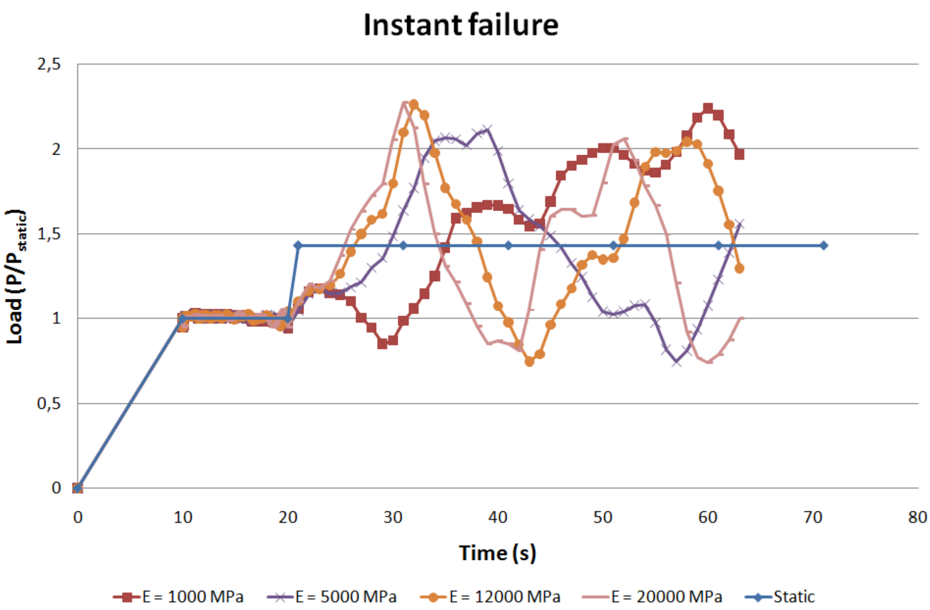

Figure 10: Maximum relative force dep. on transverse stiffness (0.1 s failure).

Table 1: Max relative interface force (dep. on stiffness (MPa) and failure duration)

Duration (s)	*E =1000*	*E = 5000*	*E = 12000*	*E = 20000*	*Static*
0.1 (instant)	2.240083	2.166364	2.264006	2.272991	**1.43**
10	2.204237	2.102571	2.020694	1.974379	
20	2.115921	1.901179	1.756142	1.646409	
60	1.885595	1.778881	1.728023	1.626378	
180	1.810653	1.665404	1.697505	1.630645	

Figure 11 presents results from simulations where the elastic modulus of the transverse beam is kept constant at $E = 12000$ MPa, but the period of failure is varied. Similar simulations have also been performed with other stiffness values of the transverse beam, and the corresponding numbers for the maximum force levels are given in Table 1. For longer failure periods, we see that the duration of the failure period in relation to the structural fundamental period comes into play. However, a considerable effect of dynamics occur in all the results, even at extremely long duration of the failure process.

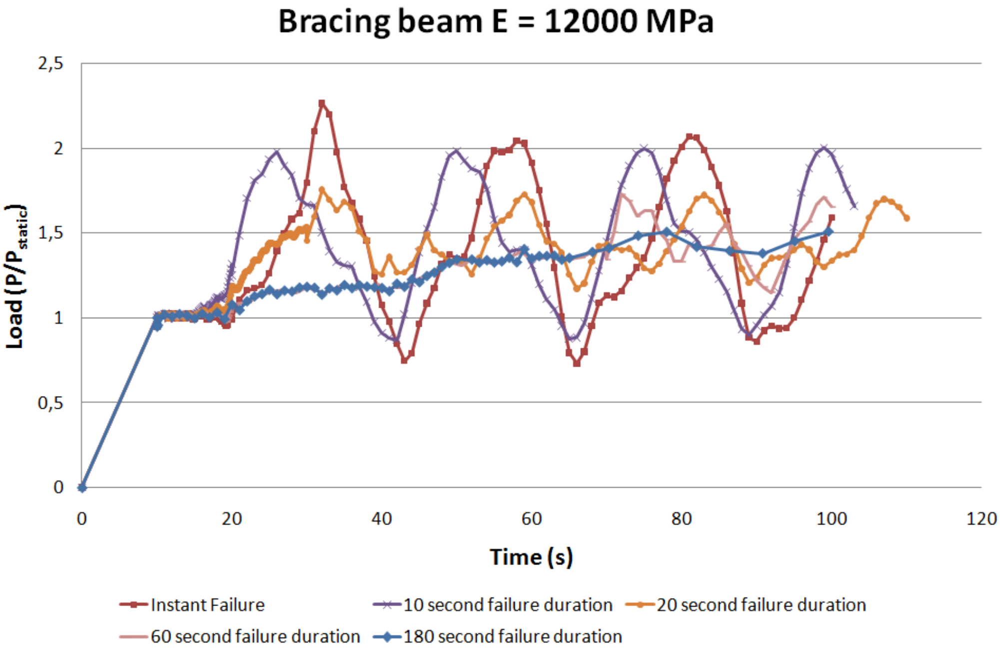

Figure 11: Maximum relative force for various failure periods.

The force responses in Figure 10 and Figure 11 are based on un-damped linear systems. In real structures nonlinearities and some damping will limit the maximum response to occur only once. In our example a release of potential energy takes place due to the failure of one of the main beams. The released energy will partly lead to kinetic energy of the moving parts and partly to an increase of the strain energy in the remaining structural components. In our example the total released energy finally has to be balanced by an increase of the strain energy, since the parts of the numerical model are not allowed to dissemble. By evaluation of the dynamic changes in the strain energy relative to a perfect static case, we find that the maximum increase of the strain energy ratio in the adjacent beams is in the range 1.3 to 2.5, increasing with decreasing failure period. The value 2.5 is obtained for instant failure. A failure or impact will hence most likely put some temporarily additional energy into the remaining parts, which has to be absorbed as strain energy or consumed by plastic work. Consequently, in design verifications, it should be documented that this additional energy does not cause failure in the adjacent parts of the main structure.

4 Deriving quantities from experimental response

4.1 Requirements

From the previous sections we see that some basic properties are needed in order to evaluate the robustness of timber structures due to accidental or impact loading. In general we need to quantify the intial slip ε_i, the linear elastic stiffness E, the ultimate strength σ_u and also the full nonlinear domain of the response, if any. (Note that we have let the term E

get an extended meaning in this section, as it here will denote the stiffness of a component and only denote the elastic modulus in the case of pure material response.) Furthermore, we let σ denote any stress or integrated stress resultant (force or moment) and ε is the strain or another integrated measure of deformation (displacement or rotation). The proportionality limit is indicated by σ_0, ε_0, the ultimate load by σ_u, ε_u and the point of fracture by σ_f, ε_f. In addition there is a need to determine the maximum strain $\varepsilon_{\max}$ measured in the experiments. The used terms are visualized in Figure 12.

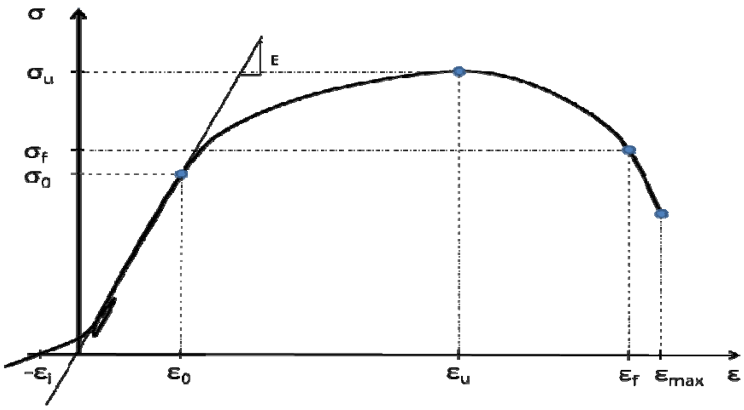

Figure 12 Parameters, load vs. deformation with initial slip removed

Traditionally the evaluation of timber structures in ultimate limit state is based on strength limitations. However, when we have dynamic effects, the short duration forces might well exceed the static force level prior to the dynamic event by more than a factor of 2. It might therefore be too conservative to make design verification using this short term load combined with long term strength values, or on strength at all. It is probably a more rational approach to perform this design verification based on energy quantities. Furthermore it should be noted that a structural load bearing system should always have a certain minimum of energy dissipation in order to avoid fracture due to a single minor stress wave. This can be accomplished by e.g. some minimum requirements with respect to the so-called ductility.

4.2 Quantifications of experimental response

The nonlinear domain represents the ability to redistribute forces and dissipate energy, which is a large benefit with respect to robustness. Design verification with respect to impact and accidental loading in ultimate limit state will probably be along two possible paths, either by design requirements in codes and simplified verification rules, or by the use of numerical models like the FEM method. In the first case the nonlinear domain has to be quantified in a simple or integrated manner, while the numerical methods call for a complete description of the experimental response including the softening part and fracture. Both needs should be available from reported experiments. In [11] a consistent method for quantification of parameters are presented and this method is also introduced here. The experimental response (“stress” vs. “strain”) can be expressed as:

$$\sigma = \begin{cases} E \cdot \varepsilon & \varepsilon < \sigma_0 / E \\ f(\varepsilon_p) & \varepsilon \geq \sigma_0 / E \end{cases} \tag{11}$$

where the strain leading to stress in the structure is $\varepsilon = \varepsilon_m - \varepsilon_i$. Moreover, ε_m is the measured deformation in experimental tests, or the total deformation in a structural calculation. The initial slip ε_i is a linearized value determined in accordance with linear elastic model in the initial regime, confer Figure 12. Remark that the nonlinear part $f(\varepsilon_p)$ is modeled solely as a function of the permanent ("plastic") deformation, which is given by:

$$\varepsilon_p = \varepsilon - \frac{\sigma}{E} \tag{12}$$

It is assumed that the total strain ε is an additive composition of elastic and fully recoverable strain $\varepsilon_e = \sigma/E$, and permanent, non-recoverable strain ε_p. The advantage of the formulation in Eq. (11) is that the mathematical requirements to a model of the nonlinear part $f(\varepsilon_p)$ become more relaxed and it complies with the standard procedures in numerical modeling of materials.

4.3 Characterization of nonlinear response

Having determined the intial slip ε_i , the linear elastic stiffness E , a characterization of the nonlinear domain of the response is needed. The choice of analytical expression for $\sigma = f(\varepsilon_p)$ is unimportant if fitted by e.g. the method of least squares and models the measured response well. After an analytical expression for $\sigma = f(\varepsilon_p)$ is determined, numerical analyses may be performed and the structural behavior evaluated, both for static and dynamical loading. It should be recognized that rate of loading can influence all of the parameters, and the nonlinear part is particularly sensitive.

Morover, the analytical expression for $\sigma = f(\varepsilon_p)$ can also be used for evaluation of ductility and impact resistance on the basis of simplified methods, or as basis for requirements in codes. According to [11] useful measures of ductility are given by Eqs. (13), (15) and (16).

The ductility measure Ds_{ue} is a strain based measure which compares the ultimate permament (plastic) strain to the corresponding elastic strain and gives directly a measure of the nonlinearity of a component or connection;

$$Ds_{ue} = \frac{\varepsilon_{pu}}{\varepsilon_{eu}} = \frac{\varepsilon_{pu}}{\sigma_u / E} \tag{13}$$

The measure Ds_{ue} is particularly useful for statements on minimum ductility requirements or evaluations of redistribution of static loads. The total deformation at ultimate load can be evaluated directly from:

$$\varepsilon_u = \frac{\sigma_u}{E}\left(1 + Ds_{ue}\right) \tag{14}$$

A similar measure of ductility based on energy is Dw_{ue}, which is calculated by:

$$Dw_{ue} = \frac{W_{pu}}{W_{eu}} = \frac{\int_0^{\varepsilon_{pu}} \sigma d\varepsilon_p}{\int_0^{\sigma_u} \sigma d\varepsilon_e} = \frac{\int_0^{\varepsilon_{pu}} f(\varepsilon_p) d\varepsilon_p}{\frac{\sigma_u^2}{2E}} \tag{15}$$

Here the permanent (plastic) dissipation up to the ultimate load level is compared to the elastic energy stored at the same load level. Classifications of experiments based on Eq. (13) and Eq. (15) will usually give similar mutual relation between the experimental results, but the actual numbers will differ.

For short duration loading (impact) the total permanent dissipation up to fracture should be taken into account, and by scaling it by the maximum elastic energy, we get

$$Dw_{fe} = \frac{W_{pf}}{W_{eu}} = \frac{\int_0^{\varepsilon_{pf}} \sigma d\varepsilon_p}{\int_0^{\sigma_u} \sigma d\varepsilon_e} = \frac{\int_0^{\varepsilon_{pf}} f(\varepsilon_p) d\varepsilon_p}{\frac{\sigma_u^2}{2E}} \tag{16}$$

It is quite straightforward to evaluate energy criterions for robustness from both Eqs. (15) and (16) [11].

5 Concluding remarks

For beam and post systems commonly used in timber structures few alternative load paths are directly available in case of a failing member. Accidental loads and impacts are usually of local nature and their possible effects should also be kept local, avoiding progressive collapse mechanisms. This structural property is commonly denoted robustness and a minimum robustness should be inherent in all load bearing structures.

Herein some structural properties like rotational and axial restraints and effects of rate of loading have been highlighted in view of local accidental loading, both statically and dynamically. The effects of end restraints, coupling stiffness between components and duration of the loading have to some extent been discussed, but clearly there is a need for a more comprehensive studies on these topics. Finally, a method which can be used for characterization of necessary quantities with respect to a simplified evaluation of robustness was introduced. It appears to be a need for more guidelines and rules on how to deal with accidental loading and impact situations with respect to the behavior of timber structures. Moreover, the material and connection behavior and their characteristics with respect to instant loading and calculations, should be paid more attention.

6 References

[1] Früwald, E. et al: Design of safe timber structures – How can we learn from structural failures in concrete, steel and timber? Report TVBK-3053. Div. of Struct. Eng. Lund University, Sweden 2007.

[2] European Standard EN 1991-1-7:2006 Eurocode 1 – Part 1-7: Actions on structures. General actions. Accidental actions, European Committee for Standardization, Bruxelles, Belgium, July 2006.

[3] European Standard EN 1990:2002 Eurocode - Basis of structural design. European Committee for Standardization, Bruxelles, Belgium, April 2002.

[4] European Standard EN 1995-1-1:2004/A1:2008 Eurocode 5: Design of timber structures – Part 1-1: General – Common rules and rules for buildings/incl Amendment A1, European Committee for Standardization, Bruxelles, Belgium, November 2004/2008.

[5] Sørensen, J.D. et al: COST – Design for Robustness of timber structures. ISBN978-3-8322-9949-1, Shaker Verlag, Germany 2011.

[6] Ellingwood, B.R. et al: Best practices for reducing the potential for progressive collapse in buildings. NISTIR 7396, US Department of Commerce, USA 2007.

[7] Enjily, V.: The performance of timber structures, elements and components. COST action E24, Oct. 2001, Denmark.

[8] Department of defence, USA: Unified Facilities criteria (UFC). Design of buildings to resist progressive collapse. UFC 4-023-03, July-2009/January 2010.

[9] European Standard EN 1998-1:2004 Eurocode 8: Design of structures for earthquake resistance– Part 1: General rules, seismic actions and rules for buildings, European Committee for Standardization, Bruxelles, Belgium, December 2004.

[10] Winter, S. and Kreuzinger, H.: The Bad Reichenhall ice arena collapse and the necessary consequences for wide span timber structures. Proceedings of WCTE 2008, Miyazaki, Japan.

[11] Malo, K.A., Siem, J. and Ellingsbø P.: Quantifying ductility in timber structures. Engineering Structures (2011), doi:10.1016/j.engstruct.2011.03.002.

CIB-W18/44-15-6

INTERNATIONAL COUNCIL FOR RESEARCH AND INNOVATION
IN BUILDING AND CONSTRUCTION

WORKING COMMISSION W18 - TIMBER STRUCTURES

ENHANCED MODEL OF THE NONLINEAR LOAD-BEARING BEHAVIOR OF WOOD SHEAR WALLS AND DIAPHRAGMS

M H Kessel
C Hall

Technische Universität Braunschweig

GERMANY

MEETING FORTY FOUR

ALGHERO

ITALY

AUGUST 2011

Presented by C Hall
M Yasumura and C Hall discussed the pin joint at the bottom of the panel. C Hall responded that there were boundary conditions for the vertical members for uplift considerations. These methods could be applied in general such that one could consider hold-downs etc.
F Lam asked whether the approach had been compared with results from experimental data or verified model predictions to support the conclusions. C Hall responded that on-going work with FEM was underway.
H Blass commented that considering our criteria for paper acceptance, this work should have been accepted as research note.

Enhanced Model of the Nonlinear Load-bearing Behaviour of Wood Shear Walls and Diaphragms

Martin H. Kessel, Christoph Hall

Institut für Baukonstruktion und Holzbau, iBHolz

Technische Universität Braunschweig, Germany

1 Introduction

Load-bearing models for the static analysis of wood shear walls and diaphragms are statically indeterminate, due to the use of numerous components as sheathing panels, framing members and fasteners. Therefore the stiffness of the structure components and their fasteners has a non negligible impact on the internal force distribution.

The analysis of loads and deformations of wood-frame structures considering the plastic ductile load-bearing behaviour of the anchoring and the interconnection between framing members and sheathing as well as the elastic brittle behaviour of the framing members and sheathing has, until now, only been possible with complex finite element modelling.

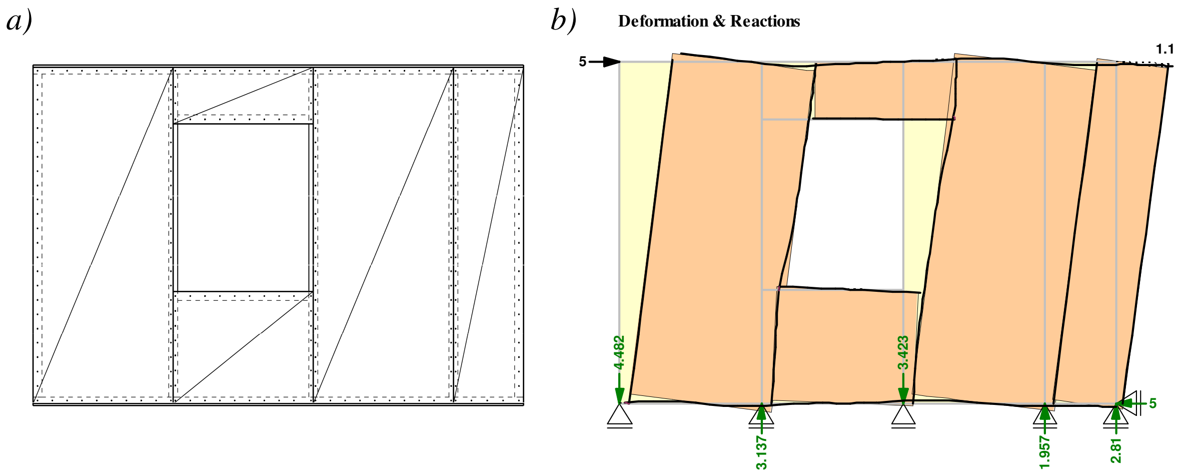

Figure 1: Example of a shear wall
a) design, b) deformation and reactions

With simplified methods suitable for manual calculations such as the segmented shear wall method of Kessel [1] in DIN 1052 and the german non-contradictory complementary information of EC5 it is only possible to define the lower limit of the load bearing capacity. The actual load bearing capacity or the deformations or stiffness of wood shear walls and diaphragms cannot be analysed by applying the segmented shear wall method.

This paper will introduce you to an enhanced member model to simulate the physical non linear load bearing behaviour up to the point where the maximum load bearing capacity is reached, which means until structure failure. For linear elastic load bearing behaviour the model can be applied to analytically determine the internal force variables, the stresses of interconnection and the deformations. For plastic behaviour an iteratively calculated solution is provided. The model can be applied to almost any problem in timber frame construction, independent of structure design. For example it is possible to consider the significant influence of plastifying anchorage against uplift as well as uplifted supports of wood shear walls.

The interaction of timber frames with structural parts other than timber frame structures, for example steel frames or reinforced concrete columns, can be modelled within the same member structure.

The results gained from this model (stresses and deformations) are comparable to the results of a Finite Element Analysis, however, requiring much less input and calculation effort.

2 The Enhanced Member Model

The enhanced member model is very similar to the member models of current software applications applying the deformation method. The main difference to the regular member models is the use of two new elements enabling the non-linear modelling of the continuous interconnection between framing members and sheathing.

The main advantage of the use of these elements compared to a detailed FE modelling of each fastener is that the single fasteners between framing member and sheathing can be "dispersed" across the total length of the structure. Thus a complete interconnection area or even the complete interconnection between a framing member and one or two panels can be simulated in a single element. Within this element the framing member acts like a beam that is continuously elastically supported along the member axis as well as vertical to the member axis. The line stiffness k of the member's continuous elastic support against the (rigid) panel edge results from slip modulus K of the individual fasteners and the fastener spacing a_v. The member's bending stiffness EI and extensional stiffness EA are closely related to interconnection stiffness k, so that framing member and interconnection can only jointly be modelled in an element.

2.1 New Elements

In the sheathing plane the framing members are usually connected to one or two panels. Therefore it is necessary to develop two different elements for the modelling of the framing members. One element is necessary to model a framing member and its connection to one panel (4-node element, Figure 2a), the other element is used to model a framing member and its connection to two panels (6-node element, Figure 2b).

a) 4-node-element to model an elastic wooden framing member and its connection to one rigid panel

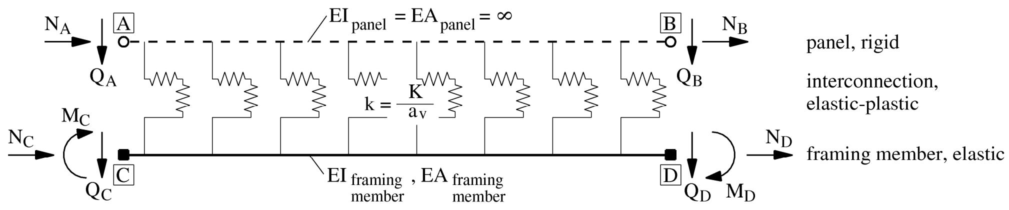

b) 6-node-element to model an elastic wooden framing member and its connection to two rigid panels

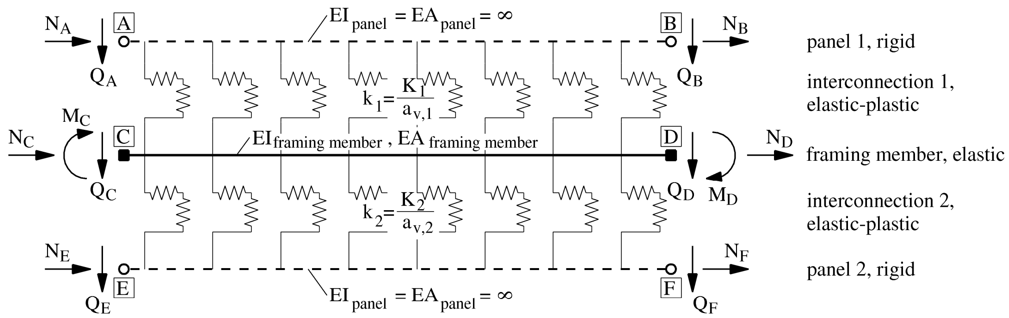

Figure 2: New Elements

While nodes A, B, E, and F connecting the element to the panel only have two degrees of freedom, member nodes C and D have three degrees of freedom. These are the displacements parallel and perpendicular to the member axis and one rotation. The four-node element has 10 degrees of freedom, the six-node element has 14 degrees of freedom. For each degree of freedom of a node there is a corresponding stress resultant (see Figure 2). If a virtual unit displacement is applied to an element node, the values of the stress resultant resulting from this deformation correspond to the values of the corresponding lines of the stiffness matrix of this element. Thus, the four-node element is described by a 10x10 stiffness matrix, the six-node element by a 14x14 stiffness matrix.

Nodes A, C, and E as well as nodes B, D, and F are coincident in an undeformed state. The more extended presentation in Figure 2 is used to present a more vivid illustration.

In the member model it is not possible to model the sheathing panels as membrane or shell elements. Instead, sheathing panels are applied with rigid coupling of their corner nodes. Thus, in the model the panels are rigid.

2.1.1 Linear Elastic Behaviour

Until yield point R is reached the force deflection behaviour of the fasteners between framing member and panel can be considered linear-elastic (see Figure 3).

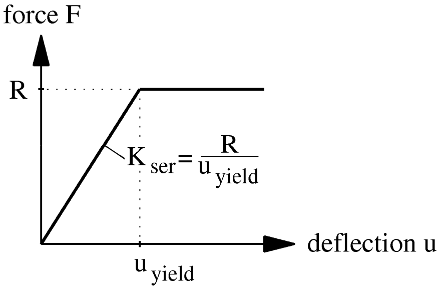

Figure 3: Simplified force-deflection relation of the fasteners

If slip modulus K_{ser} of the fasteners is put into relation to fastener spacing a_v, the member is quasi elastically supported by the rigid panels. As long as no fastener reaches its yield displacement u_{yield}, all displacement states of the 4-node and 6-node element can be described by the differential equations of the member that is elastically supported along the longitudinal member axis and vertical to the member axis. In a calculation according to first order theory the directions parallel and vertical to the member axis do not depend on each other and can be considered separately.

The stiffness matrix of the elements can be derived based on the principle of virtual displacements. According to this principle you select real unit displacement approaches (see for example Figure 4) that at the same time are used as virtual displacements.

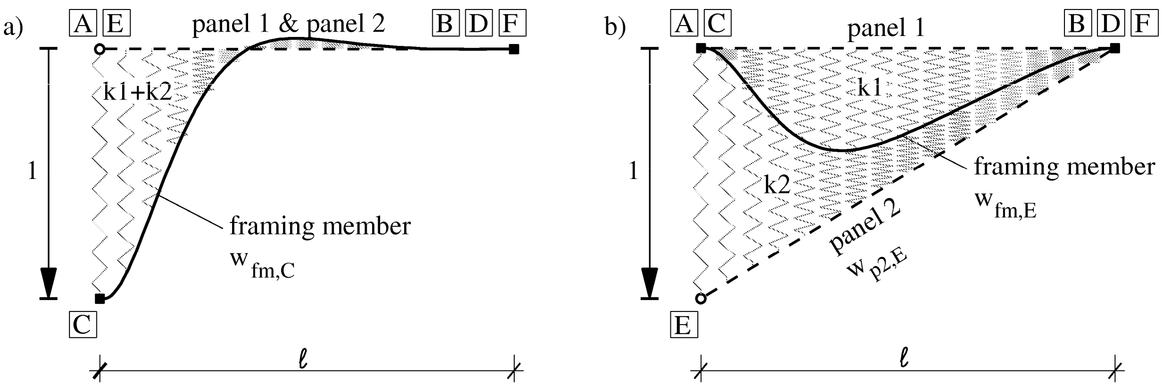

Figure 4: Deformations of the 6-node element resulting from a unit displacement of a) member node C and b) panel node E

The continuous elastic support along the longitudinal axis of the member which is only loaded by single loads at the two member ends can be described by the differential equation

$$u'' - \frac{k}{EA} u = 0$$

the solution of which is

$$u = \cosh(\lambda x)C_1 + \sinh(\lambda x)C_2 \qquad \text{with } \lambda = \sqrt{\frac{k}{EA}}$$

[2]. The differential equation for the member elastically supported perpendicular to the member axis is:

$$w'''' + 4a^4 w = 0 \qquad \text{with } a = \sqrt[4]{\frac{k}{4EI}} \text{ and } k = \frac{K_{ser}}{a_v}.$$

The general solution [2]

$$w = \cos(ax)\cosh(ax)C_1 + \cos(ax)\sinh(ax)C_2 + \sin(ax)\cosh(ax)C_3 + \sin(ax)\sinh(ax)C_4$$

includes the four integration constants C_1 to C_4. They are eliminated by the insertion of the edge conditions for each unit deformation state. If for example the vertical displacement of member node C is set to 1, and the vertical displacement degree of freedom of member node D and the rotational degrees of freedom of member nodes C and D are set to 0 (see Figure. 4a), you receive a linear equation system of four conditional equations. On the basis of these equations the integration constants are calculated. The insertion of these integration constants into the general solution leads to the function of the deflection curve shown in Figure 4a.:

$$w_{fm,C} = \frac{\cos(\xi)\cosh(ax) + \cos(ax)\cosh(\xi) - 2\cos(ax)\cosh(ax) - \sin(\xi)\sinh(ax) + \sin(ax)\sinh(\xi)}{\cos(2\ell a) + \cosh(2\ell a) - 2}$$

$$\text{with } \xi = a(2\ell - x) \qquad \text{and } a = \sqrt[4]{\frac{k_1 + k_2}{4EI}}.$$

In order to obtain, for example, value $k_{6,12}$ (entered in 6th line and 12th column of the stiffness matrix of the 6-node element) which corresponds to the shear force acting in node E resulting from a unit displacement of node C, the following integrals must be evaluated:

$$k_{6,12} = \int_0^\ell k_1 \cdot \delta w_{fm,C} \cdot w_{p2,E}\, dx + \int_0^\ell k_2 \cdot \delta w_{fm,C} \cdot \left(w_{p2,E} - w_{fm,E}\right) dx + \int_0^\ell EI \cdot \delta w''_{fm,C} \cdot w''_{fm,E}\, dx$$

The elastic forces of interconnection 1 and interconnection 2 do work on the virtual displacements of the framing member and the bending moment within the framing member does work on the virtual flection of the member. Similar to the other matrix values the result of this integration is very complex so that no further descriptions are included in this paper.

With the stiffness matrices of the elements it is now possible to define the total stiffness matrix and to calculate the unknown node displacements because the final displacements are composed of the unit displacement approaches multiplied by the node displacements. The internal force variables of all members and interconnection stresses can now be recovered from these displacement functions and their derivatives.

2.1.2 Plastic Behaviour of the Interconnection Structure

As soon as the displacement of the interconnection structure reaches the yield point u_{yield} (see Figure 3) in a 4-node or 6-node element the element is subjected to a physically nonlinear behaviour. Depending on the displacement of the member in relation to either one panel or two panels, partial or full plastification of the structure may occur. Partial plastification may occur at various points within the element length. A modelling of the plastic zones as an elastic support as described in 2.1.1 is not recommended as the equivalent elastic stiffness of the support would have to be iteratively calculated for all plastic zones of the load-bearing structure. This would not only result in a complex calculation procedure, it also runs the risk that the calculation becomes unstable.

It is rather recommended to divide the element into elastic and plastic zones. The elastic zones are modelled with the elastic 4-node and 6-node elements similar to the ones described above. For the plastic zones the elastic support stiffness of the plasticized interconnection is removed and replaced by a substitute load group. For the 4-node element this is realized by using a regular, not elastically supported member between nodes C and D which is subjected to a substitute load. In order to maintain equilibrium within the element an equivalent load is applied with the opposite orientation to panel nodes A and B. Figure 5 shows such a 4-node element in the elastic (Fig. 5a) and in the partial plastic state (Fig. 5b). The partial plastic zone extends over length ℓ_{pl}.

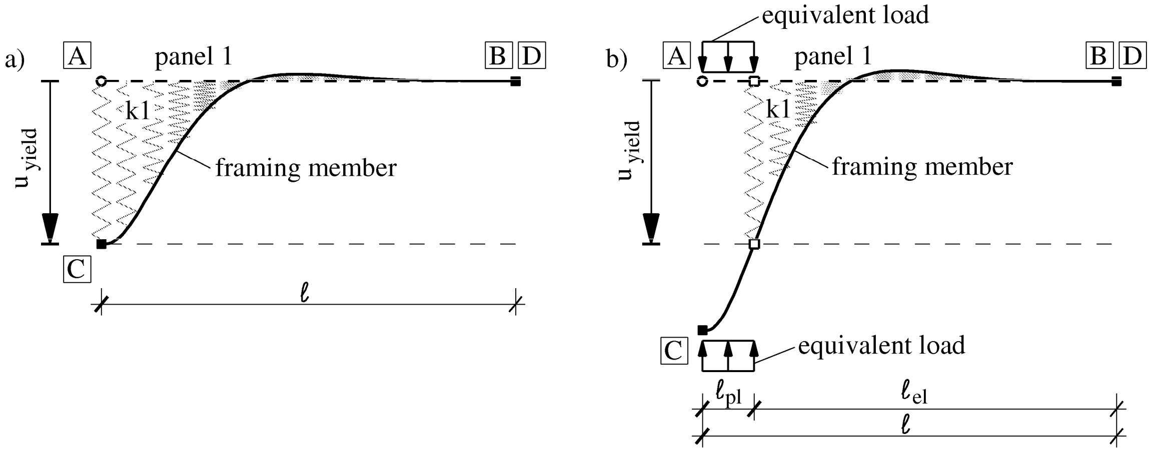

Figure 5: 4-node element when it a) reaches and b) exceeds the yield point u_{yield} of the structure

For a 6-node element it plays a decisive role if only one interconnection or both interconnections start to yield. If both interconnections yield the framing member will be modelled by a regular member element, however, it will be subjected to two substitute loads. Apart from panel nodes A and B, panel nodes E and F will also be subjected to a substitute load. If only one of the two interconnections yields, the framing member and the elastic structure will be modelled by a 4-node element, the plastic structure by substitute loads.

The different elastic and plastic zones within an element are regrouped to a 4-node or 6-node element based on a static condensation, so that the number of nodes and elements of the static model remains the same in the plastic state in relation to the elastic state.

The size of the resulting substitute loads corresponds to the linear strength R of the fasteners. As the fasteners are deflected parallel and vertical to the member axis the resulting substitute loads must be decomposed into load components acting in both directions. The ratio of the load components changes if the stiffness of the load bearing structure changes locally. This happens if other interconnections of the load bearing structure exceed their yield point due to increased loads.

Therefore it is recommended to increase the external load step by step until the target value or the kinematic chain is reached. One load step covers the yielding of one interconnection zone to the yielding of the next interconnection zone. Within the load step the ratios of the substitute load components must be iteratively varied until the displacements of the load bearing structure do not change from one iteration step to the next one within defined tolerance limits.

At the time of creating this paper the development of the algorithm for the modelling of plastic load-bearing behaviour has not been completed. Thus it is not possible to present a practical application with plasticizing interconnections.

2.2 Compression Contact between Members

If a lateral load is applied to a shear wall or a diaphragm, inplane displacement of the members will occur. Thus the members will come into contact with each other and loads are transferred from one member to the other. The parapet member of a window opening, for example, transfers its longitudinal force by compression contact to the vertical member next to the window opening. The vertical member carries this load on the one hand by deflection, on the other hand by the elastic support of the fasteners (see Figures 1, 6 and 7).

It is recommended that a model of the member elements described above should simulate the compression contact between members by using simple spring elements. These are 2-node elements that are applied between the member nodes and that only offer compression stiffness if it is applied against the penetration of the member elements. The compression stiffness is a result of the stiffness perpendicular to the grain of the wood and the contact area.

It is also possible to consider slippage. In this context it is necessary to increase the load step-by-step as the activation of the compression contact depends on the displacement of the compression contact element.

In general, these spring elements can also be used to model a compression contact between two panels to avoid the penetration of adjacent panels.

2.3 Anchorage

Similar to the compression contact element the anchorage can also be modelled by using a simple spring element. This spring element can be applied between a rigidly mounted support node and the base point node of a member. Again, slippage can be considered.

Provided that brittle failure of the anchorage of the real load bearing structure is eliminated and, instead, the anchorage shows ductile force-deflection behaviour, the spring element can be assigned a load-deflection curve as shown in Figure 3. If yield point R is reached, the strength of the spring element is set to zero and instead a substitute load R is applied to the member node.

3 Practical Application: Shear Wall with Opening

The performance of the newly developed elements shall be demonstrated by the shear wall shown in Figure 1. To this end the elements were integrated into a small analysis tool for frameworks. The modelling of the shear wall only required 52 nodes and 27 elements (Figure 6). For example, the vertical member going from the bottom member to the top member on the left side of the window was modelled with three elements. 6-node element 7 is connected to panel element 1 and to panel element 2. Node 28 is used to connect 6-node element 7 to 4-node element 8 which is also connected to panel element 1. The 6-node element 9 is connected to elements 8, 1 and 3. Contact element 26 prevents the parapet member (element 20) and the vertical member modelled by elements 7, 8 and 9 from penetration into each. The resulting deformation of the complete shear wall is illustrated in Figure 1b.

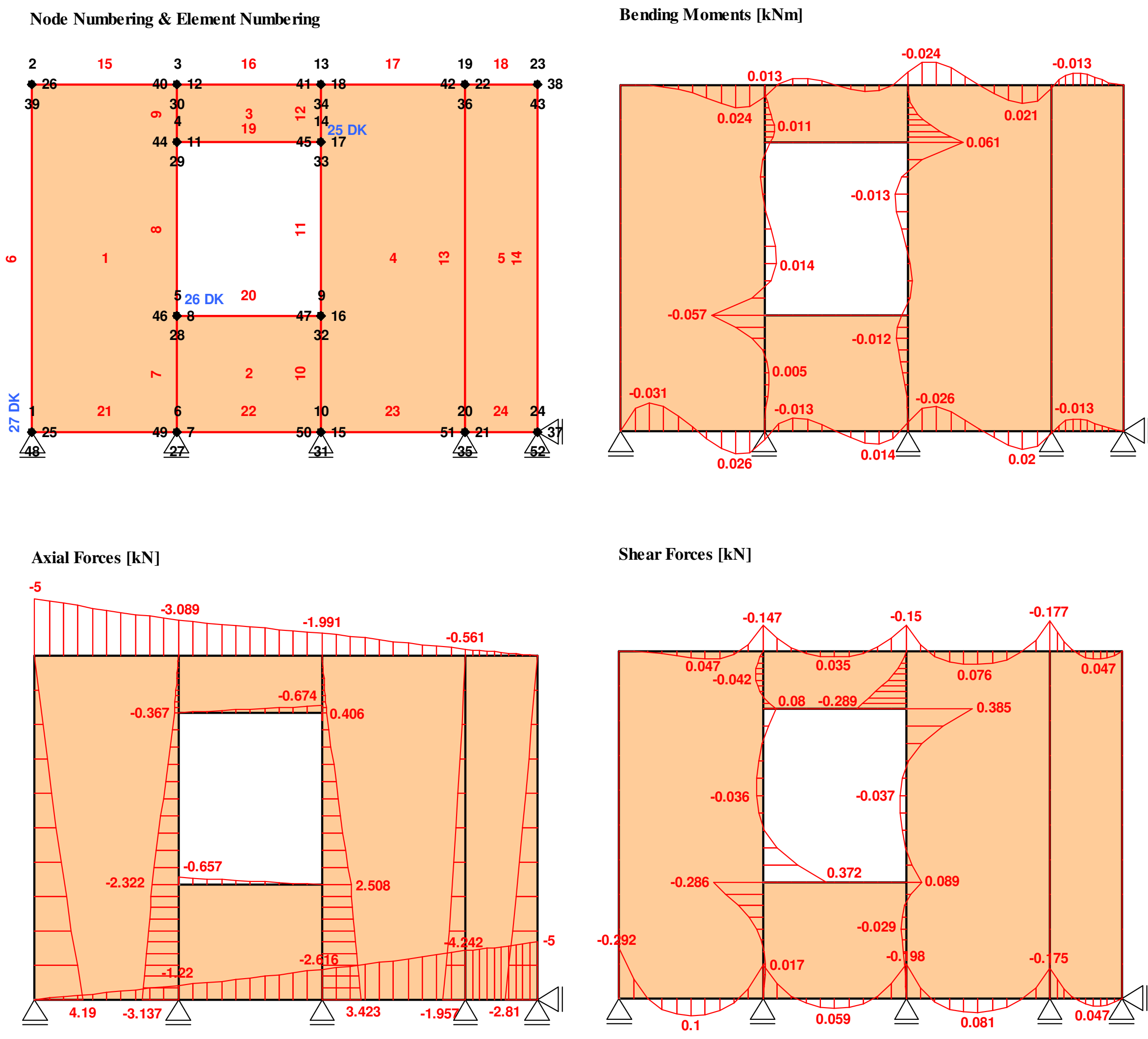

Figure 6: Element usage and stress resultants of the members of the shear wall shown in Figure 1

Figures 6 and 7 show the results of an elastic calculation. Even though the vertical members are anchored at nodes 25 and 31, interconnection stresses $s_{v,90}$ acting perpendicular to the panel edges occur at almost all panel edges. Some of these stresses are of the order of the interconnection stresses $s_{v,0}$ acting parallel to the panel edge.

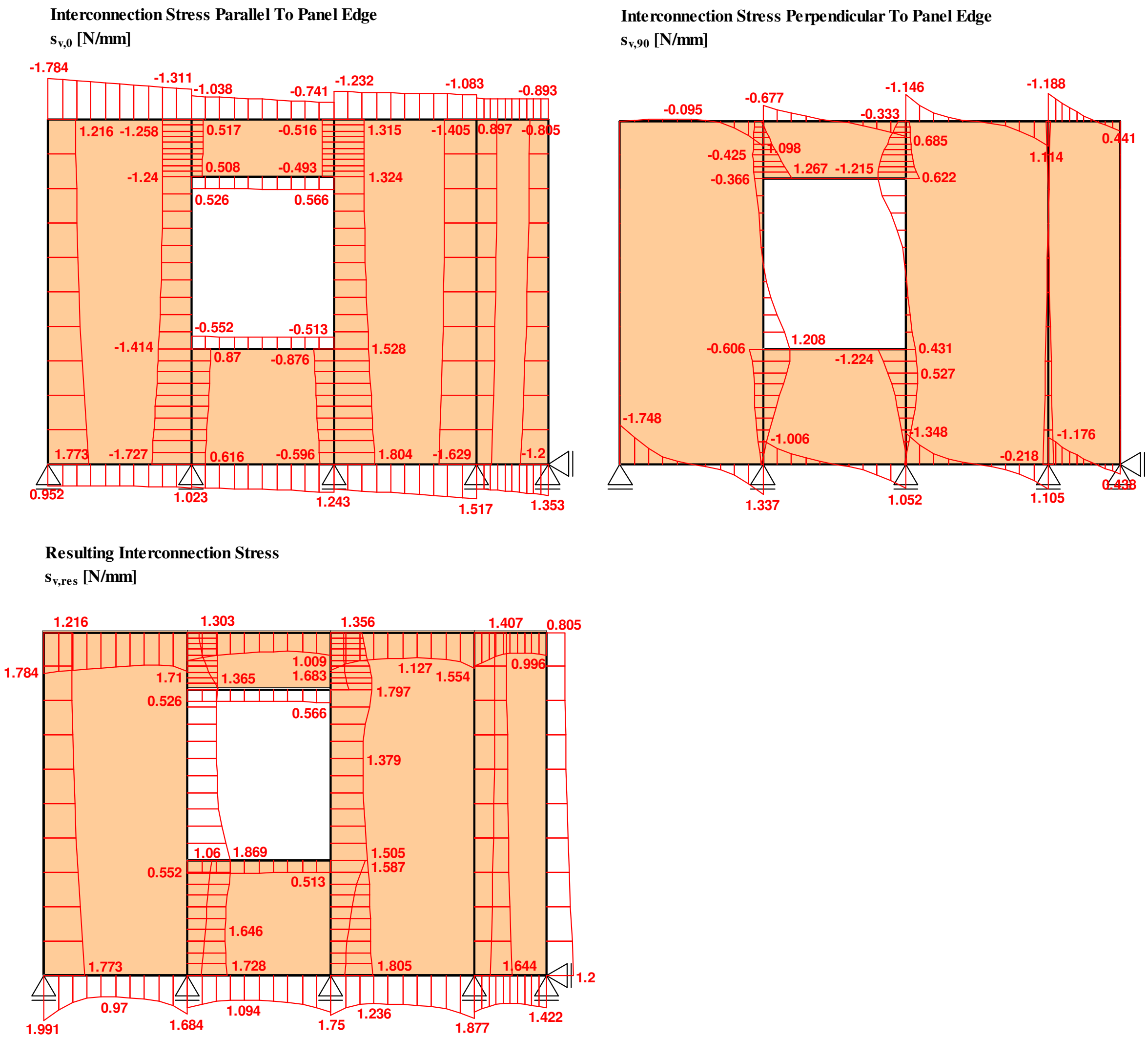

Figure 7: Interconnection stresses of the shear wall shown in Figure 1

Neither the deformation shown in Figure 1 nor the stresses shown in Figures 6 and 7 could be calculated with simplified methods with a reasonable effort.

4 Advantages of the Enhanced Member Model Compared to the Segmented Shear Wall Method of DIN 1052 and EC5

In contrast to the elastic segmented shear wall method of DIN 1052 and EC5 the new model enables a more reliable estimation of the stiffness of wood-frame structures. Thus it is possible to estimate better the load-deformation behaviour of such structures. This is for example important for wood-frame buildings if the distribution of the wind load to each of the storey walls shall be estimated.

A real load-bearing structure contains components that support force transfer but which are neglected by the segmented shear wall method (for example wall segments above and below openings). Thus the interconnection between framing member and sheathing is not only stressed parallel to the panel edge resulting from shear flow $s_{v,0}$ (apart from some exceptions) but also perpendicular to the panel edge resulting from $s_{v,90}$ (Figure 7). Thus, in a real structure, the framing members are subjected to longitudinal stresses as well as bending and shear stresses and the sheathing panels are subjected to stresses acting perpendicular to the panel edge. If the segmented shear wall method is applied it is not possible to give an estimation of the size of these stresses. The presented enhanced member model could serve as validation of the segmented shear wall method by revealing the error in terms of an error estimation.

With the presented enhanced member model it is less complex to perform parameter studies on wood-frame constructions which could be the basis for more reliable simplified calculation methods.

Furthermore the direct use of the enhanced member model is an economical option for static analysis of wood shear walls and diaphragms.

References

[1] Kessel M. H. (2004), *Erläuterungen zu den Abschnitten 8.7 und 10.6 der DIN 1052-2004*. Herausgegeben von der Deutschen Gesellschaft für Holzforschung DGfH

[2] Mehlhorn G. (1995): *Der Ingenieurbau: Grundwissen*, Ernst & Sohn, Berlin

CIB-W18/44-15-7

INTERNATIONAL COUNCIL FOR RESEARCH AND INNOVATION
IN BUILDING AND CONSTRUCTION

WORKING COMMISSION W18 - TIMBER STRUCTURES

SEISMIC PERFORMANCE OF CROSS-LAMINATED WOOD PANELS

M Popovski,

E Karacabeyli

FPInnovations, Building Systems Department

Vancouver

CANADA

MEETING FORTY FOUR

ALGHERO

ITALY

AUGUST 2011

Presented by M Popovski

A Buchanan stated that this work made comparisons between CLT and light wood frame systems. In case of light wood frame system there are many nail connectors helping the structure resist the lateral forces. In CLT only few hold down and brackets devices were available such that the entire system relied on few connectors. For CLT case with a nail strip, it is more similar to the light frame wall but still not the same. A Buchanan stated that more care would be needed to treat the CLT system. M Popovski agreed and stated in general CLT system connections are more localized but there can still be a lot of nail available.

B Dujic S Pampanin and M Popovski discussed where sliding occurred in the load CLT walls.

A Ceccotti asked about the equivalent viscous damping. M Popovski answered that it was not calculated yet.

I Smith stated that in Canada the type of building for CLT use is still unknown and 2015 target for CLT information to be in the Canadian CSA code might be too optimistic.

Seismic Performance of Cross-Laminated Wood Panels

Marjan Popovski, Erol Karacabeyli

FPInnovations, Building Systems Department, Vancouver, BC, Canada

Abstract

In this paper, some of the results are presented from a series of quasi-static tests on CLT wall panels conducted at FPInnovations. CLT walls with various configurations, connection details, aspect ratios, as well as multi-panel walls with step joints and different screws to connect them, were tested. Results showed that CLT walls have adequate seismic performance when nails or screws are used with steel brackets. Use of hold-downs with nails on each end of the wall can improve the seismic performance. Use of diagonally placed long screws to connect the CLT walls to the floor below is not recommended in high seismic zones due to less ductile wall behaviour. Use of step joints in longer walls can be an effective solution to reduce the wall stiffness and to improve the wall deformation capabilities. Timber rivets in smaller groups with custom made brackets were found to be effective connectors for CLT wall panels. Preliminary analyses suggest that an R_d factor of 2.0 and an R_o factor of 1.5 are appropriate estimates for the force modification factors for seismic design of CLT structures according to National Building Code of Canada (NBCC).

1 Introduction and Background

Cross-laminated timber (CLT) was first developed some 20 years ago in Austria and Germany. European experience shows that this system can be competitive not only in low rise but also in mid-rise and high-rise buildings. Although CLT has barely being used in North America so far, it may be used as a viable wood-based structural solution for the shift towards sustainable densification of urban and suburban centres in Canada and the US. In order to gain wide acceptance, CLT as a structural system needs to be implemented in the North American building codes arena. For these reasons FPInnovations has undertaken a multi-disciplinary research project on determining the structural properties of CLT construction. One of the important parts of the project is to quantify the seismic behaviour of CLT structures including the development of the force modification factors (R-factors) for seismic design according to NBCC. In this paper some of the results from a series of quasi-static tests on CLT wall panels are presented along with preliminary analyses of R-factors.

2 Previous Research in the Field

The most robust study to date to quantify the seismic behaviour of CLT construction was the SOFIE project undertaken by the Trees and Timber Institute of Italy (CNR-IVALSA) in collaboration with Japanese researchers from NIED, Shizuoka University, and the BRI. The testing programme included in-plane cyclic tests on CLT wall panels with different layouts of connections and openings [1], pseudo-dynamic tests on a one-storey 3-D specimen in three different layouts, and shaking table tests on a three-storey [2] and seven-storey CLT building. Shaking table tests on the 3-storey building showed that the CLT construction survived 15 destructive earthquakes without any severe damage even at peak ground accelerations (PGA) of 1.2g [3]. Similarly, the 7-storey building was able to withstand strong earthquakes such as the Kobe one (PGA of 0.6g in X-direction, 0.82g in Y-direction, and 0.34g in vertical Z-direction) without any significant damage.

A comprehensive study to determine the seismic behaviour of 2-D CLT wall panels was conducted at the University of Ljubljana. Numerous monotonic and cyclic tests were carried out on walls with different aspect ratios and boundary conditions from the cantilever type all the way to the pure shear [4]. Influence of vertical load and type of anchoring systems were evaluated, along with wall deformation mechanisms [5]. In addition, influence of openings on the shear properties of CLT wall panels was studied and formulae were suggested [6].

CLT wall tests were also carried out by the Karlsruhe Institute of Technology to compare the performance of such modern system vs. the traditional timber frame construction [7].

3. CLT Wall Specimens Tested and the Test Setup

A total of 32 monotonic (ramp) and cyclic tests were performed on 12 configurations of CLT walls. The testing matrix that includes wall configurations I to IX is given in Tables 1 and 2. Three additional wall configurations (walls with openings, 4.9 m tall walls, and two-storey CLT assemblies) were also tested but these results are not reported in this paper, but reported in [8]. All walls were 3-ply CLT panels with a thickness of 94 mm, made of European spruce and manufactured at KLH Massiveholz GmbH in Austria.

a) Bracket A b) Bracket B c) Bracket C

Figure 1 Brackets for CLT walls used in the tests

Three different types of brackets (A, B, and C) were used to connect the walls to the steel foundation beam or to the CLT floor panel bellow (Figure 1). Bracket A (BMF 90 mm x 48mm x 116 mm, and bracket B (Simpson Strong Tie 90 mm x 105 mm x 105 mm) were off-the-shelf products that are commonly used in CLT applications in Europe, while bracket C was custom made out of 6.4mm thick steel plates to accommodate the use of timber rivets. The designations of the tests shown in Tables 1 and 2 were developed to show the bracket type and the fastener type used in the tests. For example designation **CA-SNH-08A** (from configuration II) means that the **C**LT wall had brackets type **A**, **S**piral **N**ails as fasteners, had **H**old-downs and it is test number **08A**. The following acronyms were also used in the test designations: **TR** for **T**imber **R**ivets, **RN** for Annular **R**ing **N**ails, **S1** for SFS screws 4 x 70mm, **S2** for SFS screws 5x90mm, and **WT** for SFS **WT**-T type screws.

Table 1 Test matrix for 2.3m long and 2.3m high CLT walls (aspect ratio 1:1)

Wall Configuration	Test Designation	Brackets and Fasteners	Vertical Load [kN/m]	Lateral Load
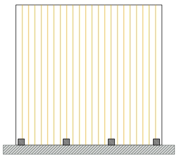 I	CA-SN-00	Bracket A at 710mm SN 16d, n = 18 D = 3.9 mm L = 89 mm	0	CUREE
	CA-SN-01		10	Ramp
	CA-SN-02		10	CUREE
	CA-SN-03		20	CUREE
	CA-RN-04	RN 10d (3.4 x 76mm), n=12	20	CUREE
	CA-S1-05	S1 (4 x 70mm) n=18	20	CUREE
	CA-S2-06	S2 (5 x 90mm) n=10	20	CUREE
	CC-TR-09	Bracket C, Rivets L=65mm, n=10	20	Ramp
	CC-TR-10A	Bracket C, Rivets L=65mm, n=10	20	CUREE
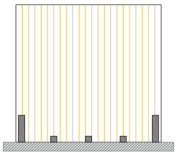 II	CA-SNH-07	SN 16d (3.9 x 89mm), n=18 Same on Hold-Down	20	Ramp
	CA-SNH-08	SN 16d (3.9 x 89mm), n=18 Same on Hold-Down	20	CUREE
	CA-SNH-08A	SN 16d (3.9 x 89mm), n=18 12d (3.3 x 63mm), n=18 on HD	20	CUREE
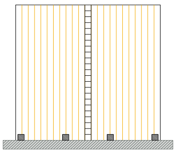 III	CA-SN-11	SN 16d (3.9 x 89mm), n=18 WT-T (3.8 x 89mm) n=12	20	CUREE
	CA-SN-12	SN 16d (3.9 x 89mm), n=18 SFS2 (5 x 90mm) n=12	20	CUREE
	CA-SN-12A	SN 16d (3.9 x 89mm), n=18 Btw panels SFS2 (5 x 90mm) n=12	20	ISO
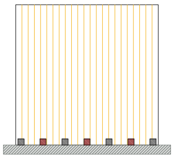 IV	CA-SN-20	Bracket A SN 16d , n=18 D=3.9mm L=89mm 3 brackets on the back side Representative of inside wall	20	CUREE
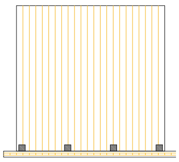 V	CA-SN-21	Bracket A at 710mm SN 16d, n=6 D = 3.9 mm L = 89 mm	20	CUREE
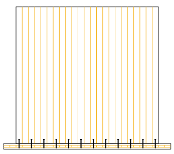 VI	CS-WT-22	WTT-T n=18 at D = 6.5 mm L = 130 mm Screws spaced at 280 mm	20	CUREE
	CS-WT-22B	WTT-T n=34 D = 6.5 mm L = 130 mm Screws spaced at 40mm/320 mm	20	CUREE
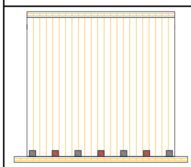 VII	CA-SN-23	Bracket A SN 16d, n=6 D=3.9mm L=89mm 3 brackets on the back side Representative of inside wall	20	CUREE

Walls from configuration III (11, 12 and 12A) consisted of two panels that were connected to each other using a continuous 65 mm step-joint with no gap, and one vertical row of screws. Twelve SFS WTT-T type screws 3.8 mm x 89 mm, spaced at 200 mm were used in the step-joint in wall 11, while walls 12 and 12A used 5 mm x 90 mm SFS screws. To investigate the effect of the foundation stiffness (walls in upper storeys), walls in configurations V, VI and

VII were placed over a 94mm thick CLT slab with a width of 400mm. The brackets were connected to the CLT floor slab using 3 SFS WFC screws (D=10mm and L=80 mm).

Table 2 Test matrix for 3.45m long and 2.3m high CLT walls (aspect ratio 1:1.5)

Wall Configuration	Test Designation	Brackets and Fasteners	Vertical Load [kN/m]	Lateral Load
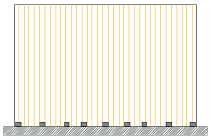 VIII	CB-SN-13	Bracket B SN 16d (3.9 x 89mm) n=10 9 brackets	20	Ramp
	CB-SN-14	Bracket B SN 16d (3.9 x 89mm), n=10 9 brackets	20	ISO
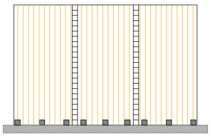 IX	CB-SN-15	Bracket B SN 16d (3.9 x 89mm) n=10 9 brackets; SFS2 (5 x 80mm) n=8	20	Ramp
	CB-SN-16	Bracket B SN 16d (3.9 x 89mm), n=10 9 brackets SFS2 (5 x 90mm) n=8	20	ISO

Wall 22 was connected to the floor slab using 9 pairs of SFS WT-T 6.5 mm x 130 mm screws placed at 45 degree angle to the slab. Wall 22B used 17 pairs of the same screws with 5 pairs being closely grouped near each end of the wall (spaced at 40 mm) to simulate a hold-down effect. The rest of the screws were spaced at 320 mm. Walls 13 and 14 were single panel walls with a total of 9, type B brackets spaced from 320 mm to 460 mm. Walls 15 and 16 of configuration IX were 3-panel walls, with the same number and position of the brackets as the walls of configuration VIII. The panels were connected between them by step joints and 8 SFS 5x90mm screws spaced at 300mm.

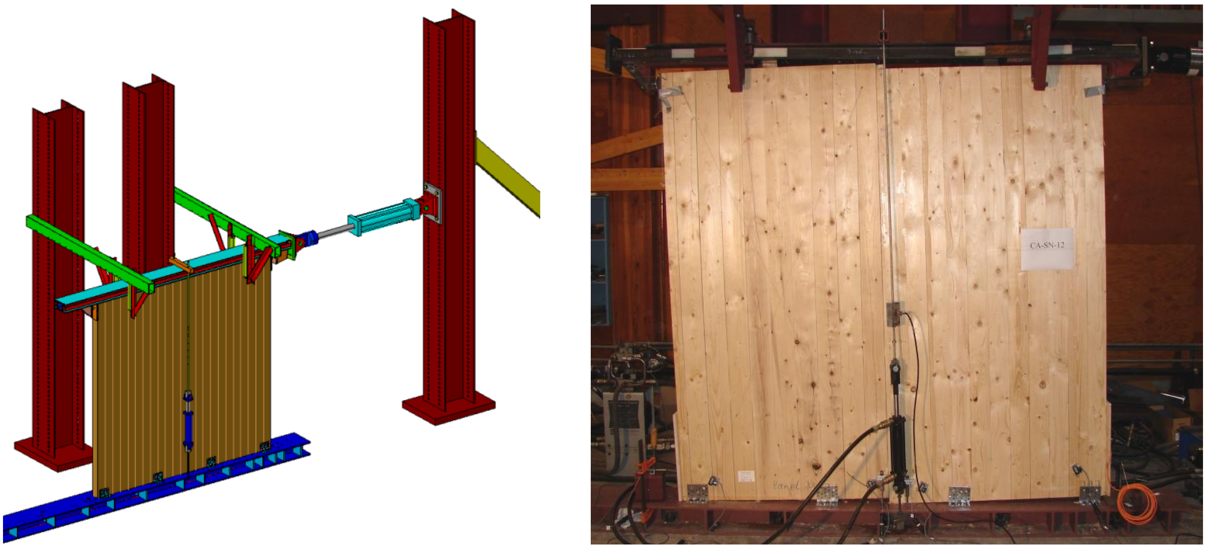

Figure 3 a) Sketch of the test setup used for CLT walls; b) CLT Wall 12 during testing

A sketch of the test set-up with a specimen ready for testing is shown in Figure 3a. Steel I beam provided a foundation to which the specimens were bolted down. Another stiff steel beam that was bolted to the CLT walls was used as lateral load spreader bar. Lateral guides with rollers were also used to ensure a steady and consistent unidirectional movement of the walls. Vertical load was applied using a single 13.3 kN hydraulic actuator placed in the middle of the wall in case of 2.3 m long walls (Figure 3a), or with two such actuators located at third points in case of 3.45 m long walls. Walls 01 and 02 were tested with 10 kN/m vertical load that approximately corresponds to a wall being at the bottom of a two storey structure. All other walls (except wall 00 with no load) were tested using 20 kN/m vertical load that corresponds to a wall being at the bottom of a four storey structure. The walls were subjected to either monotonic or cyclic lateral loading. The rate of loading for the monotonic (ramp) tests was 0.2 mm/s. Cyclic loading tests were carried using either CUREE (Method C) or ISO 16670 (Method B) testing protocols given in ASTM E2126 [9], with a rate of 5mm/s.

4. Results and Discussion

As expected, the CLT wall panels behaved almost as rigid bodies during the testing. Although slight shear deformations in the panels were measured, most of the panel deflections occurred as a result of the deformation in the joints. In case of multi-panel walls, deformations in the step joints also had significant contribution to the overall wall deflection. Selected average properties (based on both sides of the hysteretic loops) of the CLT wall tests obtained from the experimental program are given in [8]. The value of axial load had an impact on the lateral resistance of the walls. Wall 00 with no vertical load reached a maximum load of 88.9 kN while wall 02 with 10 kN/m vertical load had a lateral resistance of 90.3 kN. When the vertical load was increased to 20kN/m (wall 03) the resistance increased to 98.1 kN, an increase of 10% (Figure 4). It seems that the axial load had to be 20kN/m or higher to have any significant influence on the lateral load resistance. The amount of vertical load, however, had a higher influence of the wall stiffness. The stiffness of wall 03 was 28% higher than that of wall 00. In addition, higher values of vertical load had influence on the shape of the hysteresis loop near the origin (Figure 4).

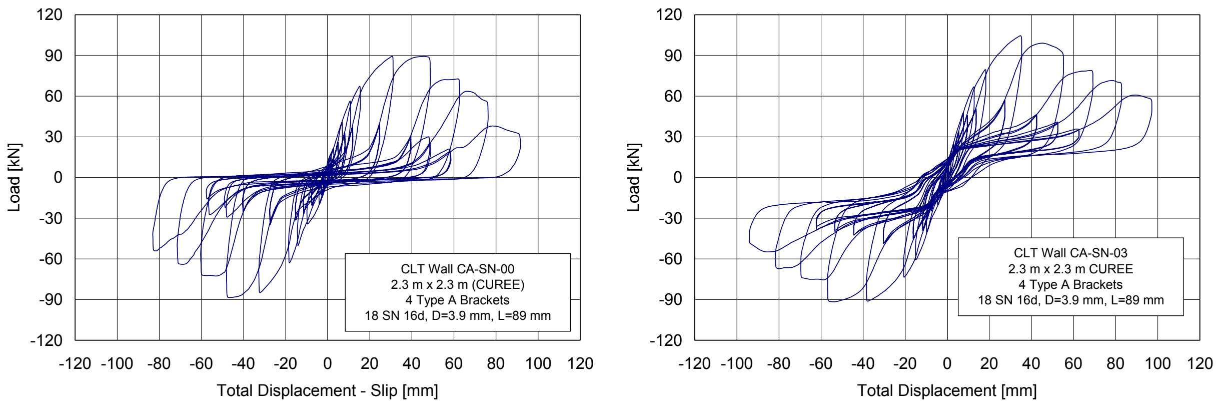

Figure 4 Hysteresis loops for wall 00 with no vertical load and wall 03 with 20kN/m load

Wall 04 with twelve, 10d ring nails per bracket exhibited slightly higher resistance than wall 03 with eighteen 16d spiral nails per bracket. This was mainly due to the higher withdrawal resistance of the ring nails. The ductility of the wall 04, however, was slightly lower than that of wall 03 (Figure 5c). The failure mode observed at the brackets for wall 04 was also slightly different than that of wall 03. While spiral nails in the brackets exhibited mostly bearing failure combined with nail withdrawal, the ring nails in withdrawal tended to pull out small chunks of wood along the way (Fig. 5a and 5b).

The walls with screws in the brackets (05 and 06) reached similar maximum loads as the walls with nails. The load carrying capacity for CLT walls with screws, however, dropped a little bit faster at higher deformation levels than in the case of walls with nails (Figure 6). CLT wall with hold-downs (wall 08A) showed one of the highest stiffness values for a 2.3 m long wall, with its stiffness being 81% higher than that of wall 03 with 18 spiral nails per bracket. CLT wall 08A also showed one of the highest ductility properties (Figure 7b) and therefore this wall configuration is highly recommended for use in regions with high seismicity. Behaviour of one corner of wall 08A during testing is shown in Figure 7a.

a)

b)

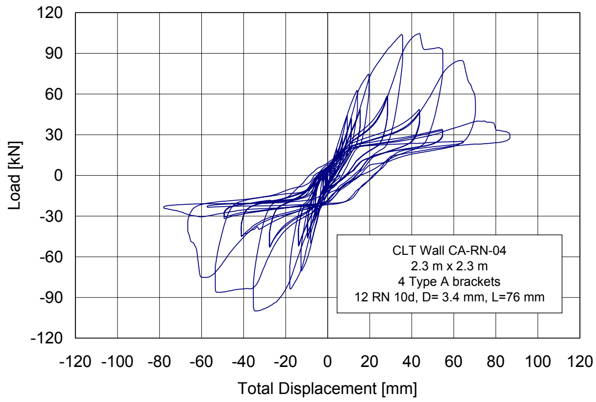

Figure 5 Failure mode of the brackets for: a) wall 02 with spiral nails, and b) wall 04 with ring nails; c) Hysteresis loop for wall 04 with 12 ring nails

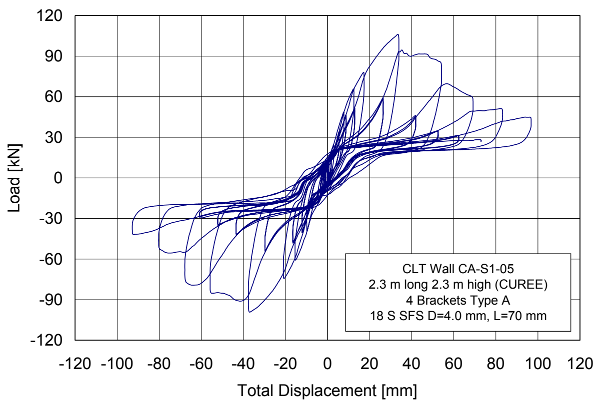

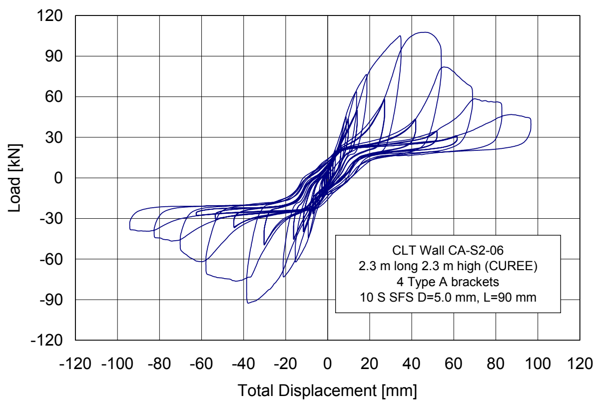

Figure 6 Hysteresis loops: a) wall 05 (18 screws 4x70mm); b)wall 06 (10 screws 5x90mm)

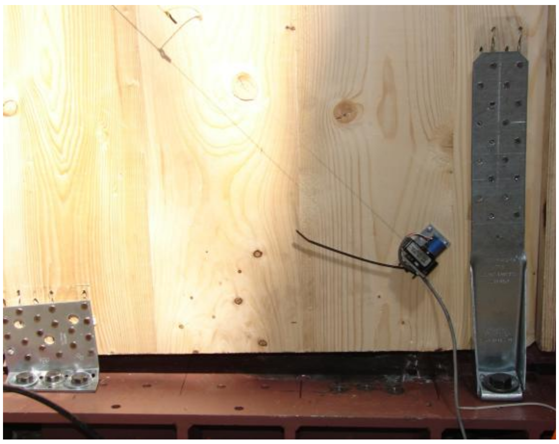

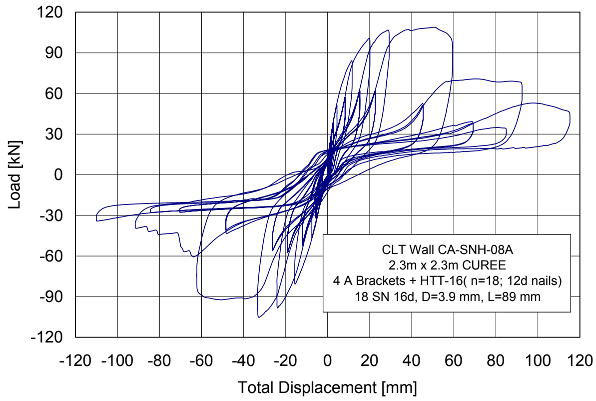

Figure 7 a) A corner of wall 08A during testing; b) Hysteresis loop for the wall 08A

Although timber rivets were developed to be used with glulam, an attempt was made to use rivets in CLT, beside the fact that when driven with their flat side along the grains in the outer layers they will be oriented across the grain in the middle layer. The CLT wall 10A with ten rivets per bracket exhibited by far the highest stiffness than any 2.3 m long wall, with its stiffness being 220% higher than that of wall 03. Timber rivets were also able to carry more load per fastener than any other fastener used in the program. In addition, the wall was able to attain high ductility levels.

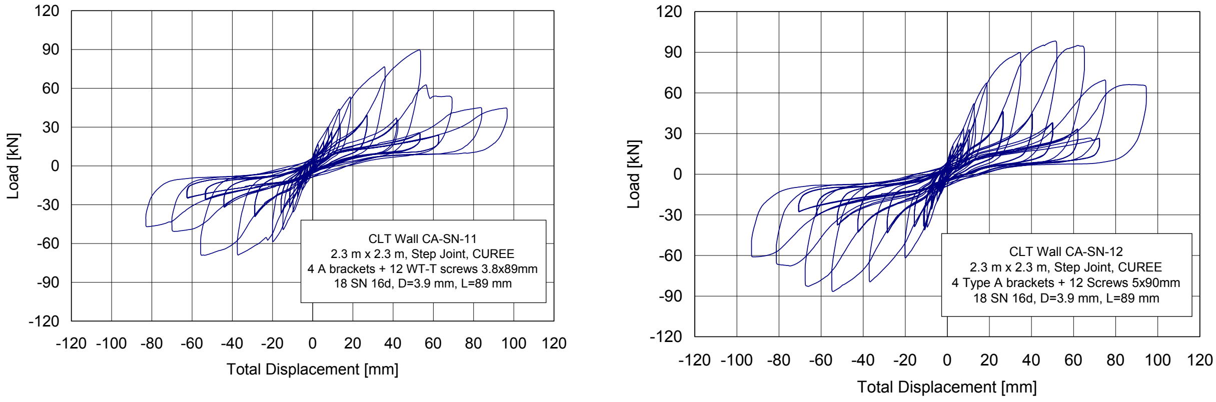

Figure 8 Hysteresis loops for 2-panel walls with different screws the step joint

By introducing a step joint in the wall (creating a wall of two separate panels), the behaviour of the wall was not only influenced by the types of fasteners in the bottom brackets, but also by the type of fasteners used in the step joint. These walls (11 and 12) showed reduced stiffness by 32% and 22% respectively, with respect to the reference wall 03. Both walls were able to shift the occurrence of the yield load F_y and ultimate load F_u at higher deflection levels, while only wall 12 was able to show an increase in its ultimate deflection. Wall 11 that used WT-T screws in the step joint showed reduced ultimate load by 19%, while wall 12 that used regular 5x90mm screws showed a reduction of only 5%. In addition, wall 11 showed higher reduction of ductility compared to the reference wall 03, while the ductility for wall 12 was only slightly lower than that of the reference wall. Based on the results, in case of having multi-panel walls with step joints, the use of regular screws is recommended in high seismic zones. A photo of wall 12 during the testing is shown in Figure 3b, while the behaviour of walls 11 and 12 are shown in Figure 8.

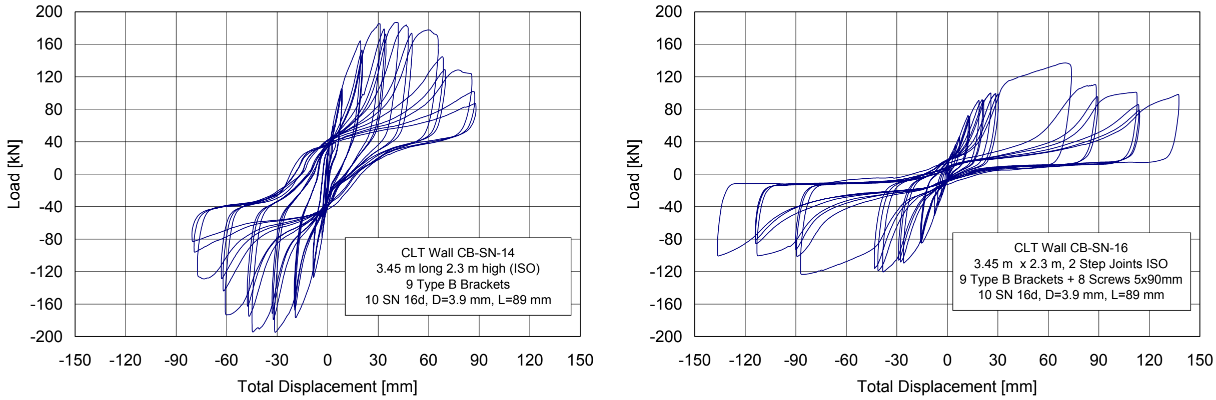

Figure 9 Hysteresis loops for: a) wall *14 (3.45 m long panel); b) wall 16 with 5x90 mm screws in the step joint*

The presence of the step joints and the type of fasteners used in them had more significant influence on the overall wall behaviour as the length of the wall increases. Comparing the results from walls 14 and 16, both with length of 3.45 m, a significant change in stiffness and strength properties of the walls was observed. Introduction of step joints enabled wall 16 to carry a significant portion of the maximum load at higher deformation levels (Figure 9b).

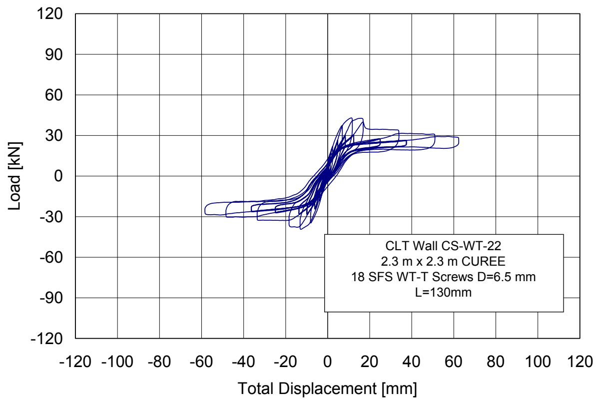

Figure 10 a) A corner of wall 22B during testing; b) Hysteresis loop for wall 22

Specimens 22 and 22B (Figure 10) that were connected to the bottom CLT floor with WT-T type screws placed at 45 degrees showed lower resistance and energy dissipation than any single storey wall in the program (Figure 10b). Grouping the screws at the ends of the panels (wall 22B) created a hold-down effect and helped increase the wall capacity for about 30% compared to that of wall 22. Based on the test results, use of screws at an angle as a primary connector for wall to floor connections is not recommended for structures in earthquake prone regions due to reduced capability for energy dissipation.

6 Preliminary Estimates of Force Modification Factors

Force modification factors in building codes (R-factors in Canada, R-factor in the US, and q-factor in Europe) account for the capability of the structure to undergo ductile nonlinear deformations and allow for the structure to be designed for lower seismic forces. In the 2010 NBCC the elastic seismic load is reduced by two R-factors, R_o-factor related to the system over-strength and R_d-factor related to the ductility of the structure. In this section, an estimate will be made for the R-factors for CLT structures based on the equivalency approach in the AC130 acceptance criteria [10]. According to the strength limit states of these criteria, assigning an R-factor for a new wood shearwall assembly in the US can be made by showing equivalency of the seismic performance of the new wall assembly in terms of maximum load, ductility, and storey drift obtained from quasi-static cyclic tests, with respect to the properties of lumber-based nailed shearwalls that are already present in the code. Although CLT wall panels as a system differ from wood-frame shearwalls, we can use the AC130 equivalency criteria for preliminary assessment of the R-factors as they are performance-based criteria. The criteria specify that for a new shearwall assembly (in our case CLT) to have the same seismic design factor (R=6.5) as regular shearwalls in the International Building Code (IBC) in the US, the assembly shall satisfy the response criteria given in equations (1) to (3):

$$\frac{\Delta_u}{\Delta_{ASD}} \geq 11 \quad (1); \qquad \Delta_u \geq 0.028 \cdot H \quad (2); \qquad 2.5 \leq \frac{P_{max}}{P_{ASD}} \leq 5.0 \quad (3);$$

where:

Δ_{ASD} = the displacement at the ASD load level according to the IBC;
P_{ASD} = the assigned Allowable Stress Design load level according to IBC ($P_{max}/2.5$);
Δ_U = ultimate displacement (displacement at which load drops to 80% of the maximum);
H = the height of the panel element;
P_{max} = the maximum load obtained from the backbone curve.

The specified strengths for shearwalls in Canada were soft converted from the ASD values in the US, which were derived as the average maximum load from monotonic tests divided by a safety factor of 2.8, or the average maximum load from cyclic tests divided by 2.5. Here we will assume that the design values for CLT panels have the same safety margin as that of regular wood-frame shearwalls. In addition, as required by the AC130 criteria, only walls tested under the CUREE protocol will be used for the analyses. The average response parameters related to the AC130 criteria obtained from the envelopes of cyclic tests on CLT wall panels are shown in Table 3.

Table 3 The average response parameters for CLT walls as per AC130 criteria

Wall	P_{ASD} [kN]	Δ_{ASD} [mm]	P_{max} [kN]	Δ_u [mm]	Δ_u [% drift]	Ductility Δ_u/Δ_{ASD}
00	35.6	7.8	88.9	66.6	2.9	9.4
02	36.1	8.5	90.3	71.5	3.1	8.5
03	39.2	7.5	98.1	63.6	2.8	8.8
04	40.9	7.5	102.3	59.6	2.6	8.1
05	41.1	8.0	102.7	53.7	2.3	6.8
06	40.0	8.1	100.1	50.1	2.2	6.2
08A	42.8	4.9	107.1	57.8	2.5	13.7
10A	41.0	3.2	102.4	49.0	2.1	16.5
12	37.0	8.6	92.5	72.0	3.1	8.5
14	76.4	3.9	190.9	67.7	2.9	17.7
16	52.1	8.2	130.2	107.1	4.7	13.2
20	60.8	8.6	152.1	70.5	3.1	8.7
21	21.6	3.6	54.1	84.9	3.7	23.8
23	28.9	5.6	72.2	79.8	3.5	15.0
Average for all CLT panels above				68.1	3.0	11.8

Although AC130 criteria do not deal with sets of different walls, one can always look at the average values of the entire set of CLT walls. As shown in Table 3, the average values for the set of CLT walls satisfy the AC130 criteria. The average ductility (as defined in AC130) is 11.8, which is greater than the required minimum of 11 in eq. (1), and the average ultimate storey drift is 3.0%, which is greater than the required 2.8% (eq. 2). Based on this, the CLT walls tested can qualify as new structural wall elements that can share the same seismic response parameters with regular wood-frame shearwalls in the US, which means using an R-factor of 6.5. This value would correspond to having the product of R_d R_o equal to 5.1 in Canada with R_d = 3.0 and R_o = 1.7 being the factors currently used in NBCC for nailed wood-frame shearwalls.

However, at this early stage of acceptance in the design practice, the authors are of the opinion that a bit more conservative set of factors be used for CLT as a structural system. It is recommended that R_o factor of 1.5 and R_d factor of 2.0 are used as early estimates of force modification factors for CLT structures that use brackets with ductile nails or screws and hold-downs. These estimates are in line with the proposed values for the q-factor in Europe [11]. This will put CLT structures in equal position in terms of the R-factors with other heavy timber systems such as braced timber frames and moment resisting frames, that have already been assigned R_o = 1.5 and R_d = 2.0 in NBCC when designed with ductile connections. A higher R_d-factor may be considered for CLT systems in the near future, based on the results from additional analytical and experimental work. Based on the research results from tests on braced timber frames [12], the performance of CLT panels with ductile connections (nails or slender screws) tends to be more ductile. In addition, the CLT as a structural system is far less susceptible to development of soft storey mechanism than braced frames or the other structural systems of the platform type. Since the nonlinear behaviour (and the potential damage) is localized to the bracket and hold-down connection areas only, the CLT panels that are also the vertical load carrying elements, are virtually left intact in place and well connected to the floor panels even after a “near collapse” state is reached. Finally, all walls in one storey in CLT construction contribute to the lateral load resistance, thus providing a system with increased degree of redundancy.

7 Conclusions

Results from quasi-static tests on CLT wall panels showed that CLT structures can have adequate seismic performance when nails or screws are used with the steel brackets. Use of hold-downs with nails on each end of the wall improves its seismic performance. Use of diagonally placed long screws to connect the CLT walls to the floor below is not recommended in seismic prone areas due to less ductile wall behaviour. Use of step joints in longer walls can be an effective solution not only to reduce the wall stiffness and thus reduce the seismic input load, but also to improve the wall deformation capabilities. Preliminary evaluation of the R-factors for the seismic design of structures according to the NBCC based on the performance comparison to already existing systems in NBCC and on the equivalency performance criteria given in AC130, values of 2.0 for the R_d factor and 1.5 for the R_o factor are recommended as conservative estimates for CLT structures that use ductile connections such as nails and slender screws.

8 References

[1] Ceccotti A. et. al. 2006. Sofie Project – Test Results on the Lateral Resistance of Cross-Laminated Wooden Panels. Proc. of the First ECEE and Seismicity, Geneva, Switzerland.

[2] Ceccotti A., Follesa M. 2006. Seismic Behaviour of Multi-Storey X-Lam Buildings. COST E29 Workshop on Earthquake Engineering on Timber Structures, Coimbra, Portugal.

[3] Ceccotti A. 2008. New Technologies for Construction of Medium-Rise Buildings in Seismic regions: The XLAM Case. Structural Engineering International SEI, 18 (2):156-165.

[4] Dujic B., Pucelj J., Zarnic R. 2004. Testing of Racking Behavior of Massive Wooden Wall Panels. Proceedings of the 37th CIB-W18 Meeting, paper 37-15-2, Edinburgh, Scotland.

[5] Dujic B., Zarnic, R. 2006. Study of Lateral resistance of Massive X-Lam Wooden Wall System subjected to Horizontal Loads. COST E29 Workshop, Coimbra, Portugal.

[6] Dujic B., Klobcar S., Zarnic, R. 2007. Influence of Openings on Shear Capacity of Wooden Walls. Proceedings of the 40th CIB-W18 Meeting, paper 40-15-6, Bled, Slovenia.

[7] Schädle, P., Blaß, H.J. 2010. Earthquake behaviour of modern timber construction systems. Proceedings of the 11th World Conference on Timber Engineering, Riva del Garda, Italy.

[8] Popovski, M., Karacabeyli, E., Ceccotti, A. 2011. Seismic Performance of Cross-Laminated Timber Buildings. Chapter 4 of the FPInnovations’ CLT Design Handbook, Canadian Edition.

[9] ASTM E 2126. Standard Test Methods for Cyclic (Reversed) Load Test for Shear Resistance of Vertical Elements of the Lateral Load Resisting Systems for Buildings. ASTM Int. 2009.

[10] ICC-ES AC130. 2009. Acceptance Criteria for Prefabricated Wood Shear Panels. ICC Evaluation Services, Inc. Whittier, California.

[11] Ceccotti A. et. al. 2006. Which Seismic Behaviour Factor for Multi-Storey Buildings made of Cross-Laminated Wooden Panels? Proc. 39th CIB W18 Meeting, paper 39-15-4, Firenze.

[12] Popovski, M., Karacabeyli, E. 2008. Force Modification Factors and Capacity design Procedures for Braced Timber Frames. Proc. 14th WCEE, Beijing, China.

CIB-W18/44-15-8

INTERNATIONAL COUNCIL FOR RESEARCH AND INNOVATION IN BUILDING AND CONSTRUCTION

WORKING COMMISSION W18 - TIMBER STRUCTURES

EVALUATION OF PLYWOOD SHEATHED SHEAR WALLS WITH SCREWED JOINTS TESTED ACCORDING TO ISO 21581

K Kobayashi

M Yasumura

Faculty of Agriculture, Shizuoka University

JAPAN

MEETING FORTY FOUR

ALGHERO

ITALY

AUGUST 2011

Presented by K Kobayashi

F Lam received confirmation that the calibration of the hysteresis rules for the model was based on single connection test results.

E Serrano asked about the single spring model and the influence of load direction in relation to wood grain. K Kobayashi responded that test results corresponding to perpendicular to grain direction was used and there could be influence from grain direction but was not considered in the study.

J Munch-Andersen asked about the brittle fracture of the screws and how much bending of the screws was experienced. K Kobayashi responded that in monotonic tests the single screws seemed ductile.

Evaluation of plywood sheathed shear walls with screwed joints tested according to ISO 21581

Kenji Kobayashi, Motoi Yasumura
Faculty of Agriculture, Shizuoka University, Japan

1. Introduction

Screws are used gradually for timber structures in Japan. Gypsum boards and some structural panels are fastened by small screws, and metal hardware such as hold-down connections are also fastened by screws at Japanese conventional post-and-beam constructions. Moreover, the structural use such as plywood sheathed shear walls are increasing. In previous studies, we conducted single shearing tests of various types of screws. And it was clarified that screw connections sometimes showed brittle behavior. Making process of the screw often includes quenching and tempering treatments. But in some conditions, these treatments cause the brittleness of the screw. So we should give special attention to the brittleness of the screw.

Shear walls are necessary to resist seismic force or wind load. The performance of the shear wall is determined by shear wall test. Each test method has designated loading protocol and the shear performance depends on the protocol. ISO 21581 [1] has been published since June 2010. In ISO 21581 protocol, reversed cyclic loading is required till the end of the test as well as ISO 16670 [2] protocol. In general, monotonic loading test results are higher than reversed cyclic ones. Especially, the difference between monotonic and cyclic loading is large in screw joints. The degradation due to cyclic displacement is taken into account by full reversed cyclic loading.

In this research, racking tests of shear walls and single shearing tests of screwed joints were conducted according to ISO protocols. And we calculated the shear resistance of shear walls from single shearing properties of screwed joints.

2. Test method

2.1. Materials

Japanese Cedar (*Cryptomeria japonica*, density: 410kg/m^3) is used for shear wall test as columns, studs and a sill materials. Douglas Fir (*Pseudotsuga menziesii*, density: 480kg/m^3) was used for shear wall as a beam material. Japanese Cedar also used for single shearing tests as main member. Pine plywood (thickness: 9.0mm, density: 500kg/m^3) was used as sheathing material for shear wall test and side member for single shearing test.

The shape of screw is shown in Figure 1 and Table 1. These sizes were specified in Japanese Industrial Standard (JIS) B1112 [3]. The names of screws were defined from nominal diameter (first double figures, without decimal point) and nominal length (last double figures). For example, “3832” means that the screw has the nominal diameter of 3.8mm and the nominal length 32mm. They were made from SWCH18A (JIS G3507) [4], and they were quenched and tempered after rolling.

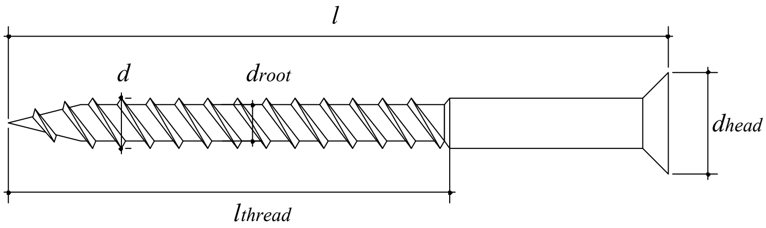

Figure 1 Shape of screw

Table 1 Size of screws (mm)

name	*d*	d_{head}	d_{root}	*l*	l_{thread}
3832	3.7	7.4	2.6	31.7	21.2
4138	4.0	8.1	2.8	37.5	25.0
4532	4.4	8.9	3.1	31.6	21.1
4550	4.4	8.9	3.1	49.0	32.7

2.2. Shear wall test

The setup of shear wall test specimen is shown in Figure 2. Specimens were determined according to Japanese conventional post-and-beam construction. They had wooden frames of 1820mm width and 2625mm height. Plywood 9mm thick was sheathed on one side of the wall by wood screws with the spacing of 150mm.

105x105mm columns were spaced 910mm apart. 105x30mm studs were located between columns. Top and bottom of columns were connected to a 105x180mm beam and a 105x105mm sill by mortise-tenon joint and two N90 nails (JIS A5508 [5]). Moreover, hold-down connections (HD-B20) were applied to connect them except for center column. The sill and steel foundation were connected by three bolts of 16mm diameter.

The monotonic and reversed cyclic loads were applied at the end of the beam by an actuator with a capacity of 150kN and a stroke of 200mm controlled by a Shimadzu 48000 system. Horizontal and vertical displacements of the wall were measured with electronic transducers. One specimen was subjected to monotonic loading; then reversed cyclic loading was applied to three specimens. The loading protocol is determined by ISO 21581, shown in Figure 4. The ultimate displacement D_u is determined from monotonic loading test.

2.3. Single shearing test

The setup of single shearing screw joints is shown in Figure 3. Main member was the same as the column of shear wall, and side member was the same as the sheathing panel of shear wall. A grain direction of outer layer of plywood was parallel to the loading direction. Above main member and each side member were connected by one screw, and below main member and each side member were fixed by six screws. Test specimen was connected to testing machine by four bolts of 16mm diameter.

The monotonic and reversed cyclic loads were applied at each main member by a universal test machine (Shimadzu Autograph AG-I). Applied load was measured by electronic loadcell with a capacity of 50kN. Relative displacements between main member and each side member were measured with electronic transducers with a capacity of 100mm. Three specimens were subjected to monotonic loading; then reversed cyclic loading was applied to six specimens. The loading protocol is determined by ISO 16670, shown in Figure 4.

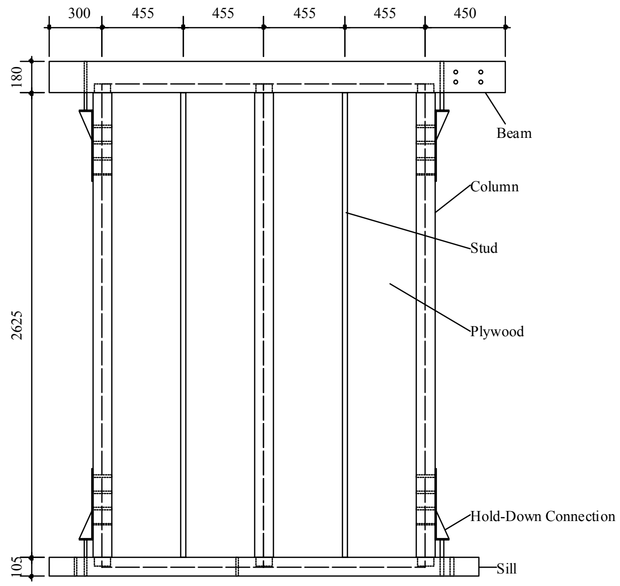

Figure 2 Shear wall test specimen

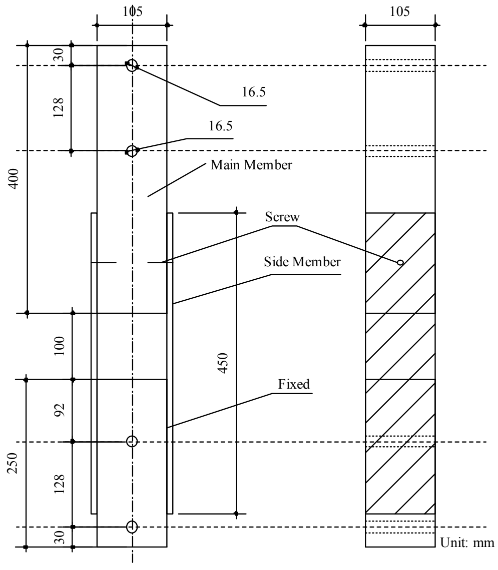

Figure 3 Single shearing test specimen

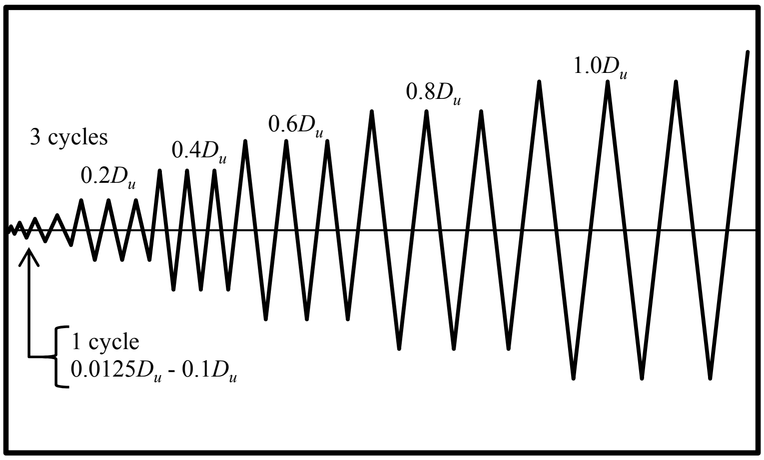

Figure 4 Loading protocol of ISO 21581 and ISO 16670

2.4. Evaluation of test results

Obtained load-displacement curves were evaluated according to the procedure which was proposed byYasumura and Kawai [6] and used in Japan [7]. The outlines were shown in Figure 5.

Line 1 was drawn to pass two points on the envelope curve at 10% and 40% of maximum load $P_{\max}$. Similarly, line 2 was drawn to pass two points at 40% and 90% of $P_{\max}$. Line 2' was a tangent to the envelope curve parallel to line 2. And yield load P_y was determined as the load at the intersection of line 1 and 2'. The yield displacement D_y was determined as the displacement at P_y on the envelope curve. The stiffness K was derived as P_y / D_y. The ultimate displacement D_u was the displacement when the load was decreased to 80% of $P_{\max}$ after the displacement at maximum load $D_{P\max}$. The area bounded by the envelope curve, line 4 and X-axis was the dissipated energy E. Line 5 was selected so that the area bounded by line 3, 4, 5, and X-axis equals to E. The ultimate load P_u was the load at line 5. The structural behavior factor Ds was calculated by the following equation:

$$Ds = \sqrt{2\mu - 1}, \mu = D_u \times \frac{K}{P_u} \qquad (1)$$

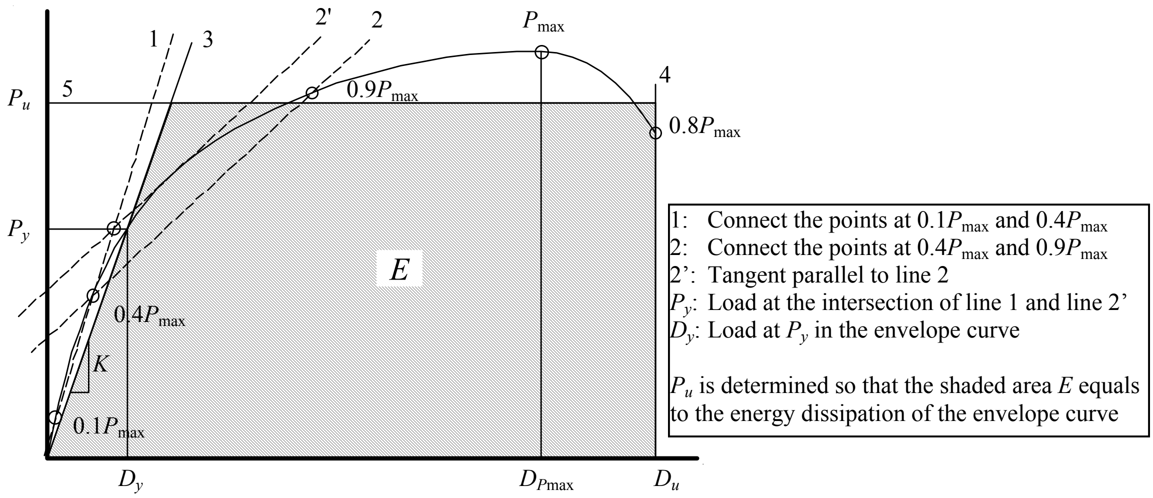

Figure 5 Evaluation procedure of test results

3. Test Results

3.1. Shear wall test

Load-displacement curves of shear wall tests are shown in Figure 6. Monotonic loading results (dash line) showed higher performance than cyclic loading results (solid line) in all test series. Especially, 4138 and 4550 screws (longer screws) showed brittle failure. On the other hand, 3832 and 4532 screws (shorter screws) showed relatively similar performance between monotonic and cyclic loading.

Characteristic values of shear wall test results are shown in Table 2. The strength values (P_y, P_{max}, and P_u) became higher as the sizes of screws increase. But in longer screws, the ratio of monotonic vs. cyclic loading test results was about 0.9, which was a little lower than that of shorter screws. The displacement values (D_y, D_{Pmax}, and D_u) in cyclic loading were relatively similar, although there were higher in longer screws with monotonic tests. In monotonic tests, it seems that the penetration length contributed to the ductility of shear wall. But in cyclic loading, high ratio of “fracture of screw” was observed in longer screws. The fracture of screw was caused by cyclic bending behavior after creation of plastic hinge.

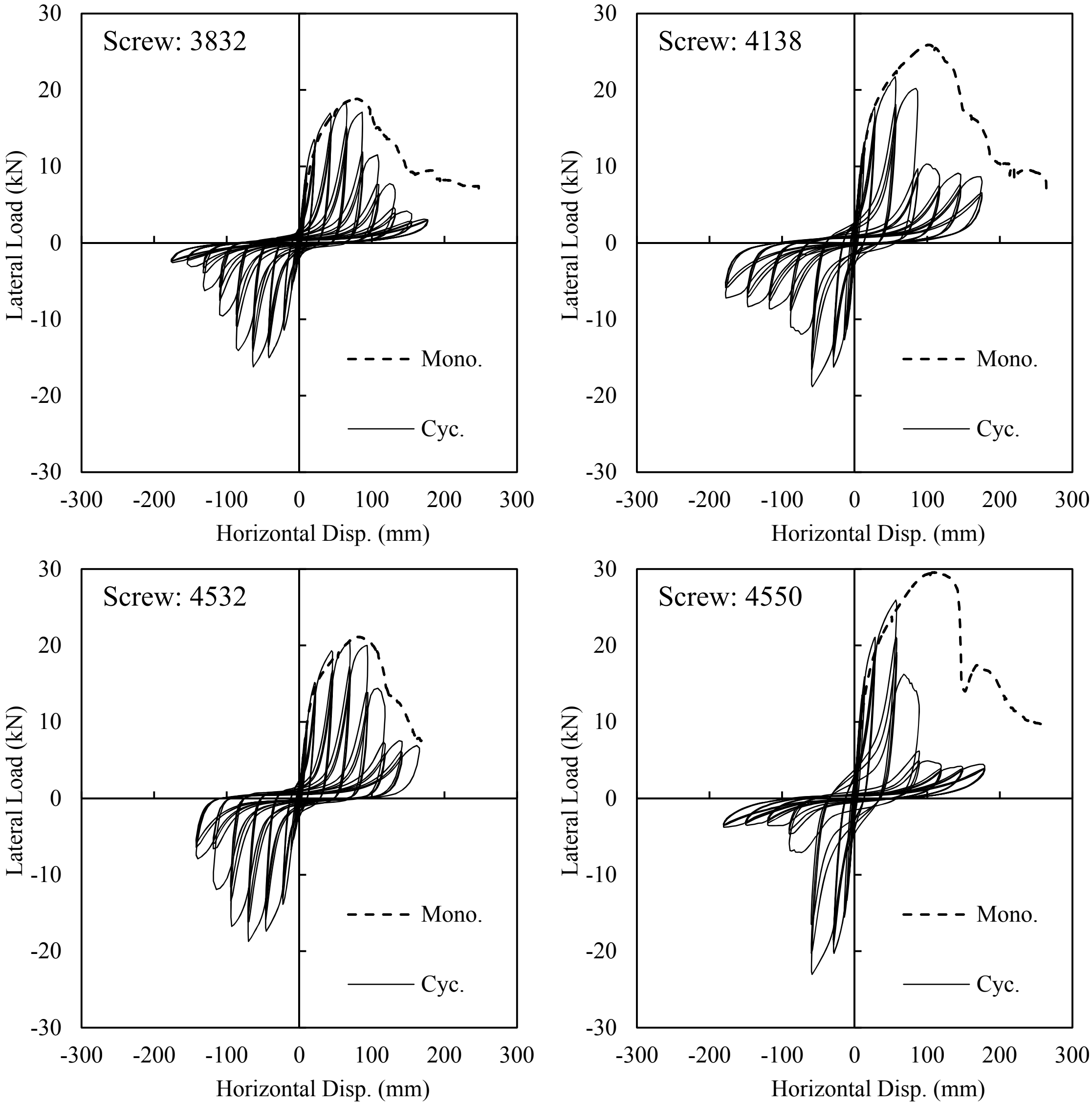

Figure 6 Load-displacement curves of shear wall tests

Table 2 Characteristic values of shear wall test results

Test series		P_y (kN)	D_y (mm)	$P_{\max}$ (kN)	$D_{P\max}$ (mm)	P_u (kN)	D_u (mm)
Cyc.	3832	10.2 (0.68)	13.1 (2.5)	17.9 (1.3)	71.3 (13.0)	15.7 (1.2)	87.1 (0.1)
	4138	13.6 (1.59)	13.8 (1.5)	23.7 (3.2)	67.2 (17.4)	21.3 (2.4)	88.0 (1.0)
	4532	13.0 (0.54)	15.1 (2.0)	20.9 (0.5)	69.2 (0.2)	18.5 (0.3)	94.1 (1.2)
	4550	15.9 (0.74)	16.5 (3.6)	27.8 (1.6)	77.5 (18.0)	24.4 (1.6)	78.9 (18.0)
Mono.	3832	11.0 (-)	17.3 (-)	18.8 (-)	80.5 (-)	17.3 (-)	110.5 (-)
	4138	15.3 (-)	19.1 (-)	25.9 (-)	101.3 (-)	23.3 (-)	142.3 (-)
	4532	12.7 (-)	16.1 (-)	21.1 (-)	80.2 (-)	19.2 (-)	115.3 (-)
	4550	16.3 (-)	19.9 (-)	29.6 (-)	109.0 (-)	26.8 (-)	144.8 (-)
Cyc./Mono. Ratio	3832	0.93	0.75	0.95	0.89	0.91	0.79
	4138	0.89	0.72	0.92	0.66	0.91	0.62
	4532	1.02	0.94	0.99	0.86	0.97	0.82
	4550	0.98	0.83	0.94	0.71	0.91	0.54

Note: Values in parenthesis were standard deviation, except for monotonic test (only one specimen).

3.2. Single shearing test

Obtained load-displacement curves of single shearing tests are shown in Figure 7. An overview of these curves was almost the same as the result of shear wall tests. But there were more differences of ductility between monotonic and cyclic loading at longer screws. In shorter screws, there were almost the same curves or slightly higher performance at cyclic loading. It is because of the variation of material properties of timber members.

Characteristic values of shear wall test results are shown in Table 3. The strength values (P_y, $P_{\max}$, and P_u) were similar between monotonic and cyclic loading tests. But the displacement values (D_y, $D_{P\max}$, and D_u) at cyclic loading were quite smaller than those at monotonic loading. The ratio of monotonic vs. cyclic loading test results was about 0.5 without 4532 screws. It is because the fracture of screw didn't occur in the test of 4532 screws.

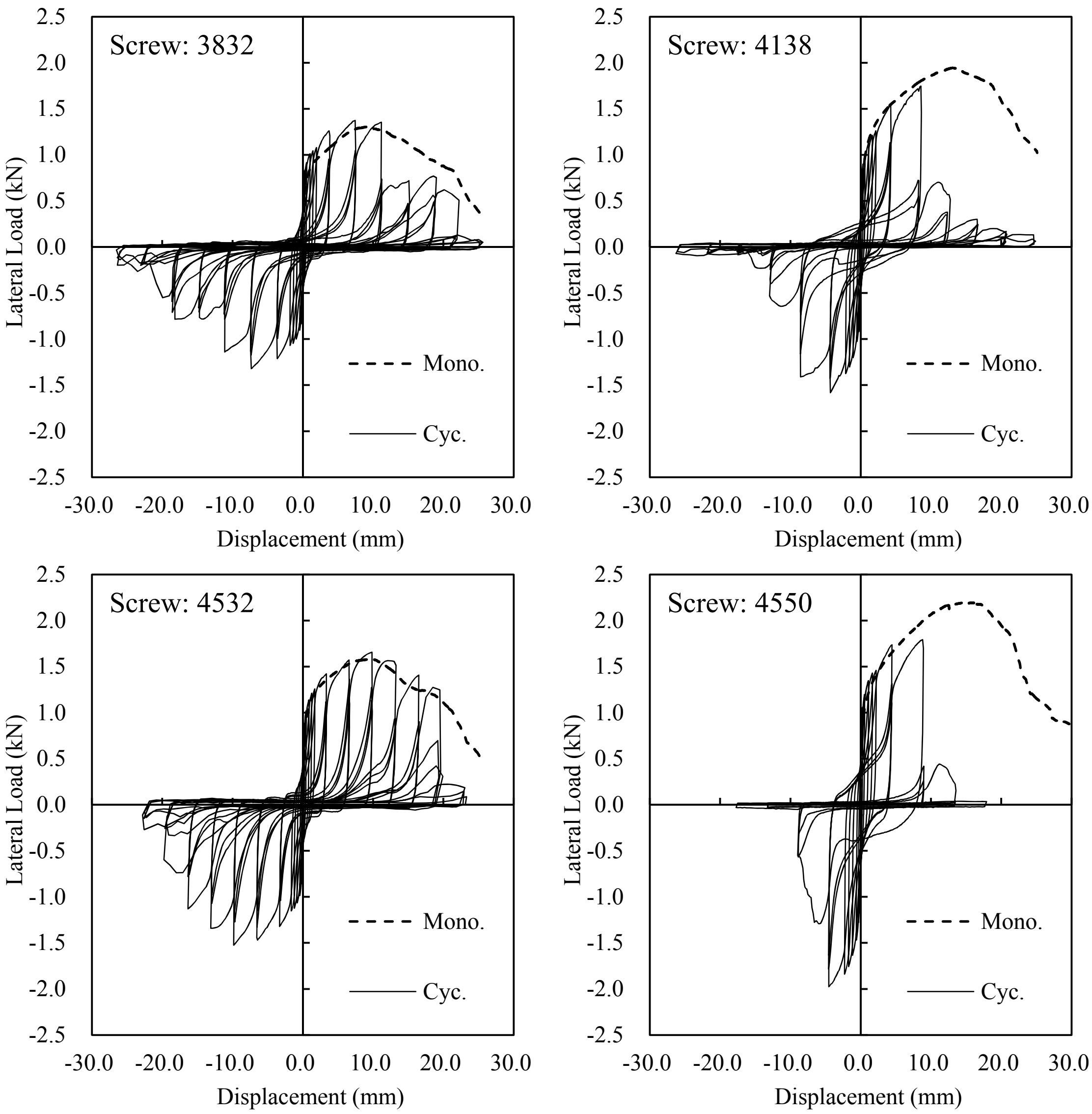

Figure 7 Load-displacement curves of single shearing tests

Table 3 Characteristic values of single shearing test results

Test series		P_y (kN)	D_y (mm)	$P_{\max}$ (kN)	$D_{P\max}$ (mm)	P_u (kN)	D_u (mm)
Cyc.	3832	0.90 (0.09)	0.38 (0.18)	1.51 (0.14)	6.4 (1.7)	1.35 (0.12)	9.3 (2.5)
	4138	1.03 (0.07)	0.45 (0.14)	1.73 (0.15)	6.8 (2.0)	1.54 (0.11)	8.7 (1.9)
	4532	1.00 (0.09)	0.49 (0.16)	1.61 (0.17)	9.4 (2.6)	1.50 (0.17)	14.8 (3.8)
	4550	1.22 (0.09)	0.43 (0.20)	2.09 (0.21)	6.6 (2.3)	1.85 (0.17)	8.8 (1.6)
Mono.	3832	0.77 (0.13)	0.70 (0.24)	1.32 (0.18)	10.4 (2.4)	1.18 (0.16)	16.6 (2.3)
	4138	0.92 (0.31)	0.99 (0.14)	1.61 (0.44)	14.9 (3.3)	1.44 (0.44)	21.0 (2.1)
	4532	0.97 (0.09)	0.56 (0.11)	1.59 (0.16)	9.7 (1.1)	1.43 (0.13)	17.3 (2.9)
	4550	1.12 (0.15)	0.97 (0.25)	2.18 (0.36)	12.8 (0.5)	1.95 (0.32)	19.4 (4.6)
Cyc./Mono. Ratio	3832	1.17	0.54	1.15	0.62	1.14	0.56
	4138	1.11	0.45	1.08	0.46	1.07	0.41
	4532	1.03	0.87	1.01	0.97	1.05	0.86
	4550	1.09	0.44	0.96	0.52	0.95	0.45

Note: Values in parenthesis were standard deviation.

4. Finite element analysis

4.1. Modeling

A finite element code EFICOBOIS were used to analyze the performance of shear walls. EFICOBOIS was developed by Richard [8] at the Laboratoire de Mécanique et Technologie, E.N.S. Cachan, France. More precise detail of EFICOBOIS is shown in the literature [9].

Beam, columns, sill, and studs were modeled as elastic beam elements with two nodes, and sheathing panels were modeled as elastic orthotropic plate elements with four nodes. Connections between beam elements (ex: mortise-tenon joints) were modeled as nonlinear spring which is valid for only compression load, and hold-down connections were modeled as elastic spring valid for only tension load.

Connections between beam and plate elements were modeled as shown in Figure 8. In this article, the model was modified for screw connections.

For monotonic loading, an exponential relation followed by two linear relation and a cutting off of the strength corresponding to the failure were adopted:

$$0 \le \Delta \le D_1 : F(\Delta) = (P_0 + K_1\Delta) \times \left(1 - \exp\left(-K_0\Delta / P_0\right)\right) \tag{2}$$

$$D_1 < \Delta \le D_2 : F(\Delta) = F(D_1) + K_2(\Delta - D_1) \tag{3}$$

$$D_2 < \Delta \le D_{\max} : F(\Delta) = F(D_1) + K_2(D_2 - D_1) + K_3(\Delta - D_2) \tag{4}$$

$$\Delta > D_{\max} : F(\Delta) = 0 \tag{5}$$

There are eight parameters to identify for monotonic loading: P_0, K_0, K_1, K_2, K_3, D_1, D_2, and $D_{\max}$. These parameters were determined from monotonic test results. In the original model, first linear stiffness (K_2) is negative and thus D_1 means the displacement at maximal load. In this article, first linear stiffness (K_2) is basically positive and second linear stiffness (K_3) is negative because it is good to describe the monotonic curve of a screwed joint.

The cyclic loading rules are based on the four exponential hysteretic curves.

$$part1 : F(\Delta) = F_{dA} + (K_4\Delta + P_2 - F_{dA}) \times \left(1 - \exp\left(K_0(U_A - \Delta) / 2P_2\right)\right) \tag{6}$$

$$part2 : F(\Delta) = F_{dB} + (K_4\Delta + P_2 - F_{dB}) \times \left(1 - \exp\left(-K_y(U_B - \Delta) / 2P_2\right)\right) \tag{7}$$

$$part3: F(\Delta) = F_{dB} + (K_5\Delta + P_1 - F_{dB}) \times \left(1 - \exp\left(K_0 (U_B - \Delta)/2P_1\right)\right) \tag{8}$$

$$part4: F(\Delta) = F_{dA} + (K_5\Delta + P_1 - F_{dA}) \times \left(1 - \exp\left(-K_y (U_A - \Delta)/2P_1\right)\right) \tag{9}$$

F_{dA} (or F_{dB}) describes a decreased strength due to cyclic loading. The decreasing coefficient α_A (or α_B) is determined by the maximum load in opposite direction F_{UB} (or F_{UA}).

$$F_{dA} = F_{UA} - \alpha_A \left(F_{UA} - (P_1 + K_5 U_A)\right) \tag{10}$$

$$F_{dB} = F_{UB} - \alpha_B \left(F_{UB} - (P_2 + K_4 U_B)\right) \tag{11}$$

where $\alpha_A = k\left|\dfrac{F_{UB}}{F_{\max}}\right|$, $\alpha_B = k\left|\dfrac{F_{UA}}{F_{\max}}\right|$, $K_4 = \dfrac{P_2}{U_A}$, $K_5 = \dfrac{P_1}{U_B}$, $K_y = \dfrac{F(D_y)}{D_y}$.

D_y is the yield displacement determined from test results, and $F(D_y)$ is calculated from the equation for monotonic loading. After yielding ($|\Delta| > D_y$), the load is decreased due to screw withdrawal, a fracture of screw, and so on. The decreased load is obtained by multiplying $(1-\beta)$ to the calculated load. β is determined by the maximum displacement at opposite direction:

$$\beta_A = \gamma\left(\frac{U_B - D_y}{D_{\max} - D_y}\right), \beta_B = \gamma\left(\frac{U_A - D_y}{D_{\max} - D_y}\right) \tag{12}$$

When $\beta > 1$, β is replaced to 1 and thus the connection has no resistance.

There are five more parameters to identify to complete the cyclic rules: P_1, P_2, D_y, k, and γ. These parameters were determined from the reversed cyclic loading tests of the screw joints. After all, the parameters were selected so that the model curves fit both monotonic and cyclic loading test results on single shearing joints. If there are no or few data about monotonic test, the parameters were determined from cyclic test results. It may be underestimate the performance of actual structures.

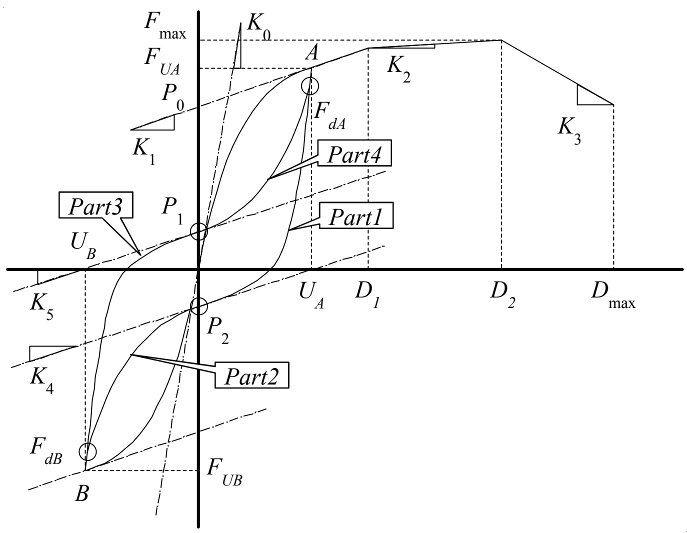

Figure 8 Load-displacement model used for screw connection

4.2. Comparison of load-displacement curves

Comparison between experimental and calculated curves is shown in Figure 9. Calculated curves fitted well to the experimental curves in both monotonic and cyclic loading. Peak load of each cycle is almost the same between experimental and calculated curves before the displacement at maximum load. After the maximum load, there is a little difference between them. This tendency is also seen in dissipated energies (in Figure 10).

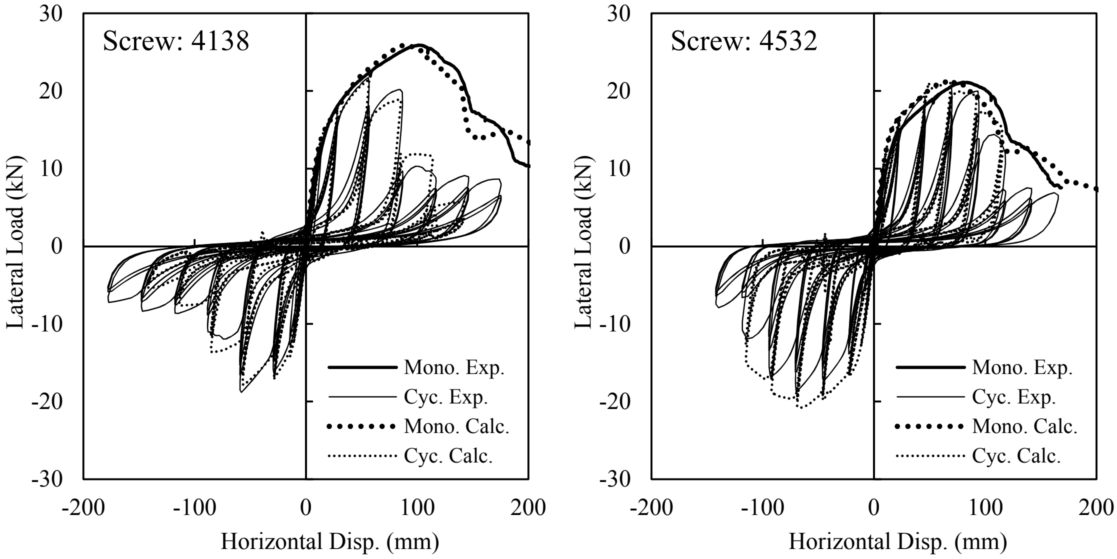

Figure 9 Comparison of load-displacement curves

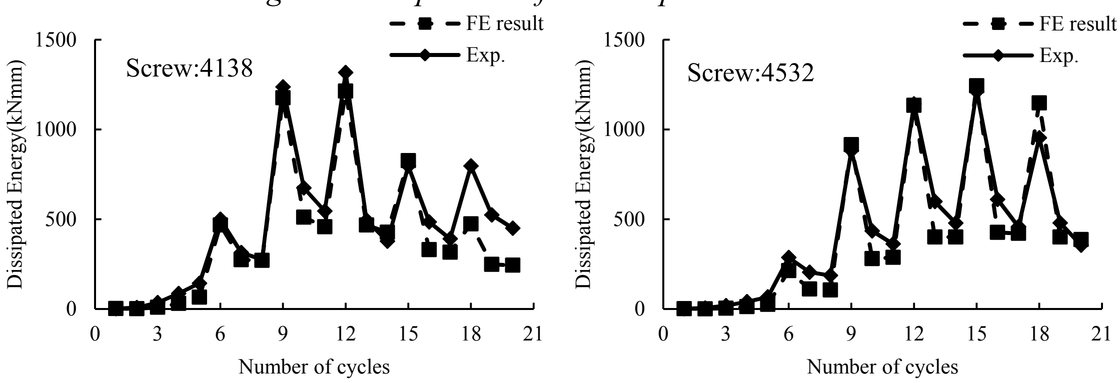

Figure 10 Dissipated energy in each cycle at cyclic loading

Figure 11 shows the comparison between calculated load-displacement curves which the parameters were determined by different way. "Envelope: Mono" means that the parameters for envelope curves (equation (2) - (5)) were determined from monotonic test results. Similarly, "Envelope: Cyc." were determined from cyclic test results. "Without degradation" means that the values of γ and k were fixed to zero. The solid line in Figure 11 takes into account the degradation, and it is the same as the small dot line in Figure 9 left.

The model curve determined by monotonic test results (small dot line) overestimated in both strength and ductility. The model curve determined by cyclic test results (large dot line) showed relatively similar performance to the solid line. In other words, the test results according to ISO 21581 could be

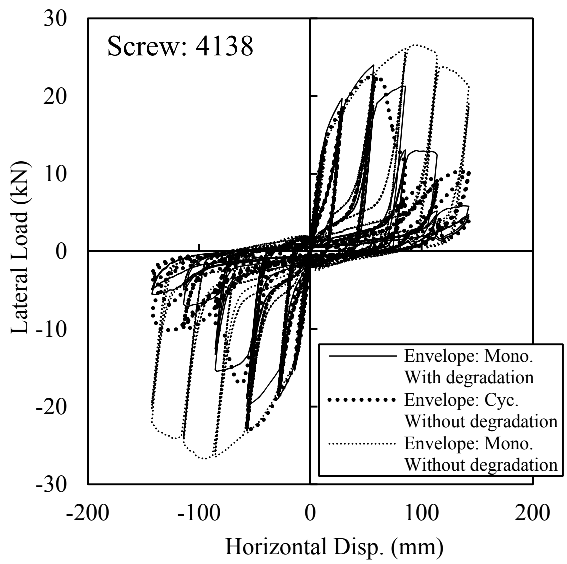

Figure 11 Comparison of calculated load-displacement Curves with different parameters

calculated from the test results according to ISO 16670. It was confirmed that these protocols were corresponded well. It may fit well by applying a little degradation to the envelope curve. Further study is required to confirm the relationship between seismic behavior and ISO protocol.

5. Conclusion

Screws are used gradually for timber structures in Japan. The structural use such as plywood sheathed shear walls are increasing. In this research, racking tests of shear walls and single shearing tests of screwed joints were conducted according to ISO protocols.

In the shear wall tests, the thickness of plywood was 9mm and different sizes of screws were selected. Monotonic tests and reversed cyclic loading tests were conducted according to ISO21581.

Single shearing tests of screwed joints were conducted to simulate the seismic behavior of shear walls. At single shearing tests, the same combination of the fasteners and the sheathing materials were selected. Monotonic tests and reversed cyclic loading tests were conducted according to ISO16670.

As a result, we observed different failure mode of screws according to the length and diameter, and the brittle failures of connections caused by the fracture of screws were observed during the reversed cyclic loading tests. Cyclic loading at large displacement caused the fracture of screws in ISO protocol. We calculated the shear resistance of shear walls from single shearing properties of screwed joints. The estimation results showed good agreement with the test results.

6. References

1. ISO 21581:2010. Timber structures - Static and cyclic lateral load test methods for shear walls. International Organization for Standardization, Geneva, Switzerland, 2010
2. ISO 16670:2003. Timber structures - Joints made with mechanical fasteners - Quasi-static reversed-cyclic test method. International Organization for Standardization, Geneva, Switzerland, 2003
3. JIS B1112:1995. Cross - recessed head wood screws. Japanese Industrial Standards Committee, Tokyo, Japan, 1995
4. JIS G3507-2:2005. Carbon steels for cold heading-Part-2:Wires. Japanese Industrial Standards Committee, Tokyo, Japan, 2005
5. JIS G5508:2009. Nails. Japanese Industrial Standards Committee, Tokyo, Japan, 2009
6. Yasumura M, Kawai N. Evaluation of wood framed shear walls subjected to lateral load. Proceedings of the 30th CIB-W18, Vancouver, paper CIB-W18/30-15-4, pp.1-10, 1997
7. Architectural Institute of Japan. Standard for structural design of timber structures (4th edition). Maruzen, Tokyo, Japan, 2009
8. Richard N, Yasumura M, Davenne L. Prediction of seismic behavior of wood-framed shear walls with openings by pseudodynamic test and FE model. Journal of Wood Science, 19:145-151, 2003
9. Richard N. Approche multi-echelles pour la modelisation des structures en bois sous solicitations sismiques. Thèse de doctorat de l'Ecole Normale Supérieure de Cachan, LMT, 2001

CIB-W18/44-15-9

INTERNATIONAL COUNCIL FOR RESEARCH AND INNOVATION IN BUILDING AND CONSTRUCTION

WORKING COMMISSION W18 - TIMBER STRUCTURES

INFLUENCE OF CONNECTION PROPERTIES ON THE DUCTILITY AND SEISMIC RESISTANCE OF MULTI-STOREY CROSS-LAM BUILDINGS

I Sustersic

B Dujic

CBD d.o.o. - Contemporary Building Design Company

SLOVENIA

M Fragiacomo

University of Sassari, Dept. of Architecture, Design and Urban Planning, Alghero

ITALY

MEETING FORTY FOUR

ALGHERO

ITALY

AUGUST 2011

Presented by I Sustersic

I Smith and I Sustersic discussed that estimating the lower strength such as 5th percentile would be easier than estimating the higher end strength and its relationship with over strength factor.

Influence of connection properties on the ductility and seismic resistance of multi-storey cross-lam buildings

Iztok Sustersic
CBD d.o.o. - Contemporary Building Design Company, Slovenia
University of Ljubljana, Faculty for Civil and Geodetic Engineering, Slovenia

Massimo Fragiacomo
University of Sassari, Dept. of Architecture, Design and Urban Planning, Alghero, Italy

Bruno Dujic
CBD d.o.o. - Contemporary Building Design Company, Slovenia

1 Introduction

The paper focuses on the influence of modelling different types of connections in multi-storey cross-lam timber buildings when performing a linear modal response spectrum analysis and nonlinear static analysis assessed with a modified N2 method.

The main parameter that defines the response of a building when performing a linear modal analysis is its stiffness. As shown in the paper, the stiffness of cross-lam buildings is predominantly governed by the stiffness of the connections between timber panels. Since the connections of walls (angular brackets or hold-downs) behave non-symmetrically in the vertical direction being characterized by a rather low stiffness in tension compared to compression due to the contact, it is necessary to transform this non-linear wall-rocking behaviour into an equivalent linear behaviour that is required in the linear modal analysis. The paper provides some information on how to model this behaviour.

By using a nonlinear static analysis and the N2 method it is shown how different connection types, vertical load on walls and friction between walls and inter-story plates influence the building's global ductility and seismic resistance in terms, for example, of maximum peak ground acceleration. The results presented herein can be used as a basis for further nonlinear dynamic analyses and provide some information for future standard development regarding the influence of connection details and other boundary conditions on the seismic response of cross-lam buildings.

Also basic values for overstrength factors of BMF 105 angular brackets and 8 mm self-tapping screws are presented and the importance of using the overstrength concept in design is demonstrated on a case study.

2 Case study

2.1 Geometry and loads

A four-storey crosslam building (Figure 1) was modelled in this study. The building has 140 mm thick 5-layer crosslam walls along its perimeter. Inside the building there are only two posts and a beam that support 140 mm thick crosslam slabs running from wall ‘A’ to wall ‘C’. Wall ‘A’ is made from two separate panels, which are connected only with a beam element pinned onto the walls (Figure 2). The other walls are made out of single panels. The wall panels are connected at the bottom and at the top with BMF105 brackets. The spacing of the brackets was determined according to the base shear force calculated with the lateral force method (explained more in detail in section 3.1). The building was modelled in SAP 2000 [1]. For modelling timber panels, shell elements and the reduction coefficients proposed by Blass and Fellmoser [2] were used. The floor diaphragms were modelled as rigid. The connections among adjacent vertical panels were schematized in different ways (explained in detail in sections 4.1 and 5.2).

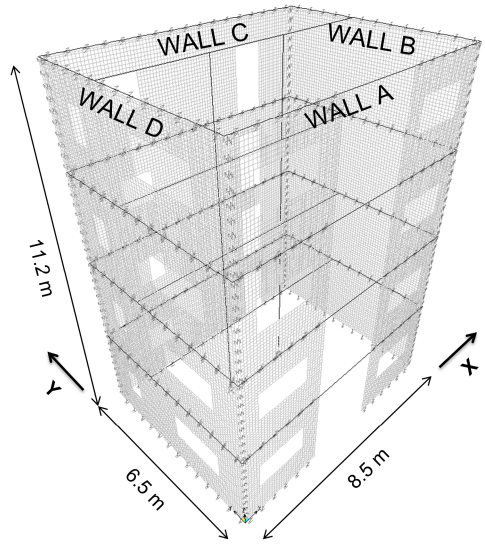

Figure 1: *FE model 3D view*

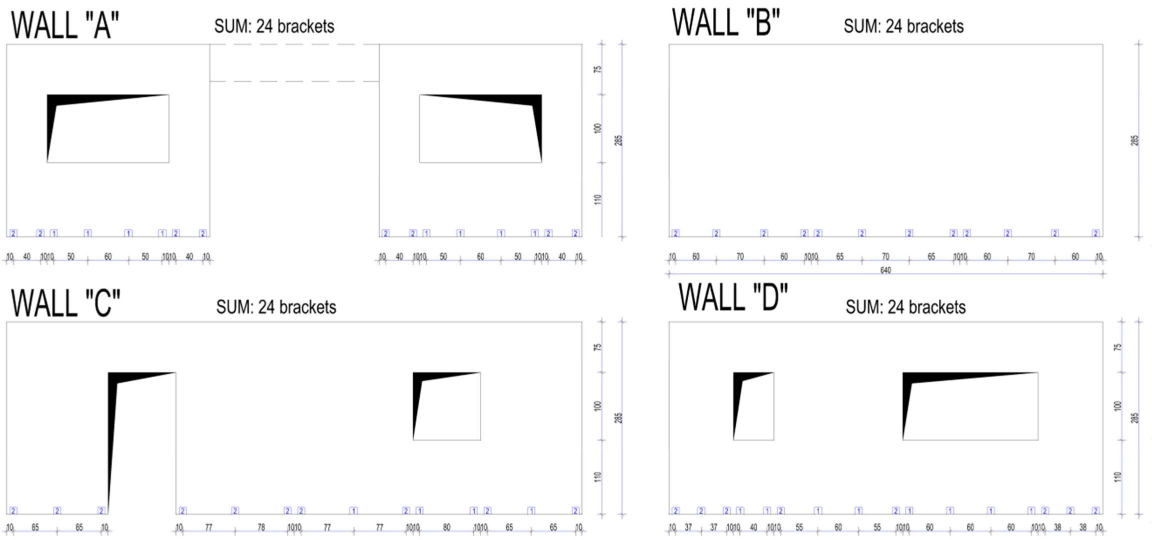

Figure 2: *Wall dimensions (in cm) and layout of bracket connectors BMF 105 used for each wall*

The following data was used for the modal response spectrum analysis of the building according to Eurocode 8 [3]: type 1 elastic response spectra and type A soil (S = 1.0, T_B = 0.15, T_C = 0.40, T_D = 2.00), behaviour factor q = 1.0 and lower bound factor for the design spectrum β = 0.20. Ground acceleration was assumed to be 0.25 g, with a building importance factor γ_I = 1.0. The permanent load of the floor and roof was 3.5 kN/m^2 and 2.0 kN/m^2, respectively. The imposed load on the floor and roof was 2.5 kN/m^2 and 2.0 kN/m^2, respectively. The self-weight of the outer walls was 1.2 kN/m^2. The building was assumed to be category of use »A« according to EN 1991-1-1 [4], so the value of ψ_{2i} for quasi-permanent load was 0.3 and the factor φ was 0.5 for all floors except for the roof where it was 1.0 assuming the roof is accessible. The mass was modelled as lumped in the centroids of the floors. Mass and radius of gyration of floor mass in plan are summarized in Table 1.

Table 1: *Mass and mass radius of gyration for each floor*

	mass [t]	mass gyration radius [t m^2]
4th storey	19.4	185.2
3rd storey	31.5	300.5
2nd storey	31.5	300.5
1st storey	31.5	300.5

2.2 Connection properties

An important issue is how to model the stiffness of the bracket connections. In this paper, it is suggested that stiffness, strength and ductility of the steel brackets and screwed connections are determined according to the procedure proposed by Yasumura and Kawai [5] for evaluation of wood framed shear walls. The yielding load is determined by the intersection of two lines (Figure 3). The first line is drawn through the points on the loading curve corresponding to 10% and 40% of the peak load F_{max}. The second line is drawn through the points corresponding to 40% and 90% of F_{max}. The line is then translated so that it becomes tangent to the actual loading curve. The intersection of this and the former line gives the yield load and the corresponding displacement. The ultimate displacement corresponds to 80% of F_{max} on the decreasing part of the loading curve. The ultimate strength F_u is calculated so that the equivalence of the deformation energies is achieved by assuming an elasto-plastic load-displacement curve, the area under which is marked gray in Figure 3. For BMF 105 angular brackets with ten 4x60 mm nails, a tensile stiffness of 6345 kN/m and shear stiffness of 2767 kN/m were calculated. The ultimate tensile strength was calculated as 21 kN and the ultimate shear strength was 16.5 kN.

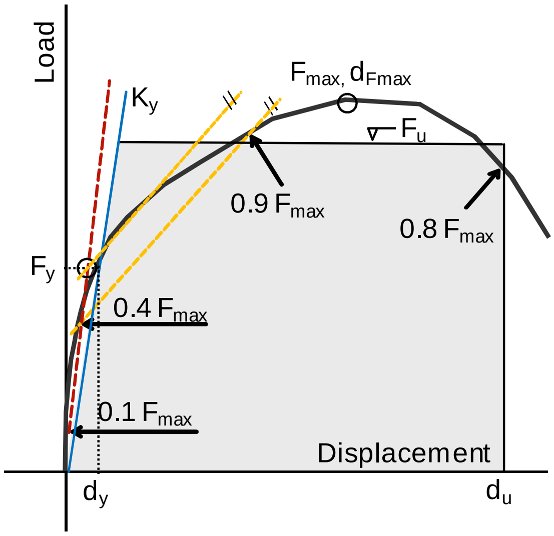

Figure 3: *Yasumura & Kawai procedure [5] for the evaluation of strength, stiffness and ductility*

3 Linear elastic analysis

The methods for linear elastic analysis are generally considered as force based design (FBD). When using linear elastic seismic analysis, the nonlinear response of a building is implicitly considered with the use of the behaviour factor q, which is employed to transform the elastic response into a design elastic spectrum characterized by reduced accelerations. On the basis of the design spectrum, seismic forces acting on the structure are calculated. According to Eurocode 8, the simplest method for calculating forces on a construction regular in plan and elevation is the lateral force method. The same method may also be used for certain types of structures irregular in plan but regular in elevation. If these requirements are not met, the modal response spectrum analysis must be used. The case study building was initially designed according to the lateral force method – the number of brackets being derived on the basis of shear forces and the overturning moment at the ground floor.

3.1 Lateral force method

The building main vibration period, base shear and story shear forces are calculated according to Eurocode 8. A behaviour factor q equal to 1 was used in design so as to compare the maximum peak ground acceleration that the building can resist calculated with a nonlinear pushover analysis with the design peak ground acceleration (0.25 g). The ratio of the former to the latter quantity provides a simplified basic value of the behaviour factor q [6]. The behaviour factor q was then calculated using the aforementioned procedure for different types of connections and wall boundary conditions.

$$T_0 = 0{,}05 \cdot H^{\frac{3}{4}} = 0{,}31 \tag{1}$$

$$W = \sum G_{kj} + \sum \psi_{EI} Q_{ki} = 1139\ kN \tag{2}$$

$$F_b = S_d(T_0) \cdot W = \alpha \cdot S \cdot \frac{2{,}5}{q} \cdot W = 0{,}25 \cdot 1 \cdot \frac{2{,}5}{1} \cdot 1139 = 712\ kN \tag{3}$$

The building connections were designed according to the base shear demand. To withstand a shear force of 712 kN of, 44 brackets are needed in every direction, hence 24 of them were installed on each of the parallel walls (Figure 2).

The resistance to overturning moment due to seismic action was conservatively assumed to be provided only by the walls running in the direction of the seismic load and their corresponding bracket connectors. Under horizontal forces the walls are assumed to rotate about the perpendicular wall on the perimeter. When considering also the beneficial contribution of the vertical load assumed to be applied in the centre of mass of each floor, the tension strength of the brackets was found to be sufficient.

3.2 Modal response spectrum analysis

When determining the elastic stiffness of brackets for use in the modal response spectrum analysis, the values of the shear and tension stiffness were calculated as described in section 2.2. Each wall was then nonlinearly modelled using elastic shell elements, gap elements (elements very rigid in compression with no stiffness in tension) at the interface with the wall underneath, and elastic links for brackets to simulate the exact boundary conditions of (rigid) contact in compression and elastic behaviour in tension and shear. The wall models were then recalibrated so that only symmetrically elastic (same stiffness in tension and compression) links were used, and the target displacements for the nonlinear and linear cases were the same under the same horizontal load (Figure 4). With the fully elastic model, a modal response spectrum analysis was carried out. The wall calibration was performed for different boundary conditions of the nonlinear load case. Natural periods, base shears and top floor lateral displacements of the building were compared for four different types of models (only the X direction of the building is analysed in the paper – therefore only the two walls running in that direction, A and C, are modelled and the connections between perpendicular walls are neglected): (i) with rigid links to model the connections with upper and lower walls and foundation; (ii) with linear elastic springs

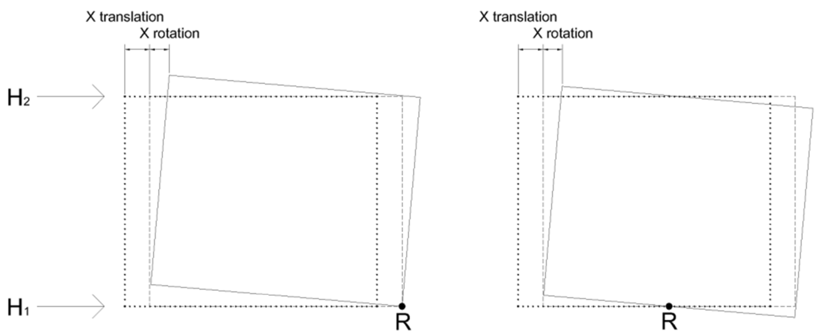

Figure 4: *Wall calibration procedure*

to model the connections with upper and lower walls and foundation; (iii) like for (ii) but considering the influence of vertical load (a higher compressive vertical load on a wall causes a higher bending stiffness due to the favourable stabilizing effect); and (iv) like for (iii) but considering also the effect of friction between walls and top and bottom plates.

It can be observed (Figure 5) that the most rigid model (i) also returns the lowest vibration period values. The base shear forces are conservative as the main vibration period (to which in our case also the majority of the effective mass belongs) is located on the plateau of the design spectrum. Model (ii) is the most flexible one. It has the longest vibration periods and generates the biggest top floor displacements. However the base shear forces are underestimated compared to all other analysed models. Accounting for vertical load on walls results in higher bending stiffness and consequently lower vibration periods. When adding also the influence of friction, the structures response is even stiffer. For the latter case the value of the first vibration period is 0.37 s. An experimentally measured first vibration period value of a 3-story SOFIE Xlam building [6] with a 10 % smaller floor plan and an almost 60 % lower mass was 0.20 s. Therefore by rough quantitative assessment, model (iv) is likely to return the most realistic vibration period values, and hence also the most realistic base shear forces and top floor displacements.

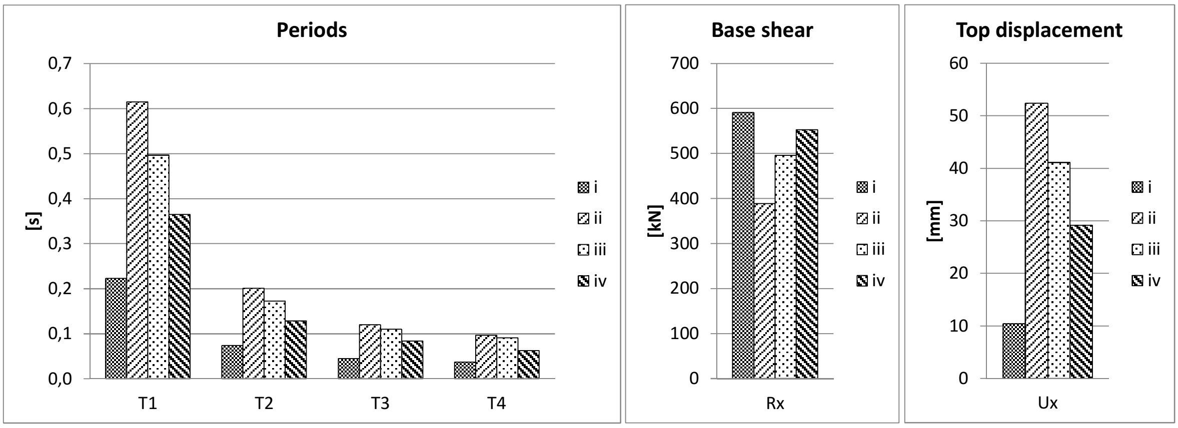

Figure 5: *Four-storey crosslam building – Comparison among different models (i, ii, iii and iv) in terms of vibration periods (T1, T2, T3 and T4), base shear (Rx) and top floor displacement (Ux) along x.*

5 Nonlinear static analysis

The nonlinear static analysis (NSA) procedure is more complex than the FBD, however it allows the designer to take into account the actual inelastic behaviour of the structure. Furthermore, it can be used for Performance-Based Design (PBD), where the design is achieved for different performance levels such as no damage, limited structural damage, important structural damage without collapse, etc. Each level is generally linked to the structural displacement by defining a damage index and by assigning a limit value for every performance level. The NSA procedures are generally based on the evaluation of the push-over curve, which represents the response of the structure under a lateral loading distribution schematising the seismic action. A number of different methods have been proposed, including the N2 method [7], which has been adopted by the Eurocode 8 [3].

5.1 N2 method

The N2 method considers a performance point defined in terms of both strength and displacement, where the structural capacity is compared with the demand of the seismic ground motion. The base shear force and the top displacement of a Multi-Degree-of-

Freedom (MDOF) system are first computed by means of a non-linear Push-Over Analysis and then converted respectively to the spectral acceleration and displacement of an equivalent Single-Degree-Of-Freedom (SDOF) system. The demand of the seismic ground motion is represented through the response spectrum in terms of pseudo-acceleration and displacement. Such an inelastic spectrum depends upon the cyclic behaviour of the SDOF system and the characteristics of the ground motion (peak ground acceleration and shape), and can be obtained from the elastic spectrum using suitable reduction factors. The N2 method was found to provide the best approximation among various NSA methods for SDOF systems with different hysteretic models and for MDOF systems [8]. However the N2 was originally not developed for the design of timber buildings with specific hysteretic behaviour. Therefore it must be noted that the results derived in this study could be non-conservative, because hysteresis loops with pinching, slip and strength degradation (typical for connections in timber structures) dissipate less energy than bilinear plastic loops with the same ductility. Nevertheless, it should be also pointed out that in the analysed setups, the SDOF systems equivalent to the multi-storey building have periods longer than T_c which is usually the value from where the reduction factor (R_μ) and ductility factor (μ) are considered to be the same (Fig. 6), regardless the type of hysteresis loop. The results of these analyses should therefore be considered as a preliminary study aimed to investigate the effect of different wall boundary conditions.

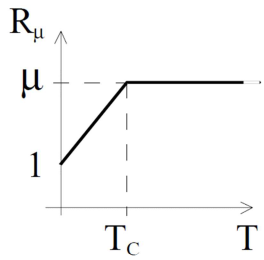

Figure 6: *Relation between $R_\mu - \mu - T$*

5.2 Modified SDOF bilinearisation procedure for the N2 method

The standard bilinearisation procedure of the pushover curve suggested within the N2 method assumes the attainment of the structure ultimate displacement when the first structural component (beam, column, wall) reaches the near collapse (NC) state. In this paper, however, the NC state was defined as a global condition on the entire Xlam building according to the Yasumura & Kawai procedure. Therefore the NC state is assumed to be attained at a displacement such that the base shear force of the structure drops by 20% from the peak value. The initial stiffness of the bilinearised pushover curve is also defined according to the aforementioned procedure instead of using the standard N2 method formula. It should be noted, however, that the results in this case could be non-conservative, as the storey shear force in an individual floor might drop below 80% of the peak value before the base shear does the same.

5.3 Parametric analysis

The following types of connectors were analysed in the parametric study:

1. BMF 105 angular brackets with ten 4x60 mm nails that exhibited ductile behaviour in experimental tests and therefore showed a desirable failure mode.

2. BMF 105 angular brackets with ten 4x60 mm nails – 1^{st} cycle backbone curve. Unlike all other cases where the 3^{rd} cycle backbone curve is used (Figure 7), the 1^{st} cycle backbone curve with an approximately 25% higher strength was considered in this analysis.

3. Fictitious angular brackets with strength equal to that of BMF 105 brackets and 4x60 mm nails but with double ductility.

4. BMF 105 angular brackets with ten 4x60 mm nails, without the influence of the vertical load. In this case the influence of vertical load on the panels, calculated in accordance with the Eurocode 8 combination $G_i + \psi_{EI} Q_i$ was neglected, as opposed to all other cases.

5. BMF 105 angular brackets with ten 4x60 mm nails, with the influence of friction. Unlike all other cases, a friction coefficient of 0.4 between walls and plates (top and bottom) was considered in this analysis.

5.

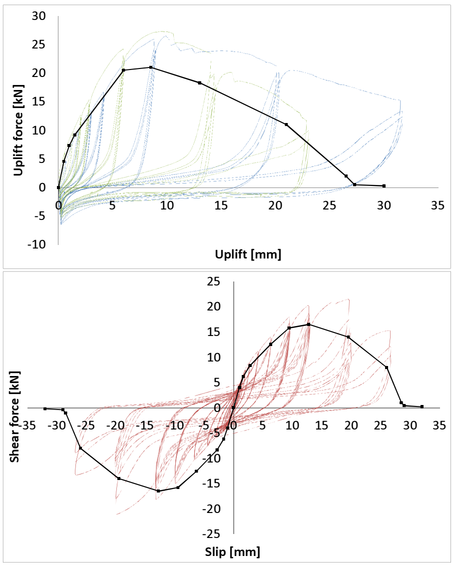

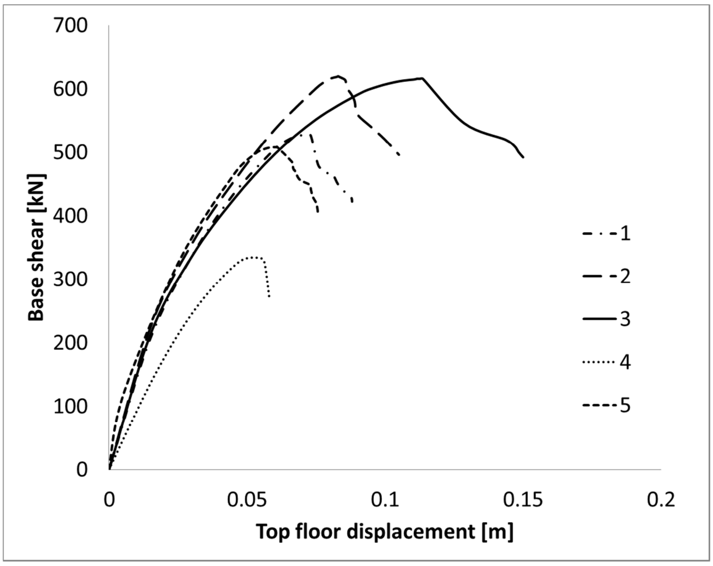

Figure 7: *Calibration of the non-linear FEM link on the backbone curve of the 3rd cycle of the experimental results for BMF105 brackets with 60 mm nails subjected to axial (top) and shear force (bottom)*

Figure 8: *Pushover curves for different types of connector (numbers follow the description above and in table 2)*

From the pushover curves in Figure 8 and values in Table 2 it can be seen that the building with the most ductile bracket connection (case #3) also demonstrates the highest displacement capacity, which also results in the highest peak ground acceleration that the building can resist, calculated as 3.48 times the initial elastic design acceleration. This clearly demonstrated the importance of ductility in seismic design.

The structure where the 1st cycle backbone is used for bracket response (case #2) comes second in terms of both ductility and maximum peak ground acceleration, the latter being about 20 % higher than the value when the 3rd cycle backbone curve is used for the bracket connection (case #1). Since a simplified nonlinear method of analysis was used, it is important to implicitly consider the effect of cyclic damage of brackets by taking into account the (roughly 25 %) lower 3rd cycle backbone curve. As demonstrated with this analysis, the results from the 1st cycle backbone curve are non-conservative.

If no vertical load is considered (case #4), the buildings bending capacity is markedly reduced. This was however expected, as the beneficial effect of the vertical load was taken into account already in the design phase of the structure (Section 3.1), reducing the tension demand on the brackets at the ground floor. The nonlinear analysis shows that a structure could withstand the design ground acceleration even in such a case, nevertheless by pointing out the importance of vertical load for seismic resistance and raising a question on the influence that the vertical ground acceleration could have on the building response.

The consideration of friction in the model (case #5) does not result in a higher peak ground acceleration capacity. Also due to the fact that the failure mechanism in all cases proved to be tension in the bracket connectors and not shear, friction does not play a significant role when performing a simplified nonlinear (pushover) analysis. The corresponding curve in Figure 8, however, demonstrates a higher initial stiffness due to higher shear resistance. When, however, the building behaviour changes from shear to bending as the lateral forces increase, this beneficial influence of friction is lost. The structure reaches lower maximum displacement – most likely due to the higher shear stiffness in the model (the edges of rocking walls generate high compression forces in the corners, which the model translates into shear forces), causing the bending mechanism to be activated at an earlier total displacement (smaller displacement due to shear). It must be noted, however, that friction would probably play a more important role when a nonlinear time history analysis is performed, where it would act as a friction damper dissipating seismic energy.

Table 2: *Ductility ratios, seismic demand and capacity of the case study building in terms of maximum acceleration depending upon the wall connection boundary conditions for loading in the "X" direction.*

	bracket uplift ductility	bracket shear ductility	building ductility	target displacement [mm]	maximum displacement [mm]	max. Peak ground acceleration [g]	$\frac{max.ground\ acc.}{design\ ground\ acc.}$
1) BMF 105 with 10 nails 4x60 mm	4.12	4.45	2.31	41	88	0.53	2.12
2) BMF 105 with 10 nails 4x 60 mm First cycle hysteresis backbone	3.50	3.29	2.47	40	105	0.65	2.60
3) BMF 105 with 10 nails 4x 60 mm Ductility doubled	8.24	8.90	3.12	42	149	0.87	3.48
4) BMF 105 with 10 nails 4x 60 mm No vertical load on walls	4.12	4.45	1.61	48	58	0.29	1.16
5) BMF 105 with 10 nails 4x 60 mm Friction coefficient 0,4	4.12	4.45	2.26	35	76	0.52	2.08

6 Overstrength factors

To ensure a structure can dissipate energy during a seismic event, capacity-based design must be used so as to avoid brittle failure mechanisms. This is achieved by designing the structural elements which may fail in a brittle manner under an increased seismic demand E'_d given by

$$E_d' = \gamma_{Rd} \cdot \gamma_{od} \cdot E_d \tag{4}$$

where E_d is the seismic demand on the structural element calculated using the design spectrum as reduced to allow for the ductile behaviour of the structure, γ_{od} is the overdesign factor, given by

$$\gamma_{od} = \frac{F_d}{E_d} \tag{5}$$

where F_d is the design strength capacity of the ductile structural element, and γ_{Rd} is the overstrength factor, given by

$$\gamma_{Rd} = \frac{F_{0.95}}{F_d} \tag{6}$$

where $F_{0.95}$ is the 95th percentile of the actual peak strength capacity of the ductile structural element. Whilst the overdesign factor depends on the rounding carried out in the actual design and execution (i.e. installing more brackets than necessary), the overstrength factor depends on the type of material and structural detail. The Eurocode 8 provides the values of the overstrength factors for steel and reinforced concrete structures, which are in the range 1–1.3, however there is no provision for timber structures. In the New Zealand timber standard [9], a value of 2 is suggested for the overstrength factor.

Dujic and Zarnic [10] carried out tests on cross-laminated wall connections with metal bracket loaded in tension and shear and self tapping screw loaded in shear. The crosslam panel had three layers of boards with 30-34-30 mm thickness. Tests were performed on BMF 105 angular brackets with ten 4x60 mm and 4x40 mm nails. The yield point was computed according to the the Yasumura & Kawai procedure. The overstrength factors were computed using Eq. (6). The design strength capacity F_d was calculated by dividing the characteristic experimental strength $F_{0.05}$ by the strength partial factor γ_M, assumed equal to one according to Eurocode 8 for dissipative timber structures. The 5th percentile $F_{0.05}$ was estimated by assuming a student's t-distribution on the basis of the maximum experimental shear and uplift strength F_{max} among the specimens tested. The same procedure was used for the calculation of the 95th percentile, $F_{0.95}$. The overstrength factors from shear tests are 1.3 for 60 mm and 2.2 for 40 mm nails (see Table 3). The results from uplift give an overstrength factor γ_{Rd} of about 1.9 for 40 mm nails and 1.2 for 60 mm nails. Since the brackets with 40 mm long nails were characterized by brittle failure, an overstrength factor of 1.3 can be recommended for the design of brittle components in crosslam buildings if ductile bracket connections such as the BMF105 ones with 60 mm long nails are used. It should be reminded, however, that too few specimens were tested to derive a final value.

An experimental investigation carried out by the same authors on screwed connections between perpendicular crosslam panels with Φ8 screws 160 mm long with an 80 mm long threaded part under cyclic shear loading led to an overstrength factor γ_{Rd}=1.6.

Table 3: *Experimental results for BMF 105 angular brackets with ten nails 40 mm and 60 mm long and Wuerth Assy II 8×160/80 self tapping screws*

		No. of specimens tested	Mean value of peak force (F_{max})	Standard deviation σ of peak force	5th percentile $F_{0.05}$	95th percentile $F_{0.95}$	Overstrength factor γ_{Rd}
BMF 105 angular brackets with ten 40 mm nails	shear	3	13.472	1.729	8.422	18.522	2.119
	uplift	3	14.830	1.514	10.408	19.252	1.850
BMF 105 angular brackets with ten 60 mm nails	shear	3	15.028	0.590	13.306	16.750	1.259
	uplift	2	23.088	0.305	21.163	25.012	1.182
Wuerth Assy II 8×160/80 self tapping screws	shear	5	4.676	0.522	3.563	5.789	1.625

6.1 Single wall case study

When dealing with full length solid wall panels the chance of a crosslam wall failing brittle itself is practically impossible if a standard connection system is used. The situation changes for walls with large openings, where concentrations of stresses in the corners may cause timber to fail brittle before the ductile mechanism in the brackets or screws can take place. In such cases the timber panels must be designed by taking into account the overstrength factors of the connections.

In the case study discussed herein (a 240 x 280 cm 3-layer Xlam panel with a 144 x 184 cm opening in the middle), load is applied horizontally on the top of the cantilevered type wall. Pushover curves are presented for the wall braced at the bottom with two BMF 105 brackets with ten 4x60 mm nails for two cases: (i) brackets with characteristic strength; and (ii) brackets with strength exceeding the characteristic value by 30% (overstrength of 1.3). It is shown that the stresses in timber are exceeded for the latter case, leading to crack formation in the wall panel at the corner of the opening. Therefore the timber panel should be redesigned for a higher load corresponding to the overstrength of the bracket connection.

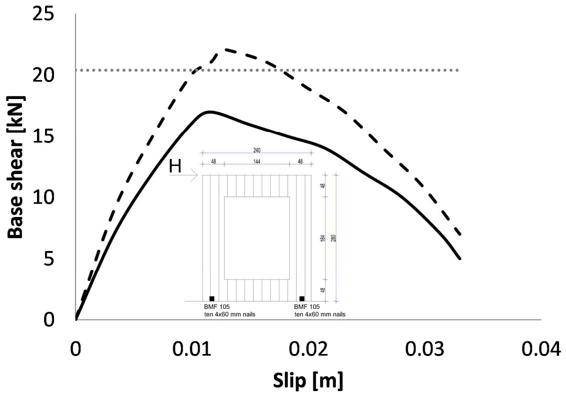

Figure 9: *Pushover curves for case "i" (full curve) and case "ii" (dashed curve). Grey dotted line (20.4 kN) is the base shear value where the Xlam timber frame cracks.*

7 Conclusions

The paper investigates how different connection properties can influence the buildings seismic response. The elastic modal analysis has shown that rigid connections between walls and plates result in very low vibration periods, hence causing too low displacements. However in the case study the prediction of the base shear force is conservative, due to the fact that the structure main vibration period fell in the plateau of the design elastic spectra. By including the influence of the vertical load and the effect of friction between walls and plates, the structure stiffens. By quantitative judgement these models should provide the most accurate values.

The results from the nonlinear static analyses have shown the important role played by ductility when designing buildings for seismic resistance. In the parametric study, the most ductile structure could withstand the highest ground acceleration. It is shown that if the first cycle hysteresis backbone is used in the analysis to model the non-linear response of angular brackets, the building can withstand 20 % more of peak ground acceleration. When including friction in the model, the pushover curves are slightly steeper but the peak load does not change and neither does ductility. It must be noted, however, that friction would probably play a more important role in nonlinear time-history analyses where it could act as a damper by dissipating energy. The beneficial effect of vertical load on walls is also presented in the parametric study.

Preliminary values of the overstrength factors for bracket connectors were also derived, suggesting the use of 1.3 in for design of brittle parts in cross-laminated buildings with BMF 105 brackets with ten 4x60 mm designed so as to achieve a ductile behaviour.

The aforementioned results, although preliminary, are important for future code development, in particular for updating Section 8 'Specific rules for timber buildings' of the Eurocode 8 Part 1. Such a part, written several years ago and never updated, does not provide information on seismic design of cross-laminated buildings including overstrength factors. Further numerical analyses including nonlinear time-history analyses and additional tests on more samples are still needed to draw final conclusions and confirm the results presented in this paper.

8 Acknowledgements

The research support provided to the first and third authors by the EU through the European Social Fund 'Investing in your future' is gratefully acknowledged.

9 References

1. Computers & Structures Inc. SAP2000—Integrated Finite Element Analysis and Design of Structures. Computers & Structures Inc.: Berkeley, CA, 2000.
2. Blass HJ, Fellmoser P. Design of solid wood panels with cross layers. 8th World Conference on Timber Engineering, WCTE 2004, Lahti, Finland; 543-548.
3. European Committee for Standardization (CEN). Eurocode 8—Design of structures for earthquake resistance. Part 1: General rules, seismic actions and rules for buildings. prEN 1998-1; Brussels, 2003.
4. European Committee for Standardization (CEN). Eurocode 1: Actions on structures – Part 1-1: General actions – Densities, self-weight, imposed loads for buildings; 2002, Brussels, Belgium.
5. Yasumura M, Kawai N. Evaluation of wood framed shear walls subjected to lateral load. Meeting 39 of the Working Commission W18-Timber Structures, CIB; 1997, Vancouver (Canada), paper CIB-W18/30-15-4.
6. Ceccotti A. New technologies for construction of medium-rise buildings in seismic regions: the XLAM case. IABSE Structural Engineering International, Special Edition on Tall Timber Buildings 2008, 18(2):156-165.
7. Fajfar P. A nonlinear analysis method for performance-based seismic design. Earthquake Spectra 2000; 16(3):573-592.
8. Fragiacomo M, Amadio C, Rajgelj S. Evaluation of the structural response under seismic actions using non-linear static methods. Earthquake Engineering & Structural Dynamics 2006; 35(12):1511-1531.
9. New Zealand Standard. Timber structures standard, NZS3603:1993. Published by Standards New Zealand, Private Bag 2439, Wellington 6020, New Zealand.
10. Dujic B, Zarnic R. Report on evaluation of racking strength of KLH system. University of Ljubljana, Faculty of civil and geodetical engineering, Slovenia, 2005.

CIB-W18/44-16-1

INTERNATIONAL COUNCIL FOR RESEARCH AND INNOVATION IN BUILDING AND CONSTRUCTION

WORKING COMMISSION W18 - TIMBER STRUCTURES

GYPSUM PLASTERBOARDS AND GYPSUM FIBREBOARDS – PROTECTIVE TIMES FOR FIRE SAFETY DESIGN OF TIMBER STRUCTURES

A Just

J Schmid

J.König

SP Trätek/Wood Technology

SWEDEN

MEETING FORTY FOUR

ALGHERO

ITALY

AUGUST 2011

Presented by A Just

A Frangi commented that the ETH data on start time of charring t_{ch} was based on mean values and the proposed equation here was very conservative. He questioned whether one would need to go with such high level of conservatism. He also question how the 1% criterion in the fire test was measured and whether 5% could be used. A Just and J Schmid responded that the high degree of conservatism was desired and the 1% was more or less a subjective criteria and difficult to assess. They claimed that there would be less difference between 1 to 5 % or 10% criteria.

S Winter commented on the issue of starting time of charring from test and supported A Frangi's point. He stated that one has to look the total system behaviour and discussed EI calculations in comparison with DIN specifications. He stated that results from Eurocode are already conservative. It would be incorrect to adopt such high degree of conservatism and 5% criterion may be more appropriate. Finally he commented that the density of gypsum board was missing in the report which would be an important parameter that could explain the validity. A Just responded that density was considered but they found no correlation.

A Buchanan commented that information of the fastening to the gypsum to the assembly was missing which could have an influence. A Just responded that the fastening of course could have an influence but they did not have more information. Also he did not believe the influence would be large.

CIB 2011 – Gypsum plasterboards and gypsum fibreboards – Protective times for fire safety design of timber structures

A. Just, J. Schmid, J.König
SP Trätek/Wood Technology, Sweden

1 Introduction

Cladding on the fire- exposed side is the first and the most important barrier for the fire resistance of structures. Reduction of cross-section by charring depth is the parameter that has most effect on the load-bearing capacity of wood. Reduction of strength and stiffness properties must be considered for small cross-sections because of the heat flux through the whole section. The time-dependent thermal degradation of wood is referred to as the charring rate, and is defined as the ratio between the distance of the charline from the original wood surface and the fire duration time [1]. The charring rate differs at different protection phases in a fire. Charring begins with slow charring behind the protective cladding. This is the case when the cladding remains in place before failure. After the cladding falls off, charring increases to a much higher rate than that of initially unprotected wood. The starting time of charring and the failure time of gypsum boards are therefore important properties for the fire safety design of timber frame construction.

EN 1995-1-2 [1] provides rules for the design of timber structures in fire. Structural design is based on the charring model by König et al [2], who performed an extensive experimental and simulation study on timber-frame assemblies in fire. For the available models start of charring t_{ch} and failure of the cladding t_{f} are crucial parameters for the load bearing and separating functions of the timber structure.

According to [1] failure times of gypsum boards are to be given by producers or to be determined by tests. In practice, there are very few producers who provide such failure times for their products. Testing, on the other hand, is costly and time-consuming, and not common in practical design of structures.

The European standard for gypsum plaster boards EN 520 [5] gives requirements for different types of gypsum plasterboards. The fire-rated gypsum plasterboard, Type F, is required to fulfil a core cohesion test, but this is not sufficient to provide all the data needed for design of timber-frame assemblies in a fire – the starting time of charring, failure time etc.

2 Gypsum boards

There are many types of gypsum plasterboards in Europe that comply with EN 520 [5]. Most common types are type A and F:

- Type A – regular common boards with porous gypsum core and no reinforcement except the paper laminated surface. This paper uses the abbreviation GtA when referring to this board or similar.
- Type F – fire protection board with improved core cohesion at high temperatures. The abbreviation GtF is used for this board in this paper.

In accordance with [5] there are also other types of gypsum plasterboards: examples include Type D, with a density over 800 kg/m^3, and Type H, with water-resistant properties etc. Furthermore combinations of the specified properties exists, e.g. DF.

Fire-protection gypsum boards (GtF) contain glass fibres which control shrinkage and provide coherence, causing a maze of fine cracks rather than a single large crack which can initiate premature failure of regular board. One of the most critical aspects of fire-resistant gypsum board is the extent to which the glass fibre reinforcement can hold the board together after the gypsum has dehydrated, to prevent the board pulling away from nailed or screwed connections when the board shrinks.

Gypsum fibreboards are high-performance building boards with cellulose reinforcement, complying with EN 15283-2 [6] and can be used as an alternative to gypsum plasterboards or for flooring. Gypsum fibreboard is made from 80-85 % burned gypsum (recycled gypsum recovered from industrial desulphurisation plants), and 15-20 % cellulose fibres (recycled newsprint). The boards are impregnated with aqueous coating-based starch and silicone. This paper uses the abbreviation GF when referring to this type of board.

3 The EN 1995-1-2 design model

The design for large timber members as well as timber frame structures in fire follows [1]. Charring is a central parameter for determining the degree of fire resistance of a timber member: the original cross-section must be reduced by the charring depth. Different charring rates apply for timber members, depending on whether they are initially protected or initially unprotected from direct fire exposure.

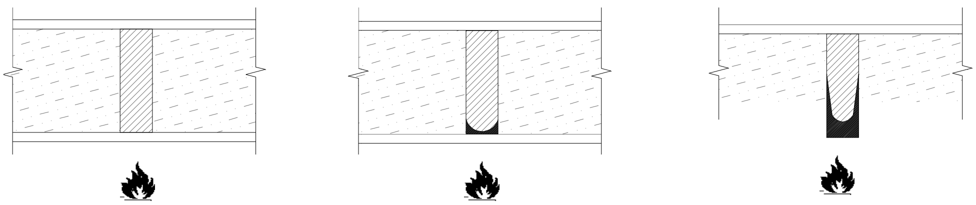

Phase 1: No charring behind the cladding　*Phase 2: Charring behind the cladding (slow charring)*　*Phase 3: Charring at post-protection phase (fast charring)*

Figure 1 – Protection phases for timber frame assemblies in fire.

Unprotected members start to char immediately when exposed to fire: see Line 1 in Figure 2. For protected members, charring is divided into different phases. No charring occurs during Phase 1 until a temperature of 300 ºC is reached behind a protective layer. Phase 2 is referred to as the *protection phase*, and protection is assumed to remain in place until the end of this phase – which is failure time t_f. The charring is relatively slow during this phase (Line 2, Figure 2). Phase 3 is the *post-protection phase*, and begins at failure time t_f. Charring is fast (Line 3a, Figure 2) due to the lack of the char coal layer as thermal barrier. For large cross-sections, there is a consolidation time t_a, when a protective char layer is built up and charring continues, but at a slow rate again.

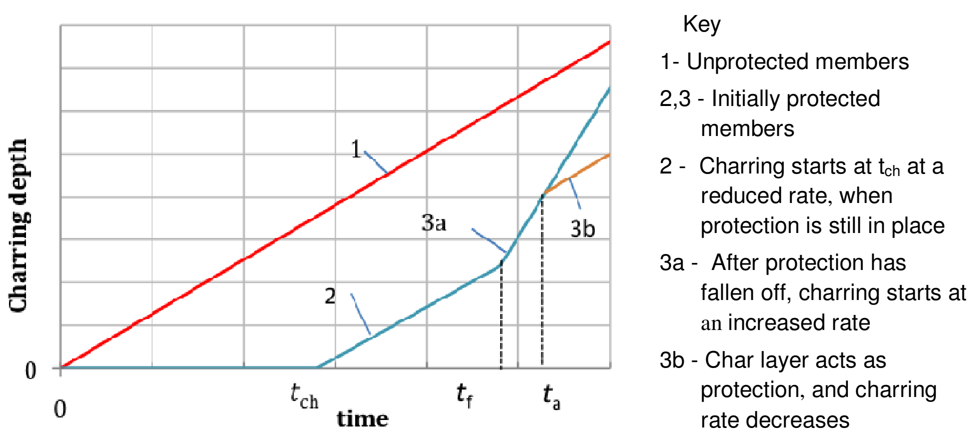

Figure 2 – Charring of unprotected and protected timber members

Small cross-sections, such as those of timber frame structures, do not have this consolidation time because of extensive heating from the wide sides; it is assumed that charring continues for those at a fast rate.

3.1 Start time of charring

Start time of charring t_{ch} is the time when charring of wood starts behind the cladding. It is a time from the beginning of fire to reaching 300 °C on wooden surfaces behind cladding. The principle is in accordance with [1].

3.2 Failure time

Today no standardized definition of failure time t_f exists. In this paper *Failure time* or *fall-off time* of cladding is the time from the start of the test when at least 1 % of the board area has fallen off, based on [7].

Regular gypsum board (GtA) may fall off a wall or ceiling as soon as the gypsum plaster has dehydrated, at about the same time as charring of the timber studs begins. Boards with glass fibre reinforcement and closely spaced fixings will not fall off until the glass fibres melt, when the entire board reaches a temperature of about 700°C [15]. König et al [2] report that the critical falling-off temperatures are 600°C for ceiling linings and 800°C for wall linings in the interlayer of a cladding and cavity insulation (mineral wool).

The time when charring starts behind the gypsum board and the failure time of cladding is an important point for the design of fire resistance of timber frame assemblies (see Figure 2). When the cladding is made of fire rated gypsum plasterboard additionally the value of failure time is needed for the adequate design of the structure.

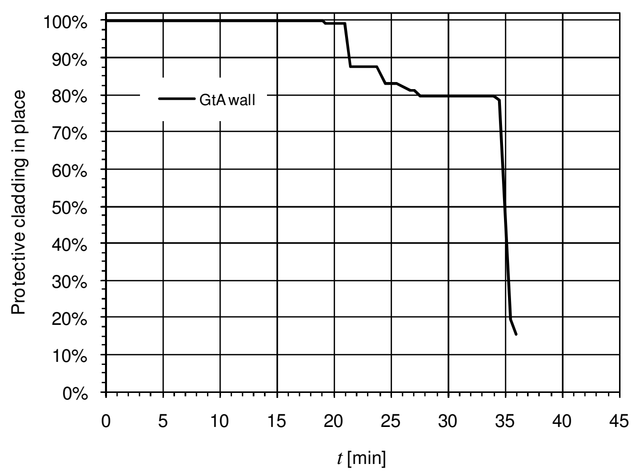

Figure 3 – Example of cladding in place on a full scale wall test specimen [8].

3.3 Different approaches

In North America, Type X gypsum boards are standardised by ASTM C 1396-09a [9]. Gypsum boards type X must provide not less than 1-hour fire-resistance rating for boards 15,9 mm thick, or 45 minutes fire-resistance rating for boards 12,7 mm thick, applied on a specified wall test specimen tested in accordance with ASTM E 119 [10]. Recently small scale tests were introduced to ensure the fire performance of fire rated boards [9] avoiding cost intensive full scale tests. Three bench tests at high temperature have to be performed to qualify fire rated boards: a core cohesion test, a shrinkage test and thermal insulation test. Nevertheless the tests don't give values for start of charring (t_{ch}) and failure time (t_f) respectively to be used in design models.

In Europe, fire-rated gypsum boards must be tested in accordance with EN 520 [5]. However the specified test method doesn't consider thermo-mechanical properties, such as fall-off times for the design of timber frame assemblies in the fire situation. According to [1] failure time due to thermal degradation of the cladding should be assessed on the bases of tests but neither instrumentation between the exposed cladding and the timber members are required in the European test methods. Thus it is hardly possible for producers to reference to standard tests.

In Finland, failure times of some typical gypsum plasterboards (A and F without further references) and combinations are given in the national Annex, somehow based on [2]. In Austria, for gypsum boards GKF [4], gypsum plaster boards type DF [5] and gypsum fibre boards [6] equations for the failure time were introduced in the national Annex based on [11] but no verification process in fire resistance tests or equivalent is given.

On the European level currently the prEN 13381-7 [12] is in revision. This standard is intended for the determination of the start of charring t_{ch}, the failure time t_f as well as of the charring rate of protected and unprotected timber members. For this full scale tests as well as small scale tests should be used but due to the complexicity this standard was not used in practice. At the present TC 127/WG1/TG12 is preparing a proposal for a useful standard to provide input data for the calculation of load bearing resistance and the separating function in [1].

4 Evaluation of database of other experiments

Since fall-off of any cladding is a failure which can’t be simulated using finite element programs due to the complex failure mechanism, easy-to-use rules were developed as the result of extensive evaluation of available test data. Different constructions and fixations were taken into account, since failure is not only a question of the cladding itself. The relationships presented in this paper are a worst-case approach to the available failure times.

A database with data from full-scale fire tests was assembled at SP Trätek to provide material for creating design rules for fire safety design of timber structures clad with gypsum boards. The database contains results from more than 340 full-scale tests from different institutes all over the world, although mainly from Europe [7].

4.1 Results

Effect of gypsum plasterboards on charring of timber

The proposed equations created in [7] from relationships of the database are shown in Table 1. The equations are conservatively created, following minimum test results: see Figure 4. The types of joints between plasterboard sheets, stud spacing, and insulation type are disregarded because effects due to them are not significant when creating conservative design equations based on minimum performance values. Minimum values were taken since the limited available results as well as the fact that most of the reports were results of successful test provided by different sponsors. Joint types shown in Figure 4 are numbered as in EN 1995-1-2 [1].

Based on the evaluations of experimental data in the database described above, conservative equations are proposed for starting times of charring and failure times of gypsum boards. The equations are presented in Tables 1 and 2, graphical explanation is provided in Figure 4 to Figure 6.

Table 1 – Start of charring behind gypsum plasterboards t_{ch} in minutes.

Cladding: gypsym plaster-board	**Start of charring behind gypsum plasterboards t_{ch} in minutes**			
	Walls		**Floors**	
Type A, F one layer	$1{,}8h_p - 7$	9 mm ≤ h_p ≤ 18 mm	$1{,}8h_p - 7$	9 mm ≤ h_p ≤ 18 mm
	25,5	h_p > 18 mm	25,5	h_p > 18 mm
Type F two layers Type F +Type A two layers	$\min\begin{cases}2{,}1h_{p,tot} - 7\\3{,}5h_p + 7\end{cases}$	25 mm ≤ $h_{p,tot}$ ≤ 31 mm 9 mm ≤ h_p ≤ 18 mm	$\min\begin{cases}2{,}1h_{p,tot} - 7\\4h_p - 14\end{cases}$	25 mm ≤ $h_{p,tot}$ ≤ 31 mm 9 mm ≤ h_p ≤ 18 mm
Type A two layers	$\min\begin{cases}2{,}1h_{p,tot} - 7\\1{,}6h_p + 13\end{cases}$	18 mm ≤ $h_{p,tot}$ ≤ 31 mm 9 mm ≤ h_p ≤ 18 mm	$\min\begin{cases}2{,}1h_{p,tot} - 7\\1{,}6h_p + 11\end{cases}$	18 mm ≤ $h_{p,tot}$ ≤ 31 mm 9 mm ≤ h_p ≤ 18 mm

Table 2 – Failure times of gypsum plasterboards t_f in minutes.

Cladding	**Failure times of gypsum boards t_f in minutes.**			
	Walls		**Floors**	
Type F, one layer	$4{,}5h_p - 24$	9 mm ≤ h_p ≤ 18 mm	$h_p + 10$	12,5 mm ≤ h_p ≤ 16 mm
	57	h_p > 18 mm	26	h_p > 16 mm
Type F, two layers	$4h_{p,tot} - 40$	25 mm ≤ $h_{p,tot}$ ≤ 31 mm	$2h_{p,tot} - 3$	25 mm ≤ $h_{p,tot}$ ≤ 31 mm
	84	$h_{p,tot}$ ≥ 31 mm	59	$h_{p,tot}$ ≥ 31 mm
Type F + Type A[a]	81	h_p ≥ 15 mm[b] $h_{p,tot}$ ≥ 27 mm	50	h_p ≥ 15 mm[b]
Type A, one layer	$1{,}9h_p - 7$	9 mm ≤ h_p ≤ 15 mm	$1{,}8h_p - 7$	12,5 mm ≤ h_p ≤ 15 mm
	21,5	h_p > 15 mm	20	h_p > 15 mm
Type A, two layers	$2{,}1h_{p,tot} - 14$[c]	25 mm ≤ $h_{p,tot}$ ≤ 30 mm		
	49	$h_{p,tot}$ ≥ 30 mm		
Type A, three layers	55	$h_{p,tot}$ ≥ 37,5 mm	–[d]	
Gypsum fibreboard, one layer	$2{,}4h_p - 4$	10 mm ≤ h_p ≤ 12,5 mm	–[d]	

[a] Outer layer Type F, inner layer type A
[b] Thickness of first layer (Type F)
[c] Same as EN 1995-1-2 Clause 3.4.3.3(3)
[d] No data available.

5 Discussion

The present study showed large variety of start times of charring related to thickness of board. See Figure 4. In most cases the charring started earlier in full-scale tests with timber frame assemblies compared to small scale tests in [16]. This might be caused by two dimensional heat flux through the cross section as well as cracks due to shrinkage of the cladding in full scale tests although Winter and Meyn [17] concluded that shrinkage of gypsum plasterboards is less than 1% at 300°C, the temperature when the start of charring occurs.

Research work has been carried out at ETH Zürich [13] to investigate the fire protection performance of different materials. The method described in [13] can also be used for calculating the start time of charring t_{ch} as a protection time for cladding layers but this method is not consistent with actual values of [1]. The curve showing the values from this method is shown in Figure 4. For comparison reason the present values from database of start time of charring for single layer gypsum plasterboards are shown in Figure 4.

Figure 5 and Figure 6 contain equations for failure times proposed in this study and also comparison with existing normative values of failure times from other sources.

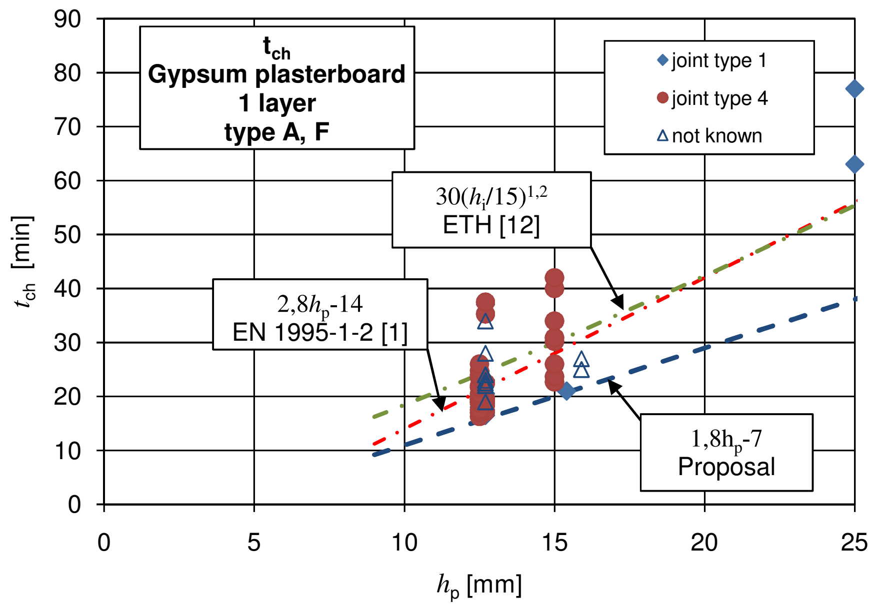

Figure 4 – Start times of charring t_{ch} from database. Comparison of different methods.

The equations provided in this paper are taking into account the large variety of available products. The values are conservative and safe to use. It is intended that producers of gypsum boards provide values of failure times to utilise possible better performance of their products if available. It is expected that it might be a long procedure to change European standards of gypsum boards [5], [6] according to the needs for fire performance of timber frame assemblies. The proposed short-term solution is to declare different protection times t_f for gypsum plasterboards type F, in accordance with the corresponding European Technical Approval Guideline (ETAG 018 [14]) procedure with certain prescribed test set-ups.

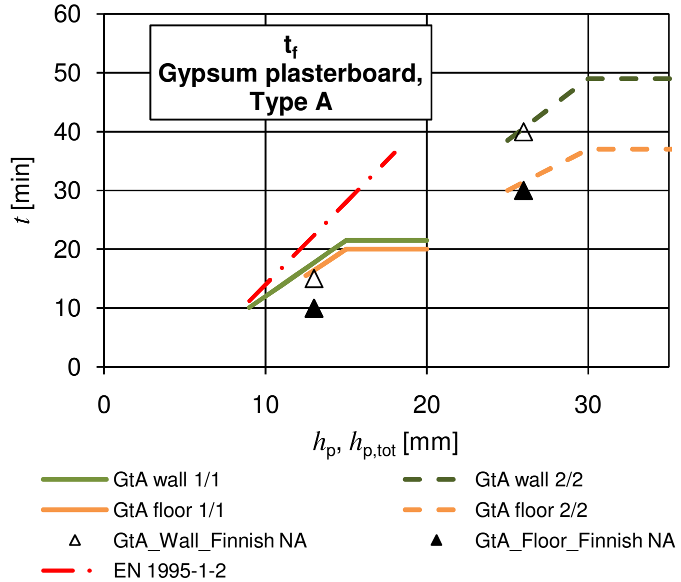

Figure 5– Failure times of Type A gypsum plasterboards. Comparison of proposed equations with other sources.

König et al [2] concluded that critical fall off temperatures are 600˚C for gypsum plasterboards in ceilings and 800˚C for walls but the critical fall-off temperature according to the results of the database [7] can vary quite noticeably: the temperature range for fall-off of gypsum plasterboards type F in wall structures is 650 to 850˚C and in floor structures it is 400 to 850˚C.

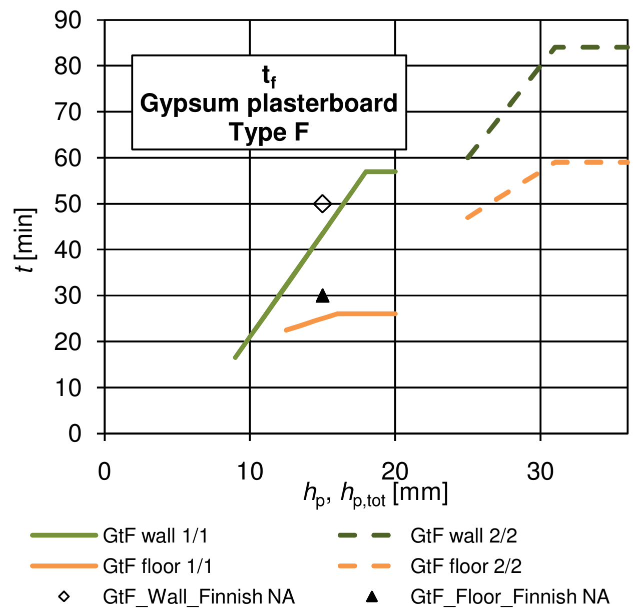

Figure 6– Failure times of Type F gypsum plasterboards. Comparison of proposed equations with other sources.

6 Conclusion, proposal, future needs

This paper presents a proposal to include minimum values for structural fire performance of gypsum plasterboards in [1] to give designers a tool to handle the wide range of products on an open European market. Producers are invited to provide better values for the start of charring t_{ch} and the failure of their boards t_f if available. Today no standard routine is available to clarify these values based on standard wall and floor full scale tests (EN 1363-1, EN 1365-1, EN 1365-2). Although work is ongoing how to determine these values based on tests [12] no bench test method is available for providing the values needed for design according to [1], neither in overseas nor in Europe. The latter would help to reduce the effort to test and classify claddings, provide continuous quality of fire protective claddings and give producers a tool to be used at their plants for development and production control.

7 References

[1] EN 1995-1-2:2004 Eurocode 5: Design of timber structures – Part 1-2: General – Structural fire design. European Standard. European Committee for Standardization, Brussels, 2004.

[2] König, J, Walleij, L. Timber frame assemblies exposed to standard and parametric fires. Part 2: A Design model for standard fire exposure. Trätek, Swedish Institute for Wood Technology Research, Report No. 0001001, Stockholm, 2000.

[3] Östman, B., König, J., Mikkola, E., Stenstad, V., Carlsson, J., and Karlsson, B., Brandsäkra trähus. Version 2. Trätek, Swedish Institute for Wood Technology Research, Publ. No. 0210034, Stockholm, 2002.

[4] ÖNORM B 3410: 2006, Plasterboards for dry construction systems (gypsum plasterboards) – Types, requirements and tests, ON Institute, Vienna, 2006.

[5] EN 520:2004, Gypsum plasterboards – Definitions, requirements and test methods. European Committee for Standardization, Brussels, 2004.

[6] EN 15283-2:2008, Gypsum boards with fibrous reinforcement – Definitions, requirements and test methods - Part 2: Gypsum fibre boards, European Standard, CEN, Brussels, 2008.

[7] Just, A, Schmid, J, König, J, Gypsum plasterboards used as fire protection – Analysis of a database. SP Report 2010:28, Stockholm, 2010.

[8] Schmid, J, Just, A, König, J, Fire exposed wooden I-joists for Wall Assemblies, SP Trätek, In preparation. SP Report 2011: 27, Stockholm, 2011.

[9] ASTM C1396 / C1396M – 09a Standard Specification for Gypsum Board, Annual Book of ASTM Standards, Vol. 4.01, ASTM International, W. Conshohocken, PA, September 2009.

[10] ASTM E119 – 10b Standard Test Methods for Fire Tests of Building Construction and Materials, Annual Book of ASTM Standards, Vol. 4.07, ASTM International, W. Conshohocken, PA, November 2010.

[11] Teibinger, M, Matzinger, I, Charwat-Pessler, J., Grundlagen zur Bewertung des Feuerwiderstandes von Holzbautelen, Endbericht, Holzforschung Austria, Vienna, 2010.

[12] prEN 13381-7:2008, Test mehod for determining the contribution to the fire resistance of structural members- Part 7: Applied protection to timber members, European Committee for Standardization, Brussels, 2008.

[13] Schleifer, V, Zum Verhalten von raumabschliessenden mehrschichtigen Holzbauteilen im Brandfall. PhD Thesis No. 18156, ETH Zürich, 2009

[14] ETAG 018, Guideline for European Technical Approval of Fire Protective products – Part 2: Reactive coatings for Fire Protection, EOTA, Brussels, 2006.

[15] Buchanan, A, Structurl Design for Fire Safety. Canterbury: John Wiley & Sons Ltd., 2001

[16] Tsantaridis, L, Östman, B, König, J, Short Communication: Fire Protection of Wood by Different Gypsum Plasterboards. Fire and Materials, 23, pp 45-48. 1999

[17] Winter, S, Meyn, W, Advanced Calculation Method fort he Fire Resistance of Timber Framed Walls. Meeting of CIB W-18. Dubbendorf, Switzerland, August, 2009.

[18] Shipp P. Thermophysical properties of fire protection membranes – a study of Type X gypsum board. ASTM Commitee E05. Research review.

[19] Fire safety in timber buildings, technical guideline for Europe, chapter 5, SP report 2010:19, Stockholm 2010.

CIB-W18/44-17-1

INTERNATIONAL COUNCIL FOR RESEARCH AND INNOVATION
IN BUILDING AND CONSTRUCTION

WORKING COMMISSION W18 - TIMBER STRUCTURES

INFLUENCE OF SAMPLE SIZE ON ASSIGNED CHARACTERISTIC STRENGTH VALUES

P Stapel
J W G. van de Kuilen
TU München

GERMANY

G J P. Ravenshorst
Delft University of Technology

THE NETHERLANDS

MEETING FORTY FOUR
ALGHERO
ITALY
AUGUST 2011

Presented by P Stapel

J Köhler questioned about 1) the confidence intervals to the design of the structure an 2) whether each subsample would be expected to have the target strength values.

P Stapel answered that question 2 should be directed to the users as to what would be their expectations. J W van de Kuilen added that on average one would like to see the samples meet the target level; however, this could not be checked if there was not enough data. Also the checks needed to be done based on the limited available data and this did not have to do the design issues.

F Rouger asked whether the approach of Ks or CI and Weibull based for 5%tile calculations in relation to the stability of small sample size.

P Stapel responded that the Weibull based for 5%tile did not matter as they also tried different approaches.

R Harris commented on the representativeness of the sample with respect to the location etc. Ks should be location dependent. P Stapel agreed and stated that this would be especially problematic for tropical hardwood where the source of the material might not be known and producers wanted to reduce testing costs.

Influence of sample size on assigned characteristic strength values

P. Stapel[1], J.W.G. van de Kuilen[1,2], G.J.P. Ravenshorst[2]
[1]TU München, Germany, [2]Delft University of Technology, The Netherlands.

Abstract

According to EN 384, characteristic values for strength need to be adjusted for sample size and number of samples. The minimum sample number is 1 and the minimum sample size allowed is 40. With decreasing number of samples the statistical punishment factor (k_s-factor) reaches a minimum value of 0.78. It means that for a single grade and species, 40 specimens may be sufficient in order to determine characteristic strength values to be used with Eurocode 5. This minimum of 40 specimens is independent of the size of the growth area, generally considered as being one country. Since the introduction of EN 384, a large number of wood species and grades have been assigned to strength classes, varying from softwoods (mainly spruce and pine), low and medium dense European hardwoods like poplar, ash and maple to heavy tropical hardwoods such as cumaru und massaranduba. In this paper, a statistical analysis has been made for a number of species for which data is available. The influence of the sample size on the derived characteristic values is studied together with an analysis of the variation in (characteristic) strength values between subsamples. It is shown that EN 384 can be too liberal. The derived characteristic strength values of species, subsamples and grades are studied using the ranking method and 2-parameter weibull distributions. A proposal for an improvement in the current procedure to determine characteristic strength values on the basis of small samples is made.

1 Introduction

In the assignment procedure of grades to strength classes it is required that the sampling is representative for the structural timber that is brought onto the market. This would require comprehensive testing programmes to determine the characteristic values, as well as a continuous monitoring testing programme to discover possible deviations from the original assumption of being representative. In practice it is hardly possible to determine whether this is actually the case, as strength values assigned to certain grades are often based on few samples. Even with as few as 40 test pieces large areas can be covered.

In this paper the influence of the sample size and the growth area for which the sampling should be representative is discussed for both softwoods and hardwoods for visual and machine grading. This paper focuses on the assigned bending strength.

2 Requirements according to EN 384 and backgrounds

2.1 Requirements according to EN 384

According to its scope, EN 384 "gives a method for determining characteristic values of mechanical properties and density, for defined populations of visual and/or mechanical strength grades of sawn timber". This allows assigning grades and species to strength classes according to EN 338.

The following aspects need to be considered for the sampling:

- The sampling should be representative for production.
- Any suspected difference in strength should be incorporated in the sampling by taking different subsamples where these suspected differences are incorporated.
- The minimum amount of pieces in a visual grade is 40 pieces. A sample is defined as a number of specimens of one cross section size and from one population.

The characteristic value for the species and the grade has to be calculated as follows:

- For every subsample the 5%-percentile of the visual grade should be determined by ranking (non-parametric method)
- The characteristic value of the visual grade of the whole sample should be determined by calculating the weighted average 5%-percentile value of the subsamples. The weight is determined by the number of pieces in a subsample.
- The determined characteristic value should be multiplied by a factor k_s, which depends on the number of samples and the number of pieces in the smallest sample.
- The determined characteristic value should not be greater than the lowest 5^{th} percentile of the individual subsamples multiplied by 1.2.

Some consequences from the method described above are:

- The characteristic value of the grade is a weighted average value for the whole growth area.
- When timber from the entire growth area is not mixed during production, but is produced from regions represented by the subsamples, this timber may have an expected characteristic value of 1.0/1.2 = 83% of the assigned strength value for the case that k_s=1.0.

2.2 Background

The background for the k_s factor can be found in Fewell and Glos (1988). To bring into account the variability between the 5^{th} percentile values of subsamples 20 subsamples of 100, 200 and 300 pieces were randomly selected from a parent sample of 652 pieces of European redwood/whitewood. This result is shown in figure 1. This figure was adopted and modified to the k_s factor that is at present incorporated in EN 384 and shown in figure 2. Figure 2 is a result of a statistical exercise on a parent sample of European redwood/whitewood, but has not been verified on any actual sample analysis with test data or on any other wood species with possible different characteristics.

EN 384 requires that sampling is representative for the whole population. Proof of representativeness is however difficult to achieve. A number of parameters influence the population characteristics (a.o. growth area, climate conditions, forestry practices, sawmill operations) but it is virtually impossible to cover these influences in a test programme to determine engineering values for timber. From EN 384, it can be read that a minimum of 40 specimens is enough, but with the consequence of a statistical punishment (k_s-factor of

0.78). This is done to account for the uncertainty in characteristic strength values caused by the small sample size. In the following, an analysis on the k_s is performed, using a number of different wood species covering EN 338 strength classes from C 24 to D 70. It might be a coincidence, but the minimum ratio in figure 1 for a subsample of 100 beams is around 0.78, exactly the same as the minimum k_s factor in EN 384 for a single subsample with the minimum required 40 specimens.

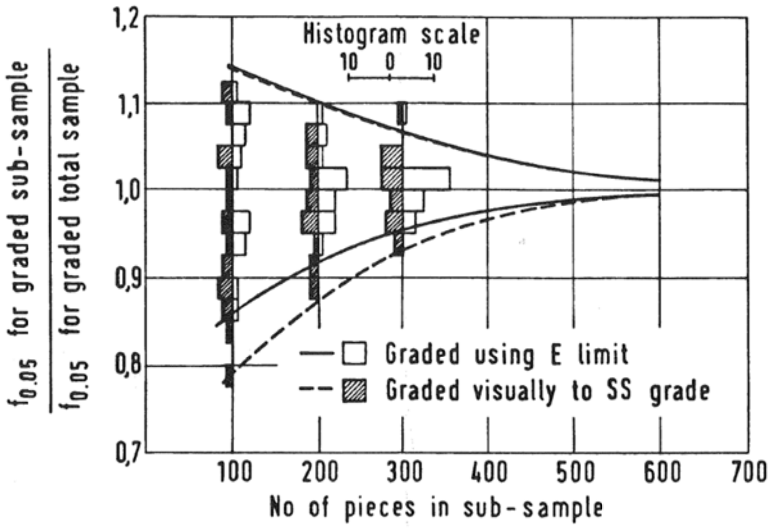

Figure 1: Ratios of lower 5% bending strength values of randomly selected sub-samples from a parent sample of 652 pieces. Taken from Fewell and Glos (1988).

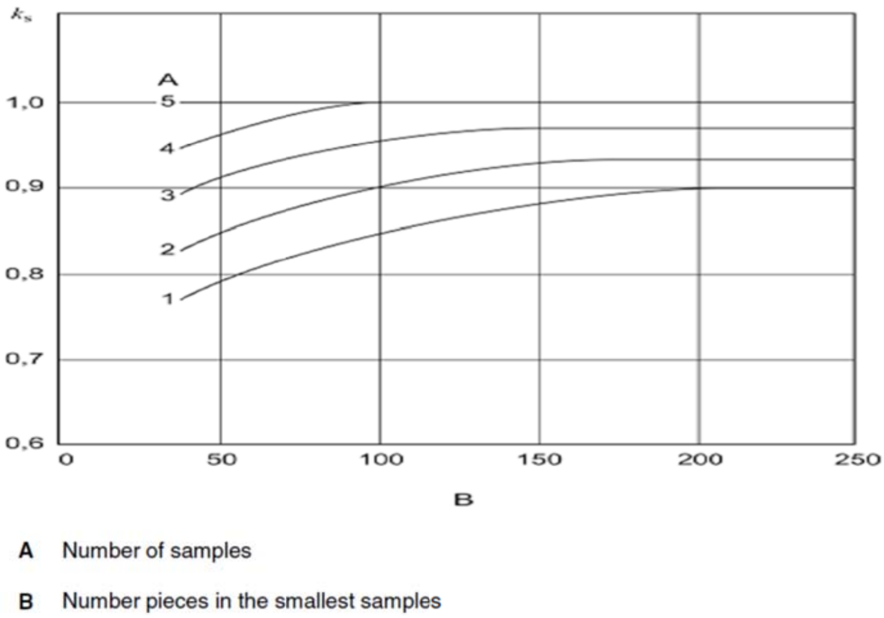

Figure 2: Required k_s-factor depending on the number of samples and sample size according to EN 384.

3 Materials and Methods

3.1 Materials

Bending test data is available for European soft- and hardwoods, as well as for tropical hardwoods from South-America. The data is separated with respect to origin and sample size. Depending on the available non-destructive test data used for grading the timber, datasets are used for analysing the results of visual grading, machine grading or both.

European Softwood

For machine grading 4893 datasets of Norway spruce (*Picea abies*) from Europe are analysed. The data covers many parts of Central, North and Eastern Europe. The sampling was carried out in different regions within 11 different countries. The cross section also covers a broad range: the thickness varies from 20 to 167 mm and the width (depth) from 63 to 284 mm. A more detailed description of the samples was given by Stapel et al. (2010). Separating the dataset according to EN 384 requirements leads to 53 samples. The minimum number of pieces in one subsample was 20, the maximum 518. For machine grading it is not mandatory to separate samples for cross-sections. As EN 384 requires this, 4 subsamples with less than 40 pieces are formed.
Less visual grading data is available. In addition to 1547 specimens of Norway spruce, 391 specimens of Scots pine (*Pinus sylvestris*) and 157 specimens of Douglas fir (*Pseudotsuga menziesii*) are available. Norway spruce was sampled in Central Europe, Scots pine and Douglas fir originated from German forest stands. The thickness varies from 20 mm to 165 mm and the width (depth) from 70 mm to 252 mm.

European Hardwood

Three European hardwood species are included in the analysis: European ash (*Fraxinus excelsior*), Sycamore Maple (*Acer pseudoplatanus*) and black poplar (*Populus nigra*) 1250 specimens from different stands within Germany were analysed. Compared to the softwood species, the range of the cross-sections was small. All pieces had a thickness of 50 mm and widths between 100 mm and 175 mm.

Tropical Hardwood

Two tropical hardwoods are analysed: cumaru (*Dypterix spp.*) and massaranduba (*Manilkara spp.*). For cumaru and massaranduba the trade name represents a genus with more species, indicated by the extension spp. Since some wood species are distributed over a whole continent, the source area of the samples is not always clear. As a result the samples can represent a small or huge growth area. The cumaru samples originate from Brazil, Peru and Bolivia, while massaranduba was sampled only within Brazil. Tested width for massaranduba was between 100 mm and 150 mm, for cumaru between 100 mm and 170 mm. Thickness for both species was between 40 mm and 64 mm. Only graded material was available.

Testing of the Material

All destructive tests were performed according to EN 408. The factors given in EN 384 (k_h-factor, k_l-factor) were applied. A symmetrical two point loading was used for the determination of bending strength, usually over a span of 18 times the depth. If possible the weakest section along the beam axis was tested. For tropical hardwoods the weak zone is mostly not visually recognizable. This means that the weakest zone is randomly present over the specimen length. The orientation of the board in edgewise bending tests was chosen randomly.

Table 1 summarizes the available data and gives basic statistical values for the tested species.

Table 1: Number of pieces, number of samples and bending strength values for tested species.

Species	n	no of subsamples	bending strength	
			mean	cov
European Softwood				
spruce	1547	14	39.3	30.6
douglas	157	2	49.4	35.0
pine	391	4	37.6	34.5
machine graded spruce	4893	53	40.6	32.4
European Hardwood				
maple	459	4	56.6	33.4
ash	324	4	69.8	23.1
poplar	467	5	44.5	33.0
Tropical Hardwood				
massaranduba	146	3	99.4	31.6
cumaru	223	5	106.8	25.0

3.2 Methods

For the analysis all specimens are graded either visually or by machine.

Based on the 4893 datasets for which laboratory data for density, eigenfrequency and knot value are available Stapel et al. 2010 calculated a model by means of (multiple) linear regression analysis. This model reflects real machine strength grading and is used here. The settings were derived for a so called "machine controlled system" in compliance with the current standard EN 14081. Single countries are used as subsamples on which the derivation of settings is based. The resulting settings would be valid for large parts of Europe.
Settings for a low grade (C 24) and a high grade (C 35) were used to check the effects for machine strength grading. The grades were not analysed in strength class combinations.

DIN 4074-2 was used to grade European softwood species for which the necessary visual data was recorded. DIN 4074-5 was used for hardwoods. Each standard gives the same eleven features which need to be considered for the assignment into a visual strength class. However limit values differ depending on the species. For the grading we focused only on the following three major criteria: knot size, existence of pith, year ring width. Depending on its properties, a board can be assigned to the visual strength class 7, 10 or 13. The higher the number is, the higher is the expected strength values. Softwoods get the prefix S, Hardwoods LS.
The visual strength class 7 was not analyzed. Both of the higher strength classes were analysed separately. Additionally, boards graded into the visual strength classes 10 and 13 were analysed combined in a so called strength class "10 and better" (L 10+ / LS 10+).

Visual strength grading of dense tropical hardwoods is generally restricted to slope of grain and some limit on growth defects such as knots or other growth disturbances that may be present in hardwoods. In most cases, such as NEN 5493 and BS 5756, the growth defect size is limited to 0.2 times the size of the face on which the defect is visible. Slope of grain has a typical limit of 1:10, but when sampling is done timber with exactly these defects are often difficult to find. Consequently, the limits present in the standards are also meant to prevent too big defects coming onto the market for which no test data is available, without reducing the strength to an unsafe level. For ring width generally no requirement is given.
The two tropical hardwood samples were graded into grade C3 STH according to

NEN 5493, which is equal to BS 5756, except for a minor difference in slope of grain which is 1:10 for NEN 5493 and 1:11 for BS 5756.

Bending strength values were determined, if 40 or more pieces were graded into the same grade. For the 5th percentile characteristic value this was done by ranking and by a two parameter Weibull distribution using SPSS software. Multiplying the 5th percentile characteristic value determined by ranking with the k_s-value for the subsample leads to the characteristic strength value which would have been assigned to the species if only this sample had been tested. Depending on the number of specimens in this subsample, the used k_s-factor in the analysis varies between 0.78 and 0.9.

In addition, all samples of each species were analysed together. The 5th percentile characteristic value was determined by calculating the weighted mean of the 5th percentile characteristic value of each sample. The values were weighted by the number of pieces in each sample. Additionally, the lowest of all 5th percentile characteristic sample values was multiplied by 1.2 according to EN 384. This results in two 5th percentile characteristic values. The lower value was chosen and multiplied by a k_s-factor for the species, resulting in the ´real´ characteristic value. Depending on the number of specimens and the number of samples available for the species and grade, the used k_s-factor can vary between 0.78 and 1.0.

Then, for each subsample, the ratio between the characteristic value of the sample and the ´real´ value was determined. In principle, the characteristic 5th percentile value of the subsample, multiplied with k_s should lead to a safe design value, i.e. a value equal to or higher than the ´real´ characteristic value. If ratios higher than 1.0 are found for subsamples, the current method in EN 384 is on the unsafe side, assuming that the ´real´ characteristic value is accurate. The following equation summarizes the procedure mathematically.

$$Ratio = \frac{k_{s,i}\, f_{m,0.05,i}}{k_{s,j} \cdot \min\left(1.2\, f_{m,0.05,i,\min}, \frac{\sum_{i=1}^{j} n_i\, f_{m,0.05,i}}{\sum n}\right)} \qquad (1)$$

in which:

$f_{m,0.05,i}$	= 5-th percentile bending strength of subsample i
$f_{m,0.05,i,\min}$	= lowest 5-th percentile bending strength of i – subsamples
j	= the number of subsamples
n_i	= the number of specimens in subsample i
n	= the total number of specimens
$k_{s,i}$	= factor taking into account the size of subsample i
$k_{s,j}$	= factor taking into account the number of specimens in the smallest subsample i and total number of subsamples j (for $j \geq 5$, $k_{s,j} = 1$)

4 Results

The grading results for the single species are given in Table 2. The separation into different cross-sections and origins had the effect that less than 40 pieces are found for certain species and grades. For European softwoods not enough pieces were available in the visual strength class S 13. For Douglas fir, the total number of pieces was too low to have separate results neither for S 10 nor for S 13. For European hardwoods the share of timber in class LS 10 was too low.

Table 2: Grading results for different species and grades.

grade	species	n	mean	cov	f_0,05_weibull	f_0,05_rank	$k_{s,j}$	f_EN_384
S 10	pine	185	39.9	27.9	21.9	22.7	0.90	18.7
S 10	spruce	832	42.7	26.0	24.2	23.6	1.00	22.6
S 10 +	douglas	96	56.4	28.4	29.3	27.4	0.83	24.7
S 10 +	pine	246	42.4	29.2	22.7	23.6	0.96	22.0
S 10 +	spruce	969	43.3	26.2	24.5	24.3	1.00	22.7
LS 10 +	maple	311	59.6	30.8	28.6	30.0	0.97	28.6
LS 10 +	poplar	317	49.4	27.1	26.1	26.9	1.00	20.6
LS 10 +	ash	257	72.2	20.8	45.7	44.9	0.96	37.0
LS 13	ash	207	75.3	18.1	51.1	52.8	0.95	46.9
LS 13	poplar	216	54.1	20.8	34.7	36.4	0.90	31.2
LS 13	maple	242	62.8	28.2	31.4	32.3	0.95	28.0
C 24	spruce	4773	41.1	31.3	20.4	21.4	1.00	16.1
C 35	spruce	1391	53.2	20.0	34.8	35.1	1.00	33.9
C3 STH	massaranduba	146	99.4	31.6	47.0	51.0	0.89	43.8
C3 STH	cumaru	223	106.8	25.0	59.7	56.8	1.00	56.3

The lowest $k_{s,j}$-factor on the complete species is used on douglas fir, as only two samples were available from the beginning. For several grades $k_{s,j}$ = 1.0 as at least five samples are present for the grade. Only for S 10+ for douglas fir and pine and for S 10 for pine, the weighted mean of the 5th percentile strength values was used to get the characteristic strength value according to EN 384. In all other cases this value can be explained by one weak sample. In most cases the difference between the minimum value and the weighted mean is less than 5 N/mm². Differences are bigger for machine graded C 24 and tropical hardwoods. The extreme is reached for massaranduba, showing a difference between both values of 17.7 N/mm².

5th percentile values determined by ranking method are close to the results for 5th percentile values based on weibull distributions. As this can even be found on the basis of the single subsamples, no distinction between the two is made in the following analysis and only the ranking results are used.

Figure 3 shows the ratio for the EN 384 value which would have been calculated for single subsamples and the value which would result determining the expected strength value for all samples - also based on EN 384. The results are shown separated by countries, for which a country code is given on the x-axis. As there are 42 subsamples with more than 40 pieces in a grade it is obvious, that the subsample with the lowest 5th percentile value is responsible for the ´real´ characteristic value. This value resulting from one subsample has a 5th percentile characteristic value as low as 13.4 N/mm². This results in a reference value of 16.1 N/mm², while the value for the weighted mean is 22.1 N/mm². According to

EN 14081-2 the required characteristic strength for C 24 is 21.4 N/mm². This value is indicated by the red dotted line.
The results for C 35 are also shown in Figure 3. The dots indicate the ratio. For countries with low quality timber or small sample sizes it is not possible to grade at least 40 pieces into C 35. Only the ratio value for one sample lies slightly above 1.0. This is the case even though the reference value again depends on one single subsample. Compared to C 24 the difference between the value based on the one SI sample (33.9 N/mm²) is much closer to the value for the weighted mean (36.1 N/mm²).

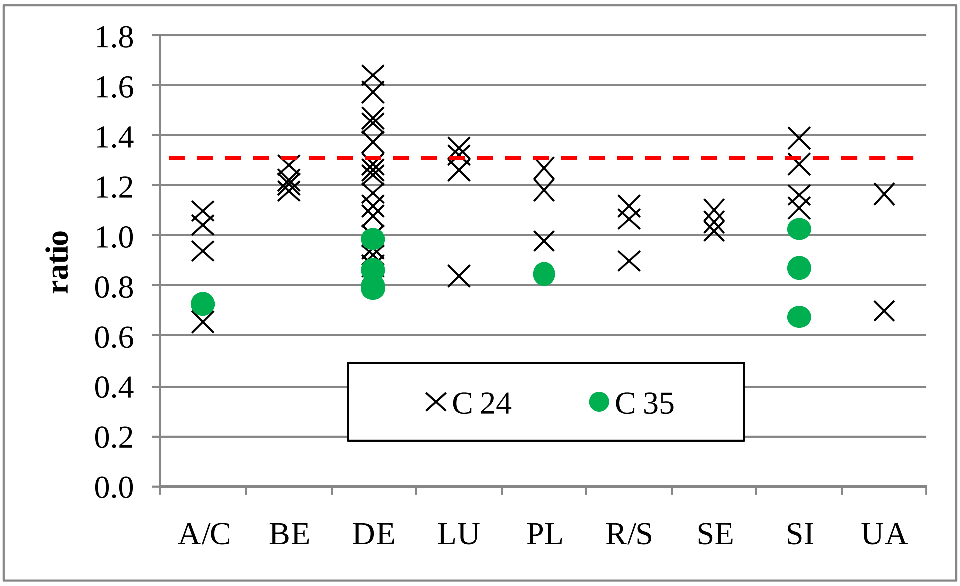

Figure 3: Ratio for machine graded timber in grade C 24 and in grade C 35 separated for countries. The red dotted line indicates the required characteristic strength for C 24 according to EN 14081-2.

Visual grading results are shown in Figure 4. Results for 33 subsamples are available in S 10+ for softwoods and LS 10+ for European hardwoods. The highest characteristic strength difference can be found for poplar: The sample with the lowest strength reaches a characteristic value of 17.2 N/mm², while the highest one reaches a value of 30.4 N /mm².
When the visual grades are more specific and grading is done to visual classes 10 and 13 separately subsamples become smaller and k_s-factors decrease for subsamples. For one subsample of maple this still leads to a recognizable high ratio, as the decrease of the characteristic strength of this sample from 48.1 N/mm² to 37.5 N/mm² is not big enough. For softwoods graded into S 10 most ratio values are below 1.0 with few values being slightly higher than 1.0.
For tropical hardwoods the situation is quite different. For both species the 5th percentile strength values of the different samples show a large scatter. For cumaru the values range from 47.0 N/mm² to 100.9 N/mm², for massaranduba from 41.1 N/mm² to 86.2 N/mm².

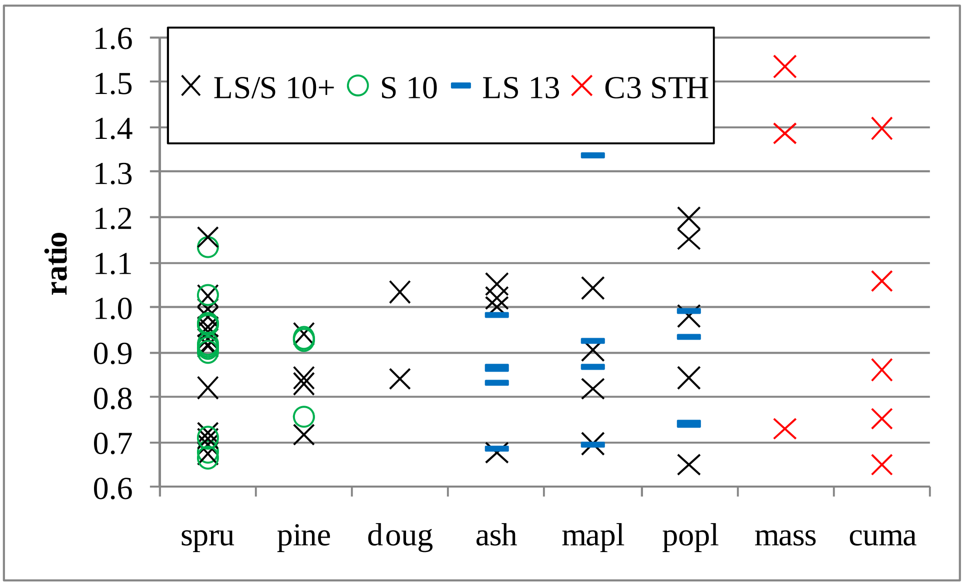

Figure 4: Ratio for visual graded timber in grades S 10+, LS 10+, S 10, LS 13 (according to DIN 4074-1 & DIN 4074-5) and C3 STH (according to NEN 5493).

In Figure 5 the ratios given in Figure 3 are Figure 4 are used, but now plotted over the number of pieces per subsample. For better visualization only sample sizes below 200 pieces are shown. For the machine grade C 24 there are 6 samples with more specimens. The biggest sample has 516 specimens with a maximum ratio of 1.29, which is still considered high.

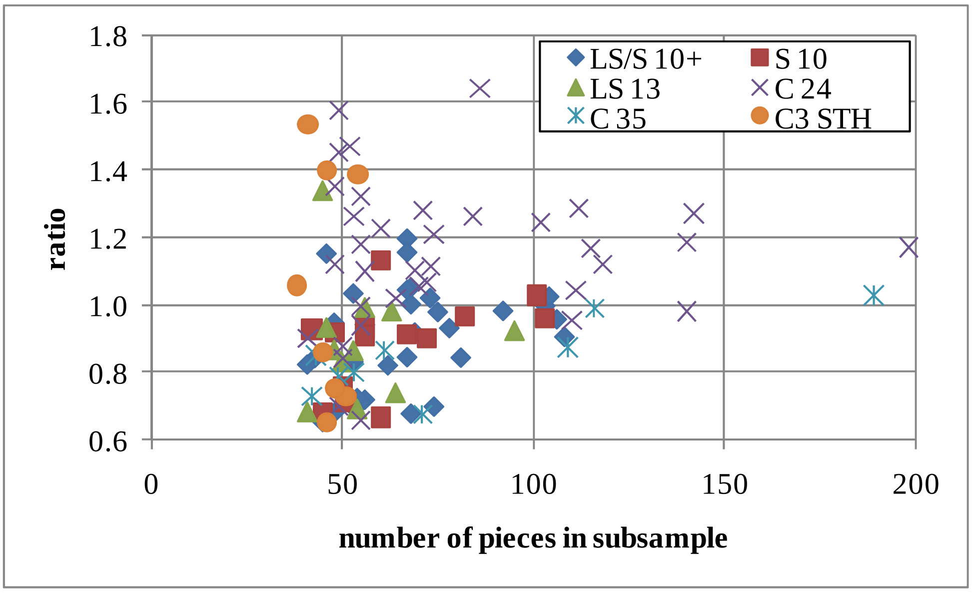

Figure 5: Ratio of single samples compared to the number of specimens in each grade - for sample sizes below 200 pieces.

In Figure 6, the ratio of Fewell and Glos is presented, where the ratio between the ranked 5^{th}-percentile of the individual sample (without $k_{s,i}$) and the ranked 5^{th} percentile of the whole sample (without $k_{s,j}$) is used. This Figure can directly be compared to Figure 1, but now subsamples smaller than 100 specimens are included, showing a considerable increase in the ratio.

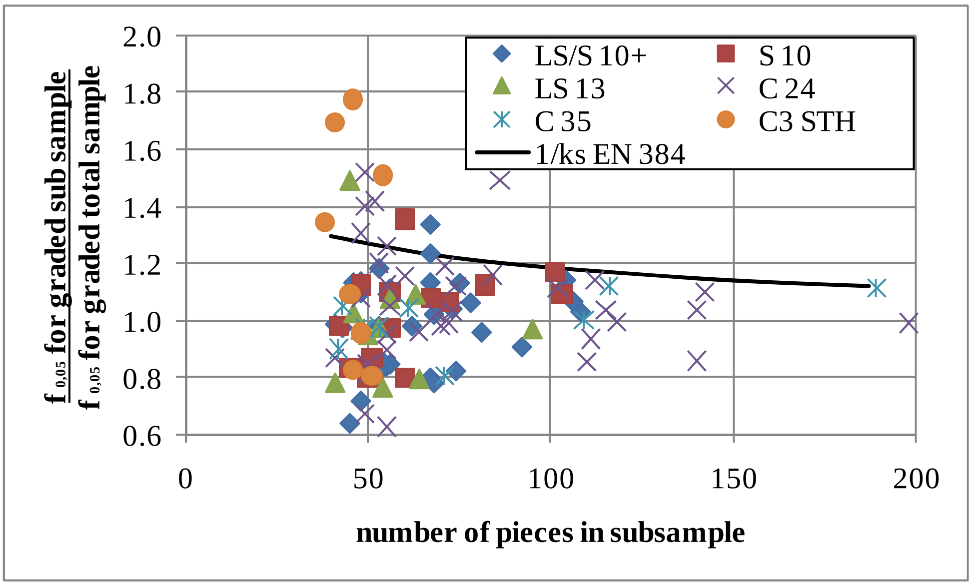

Figure 6: Ratio used by Fewell and Glos (1988). k_s-line according to EN 384.

The coefficient of variation for the individual subsamples, plotted in Figure 7 also seems to have an influence on the calculated ratio. Machine graded C 24 (and better) shows similar COV´s per subsample as visually graded timber, but with much higher ratios.

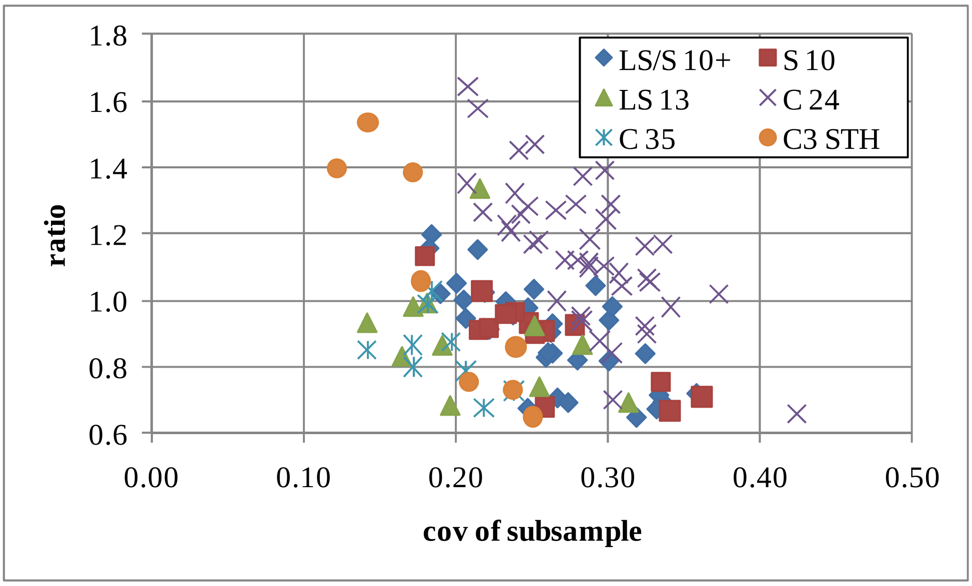

Figure 7: Characteristic value ratio as a function of the coefficient of variation in subsamples.

5 Discussion

In 49 out of 117 cases the value of the ratio between a single sample and the full sample is higher than 1.0. If characteristic values would have been derived on the basis of this sample instead of on all available data for the species, the assigned characteristic strength value would have been higher than the declared value. This is the case even though the k_s-factor, which should prevent this effect, has been applied in the derivation. Consequently the $k_{s,i}$-factor according to EN 384 is too small.

The effect can be small or in practice not recognizable at all, depending on the absolute 5th percentile strength value. However, for species in high strength classes and small COV´s in the subsamples, the effect can be considerable. The highest 5th percentile strength value of

all samples was reached for a cumaru sample from Brazil (100.9 N/mm²). Based on all five samples, cumaru would be assigned to D 50, while using a minimum k_s-factor of 0,78 on the maximum value would have allowed for an assignment in D 70. (D 55 and D 75 would be possible, if these classes existed).
Grading quality has a big influence on the assignment of a strength class. This is especially true if many samples are available. In this case strength values can become very low, which can be seen for C 24. As samples are separated due to source and cross-section, single values of small samples are responsible for the overall assigned characteristic value. That is one reason for the high ratio values of C 24. If the characteristic strength values of the sub-samples multiplied by the corresponding k_s-factor were compared to the required strength value for machine graded C 24 (21.4 N/mm²) the maximum ratio would be 1.23.

A tendency for a smaller COV for tropical hardwood subsamples can be noticed, at the same time observing high ratios for subsamples with low COV´s. As a consequence, the smaller the COV of subsamples, the more subsamples should be taken in order to cover the variety in the timber production for the large growth areas of tropical hardwoods. For European data this effect seems however much less present.

6 Conclusions

Sample size and number of samples have a significant influence on the characteristic strength values which are assigned to certain species and grades.
Assigning strength class to certain grade and species based only on 40 pieces is unsafe using the current rules. Especially if assignments are made for complete continents, as is currently the case in EN 1912.
Clearly, from Figure 3 to 6 it can be concluded that the value of k_s for a single subsample with up to around 100 specimens is on the unsafe side. The value of k_s should be lowered to around 0.5 for a subsample size of 40 specimens and to around 0.8 for a single subsample with around 100 specimens. Based on the ratio between the characteristic strength value of the subsamples and the strength value for the total sample calculated according EN 384, a proposal for a new line is given in Figure 8. It is expected that curves for more than 1 subsample need to be adjusted accordingly. The subdivision of subsamples is different for EN 384 and EN 14081-2. As a consequence the suggested line can only be applied for visual grades.

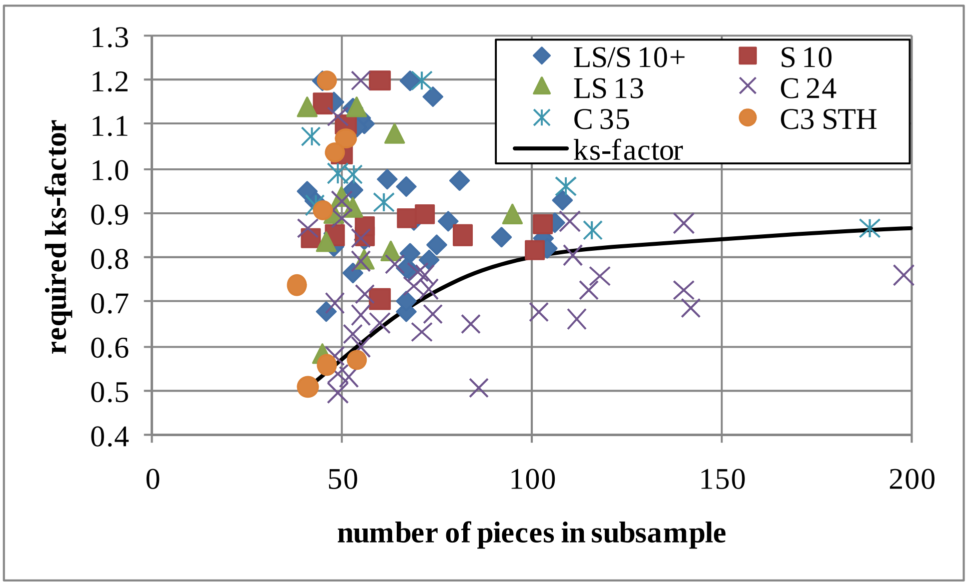

Figure 8: Suggestion for the EN 384 k_s-factor for 1 subsample.

7 References

BS 5756:2007. Visual grading of hardwood. Specification. BSI.

EN 338:2009 Structural timber - Strength classes. CEN European Committee for Standardization, Brussels.

EN 384:2010 Structural Timber – Determination of characteristic values of mechanical properties and density. CEN European Committee for Standardization, Brussels.

EN 408:2003 Timber structures – Structural timber and glued laminated timber- Determination of some physical and mechanical properties. CEN European Committee for Standardization, Brussels.

EN 1912:2004+A4 Structural timber - Strength classes - Assignment of visual grades and species. CEN European Committee for Standardization, Brussels.

EN 14081-2:2010 Timber structures - Strength graded structural timber with rectangular cross section - Part 2: Machine grading; additional requirements for initial type testing. CEN European Committee for Standardization, Brussels.

Fewell, A.R. and Glos,P. 1988. The determination of characteristic strength values for stress grades of structural timber. Part 1. CIB W18 proceedings paper 21-6-2. Parksville, Canada.

NEN 5493:2010. Quality requirements for hardwoods in civil engineering works and other structural applications.

Stapel P., v. d. Kuilen J.-W. G., Rais A. 2010. Influence of origin and grading principles on the engineering properties of European timber. CIB W18, proceedings paper 43-5-2, Nelson, New Zealand.

INTERNATIONAL COUNCIL FOR RESEARCH AND INNOVATION IN BUILDING AND CONSTRUCTION

WORKING COMMISSION W18 - TIMBER STRUCTURES

NOTES

MEETING FORTY FOUR

ALGHERO

ITALY

AUGUST 2011

Considerations for the inclusion of expressions in Eurocode 5 to assess the vibrational performance of timber-concrete composites

Jonathan Skinner, Richard Harris, Kevin Paine and Peter Walker

BRE Centre for Innovative Construction Materials, University of Bath, UK

1 Introduction

The use of timber-concrete composites in the UK is not widespread. Research at the University of Bath is focused on the upgrade and refurbishment of existing timber floors by applying a thin cementitious topping to increase the effective stiffness of the floor section. Serviceability rather than strength has been identified as the key performance upgrade. Of the serviceability requirements the vibration performance of the floor has been found to be the most important, as occupants often tolerate large static deflections.

Eurocode 5 provides criteria to ensure that timber floors achieve satisfactory vibration performance but does not include criteria for timber-concrete composite (TCC) floors. As there are significant differences between the vibration behaviour of TCC floors and timber floors the current design guidelines cannot be applied to TCC floors without modification. This note does not seek to propose new formula but highlights the salient features of TCC floor vibration which would have to be considered for new criteria to be adopted. It first describes the rationale for a new approach to timber TCCs which takes advantage of a thin topping to maximise the improvement in vibration frequency. This will be followed by a discussion of the perpendicular stiffness of TCCs and their damping properties.

2 Rationale for thin toppings

Previous work by van der Linden [1] considered how the arrangement of the timber joists and the stiffness of both timber and concrete elements affect the stiffness of the composite section. By expanding this work, to include the change in mass of the floor due to the addition of the topping, the change in the natural frequency of the floor can be expressed as described by Equation 1 and Figures 1 and 2. In Figure 2 n is the modular ratio, h_t is 200mm, Δ_m is the change in mass due to the addition of the topping and EI_{max} and EI_{min} are the stiffness of the composite with full and zero composite action respectively. For a timber floor, with $n * b_c / b_t = 24$ and spans likely to require upgrade, the optimal topping thickness to increase the natural frequency of floor vibrations is approximately 20mm (h_c/h_t = 0.1). This is far thinner than in existing timber-concrete composite floors which tend to be between 50mm and 100mm thick.

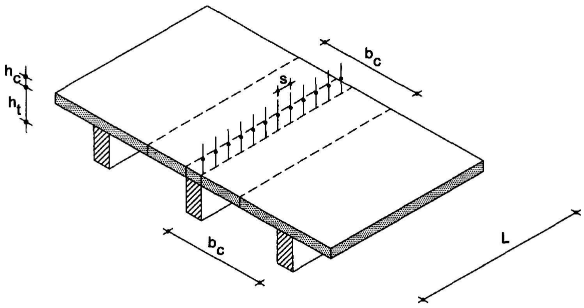

Figure 1: Arrangement of beams and topping [1]

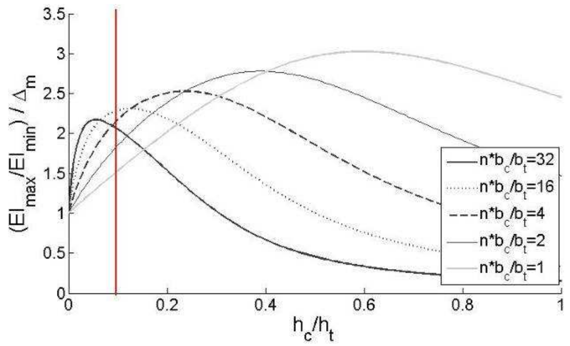

Figure 2: Max. change in bending stiffness / mass

$$f_n \propto \sqrt{\frac{k}{m}} \tag{1}$$

3 Stiffness perpendicular to the joists

The current formula in Eurocode 5, which is used to calculate the fundamental frequency of timber floor vibrations, can be seen to be a simplification of the equation for the vibration of an orthotropic plate, simply supported on all four sides. The equation for the vibration of an orthotropic plate, derived by Hearmon [2], was later simplified by Ohlsson [3] to Equation 2, by assuming the torsional rigidty is approximately equal to the transverse stiffness. Equation 3, adopted by Eurocode 5, introduces a further simplification by presuming that the ratio of transverse and longitudinal stiffness of a timber floor is always small and therefore the second square root term of Equation 2 can be assumed to be equal to 1. As timber floors are often assumed to have little or negligible stiffness perpendicular to the joists this assumption is valid for many floors. For countries (e.g. Finland) where this is deemed inappropriate due to contributions to the transverse stiffness from strutting, floorboards and plasterboard, Equation 2 is included in the National Annex.

$$f_{1,n} = \frac{\pi}{2l^2}\sqrt{\frac{(EI_l)}{m}} \cdot \sqrt{1 + \left[2n^2\left(\frac{l}{b}\right)^2 + n^4\left(\frac{l}{b}\right)^4\right] \cdot \frac{(EI)_b}{(EI)_l}} \tag{2}$$

For a TCC floor the stiffness perpendicular to the joists is far greater than that of a timber floor and, if ignored, leads to unnecessarily conservative designs. The error would be largest for TCC floors, constructed with cross-laminated timber, where the transverse stiffness of the timber alone is substantial, or for conventional timber floors upgraded with a topping but without a large degree of composite action. A conventional, upgraded timber floor with very good composite action, would be least affected. Nonetheless, an error of 10-11% is found for a TCC floor simply supported on all sides with, dimensions L=6m and B=4m, full composite action, 200 x 50mm softwood joists, 20mm thick floorboards and optimal topping thickness as defined by Figure 2. Therefore it is suggested that for TCC floors Equation 2 suggested by Ohlsson would be more appropriate than Equation 3.

$$f_{1,1} = \frac{\pi}{2l^2}\sqrt{\frac{(EI)_l}{m}} \tag{3}$$

4 Damping

Previous authors [4] have commented that damping has a large effect on the human perception of occupant induced vibrations. The damping ratio is $\xi = c/c_r$, where $c_r = 2\sqrt{km}$ and c is the energy dissipated per cycle of vibration. Eurocode 5 currently stipulates that for timber floors "*unless other values ares proven to be more appropriate, a modal damping ratio of ξ=1% should be assumed*". However the UK NA overrides this and suggests that 2% damping is appropriate for UK floors. Damping values for timber floors have been suggested on the basis of experimental tests. As yet there have been few tests on full-scale TCC floors, with comparative tests of sections of floors being preferred to validate vibration performance [5, 6]. For appropriate damping values to be suggested for TCC floors full-scale tests need to be conducted; preferably insitu to properly allow for the effects of realistic support conditions, stud walling and furniture.

Both material and friction damping contribute to the total energy loss per cycle of vibration. Of these, friction damping, energy lost in connections and supports, is of most interest as the connectors used to create composite action between the timber and concrete elements almost certainly dissipate energy. This inevitably poses the following questions:

- Do different connector types dissipate more or less or energy?
- What proportion of the total energy dissipated in a timber-concrete composite floor is attributable to the connectors?
- If the proportion is significant, should Eurocode 5 allow for this considering the difficulty in quantifying damping in timber only floors?

5 Discussion

This note has highlighted the importance of designing TCC floors based on their serviceability performance. It has been shown that there is scope to expand existing clauses for vibration of timber floors in Eurocode 5 to include the vibration performance of TCC. However there are key differences between the vibration of timber floors and TCC floors which need to be accounted for in the formation of new criteria. Full scale studies are required to determine available damping.

6 References

[1] van der Linden, M. Timber-Concrete composite oor systems. Ph.D. thesis, DelftUniversity, 1999

[2] Hearmon, R. F. S. (1946). The fundamental frequency of vibration of rectangular wood and plywood plates. Proceedings of the Physical Society, 58 (1), 78-92.

[3] Ohlsson, S. Springiness and Human-Induced Floor Vibrations: a Design Guide. Swedish Council for Building Research, 1988

[4] Chui, Y. H., & Smith, I. Quantifying damping in structural timber components. In Proceedings of the 2nd Pacific Timber Engineering Conference, vol. 2, 57-60. Auckland, 1989

[5] Lukaszewska, E., & Fragiacomo, M. Static and Dynamic (Vibration) Performance of Composite Beams with Prefabricated Concrete Slab. vol: CD. Riva del Garda, Trentino, Italy, 2010

[6] Rijal, R., Samali, B., & Crews, K. Dynamic performance of timber-concrete composite flooring systems. In Incorporating Sustainable Practice in Mechanics of Structures and Materials, pp. 315-319. London: Taylor and Francis Group, 2011

Splitting of beams loaded perpendicular to grain by connections – some issues with EC5

Jørgen L. Jensen
Pierre Quenneville
The University of Auckland, New Zealand

1 Introduction

EC5 [1] contains an equation for calculation of the splitting capacity of beams loaded at an angle to grain by connections. The equation is based on a linear elastic fracture mechanics model considering a simply supported beam loaded by a single force at mid-span [2], [3]. EC5 [1] applies the model to all support conditions and all locations of the connection by requiring that the maximum shear force on either side of the connection must be less than half the total capacity as determined by the theoretical model [2], [3]. This implies for instance that the splitting capacity of a simply supported beam loaded by a connection at mid-span according to EC5 [1] is 50% higher than the capacity of the same beam loaded by the same connection at quarter-span.

The splitting capacity equation in EC5 [1] contains a constant (C_1) of value 14 N/mm$^{1.5}$. According to the theoretical model [2], [3], C_1 is given by the shear modulus and the fracture energy. Test results show that characteristic values of this constant may easily vary in a range from 9 N/mm$^{1.5}$ to 19 N/mm$^{1.5}$ depending on the wood species and product.

The scientific literature [2], [4], [5] suggests that a characteristic value of C_1 = 10 N/mm$^{1.5}$ or less is appropriate for wood species normally used in Europe.

2 Experiments

2.1 Plate specimen tests

Plate specimens [4] as shown in Fig. 1 were tested. Material properties and test results are given in Table 1, where GL is glulam and MSG is machine stress graded sawn timber. The MOE given is the dynamic modulus of elasticity. 16 mm bolts in 17 mm holes were used.

C_1 was calculated by means of Eq. (1), where P_u is the ultimate load.

$$C_1 = \frac{P_u}{2b\sqrt{h_e}} \qquad (1)$$

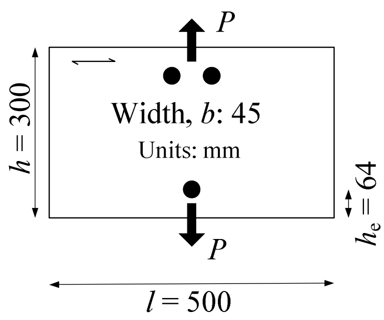

Fig. 1. *Specimen geometry*

Table 1. *Plate specimens, material properties and test results*

Species	Radiata pine				Douglas fir	
Product/grade	LVL	GL8	MSG8	MSG12	GL8	GL10
Density [kg/m^3]	548	N/A	522	569	516	516
MOE [GPa]	12.2	N/A	9.4	11.5	12.8	13.0
MC [%]	12	11	16	16	13	12
Number of replicates	10	24	36	31	21	12
C_1, mean [N/mm$^{1.5}$]	22.9	18.4	18.2	19.5	12.4	13.0
C_1, COV [%]	9	16	16	10	15	20
C_1, charact. [N/mm$^{1.5}$]	19.0	13.9	13.5	16.4	9.0	8.7

2.2 Beam tests

Six Douglas fir glulam beams of each grade (GL8 and GL10) with cross section 45x300 mm^2 were purchased. The plate specimens described above and the beam specimens shown in Fig. 2 were all cut from these 12 beams. 16 mm bolts were used in 17 mm holes also in the beam tests. In order to avoid embedment, two bolts were needed for 8*d* edge distances, in which case two different configurations were used, see Fig. 2.

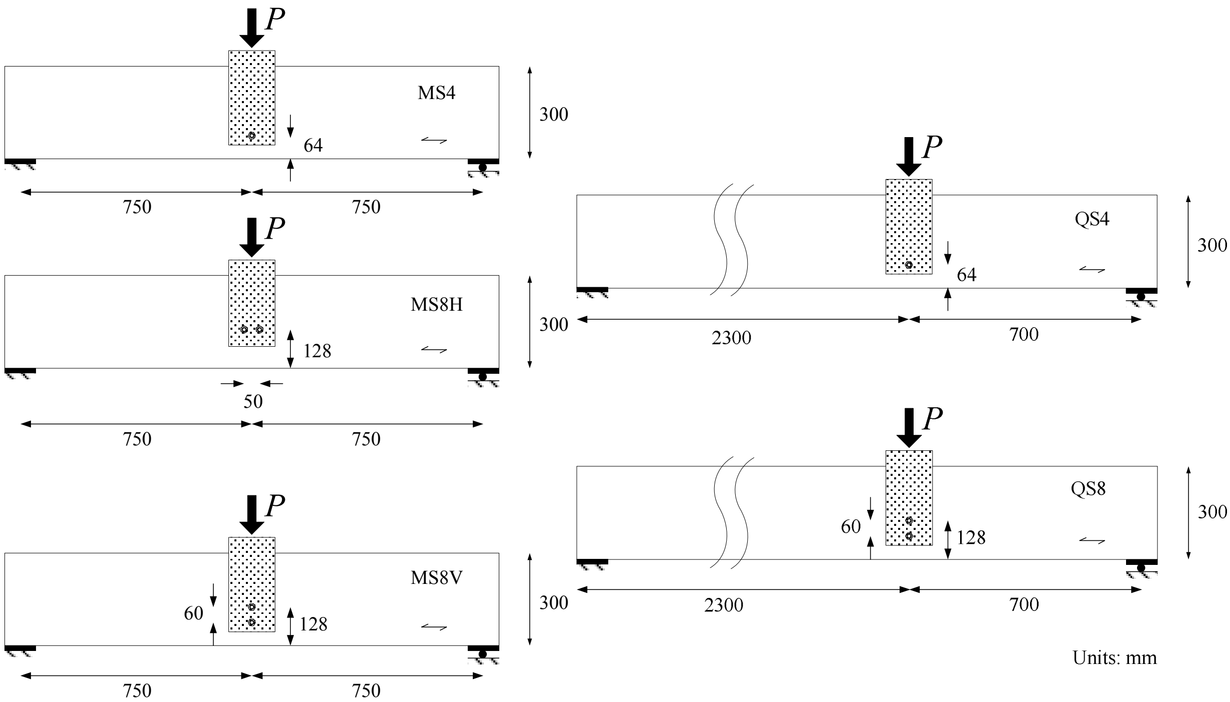

Fig. 2. *Geometry of beam specimens (in mm)*

Table 2 shows the experimental results of the beams loaded at mid-span as compared with the theoretical predictions [2], [3] using the mean values of C_1 as given in Table 1. The theoretical failure loads are calculated by means of Eq. (2). Table 3 shows the ratio of the failure load of beams loaded at mid-span to beams loaded at quarter-span. In parenthesis is given the ratio using the pooled results of MS8H and MS8V.

$$P_u = 2bC_1\sqrt{\frac{h_e}{1-\frac{h_e}{h}}} \tag{2}$$

Table 2 *Failure load of beams loaded at mid-span*

Specimen	h_e [mm]	C_1 [N/mm$^{1.5}$]	Experimental P_u [kN]	Experimental Mean [kN]	Eq. (2) P_u [kN]
MS4-1	64	12.4	9.8	9.3	10.0
MS4-2	64	12.4	9.1		
MS4-3	64	12.4	7.9		
MS4-4	64	12.4	8.4		
MS4-5	64	12.4	10.8		
MS4-6	64	12.4	9.6		
MS8H-1	128	13.0	15.8	16.8	17.5
MS8H-2	128	13.0	19.4		
MS8H-3	128	13.0	15.3		
MS8V-1	128	13.0	19.4	18.5	17.5
MS8V-2	128	13.0	20.2		
MS8V-3	128	13.0	15.8		

Table 3 *Failure load of beams loaded at quarter-span*

Specimen	h_e [mm]	Experimental P_u [kN]	Experimental Mean [kN]	Experimental $R_{mid/quarter}$	EC5 $R_{mid/quarter}$
QS4-1	64	10.3	9.7	0.96	1.5
QS4-2	64	9.5			
QS4-3	64	9.3			
QS8-1	128	24.1	20.1	0.92 (0.88)	1.5
QS8-2	128	17.1			
QS8-3	128	19.0			

$R_{mid/quarter}$: Failure load of beams loaded at mid-span/failure load of beams loaded at quarter-span

3 Conclusions

EC5 [1] uses C_1 = 14 N/mm$^{1.5}$, which is a considerable overestimation for wood species commonly used in Europe. A constant value of C_1 grossly favours some wood products. The principle of comparing the maximum shear force on either side of a connection with a constant splitting capacity seems also not appropriate.

4 References

[1] EN 1995-1-1 (2004) Eurocode 5 – Design of timber structures. CEN, Brussels, Belgium.

[2] van der Put TCAM, Leijten AJM (2000) Fracture of beams loaded by joints perpendicular to grain. CIB-W18/33-7-7, Delft, The Netherlands.

[3] Jensen JL (2005) Splitting strength of beams loaded perpendicular to grain by dowel joints. J Wood Sci 51:480-485.

[4] Yasumura M (2002) Determination of fracture parameter for dowel-type joints loaded perpendicular to wooden grain and its application. CIB-W18/35-7-9, Kyoto, Japan.

[5] Ballerini M and Rizzi M (2007) Numerical analysis for the prediction of the splitting strength of beams loaded perpendicular-to-grain by dowel-type connections. Materials and Structures 40:139-149.

Mechanical behaviour of in-plane shear connections between CLT wall panels

Tom Joyce[1], Marco Ballerini[2], Ian Smith[1]

[1] University of New Brunswick, Fredericton, Canada
[2] Università degli Studi di Trento, Trento, Italy

1 Introduction

The use of timber in building construction has recently increased due to the development of a new timber panel product known as cross laminated timber (CLT, or X-lam). The high strength and stiffness properties of this new material mean that it can be used in many different situations, including for floors and walls, and this allows for the realization of timber buildings of solid construction. Other benefits, such as the potential for rapid and low cost construction, are generating interest for this material in areas with a tradition for light-frame timber construction and are spreading the use of wood to areas that customarily prefer massive building construction (for instance, southern European countries).

CLT panels have very high in-plane stiffness and as such remain elastic when in service. In order to dissipate energy the connections must be designed to achieve a high degree of ductility. In platform construction with massive CLT plate elements this ductility can be obtained only in connections between CLT panels, for instance in wall-to-wall connections and hold-downs [1]. In structures that make use of CLT for rigid building cores or shear walls the ductility can be achieved in the connections between the elements of the gravity load-resisting frame.

In order to better understand the performance of wall-to-wall connections a study was initiated to investigate the static and dynamic properties of common connections. The study is divided into two parts: first an experimental program is investigating the behaviour of connections subjected to tensile and in-plane shear forces; and second, numerical models will be used to find the forces acting on wall-to-wall connections.

2 Test program and procedures

Two connections were investigated, double spline and angled screws (Fig. 1), and two fastener variations each were considered (Table 1). The monotonic tests were carried out with displacement controlled ramping at a loading rate of 0.05 mm/s. Specimens were tested until a load equal to 50% of the peak load was reached on the post-peak branch of the load-slip curve and five repetitions were made for each connection. Two cyclic tests were conducted for each connection using a non-reversed modification of the procedure outlined in EN12512 [2]. Displacement at yielding was calculated with the same standard on the basis of the results of the monotonic tests.

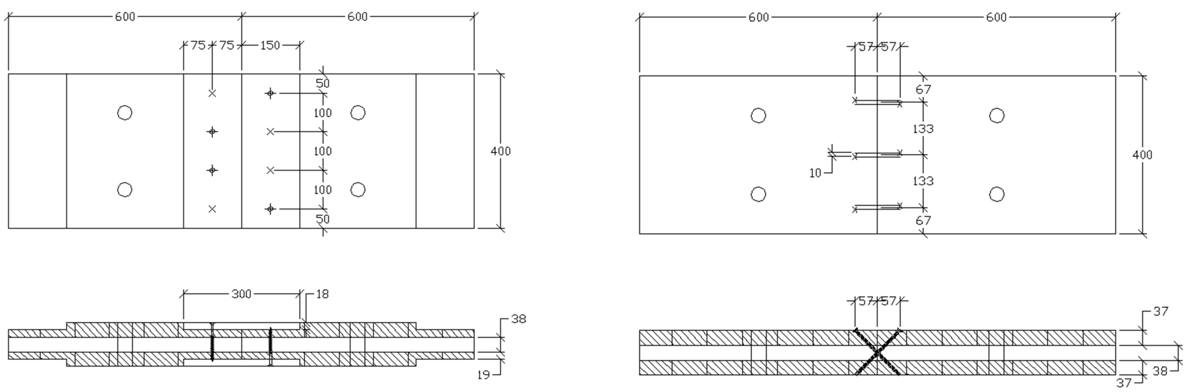

Fig. 1 – Tested wall-to-wall connections: double spline (left) and angled screws (right).

Table 1 – Details of tested wall-to-wall connections.

Connection	Series Name	Diameter and Length	Threaded Length	Fastener Spacing
Double	J1 T 08	08x100	60	100
Spline	J1 T 10	10x100	60	100
Angled	J2 T PT 08	08x160	80	133
Screws	J2 T FT 08	08x160	150	133

The CLT used was 3-layer pre-commercial Nordic X-Lam with a thickness of 112mm. The average density was 461 kg/m^3 at a moisture content of 10.2%. For the double spline connections the boundaries of the panels were notched to enclose 18mm thick Douglas Fir plywood splines. Tests were conducted using a 250kN MTS universal machine operated by an external MTS controller and with an automatic data acquisition system. Two LVDTs were used on the sides of the specimens to measure the displacement of the ends of the connections.

3 Results

The main results of the monotonic tests are shown in Fig. 2 and summarized in Table 2. The peak measured load has been divided by the number of shear planes for the double spline connections (4 planes) and by the number of fastener pairs for the angled screws (3 pairs). The data shows a low degree of scatter for all of the connections except the partially threaded angled screws (J2 T PT 08).

In the angled screws connection the fasteners are partially loaded axially. This results in a stiffer connection performance, with average elastic stiffness values (as per [3]) of 6830 and 68000 kN/mm for the partially and fully threaded screw connections as compared with 4490 and 5020 kN/mm for the 8 and 10 mm diameter double spline connections, respectively.

The failure of the double spline connections was found to be due to the formation of a plastic hinge in the CLT element (EYM failure mode IIa [4]). The failures occurred concurrently with pull-through of the screw head through the plywood. For the angled screw the failure was found to be due to splitting of the outer

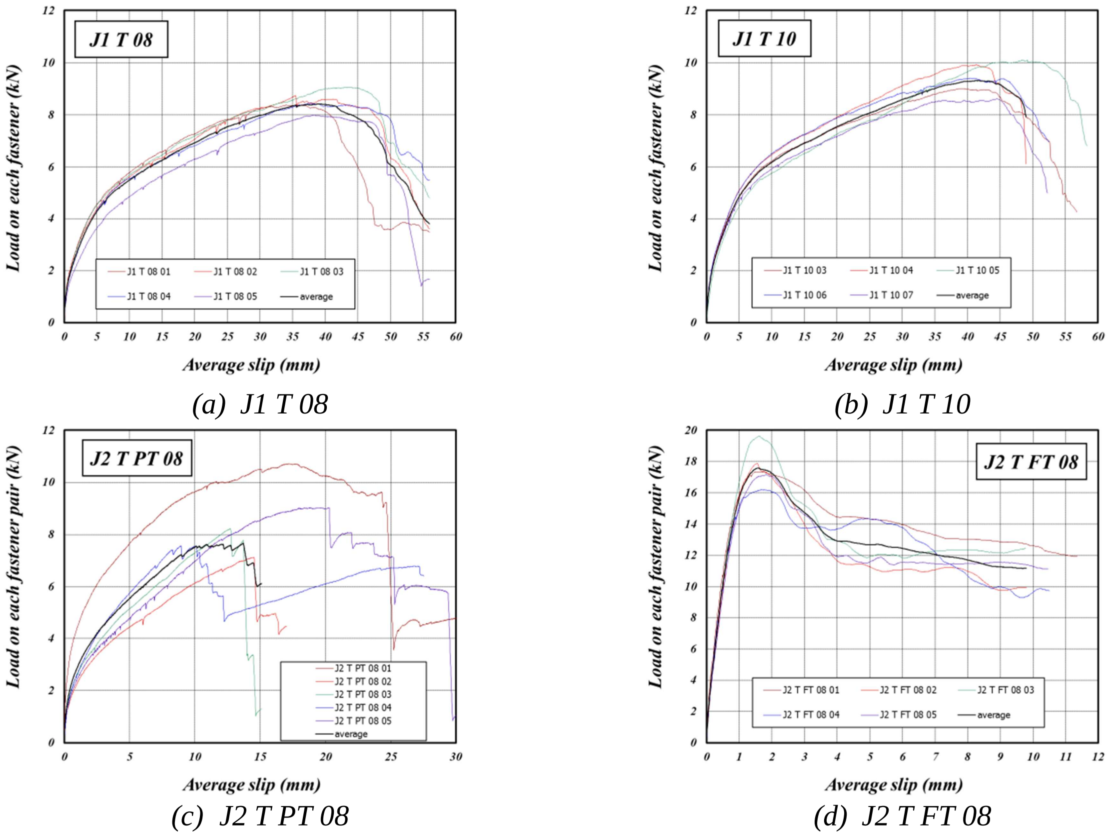

(a) J1 T 08 *(b) J1 T 10*

(c) J2 T PT 08 *(d) J2 T FT 08*

Fig. 2 – Load-slip response of monotonic tensile tests and computed average curves.

lamination of the CLT due to the forces acting perpendicular to the grain generated by the penetration of the screw head. For all cases the failure occurred on the head-side of the CLT elements. This effect was reduced when fully threaded screws were used, as the threading through the head-side CLT element provided additional embedment resistance through mechanical adhesion. Sometimes a partial withdrawal of the point-side of the screws with considerable bending was observed.

Table 2 – Summary of monotonic test results for double spline specimens.

Series	Peak Load			Allowable Load		Yield			Ductility Ratio	$k_{elastic}$ (kN/mm)
	P_{max} (kN)	$P_{max,screw}$ (kN)	Δ_{max} (mm)	P_{30} (kN)	$P_{30,screw}$ (kN)	P_y (kN)	$P_{y,screw}$ (kN)	Δ_y (mm)		
J1 T 08	33.7	8.42	39.05	31.9	7.97	17.2	4.29	3.66	8.2	4490
J1 T 10	37.2	9.31	41.35	34.3	8.58	19.2	4.80	3.56	8.4	5020
J2 T PT 08	22.9	7.63	12.06	-	-	12.1	4.02	1.51	9.9	6830
J2 T FT 08	52.7	17.58	1.57	-	-	44.0	14.66	0.65	5.2	68060

Two cyclic tests have been performed for the double spline connection for each screw diameter and the recorded load-slip curves are reported in Fig. 3 together with the average response of the monotonic tests. The results show strong agreement with the monotonic tests and a high degree of energy dissipation between the first and section cycles at each level.

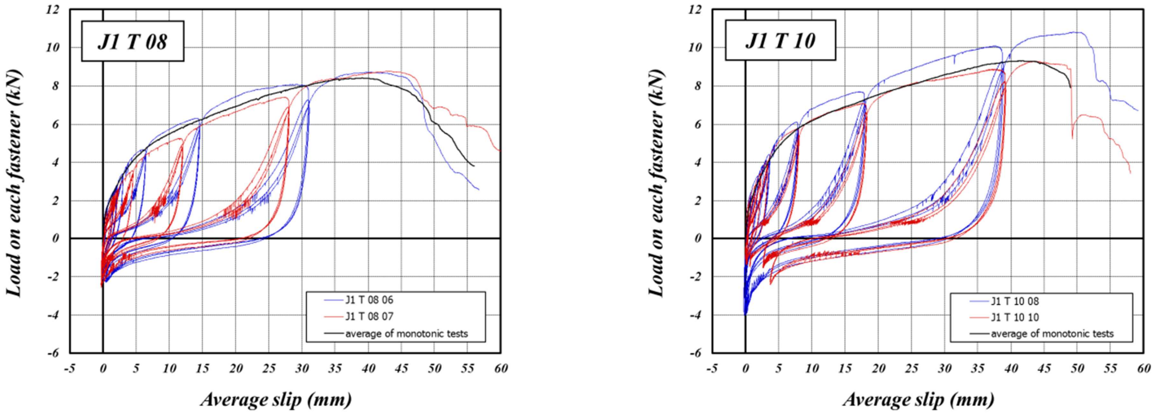

Fig. 3 – Load-slip response of cyclic tensile tests for specimens J1 T 08 (left) and J1 T 10 (right) with the corresponding backbone curves.

4 Conclusions

The main preliminary results of an on-going research on the structural behaviour of wall-to-wall connections in CLT construction have been presented. The tensile tests that have been performed up to now show good behaviour of the double spline connections and poorer behaviour of connections with angled screws. The ductility of the double spline connections was found to be high; however in situations where the elastic stiffness is importance the fully threaded angled screws option provides a significantly higher stiffness than any of the other options investigated.

References

[1] Sandhaas, C.; Boukes, J.; van de Kuilen, J. W. G.; Ceccotti, A.: *Analysis of X-lam Panel-to-Panel Connections Under Monotonic and Cyclic Loading*. Paper 42-12-2, CIB W18 Meeting 42, Dübendorf. Switzerland, 2009.

[2] EN 12512: 2001, *Timber structures – Test methods – Cyclic testing of joints made with mechanical fasteners*, CEN, 2001, Brussels, Belgium.

[3] EN 26891: 1991, *Timber structures – Joints made with mechanical fasteners – General principles for the determination of strength and deformation characteristics*, CEN, 1991, Brussels, Belgium.

[4] UNI EN 1995 1-1: 2009, *Eurocode 5: Design of timber structures – Part 1-1: General – Common rules and rules for buildings*. CEN, 2009, Brussels, Belgium.

Research note: Compression perpendicular to the grain – the Norwegian approach

Sigurd Eide, Kristine Nore and Erik Aasheim, Norwegian Institute of Wood Technology, Oslo, Norway

Introduction

Since the 1950s, thousands of buildings with light timber frames have been erected in Norway. Structural calculations based on EN 1995-1-1:2010 item 6.1.5, Compression perpendicular to the grain, provide significantly lower capacities for special building parts compared to what was allowed in the previous standard NS 3470:1999. The design criteria were deformation in service, which does not cause fracture. NS 3470:1999 allowed for more deformation compared to EN 1995-1-1:2010. No critical conditions have been observed with timber constructions designed by previous standards and built within Nordic craft traditions, regarding compression perpendicular to the grain.

In 2010 a working group was established with members from the research institutes; SINTEF Building and Infrastructure, Norwegian Institute of Wood Technology and Norwegian University of Life Science. The group's task was to create an improved assessment where the NS-EN 1995-1-1 provides too strict rules for uncritical construction parts.

This note shows the current Norwegian approach to control compressive strength perpendicular to the grain, $f_{c,90,k}$.

Background

In the first version of the strength classes for structural timber, EN 338:1995, a characteristic compressive strength perpendicular to grain ($f_{c,90,k}$) was listed, see Table 1. These values were also implemented in the Norwegian design rules for timber structures, NS 3470-1:1999. The values were given in EN 384:1995 Structural timber – Determination of characteristic values of mechanical properties and density, which stated that $f_{c,90,k}$ should be calculated as 0,015 x ρ_k (characteristic density) for the strength class. This relationship was questioned by Gehri (1997). He claimed that these values were too high if tests were performed according to the test standard EN 1193:1998, namely by applying pressure over the entire length of a specimen. He referred to a number of German tests that showed values of about half, and suggested that the value should be changed to $0.007 \times \rho_k$ for the strength class.

The revised EN 338:2003 and EN 384:2004 implemented Gehris point of view, and how to determine the various characteristic values for other properties than bending strength, stiffness and density, including $f_{,c,90,k}$, was also included as an informative annex A in EN 338:2003. Table 1 compares the different values of the various versions of EN 338.

For glulam, the first version of EN 1194:1999 used $f_{c,90,k}$ based on $0.007 \times \rho_k$ for the strength class.

Table 1. Comparison of the capacity of characteristic compressive strength perpendicular to the grain ($f_{c,90,k}$) for various standard versions.

Standard	Version	Strength class	$f_{c,90,k}$ N/mm^2
NS 3470	3. ed. 1979	T24	4.0
NS 3470	4. ed. 1989	C24	7.0
NS 3470	5. ed. 1999	C24	5.3
NS-EN 338	2003	C24	2.5

Implications for the Nordic building industry

For sills and beams, which are typical structural components in Nordic buildings, the load will only be applied on parts of the design piece. This is similar to the force application for the test in ASTM-D143, where load is applied on parts of the length of the specimen, as shown in Table 2. Calculations based on NS-EN 1995-1-1:2010, 6.1.5, Compression perpendicular to the grain, with material strengths from EN 338:2003, gives lower capacities compared to previous Norwegian standards, where material strengths are derived from testing according to ASTM-D143.

Table 2. Comparison of capacity compressive strength perpendicular to the grain ($f_{c,90,k}$), different test methods.

Construction timber *Compressive strength perpendicular to the grain* $f_{c,90,k}$					
		Strength class			
Test method		C14	C18	C24	C30
ASTM-D143	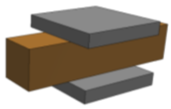	4.3	4.8	5.3	5.7
EN 1193 / EN 408:2003	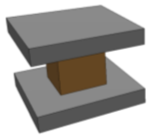	2.0	2.2	2.5	2.7

The Norwegian approach prior to EN 1995-1-1:2015

The values of $f_{c,90,k}$ in EN 338 appear reasonable based on the given test method in EN:408. ASTM-D143, where testing is performed with partial loading, provides $f_{c,90,k}$ values just above 5 N/mm^2. With this test method the "rope effect" increase the material strength. This seems to be a more accurate test method in relation to the Norwegian timber construction practice. The increased area with 30 mm added according to EN 1995-1-1 does not provide satisfying values, neither in strength or precision. Thus, calculations made according to the previous Norwegian standard NS 3470, where material strength is derived from testing according to ASTM-D143, are more representative to construction current timber constructions built in Norway.

Recommendation

For design of timber structures according to Eurocode 5, NS-EN 1995-1-1 with National Annex (NA), the following method is recommended for structural timber and glulam as an alternative for design according to item 6.1.5 in the standard. Annex 1 is a translation of the Norwegian recommendation.

Further work

From august 2011, Norwegian Institute of Wood Technology is leading a project on how to develop the EN 1995 -1-1 towards improved timber constructions and simplified engineer understanding.

References

Damkilde, L, Hoffmeyer, P, and Pedersen, TN (1998). Compression strength perpendicular to grain of structural timber and glulam. CIB-W18 Meeting thirty-one, Savonlinna, Finland

Gehri, E (1997). Timber in compression perpendicular to the grain. P. 355-374 in IUFRO S5.02 Timber engineering. Department of Structrual Engineering and Materials, Techincal University of Denmark

Poussa, M, Tukiainen, P, and Ranta-Maunus, A (2007). Experimental study of compression and shear strength of spruce timber. CIB-W18 Meeting forty, Bled, Slovenia

Treteknisk (2009) Treteknisk Håndbok. (In Norwegian). Norwegian Institute of Wood Technology

EN 1995-1-1:2010 Eurocode 5 with National Annex (NA)

ASTM-D143 Standard Test Methods for Small Clear Specimens of Timber

EN:408:2010 Timber Structures, Structural timber and glued laminated timber, Determination of some Physical and mechanical properties.

EN 338:2003 Structural timber, Strength classes

Annex 1: Recommendation

For sills and beams (see Figure 1 and 2) only compressive stress in the ultimate limit state is controlled (deformation control in the serviceability limit state is considered redundant).

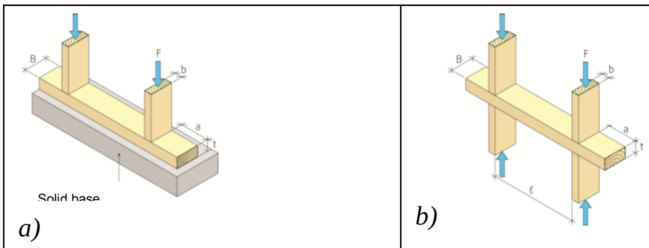

Figure 1. Sills.

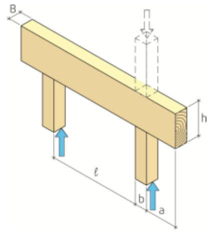

Figure 2. Beams / trusses / rafters.

The compressive stress, $\sigma_{c,90}$, at load in the ultimate limit state on the loaded area shall be limited to the following:

$$\sigma_{c,90,d} \leq k_{c90} * f_{c,90,d} \quad \text{where} \quad \sigma_{c,90,d} \leq \frac{F_{c,90,d}}{A} \qquad f_{c,90,d} = f_{c,90,k} * \frac{k_{\text{mod}}}{\gamma_m}$$

Table 1. Characteristic compressive strength $f_{c,90,k}$ perpendicular to the grain.

Structural timber Compressive strength $f_{c,90,k}$			
Strength class			
C14	C18	C24	C30
4.3	4.8	5.3	5.7

Table 2. Characteristic compressive strength $f_{c,90,k}$ perpendicular to the grain.

Glulam Compressive strength $f_{c,90,k}$					
Glulam class, combined glulam			Glulam class, homogenous glulam		
GL28c	GL32c	GL36c	GL28h	GL32h	GL36h
5.3	5.7	6.3	5.3	5.7	6.3

NOTE: The values in Table 1 and 2 refer to testing of longer specimens that are partially loaded according to ASTM-D143. In Eurocode 5, NS-EN 1995-1-1, 6.1.5 calculations are based on the strength values in NS-EN 338:2003 and NS-EN 1194:2010. These calculations are based on testing of small specimens with load across the entire cross section. This gives lower values than ASTM.

Table 3. Factor $k_{c,90}$ for load configuration.

Configuration (Figure 4 a and b and Figure 5)	$k_{c,90}$ for l < 150 mm	$k_{c,90}$ for l >150 mm	
		a ≥ 100 mm	a < 100 mm
b ≥150 mm	1.0	1.0	1.0
150 > b ≥15 mm	1.0	$1+\frac{150-b}{170}$	$1+\frac{a(150-b)}{17000}$
15 mm > b	1.0	1.8	$1+\frac{a}{125}$

For a load situation as shown in Figure 1 b and where a < t, the values in Table 3 shall be halved.

Bending Strength of Finger Jointed Solid Lumber

Gordian Stapf, Simon Aicher
MPA University Stuttgart, Germany

1 Introduction

Finger jointed solid lumber is continuously substituting unjointed sawn solid timber in Central Europe and many other parts of the world. The reasons for this are manifold including a higher yield from the timber source thanks to cutting out the timber defects (e. g. knots), considerably higher dimensional stability due to drying of shorter lumber lengths, just in time delivery of quasi deliberate length and compliance with decreasing log-lengths in todays sawmills.

Finger jointed lumber production has a large dimensional range, whereby the smallest commercially available cross-sections are about 60 x 100 mm² and the largest are approximately 160 x 240 mm². In Europe, so far, the product is subjected to several national product and design standards. In the future this will be dealt under the upcoming harmonized product standard EN 15497, hereby being subject to level of attestation of conformity 1.

The bending strength of finger jointed lumber is influenced by many parameters: the most important are strength class and density of the lumber; distance of knots from the finger joint; finger joint profile and cutting orientation; adhesive; wood moisture content; size of the cross-section and several production conditions such as precise cutting of the fingers; end pressure as well as adequate transport and curing conditions.

1 Factor k_f

In case of factory production control according to EN 385 the specimens are usually tested in flatwise bending for the sake of economics; in that case the bending strength requirement $f_{k,req}$ is increased by a factor k_f. The factor k_f can be determined by initial testing with each 15 specimens tested in flatwise and edgewise bending, respectively. Other from that, the value for k_f can be taken from EN 385 depending on the finger joint profile in cases when the fingers are visible on the face perpendicular to the load direction, see Table 1. The consequence of this approach is that the bending strength required in factory testing in cases of flatside bending and fingers visible on the flatside is $f_{k,l,req} = k_f \cdot f_k$ with f_k being the declared bending strength value of the timber. This procedure reflects the empiric fact that the bending strength in bending tests with the grooves of the finger joints parallel to the load direction (“vertical finger grooves”) $f_{m,\parallel}$ is higher than the bending strength in lumber with the grooves of the fingers perpendicular to the load direction (“horizontal finger grooves”) $f_{m,\perp}$. The mentioned relationship can be expressed as $k_f = f_{m,\parallel} / f_{m,\perp}$.

Table 1: *Factors k_f for flatwise bending tests according to EN 385 depending on the profile.*

Profile	Fingers visible on flatside “horizontal finger grooves”	Fingers visible on edgeside “vertical finger grooves”
15/3,8	k_f = 1,25	k_f = 1,0
20/6,2	k_f = 1,25	k_f = 1,0
10/3,7	k_f = 1,10	k_f = 1,0
32/6,2	-	k_f = 1,0

The lower bending strength of joints with finger grooves perpendicular to the load direction results from two main factors. Firstly, the outermost finger is more frequently exposed to manufacturing errors than the rest of the joint. This is partially due to comparatively lower pressure exerted on the glueline. Secondly, depending on the geometry of the lower lateral finger due to planing, a stress peak can occur over the whole lower side of the specimen that is subjected to flexural tension. Additionally to that, the insufficient glueline mentioned above can facilitate crack propagation, see Figure 1.

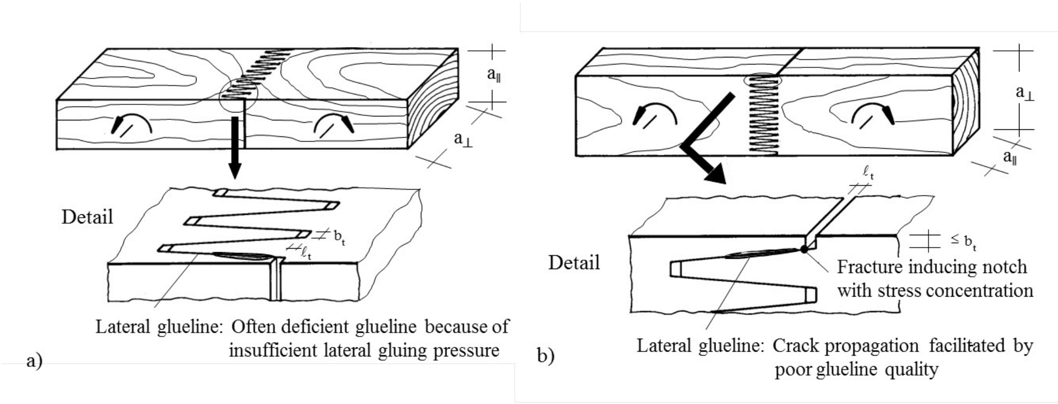

***Figure 1:** a) Vertical finger grooves. The deficient glueline has only minor effects on the bending strength. b) Horizontal finger grooves. Depending on the planing of the specimen, a fracture inducing notch can occur. The crack propagation is facilitated by the poor glueline quality of the lateral finger.*

This means that on the side of the tested beam perpendicular to the finger grooves, width $a_{\perp}$ is reduced by the width of sub-optimally glued section or the width weakend by peak stresses a_{def}. This results in the effective width $a_{\perp,eff} = a_{\perp} - a_{def}$. A possible assumption for a_{def} is the width of one finger (e. g. 6,2 mm for the 20/6,2 profile). The effective width $a_{\perp,eff}$ results in a discrepancy, say $k_{\perp,eff} = S_{\perp,cal} / S_{\perp,eff} = (a_{\perp} / a_{\perp,eff})^2$, between the calculated section modulus $S_{\perp,cal} = a_{\perp}^2 \cdot a_{\|} / 6$ and the effective section modulus $S_{\perp,eff} = a_{\perp,eff}^2 \cdot a_{\|} / 6$. Depending on how much a_{def} is based on fracture mechanics or on productional deficits, a discrepancy for joints with vertical finger grooves has to be considered, too. Assuming the latter case, it can be calculated similarly as $k_{\|,eff} = S_{\|,cal} / S_{\|,cal} = a_{\perp} / a_{\perp,eff}$. Finally, the difference between the bending strength of joints with vertical finger grooves $f_{m,\|}$ and that of joints with horizontal finger grooves $f_{m,\perp}$ can be computed as

$$k_f = f_{m,\|} / f_{m,\perp} = k_{\|,eff} / k_{\perp,eff} = a_{\perp} / a_{\perp,eff} = a_{\perp} / (a_{\perp} - a_{def}). \tag{1a}$$

Considering the weakening of the cross-section only taking place with the finger joints lying there is a square dependency between k_f and a_{def}:

$$k_f = f_{m,\|} / f_{m,\perp} = k_{\|,eff} / k_{\perp,eff} = a_{\perp}^2 / a_{\perp,eff}^2 = a_{\perp}^2 / (a_{\perp} - a_{def})^2. \tag{1b}$$

Assuming a_{def} being a constant, there must be a size effect in k_f, e. g. larger width perpendicular to the finger grooves $a_{\perp}$ result in smaller k_f. This size effect in k_f only shows up immediately in timber beams with a square cross section. Beams with a rectangular cross section are additionally prone to the regular size effect k_{size}, e. g. larger width parallel to the load direction results in smaller bending strength. This leads to the measured factor $k_{f,measured} = k_{size} \cdot k_f$. Considering a size-effect governed by a power-law

$$k_{size} = f_{m,\|} / f_{m,\perp} = (a_{\perp} / a_{\|})^s,$$

the factor k_f can be written size-corrected for equation (1a)

$$k_f = k_{f,measured} / k_{size} = k_{f,measured} / (a_{\perp} / a_{\|})^s = a_{\perp} / (a_{\perp} - a_{def}). \tag{2a}$$

For equation (1b) one obtains

$$k_f = k_{f,measured} / k_{size} = k_{f,measured} / (a_{\perp} / a_{\|})^s = a_{\perp}^2 / (a_{\perp} - a_{def})^2. \tag{2b}$$

2 Materials and Methods

This paper presents the results of third party bending strength tests with about 2000 spruce specimens (strength class C24) by 40 different companies in Europe. The data were collected over a time span of more than 15 years. The data source encompasses *inter alia* 116 comparative test series with flatwise and edgewise bending, enabling the assessment /

determination of the factor k_f. The data comprise two major finger joint profiles and different adhesive families, being One Component Polyurethanes (1K-PU), Melamine-Urea-Formaldehyde (MUF) adhesives and EPI adhesives. Due to the length restriction of the "research note", only finger joints with the profile 20/6,2 are regarded. Specimens with failure modes mainly outside of the finger joint were excluded. The factor k_f was calculated via the means of each test series. This resulted in 90 test series with around 8 specimens per bending direction (flatwise and edgewise). With the exception of two test series, all the specimens were produced with the fingers visible on the wider side of the cross section ($a_\perp > a_{||}$). The cross-sectional side ratios and areas range from 1–3,7; the width perpendicular and parallel to the finger grooves were $a_\perp$ = 60–240 mm and $a_{||}$ = 40–160 mm, respectively.

3 Test Results and Discussion

The results of the data evaluation can be seen in Figure 2. Due to the small size of the single test series, the scatter is considerably high, e. g. there are 20 test results with values smaller than 1, which can only be explained statistically. Nevertheless, a clear size dependency on the already size-corrected factor k_f can be seen.

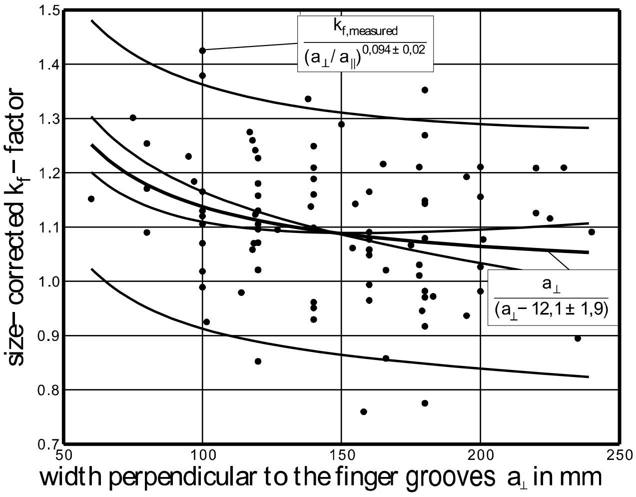

***Figure 2:** Relationship between the widt with fingers visible a_l and the size-korrected factor k_f. The dotted lines represent upper and lower borders of the 95%-confidence-interval and for the 95%-prediction-interval respectively.*

The non-linear fit of the data via equation (2a) results in a size factor s = 0,094 and a defective width a_{def} = 12 mm. In comparison, equation (2b) does not change the size factor much (s = 0,093) but decreases the defective width a_{def} = 6 mm considerably.

4 Conclusion and Recommendations

The results of the 80 samples taken from over 70 different factories scatter a lot, which is normal for a very production-dependent value. Nevertheless, the presented size-dependent approach for the differences between edgewise and flatwise bending illustrates that, dependent of the production defects at the outer finger, the size and the width-height-relationship have a clear influence on the factor k_f of a tested sample of timber. Based on these findings, we propose the following for the evaluation of the factor k_f in initial factory testing:

- Factor k_f should be evaluated using the smallest cross-section produced in the factory in question. This is because factor k_f resulting from production deficits has a greater effect on smaller cross-sections.
- Because a good portion between edgewise and flatwise bending is due to the regular size-effect, factor k_f should not be permitted to be smaller than $k_f = R^{0,1}$ where R is the largest height to width ratio produced at the particular factory.
- The number of specimens for initial testing should be raised to a number of at least 30 specimens with vertical finger grooves and 30 specimens with horizontal finger grooves.

2011 Christchurch Earthquakes

Damage to houses and timber buildings

Professor Andy Buchanan
University of Canterbury

New Zealand's tectonic setting

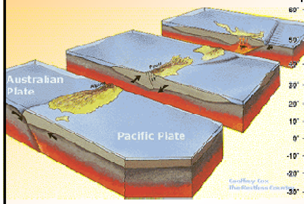

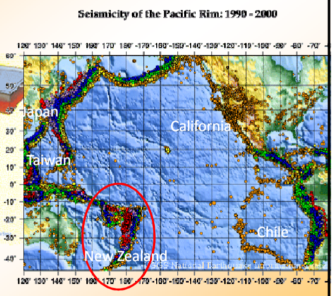

22 February, 1pm. M6.3

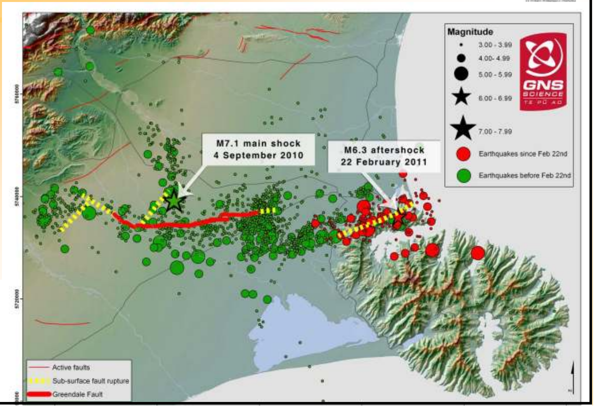

Spectral acceleration, 22 February

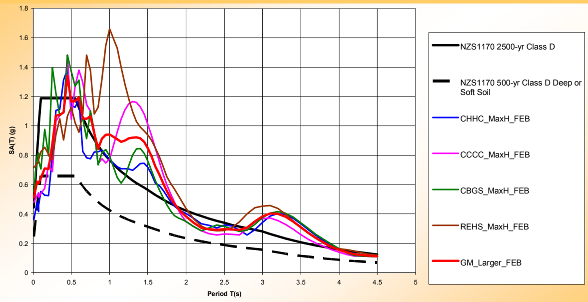

Rockfall

Liquefaction and lateral spreading

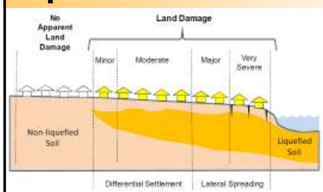

Pipes and manholes floated up

Differential foundation settlement

Differential settlement
Veneer damage
Timber structure held together

Houses – vertical accelerations

Roof shaken off

Timber house structurally safe

Falling chimneys

Internal linings

Gypsum plasterboard

Provided bracing for most houses

Good performance
Thousands of repairs necessary

Lath and plaster
Poorer performance

Timber houses - veneer failures

Wall bracing failures

Soft storey collapse

Before

Larger cantilever floor at rear

Solid wood houses

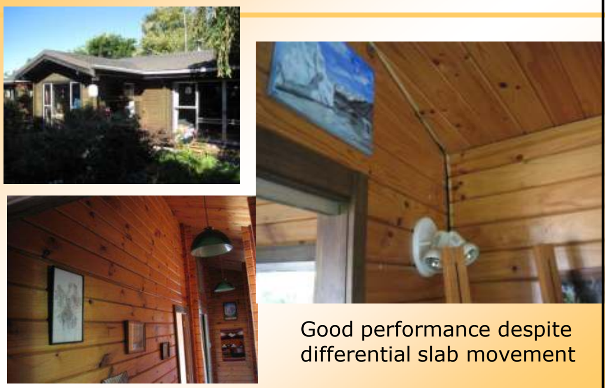

Good performance despite differential slab movement

Concrete slab floors

Differential sinking

Lateral spreading

No reinforcing

Engineered timber buildings

Shear failure in column

Buckled bracing

UC test building

Post-tensioned timber technology

EXPAN office, Christchurch

EXPAN building with Pres-Lam technology

No damage in the earthquake

Why not rebuild Christchurch with multi-storey timber?

Professor Stefano Pampanin
University of Canterbury

Associate Professor Stefano Pampanin | National Hazard Research Platform: Resilient Buildings and Infrastructure

How many **"Lessons"** do we still need?

1999 → **2009** → **2011**

Izmit-Kocaeli, 1999 (photo courtesy: Berkeley Library)
L'Aquila, 2009 (photo courtesy: Anna Brignola)
Christchurch, 2011 (photo courtesy: Kam Weng)

NZCS | NZ Society for Earthquake Engineering Incorporated | SESOC | Seismic Retrofit Solutions

---

Associate Professor Stefano Pampanin | National Hazard Research Platform: Resilient Buildings and Infrastructure

The Past and Present: a Factual Damage Report

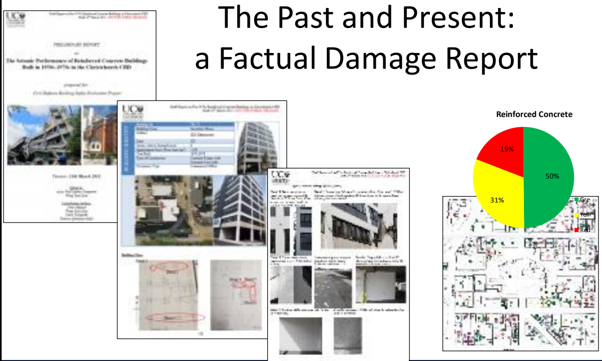

NZCS | NZ Society for Earthquake Engineering Incorporated | SESOC | Seismic Retrofit Solutions

---

Associate Professor Stefano Pampanin | National Hazard Research Platform: Resilient Buildings and Infrastructure

Precast RC high-rise (20+ storey)

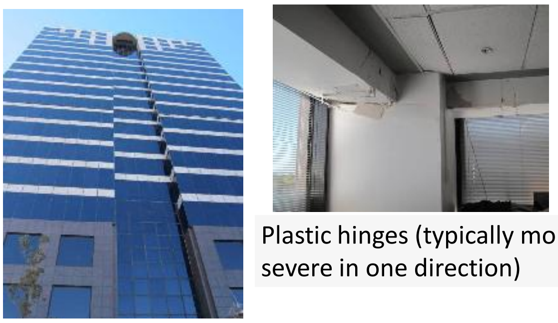

Plastic hinges (typically more severe in one direction)

Many buildings "just did what you asked them to do"... - Tom Paulay

---

Short confined columns

Internal core wall

15m long
200mm thick
T-shaped wall

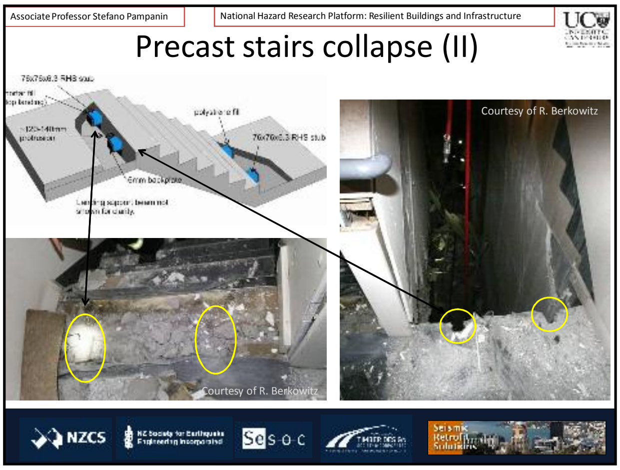

Associate Professor Stefano Pampanin
National Hazard Research Platform: Resilient Buildings and Infrastructure
Precast stairs collapse (II)
Courtesy of R. Berkowitz
Courtesy of R. Berkowitz
NZCS

Associate Professor Stefano Pampanin
National Hazard Research Platform: Resilient Buildings and Infrastructure
Is this really THE BEST
we can do in 2011?
Christchurch Rebuild:
Vision 2050
NZCS

Associate Professor Stefano Pampanin
National Hazard Research Platform: Resilient Buildings and Infrastructure
The Opportunity for the Future:
the best know-how for the rebuild
Base Isolation
(Christchurch Womens Hospital)
PRESSS-Technology
(Southern Cross Hospital Endoscopy Building)
Unbonded post-tensioned tendons
Energy Dissipation Devices
NZCS

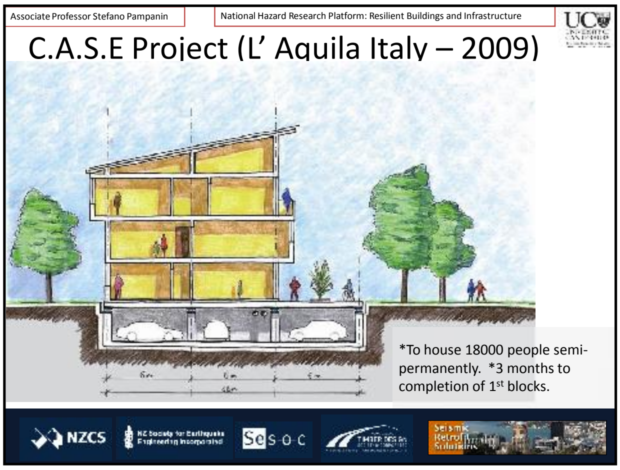

Associate Professor Stefano Pampanin
National Hazard Research Platform: Resilient Buildings and Infrastructure
C.A.S.E Project (L' Aquila Italy – 2009)
*To house 18000 people semi-permanently. *3 months to completion of 1st blocks.
NZCS

Associate Professor Stefano Pampanin
National Hazard Research Platform: Resilient Buildings and Infrastructure
Learning from our Ancestors..
Rocking Section
Multi-block Rocking: Ancient Greek Columns (Athens)

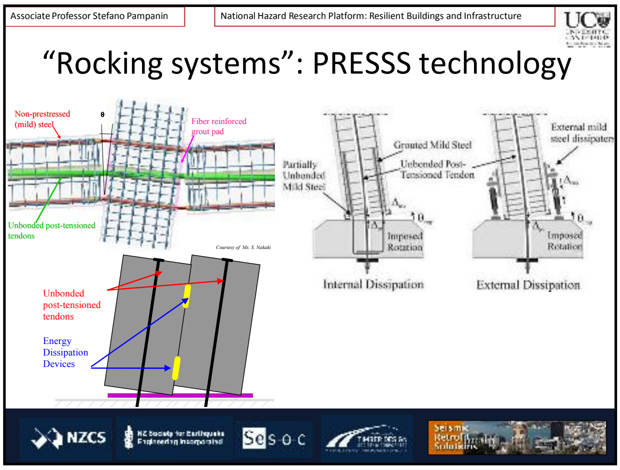

Associate Professor Stefano Pampanin
National Hazard Research Platform: Resilient Buildings and Infrastructure
"Rocking systems": PRESSS technology
Non-prestressed (mild) steel
Fiber reinforced grout pad
Unbonded post-tensioned tendons
Partially Unbonded Mild Steel
Grouted Mild Steel
Unbonded Post-Tensioned Tendon
External mild steel dissipaters
Imposed Rotation
Internal Dissipation
External Dissipation
Unbonded post-tensioned tendons
Energy Dissipation Devices
NZCS

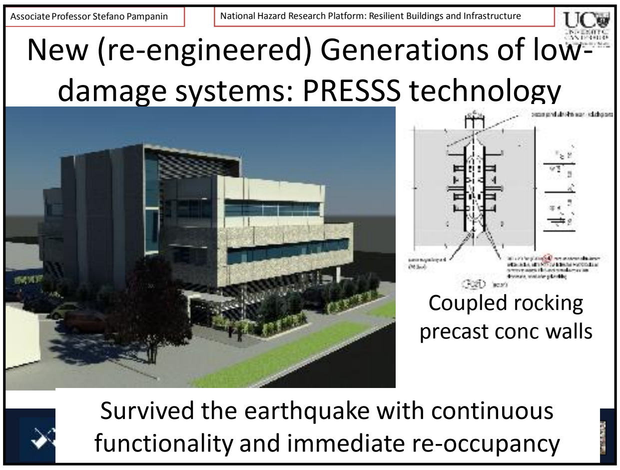
Associate Professor Stefano Pampanin
National Hazard Research Platform: Resilient Buildings and Infrastructure
New (re-engineered) Generations of low-damage systems: PRESSS technology
Coupled rocking precast conc walls
Survived the earthquake with continuous functionality and immediate re-occupancy

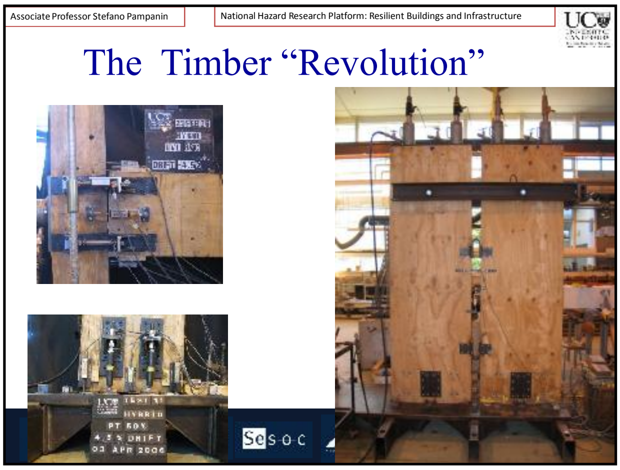
Associate Professor Stefano Pampanin
National Hazard Research Platform: Resilient Buildings and Infrastructure
The Timber "Revolution"

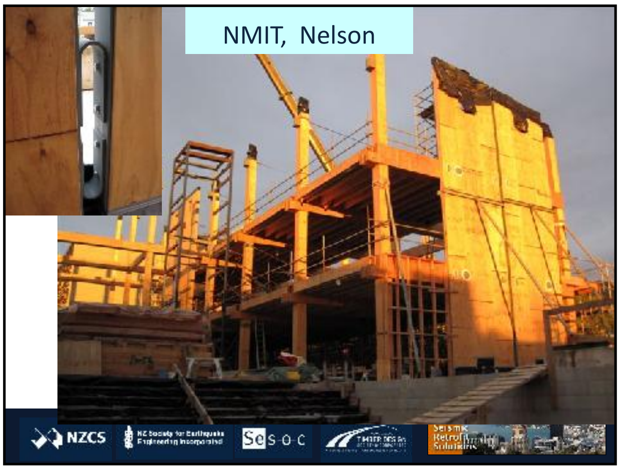
NMIT, Nelson
NZCS


Associate Professor Stefano Pampanin
National Hazard Research Platform: Resilient Buildings and Infrastructure
Massey Univ, Wellington
NZCS


Platform: Resilient Buildings and Infrastructure
Progetti Concorsi
Provincia di Parma, uffici in legno hi-tech
First Pres-Lam Building to appear soon in Europe?!


How will this look like in 2050?
Re-building Christchurch in wood

Damage of wooden houses due to *Tsunami* caused by the 2011 off the Pacific coast of Tohoku Earthquake

Motoi Yasumura

Shizuoka University, Japan

1 Introduction

A severe earthquake of Magnitude 9.0 occurred off the Pacific coast of Tohoku in March 11, 2011. The epicentral area attained to the large area of about 500 km of north and south from the offing of Iwate to the offing of Ibaraki, and about 200 km of east and west. The *tsunami* caused by this earthquake went up to not less than 10 m of wave height and 40.5 m of the maximum ascension in particular places, and brought destructive damage to the Pacific coast of the Tohoku district and the Kanto district. This prompt report presents an outline of the damage of wooden houses in *tsunami* area and what we should consider about the design of timber structures related to *tsunami*.

2 Outline of earthquake

The outline of the main shock is shown as follows;

- Epicenter: Off Sanriku, Japan
- Origin time: March 11, 2011 at 14:46 JST (JMA)
- Location: 38.103°N 142.860°E (JMA)
- Depth: 24 km (JMA)
- Magnitude: 9.0 (JMA)
- The dead: 15,707 persons (18 August, 2011)
- Missing: 4,642 persons (18 August, 2011)
- Completely destroyed houses: 112,962 units
- Partially destroyed houses: 145,051 units

More than 90% of the dead were drowned and more than 90% of completely destroyed houses were caused by *tsunami*.

3 Damage of wooden houses

In general the number of collapsed wooden houses due to the ground motion of this earthquake was very limited. However timber buildings did not remain in the area where the maximum flood depth by *tsunami* attained 13-14m (photos. 1,2). Some wooden houses were not swept away in the vicinities of the Ishinomaki harbor and Yuriage, Natori-city

Photo.1 General view of damaged area by ***tsunami*** in Onagawa. Flood depth attained about twenty meters at the city center.

Photo.2 General view of damaged area by ***tsunami*** in Minami-sanriku. Almost no buildings remain except for some reinforced concrete buildings.

whose flood depth is presumed more or less 6m (photos. 3, 4). In the slope of hills near the coast, the damage of wooden houses depends on the flood depth (photos. 5, 6). Most houses were collapsed and swept away at the foot of the slope. In the upper area, the wooden houses flooded to the second storey above the floor level remained without serious structural damage (photos 5 and 6).

Photo.3 The house remained resisting against the flood in the flatlands despite of the collapse of the corner room (Natori).

Photo.4 The house remained resisting against the flood in the flatlands. (Natori).

Photo.5 Overview of damage of houses on the slope (Onagawa)

Photo.6 Overview of damage of houses on the slope. Damages depend a lot on the height above the sea level (Onagawa).

4 Design of timber structures against *Tsunami*

It seems impossible to design timber structures so that they resist against higher flood level than the height of the building, but it may be possible to design them for some lower criteria. Such design and criteria should be studied by looking at the results of investigation on damage of timber structures due to Tsunami caused by this earthquake (Photos 7-12).

Photo.7 The house standing on the slope and flooded up to the top of the building (Onagawa).

Photo.8 The house standing on the slope and flooded up to the second floor level (Minami-sanriku).

Photo.9 Floating house may cause the secondary disaster such as a crash to other houses (Onagawa)

Photo.10 Three storey wooden building that resisted against flood up to the third floor level (Onagawa).

Photo.11 Well designed glulam warehouse resisted well against the flood although it lost all the exterior walls (Ishinomaki).

Photo.12 The wooden building having the reinforced concrete piloti in the first storey resisted well against the flood (Natori)

CIB 2011 – Research note ”Mineral wool in timber structures exposed to fire”

J. Schmid, A. Just

1 Introduction

Mineral wool is used for cavity insulation in many types of structures. As other building elements mineral wool has to satisfy different needs, among others heat and acoustic insulation during the service life but it may also contribute the fire resistance of the structure. When EN 1995-1-2 [1] was drafted the terms “insulation made of glass fibre” (glass wool) and “insulation made of rock fibre” (stone wool) were introduced without any further definition. A later European standard, EN 13162 [2], for thermal insulation products defines mineral wool but the only difference between glass and stone wool is the raw material: No classification of mineral wool in terms needed for structural fire design is given although it is widely known from fire resistance tests that stone wool performs better than glass wool when directly exposed to fire. At the moment no standardized test method exists to quantify the difference in terms of product properties. In a revision of 1995-1-2 [1] these facts have to be considered due to discovered differences in the fire performance of stone wool and the availability of a novel product on the market which is a glass wool but performs in fire as stone wool.

2 Limitation of existing models for the verification of fire resistance

In the main part of [1] as well as the Annex C (based on [3]) for light weight timber floors and walls the constructions can be filled with any mineral wool as long as any cladding is in place, protecting the members and the cavity insulation. As soon as the cladding fails (t_f) verification can be done only if stone wool is used since glass wool will undergo decomposition, although models exist for void cavities (Annex D of [1], [4]). A proposal for an intermediate stage exists which takes into account a recession speed of the insulation; for glass wool a value of $v = 30\ mm/min$ is proposed, see Figure 2, (trapezoid model for shrinking cavity insulation) [5].

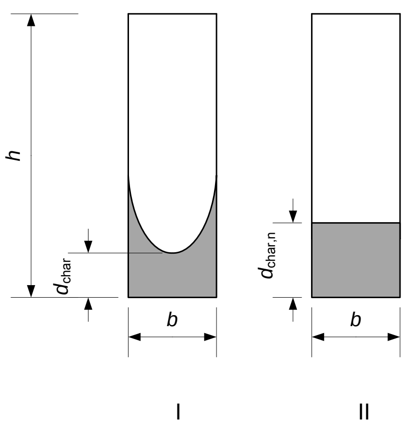

Figure 1: Charring during different phases of fire exposure according to [1] . Using the charring in the centre of the cross-section and the real shape of the residual cross-section (I) a one-dimensional charring rate is applied which results in a rectangular residual cross-section (II).

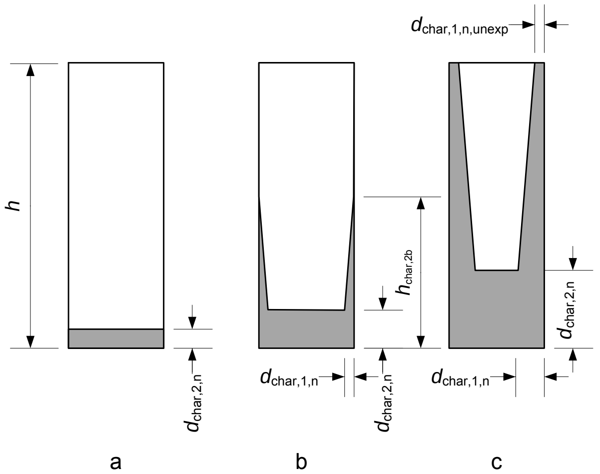

Figure 2: Charring during different phases of fire exposure. One dimensional charring during the protective phase (a), charring during recession of the cavity insulation (b) and during the final stage with a void (c). [5]

In Annex E of EN 1995-1-2 [1] the assumption is taken that the quality of protection ability of glass and stone wool is related to the density but recent research showed that density might not be the determining factor [10]. The models of [1] are based on a 29,4 kg/m^3 dense product available in Scandinavia [2]. A new model for the calculation of the separating function developed at ETH Zurich [6], [7] uses the density of stone wool and glass wool to describe their ability to contribute to the protection of an insulating layer. In recent research [10] different products, both stone wool and heat resistant glass wool were compared in a full scale wall test with direct fire exposure, see Figure 4. It shows that [1] is based on one of the best products while other products satisfying the description stone wool and representing high densities do not lead to comparable good results.

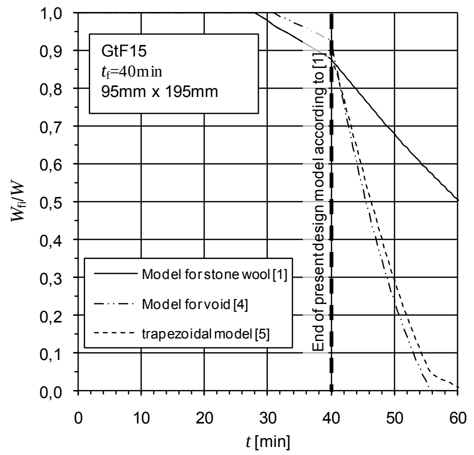

Figure 3: Example of new design model for structure with gypsum plasterboard type F (h_p=15 mm) and timber studs 95 mm x 195 mm.[5]

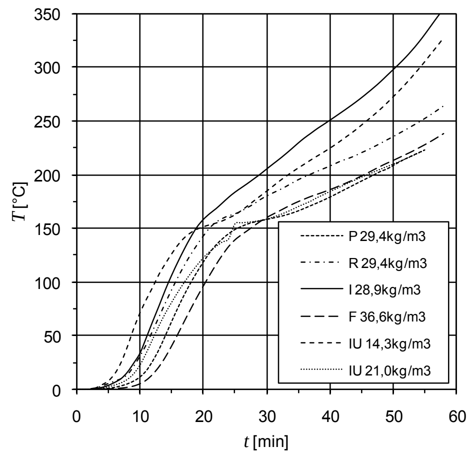

Figure 4: Temperature rise behind mineral wool of 145 mm thickness exposed to standard fire. [10]

During the last years a novel product combining the traditional advantages of glass wool (high flexibility, lower self weight) and fire resistance ability was introduced on the market. Due to the limitations of [1] described above it can't be used after the failure of the cladding (post protection phase) although the protection ability was proven in both non load bearing and load bearing model scale and full scale tests [10]. The charring rate of timber frame structures insulated with this heat-resistant glass wool is in good agreement with results of stone wool, see Figure 5. In loaded beam tests (unprotected phase) the interaction of insulation and timber can be evaluated. Results of tests done to develop the existing model for stone wool of [1] were compared with new test results, see Figure 6. It can be observed that all test results with heat-resistant glass wool are on the safe side compared to the model curve and the results for stone wool. All results were determined according the same internal SP model scale standard method.

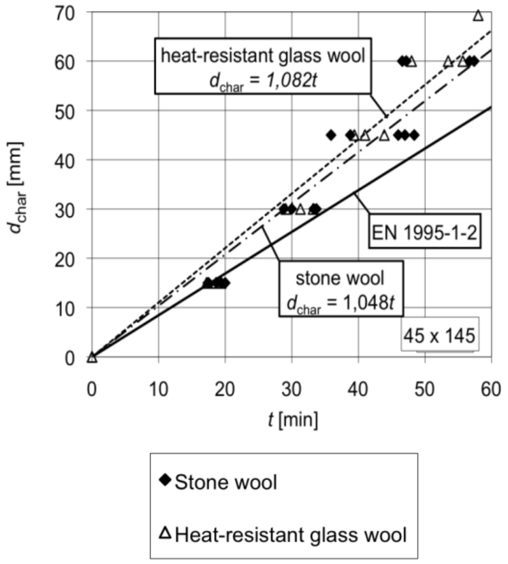

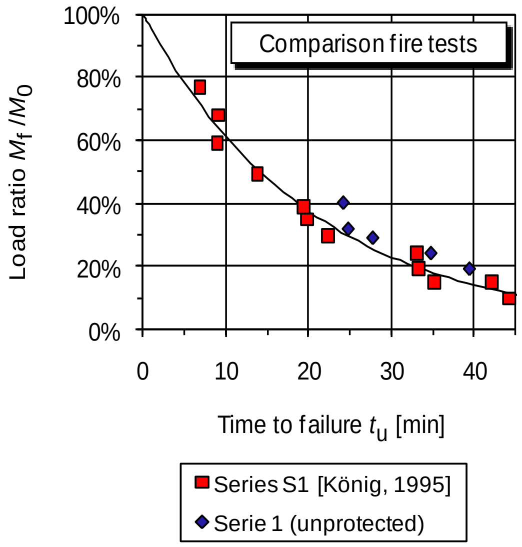

Figure 5: Linear equations for the charring rates of studs insulated by heat-resistant glass wool and stone wool. [9]

Figure 6: Comparison of failure times in fire tests with stone wool (squares) and tests with heat resistant glass wool (rhombuses). [11]

3 Conclusion, proposal, future needs

It might be difficult to keep terms for stone wool and glass wool as distinguishing parameter in [1]; however no official testing method is available to verify the fire performance of insulation materials to be used in construction (resistance to fire). The lowest common denominator would be that failure of claddings is not acceptable, that means after a cladding's failure a void has to be assumed for any mineral wool, compare Figure 3 This would be design on the safe side but would be a clear change for the worse for timber structures and thus not preferable.

For better specification of mineral wool, a new classification of mineral wool is needed with respect to its performance in fire. Such classification should permit the inclusion of new types of mineral wool in accordance with EN 13162.

Since glass wool will undergo decomposition between 550-650°C and traditional fire resistance requirements of 30, 60 and 90 minutes standard fire exposure correspond to furnace temperatures of 884, 969 and 1031°C a proposal could be that the "stability of insulation" has to be assessed by tests up to the corresponding temperature for any insulation product; alternatively a recession speed is to be declared, compare [5]. However there is no test method available to proof the "stability of insulation". Furthermore stability, which means the existence of a material at a certain temperature, is a very rough characterization of the material since the thermal performance has to be considered.

4 References

[1] EN 1995-1-2:2004 Eurocode 5: Design of timber structures – Part 1-2: General – Structural fire design. European Standard. European Committee for Standardization, Brussels, 2004.

[2] EN 13162:2008. Thermal insulation products for buildings - Factory made mineral wool products - Specification. European Standard. European Committee for Standardization, Brussels, 2008.

[3] König J, Walleij L. Timber frame assemblies exposed to standard and parametric fires. Part 2: A Design model for standard fire exposure. Trätek, Swedish Institute for Wood Technology Research, Report No. 0001001, Stockholm, 2000.

[4] Frangi, A, Erchinger, C, Fontana, M, 2008, Charring model for timber frame floor assemblies with void cavities. Fire Safety Journal 43 (2008) 551–564.

[5] Just, A, Schmid, J and König, J, Post protection behaviour of wooden wall and floor structures completely filled with glass wool, Structures in Fire (SIF) 2010.

[6] Fire safety in timber buildings, technical guideline for Europe, chapter 5, SP report 2010:19, Stockholm 2010.

[7] Schleifer V., Zum Verhalten von raumabschliessenden mehrschichtigen Holzbauteilen im Brandfall, PhD Thesis ETH No. 18156, ETH Zurich, 2009.

[8] CEN/TC88. prEN ISO 9229 Thermal insulation - Definitions of terms. European Standard. European Committee for Standardization, Brussels, 2006.

[9] Just, A, Schmid, J and König, J, Post protection effect of heat-resistant insulations on timber frame members exposed to fire, Fire and materials, in print.

[10] Just, A, Schmid, J and König, J, Effect of insulation on charring of timber frame members, SP report 2010:30, Stockholm, 2010.

[11] Schmid, J, König, J, Just, A., Model scale fire tests of Isover Ultimate – Step 1.2: Load bearing capacity, SP report 2010:26, Stockholm. 2010.

Reliability Based Code Calibration
– note on basic principles and possible misunderstandings

Jochen Köhler, ETH Zurich

Synopsis:
This note refers to an on-going controversy about the meaning and consistency of the present LRFD format prescribed in the Eurocodes. The debate is driven by mainly one individual researcher who fundamentally criticised the consistency of the present timber structural design basis (EC5 in particular) at the annual meetings of the CIB W18 community in 2009 [1] and 2010 [2]. The importance of this topic necessitates a brief following up of this discourse. The aim of this note is to clarify whether the basis on which the arguments are raised can be scientifically proven.
It is underlined that the personalized style of discussion followed in this document does originate in the rather exclusive argumentation of T.Poutanen as an individual researcher, i.e. his statements and conclusions are entirely based on his personal reasoning and therefore his name is addressed repeatedly in the text.

Basic principles of reliability based code calibration:
A large proportion of the societal wealth is invested in the continuous development and maintenance of the built infrastructure. It is therefore essential that decisions in this regard are made on a rational basis. A structural design code should be such a rationale that facilitates design solutions that balance expected adverse consequences (e.g. in case of failure or deterioration) with investments into more safety (e.g. larger cross sections). Structural design codes are therefore calibrated on the basis of associated risks or, simplified, on the basis of associated failure probability. In this note it is focused on the latter, the interested reader should refer to e.g. [3] for more complete information on this topic.

Modern design codes are based on the so-called load and resistance factor design (LRFD) format. For the case of two loads (one constant and the other variable over time) a LRFD equation could be written as

$$z\frac{R_k}{\gamma_m} - \gamma_G G_k - \gamma_Q Q_k = 0 \qquad (1)$$

R_k is the characteristic value for the resistance, G_k is the characteristic value for the permanent load, Q_k is the characteristic value for the load variable over time, $\gamma_m, \gamma_G, \gamma_Q$ are the corresponding partial safety factors for the resistance and for the load. z is the so-called design variable, i.e. it is defined by the chosen dimensions of the structural component. The characteristic values for the resistance and the loads are conventionally defined as certain fractile values of the probability distributions of the random variables representing resistance and load, correspondingly. For EC 5, R_k corresponds to the 5% fractile value of a Lognormal distributed resistance, G_k to a 50% fractile value (or mean value) of the Normal distributed load constant in time. Q_k is the 98% fractile value of the Gumbel distributed yearly maxima of the load variable in time. Based on the conventional choice of R_k, G_k and Q_k the corresponding partial safety factors can be calibrated to provide design solutions (z) with an acceptable failure probability. The failure probability P_F is expressed as

$$\begin{aligned} &P_F = \Pr\left(g(X,R,G,Q) < 0\right) \\ &\text{with} \\ &g(X,R,G,Q) = z^* XR - G - Q = 0 \end{aligned} \qquad (2)$$

$g(.)$ is the Limit State Equation R. G and Q are resistance and loads represented as random variables. $z^* = z(\gamma_m, \gamma_G, \gamma_Q)$ is the design solution identified with Equation (1) as a function of the selected partial safety factors. X is the model uncertainty.

In general, different design situations are relevant in terms of different contributions of the permanent and variable load. With the following modification of Equations (1) and (2) this can be considered:

$$z_i \frac{\hat{R}_k}{\gamma_m} - \gamma_G \alpha_i \hat{G}_k - \gamma_Q (1-\alpha_i)\hat{Q}_k = 0 \tag{3}$$

$$g_i\left(X,\hat{R},\hat{G},\hat{Q}\right) = z_i^* X\hat{R} - \alpha_i \hat{G} - \left(1-\alpha_i\right)\hat{Q} = 0 \tag{4}$$

Here, α_i might take values between and including 0 and 1, representing different relative contributions of permanent and variable load. The hat "^" indicates that the variables R, G and Q are normalized to a mean value of 1, resulting in $\hat{R}$, $\hat{G}$ and $\hat{Q}$; with $\alpha = \left[0, 0.1, 0.2, \ldots, 1.0\right]$ - 11 different design equations are considered.
The partial safety factors $\boldsymbol{\gamma} = \left(\gamma_m, \gamma_G, \gamma_Q\right)$ can now be calibrated by solving the following optimisation problem:

$$\min_{\gamma}\left[\sum_{j=1}^{L}\left(P_{F,target} - P_{F,j}\right)^2\right] \tag{5}$$

for $L = 11$ different design situations.

Example:
The software CodeCal [4] is used to consider the following example:

	X	R	G	Q
mean value	1	1	1	1
st.dev.	0.1	0.25	0.1	0.4
dist. type	lognormal	lognormal	normal	Gumbel
fractile	-	0.05	0.5	0.98
char. value	-	0.647	1	2.037

The target probability of failure is set to $P_{F,target} = 10^{-5}$. If the partial safety factors for the constant and variable over time load are fixed to $\gamma_G = 1.35$ and $\gamma_Q = 1.5$ the optimal value of the partial safety factor for the resistance results in $\gamma_m = 1.38$ if the entire range $\alpha = \left[0, 0.1, 0.2, \ldots, 1.0\right]$ is considered. However, the range $\alpha = \left[0.1, 0.2, \ldots, 0.8\right]$ might more realistically represent design equations in timber design and the corresponding optimal value of the partial safety factor for the material resistance would be $\gamma_m = 1.33$.

Discussion on the scientific validity of the presented approach
The correct application of the procedure for reliability based code calibration summarized above necessitates that common text book knowledge about statistics, probability theory and structural reliability as well as basic calculus is implemented. In regard to the procedural content of the method it should be noted that a differentiation can be made between 'right' and 'wrong' in the sense of the philosophical basis of scientific reasoning e.g. [5], i.e. the procedural content is falsifiable on the basis of deductive reasoning. The procedural content of reliability based code calibration includes:

- the abstraction of an identified limit state, including the choice of a set of basic random variables,
- the use of statistics and probability theory to set up probabilistic models for the basic random variables,
- the use of structural reliability methods for computing failure probability.

However, reliability based code calibration rests also on many assumptions and simplifications, and the results are highly sensitive to these, including:

- identification of relevant limit states,

- format of the design equation,
- choice of probabilistic models, distribution types to represent the basic random variables.

The assumptions are made based on expert agreement, however, they can hardly be attributed as ‘right’ or ‘wrong’ in a scientific sense outlined above.

Evaluation of the current debate

The discussion about the consistency of the current EC format driven by T. Poutanen clearly relates to attributes that can be falsified based on scientific reasoning. Basis for T. Poutanen`s criticism is a misunderstanding of the meaning of a random property and random variable in general. However, the rather basic mistake that is made at the very beginning of T. Poutanens’ argumentation is obviously hard to see even for experts leading to many unstructured and inconclusive discussions.

The starting point of T. Poutanen’s argumentation is related to ‘dependence’, ‘independence’, ‘correlation’ and ‘non-correlation’ of loads. From an observation of the behaviour of the sum of two independent random variables that appears non-logical to him, T. Poutanen finds that the probabilistic representation of the two random variables should be modified to match his expectations.

T. Poutanen tries to illustrate his reasoning usually along an example similar to the following:
A constant material resistance r is considered together with a permanent and a time variable load, X_1 and X_2 that are represented with normal distributed random variables, i.e. X_1 and X_2 with corresponding mean values μ_{X_1}, μ_{X_2} and coefficients of variation ν_{X_1}, ν_{X_2}. Three different design situations are considered, which are expressed with the following limit state equations:

Design situation 1: $z_1 r - X_1 \geq 0$
Design situation 2: $z_2 r - X_2 \geq 0$
Design situation 3: $z_3 r - X_3 \geq 0$ with $X_3 = 0.5X_1 + 0.5X_2$

z_1, z_2, z_3 are the design variables that have to be chosen in a way that a predefined target probability of failure P_F is obtained:

$$\begin{aligned} &\Pr\left(z_i r - X_i \leq 0\right) \overset{!}{=} P_F \Leftrightarrow \Phi\left(\frac{\mu_{X_i} - z_i r}{\mu_{X_i}\nu_{X_i}}\right) \overset{!}{=} P_F \\ &z_i r = \mu_{X_i}\left(1 - \Phi^{-1}\left(P_F\right)\nu_{X_i}\right) \end{aligned} \tag{6}$$

Based on Equation (6) the design variables z_1 and z_2 can be computed for the given values of $\mu_{X_1}, \nu_{X_1}, \mu_{X_2}$ and ν_{X_2}; z_3 is calculated based on

$$\mu_{X_3} = 0.5\mu_{X_1} + 0.5\mu_{X_2} \tag{7}$$

and

$$\nu_{X_3} = \sqrt{0.5^2\nu_{X_1}^2 + 0.5^2\nu_{X_2}^2} \Big/ \mu_{X_3} \tag{8}$$

assuming X_1 and X_2 are independent.

In T. Poutanen`s examples $\mu_{X_1}, \nu_{X_1}, \mu_{X_2}$ and ν_{X_2} are chosen in a way that design situation 1 and 2 lead to the same design variable for a given target probability of failure P_F i.e. $z_1 = z_2$.

For given coefficients of variation ν_{X_1}, ν_{X_2} μ_{X_2} is selected based on μ_{X_1} as

$$\mu_{X_2} = \frac{\mu_{X_1} - \Phi^{-1}\left(P_F\right)\nu_{X_1}}{1 - \Phi^{-1}\left(P_F\right)\nu_{X_2}} \tag{9}$$

It is now argued by T. Poutanen that it has to be expected that design variable z_3 should also be the same if μ_{X_2} is selected based on Equation (9). It is seen from Equations (7) and (8) together with equation (6) that this is not the case. T. Poutanen concludes that a correlation between X_1 and X_2 must be introduced and quantified specifically based on v_{X_1}, v_{X_2}, μ_{X_1} and P_F to satisfy the condition $z_1 = z_2 = z_3$.

Summary

The probabilistic representation of loads and resistances should be guided by the nature of the corresponding phenomena. It is common sense that in most cases the assumption of independence of load (e.g. wind, snow, traffic) and resistance (i.e. material strength and geometry) is appropriately reflecting reality. However, T. Poutanen's conclusion that loads must be considered as dependent variables does not originate from a study of the physical behaviour of loads and the proper probabilistic representation; it originates from a misunderstanding in probability theory.

A simple illustration based on the example presented above is given in Figure 1. Here, X_1 and X_2 are represented by independent normal distributed random variables with identical mean values and coefficient of variations (2 and 0.5) and plotted with the blue line. It can be seen that for different target failure probabilities the corresponding design solutions are obtained, as indicated with the red lie for a target failure probability of 0.1. It is also seen that the solutions for the combined variables $X_3 = 0.5X_1 + 0.5X_2$ are different.

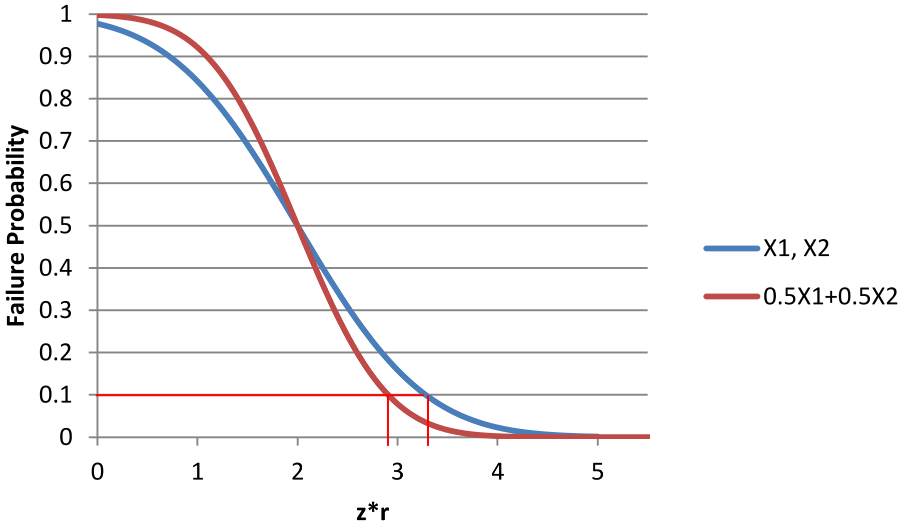

Figure 1: Failure Probability for different design solutions.

References

[1] Poutanen T. (2009) Calculation of partial safety factors. Paper CIB-W18/42-1-1 (not published).

[2] Poutanen T. (2010) Dependent versus independent loads in structural design. Paper CIB-W18/43-101-1.

[3] Faber M. H., Sorensen J. D. (2002) Reliability Based Code Calibration - Joint Committee on Structural Safety; http://www.jcss.ethz.ch.

[4] CodeCal (2002) An EXCEL® based software tool for reliability based code calibration. Available on-line; http://www.jcss.ethz.ch.

[5] Popper K. R. (1973) The aim of science. *Ratio.* Volume 1, Oxford University Press.